NEUROMODULATORY FUNCTION IN AUDITORY PROCESSING

EDITED BY: R. Michael Burger and Conny Kopp-Scheinpflug
PUBLISHED IN: Frontiers in Neural Circuits

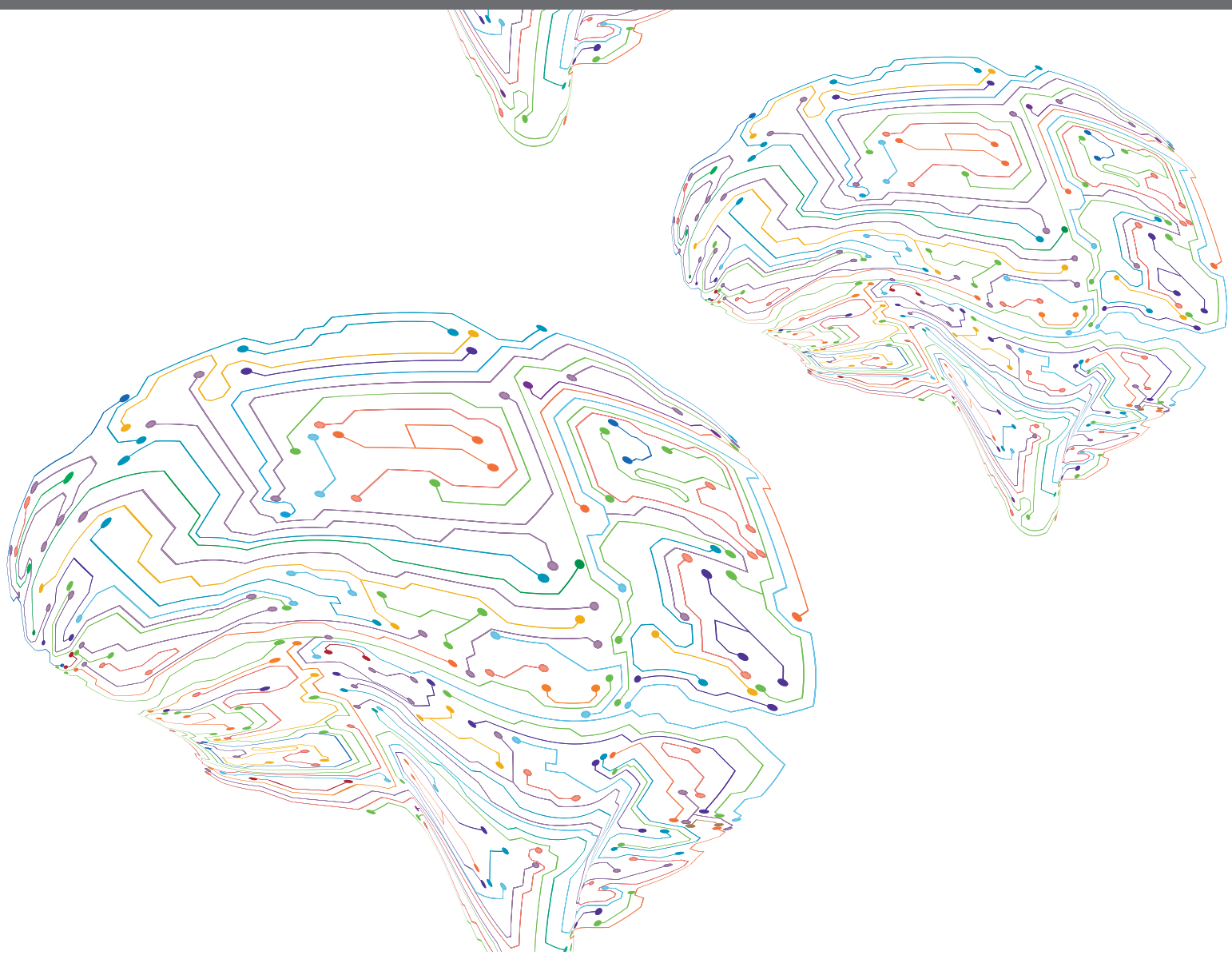

frontiers Research Topics

frontiers

ISSN 1664-8714
ISBN 978-2-88976-315-3
DOI 10.3389/978-2-88976-315-3

About Frontiers

Frontiers is more than just an open-access publisher of scholarly articles: it is a pioneering approach to the world of academia, radically improving the way scholarly research is managed. The grand vision of Frontiers is a world where all people have an equal opportunity to seek, share and generate knowledge. Frontiers provides immediate and permanent online open access to all its publications, but this alone is not enough to realize our grand goals.

Frontiers Journal Series

The Frontiers Journal Series is a multi-tier and interdisciplinary set of open-access, online journals, promising a paradigm shift from the current review, selection and dissemination processes in academic publishing. All Frontiers journals are driven by researchers for researchers; therefore, they constitute a service to the scholarly community. At the same time, the Frontiers Journal Series operates on a revolutionary invention, the tiered publishing system, initially addressing specific communities of scholars, and gradually climbing up to broader public understanding, thus serving the interests of the lay society, too.

Dedication to Quality

Each Frontiers article is a landmark of the highest quality, thanks to genuinely collaborative interactions between authors and review editors, who include some of the world's best academicians. Research must be certified by peers before entering a stream of knowledge that may eventually reach the public - and shape society; therefore, Frontiers only applies the most rigorous and unbiased reviews.
Frontiers revolutionizes research publishing by freely delivering the most outstanding research, evaluated with no bias from both the academic and social point of view. By applying the most advanced information technologies, Frontiers is catapulting scholarly publishing into a new generation.

What are Frontiers Research Topics?

Frontiers Research Topics are very popular trademarks of the Frontiers Journals Series: they are collections of at least ten articles, all centered on a particular subject. With their unique mix of varied contributions from Original Research to Review Articles, Frontiers Research Topics unify the most influential researchers, the latest key findings and historical advances in a hot research area! Find out more on how to host your own Frontiers Research Topic or contribute to one as an author by contacting the Frontiers Editorial Office: frontiersin.org/about/contact

NEUROMODULATORY FUNCTION IN AUDITORY PROCESSING

Topic Editors:
R. Michael Burger, Lehigh University, United States
Conny Kopp-Scheinpflug, Ludwig Maximilian University of Munich, Germany

Citation: Burger, R. M., Kopp-Scheinpflug, C., eds. (2022). Neuromodulatory Function in Auditory Processing. Lausanne: Frontiers Media SA.
doi: 10.3389/978-2-88976-315-3

Table of Contents

frontiers | Frontiers in Neural Circuits

EDITORIAL
published: 17 May 2022
doi: 10.3389/fncir.2022.898646

Editorial: Neuromodulatory Function in Auditory Processing

R. Michael Burger[1]* *and Conny Kopp-Scheinpflug*[2]

[1] Department of Biological Sciences, Lehigh University, Bethlehem, PA, United States, [2] Division of Neurobiology, Department Biology II, Ludwig Maximilian University, Munich, Germany

Keywords: neuromodulation, inferior colliculus, superior olive, auditory cortex, acetylcholine, auditory

Editorial on the Research Topic

Neuromodulatory Function in Auditory Processing

Neuromodulatory systems are generally known to play roles in complex behaviors such as the sleep/wake cycle, attention, arousal and learning (Picciotto et al., 2012). Canonical modulatory circuitry emanates from discrete nuclei throughout the brain, and projects broadly to virtually every region. However, most scientific investigation of modulatory signaling has focused on higher order computational centers in the forebrain, where its impact on neural response properties may be understood in the context of complex functions such as attention or arousal (McGinley et al., 2015; Carcea et al., 2017). Much less is understood about how neuromodulation shapes processing in subcortical sensory regions, or how it may influence circuitry during development.

The works presented here provide a broader view of how neuromodulation may influence auditory processing; from brainstem to cortex, from computationally simple regions to the complex, and on time scales ranging from transient to long-term. The challenges of investigating neuromodulation in vertebrates stem from poor understanding of the conditions under which modulatory ligands are released, the wide variety of receptors that bind each of them, and the spatial and temporal ranges of action which is so different from classical neurotransmitters. In tackling these challenges in the vertebrate brain, the auditory system provides the experimental advantages of a robust functional understanding of auditory processing from the ear to cortex.

OPEN ACCESS

Edited and reviewed by:
Edward S. Ruthazer, McGill University, Canada

***Correspondence:**
R. Michael Burger
burger@lehigh.edu

Received: *17 March 2022*
Accepted: *28 April 2022*
Published: *17 May 2022*

Citation:
Burger RM and Kopp-Scheinpflug C (2022) Editorial: Neuromodulatory Function in Auditory Processing. Front. Neural Circuits 16:898646. doi: 10.3389/fncir.2022.898646

NEW MODULATORY PATHWAYS

This topic's contents include what are likely to be enduring discoveries providing new insights into the anatomy of cholinergic circuitry influencing auditory nuclei. Beebe et al. focused on cholinergic input to the superior olive, a cluster of nuclei that processes several fundamental aspects of auditory input, and Noftz et al. documented cholinergic inputs to the inferior colliculus (IC) in unprecedented detail using viral vectors, tract tracing, and immunohistochemistry. Together they describe major output projections of cholinergic neurons in the pontomesencephalic tegmentum (PMT), which is not just a primary source of cholinergic output in the brain, but may serve as a hub for multiple neuromodulators.

MODULATION OVER SHORT TIME SCALES

Several works appearing in this volume illustrate the power of investigating neuromodulatory physiology in the auditory system, where modulation of stimulus driven activity in real-time can be interpreted in its functional context. Instkerveli and Metherate demonstrated how activation of nicotinic signaling increases response gain and shortens response latency across populations

of auditory cortex neurons. These changes improved response reliability across trials and countered adaptation to repeated stimuli which may be important for processing ongoing signals including speech. Similarly, Rivera-Perez et al. revealed the cellular mechanisms for nicotinic gain control in a genetically defined population of neurons in the IC. Specifically, they showed that $\alpha_3\beta_4$ nicotinic receptors are primarily responsible for mediating a depolarizing inward current that both boosts membrane excitability and enhances summation of excitatory inputs. Together these papers show that modulation by acetylcholine can rapidly and consequentially enhance responses to sound in two major auditory centers.

Auditory modulation is not limited to cholinergic input however, and several studies collectively demonstrated the wide variety of factors that are brought to bear on auditory computation. Serotonin is a neurotransmitter well known to be released in specific behavioral contexts such as mating. Polese et al. presented anesthetized mice with broadband vocalizations while recording IC neuron responses in the presence or absence of serotonin agonists. They showed that serotonin released in the context of mating has the potential to sharpen neural selectivity for specific vocalizations and call features.

Two review contributions highlight bodies of work that reveal complex and varied influences of metabotropic glutamate receptors (mGluRs) and nitric oxide (NO) signaling. Goel et al. illustrate the many ways that mGluRs control both presynaptic release at excitatory synapses and simultaneously modulate the excitability of the postsynaptic cells in the sound localization circuitry of both birds and mammals. Kopp-Scheinpflug and Forsythe review how NO, synthesized in response to Ca^{++} entry during synaptic activity, can mediate a myriad of effects in both postsynaptic and presynaptic neurons. Importantly, NO as a soluble messenger has the potential to act on neurons away from its site of production and independently of synaptic connections, including non-auditory or multisensory neurons.

MODULATORS MAY SHAPE CIRCUITRY OVER LONG TIME PERIODS

Modulation may not necessarily derive from discrete clusters of functionally similar neurons releasing a canonical transmitter, nor is modulatory function temporally constrained to influence processing in time scales limited to stimulus duration or behavioral state. One example of modulatory release from principal auditory neurons themselves is provided by Wollet and Kim. Activity-dependent BDNF release is known to influence synaptic plasticity during long term potentiation Xu et al. (2010). Here, Wollet and Kim demonstrate that sound driven BDNF signaling also influences auditory circuitry on developmental time scales. Heterozygous BDNF (+/−) mutant mice failed to develop normal frequency-dependent patterning of intrinsic neural properties. A second compelling example is presented by Pagella et al., who showed that Urocortin 3, a neuropeptide transmitter released during stress, and its receptor CRFR2, are expressed broadly in the auditory pathway by principal and interneurons, respectively, suggesting a reverse modulation from principal neurons to the canonical modulatory neurons. Urocortin 3 knockout animals have been shown to be particularly sensitive to noise damage suggesting that the auditory pathways express modulators that confer an auto-protective function (Fischl et al., 2019). Finally, Knipper et al. propose a model by which trauma induced hyperexcitability along the auditory pathway influences BDNF signaling to disrupt the balance of excitation and inhibition. They go on to propose that downstream changes to NO signaling may disrupt the neural-vascular interface which may cause deficits beyond the auditory system.

These studies open new lines of inquiry beyond investigations of excitation and inhibition in principal auditory neurons to include the additional layers of complexity provided by modulation from the ear to cortex and back again. Further, it is evident that modulatory circuitry shapes neural responses on time scales ranging from long-lasting developmental processes to immediate effects in the mature organisms. We hope the work presented here will stimulate further exploration into what promises to be a rich and emerging field of auditory neuroscience.

AUTHOR CONTRIBUTIONS

All authors listed have made a substantial, direct, and intellectual contribution to the work and approved it for publication.

ACKNOWLEDGMENTS

We wish to express our gratitude to the 31 authors who contributed their effort to this Research Topic.

REFERENCES

Carcea, I., Insanally, M., and Froemke, R. (2017). Dynamics of auditory cortical activity during behavioural engagement and auditory perception. *Nat. Commun.* 8, 14412. doi: 10.1038/ncomms14412

Fischl, M. J., Ueberfuhr, M. A., Drexl, M., Pagella, S., Sinclair, J. L., Alexandrova, O., et al. (2019). Urocortin 3 signalling in the auditory brainstem aids recovery of hearing after reversible noise-induced threshold shift. *J. Physiol.* 597, 4341–4355. doi: 10.1113/JP278132

McGinley, M. J., Vinck, M., Reimer, J., Batista-Brito, R., Zagha, E., Cadwell, C. R., et al. (2015). Waking state: rapid variations modulate neural and behavioral responses. *Neuron.* 87, 1143–1161. doi: 10.1016/j.neuron.2015.09.012

Picciotto, M. R., Higley, M. J., and Mineur, Y. S. (2012). Acetylcholine as a neuromodulator: cholinergic signaling shapes nervous system function and behavior. *Neuron.* 76, 116–29. doi: 10.1016/j.neuron.2012.08.036

Xu, H., Kotak, V. C., and Sanes, D. H. (2010). Normal hearing is required for the emergence of long-lasting inhibitory potentiation

in cortex. *J. Neurosci.* 30, 331–341. doi: 10.1523/JNEUROSCI.4554-09.2010

Conflict of Interest: The authors declare that the research was conducted in the absence of any commercial or financial relationships that could be construed as a potential conflict of interest.

Publisher's Note: All claims expressed in this article are solely those of the authors and do not necessarily represent those of their affiliated organizations, or those of the publisher, the editors and the reviewers. Any product that may be evaluated in this article, or claim that may be made by its manufacturer, is not guaranteed or endorsed by the publisher.

frontiers in Neural Circuits

ORIGINAL RESEARCH
published: 16 July 2020
doi: 10.3389/fncir.2020.00043

Cholinergic Projections From the Pedunculopontine Tegmental Nucleus Contact Excitatory and Inhibitory Neurons in the Inferior Colliculus

William A. Noftz[1,2], *Nichole L. Beebe*[2], *Jeffrey G. Mellott*[2] *and Brett R. Schofield*[1,2]*

[1]School of Biomedical Sciences, Kent State University, Kent, OH, United States, [2]Department of Anatomy and Neurobiology, Hearing Research Group, Northeast Ohio Medical University, Rootstown, OH, United States

The inferior colliculus processes nearly all ascending auditory information. Most collicular cells respond to sound, and for a majority of these cells, the responses can be modulated by acetylcholine (ACh). The cholinergic effects are varied and, for the most part, the underlying mechanisms are unknown. The major source of cholinergic input to the inferior colliculus is the pedunculopontine tegmental nucleus (PPT), part of the pontomesencephalic tegmentum known for projections to the thalamus and roles in arousal and the sleep-wake cycle. Characterization of PPT inputs to the inferior colliculus has been complicated by the mixed neurotransmitter population within the PPT. Using selective viral-tract tracing techniques in a ChAT-Cre Long Evans rat, the present study characterizes the distribution and targets of cholinergic projections from PPT to the inferior colliculus. Following the deposit of viral vector in one PPT, cholinergic axons studded with boutons were present bilaterally in the inferior colliculus, with the greater density of axons and boutons ipsilateral to the injection site. On both sides, cholinergic axons were present throughout the inferior colliculus, distributing boutons to the central nucleus, lateral cortex, and dorsal cortex. In each inferior colliculus (IC) subdivision, the cholinergic PPT axons appear to contact both GABAergic and glutamatergic neurons. These findings suggest cholinergic projections from the PPT have a widespread influence over the IC, likely affecting many aspects of midbrain auditory processing. Moreover, the effects are likely to be mediated by direct cholinergic actions on both excitatory and inhibitory circuits in the inferior colliculus.

Keywords: acetylcholine, auditory, choline acetyltransferase, midbrain, viral tracing, hearing, neuromodulation, arousal

OPEN ACCESS

Edited by:
Conny Kopp-Scheinpflug, Ludwig Maximilian University of Munich, Germany

Reviewed by:
Susanne Schmid, University of Western Ontario, Canada
Troy Hackett, Vanderbilt University, United States

***Correspondence:**
Brett R. Schofield
bschofie@neomed.edu

Received: *22 April 2020*
Accepted: *19 June 2020*
Published: *16 July 2020*

Citation:
Noftz WA, Beebe NL, Mellott JG and Schofield BR (2020) Cholinergic Projections From the Pedunculopontine Tegmental Nucleus Contact Excitatory and Inhibitory Neurons in the Inferior Colliculus. Front. Neural Circuits 14:43. doi: 10.3389/fncir.2020.00043

INTRODUCTION

Acetylcholine (ACh) plays a wide range of roles in normal auditory function, exerting influence from the cochlea to the auditory cortex. In the forebrain, ACh contributes to memory, learning, and attention (Hasselmo and Sarter, 2011; Leach et al., 2013). In the thalamus, ACh differentially influences the efficacy of inputs to a cell, affecting the gating of information flow and possibly biasing a cell toward top-down vs. bottom-up modulation (Sottile et al., 2017). At many levels

of the auditory system, ACh can increase spontaneous activity and excitability of auditory neurons and can alter tuning profiles of cells (Farley et al., 1983; Sarter and Bruno, 1997; Ji et al., 2001; Metherate, 2011; Suga, 2012). Finally, ACh is a primary neurotransmitter in the olivocochlear system and plays a critical role in the cochlear amplifier (Dallos et al., 1996; Ryugo et al., 2011). Although much of the previous research on ACh in the auditory system has been done at the levels of forebrain and cochlea, the evidence is accumulating for widespread and varied effects of ACh in the inferior colliculus (IC), a midbrain hub for both ascending and descending auditory pathways (Winer and Schreiner, 2005; Schofield and Beebe, 2019).

Application of ACh to the IC affects the responses to auditory stimuli of a majority of IC neurons (Watanabe and Simada, 1973; Farley et al., 1983; Habbicht and Vater, 1996). Such effects can modify temporal processing and forward masking (Felix et al., 2019). Supporting the idea of widespread effects of ACh in the IC, both nicotinic and muscarinic ACh receptors are present throughout the IC, as is acetylcholinesterase, the enzyme that degrades ACh (Shute and Lewis, 1967; Cortes et al., 1984; Glendenning and Baker, 1988; Henderson and Sherriff, 1991; Happe and Morley, 2004). This is relevant because the physiological studies described above focused on cells in the central nucleus of the IC (ICc), the main lemniscal division of the IC. The dorsal cortex (ICd) and the lateral cortex (IClc) are extralemniscal subdivisions that give rise to parallel ascending pathways that terminate in different parts of the thalamus and serve a variety of functions. These three subdivisions vary concerning cholinergic innervation; in fact, the extralemniscal divisions typically exhibit the highest levels of cholinergic receptors. Staining for β4 nicotinic cholinergic receptor subunits is heaviest in layer 2 of the IClc, with moderate expression in the ICc and less in the ICd (Gahring et al., 2004). These receptors have recently been reported to aid in the modulation of spike timing and forward masking in the IC (Felix et al., 2019). The IClc has also been noted for its comparatively high levels of the α7 nicotinic receptor subunit and high levels of acetylcholinesterase (Happe and Morley, 2004; Dillingham et al., 2017). Muscarinic receptors also stained differentially in the IC, with an expression of m2 receptors highest in the IClc and ICd and less so in the ICc (Hamada et al., 2010). All of this points to a diverse effect of ACh onto several different regions of IC which are known to participate in different parallel ascending auditory and multisensory pathways (Calford and Aitkin, 1983; Rouiller, 1997; Mellott et al., 2014).

Despite the numerous studies of cholinergic receptors in the IC, there is very little information about the identity of IC cells that are directly targeted by the cholinergic inputs. Neurons of the IC are glutamatergic or GABAergic, with GABAergic neurons constituting 20–40% of this population (Oliver et al., 1994; Winer et al., 1996; Merchán et al., 2005; Mellott et al., 2014). Both glutamatergic and GABAergic IC cells likely receive direct cholinergic inputs. Yigit et al. (2003) provided evidence that cholinergic inputs directly activate GABAergic IC cells during development. Sottile et al. (2017) showed that both GABAergic and glutamatergic IC cells can express nicotinic receptors, but their methods did not provide information on the subcellular localization of those receptors (in fact, their study was focused on cholinergic effects on the axon terminals of IC cells that project to the thalamus). An understanding of cholinergic effects in the IC will require identification of the cell types that receive direct cholinergic inputs.

The major source of cholinergic input into the IC is from the pontomesencephalic tegmentum (PMT; Motts and Schofield, 2009, 2011; Schofield et al., 2011). The PMT is the primary source of cholinergic innervation of the thalamus and brainstem and is closely associated with the sleep-wake cycle, sensory gating and attention (Reese et al., 1995a,b,c; Jones, 2017; Cissé et al., 2018). It comprises two groups of neurons: the laterodorsal tegmental nucleus (LDT) which is situated largely within the periaqueductal gray (PAG), and the pedunculopontine tegmental nucleus (PPT). Of the two components, the PPT is the predominant source of cholinergic inputs to the IC (Motts and Schofield, 2009). At its caudal end, the PPT is ventrolateral to the PAG and surrounds the superior cerebellar peduncle. The PPT extends rostro-ventrally from this location almost as far as the substantia nigra in the rostral and ventral midbrain. Nearly half of the neurons in the PPT region respond to sound, and the cholinergic neurons have been implicated in acoustic startle and tone-specific plasticity (e.g., Reese et al., 1995a,b,c; Xiong et al., 2009; Suga, 2012; Azzopardi et al., 2018).

Here we take advantage of viral vectors and a transgenic rat line to allow for the selective tracing of cholinergic projections into the IC. This is important because the PMT contains a mixed population of neuronal neurotransmitter phenotypes, including cholinergic, GABAergic, and glutamatergic cells (Wang and Morales, 2009). Traditional tract-tracing methods rely on axonal transport of tracers without regard for neurotransmitter phenotype, making it difficult to identify the neurotransmitter associated with any particular axon. We used viral vectors that express fluorescent protein only in cells that contain Cre-recombinase. The vectors were injected into the PPT in ChAT-Cre rats, in which Cre-recombinase is expressed only in cholinergic cells. We then use antibodies against glutamic acid decarboxylase (GAD), a specific marker of GABAergic neurons, to distinguish GABAergic from glutamatergic IC neurons. Our analyses focus on the central nucleus (ICc), the lateral cortex (IClc), and the dorsal cortex (ICd), three of the largest IC subdivisions, and the focus of most previous studies of cholinergic effects in the IC. We observed cholinergic axons from the PPT throughout the IC ipsilateral and contralateral to the labeled PPT cholinergic neurons. The axons typically possessed many boutons, including ones in close apposition to GAD-immunopositive (GAD^+) and GAD-immunonegative (GAD^-) neurons in all the IC subdivisions examined. These results suggest that cholinergic axons from the PPT directly contact glutamatergic and GABAergic IC neurons and thus could modulate both excitatory and inhibitory circuits that arise from these cells.

MATERIALS AND METHODS

All procedures were conducted following the Northeast Ohio Medical University Institutional Animal Care and Use Committee and National Institutes of Health guidelines. Eighteen Long Evans LE tg (ChAT-Cre) 5.1 Deis rats (Rat Resource and Research Center, University of Missouri; 12 female; six male) received injections of the vector into the PPT. Efforts were made to minimize the number of animals and their suffering. A list of all key resources used in this study are presented in **Table 1**.

Surgery

Each rat was deeply anesthetized with isoflurane in oxygen (3.5%–5% isoflurane for induction; 1.75%–3% for maintenance). The rat's head was shaved and disinfected with Betadine (Perdue Products L.P., Stamford, CT, USA). Atropine sulfate (0.08 mg/kg, i.m.) was given to minimize respiratory secretions and Ketofen (ketoprofen; 5 mg/kg, s.c.; Henry Schein, Melville, NY, USA) or Meloxicam SR (1.5 mg/kg, s.c.; ZooPharm, Laramie, WY, USA) was given for pain management. Moisture Eyes PM ophthalmic ointment (Bausch and Lomb, Rochester, NY, USA) was applied to each eye to protect the cornea. The animal's head was positioned in a stereotaxic frame with a mouth bar positioned 3.5 mm ventral to the horizontal plane through interaural zero. Body temperature was maintained with a feedback-controlled heating pad. Sterile instruments and aseptic techniques were used for all surgical procedures. An incision was made in the scalp and the surrounding skin was injected with 0.5% bupivacaine (Hospira, Inc., Lake Forest, IL, USA), a long-lasting local anesthetic. A craniotomy was made using a dental drill. A 1 μl Hamilton microsyringe was mounted in a manipulator that was rotated caudally in the sagittal plane so that the syringe came in at a 30° angle above the horizontal axis. Following viral injection, Gelfoam (Harvard Apparatus, Holliston, MA, USA) was placed in the craniotomy and the scalp sutured. The animal was then removed from the stereotaxic frame and placed in a clean cage. The animal was monitored until it could walk, eat, and drink without difficulty.

Viral Tracing

Long Evans LE tg (ChAT-Cre) 5.1 Deis rats were obtained from the Rat Resource and Research Center (University of Missouri). Cre-recombinase is expressed in nearly all cholinergic neurons in these animals (Witten et al., 2011). Two viral vectors were used. Each vector delivers a gene for the expression of fluorescent protein (EYFP or mCherry). The gene is in double-inverted orientation (DIO), so it is expressed only in neurons that contain Cre-recombinase (i.e., in cholinergic neurons). rAAV2/EF1a-DIO-EYFP (titer: 4.6×10^{12}; UNC Vector Core) or rAAV2/EF1a-DIO-mCherry (titer: 3.2×10^{12}; UNC Vector Core) was injected in the right PPT of each animal. Coordinates for the injections were chosen to target the caudal PPT, where the cholinergic cells that project to the IC are concentrated (Motts and Schofield, 2009). In two animals, 50 nl vectors were deposited over 2 min at a single site. In the remaining animals, 300–400 nl was delivered over 10 min at one site (12 animals) or each of two sites (four animals). In the latter cases, the syringe was inserted twice, so that one deposit was positioned 0.4–0.5 mm dorsal to the other. After each deposit, the syringe was left in place for 2 min before being withdrawn.

Perfusion and Tissue Processing

Four weeks after surgery, the animal was deeply anesthetized with isoflurane and perfused transcardially with Tyrode's solution, followed by 250 ml of 4% paraformaldehyde in 0.1 M phosphate buffer, pH 7.4 and then by 250 ml of the same fixative with 10% sucrose. The brain was removed and stored at 4°C in fixative with 25–30% sucrose for cryoprotection. The following day, the brain was prepared for processing by removing the cerebellum and cortex and blocking the remaining piece with transverse cuts posterior to the cochlear nucleus and anterior to the medial geniculate body. The tissue was frozen and cut on a sliding microtome into 40 μm thick transverse sections, collected in six sets. Before staining, sections were permeablized in 0.2% Triton X-100 in phosphate-buffered saline (PBS) for 30 min at room temperature, then blocked in 10% normal goat serum in 0.2% Triton X-100 and PBS for 1 h, also at room temperature. Sections were then processed for markers as described below. EYFP label was amplified using an antibody against the green fluorescent protein (GFP, 1:400, Molecular Probes A10262; RRID: AB_2534023; note this antibody cross-reacts with EYFP) in combination with a Tyramide Signal Amplification Kit (Molecular Probes). In two cases, an antibody against ChAT (Chemicon AB144P 1:100; RRID: AB_2079751) was used to verify that viral expression was limited to cholinergic neurons. Putative GABAergic cells were stained with an antibody against GAD67 (1:400; Millipore MAB5406; RRID: AB_2278725). Neurons were counterstained with an antibody against the neuronal nuclear protein (NeuN; 1:500; Millipore ABN78; RRID: AB_10807945). In cases where the ChAT antibody was used, a biotinylated anti-goat antibody (1:100; Vector BA-5000; AB_2336126) was used followed by an AF546 Streptavidin tag (1:100; Thermo Fisher Scientific Cat# S-11225; RRID: AB_2532130) to label ChAT-positive neurons in the PPT. In all other cases, a mixture of an AF488 streptavidin tag (1:100; Thermo Fisher Scientific Cat# S11223; RRID: AB_2336881), an AF564 conjugated anti-mouse secondary (1:100; Thermo Fisher Scientific Cat# A10036, RRID: AB_2534012), and an AF750 conjugated anti-rabbit secondary (1:100; Thermo Fisher Scientific Cat# A21039; RRID: AB_10375716) were used to label GFP, GAD67, and NeuN, respectively. Stained sections were mounted on gelatin-coated slides, allowed to dry and coverslipped with DPX.

Data Analysis

Cholinergic neurons stained with anti-ChAT or labeled by the viral vector injections were used to identify the cholinergic nuclei according to previously published criteria (Motts et al., 2008). In the original study describing the generation of the ChAT-Cre rats, the authors tested the specificity of labeling after injection of a viral vector carrying a gene for Cre-dependent

TABLE 1 | Key resources.

Reagent type (species) or resource	Designation	Source or Reference	Identifiers	Additional Information
Genetic reagent *(Rattus norvegicus)*	LE-Tg(Chat-Cre)5.1Deis	Rat Resource and Research Center Donor: Dr. Karl Deisseroth (Stanford)	RRRC:00658 RRID: RGD_10401204	
Recombinant DNA reagent	rAAV2/EF1a-DIO-EYFP	UNC Vector Core Donor: Dr. Karl Deisseroth (Stanford)	N/A	titer: 4.6×10^{12} http://www.everyvector.com/sequences/show_public/8791
Recombinant DNA reagent	rAAV2/EF1a-DIO-mCherry	UNC Vector Core Donor: Dr. Karl Deisseroth (Stanford)	N/A	titer: 3.2×10^{12} http://www.everyvector.com/sequences/show_public/4897
Antibody	anti-GFP (chicken polyclonal)	Thermo Fisher Scientific	Cat#: A10262 RRID: AB_2534023	IHC (1:400)
Antibody	anti-ChAT (goat polyclonal)	Millipore	Cat#: AB144P RRID: AB_2079751	IHC (1:100)
Antibody	anti-GAD67 (mouse monoclonal)	Millipore	Cat#: MAB5406 RRID: AB_2278725	IHC (1:400)
Antibody	anti-NeuN (rabbit polyclonal)	Millipore	Cat#: ABN78 RRID: AB_10807945	IHC (1:500)
Antibody	biotinylated anti-goat (rabbit)	Vector	Cat#: BA-5000 RRID: AB_2336126	IHC (1:100)
Antibody	AF546 streptavidin	Thermo Fisher Scientific	Cat#: S11225 RRID: AB_2532130	IHC (1:100)
Antibody	AF488 streptavidin	Thermo Fisher Scientific	Cat#: S11223 RRID: AB_2336881	IHC (1:100)
Antibody	AF564 anti-mouse (donkey polyclonal)	Thermo Fisher Scientific	Cat#: A10036 RRID: AB_2534012	IHC (1:100)
Antibody	AF750 anti-rabbit (goat)	Thermo Fisher Scientific	Cat#: A21039 RRID: AB_10375716	IHC (1:100)
Software	Neurolucida	MBF Bioscience	RRID: SCR_001775	

expression of YFP (Witten et al., 2011). Their results showed that over 90% of the YFP-labeled neurons were immunoreactive for ChAT, a specific marker of cholinergic neurons. To ensure that subsequent mutations had not interfered with that specificity, we immunostained sections from two animals with anti-ChAT. IC subdivisions were also identified based on previous criteria (Coote and Rees, 2008; Beebe et al., 2016). Plots and analyses were performed using a Neurolucida system (MBF Bioscience; RRID: SCR_001775) attached to a Zeiss AxioImager Z2 fluorescence microscope (Carl Zeiss MicroImaging, Inc., Thornwood, NY, USA).

For each experiment, fluorescent neurons in the PMT were plotted to visualize the extent of the injection site. The IC was then examined at high magnification in every sixth section through its entire rostral-caudal extent (typically 4–6 sections per animal). The amount of labeling varied across animals. In some cases, especially those with fewer labeled cells in the PPT, there were no labeled axons in the IC; this was not unexpected, given that PPT cholinergic cells projects to many structures throughout the brainstem and thalamus. Those cases were excluded from the present study. Labeled axons were examined to assess possible routes from the PPT to the IC. The results were consistent across cases and suggested several possible routes to both ipsilateral and contralateral IC. To illustrate routes to and within the IC, a representative case with many labeled axons was chosen for detailed plotting. The labeled axons were drawn in every sixth section through the midbrain. The distribution of boutons within the IC was also documented by visual examination of every sixth section through the ipsilateral and contralateral IC. The overall pattern of labeling was consistent across cases, with variations appearing to relate generally to the relative size of the injections (i.e., the relative number of labeled cells in the PMT). For a quantitative description of the labeled boutons, we selected two cases with a large number of labeled axons. We then plotted the labeled boutons, identified as distinct swellings along a labeled axon, in every sixth section through the IC.

A substantial number of labeled boutons appeared to be in close apposition to an IC neuron that was labeled with anti-NeuN and, in some cases, anti-GAD67. Such contacts were apparent across animals; two with a large number of labeled axons and robust immunostaining for both NeuN and GAD were chosen for quantitative analysis. Sections spaced 240 μm apart were chosen to include large parts of the major IC subdivisions in each animal (two sections from one case and three from the second case). The IC in each section was examined at high magnification (63× objective, NA 1.4) and the location of each neuron that appeared to be contacted by a cholinergic axon was plotted with a symbol indicating whether the neuron was GAD^- or GAD^+.

Photomicrographs were taken with a Zeiss AxioImager Z2 fluorescence microscope with either an AxioCam HRm camera (Zeiss) or an Orca Flash 4.0 camera (Hamamatsu). Additions of color, scale bars, and arrows as well as, cropping and global adjustment of levels were done in Adobe Photoshop (Adobe Systems).

RESULTS

Injection of Viral Vector Into PPT Labels Cholinergic Neurons

Injection of either AAV-EF1a-DIO-mCherry or AAV-EF1a-DIO-EYFP into the PPT of Long Evans ChAT-Cre transgenic rats yielded expression of fluorescent protein in neurons associated with the PPT (**Figure 1**). The number of labeled cells varied across cases, leading to quantitative differences, but qualitatively the results were similar with the two vectors and across sexes. In one case, we saw labeled neurons in the adjacent LDT, the other component nucleus of PMT (not shown). Results, in this case, did not differ from cases in which the label was confined to PPT. In some cases, additional labeled cells were present in the parabigeminal nucleus, a nucleus on the lateral edge of the rostral midbrain that includes a dense cluster of cholinergic cells. These cases were excluded from the analysis in the present study. In the remaining 18 cases, all produced labeled axons in the IC. Twelve of these cases had substantial labeling ("good to very good") while the remaining cases had fewer labeled axons that served to support and confirm the conclusions. By plotting the labeled cells in every 6th section, we could assess both the viral spread and the efficacy of the labeling. In the twelve better cases, the labeled cell bodies were located across 1–5 sections, indicating that the injection site extended rostrocaudally from a minimum of less than 240 μm to a maximum of ∼1,200 μm. The number of fluorescent cells in these cases ranged from 7 (in a single section) to 328 across five sections. Interestingly, the cases that yielded the most labeled axons in the IC were not those with the most labeled PMT cells; we believe this reflects the fact that only a subset of PMT cells projects to the IC, and these cells are interspersed with those that project to other targets (see Motts and Schofield, 2009; Motts and Schofield, 2010).

Within the PPT, our injections labeled cells mostly in the caudal portion of the nucleus, surrounding the superior cerebellar peduncle at the same rostrocaudal levels as the IC. An example of a large injection site is shown in **Figure 1C**, where each green marker represents a single EYFP-labeled PPT neuron. Cholinergic neurons are not as densely packed in more rostral regions of the nucleus (which extends as far as the substantia nigra in the ventral midbrain; Mesulam et al., 1983). Our cases contained few or no labeled cells in these rostral regions, so we may have missed a portion of the cholinergic projections to the IC. If so, it is likely to be a very small component because the majority of PPT cells that project to the IC are concentrated in the caudal PPT (Motts and Schofield, 2009).

We stained sections with antibodies against ChAT to determine whether the expression of the fluorescent protein was limited to cholinergic (i.e., ChAT$^+$) cells (**Figure 2**). In these sections, all virally-labeled PPT neurons were co-labeled with the ChAT antibody (**Figure 2**, green arrows), indicating that the viral vector is selective for cholinergic neurons. However, it was common to see ChAT$^+$ neurons that were not labeled by the viral gene, even though adjacent neurons were so labeled (**Figure 2**). It is impossible to determine whether this

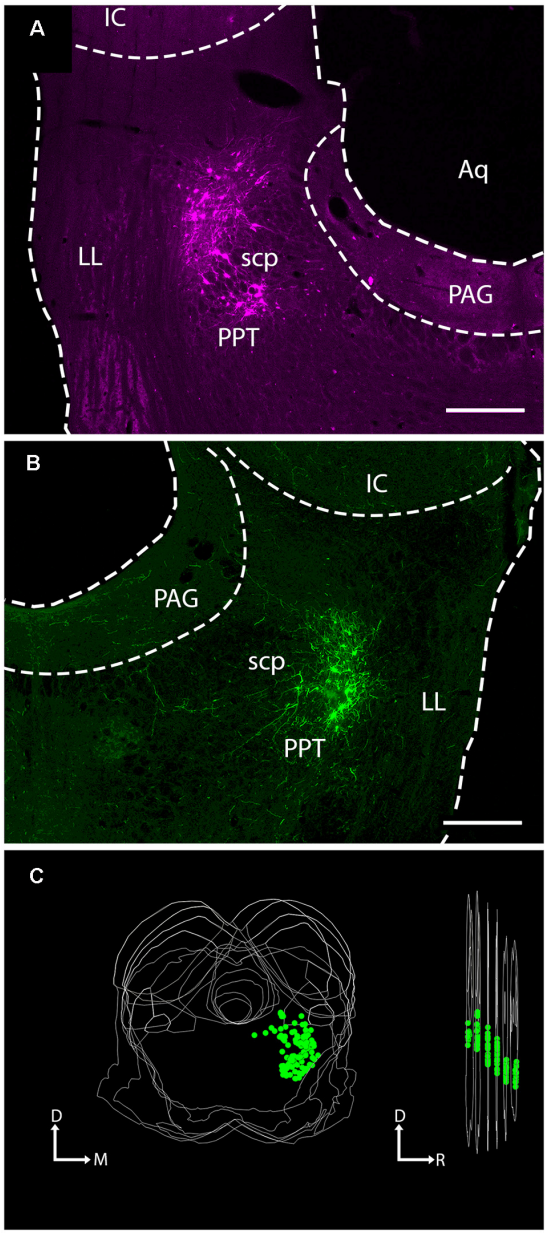

FIGURE 1 | Injection of viral vector into the PPT of ChAT-Cre transgenic rats labeled neurons at the site of injection. Photomicrographs show virally-expressed fluorescent protein in PPT neurons. **(A)** A representative example of mCherry expression in neurons of the left PPT following injection of rAAV2/EF1a-DIO-mCherry. Transverse section; lateral is left, dorsal is up. Scale bar = 500 μm. **(B)** A representative example of EYFP expression in neurons of the right PPT following injection of rAAV2/EF1a-DIO-EYFP. Transverse section; lateral is right, dorsal is up. Scale bar = 500 μm. **(C)** A representative three-dimensional reconstruction showing the extent of labeled neurons in the PPT through six transverse sections (spacing: 240 μm between sections). The image on the left shows the six sections stacked, with each EYFP-labeled cell indicated by a green circle. The image on the right shows the stack rotated for a lateral view. The "cloud" of labeled cells shifts ventrally moving from caudal to rostral, reflecting the orientation of the PPT. Aq, cerebral aqueduct; D, dorsal; IC, inferior colliculus; LL, lateral lemniscus; M, medial; PAG, periaqueductal gray; PPT, pedunculopontine tegmental nucleus; R, rostral, scp, superior cerebellar peduncle.

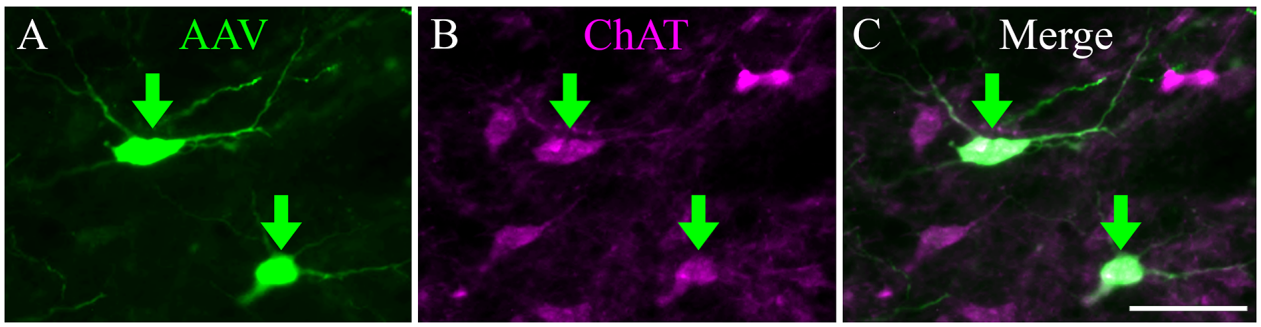

FIGURE 2 | Viral injection selectively labeled ChAT-positive neurons in the PPT. **(A)** EYFP-expressing PPT neurons (green arrows) following AAV injection. **(B)** Same region as shown in **(A)**, but imaged to show immunostaining for ChAT. **(C)** Merged image showing colocalization of ChAT antibody and viral EYFP expression (green arrows). Scale = 100 μm.

was a failure of the transgene (i.e., Cre-recombinase was not expressed in the cholinergic neuron) or a failure of viral uptake of fluorescent gene expression by the presumptive cholinergic neurons. We chose three cases that produced the most labeled axons in the IC and counted both the virally-labeled cells and the ChAT$^+$ PPT cells in the same sections. On average, 18% of the ChAT$^+$ cells were labeled by the viral vector (range: 14–23%), suggesting that the efficacy of viral labeling is limited. We completed a similar analysis for a fourth case that had fewer labeled axons in the IC despite having many more labeled cells in the PPT. This case had 155 virally-labeled cells in five sections, which constituted 72% of the ChAT$^+$ cells. Clearly, some cases had greater efficacy of labeling, although we never observed 100% labeling. We conclude that the labeled axons and boutons that we observed in the IC are cholinergic and likely underrepresent the PPT-to-IC cholinergic pathway.

Cholinergic Axons Course Through the Tegmentum to Reach Ipsilateral and Contralateral IC

From the PPT, cholinergic axons travel to many regions of the brainstem and thalamus. Labeled axons were present in the IC bilaterally, with more axons present on the ipsilateral side (**Figure 3**). Axons coursing toward the IC take multiple routes. Axons leave the PPT dorsally and dorsolaterally to enter the ICc through its ventral border. Axons reaching the ipsilateral IClc do so either through the ventrolateral border of the IC or by coursing through the ICc and turning laterally. Axons traveling to the ICd travel first through either the ICc or the IClc.

The organization of labeled axons suggests several possible routes from the PPT to the contralateral IC. First, axon fragments could be followed from the PPT across the midline, traveling ventral to the PAG or even through the ventral PAG to the ventral border of the contralateral IC. At this point, the axons entered the contralateral IC all along its ventral border and were distributed to each major subdivision in a pattern similar to that in the ipsilateral IC. Also, labeled axons were present in the IC commissure. The directionality of these axons could not be determined, so they could represent a projection from one PPT through the ipsilateral IC to the contralateral IC, or a recurrent loop from the PPT to the contralateral IC and then back to the ipsilateral side.

Cholinergic Boutons Are Present in all IC Subdivisions

Labeled axons typically were thin and studded with en passant and terminal boutons. **Figure 4** shows results from a case that had substantial labeling of axons in the IC. Cases with fewer labeled axons had fewer boutons but otherwise were similar to one another. In all cases, more boutons were present ipsilaterally than contralaterally and typically were present in all the IC subdivisions on both sides. Individual axons were observed to cross any of the borders between IC subdivisions, with boutons clearly visible in each subdivision; **Figure 4G** (asterisks) shows examples of axons crossing the ICc/IClc border. Within a subdivision, there was no obvious relationship between the axons or boutons and other features of the subdivision architecture. In the ICc, labeled axons were oriented in several directions without any clear relationship to the orientation of fibrodendritic laminae. In the shell areas (ICd and IClc), the labeled axons showed no particular relationship to borders between layers or between the "GABA modules" and the extramodular domains (see Chernock et al., 2004).

As described above, the labeled axons in the IC were typically studded with boutons, suggesting many sites of ACh release. **Figure 5** plots the distribution of labeled boutons (green circles), demonstrating their wide distribution throughout the ipsilateral and contralateral IC. Consistent with the axonal pattern, the boutons were more numerous on the ipsilateral side than on the contralateral side. Also, labeled boutons were more numerous in the caudal part of the IC, even within a subdivision (compare **Figure 5C** vs. **Figure 5A**).

Cholinergic PPT Axons Contact GAD$^+$ and GAD$^-$ Neurons in the IC

A majority of the labeled boutons were located in the neuropil between the labeled neuronal cell bodies, but a substantial

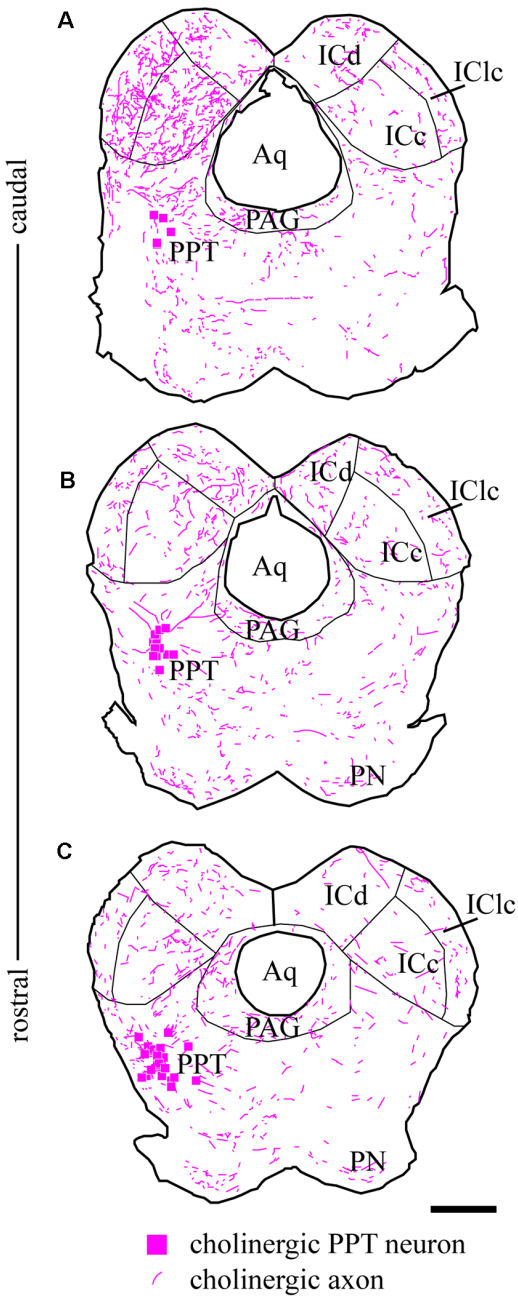

FIGURE 3 | Cholinergic axons travel through the tegmentum to reach ipsilateral and contralateral IC. Fluorescent-labeled axons (magenta lines) were observed throughout transverse IC sections after labeling cholinergic cells in the left PPT (magenta squares). The plots show the axons in a series of transverse sections through the IC at caudal **(A)**, middle **(B)**, and rostral levels **(C)**. On both sides, labeled axons appear to enter the IC all along its ventral border. Sections are 40 μm thick and 240 μm apart. Scale bar = 1 mm.

number of boutons were in close apposition to the cell bodies, suggesting possible synaptic contacts. By staining the tissue with an antibody to GAD, we could examine the relationship of the labeled cholinergic boutons to presumptive GABAergic cells. **Figure 6** shows examples of virally-labeled cholinergic boutons (green) in close contact (arrows) with GAD$^+$ IC neurons (magenta). We also stained the tissue with a neuron-specific marker (NeuN), allowing us to distinguish GAD$^+$ cells from GAD$^-$ cells (presumptive glutamatergic neurons). A neuron that is NeuN$^+$ and GAD$^-$ located close to GAD$^+$ profiles is considered to be non-GABAergic. GAD$^-$ neurons are likely glutamatergic neurons as IC neurons are either GABAergic or glutamatergic (reviewed by Schofield and Beebe, 2019). Glutamatergic neurons make up the majority of IC neurons and were frequently contacted by labeled cholinergic PPT boutons (**Figures 7A,B**, arrows).

We observed cholinergic contacts onto neurons in both the ipsilateral and contralateral IC. **Figure 8** shows the distribution of contacted cell bodies in two sections through the IC in a representative case. Several points are clear. First, contacts occur bilaterally in all three IC subdivisions, with more contacts ipsilateral than contralateral. Second, contacts occurred on both GAD$^-$ cells (presumptive glutamatergic cells, **Figure 8**, cyan symbols) and GAD$^+$ cells (presumptive GABAergic cells, **Figure 8**, magenta symbols). Thus, cholinergic axons from a single PPT appear to contact GAD$^+$ and GAD$^-$ neurons in each major IC subdivision both ipsilateral and contralateral to the injected PPT.

Individual Cholinergic Axons Can Contact Both GAD$^+$ and GAD$^-$ Neurons

Individual sections often contained relatively long segments of labeled axons that allowed several observations. In each of the IC subdivisions, individual axons appeared to contact multiple IC neurons. **Figure 7** includes examples of single cholinergic axons that appear to contact multiple GAD$^-$ neurons. **Figure 9** shows additional patterns of multiple targets, including multiple GAD$^+$ neurons (**Figure 9B**) and axons that contact both GAD$^+$ and GAD$^-$ neurons (**Figures 9A,B**). Each pattern of contact—onto multiple GAD$^+$ neurons, multiple GAD$^-$ neurons, or both GAD$^+$ and GAD$^-$ neurons—was observed ipsilateral and, less often, contralateral to the injection site.

DISCUSSION

We used selective viral tract-tracing of cholinergic PPT neurons to identify cholinergic projections to the IC. The PPT is a prominent source of cholinergic innervation of the thalamus and brainstem and is involved in wide-ranging functions such as arousal, sensory gating, sleep-wake cycle, and plasticity (reviewed by Schofield et al., 2011; Schofield and Hurley, 2018). The present results demonstrate that cholinergic axons from the PPT terminate in the three largest IC subdivisions: the ICc, ICd, and IClc (**Figure 10**). These subdivisions contribute to different aspects of hearing, each of which may be affected by cholinergic modulation. The cholinergic axons typically contain many boutons and can cross borders between IC subdivisions as well as within subdivisions (e.g., the laminar boundaries in the IClc). Cholinergic axons contact IC cells that are GAD$^+$ (presumptive GABAergic) and GAD$^-$ (presumptive

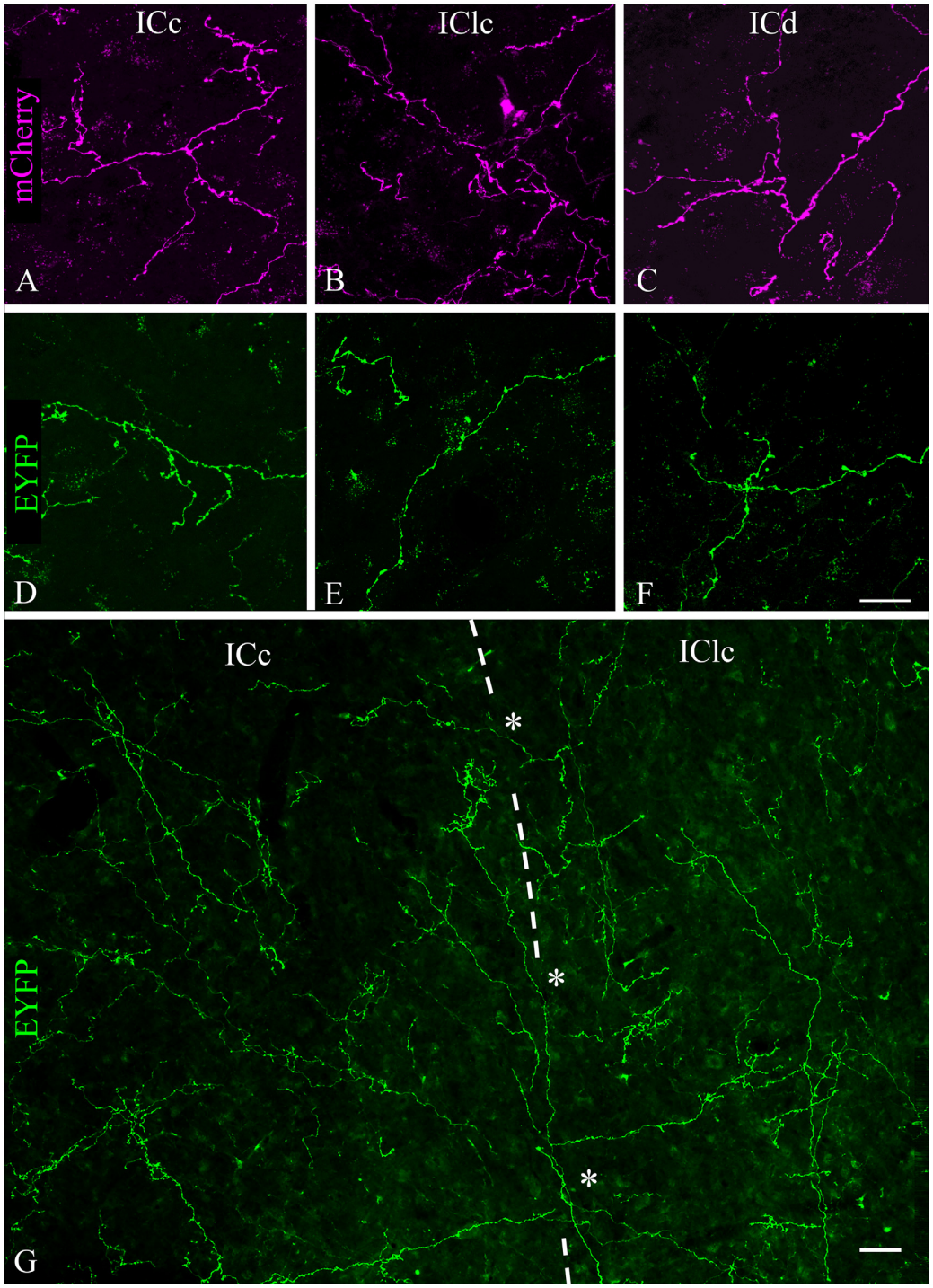

FIGURE 4 | Labeled cholinergic axons with many boutons were present in each subdivision of the IC. **(A–C)** Expression of mCherry in axons from PPT in **(A)** ICc, **(B)** IClc, and **(C)** ICd. **(D–F)** Expression of EYFP in axons from PPT in **(D)** ICc, **(E)** IClc, and **(F)** ICd. Scale bar in **(F)** = 25 μm and applies to **(A–F)**. **(G)** Montage showing EYFP-labeled cholinergic axons in the ICc and IClc (separated by the dashed line), including individual axons that cross the border (asterisks), providing boutons to both subdivisions. Scale = 25 μm.

glutamatergic), suggesting that ACh acts on both excitatory and inhibitory IC circuits. Moreover, an individual cholinergic axon can contact cells of both neurotransmitter phenotypes. Taken together, PPT cholinergic neurons appear to contact many excitatory and inhibitory cells across multiple IC subdivisions, suggesting wide-ranging effects of ACh in the IC.

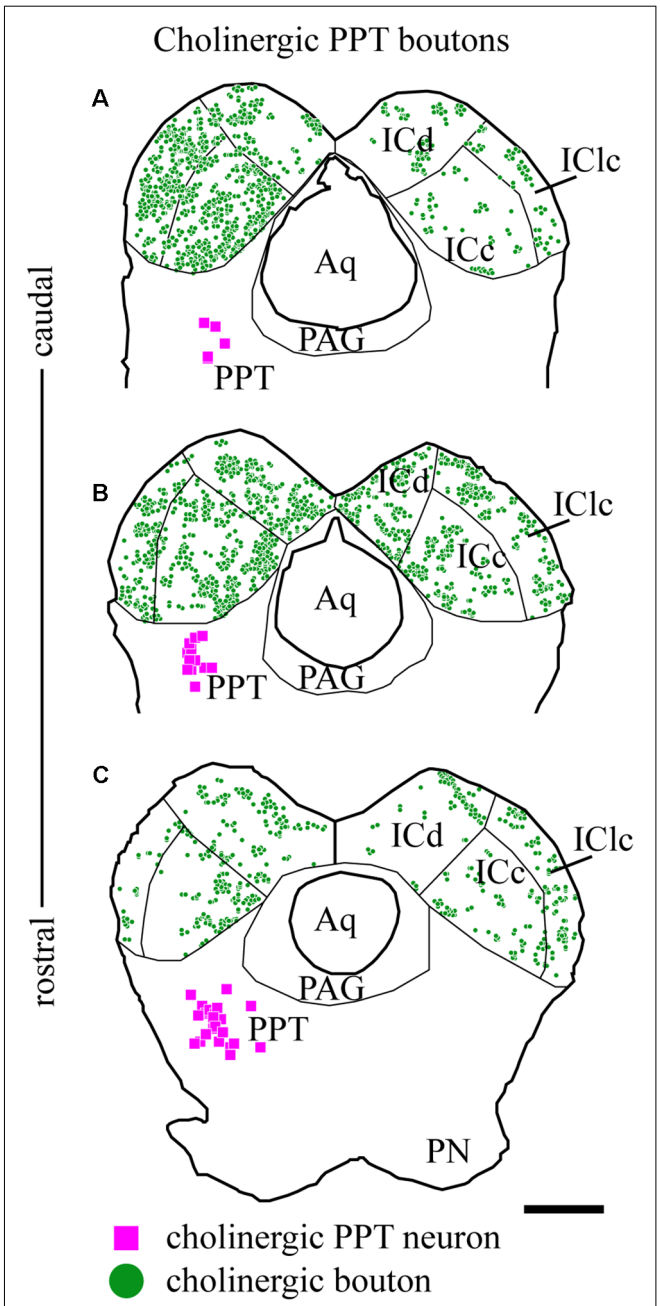

FIGURE 5 | Cholinergic boutons are present in multiple IC subdivisions. Plots of transverse sections through the IC (the same sections illustrated in **Figure 2**) showing the distribution of labeled boutons (green circles) in the IC after fluorescent labeling of cholinergic cells (magenta squares) in the left PPT. Cholinergic boutons were found in **(A)** caudal, **(B)** mid-IC, and **(C)** rostral sections of IC, where they terminated in the three major subdivisions: dorsal cortex (ICd), lateral cortex (IClc) and central nucleus (ICc). Scale bar = 1 mm.

Technical Issues

The combination of Cre-expressing cholinergic cells in transgenic animals and Cre-dependent expression of fluorescent proteins delivered *via* viral vectors provides an opportunity for highly selective labeling of a cholinergic pathway (e.g., Stornetta et al., 2013). Following immunostaining with anti-ChAT, we found that fluorescent protein expression was limited to ChAT$^+$ cells. We conclude that the labeled axons were cholinergic. The same analysis showed numerous ChAT$^+$ cells that did not express fluorescent protein despite being among other cells that were so labeled. It is unclear whether this reflects a failure of Cre expression or failure of viral uptake and subsequent expression of the fluorescent label. The two vectors used here were serotype 2, selected because of relatively high efficiency in anterograde labeling of neuronal pathways (Aschauer et al., 2013; Salegio et al., 2013). However, possibly a different serotype would label some of the cholinergic cells that were unlabeled here. We conclude that our experiments probably labeled <100% of the pathway of interest, and cannot rule out the possibility that a specific subtype of cholinergic cell failed to express the fluorescent proteins.

There are disparate views on volume vs. synaptic cholinergic transmission (Descarries et al., 1997; Zoli et al., 1999; Parikh et al., 2007; Lendvai and Vizi, 2008; Sarter et al., 2009; Muñoz and Rudy, 2014; Takács et al., 2018), with no data to argue strongly for one mode or the other in the IC. Of course, the specificity of cholinergic action also depends on the nature and location of cholinergic receptors, with opportunities for both presynaptic and postsynaptic effects. As discussed above (Introduction), the IC contains a variety of nicotinic and muscarinic receptor types, but as yet little is known about the specific cells and circuits associated with these receptors. By using light microscopy, we have been able to assess the distribution of cholinergic axons and likely release sites over a large area. The results suggest that a single PPT releases ACh across a wide expanse of both ipsilateral and contralateral IC. Although a majority of boutons were located in the neuropil, many of the cholinergic boutons were in close apposition to neuronal (NeuN$^+$) cell bodies, allowing us to assess some of the cell types most likely affected by ACh. By adding immunostain for NeuN and GAD67, we were able to conclude that ACh is likely to have direct effects on both GAD$^+$ (likely GABAergic) and GAD$^-$ neurons. Given that IC neurons are mostly either GABAergic or glutamatergic, the GAD$^-$ neurons are likely to be glutamatergic cells. Our conclusion that ACh affects both glutamatergic and GABAergic IC cells is consistent with previous studies showing physiologic activation of GABAergic cells (Yigit et al., 2003) and the presence of cholinergic receptor mRNA in both cell types (e.g., Sottile et al., 2017). Ultimately, electron microscopy will be needed to identify synaptic release sites for ACh. The present results indicate that such studies will be needed in each of the IC subdivisions.

Functional Implications

The present results extend the conclusions reached *via* retrograde tracing experiments that identified the PPT as the largest source of cholinergic input to the IC (Motts and Schofield, 2009). Those experiments were based on large injections of tracer that typically encroached on multiple IC subdivisions. The present results show that cholinergic PPT axons innervate each of the large IC subdivisions: ICc, ICd, and IClc. Also, the retrograde tracing studies

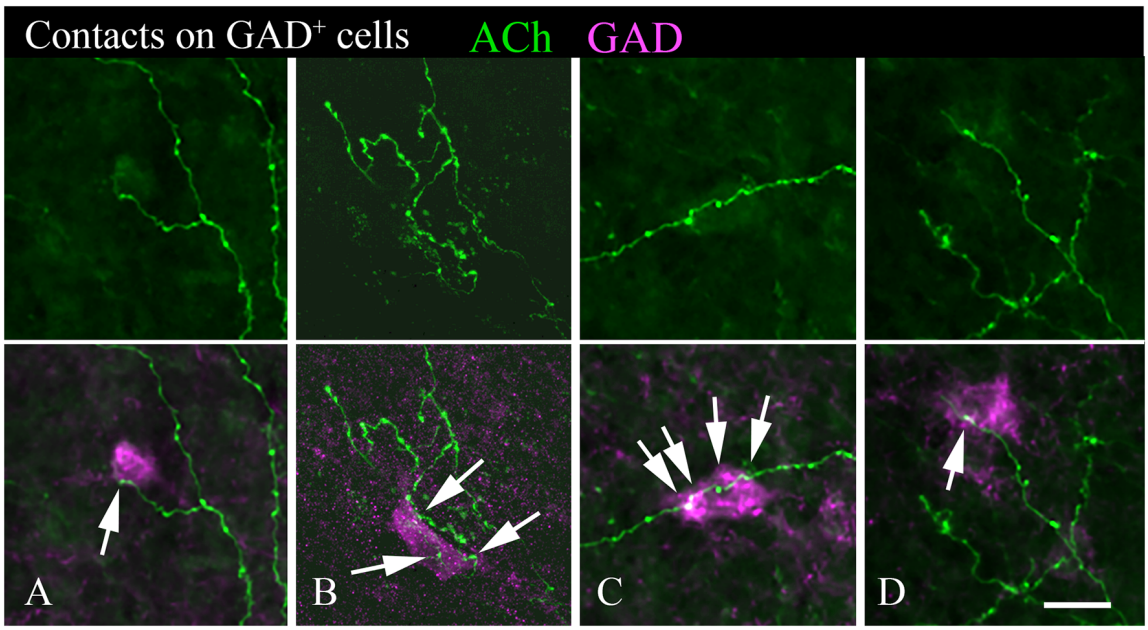

FIGURE 6 | Cholinergic axons contact GAD$^+$ neurons in the IC. The upper panel in each column shows fluorescent-labeled cholinergic axons in the IC (green). The lower panel in each column shows the same axons overlaid with an image of the GAD stain (magenta). Arrows show points of close contact between labeled boutons and the GAD$^+$ cells. Images **(A,C,D)** are from the IC central nucleus; **(B)** is from IC lateral cortex. Scale bar = 20 μm.

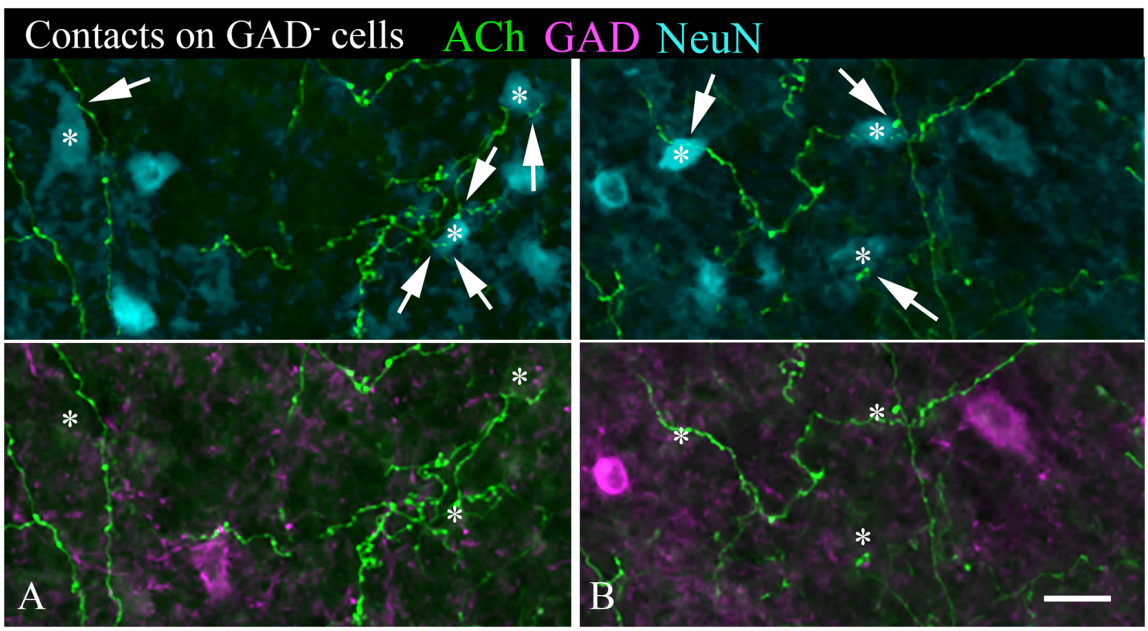

FIGURE 7 | (A,B) Cholinergic axons contact GAD$^-$ neurons in the IC. The upper panel in each column shows fluorescent-labeled cholinergic axons (green) and NeuN$^+$ neurons (cyan). Labeled boutons are in close contact (arrows) with several of the NeuN$^+$ cells (*). That these contacted cells are non-GABAergic is shown by the lower panel, which shows GAD immunostain in magenta. None of the asterisk-marked cells are GAD$^+$, despite the presence of GAD$^+$ cells nearby. IC, lateral cortex. Scale bar = 20 μm.

indicated that, overall, more PPT cells project to the ipsilateral IC and fewer project to the contralateral IC. The present results indicate that the axonal distribution reflects a similar pattern, with denser projections to the ipsilateral IC than contralateral IC. Ipsilateral dominance applies to each of the IC subdivisions.

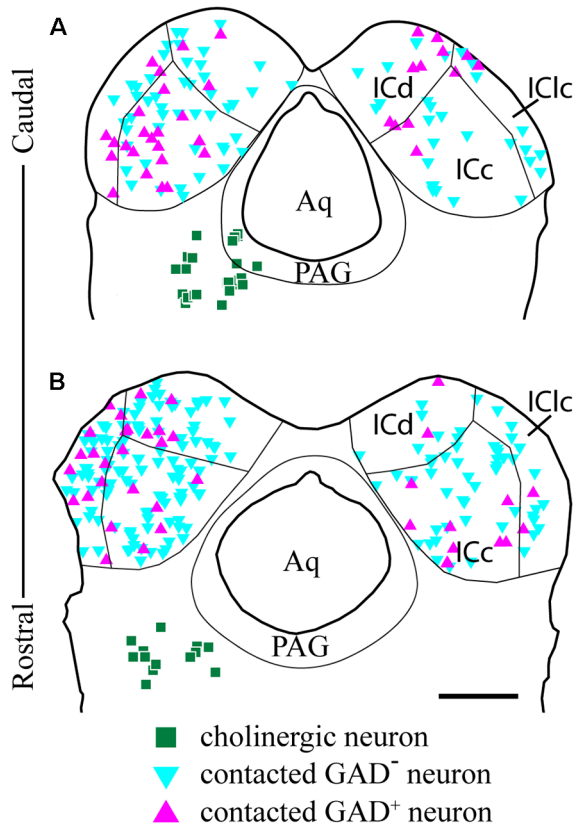

FIGURE 8 | GAD-positive and GAD-negative IC neurons are contacted throughout the IC. Plots of transverse sections through the caudal **(A)** and rostral **(B)** IC show the distribution of neurons contacted by cholinergic boutons after labeling cholinergic cells in the left PPT and laterodorsal tegmental nucleus (LDT; green squares). Contacted cells included both GAD$^+$ neurons (magenta triangles) and GAD$^-$ neurons (cyan triangles) in each of the major IC subdivisions. Contacted IC neurons were more numerous on the ipsilateral side than the contralateral side. Contacted GAD$^-$ neurons outnumbered contacted GAD$^+$ neurons. Scale bar = 1 mm.

The widespread distribution of PPT cholinergic axons is consistent with studies of cholinergic receptors, which describe nicotinic and muscarinic receptors throughout the IC (Schwartz, 1986; Glendenning and Baker, 1988; Morley and Happe, 2000; Gahring et al., 2004; Happe and Morley, 2004). Given that cholinergic axons are distributed widely in the IC, one would expect that a majority of IC cells are affected by cholinergic inputs. The available studies are consistent with such a view, but the data are limited to studies in which the location of recorded units was not related to IC subdivision (Curtis and Koizumi, 1961; Watanabe and Simada, 1973; Farley et al., 1983), or to studies in which the units were restricted to the ICc (Habbicht and Vater, 1996; Ji et al., 2001; Yigit et al., 2003). The present results suggest that direct cholinergic effects would be observed upon recording neurons in the ICd and the IClc.

Cholinergic Effects in the ICc

Information on cholinergic effects within specific IC subdivisions has been limited to the ICc. Previous studies showed that cholinergic agents affect the firing rate but not the temporal response patterns of IC neuronal responses to sounds (Farley et al., 1983; Habbicht and Vater, 1996). They suggested that ACh acted through nicotinic and muscarinic receptors to set the level of neuronal activity in the IC, likely modulating neuronal sensitivity as well as gain. Cholinergic effects in other subcortical auditory nuclei have led to similar conclusions. Oertel and colleagues (Fujino and Oertel, 2001; Oertel and Fujino, 2001; Oertel et al., 2011) suggested that ACh enhances responses of T stellate cells in the cochlear nucleus, perhaps to enhance coding of spectral peaks and thus to improve interpretation of sounds in noise. Caspary and colleagues have suggested that cholinergic effects in auditory thalamus similarly support hearing in a noisy environment, and further that deterioration of the cholinergic system with aging could relate to presbycusis (Sottile et al., 2017). It is worth noting that the PPT is a source of cholinergic innervation to the cochlear nucleus and auditory thalamus, as well as the inferior colliculus. Moreover, individual PPT cells can send branching axons to innervate two or more of these target structures (e.g., one IC as well as left and right auditory thalamus; Motts and Schofield, 2011). Such divergent projections are typical of many modulatory systems and may reflect a common effect across auditory nuclei (reviewed by Schofield and Hurley, 2018).

The origin of the inputs from the PPT may provide additional insight into cholinergic functions. Within the context of auditory processing, the PPT has been associated with arousal, plasticity (especially driven by top-down circuits) and sensory gating (Xiong et al., 2009; Schofield et al., 2011; Schofield and Hurley, 2018). The PPT projections to the auditory thalamus have been implicated in the enhancement of hearing in a noisy environment, in part by cholinergic enhancement of ascending inhibitory pathways as well as enhancement of top-down modulation (*via* effects on corticothalamic circuits; Sottile et al., 2017). Gut and Winn (2016) proposed that the PPT, particularly the caudal part (as studied here), is especially important for an organism's ability to act quickly in response to sensory stimuli. This proposal ties together the sensory aspects of the PPT with its well-known ties to the basal ganglia. Many cells in the PPT respond to acoustic stimuli, so it is not surprising that they would contribute to auditory function (Reese et al., 1995a,b,c). Slee and David (2015) have shown that IC cells respond differently depending on whether the subject is performing a task. They concluded that arousal associated with task performance likely accounted for part of the difference in responses. Cholinergic projections as demonstrated in the present study may contribute to such responses. Kuenzel and colleagues (Goyer et al., 2016; Gillet et al., 2018; Kuenzel, 2019) have suggested a similar role for projections from the PPT to the cochlear nucleus, where ACh can modulate neuronal sensitivity in accord with an animal's behavioral state and level of arousal.

Suga and colleagues have shown evidence for a cholinergic role in corticofugal-driven plasticity of subcortical auditory nuclei, including plasticity in the IC (Xiong et al., 2009; Suga, 2012). Stimulation of the auditory cortex can lead to the retuning of an IC cell's response selectivity. Such plasticity can involve a variety of stimulus parameters, such as shifting the

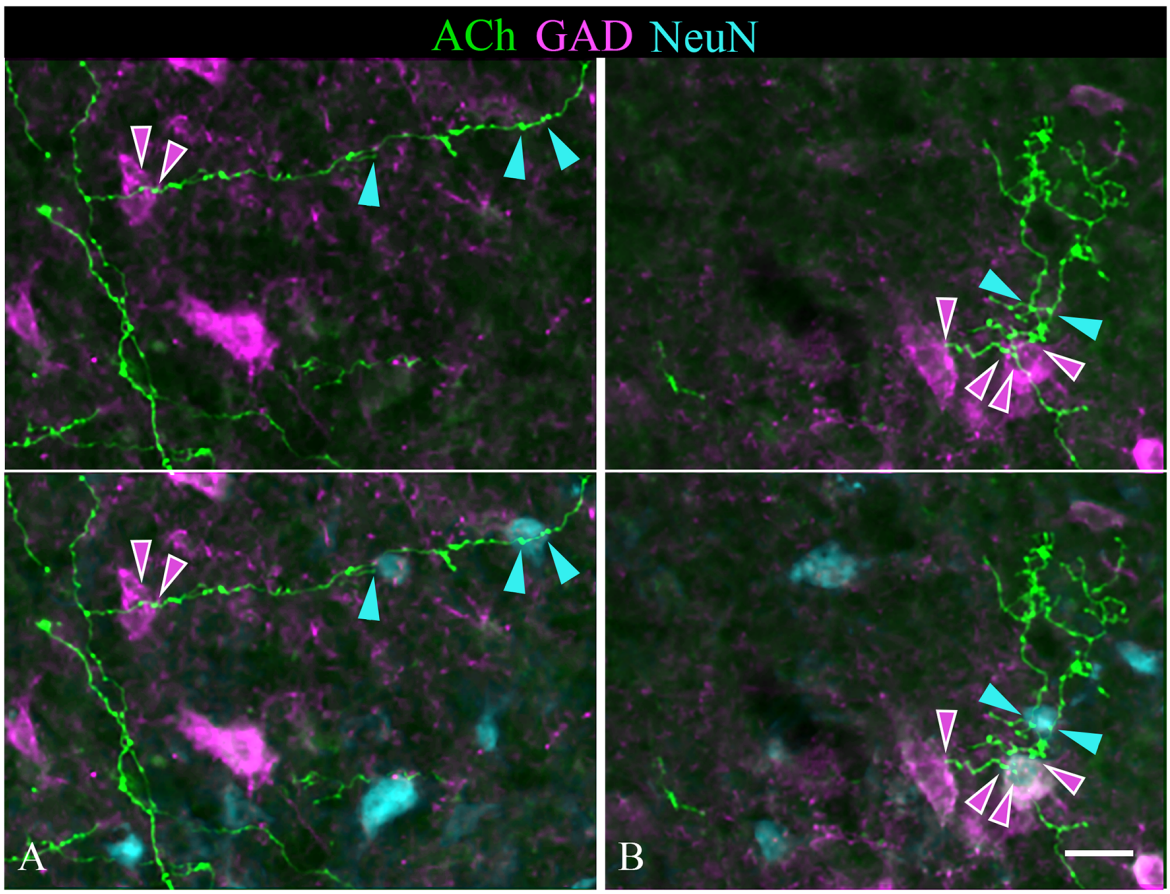

FIGURE 9 | Single cholinergic axons contact both GAD$^+$ and GAD$^-$ IC neurons. The upper panel in each column shows fluorescent-labeled cholinergic axons (green) overlaid with an image of GAD staining (magenta). The lower panel in each column shows the same image overlaid with an image of the NeuN stain (cyan). **(A)** An axon segment in the IC lateral cortex appears to contact one GAD$^+$ neuron (magenta arrowheads) and two different GAD$^-$ neurons (cyan arrowheads). **(B)** shows an axon segment from the IC central nucleus that appears to contact two GAD$^+$ neurons (magenta arrowheads) and a nearby GAD$^-$ neuron (cyan arrowheads). Scale bar = 20 μm.

frequency to which the IC cell responds most readily. The retuning of IC responses can outlast the period of cortical stimulation by minutes to hours as a result of plasticity in both cortical and subcortical circuits. Significantly, that plasticity is dependent on ACh in the IC. We believe that the details of the retuning (e.g., whether a given cell retunes to a higher or a lower acoustic frequency) is determined by the massive direct projections from the auditory cortex to the IC, with cortical axons activating both excitatory and inhibitory circuits within the IC. ACh, on the other hand, provides a permissive signal that allows synaptic plasticity to sustain the effects of the cortical stimulation. Such a permissive signal could: (1) be elicited by direct auditory cortical projections to cholinergic PPT cells that project to the IC (Schofield and Motts, 2009; Schofield, 2010); and (2) affect multiple IC cells *via* highly divergent cholinergic axons, including axons that contact both glutamatergic and GABAergic IC cells (current results).

Interestingly, the work by Suga (2012) like that cited earlier regarding cholinergic effects on IC cells, focused on responses of cells in the ICc. It will be of interest in future studies to identify the effects of ACh on responses of IC cells outside the central nucleus, particularly given these non-central regions being the prime targets of cortical inputs as well as centers for multisensory processing.

Cholinergic PPT Axons Likely Modulate Lemniscal and Extralemniscal Auditory Pathways

The termination of cholinergic axons across IC subdivisions is significant when we consider that each IC subdivision contributes differentially to three parallel auditory pathways: a lemniscal pathway, a polysensory pathway, and a diffuse pathway (Calford and Aitkin, 1983; Rouiller, 1997; Mellott et al., 2014). Each pathway is thought to serve different aspects of hearing. The lemniscal pathway is tonotopically organized and provides the primary-like representation of sound. It encompasses projections from the ICc to the ventral medial geniculate nucleus and on to tonotopically organized regions of the auditory cortex. The polysensory pathway incorporates inputs from other sensory systems, especially the somatosensory system. These inputs terminate heavily in the IClc. Projections from the IClc, along

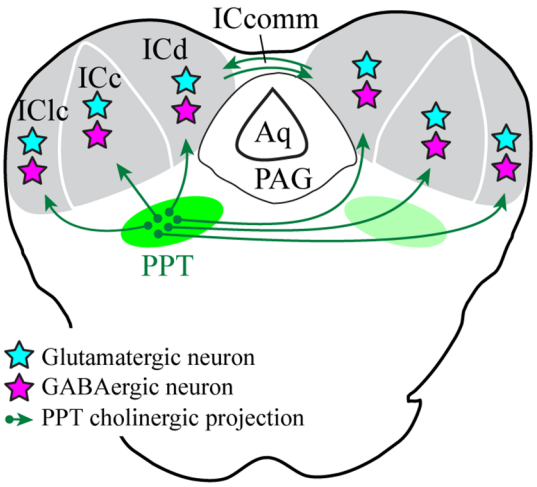

FIGURE 10 | Cholinergic PPT cells project throughout the IC and contact GABAergic and presumptive glutamatergic cells. Green arrows show cholinergic projections from PPT to all three subdivisions of the IC. Cyan stars represent cholinergic-contacted glutamatergic neurons and magenta stars represent cholinergic-contacted GABAergic neurons. Aq, cerebral aqueduct; ICc, d, lc, inferior colliculus central nucleus, dorsal cortex, and lateral cortex; ICcomm, commissure of the IC; PAG, periaqueductal gray; PPT, pedunculopontine tegmental nucleus.

with projections from ICc, converge in the medial division of the medial geniculate nucleus, which then projects widely to auditory cortical areas and other forebrain targets to form the polysensory pathway (De Ribaupierre, 1997). Finally, the diffuse pathway originates from the ICd, which projects to the dorsal medial geniculate nucleus and then on to secondary and temporal auditory cortical areas. The ICd has long stood out as unique among IC subdivisions, with descending inputs from the auditory cortex appearing to dominate over ascending inputs (Ehret, 1997). ICd cells are typically broadly-tuned and respond only weakly to simple auditory stimuli, but respond more robustly to complex contextual stimuli (such as the cries of isolated offspring; De Ribaupierre, 1997). Early lesion studies suggested that ICd plays a particularly important role in auditory attention (Jane et al., 1965). The present results show that cholinergic axons from the PPT terminate broadly in each of the large IC subdivisions and are in a position to modulate the activity in each of the ascending parallel pathways. At the level of the thalamus (another target of PPT cholinergic projections), ACh can have different effects on lemniscal vs. extra-lemniscal cells (Mooney et al., 2004). The differences are thought to be mediated through different cholinergic receptors. In the IC, Gahring et al. (2004) noted higher levels of the nicotinic receptor subunit β4 in the IClc compared to other IC subdivisions. Happe and Morley (2004) noted high levels of the nicotinic receptor α7 subunits in the IClc. To the best of our knowledge, none of these receptors have been associated with specific output pathways from the IClc or ICd. Nonetheless, the current data, along with the prominent contributions of each IC subdivision to the parallel ascending pathways, suggests that PPT cholinergic modulation could affect a wide range of auditory functions.

Cholinergic Axons Target Both GABAergic and Glutamatergic IC Neurons

Several studies have shown that ACh affects the majority of IC cells' response to sound (Watanabe and Simada, 1973; Farley et al., 1983; Habbicht and Vater, 1996). The effects can be mediated *via* nicotinic and muscarinic receptors. In general, cholinergic agents can affect response rate but appear to have little effect on the temporal patterns of a neuron's response to a sound, or on the selectivity for specific stimulus parameters. These studies could not discern direct from indirect cholinergic effects on the recorded cell, so the underlying mechanisms remain unclear. The present study suggests that the cholinergic effects are mediated by direct actions on both excitatory and inhibitory IC cells. We showed that PPT cholinergic axons are closely associated with both glutamatergic and GABAergic IC neurons. This sets the stage for postsynaptic effects on the closely apposed cell bodies or dendrites (without ruling out presynaptic effects on nearby axon terminals that contact the same postsynaptic cell). Evidence for cholinergic effects on identified GABAergic or glutamatergic IC cells is limited. Sottile et al. (2017) showed that GABAergic and presumptive glutamatergic IC cells express mRNA for nicotinic receptor subunits. These results do not indicate where the receptors are expressed on the cells [indeed, Sottile et al. (2017) were examining cholinergic effects on the collicular axon terminals in the thalamus]. *In vitro* recordings from the IC provide additional support. Yigit et al. (2003) provided physiological evidence that GABAergic IC cells are activated *via* muscarinic receptors. Those experiments were conducted in young animals and could potentially reflect mechanisms that disappear after the system has developed (see Morley and Happe, 2000 for a discussion of separate cholinergic roles during and after the development of the auditory system). In a preliminary study, Rivera-Perez et al. (2020) demonstrated direct nicotinic depolarization of VIP-expressing IC cells (which are known to be glutamatergic; Goyer et al., 2019). Additional experiments will be needed to identify the receptor types on glutamatergic and GABAergic IC cells and to differentiate presynaptic vs. postsynaptic effects.

CONCLUSION

The PPT, the largest source of cholinergic projections to the IC, sends axons to terminate bilaterally throughout the three major subdivisions of the IC. This termination pattern suggests that ACh modulates auditory processing associated with all three parallel ascending pathways to the thalamus—the tonotopic, multisensory, and diffuse pathways—and thus affects most aspects of auditory processing. Cholinergic boutons are found in close association with both glutamatergic and GABAergic IC cells, suggesting that ACh modulates both excitatory and inhibitory IC circuits. Overall, the PPT is likely to set the sensitivity of IC cells, modulating neuronal responses according to behavioral state and level of arousal. Further, by providing a permissive signal for plasticity in IC cells driven by top-down (corticofugal) mechanisms, ACh is likely to have both long-term as well as short-term effects on midbrain auditory processing.

DATA AVAILABILITY STATEMENT

The original contributions presented in this study are included in the article. Further inquiries can be directed to the corresponding author.

ETHICS STATEMENT

The animal study was reviewed and approved by Northeast Ohio Medical University Institutional Animal Care and Use Committee.

AUTHOR CONTRIBUTIONS

All authors contributed to the conception and design of the study and data collection. WN analyzed the data and wrote the first draft of the manuscript. All authors contributed to manuscript revision, and read and approved the submitted version.

FUNDING

This work was supported by the National Institutes of Health Grant R01 DC004391.

ACKNOWLEDGMENTS

We acknowledge Dr. Karl Deisseroth (Stanford University) as the donor of the transgenic rat model and the viral vectors used in the study, and also the Rat Resource and Research Center for providing the transgenic rat model. We gratefully acknowledge Colleen Sowick for technical support throughout the process.

REFERENCES

Aschauer, D. F., Kreuz, S., and Rumpel, S. (2013). Analysis of transduction efficiency, tropism and axonal transport of aav serotypes 1, 2, 5, 6, 8 and 9 in the mouse brain. *PLoS One* 8:e76310. doi: 10.1371/journal.pone.0076310

Azzopardi, E., Louttit, A. G., DeOliveira, C., Laviolette, S. R., and Schmid, S. (2018). The role of cholinergic midbrain neurons in startle and prepulse inhibition. *J. Neurosci.* 38, 8798–8808. doi: 10.1523/jneurosci.0984-18.2018

Beebe, N. L., Young, J. W., Mellott, J. G., and Schofield, B. R. (2016). Extracellular molecular markers and soma size of inhibitory neurons: evidence for four subtypes of GABAergic cells in the inferior colliculus. *J. Neurosci.* 36, 3988–3999. doi: 10.1523/jneurosci.0217-16.2016

Calford, M., and Aitkin, L. (1983). Ascending projections to the medial geniculate body of the cat: evidence for multiple, parallel auditory pathways through thalamus. *J. Neurosci.* 3, 2365–2380. doi: 10.1523/jneurosci.03-11-02365.1983

Chernock, M. L., Larue, D. T., and Winer, J. A. (2004). A periodic network of neurochemical modules in the inferior colliculus. *Hear. Res.* 188, 12–20. doi: 10.1016/s0378-5955(03)00340-x

Cissé, Y., Toossi, H., Ishibashi, M., Mainville, L., Leonard, C. S., Adamantidis, A., et al. (2018). Discharge and role of acetylcholine pontomesencephalic neurons in cortical activity and sleep-wake states examined by optogenetics and juxtacellular recording in mice. *eNeuro* 5:ENEURO.0270–18.2018. doi: 10.1523/eneuro.0270-18.2018

Coote, E. J., and Rees, A. (2008). The distribution of nitric oxide synthase in the inferior colliculus of guinea pig. *Neuroscience* 154, 218–225. doi: 10.1016/j.neuroscience.2008.02.030

Cortes, R., Probst, A., and Palacios, J. M. (1984). Quantitative light microscopic autoradiographic localization of cholinergic muscarinic receptors in the human brain: brainstem. *Neuroscience* 12, 1003–1026. doi: 10.1016/0306-4522(84)90001-0

Curtis, D. R., and Koizumi, K. (1961). Chemical transmitter substances in the brain stem of cat. *J. Neurophysiol.* 24, 80–90. doi: 10.1152/jn.1961.24.1.80

Dallos, P., Popper, A. N., and Fay, R. R. (Eds.) (1996). *The Cochlea.* New York, NY: Springer New York.

De Ribaupierre, F. (1997). "Acoustical information processing in the auditory thalamus and cerebral cortex," in *The Central Auditory System*, eds G. Ehret and R. Romand (New York, NY: Oxford University Press), 317–397.

Descarries, L., Gisiger, V., and Steriade, M. (1997). Diffuse transmission by acetylcholine in the CNS. *Prog. Neurobiol.* 53, 603–625. doi: 10.1016/s0301-0082(97)00050-6

Dillingham, C. H., Gay, S. M., Behrooz, R., and Gabriele, M. L. (2017). Modular-extramodular organization in developing multisensory shell regions of the mouse inferior colliculus. *J. Comp. Neurol.* 525, 3742–3756. doi: 10.1002/cne.24300

Ehret, G. (1997). "The auditory midbrain, a 'shunting-yard' of acoustical information," in *The central auditory system*, eds G. Ehret and R. Romand (New York, NY: Oxford University Press), 3–96.

Farley, G. R., Morley, B. J., Javel, E., and Gorga, M. P. (1983). Single-unit responses to cholinergic agents in the rat inferior colliculus. *Hear. Res.* 11, 73–91. doi: 10.1016/0378-5955(83)90046-1

Felix, R. A. II., Chavez, V. A., Novicio, D. M., Morley, B. J., and Portfors, C. V. (2019). Nicotinic acetylcholine receptor subunit α_7 -knockout mice exhibit degraded auditory temporal processing. *J. Neurophysiol.* 122, 451–465. doi: 10.1152/jn.00170.2019

Fujino, K., and Oertel, D. (2001). Cholinergic modulation of stellate cells in the mammalian ventral cochlear nucleus. *J. Neurosci.* 21, 7372–7383. doi: 10.1523/JNEUROSCI.21-18-07372.2001

Gahring, L. C., Persiyanov, K., and Rogers, S. W. (2004). Neuronal and astrocyte expression of nicotinic receptor subunit β4 in the adult mouse brain. *J. Comp. Neurol.* 468, 322–333. doi: 10.1002/cne.10942

Gillet, C., Goyer, D., Kurth, S., Griebel, H., and Kuenzel, T. (2018). Cholinergic innervation of principal neurons in the cochlear nucleus of the Mongolian gerbil. *J. Comp. Neurol.* 526, 1647–1661. doi: 10.1002/cne.24433

Glendenning, K. K., and Baker, B. N. (1988). Neuroanatomical distribution of receptors for three potential inhibitory neurotransmitters in the brainstem auditory nuclei of the cat. *J. Comp. Neurol.* 275, 288–308. doi: 10.1002/cne.902750210

Goyer, D., Kurth, S., Gillet, C., Keine, C., Rübsamen, R., and Kuenzel, T. (2016). Slow cholinergic modulation of spike probability in ultra-fast time-coding sensory neurons. *eNeuro* 3:ENEURO.0186–16.2016. doi: 10.1523/eneuro.0186-16.2016

Goyer, D., Silveira, M. A., George, A. P., Beebe, N. L., Edelbrock, R. M., Malinski, P. T., et al. (2019). A novel class of inferior colliculus principal neurons labeled in vasoactive intestinal peptide-Cre mice. *eLife* 8:e43770. doi: 10.7554/elife.43770

Gut, N. K., and Winn, P. (2016). The pedunculopontine tegmental nucleus-a functional hypothesis from the comparative literature: the pedunculopontine-a functional hypothesis. *Mov. Disord.* 31, 615–624. doi: 10.1002/mds.26556

Habbicht, H., and Vater, M. (1996). A microiontophoretic study of acetylcholine effects in the inferior colliculus of horseshoe bats: implications for a modulatory role. *Brain Res.* 724, 169–179. doi: 10.1016/0006-8993(96)00224-7

Hamada, S., Houtani, T., Trifonov, S., Kase, M., Maruyama, M., Shimizu, J.-I., et al. (2010). Histological determination of the areas enriched in cholinergic terminals and m2 and m3 muscarinic receptors in the mouse central auditory system. *Anat. Rec.* 293, 1393–1399. doi: 10.1002/ar.21186

Happe, H. K., and Morley, B. J. (2004). Distribution and postnatal development of α7 nicotinic acetylcholine receptors in the rodent lower auditory brainstem. *Dev. Brain Res.* 153, 29–37. doi: 10.1016/j.devbrainres.2004.07.004

Hasselmo, M. E., and Sarter, M. (2011). Modes and models of forebrain cholinergic neuromodulation of cognition. *Neuropsychopharmacol* 36, 52–73. doi: 10.1038/npp.2010.104

Henderson, Z., and Sherriff, F. E. (1991). Distribution of choline acetyltransferase immunoreactive axons and terminals in the rat and ferret brainstem. *J. Comp. Neurol.* 314, 147–163. doi: 10.1002/cne.903140114

Jane, J. A., Masterton, R. B., and Diamond, I. T. (1965). The function of the tectum for attention to auditory stimuli in the cat. *J. Comp. Neurol.* 125, 165–191. doi: 10.1002/cne.901250203

Ji, W., Gao, E., and Suga, N. (2001). Effects of acetylcholine and atropine on plasticity of central auditory neurons caused by conditioning in bats. *J. Neurophysiol.* 86, 211–225. doi: 10.1152/jn.2001.86.1.211

Jones, B. E. (2017). Principal cell types of sleep-wake regulatory circuits. *Curr. Opin. Neurobiol.* 44, 101–109. doi: 10.1016/j.conb.2017.03.018

Kuenzel, T. (2019). Modulatory influences on time-coding neurons in the ventral cochlear nucleus. *Hear. Res.* 384:107824. doi: 10.1016/j.heares.2019.107824

Leach, N. D., Nodal, F. R., Cordery, P. M., King, A. J., and Bajo, V. M. (2013). Cortical cholinergic input is required for normal auditory perception and experience-dependent plasticity in adult ferrets. *J. Neurosci.* 33, 6659–6671. doi: 10.1523/jneurosci.5039-12.2013

Lendvai, B., and Vizi, E. S. (2008). Nonsynaptic chemical transmission through nicotinic acetylcholine receptors. *Physiol. Rev.* 88, 333–349. doi: 10.1152/physrev.00040.2006

Mellott, J. G., Foster, N. L., Ohl, A. P., and Schofield, B. R. (2014). Excitatory and inhibitory projections in parallel pathways from the inferior colliculus to the auditory thalamus. *Front. Neuroanat.* 8:124. doi: 10.3389/fnana.2014.00124

Mooney, D. M., Zhang, L., Basile, C., Senatorov, V. V., Ngsee, J., Omar, A., et al. (2004). Distinct forms of cholinergic modulation in parallel thalamic sensory pathways. *Proc. Natl. Acad. Sci. U.S.A.* 101, 320–324. doi: 10.1073/pnas.0304445101

Merchán, M., Aguilar, L. A., Lopez-Poveda, E. A., and Malmierca, M. S. (2005). The inferior colliculus of the rat: quantitative immunocytochemical study of GABA and glycine. *Neuroscience* 136, 907–925. doi: 10.1016/j.neuroscience.2004.12.030

Mesulam, M.-M., Mufson, E. J., Wainer, B. H., and Levey, A. I. (1983). Central cholinergic pathways in the rat: an overview based on an alternative nomenclature (Ch1-Ch6). *Neuroscience* 10, 1185–1201. doi: 10.1016/0306-4522(83)90108-2

Metherate, R. (2011). Functional connectivity and cholinergic modulation in auditory cortex. *Neurosci. Biobehav. Rev.* 35, 2058–2063. doi: 10.1016/j.neubiorev.2010.11.010

Morley, B. J., and Happe, H. K. (2000). Cholinergic receptors: dual roles in transduction and plasticity. *Hear. Res.* 147, 104–112. doi: 10.1016/s0378-5955(00)00124-6

Motts, S. D., and Schofield, B. R. (2009). Sources of cholinergic input to the inferior colliculus. *Neuroscience* 160, 103–114. doi: 10.1016/j.neuroscience.2009.02.036

Motts, S. D., and Schofield, B. R. (2011). Cholinergic cells in the tegmentum send branching projections to the inferior colliculus and the medial geniculate body. *Neuroscience* 179, 120–130. doi: 10.1016/j.neuroscience.2011.01.044

Motts, S. D., Slusarczyk, A. S., Sowick, C. S., and Schofield, B. R. (2008). Distribution of cholinergic cells in guinea pig brainstem. *Neuroscience* 154, 186–195. doi: 10.1016/j.neuroscience.2007.12.017

Motts, S. D., and Schofield, B. R. (2010). Cholinergic and non-cholinergic projections from the pedunculopontine and laterodorsal tegmental nuclei to the medial geniculate body in guinea pigs. *Front. Neuroanat.* 4:137. doi: 10.3389/fnana.2010.00137

Muñoz, W., and Rudy, B. (2014). Spatiotemporal specificity in cholinergic control of neocortical function. *Curr. Opin. Neurobiol.* 26, 149–160. doi: 10.1016/j.conb.2014.02.015

Oertel, D., and Fujino, K. (2001). Role of biophysical specialization in cholinergic modulation in neurons of the ventral cochlear nuclei. *Audiol. Neurootol.* 6, 161–166. doi: 10.1159/000046825

Oertel, D., Wright, S., Cao, X.-J., Ferragamo, M., and Bal, R. (2011). The multiple functions of T stellate/multipolar/chopper cells in the ventral cochlear nucleus. *Hear. Res.* 276, 61–69. doi: 10.1016/j.heares.2010.10.018

Oliver, D. L., Winer, J. A., Beckius, G. E., and Marie, R. L. S. (1994). Morphology of GABAergic neurons in the inferior colliculus of the cat. *J. Comp. Neurol.* 340, 27–42. doi: 10.1002/cne.903400104

Parikh, V., Kozak, R., Martinez, V., and Sarter, M. (2007). Prefrontal acetylcholine release controls cue detection on multiple timescales. *Neuron* 56, 141–154. doi: 10.1016/j.neuron.2007.08.025

Reese, N. B., Garcia-Rill, E., and Skinner, R. D. (1995a). Auditory input to the pedunculopontine nucleus: I. Evoked potentials. *Brain Res. Bull.* 37, 257–264. doi: 10.1016/0361-9230(95)00002-v

Reese, N. B., Garcia-Rill, E., and Skinner, R. D. (1995b). Auditory input to the pedunculopontine nucleus: II. Unit responses. *Brain Res. Bull.* 37, 265–273. doi: 10.1016/0361-9230(95)00001-u

Reese, N. B., Garcia-Rill, E., and Skinner, R. D. (1995c). The pedunculopontine nucleus—auditory input, arousal and pathophysiology. *Prog. Neurobiol.* 47, 105–133. doi: 10.1016/0301-0082(95)00023-o

Rivera-Perez, L. M., Cruz-Colon, K. O., and Roberts, M. T. (2020). "Cholinergic signaling modulates the excitability of VIP neurons in the mouse inferior colliculus *via* nicotinic acetylcholine receptor-dependent mechanisms," in *Associaton for Research in Otolaryngology MidWinter Meeting 43, 571. Abstract retrieved from Association for Research in Otolaryngology MidWinter Meeting Archives*.

Rouiller, E. M. (1997). "Functional organization of the auditory pathways," in *The Central Auditory System*, eds G. Ehret and R. Romand (New York, NY: Oxford University Press), 3–96.

Ryugo, D. K., Fay, R. R., and Popper, A. N. (Eds.) (2011). *Auditory and Vestibular Efferents*. New York, NY: Springer.

Salegio, E. A., Samaranch, L., Kells, A. P., Mittermeyer, G., San Sebastian, W., Zhou, S., et al. (2013). Axonal transport of adeno-associated viral vectors is serotype-dependent. *Gene Ther.* 20, 348–352. doi: 10.1038/gt.2012.27

Sarter, M., and Bruno, J. P. (1997). Cognitive functions of cortical acetylcholine: toward a unifying hypothesis. *Brain Res. Rev.* 23, 28–46. doi: 10.1016/s0165-0173(96)00009-4

Sarter, M., Parikh, V., and Howe, W. M. (2009). Phasic acetylcholine release and the volume transmission hypothesis: time to move on. *Nat. Rev. Neurosci.* 10, 383–390. doi: 10.1038/nrn2635

Schofield, B. R. (2010). Projections from auditory cortex to midbrain cholinergic neurons that project to the inferior colliculus. *Neuroscience* 166, 231–240. doi: 10.1016/j.neuroscience.2009.12.008

Schofield, B. R., and Beebe, N. L. (2019). "Descending auditory pathways and plasticity," in *The Oxford Handbook of the Auditory Brainstem*, ed. K. Kandler (New York, NY; Oxford University Press), 610–638.

Schofield, B. R., and Hurley, L. (2018). "Circuits for modulation of auditory function," in *The Mammalian Auditory Pathways Springer Handbook of Auditory Research*, eds D. L. Oliver, N. B. Cant, R. R. Fay and A. N. Popper (Cham: Springer International Publishing), 235–267.

Schofield, B. R., and Motts, S. D. (2009). Projections from auditory cortex to cholinergic cells in the midbrain tegmentum of guinea pigs. *Brain Res. Bull.* 80, 163–170. doi: 10.1016/j.brainresbull.2009.06.015

Schofield, B. R., Motts, S. D., and Mellott, J. G. (2011). Cholinergic cells of the pontomesencephalic tegmentum: connections with auditory structures from cochlear nucleus to cortex. *Hear. Res.* 279, 85–95. doi: 10.1016/j.heares.2010.12.019

Schwartz, R. D. (1986). Autoradiographic distribution of high affinity muscarinic and nicotinic cholinergic receptors labeled with [3H]acetylcholine in rat brain. *Life Sci.* 38, 2111–2119. doi: 10.1016/0024-3205(86)90210-9

Shute, C. C. D., and Lewis, P. R. (1967). The ascending cholinergic reticular system: neocortical, olfactory and subcortical projections. *Brain* 90, 497–520. doi: 10.1093/brain/90.3.497

Slee, S. J., and David, S. V. (2015). Rapid task-related plasticity of spectrotemporal receptive fields in the auditory midbrain. *J. Neurosci.* 35, 13090–13102. doi: 10.1523/jneurosci.1671-15.2015

Sottile, S. Y., Hackett, T. A., Cai, R., Ling, L., Llano, D. A., and Caspary, D. M. (2017). Presynaptic neuronal nicotinic receptors differentially shape select inputs to auditory thalamus and are negatively impacted by aging. *J. Neurosci.* 37, 11377–11389. doi: 10.1523/jneurosci.1795-17.2017

Stornetta, R. L., Macon, C. J., Nguyen, T. M., Coates, M. B., and Guyenet, P. G. (2013). Cholinergic neurons in the mouse rostral ventrolateral medulla target sensory afferent areas. *Brain Struct. Funct.* 218, 455–475. doi: 10.1007/s00429-012-0408-3

Suga, N. (2012). Tuning shifts of the auditory system by corticocortical and corticofugal projections and conditioning. *Neurosci. Biobehav. Rev.* 36, 969–988. doi: 10.1016/j.neubiorev.2011.11.006

Takács, V. T., Cserép, C., Schlingloff, D., Pósfai, B., Szőnyi, A., Sos, K. E., et al. (2018). Co-transmission of acetylcholine and GABA regulates hippocampal states. *Nat. Commun.* 9:2848. doi: 10.1038/s41467-018-05136-1

Wang, H.-L., and Morales, M. (2009). Pedunculopontine and laterodorsal tegmental nuclei contain distinct populations of cholinergic, glutamatergic and GABAergic neurons in the rat. *Eur. J. Neurosci.* 29, 340–358. doi: 10.1111/j.1460-9568.2008.06576.x

Watanabe, T., and Simada, Z. (1973). Phamacological properties of cat's collicular auditory neurons. *Jpn. J. Physiol.* 23, 291–308. doi: 10.2170/jjphysiol.23.291

Winer, J. A., and Schreiner, C. E. (Eds.) (2005). *The Inferior Colliculus.* New York, NY: Springer-Verlag.

Winer, J. A., Saint Marie, R. L., Larue, D. T., and Oliver, D. L. (1996). GABAergic feedforward projections from the inferior colliculus to the medial geniculate body. *Proc. Natl. Acad. Sci. U S A* 93, 8005–8010. doi: 10.1073/pnas.93.15.8005

Witten, I. B., Steinberg, E. E., Lee, S. Y., Davidson, T. J., Zalocusky, K. A., Brodsky, M., et al. (2011). Recombinase-driver rat lines: tools, techniques, and optogenetic application to dopamine-mediated reinforcement. *Neuron* 72, 721–733. doi: 10.1016/j.neuron.2011.10.028

Xiong, Y., Zhang, Y., and Yan, J. (2009). The neurobiology of sound-specific auditory plasticity: a core neural circuit. *Neurosci. Biobehav. Rev.* 33, 1178–1184. doi: 10.1016/j.neubiorev.2008.10.006

Yigit, M., Keipert, C., and Backus, K. H. (2003). Muscarinic acetylcholine receptors potentiate the GABAergic transmission in the developing rat inferior colliculus. *Neuropharmacology* 45, 504–513. doi: 10.1016/s0028-3908(03)00197-7

Zoli, M., Jansson, A., Syková, E., Agnati, L. F., and Fuxe, K. (1999). Volume transmission in the CNS and its relevance for neuropsychopharmacology. *Trends Pharmacol. Sci.* 20, 142–150. doi: 10.1016/s0165-6147(99)01343-7

Conflict of Interest: The authors declare that the research was conducted in the absence of any commercial or financial relationships that could be construed as a potential conflict of interest.

frontiers in Neural Circuits

MINI REVIEW
published: 05 November 2020
doi: 10.3389/fncir.2020.599600

Neuromodulation by mGluRs in Sound Localization Circuits in the Auditory Brainstem

*Nupur Goel†, Kang Peng† and Yong Lu**

Department of Anatomy and Neurobiology, Hearing Research Group, College of Medicine, Northeast Ohio Medical University, Rootstown, OH, United States

The ability of humans and animals to localize the source of a sound in a complex acoustic environment facilitates communication and survival. Two cues are used for sound localization at horizontal planes, interaural time and level differences (ITD and ILD), which are analyzed by distinct neural circuits in the brainstem. Here, we review the studies on metabotropic glutamate receptor (mGluR)-mediated neuromodulation of both intrinsic and synaptic properties of brainstem neurons in these circuits. Both mammalian and avian animal models have been used, with each having their advantages that are not present in the other. For the mammalian model, we discuss mGluR neuromodulation in the ILD circuit, with an emphasis on the recent discovery of differential modulation of synaptic transmission of different transmitter release modes. For the avian model, we focus on reviewing mGluR neuromodulation in the ITD pathway, with an emphasis on tonotopic distribution and synaptic plasticity of mGluR modulation in coincidence detector neurons. Future works are proposed to further investigate the functions and mechanisms of mGluRs in the sound localization circuits.

Keywords: neuromodulation, mGluR, sound localization, ITD, ILD

OPEN ACCESS

Edited by:
Conny Kopp-Scheinpflug, Ludwig Maximilian University of Munich, Germany

Reviewed by:
Harunori Ohmori, Kyoto University, Japan
Christopher Kushmerick, Federal University of Minas Gerais, Brazil

****Correspondence:***
Yong Lu
ylu@neomed.edu

†These authors have contributed equally to this work

Received: *27 August 2020*
Accepted: *05 October 2020*
Published: *05 November 2020*

Citation:
Goel N, Peng K and Lu Y (2020) Neuromodulation by mGluRs in Sound Localization Circuits in the Auditory Brainstem. Front. Neural Circuits 14:599600. doi: 10.3389/fncir.2020.599600

INTRODUCTION

Glutamate, the most ubiquitous excitatory neurotransmitter used in the nervous system, activates two types of receptors, ionotropic and metabotropic receptors (iGluRs and mGluRs). These receptors are tasked with fast and slow neurotransmission respectively. Soon after mGluRs were discovered (Sladeczek et al., 1985; Nicoletti et al., 1986a,b), studies on their structure, functional expression, and signaling pathways followed (Sugiyama et al., 1987; Houamed et al., 1991; Masu et al., 1991). To date, eight members of mGluRs have been identified. They are classified into three groups based on signaling mechanisms and amino acid sequences (reviewed by Niswender and Conn, 2010). Group I mGluRs consist of two members, mGluR1 and mGluR5. They are typically expressed in postsynaptic cells, and function through G_q/G_{11} proteins. Group II mGluRs consist of mGluR2 and mGluR3, and group III mGluRs have four members (mGluR4, 6, 7, and 8). Both group II and group III mGluRs are expressed primarily on presynaptic loci and function through G_i/G_o proteins. Since mGluRs play a crucial role in modulating many neural circuits, mGluRs have been targets for drug development to treat various psychiatric conditions such as anxiety disorders, depression, schizophrenia, and chronic pain (reviewed by Swanson et al., 2005; Krystal et al., 2010; Crupi et al., 2019).

This review focuses on mGluR modulation of sound localization circuits in the brainstem. The general topics of mGluRs can be found in other reviews (reviewed by Krystal et al., 2010; Niswender and Conn, 2010; Nicoletti et al., 2011; Tharmalingam et al., 2012; Lodge et al., 2013). Additionally, mGluR modulation of both synaptic transmission and intrinsic excitability of auditory neurons, which is important for modulation of auditory processing, has been reviewed previously (reviewed by Lu, 2014; Tang and Lu, 2018).

Sound localization allows an organism to discern spatial characteristics of sounds, providing a clear evolutionary advantage in terms of communication and survival skills. For sound localization in the horizontal plane, two cues are used, interaural time differences (ITD) and interaural level differences (ILD; reviewed by Grothe et al., 2010). While ITD cues help process low-frequency sounds, ILD cues are well suited for high-frequency sounds (Goupell and Stakhovskaya, 2018). It is conceivable that mGluRs are involved in sound localization pathways, because glutamate is the principal excitatory neurotransmitter expressed from the cochlea to the auditory cortex, and mGluRs are found to be expressed in all these auditory stations (reviewed by Lu, 2014; Tang and Lu, 2018). The brainstem is the preliminary location of integrating complex auditory processes such as sound localization. Understanding the functions of mGluRs in auditory circuits will provide a deeper appreciation for modulatory mechanisms involved with auditory processing and help cultivate potential therapeutic approaches targeting mGluRs in treating hearing disorders such as tinnitus (ringing of the ear without external sound stimuli; reviewed by Galazyuk et al., 2019). Here, we review the studies on mGluRs in the avian ITD and the mammalian ILD circuits with a focus on brainstem structures.

mGluRs IN MAMMALIAN ILD PATHWAY

The mammalian ILD pathway is extensive and spans many subcortical and cortical structures. The auditory nerve enters the brainstem and innervates the cochlear nucleus (CN). The CN has three sub-nuclei: dorsal CN, anteroventral CN (AVCN), and posteroventral CN (PVCN). These sub-nuclei have diverse functions and neuromodulation (Farago et al., 2006). Outputs from the AVCN lead to excitation of the ipsilateral lateral superior olivary (LSO) complex. The LSO also receives synaptic inhibition from the ipsilateral medial nucleus trapezoid body (MNTB), which receives excitatory input from the contralateral AVCN and converts the excitation to an inhibitory output. The integration of ipsilateral excitation and contralateral inhibition allows LSO to encode ILDs (reviewed by Tollin, 2003). Thus, our discussion will be focused on mGluRs in AVCN, MNTB, and LSO (**Figure 1**).

In AVCN, at the mRNA and protein levels, mGluR1 (a subtype of group I mGluRs) is moderately expressed (Shigemoto et al., 1992; Petralia et al., 1997; Bilak and Morest, 1998; Kemmer and Vater, 2001). Chanda and Xu-Friedman (2011) have provided physiological evidence for the presence of tonic activity of group I mGluRs in AVCN. Depolarization of bushy cells by activation of mGluR1 and/or mGluR5 is believed to enhance the excitability of these cells (Chanda and Xu-Friedman, 2011), forming a contrast with the inhibition mediated by $GABA_B$ receptors ($GABA_B$Rs). For groups II and III mGluRs, very little is known about their expression or function in the AVCN (Ohishi et al., 1998).

The expression and *in vitro* physiology of mGluRs in MNTB has been relatively extensively studied. Group I mGluRs are expressed primarily on the postsynaptic membrane of MNTB neurons (mGluR1: Kushmerick et al., 2004; mGluR5: Peng et al., 2020). Kushmerick et al. (2004) has shown that *via* retrograde signaling, a postsynaptic group I mGluRs (predominantly mGluR1) inhibit glutamatergic transmission at the calyx-MNTB synapse. Remarkably, mGluR5 (and maybe mGluR1 too) is also expressed presynaptically in the calyx of Held, and enhances spontaneous glutamate release, *via* regulating a persistent voltage-gated Na^+ channel current (Peng et al., 2020). The differential mGluR modulation on spontaneous vs. evoked glutamate release is consistent with our finding that group I mGluRs differentially modulate spontaneously vs. evoked inhibitory postsynaptic currents (sIPSCs and eIPSCs, respectively) based on the neurotransmitter (glycine or GABA; Curry et al., 2018). Group I mGluRs selectively increase glycine sIPSCs while depressing GABA eIPSCs and having minimal effect on glycine eIPSCs and GABA sIPSCs (Curry et al., 2018). Our results (Curry et al., 2018; Peng et al., 2020) support the theory of different synaptic vesicular pools for spontaneous and evoked release and provide potential evidence of multivesicular spontaneous release under mGluR modulation. Besides modulating synaptic properties, the group I mGluRs can also increase the excitability of MNTB neurons *via* different mechanisms from the presynaptic modulation (dos Santos E Alhadas et al., 2019). Activation of these receptors leads to MNTB membrane depolarization, inhibition of inward rectifier K^+ channels, promotion of action potentials (APs), improvement in the neuron's ability to follow high-frequency excitatory inputs, and these effects persist into adulthood (P90; dos Santos E Alhadas et al., 2019). The enhancement of cellular excitability of MNTB neurons by the group I mGluRs remains in the presence of the antagonists for the major known ionotropic receptors (Peng et al., 2020), indicating postsynaptic actions of these receptors. Also, $K_V3.1b$ phosphorylation, which underlies the high-threshold K_V conductances, is subject to modulation by the group I mGluRs (Song and Kaczmarek, 2006). Because the high-threshold K_V conductances critically define the ability of MNTB neurons to follow spike inputs at high frequency (HF; Johnston et al., 2010), the mGluR modulation of their phosphorylation status affects the inhibitory output of MNTB. Other mGluRs in MNTB are less well understood. Group II mGluRs are shown to be present at synapses of MNTB (Elezgarai et al., 2001). One group III member, mGluR4, is identified at the presynaptic glutamatergic terminals, and its activity is developmentally regulated (functioning before hearing onset; Elezgarai et al., 1999). Functionally, mGluRs make a small (10%) yet physiologically relevant contribution to the presynaptic depression of the excitatory input to MNTB from the calyx (von Gersdorff et al., 1997). Limited data also showed that the

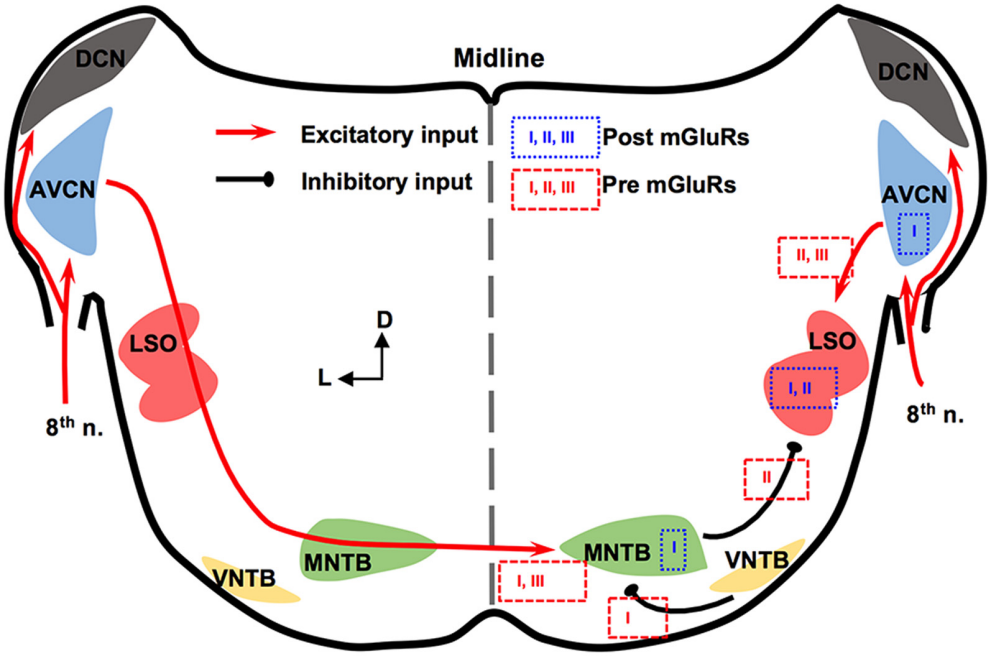

FIGURE 1 | Metabotropic glutamate receptor (mGluR) modulation in the mammalian brainstem interaural level differences (ILD) pathway. Modulation of neuronal properties by mGluRs has been observed at the ILD-coding site lateral superior olivary (LSO), as well as the input nuclei, anteroventral cochlear nucleus (AVCN) and medial nucleus trapezoid body (MNTB). At the LSO, groups I and II mGluRs at the postsynaptic site generate Ca^{2+} signaling. Presynaptic group II mGluRs regulate the inhibitory input from MNTB while groups II and III mGluRs regulate the excitatory input from AVCN. At the AVCN, the group I mGluRs facilitate the excitability of bushy cells. At the MNTB, besides facilitating the excitability, the group I mGluRs exert release-mode dependent modulation on both the excitatory and inhibitory inputs to MNTB. Group III mGluRs may also be involved in modulating the excitatory input to MNTB. The text boxes containing the subtypes of mGluRs indicate postsynaptic (within a particular nucleus) or presynaptic (outside of the nucleus) modulation.

excitatory input to MNTB is negatively regulated *via* group III mGluRs (Billups et al., 2005). These studies demonstrate multi-directional regulations by mGluRs of neuronal properties of MNTB. Although MNTB has been considered a simple sign-inverting relay station, the evidence reviewed above suggests rich possibilities for neural plasticity.

In the LSO, mGluR modulation seems to be limited during development. The expression of group II mGluRs is mostly detected in early development (P4) but not after hearing onset (Nishimaki et al., 2007). Supporting this anatomical observation, Ene et al. (2003) showed that the intracellular Ca^{2+} concentration is increased by activation of groups I and II mGluRs in LSO neurons obtained in P0-P4 mice. This mGluR-triggered response in the intracellular Ca^{2+} concentration reduces its amplitude in later animal ages (P20; Ene et al., 2007). Activation of mGluRs (likely groups II and III) inhibits evoked glutamate release at LSO in P14–22 rats, forming feedback control of the excitatory input (Wu and Fu, 1998). Meanwhile, Nishimaki et al. (2007) reported suppression of the inhibitory input to LSO neurons, apparently *via* activation of mGluRs on the inhibitory terminals by glutamate spillover escaped from the synaptic cleft of the excitatory terminals, and the effects diminish a few days after hearing onset. These results suggest a role of mGluRs in the development of the neural circuits involving the LSO.

In summary, mGluRs modulate synaptic inputs to the LSO, and extensively modulate the neuronal properties of the projecting neurons in AVCN and MNTB, constituting a network modulation of the ILD circuit in mammals.

mGluRs IN AVIAN ITD PATHWAY

For studies of mGluRs in the avian ITD circuit, the chicken auditory brainstem represents an excellent model because of its defined and specialized anatomy, and its well-characterized functions (reviewed by Rubel et al., 1990; Grothe, 2003; Burger et al., 2011). There are two subnuclei in the avian CN, the cochlear nucleus angularis (NA) and nucleus magnocellularis (NM), both of which receive excitatory inputs from the auditory nerve (8th nerve). Cells in NM are primarily bushy cells equivalent to bushy cells in mammalian AVCN. The nucleus laminaris (NL), the avian equivalent of MSO in mammals, receives bilateral excitatory inputs from the NM. These two excitatory inputs are morphologically and physiologically symmetrical (Lu et al., 2018). While the NA is tasked with intensity (ILD) cues, NM and NL circuits process temporal (ITD) characteristics. Besides the excitatory inputs, all these three lower brainstem nuclei (NM, NL, and NA) receive synaptic inhibition from projection neurons in the ipsilateral superior olivary nucleus (SON; Burger et al., 2005), as well as from local GABAergic interneurons (Yamada et al., 2013). The SON is driven by excitatory inputs originating from the NA and NL. Therefore, the inhibitory input from the SON onto these lower

brainstem nuclei forms a functionally important feedback loop, regulating the synaptic strength of the excitatory inputs to the ITD-coding circuit. The local interneurons are driven by the auditory nerve input and form feedforward inhibition, regulating ITD sensitivity in low-frequency NL neurons (Yamada et al., 2013). Compared to their mammalian counterparts, cells of NM and NL are more homogenous. Our discussion will be focused on mGluRs in NM and NL (**Figure 2**).

Immunohistochemistry has revealed the expression of group I and II mGluRs in NM neurons (Zirpel and Parks, 2001; Tang et al., 2013). The activity of mGluRs in NM neurons was first reported by Zirpel et al. (1994), in which an increase in the phosphatidylinositol metabolism was observed in response to glutamate. A series of subsequent studies demonstrated the importance of mGluRs in the regulation of Ca^{2+} signaling in NM neurons (Lachica et al., 1995, 1998; Zirpel et al., 1995, 1998; Kato et al., 1996; Zirpel and Rubel, 1996; Kato and Rubel, 1999; Zirpel and Parks, 2001). Because of the high activity of the excitatory input to NM neurons from the auditory nerve, these neurons need to buffer efficiently the activity-induced increase in Ca^{2+} concentration and maintain Ca^{2+} homeostasis for their survival. Modulation of Ca^{2+} signaling by mGluRs constitutes one of the mechanisms, e.g., *via* reduction of Ca^{2+} influx mediated by voltage-gated Ca^{2+} channels in NM neurons (Lachica et al., 1995; Lu and Rubel, 2005). In addition to postsynaptic neuromodulation, multiple mGluRs from all three groups also regulate presynaptic properties of NM neurons, *via* regulation of the inhibitory transmission originating from the ipsilateral SON. The SON inhibitory inputs to NM neurons are unusual because unlike other inhibitory transmissions in the adult brain the GABAergic input to NM elicits depolarizing responses, which exerts an inhibitory action through shunting inhibition (Hyson et al., 1995; Lu and Trussell, 2001; Monsivais and Rubel, 2001). Paradoxically, the GABAergic input could drive the postsynaptic cells to fire APs (Lu and Trussell, 2001; Kuo et al., 2009; Tang et al., 2009), which would be unlikely phase-locked to the excitatory inputs. Such unusual spiking activity could disrupt NM response to excitatory inputs and reduce the phase-locking fidelity of NM neurons, a property essential for accurate ITD coding. Multiple mechanisms have been discovered as a means to regulate inhibitory signals and prevent GABA-induced spiking. One of the important mechanisms, as we review here, is that mGluRs may tonically reduce the inhibitory synaptic strength to NM neurons (Lu, 2007), while a feedback regulation of the GABAergic system is provided by $GABA_B$Rs (Monsivais and Rubel, 2001), which may help ensure precise coincidence detection process and ITD coding in the NL.

Synaptic excitation to NL neurons is tonotopically distributed. EPSCs recorded in neurons in HF-coding regions are faster in kinetics and stronger in amplitude compared to low frequency (LF)-coding neurons (Sanchez et al., 2010; Slee et al., 2010). Conversely, synaptic inhibition in NL is also tonotopically distributed. In LF neurons, phasic IPSCs are fast in kinetics and the tonic inhibition is minimal. In contrast, phasic IPSCs are slower and the tonic inhibition is stronger in middle frequency (MF) and HF neurons (Tang et al., 2011; Tang and Lu, 2012a; Yamada et al., 2013). Group II mGluRs are found to be expressed in a graded manner along the frequency axis of NL (Tang et al., 2013). The greatest expression of mGluRs within the NL is in the LF neurons, lesser mGluR expression in the MF neurons, and the smallest expression in the HF neurons. Consistent with the anatomical evidence, physiological results by Okuda et al. (2013) demonstrated that mGluRs regulate EPSCs in NL with different modulation strength depending on the frequency-coding region. In LF neurons, activation of groups II and III mGluRs substantially suppresses the glutamatergic transmission. In contrast, in the MF and HF neurons, the modulation is less strong. This forms a complementary regulation when compared to the modulation by mGluRs of the inhibitory transmission across different frequency regions. Groups II and III mGluRs modulate the inhibitory input to NL neurons (primarily in MF and HF neurons), controlling the synaptic inhibitory strength *via* a mechanism similar to that in NM (Tang et al., 2009). Taken together, mGluR modulation of both the excitatory and inhibitory inputs to NL may help maintain a balance in excitation and inhibition and improve synaptic integration at particular sound frequencies.

Given the symmetrical bilateral excitatory inputs each NL neuron receives from the two ears, the NL serves as an excellent model to address possible plasticity of mGluR modulation. After removing the cochlea from one ear, we witnessed a dramatic reduction of evoked EPSCs and surprisingly a selective increase in group II mGluR expression and physiological suppression of the excitatory input from the deafferented pathway (Lu et al., 2018). The results suggest that unilateral cochlear ablation disrupts the animal's binaural processing capacity, and the upregulation of mGluRs modulation over eEPSCs presents an interesting case of anti-homeostatic plasticity. It is worth to point out that most of the studies on mGluRs in the avian auditory system have used relatively mature chicken tissues, and the developmental aspects of mGluRs have not been examined except for one study in which the modulatory strength of mGluRs on the inhibitory input to NL gradually increases over age (Tang and Lu, 2012b), in contrast to the mammalian system where mGluRs usually diminish over development. Therefore, the anti-homeostatic plasticity observed after hearing deprivation is unlikely a reversion to the pre-hearing status. Besides, the intrinsic neuronal properties of NL neurons are also regulated by mGluRs in a coding frequency-dependent manner (Hamlet and Lu, 2016). By using a technique that preserves intracellular signaling pathways (perforated patch-clamp recording), we reported that the high threshold K_V currents in NL neurons are enhanced, with the strongest modulation in LF neurons. This mGluR enhancement of K_V currents renders NL neurons the ability to follow high-frequency inputs, *via* an increase in the membrane outward rectification and sharpening of the waveform of APs (Hamlet and Lu, 2016). We propose that this modulation provides a feedforward modulatory mechanism that enhances temporal processing, especially when the peripheral input is of high intensity. Based on these studies, we conclude that mGluR modulation of neuronal properties in the ITD-coding NL neurons is tonotopically distributed, consistent with the tonotopic distribution of the

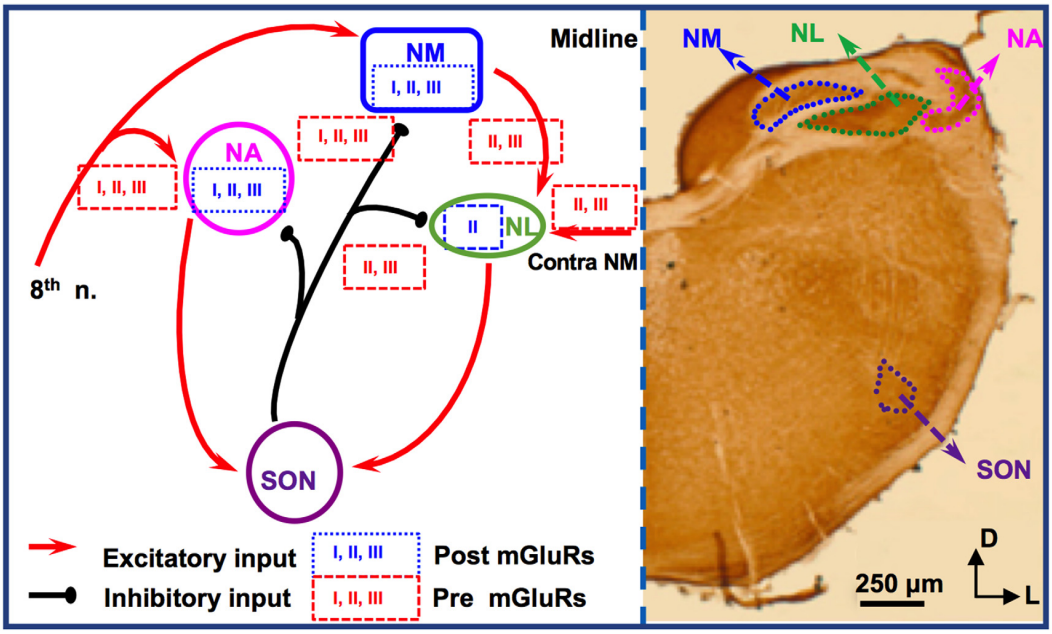

FIGURE 2 | mGluR modulation in the avian brainstem interaural time differences (ITD) pathway. Modulation of neuronal properties by mGluRs has been observed at the ITD-coding site nucleus laminaris (NL), as well as the excitatory input nucleus, nucleus magnocellularis (NM). At the NL, postsynaptic group II mGluRs interact with K_V channels, enhancing high frequency (HF) following ability. Presynaptic groups II and III mGluRs co-regulate both the excitatory and inhibitory transmission at NL. Importantly, this modulation varies depending on the coding-frequency region. At the NM, mGluRs on the presynaptic terminals exert fine control on the strength of the inhibitory input from superior olivary nucleus (SON), and postsynaptic mGluRs help maintain Ca^{2+} homeostasis. Data on mGluR modulation of neuronal properties of SON neurons is still lacking.

synaptic excitation and inhibition mediated by their respective ionotropic receptors. The differential modulation by mGluRs of the neuronal properties in different frequency coding regions of the NL represents a great example of fine-tuning of auditory processing within a single nucleus.

CONCLUDING REMARKS AND FUTURE WORKS

Here, we reviewed the studies on mGluRs in the sound localization circuits in both the mammalian and avian auditory brainstem, with an emphasis on the latest discoveries regarding mGluR modulation in the mammalian MNTB and the avian NL. While we have a decent grasp of mGluR expression in these circuits, a huge gap remains in our knowledge about mGluR physiology at the cellular and systems levels. There is no data on mGluRs for ITD-coding neurons in the mammalian MSO and the ILD-coding neurons (in the posterior portion of the dorsal nucleus of the lateral lemniscus). Thus, more studies regarding mGluR modulation of those circuits need to be performed. Research conducted from the 1980s up until 2010s of human brain slices concludes that humans possess an MNTB, MSO, and LSO (Kulesza and Grothe, 2015). These structures play a vital role in auditory processing and provide evidence to believe that ITD and ILD coding are interlinked and multi-dimensional in humans. Thus, our understanding of their proper function in different animal species directly correlates to the understanding we have of their function, or lack thereof, in our species. There are many vital questions about the roles of mGluR in sound localization circuits that still need to be answered. Are the presence and activity of mGluRs essential to the development of the auditory circuits underlying sound localization? Whether and how mGluRs regulate binaural sound processing at the systems level? Can mGluRs be used as potential targets for developing therapeutics to improve binaural auditory processing in cochlear implant patients? These questions warrant more active research in this field and our lab's ongoing works aim to address some of these unknowns.

AUTHOR CONTRIBUTIONS

YL perceived and supervised the project. NG wrote the draft of the main text. KP prepared the figures. NG, KP, and YL edited the article. All authors contributed to the article and approved the submitted version.

FUNDING

This work was supported by National Institute on Deafness and Other Communication Disorders Grant R01DC016054 (YL).

ACKNOWLEDGMENTS

We thank our former lab members for their contributions, and Lin Cai for editorial proofreading of the manuscript.

REFERENCES

Bilak, S. R., and Morest, D. K. (1998). Differential expression of the metabotropic glutamate receptor mGluR1α by neurons and axons in the cochlear nucleus: *in situ* hybridization and immunohistochemistry. *Synapse* 28, 251–270. doi: 10.1002/(SICI)1098-2396(199804)28:4<251::AID-SYN1>3.0.CO;2-8

Billups, B., Graham, B. P., Wong, A. Y., and Forsythe, I. D. (2005). Unmasking group III metabotropic glutamate autoreceptor function at excitatory synapses in the rat CNS. *J. Physiol.* 565, 885–896. doi: 10.1113/jphysiol.2005.086736

Burger, R. M., Cramer, K. S., Pfeiffer, J. D., and Rubel, E. W. (2005). Avian superior olivary nucleus provides divergent inhibitory input to parallel auditory pathways. *J. Comp. Neurol.* 481, 6–18. doi: 10.1002/cne.20334

Burger, R. M., Fukui, I., Ohmori, H., and Rubel, E. W. (2011). Inhibition in the balance: binaurally coupled inhibitory feedback in sound localization circuitry. *J. Neurophysiol.* 106, 4–14. doi: 10.1152/jn.00205.2011

Chanda, S., and Xu-Friedman, M. A. (2011). Excitatory modulation in the cochlear nucleus through group I metabotropic glutamate receptor activation. *J. Neurosci.* 31, 7450–7455. doi: 10.1523/JNEUROSCI.1193-11.2011

Crupi, R., Impellizzeri, D., and Cuzzocrea, S. (2019). Role of metabotropic glutamate receptors in neurological disorders. *Front. Mol. Neurosci.* 12:20. doi: 10.3389/fnmol.2019.00020

Curry, R. J., Peng, K., and Lu, Y. (2018). Neurotransmitter- and release-mode-specific modulation of inhibitory transmission by group I metabotropic glutamate receptors in central auditory neurons of the mouse. *J. Neurosci.* 38, 8187–8199. doi: 10.1523/JNEUROSCI.0603-18.2018

dos Santos E Alhadas, É. S., Correa, A. M., Naves, L. A., and Kushmerick, C. (2019). Mechanisms and functional impact of Group I metabotropic glutamate receptor modulation of excitability in mouse MNTB neurons. *Synapse* 74:e22137. doi: 10.1002/syn.22137

Elezgarai, I., Benítez, R., Mateos, J. M., Lázaro, E., Osorio, A., Azkue, J. J., et al. (1999). Developmental expression of the group III metabotropic glutamate receptor mGluR4a in the medial nucleus of the trapezoid body of the rat. *J. Comp. Neurol.* 411, 431–440. doi: 10.1002/(sici)1096-9861(19990830)411:3<431::aid-cne6>3.0.co;2-r

Elezgarai, I., Bilbao, A., Mateos, J. M., Azkue, J. J., Benítez, R., Osorio, A., et al. (2001). Group II metabotropic glutamate receptors are differentially expressed in the medial nucleus of the trapezoid body in the developing and adult rat. *Neuroscience* 104, 487–498. doi: 10.1016/s0306-4522(01)00080-x

Ene, F. A., Kalmbach, A., and Kandler, K. (2007). Metabotropic glutamate receptors in the lateral superior olive activate TRP-like channels: age- and experience-dependent regulation. *J. Neurophysiol.* 97, 3365–3375. doi: 10.1152/jn.00686.2006

Ene, F. A., Kullmann, P. H., Gillespie, D. C., and Kandler, K. (2003). Glutamatergic calcium responses in the developing lateral superior olive: receptor types and their specific activation by synaptic activity patterns. *J. Neurophysiol.* 90, 2581–2591. doi: 10.1152/jn.00238.2003

Farago, A. F., Awatramani, R. B., and Dymecki, S. M. (2006). Assembly of the brainstem cochlear nuclear complex is revealed by intersectional and subtractive genetic fate maps. *Neuron* 50, 205–218. doi: 10.1016/j.neuron.2006.03.014

Galazyuk, A. V., Longenecker, R. J., Voytenko, S. V., Kristaponyte, I., and Nelson, G. L. (2019). Residual inhibition: from the putative mechanisms to potential tinnitus treatment. *Hear. Res.* 375, 1–13. doi: 10.1016/j.heares.2019.01.022

Goupell, M. J., and Stakhovskaya, O. A. (2018). Across-frequency processing of interaural time and level differences in perceived lateralization. *Acta Acust. United Acust.* 104, 758–761. doi: 10.3813/AAA.919217

Grothe, B. (2003). New roles for synaptic inhibition in sound localization. *Nat. Rev. Neurosci.* 4, 540–550. doi: 10.1038/nrn1136

Grothe, B., Pecka, M., and McAlpine, D. (2010). Mechanisms of sound localization in mammals. *Physiol. Rev.* 90, 983–1012. doi: 10.1152/physrev.00026.2009

Hamlet, W. R., and Lu, Y. (2016). Intrinsic plasticity induced by group II metabotropic glutamate receptors *via* enhancement of high-threshold K_V currents in sound localizing neurons. *Neuroscience* 324, 177–190. doi: 10.1016/j.neuroscience.2016.03.010

Houamed, K. M., Kuijper, J. L., Gilbert, T. L., Haldeman, B. A., O'Hara, P. J., Mulvihill, E. R. et al. (1991). Cloning, expression, and gene structure of a G protein-coupled glutamate receptor from rat brain. *Science* 252, 1318–1320. doi: 10.1126/science.1656524

Hyson, R. L., Reyes, A. D., and Rubel, E. W. (1995). A depolarizing inhibitory response to GABA in brainstem auditory neurons of the chick. *Brain Res.* 677, 117–126. doi: 10.1016/0006-8993(95)00130-i

Johnston, J., Forsythe, I. D., and Kopp-Scheinpflug, C. (2010). Going native: voltage-gated potassium channels controlling neuronal excitability. *J. Physiol.* 588, 3187–3200. doi: 10.1113/jphysiol.2010.191973

Kato, B. M., and Rubel, E. W. (1999). Glutamate regulates IP3-type and CICR stores in the avian cochlear nucleus. *J. Neurophysiol.* 81, 1587–1596. doi: 10.1152/jn.1999.81.4.1587

Kato, B. M., Lachica, E. A., and Rubel, E. W. (1996). Glutamate modulates intracellular Ca^{2+} stores in brain stem auditory neurons. *J. Neurophysiol.* 76, 646–650. doi: 10.1152/jn.1996.76.1.646

Kemmer, M., and Vater, M. (2001). Cellular and subcellular distribution of AMPA-type glutamate receptor subunits and metabotropic glutamate receptor 1α in the cochlear nucleus of the horseshoe bat (Rhinolophus rouxi). *Hear. Res.* 156, 128–142. doi: 10.1016/s0378-5955(01)00266-0

Krystal, J. H., Mathew, S. J., D'Souza, D. C., Garakani, A., Gunduz-Bruce, H., and Charney, D. S. (2010). Potential psychiatric applications of metabotropic glutamate receptor agonists and antagonists. *CNS Drugs* 24, 669–693. doi: 10.2165/11533230-000000000-00000

Kulesza, R. J. Jr., and Grothe, B. (2015). Yes, there is a medial nucleus of the trapezoid body in humans. *Front. Neuroanat.* 9:35. doi: 10.3389/fnana.2015.00035

Kuo, S. P., Bradley, L. A., and Trussell, L. O. (2009). Heterogeneous kinetics and pharmacology of synaptic inhibition in the chick auditory brainstem. *J. Neurosci.* 29, 9625–9634. doi: 10.1523/JNEUROSCI.0103-09.2009

Kushmerick, C., Price, G. D., Taschenberger, H., Puente, N., Renden, R., Wadiche, J. I., et al. (2004). Retroinhibition of presynaptic Ca^{2+} currents by endocannabinoids released *via* postsynaptic mGluR activation at a calyx synapse. *J. Neurosci.* 24, 5955–5965. doi: 10.1523/JNEUROSCI.0768-04.2004

Lachica, E. A., Kato, B. M., Lippe, W. R., and Rubel, E. W. (1998). Glutamatergic and GABAergic agonists increase $[Ca^{2+}]_i$ in avian cochlear nucleus neurons. *J. Neurobiol.* 37, 321–337. doi: 10.1002/(sici)1097-4695(19981105)37:2<321::aid-neu10>3.0.co;2-m

Lachica, E. A., Rübsamen, R., Zirpel, L., and Rubel, E. W. (1995). Glutamatergic inhibition of voltage-operated calcium channels in the avian cochlear nucleus. *J. Neurosci.* 15, 1724–1734. doi: 10.1523/JNEUROSCI.15-03-01724.1995

Lodge, D., Tidball, P., Mercier, M. S., Lucas, S. J., Hanna, L., Ceolin, L., et al. (2013). Antagonists reversibly reverse chemical LTD induced by group I, group II and group III metabotropic glutamate receptors. *Neuropharmacology* 74, 135–146. doi: 10.1016/j.neuropharm.2013.03.011

Lu, Y. (2007). Endogenous mGluR activity suppresses GABAergic transmission in avian cochlear nucleus magnocellularis neurons. *J. Neurophysiol.* 97, 1018–1029. doi: 10.1152/jn.00883.2006

Lu, Y. (2014). Metabotropic glutamate receptors in auditory processing. *Neuroscience* 274, 429–445. doi: 10.1016/j.neuroscience.2014.05.057

Lu, Y., Liu, Y., and Curry, R. J. (2018). Activity dependent synaptic integration and modulation of bilateral excitatory inputs in an auditory coincidence detection circuit. *J. Physiol.* 596, 1981–1997. doi: 10.1113/JP275735

Lu, Y., and Rubel, E. W. (2005). Activation of metabotropic glutamate receptors inhibits high-voltage-gated calcium channel currents of chicken nucleus magnocellularis neurons. *J. Neurophysiol.* 93, 1418–1428. doi: 10.1152/jn.00659.2004

Lu, T., and Trussell, L. O. (2001). Mixed excitatory and inhibitory GABA-mediated transmission in chick cochlear nucleus. *J. Physiol.* 535, 125–131. doi: 10.1111/j.1469-7793.2001.t01-1-00125.x

Masu, M., Tanabe, Y., Tsuchida, K., Shigimoto, R., and Nakanishi, S. (1991). Sequence and expression of a metabotropic glutamate receptor. *Nature* 349, 760–765. doi: 10.1038/349760a0

Monsivais, P., and Rubel, E. W. (2001). Accommodation enhances depolarizing inhibition in central neurons. *J. Neurosci.* 21, 7823–7830. doi: 10.1523/JNEUROSCI.21-19-07823.2001

Nicoletti, F., Bockaert, J., Collingridge, G. L., Conn, P. J., Ferraguti, F., Schoepp, D. D., et al. (2011). Metabotropic glutamate receptors: from the workbench to the bedside. *Neuropharmacology* 60, 1017–1041. doi: 10.1016/j.neuropharm.2010.10.022

Nicoletti, F., Iadarola, M. J., Wroblewski, J. T., and Costa, E. (1986a). Excitatory amino acid recognition sites coupled with inositol phospholipid metabolism: developmental changes and interaction with α1-adrenoceptors. *Proc. Natl. Acad. Sci. U S A* 83, 1931–1935. doi: 10.1073/pnas.83.6.1931

Nicoletti, F., Wroblewski, J. T., Novelli, A., Alho, H., Guidotti, A., and Costa, E. (1986b). The activation of inositol phospholipid metabolism as a signal-transducing system for excitatory amino acids in primary cultures of cerebellar granule cells. *J. Neurosci.* 6, 1905–1911. doi: 10.1523/JNEUROSCI.06-07-01905.1986

Nishimaki, T., Jang, I. S., Ishibashi, H., Yamaguchi, J., and Nabekura, J. (2007). Reduction of metabotropic glutamate receptor-mediated heterosynaptic inhibition of developing MTNB-LSO inhibitory synapses. *Eur. J. Neurosci.* 26, 323–330. doi: 10.1111/j.1460-9568.2007.05656.x

Niswender, C. M., and Conn, P. J. (2010). Metabotropic glutamate receptors: physiology, pharmacology, and disease. *Annu. Rev. Pharmacol. Toxicol.* 50, 295–322. doi: 10.1146/annurev.pharmtox.011008.145533

Ohishi, H., Neki, A., and Mizuno, N. (1998). Distribution of a metabotropic glutamate receptor, mGluR2, in the central nervous system of the rat and mouse: an immunohistochemical study with a monoclonal antibody. *Neurosci. Res.* 30, 65–82. doi: 10.1016/s0168-0102(97)00120-x

Okuda, H., Yamada, R., Kuba, H., and Ohmori, H. (2013). Activation of metabotropic glutamate receptors improves the accuracy of coincidence detection by presynaptic mechanisms in the nucleus laminaris of the chick. *J. Physiol.* 591, 365–378. doi: 10.1113/jphysiol.2012.244350

Peng, K., Wang, X., Wang, Y., Li, D., Huang, H., and Lu, Y. (2020). Mechanisms underlying enhancement of spontaneous glutamate release by group I mGluRs at a central auditory synapse. *J. Neurosci.* 40, 7027–7042. doi: 10.1523/JNEUROSCI.2771-19.2020

Petralia, R. S., Wang, Y. X., Singh, S., Wu, C., Shi, L., Wei, J., et al. (1997). A monoclonal antibody shows discrete cellular and subcellular localizations of mGluR1α metabotropic glutamate receptors. *J. Chem. Neuroanat.* 13, 77–93. doi: 10.1016/s0891-0618(97)00023-9

Rubel, E. W., Hyson, R. L., and Durham, D. (1990). Afferent regulation of neurons in the brain stem auditory system. *J. Neurobiol.* 21, 169–196. doi: 10.1002/neu.480210112

Sanchez, J. T., Wang, Y., Rubel, E. W., and Barria, A. (2010). Development of glutamatergic synaptic transmission in binaural auditory neurons. *J. Neurophysiol.* 104, 1774–1789. doi: 10.1152/jn.00468.2010

Shigemoto, R., Nakanishi, S., and Mizuno, N. (1992). Distribution of the mRNA for a metabotropic glutamate receptor (mGluR1) in the central nervous system: an *in situ* hybridization study in adult and developing rat. *J. Comp. Neurol.* 322, 121–135. doi: 10.1002/cne.903220110

Sladeczek, F., Pin, J. P., Récasens, M., Bockaert, J., and Weiss, S. (1985). Glutamate stimulates inositol phosphate formation in striatal neurones. *Nature* 317, 717–719. doi: 10.1038/317717a0

Slee, S. J., Higgs, M. H., Fairhall, A. L., and Spain, W. J. (2010). Tonotopic tuning in a sound localization circuit. *J. Neurophysiol.* 103, 2857–2875. doi: 10.1152/jn.00678.2009

Song, P., and Kaczmarek, L. (2006). Modulation of Kv3.1b potassium channel phosphorylation in auditory neurons by conventional and novel protein kinase C isozymes. *J. Biol. Chem.* 281, 15582–15591. doi: 10.1074/jbc.M512866200

Sugiyama, H., Ito, I., and Hirono, C. (1987). A new type of glutamate receptor linked to inositol phospholipid metabolism. *Nature* 325, 531–533. doi: 10.1038/325531a0

Swanson, C. J., Bures, M., Johnson, M. P., Linden, A. M., Monn, J. A., and Schoepp, D. D. (2005). Metabotropic glutamate receptors as novel targets for anxiety and stress disorders. *Nat. Rev. Drug Discov.* 4, 131–144. doi: 10.1038/nrd1630

Tang, Z.-Q., Dinh, E. H., Shi, W., and Lu, Y. (2011). Ambient GABA-activated tonic inhibition sharpens auditory coincidence detection *via* a depolarizing shunting mechanism. *J. Neurosci.* 31, 6121–6131. doi: 10.1523/JNEUROSCI.4733-10.2011

Tang, Z.-Q., Gao, H., and Lu, Y. (2009). Control of a depolarizing GABAergic input in an auditory coincidence detection circuit. *J. Neurophysiol.* 102, 1672–1683. doi: 10.1152/jn.00419.2009

Tang, Z.-Q., Liu, Y. W., Shi, W., Dinh, E. H., Hamlet, W. R., Curry, R. J., et al. (2013). Activation of synaptic group II metabotropic glutamate receptors induces long-term depression at GABAergic synapses in CNS neurons. *J. Neurosci.* 33, 15964–15977. doi: 10.1523/JNEUROSCI.0202-13.2013

Tang, Z.-Q., and Lu, Y. (2012a). Two $GABA_A$ responses with distinct kinetics in a sound localization circuit. *J. Physiol.* 590, 3787–3805. doi: 10.1113/jphysiol.2012.230136

Tang, Z.-Q., and Lu, Y. (2012b). Development of GPCR modulation of GABAergic transmission in chicken nucleus laminaris neurons. *PLoS One* 7:e35831. doi: 10.1371/journal.pone.0035831

Tang, Z.-Q., and Lu, Y. (2018). Anatomy and physiology of metabotropic glutamate receptors in mammalian and avian auditory system. *HSOA Trends Anat. Physiol.* 1:001. doi: 10.24966/TAP-7752/100001

Tharmalingam, S., Burns, A. R., Roy, P. J., and Hampson, D. R. (2012). Orthosteric and allosteric drug binding sites in the caenorhabditis elegans mgl-2 metabotropic glutamate receptor. *Neuropharmacology* 63, 667–674. doi: 10.1016/j.neuropharm.2012.05.029

Tollin, D. J. (2003). The lateral superior olive: a functional role in sound source localization. *Neuroscientist* 9, 127–143. doi: 10.1177/1073858403252228

von Gersdorff, H., Schneggenburger, R., Weis, S., and Neher, E. (1997). Presynaptic depression at a calyx synapse: the small contribution of metabotropic glutamate receptors. *J. Neurosci.* 17, 8137–8146. doi: 10.1523/JNEUROSCI.17-21-08137.1997

Wu, S. H., and Fu, X. W. (1998). Glutamate receptors underlying excitatory synaptic transmission in the rat's lateral superior olive studied *in vitro*. *Hear. Res.* 122, 47–59. doi: 10.1016/s0378-5955(98)00085-9

Yamada, R., Okuda, H., Kuba, H., Nishino, E., Ishii, T. M., and Ohmori, H. (2013). The cooperation of sustained and phasic inhibitions increases the contrast of ITD-tuning in low-frequency neurons of the chick nucleus laminaris. *J. Neurosci.* 33, 3927–3938. doi: 10.1523/JNEUROSCI.2377-12.2013

Zirpel, L., Lachica, E. A., and Rubel, E. W. (1995). Activation of a metabotropic glutamate receptor increases intracellular calcium concentrations in neurons of the avian cochlear nucleus. *J. Neurosci.* 15, 214–222. doi: 10.1523/JNEUROSCI.15-01-00214.1995

Zirpel, L., Lippe, W. R., and Rubel, E. W. (1998). Activity-dependent regulation of $[Ca^{2+}]_i$ in avian cochlear nucleus neurons: roles of protein kinases A and C and relation to cell death. *J. Neurophysiol.* 79, 2288–2302. doi: 10.1152/jn.1998.79.5.2288

Zirpel, L., Nathanson, N. M., Rubel, E. W., and Hyson, R. L. (1994). Glutamate-stimulated phosphatidylinositol metabolism in the avian cochlear nucleus. *Neurosci. Lett.* 168, 163–166. doi: 10.1016/0304-3940(94)90441-3

Zirpel, L., and Parks, T. N. (2001). Zinc inhibition of group I mGluR-mediated calcium homeostasis in auditory neurons. *J. Assoc. Res. Otolaryngol.* 2, 180–187. doi: 10.1007/s101620010082

Zirpel, L., and Rubel, E. W. (1996). Eighth nerve activity regulates intracellular calcium concentration of avian cochlear nucleus neurons *via* a metabotropic glutamate receptor. *J. Neurophysiol.* 76, 4127–4139. doi: 10.1152/jn.1996.76.6.4127

Conflict of Interest: The authors declare that the research was conducted in the absence of any commercial or financial relationships that could be construed as a potential conflict of interest.

frontiers in Neural Circuits

ORIGINAL RESEARCH
published: 18 February 2021
doi: 10.3389/fncir.2021.597401

Nicotine Enhances Amplitude and Consistency of Timing of Responses to Acoustic Trains in A1

*Irakli Intskirveli and Raju Metherate**

Department of Neurobiology and Behavior, Center for Hearing Research, University of California, Irvine, Irvine, CA, United States

Systemic nicotine enhances neural processing in primary auditory cortex (A1) as determined using tone-evoked, current-source density (CSD) measurements. For example, nicotine enhances the characteristic frequency (CF)-evoked current sink in layer 4 of A1, increasing amplitude and decreasing latency. However, since presenting auditory stimuli within a stream of stimuli increases the complexity of response dynamics, we sought to determine the effects of nicotine on CSD responses to trains of CF stimuli (one-second trains at 2–40 Hz; each train repeated 25 times). CSD recordings were obtained using a 16-channel multiprobe inserted in A1 of urethane/xylazine-anesthetized mice, and analysis focused on two current sinks in the middle (layer 4) and deep (layers 5/6) layers. CF trains produced adaptation of the layer 4 response that was weak at 2 Hz, stronger at 5–10 Hz and complete at 20–40 Hz. In contrast, the layer 5/6 current sink exhibited less adaptation at 2–10 Hz, and simultaneously recorded auditory brainstem responses (ABRs) showed no adaptation even at 40 Hz. Systemic nicotine (2.1 mg/kg) enhanced layer 4 responses throughout the one-second stimulus train at rates $\leq$10 Hz. Nicotine enhanced both response amplitude within each train and the consistency of response timing across 25 trials. Nicotine did not alter the degree of adaptation over one-second trials, but its effect to increase amplitudes revealed a novel, slower form of adaptation that developed over multiple trials. Nicotine did not affect responses that were fully adapted (20–40 Hz trains), nor did nicotine affect any aspect of the layer 5/6 current sink or ABRs. The overall effect of nicotine in layer 4 was to enhance all responses within each train, to emphasize earlier trials across multiple trials, and to improve the consistency of timing across all trials. These effects may improve processing of complex acoustic streams, including speech, that contain information in the 2–10 Hz range.

Keywords: nicotine, auditory cortex, hearing, mouse, frequency following, current source density

OPEN ACCESS

Edited by:
Conny Kopp-Scheinpflug, Ludwig Maximilian University of Munich, Germany

Reviewed by:
Michael Wehr, University of Oregon, United States
Feng Luo, National Institute of Neurological Disorders and Stroke (NINDS), United States

***Correspondence:**
Raju Metherate
raju.metherate@uci.edu

Received: *21 August 2020*
Accepted: *25 January 2021*
Published: *18 February 2021*

Citation:
Intskirveli I and Metherate R (2021) Nicotine Enhances Amplitude and Consistency of Timing of Responses to Acoustic Trains in A1. Front. Neural Circuits 15:597401. doi: 10.3389/fncir.2021.597401

INTRODUCTION

Activation of nicotinic acetylcholine receptors (nAChRs) increases neural excitability due to the influx of cations through the receptor ion channel (Dani and Bertrand, 2007; Albuquerque et al., 2009). However, the effect of nicotine on neural processing cannot be inferred from this cellular action alone since nAChRs are found on both excitatory and inhibitory neurons and in different neural compartments, regulating, for example, presynaptic release of neurotransmitter, postsynaptic depolarization, and action potential propagation along axons (Dani and Bertrand, 2007; Albuquerque et al., 2009; Poorthuis et al., 2013). Since sensory-evoked current-source density (CSD) profiles reflect integrated synaptic activity within neural circuits, they provide a circuit-level measure that can be used to evaluate nicotinic regulation of neural processing (Muller-Preuss and Mitzdorf, 1984; Metherate et al., 2012). In primary auditory cortex (A1) of rodents, for example, nicotine enhances the characteristic frequency (CF)-evoked thalamocortical response (layer 4 current sink), increasing peak amplitude and decreasing both onset and peak latencies (Intskirveli and Metherate, 2012; Askew et al., 2017). This effect is likely due to multiple nAChR-mediated cellular actions in A1, including increased excitability of thalamocortical axons, excitation of a subset of inhibitory interneurons, and depolarization of pyramidal neurons due to disinhibition (i.e., excitation of interneurons that innervate other interneurons) (Kawai et al., 2007; Intskirveli and Metherate, 2012; Askew et al., 2019).

However, acoustic stimuli rarely occur in isolation and can trigger complex response dynamics when presented within a stream of auditory stimuli (Todorovic et al., 2011; Phillips et al., 2017). A simple example is the response adaptation that occurs when a stimulus is presented repetitively; i.e., evoked responses become progressively weaker during a train of CF stimuli, with the degree of adaptation increasing with repetition rate. Response adaptation is weak in the lower auditory pathway and increasingly prominent in the auditory forebrain, especially cortex. In A1, CF-evoked responses begin to adapt at very low repetition rates, e.g., 1–2 Hz, and adapt fully at rates of 15–20 Hz (Creutzfeldt et al., 1980; Wang et al., 2008; Yao et al., 2015).

Since repetitive stimulation produces strong adaptation in A1 and systemic nicotine enhances cortical responses, here we examined the effects of nicotine on response adaptation during CF stimulus trains (one-second trials of 2–40 Hz stimuli; trials repeated 25 times). For the CF-evoked current sink in layer 4, nicotine enhanced responses throughout the stimulus train at rates $\leq$10 Hz. Nicotine increased response amplitude, and notably, also enhanced the consistency of response timing. While nicotine did not affect the *degree* of adaptation over one-second trials, the drug revealed a novel, slower adaptation that emerged over multiple trials after initial response enhancement. The overall effect of nicotine was to enhance all responses within each train, to emphasize earlier trials across multiple trials, and to improve the consistency of timing across trials.

MATERIALS AND METHODS

Animal Preparation

Adult (60–80 days old) male FVB mice were used for all procedures in accordance with the National Institutes of Health Guide for the Care and Use of Laboratory Animals and as approved by the University of California, Irvine Institutional Animal Care and Use Committee (IACUC). Mice were anesthetized with urethane (Sigma; 0.7 g/kg i.p.) and xylazine (Phoenix Pharmaceutics; 13 mg/kg i.p.) in saline, placed in a sound-attenuating chamber (model AC-3, IAC, Bronx, NY, United States) and maintained at 36–37°C. Anesthesia was supplemented as necessary (0.13 g/kg urethane, 1.3 mg/kg xylazine i.p.) via a catheter to avoid movement of the mice. The head was secured in a stereotaxic frame (model 923, Kopf Instruments, Tujunga, CA, United States). After a midline incision, the skull was cleared and secured to a custom-made head holder. A craniotomy was performed over the right auditory cortex and the exposed brain was kept moist with warm saline. A burr hole was made over vertex and a dental screw with connector inserted for recording the auditory brainstem response (ABR).

Electrophysiology

For mapping A1, stimulus-evoked local field potentials (LFPs) were recorded with a glass micropipette filled with 1 M NaCl ($\sim$1 MΩ at 1 kHz). ABR and LFP recordings were filtered and amplified (1–1000 Hz, AI-401, CyberAmp 380; Axon Instruments), digitized, and stored on a computer (AxoGraph software). LFPs for CSD profiles were recorded using a 16-channel silicon multiprobe ($\sim$2–3 MΩ at 1 kHz for each 177-μm^2 recording site, 100-μm separation between recording sites; NeuroNexus Technologies), filtered and amplified (1 Hz to 10 kHz, AI-405, CyberAmp 380), digitized and stored on a computer.

Acoustic Stimulation

Acoustic stimuli were digitally synthesized and controlled with custom software and delivered through an open-field speaker (FF-1 with SA1 amplifier and RP2.1 Real Time-Processor; Tucker-Davis Technologies) positioned $\sim$3 cm in front of the left ear. For calibration [sound pressure level (SPL), in dB re: 20 μPa] a microphone (model 4939 and Nexus amplifier; Bruel and Kjaer) was positioned in place of the animal at the tip of the left earbar. For mapping A1, tones were 100 ms in duration with 5-ms linear rise and fall ramps (range 5–40 kHz and 0–70 dB SPL). For determining ABR threshold, white-noise stimuli (10 ms duration, 3 ms rise/fall ramps) were delivered at 2/s for 100 repetitions and repeated at 0–70 dB SPL. For multiprobe recordings, 10 ms tones (3 ms rise/fall ramps) were delivered at 2, 5, 10, 20, and 40 Hz for 1 s trials in sets of 25 trials at 30 dB above threshold.

Determining the A1 Recording Site

To find a recording site in A1 we used our method previously described (Intskirveli and Metherate, 2012). Briefly, we recorded tone-evoked responses from multiple sites $\sim$250 μm apart along

the anterior-posterior axis in auditory cortex at a depth of ∼400 μm (approximately layer 4). Based on responses to a standard set of tones (5–40 kHz in 2.5-kHz steps, 0–70 dB SPL in 5-dB steps), we determined CF (frequency with the lowest threshold) for each recording site. After constructing a CF map and confirming the tonotopy expected for A1, including a reversal of tonotopy at the border with the anterior auditory field (Stiebler et al., 1997), we chose a region within A1 and mapped along the dorsoventral axis to identify a recording site (CF 10–20 kHz) with a short-latency, large-amplitude response in layer 4 for all subsequent procedures. At this site we inserted a 16-channel multiprobe perpendicular to the pia surface to record LFPs throughout the cortical depth and re-determined CF (1-kHz steps) and threshold (5-dB steps) based on LFPs at a depth of 300–400 μm. Threshold responses exceeded three standard deviations of the mean baseline determined over 100 ms preceding the tone.

Drug Application

(−)-Nicotine hydrogen tartrate (Sigma) was dissolved in saline, adjusted to pH 7.0 and delivered subcutaneously (2.1 mg/kg, free base). This dose is reliably suprathreshold for nicotine effects in mouse A1 (Intskirveli and Metherate, 2012).

Data Analysis

For each one-second trial, tone-evoked LFP responses were baselined using the 10 ms period before the first stimulus, and one-dimensional CSD profiles constructed off-line using custom Matlab script. CSD profiles are the second spatial derivative of the LFP laminar profile (Muller-Preuss and Mitzdorf, 1984); conventionally, a current sink implies the location, timing, and magnitude of underlying synaptic excitation. In each CSD profile we identified two prominent current sinks based on onset latency and depth. First, the current sink in the middle layers (typically 200–400 μm depth) with shortest onset latency was designated the "layer 4" current sink. A second, deeper current sink, typically 300 μm below the layer 4 sink, was designated the "layer 5/6" current sink. Current-sink peak amplitudes and latencies (for the max peak within 100 ms from stimulus onset) were measured in each condition. Coefficient of variance was calculated to show changes in latency variability after nicotine injection. Adaptation ratio during a train stimulus was calculated as the peak amplitude of the mean adapted response divided by the first response ("mean adapted response" is 2nd response for 2 Hz, mean 3rd–5th response for 5 Hz and mean 3rd–10th response for 10 Hz). Statistical comparisons were performed with GraphPad Prism. Related means (for pre-drug, saline, and nicotine responses) were compared using repeated measures (RM-) ANOVA and Tukey's *post hoc* test for multiple comparisons. Since for each mouse all data were obtained at a single recording site, for group statistics "n" refers to the number of animals.

RESULTS

After mapping with a microelectrode to determine the location of A1 in each animal, we selected a single recording site from among those exhibiting robust CF-evoked LFPs in the middle layers. The selected recording sites exhibited CFs of 10–20 kHz. At the selected site we inserted a 16-channel linear multiprobe to record LFPs and derive CSD profiles. We analyzed two prominent CF-evoked current sinks: the shortest-latency middle-layer current sink ("layer 4") and the infragranular sink in layer 5/6. For stimulus trains, CF tones (10 ms duration, 30 dB above threshold) were presented at each rate (2, 5, 10, 20, and 40 Hz) for one second, repeated 25 times (2.5 s between trial onsets, total duration of each set ∼1 min). Stimulus sets for each rate (2–40 Hz) were presented in random order and the entire series (five rates) repeated so that results for each rate were averaged from two stimulus sets per condition. Stimulus sets were presented under three conditions: before any manipulation (Pre), after systemic saline (Saline) and after systemic nicotine (Nicotine; 2.1 mg/kg, s.c.). The total duration of acoustic stimulation in each condition was ∼12–15 min, which is less than the typical duration (∼30 min) of nicotine effects from a single injection (Intskirveli and Metherate, 2012).

Figure 1A depicts one stimulus set for a 5-Hz CF train (left) alongside a representative set of responses (right) showing the layer 4 current sink evoked in the Pre (black traces) and Nicotine (red traces) conditions. Averaged responses for this animal are in **Figure 1B** and exhibit typical response adaptation in the pre-drug condition (each trace is average of two sets of 25 trials): adaptation was minimal at 2 Hz but increased with stimulus rate until complete adaptation occurred at 20 and 40 Hz. Inset traces above 5 and 40-Hz responses show ABR recordings that exhibited no adaptation even at 40 Hz. Since, in most animals, stimulus rates of 20–40 Hz produced complete adaptation of cortical responses, only data for rates up to and including 10 Hz were analyzed for effects of nicotine. Data were obtained from 10 mice, but three early experiments did not include 2 Hz stimulation. In four animals, 10 Hz produced complete adaptation and the results were not analyzed further. One experiment had a faulty ABR electrode and was excluded from ABR analysis.

Systemic Nicotine Enhances Layer 4 Response to CF Stimulus Trains

Consistent with previous studies (see section "Introduction"), systemic nicotine enhanced the layer 4 response to the first stimulus in each train. The example in **Figure 1B** and group data in **Figure 2** show that nicotine increased the peak amplitude of each first response compared to pre-drug and saline responses and reduced its peak latency. For subsequent responses within each train, nicotine similarly enhanced response amplitude despite adaptation that increased with stimulus rate (**Figures 2A,B**; inset traces are examples of adapted responses at 5 and 10 Hz). When normalized to pre-drug amplitude, nicotine's enhancement of adapted responses was similar to its effect on the first response (**Figure 2**; first response to 2–10 Hz trains enhanced 32–44%, adapted responses enhanced 33–60%). Fully adapted responses at the highest rates (20–40 Hz) were not enhanced by nicotine (**Figure 1B**). Systemic saline had no effect on any measure (**Figures 1**, **2**, blue traces, graphs, and histograms).

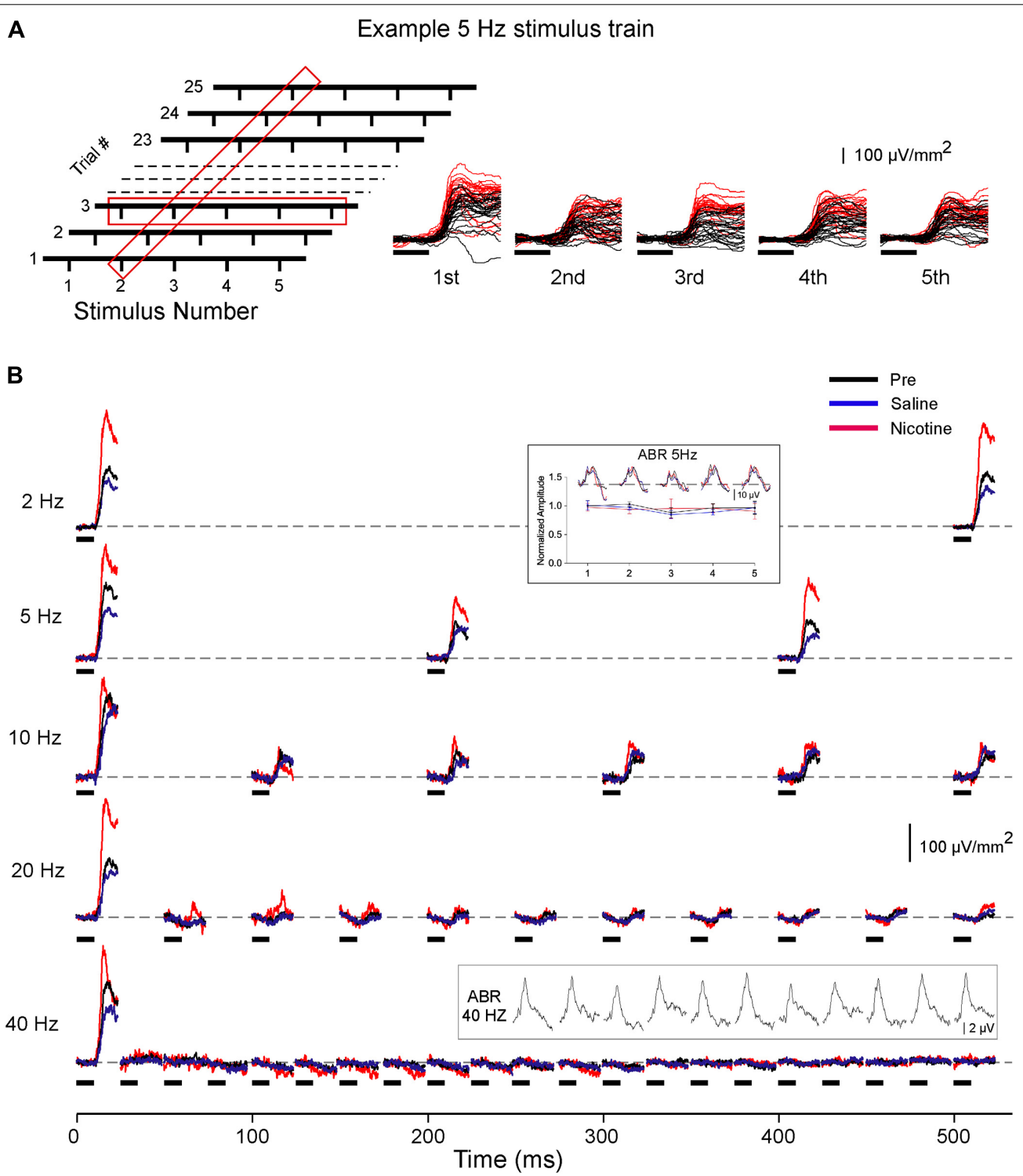

FIGURE 1 | Effects of systemic nicotine on layer 4 current sink evoked by CF stimulus trains. **(A)** Schematic of 5 Hz stimulus set (left): 25 trials, each with five CF stimuli presented over one second; 1.5 s inter-trial interval. Red boxes represent data averaged across 25 trials, as in panel B and **Figures 2**, **4**, or averaged within each trial, as in **Figure 3**. Traces (right) show example 5 Hz responses in pre-drug condition (black traces) and after systemic nicotine (2.1 mg/kg; red traces). In this and the following figures, horizontal marks indicate 10 ms tone presentation. **(B)** Representative layer 4 current sinks evoked by CF stimuli presented at different rates (2–40 Hz); responses shown are for the first half of each 1-s trial and traces are average from two sets of 25 trials. Inset above 5 Hz response shows simultaneously recorded ABR (example traces) and group data for ABR peak amplitude in each condition. Inset above 40 Hz response shows separately recorded ABR (10 ms white noise stimulus).

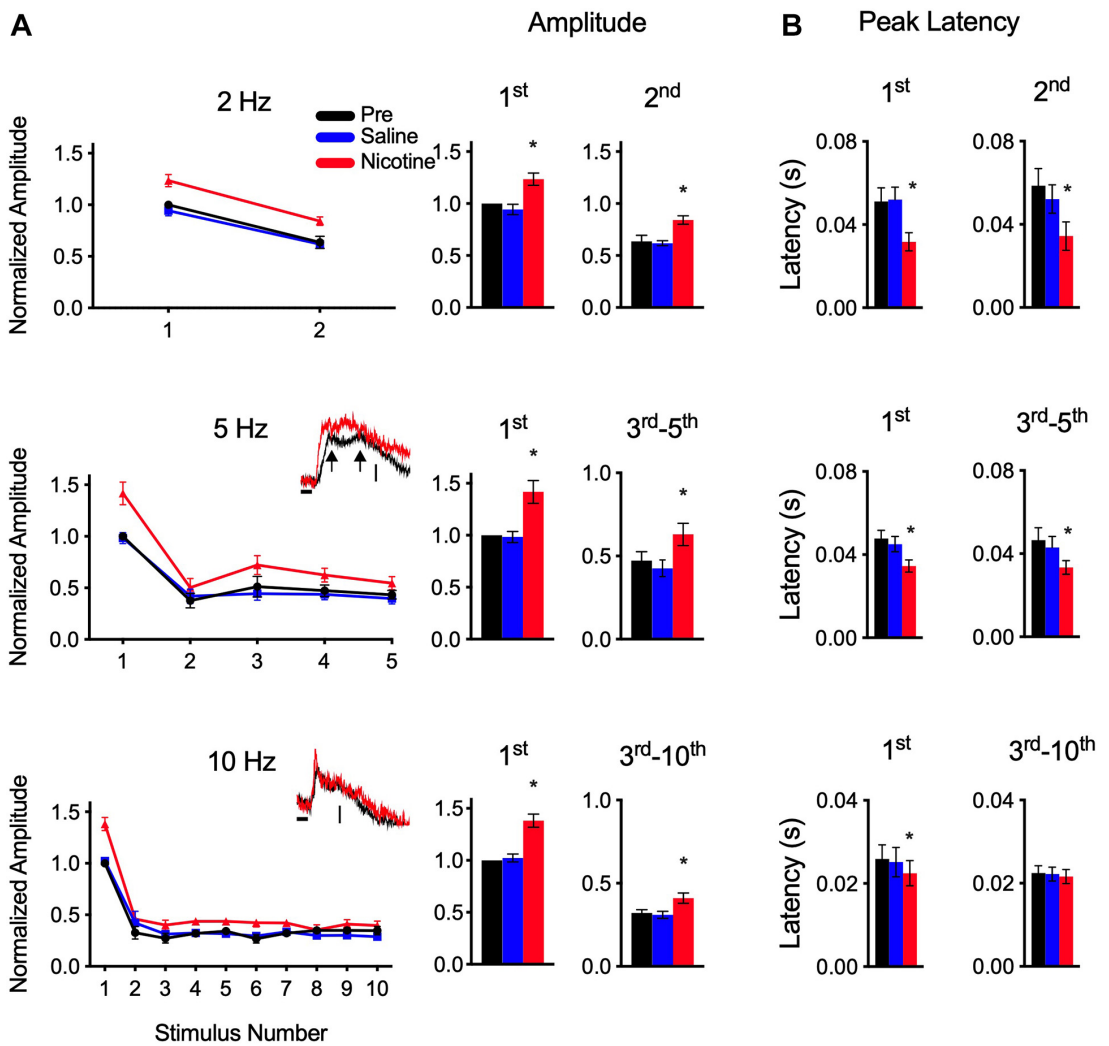

FIGURE 2 | Nicotine increased peak amplitude and decreased peak latency for responses to CF stimulus trains. **(A)** Group data show peak amplitude (normalized to value of first pre-drug response) for trains at 2, 5, and 10 Hz. Insets for 5 and 10 Hz show example traces for adapted responses, vertical scales represent 25 mV/mm^2. Histograms show amplitudes separately for first response and adapted responses combined. In this and following figures, *indicates $p < 0.05$. **(B)** Group data show peak latency separately for first response and adapted responses.

Graphs in **Figure 2A** (left), suggest enhancement of peak amplitude for nicotine compared to pre-drug and saline responses. For statistical analysis (**Figure 2A**, right), data are grouped separately for the first response at each rate and for subsequent adapted responses (for this and the following analyses, data for 5 and 10 Hz exclude 2nd response due to variable reduction before a plateau level of adaptation); asterisks indicate significant enhancement compared to pre-drug and saline values (RM-ANOVA with Tukey *post hoc* tests; 2 Hz: 1st response $p = 0.0004$, 2nd response $p = 0.0020$, $n = 7$; 5 Hz: 1st response $p = 0.0009$, 3rd–5th response $p = 0.0035$, $n = 10$; 10 Hz: 1st response $p = 0.0005$, 3rd–10th response $p = 0.0023$, $n = 6$). *Post hoc* tests confirmed no effect of saline on any measure of amplitude or latency (p's $\gg$ 0.05).

Despite enhanced amplitudes, nicotine did not alter the *degree* of adaptation as estimated by the ratio of adapted responses to the first response. This adaptation ratio for pre-drug responses averaged 0.67 $\pm$ 0.04 for 2 Hz, 0.43 $\pm$ 0.04 for 5 Hz and 0.3 $\pm$ 0.02 for 10 Hz and did not change with saline or nicotine (RM-ANOVA, p's $\gg$ 0.05). Thus, nicotine enhanced response amplitudes, but did not affect adaptation, within each stimulus train.

Simultaneous ABR recordings showed no effect of nicotine or saline on brainstem responses (**Figure 1B**, inset data at 5 Hz; peak amplitude averaged for 1st–5th response; RM-ANOVA, $p = 0.331$, $n = 9$), indicating that the locus of nicotine's effect is more central.

As in prior studies, nicotine reduced the peak latency of the first response at all rates (**Figure 2B**; RM-ANOVA, 2 Hz: $p = 0.0065$, $n = 7$; 5 Hz: $p = 0.0051$, $n = 10$; 10 Hz: $p = 0.0020$, $n = 6$). Note, as shown in **Figure 2A**, inset traces, that adapted responses to 5 Hz trains (and 2 Hz, not shown) had longer-latency peaks than did 10 Hz responses, and at times exhibited

two peaks, at short and long latencies (arrows in inset traces, **Figure 2A**). In contrast, 10 Hz responses exhibited only short-latency peaks (inset traces, **Figure 2A**). Since short and long latency peaks were not always evident, only a single value (max peak) was used for analysis. For 2 Hz and 5 Hz adapted responses, max peaks were altered by nicotine, exhibiting larger amplitudes (above, **Figure 2A**) and shorter latencies (**Figure 2B**; RM-ANOVA; 2 Hz: 2nd response $p = 0.0120$, $n = 7$; 5 Hz: 3rd–5th response $p = 0.0065$, $n = 10$). However, for the 10 Hz responses, nicotine had no effect on peak latencies of adapted responses (3rd–10th response $p = 0.447$, $n = 6$). The 10 Hz data likely reflect adaptation of longer-latency response components that did not recover between stimulus trials, leaving only a shorter-latency peak (latency ∼20 ms) that was not affected by nicotine.

Thus, nicotine enhanced partially adapted responses throughout one-second stimulus trains at 2–10 Hz by increasing peak amplitude, and for 2–5 Hz trains also reduced peak latency. However, nicotine did not change the *degree* of adaptation and did not affect fully adapted responses at 20–40 Hz.

Nicotine Improves Timing Consistency of Layer 4 Response to Repeated Trials

We next examined the degree to which nicotine altered response consistency from trial to trial (over 25 trials). As illustrated schematically in **Figure 1A**, this analysis involved averaging all responses *within* each trial (i.e., averaging 2, 5, or 10 responses per trial) and plotting the result for the 25 trials in each stimulus set. An example for a 5 Hz stimulus set is in **Figure 3A** and group data are in **Figures 3B,C**. For peak amplitude (**Figure 3B**), control responses (pre-drug and saline) exhibited little change over 25 trials, suggesting weak or no effects of stimulation that outlasted the 1.5 s interval between the end of one trial and the beginning of the next (pre-drug adaptation ratio for trials 20–25: 2 Hz: 0.95 ± 0.07; 5 Hz: 0.92 ± 0.07; 10 Hz: 1.13 ± 0.16). Nicotine, however, revealed an additional effect: while the drug increased response amplitude across all 25 trials, its effect was more prominent in early trials (**Figure 3B**). At each rate, nicotine enhanced response amplitudes for both the first six and last six trials in the stimulus set (RM-ANOVA; 2 Hz: first six trials $p = 0.0005$, last six trials $p = 0.0203$, $n = 7$; 5 Hz: first six trials $p = 0.0048$, last six trials $p = 0.0028$, $n = 10$; 10 Hz: first six trials $p = 0.0119$, last six trials $p = 0.0154$, $n = 6$). And, for 2 and 5 Hz stimuli, the increase in amplitude for the first six responses was greater than that for the last six responses (t-tests, 2 Hz: $p = 0.0066$; 5 Hz: $p = 0.0062$; 10 Hz: $p = 0.983$), indicating a more prominent effect of nicotine early in the stimulus set. Similarly, for 2 and 5 Hz stimuli the initial response in nicotine showed greater adaptation than in controls (RM-ANOVA, 2 Hz, $p = 0.009$; 5 Hz, $p = 0.0139$; 10 Hz, $p = 0.925$). Overall, nicotine enhanced response amplitude across 25 trials in the stimulus set and its effects were more prominent for early trials.

Note that data for all stimulus rates (2–40 Hz) were collected after a single nicotine injection and that stimulus sets at different rates were presented in random order. Moreover, group data (**Figure 3B**) are based on two stimulus sets for each rate, delivered at different times after the nicotine injection. Thus, the greater effect of nicotine on early trials is not due to stronger effects immediately after the nicotine injection that dissipate over time. Rather, the results suggest a nicotinic effect on auditory processing that strongly enhances initial responses then adapts slowly to a lower level where it remains for the entire stimulus set. The degree of adaptation is estimated by the adaptation ratio (above), whereas the *rate* of adaptation can be estimated by fitting the nicotine data with an exponential decay function (smooth red line in **Figure 3B**); the decay rates (tau, 2 Hz: 1.6 trials; 5 Hz: 2.5 trials; 10 Hz: 1.0 trials) are similar over a five-fold range of stimulus frequency, suggesting a mechanism independent of frequency.

The effect of nicotine on peak latency across 25 trials is shown in **Figure 3C**. Control latencies (pre-drug and saline) exhibited trial-to-trial variability that changed little over 25 trials (**Figure 3C**, left). For 2 and 5 Hz trains, nicotine reduced peak latencies, as expected (cf. **Figure 2B**), but also reduced trial-to-trial variability so that latencies were more consistent across the stimulus set. We compared variability among conditions by determining the coefficient of variation (CV; **Figure 3C**, right) and found that nicotine reduced CV (RM-ANOVA; 2 Hz: $p = 0.0087$, $n = 7$; 5 Hz: $p = 0.0100$, $n = 10$). For 10 Hz, peak latencies in control conditions were already short (as described above), exhibited little variability, and were not affected by nicotine ($p = 0.4443$). Note that while slower stimulus rates (2–5 Hz) could generate current sinks with one or two peaks (arrows in **Figure 2A**, inset trace for 5 Hz), 10 Hz stimuli generated only single, short-latency peaks (**Figure 2A**, inset trace for 10 Hz stimulus). It appears, therefore, that longer-latency peaks adapt with 10 Hz stimulation and that nicotine does not regulate the latency of the remaining peak (but does regulate its amplitude; **Figure 3B**).

Overall, this analysis of nicotine's effects across 25 trials shows that the drug enhances response amplitude for 2–10 Hz trains, as expected (**Figure 2A**), but responses early in the stimulus set are affected more strongly. Nicotine also reduced response latency, and latency variability, for 2–5 Hz trains so that trial-to-trial consistency was enhanced. Thus, over a stimulus set, nicotine served to enhance response amplitude and consistency, emphasizing response amplitude to initial stimuli in particular. A comparison of within-trial (**Figure 2**) and across-trial (**Figure 3**) responses reveals two mechanisms of adaptation: the well-documented, within-trial adaptation is unaffected by nicotine (even as response amplitudes are enhanced), whereas a novel, comparatively slow, across-trial adaptation is prominent only when responses are initially enhanced by the presence of nicotine.

Nicotine Does Not Affect Train-Evoked Responses in Layer 5/6

Finally, we examined the infragranular CSD profile to determine the effects of systemic nicotine (**Figure 4**). The CF-evoked layer 5/6 current sink reflects synaptic activity in infragranular neurons (Cruikshank et al., 2002; Zhou et al., 2010), though compared to the layer 4 current sink it is smaller (inset in **Figure 4A**) and exhibits a shorter-latency peak (**Figure 4B**). Results for

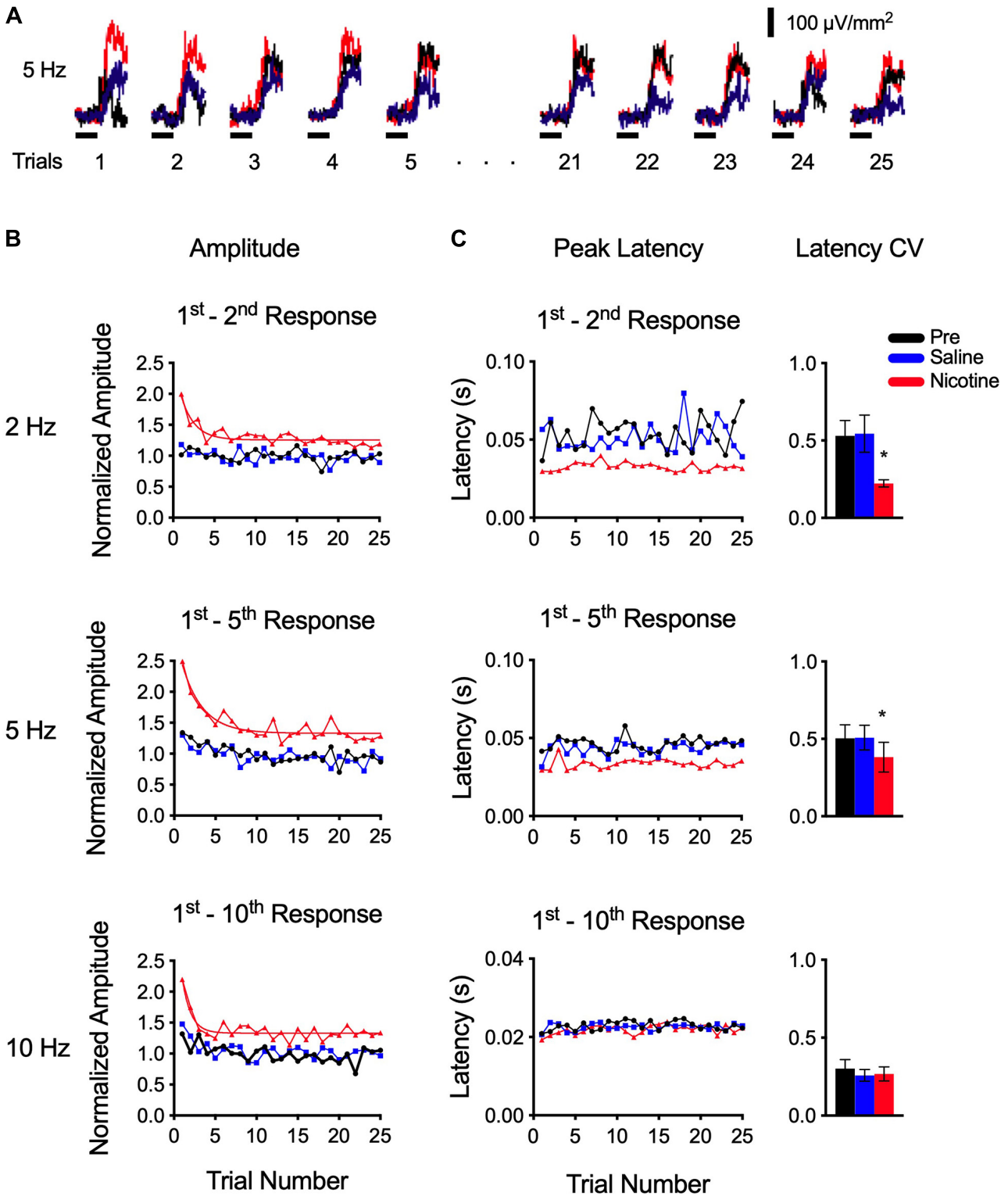

FIGURE 3 | Nicotine enhanced responses across 25 trials—preferentially for initial trials—and improved timing consistency. **(A)** Example response to 5 Hz stimulus set. Each trace is average of all five responses within a trial (see horizontal red box in **Figure 1A**); figure depicts responses across 25 trials. **(B)** Group data show that nicotine enhanced response amplitudes for 2–10 Hz trains (as expected, cf. **Figure 2A**), but enhancement was greater early in the stimulus set, whereas pre-drug and saline controls show little change over 25 trials (group data are average of two stimulus sets in each of 6–10 animals; for clarity, error bars are not shown). **(C)** Nicotine reduced peak latency (as expected, cf. **Figure 2B**) and reduced latency variability across 25 trials (left), as reflected in coefficient of variation (right), for 2 and 5 Hz trains.

the layer 5/6 current sink were obtained simultaneously with data in layer 4. In response to CF stimulus trains of 2–10 Hz, the layer 5/6 current sink exhibited weaker adaptation (**Figure 4A**) than observed in layer 4 (**Figure 2A**). However, unlike in layer 4, systemic nicotine had no effect on either the peak amplitude (**Figure 4A**) or peak latency (**Figure 4B**) of the CF-evoked layer 5/6 current sink (RM-ANOVA; $p \gg 0.05$, n = 6–10). It may be worth noting that the peak latency of the layer 5/6 current sink is short (∼20 ms) and similar to that of adapted 10-Hz responses in layer 4 whose latencies also are not affected by nicotine (**Figures 2B**, **3C**). These short-latency responses may reflect a greater contribution of afferent thalamocortical, rather than intracortical, processes.

DISCUSSION

We examined the effects of systemic nicotine on CSD responses to CF stimulus trains of 2–40 Hz in urethane/xylazine-anesthetized mice. Nicotine generally enhanced the tone-evoked current sink in layer 4 resulting in three novel findings: (i) *within* each one-second trial of CF trains at rates of 2–10 Hz, nicotine enhanced the first response and subsequent, partially adapted responses without affecting the degree of adaptation (adaptation ratio); (ii) *across* 25 trials in each stimulus set, nicotine preferentially enhanced early-trial responses revealing a novel, slower form of adaptation with a time-course of seconds; (iii) across trials, nicotine also enhanced the consistency of response timing for 2–5 Hz trains. Nicotine had no effect on the layer 5/6 current sink in A1, nor on brainstem ABRs. The overall effect of nicotine in layer 4 was to enhance all responses within each trial, to emphasize earlier trials across multiple trials, and to improve the consistency of timing across trials. These effects may improve cortical processing of acoustic streams, such as speech envelopes, that encode information in the 2–10 Hz range.

Adaptation of CSD Responses Evoked by Acoustic Trains

An advantage of using CSD recordings for this study is that current sinks reflect summed synaptic integration within local circuits rather than simply their output (action potentials) (Muller-Preuss and Mitzdorf, 1984; Metherate et al., 2012). The middle-layer current sink with the earliest onset is considered to be the site of thalamocortical input (designated "layer 4"). However, although the layer 4 current sink is triggered by thalamocortical input, by the time the response reaches peak amplitude at a latency of ∼30–50 ms it is dominated by intracortical activity (Intskirveli et al., 2016). Thus, the layer 4 current sink reflects both monosynaptic thalamic input, especially at short latencies, and progressively greater contributions of intracortical activity at longer latencies. It follows that the preferential adaptation of longer-latency components at moderate stimulus rates (e.g., 10 Hz, **Figure 2A**) likely reflects the failure of multi-synaptic intracortical activity, whereas adaptation of shorter-latency components at all rates could also reflect reduced thalamic input (Creutzfeldt et al., 1980). The present study demonstrates that current-sink adaptation—which increased with stimulus rate and was complete at ≥ 20 Hz—resembles that described for single units in anesthetized and waking animals (Creutzfeldt et al., 1980; Wang et al., 2008; Yao et al., 2015). Studies in waking animals including humans describe more complex response dynamics in addition to simple adaptation (Todorovic et al., 2011; Phillips et al., 2017), indicating that the present study targets only a subset of mechanisms. Still, the results illustrate the usefulness of CSD recordings for studying nicotinic regulation of adaptation.

In the present study, urethane anesthetic was preferred for its limited depressive effects on nicotinic responses compared to other anesthetics (Hara and Harris, 2002). Still, urethane does reduce sensory cortex responsiveness (Sceniak and Maciver, 2006), though not synaptic activity mediated by glutamate or GABA (Sceniak and Maciver, 2006), and the present studies should be extended to awake animals. However, since nicotine can alter cognition-related electrophysiological responses (Harkrider and Hedrick, 2005), tests in awake animals should control behavioral state as well.

CF train stimuli can be useful for understanding auditory processing since stimuli within an acoustic stream elicit more complex response dynamics than tones in isolation. The present results point to potential consequences of activating nAChRs during an acoustic stream, with the caveat that some effects will likely depend on brain state, especially states such as arousal and attention that are associated with release of endogenous acetylcholine (Celesia and Jasper, 1966; Parikh et al., 2007). That is, dose-dependent effects of nicotine will depend on endogenous, as well as exogenous, activation of nAChRs. Consistent with this notion, studies in human subjects have found that effects of nicotine can vary with baseline measures, i.e., enhancement of performance in subjects with weaker baseline performance, but not in subjects with stronger baselines (Baschnagel and Hawk, 2008; Knott et al., 2014a,b; Behler et al., 2015). Notably, during attention, adaptation is sensitive to "top-down" regulation, being reduced for unexpected stimulus trains and enhanced for expected trains (Todorovic et al., 2011). While it is unclear to what extent top-down regulation is cholinergic, the effects demonstrated in the present study reflect potential mechanisms by which endogenous acetylcholine and/or exogenous nicotine can regulate processing. A better understanding of these mechanisms may be therapeutically useful, e.g., for development of drug treatments for auditory processing deficits (see final section, below).

Nicotinic Enhancement of Acoustic Train-Evoked Responses

The effects of systemic nicotine on the CF-evoked layer 4 current sink likely involve actions within the auditory thalamocortical pathway and intracortical circuits in A1 (Kawai et al., 2007; Intskirveli and Metherate, 2012; Askew et al., 2017, 2019).

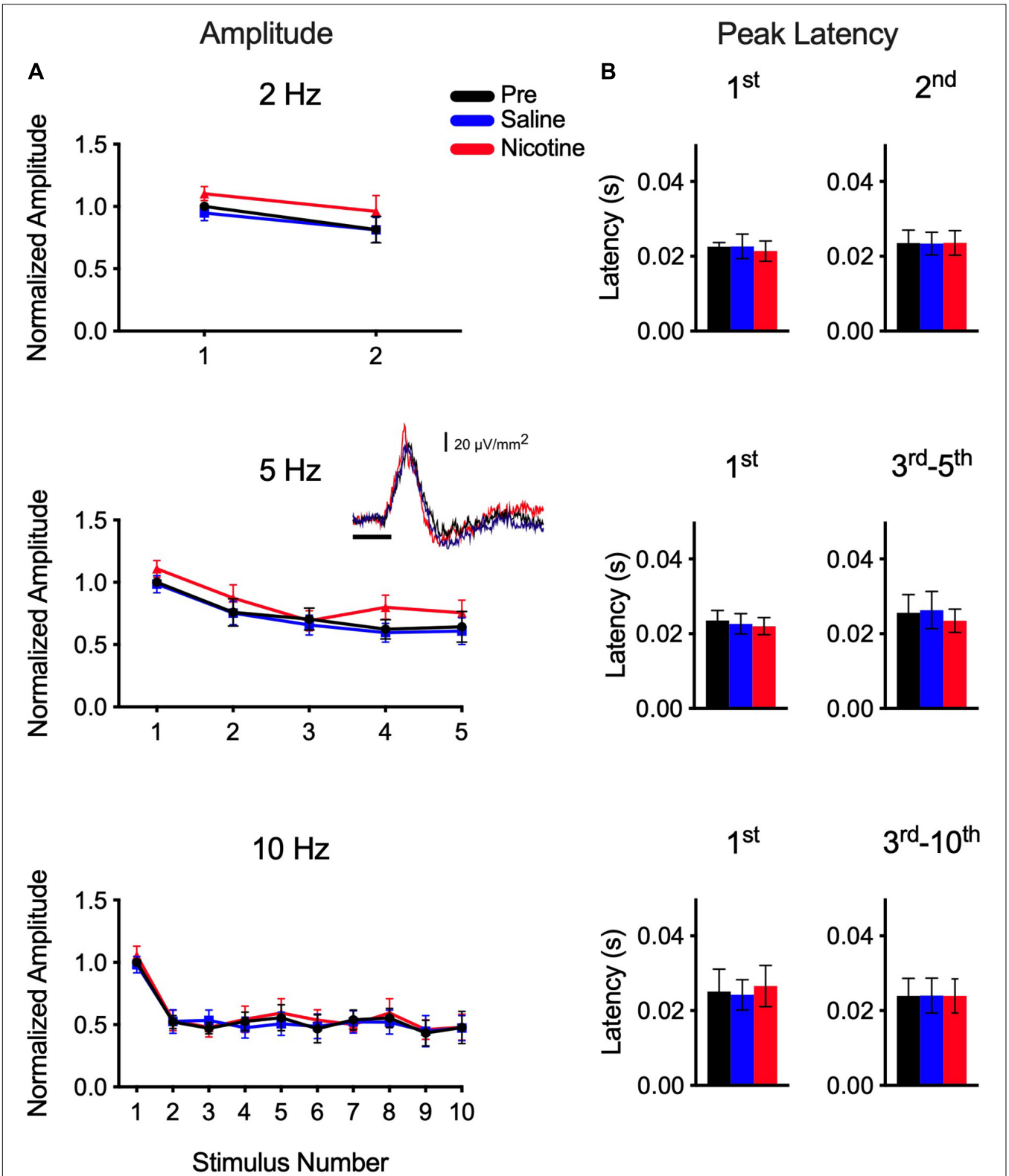

FIGURE 4 | Nicotine had no effect on CF-evoked current sink in layer 5/6. Infragranular current sink recorded simultaneously with current sink in layer 4. **(A)** Systemic nicotine did not affect peak amplitude of responses to stimulus sets (2–10 Hz). Inset shows example "first response" to CF stimulus in layer 5/6. **(B)** Group data for peak latency, separately for first response of train and for adapted responses combined.

Activation of nAChRs within the thalamocortical pathway increases axon excitability to decrease the latency of thalamic-evoked axon spikes and increase the consistency of spike timing (decreased latency CV). Increased synchrony within a population of thalamocortical axons should enhance summation of converging inputs to cortical neurons, thereby enhancing cortical responses. Intracortical actions include recently identified mechanisms by which robust nicotinic excitation of inhibitory interneurons expressing Vasoactive Intestinal Peptide (VIP) produces disinhibition of pyramidal neurons—likely via VIP-interneuron projections to other interneurons—thereby enhancing responsiveness to afferent inputs (Askew et al., 2019). Although nicotine is delivered systemically and nAChRs are found throughout the auditory pathways (Morley and Happe, 2000; Sottile et al., 2017; Noftz et al., 2020), we have not observed effects of systemic nicotine in the auditory brainstem (ABR, present study) or midbrain and thalamus (Askew et al., 2017) that might contribute to enhanced CF-evoked cortical responses [although midbrain and thalamic effects of systemic nicotine do contribute to the narrowing of cortical receptive fields (Askew et al., 2017)].

The present study describes three novel findings: First, systemic nicotine enhanced the peak response (increased amplitude, decreased latency) of partially adapted responses to CF trains at rates of 2–10 Hz (**Figure 2**). Adaptation *per se* is not affected by nicotine since the adaptation ratio was not altered and nicotine did not prevent complete adaptation at higher rates (20–40 Hz). Thus, nicotine enhances responses to CF trains but does not affect within-trial adaptation (time-course of hundreds of milliseconds).

Second, analysis *across* the 25 trials of each stimulus set revealed a slower adaptation (time-course of seconds), that is evident only in the presence of nicotine to enhance initial responses (**Figure 3B**). Nicotine does regulate this slower adaptation since it is weak or absent in controls, and the adaptation may depend on nicotinic mechanisms since the adaptation rate is similar across a five-fold range of stimulus frequency. For example, the slow adaptation could involve neuromodulatory mechanisms since nicotinic regulation of tone-evoked responses in A1 requires activation of intracellular MAP kinase (Intskirveli and Metherate, 2012). Previous studies have demonstrated multiple forms of adaptation in A1 with time-courses ranging from hundreds of milliseconds to tens of seconds (Ulanovsky et al., 2004). Similarly, fast and slow forms of adaptation over hundreds of milliseconds and tens of seconds, respectively, can be observed in the *in vitro* auditory cortex with stimulation of afferent inputs (Metherate and Ashe, 1995), suggesting mechanisms that are cortical (or thalamocortical) in origin. Nicotinic regulation of these mechanisms may contribute to top-down regulation of auditory cortex, e.g., during attention-related release of acetylcholine that activates nAChRs.

Third, a striking effect of nicotine in the present study is the enhanced consistency of response timing across trials for 2–5 Hz trains (**Figure 3C**). That is, nicotine reduced trial-to-trial variability of peak latency even as peak amplitude was enhanced and then adapted. This regulation of peak latency only occurred in responses with longer-latency response components (peak latency ∼30–50 ms), whereas the absence of such responses for 10 Hz trains, likely due to adaptation of intracortical response components, precluded this effect. The nicotinic effect on peak timing is reminiscent of effects on axon spike timing in thalamocortical axons described above (Kawai et al., 2007) and may reflect, in part, increased synchrony of discharge among afferent inputs. Given the importance of timing in auditory processing, it is likely that increased consistency could enhance auditory processing generally.

Finally, in contrast to the effects of nicotine on the layer 4 current sink, we observed no effect on the simultaneously recorded infragranular current sink (layer 5/6; **Figure 4**) or brainstem responses (ABR; **Figure 1B**). The infragranular sink exhibits very short latencies (e.g., onset <10 ms, peak ∼20 ms) and likely reflects collateral projections of the main thalamocortical input (Cruikshank et al., 2002; Zhou et al., 2010). Compared to the layer 4 response, the infragranular current sink exhibited weaker adaptation at each stimulus rate tested, and neither its peak amplitude nor peak latency was affected by systemic nicotine. The ABR exhibited no adaptation even at the highest rate tested (40 Hz) and its peak amplitude and latency were not affected by nicotine. Although the ABR recordings were of insufficient resolution to measure individual components, ABR studies in human subjects also found limited effects (reduced Wave I; no effect on Waves III and V) by systemic nicotine (transdermal patch) (Harkrider et al., 2001). However, studies in human subjects did observe nicotinic enhancement (increased amplitude, decreased latency) for longer-latency potentials of presumed thalamocortical and cortical origin (Harkrider and Champlin, 2001) and improved consonant-vowel discrimination measured both behaviorally and electrophysiologically (Harkrider and Hedrick, 2005).

Implications for Possible Therapeutic Use of Nicotine

In human subjects, cortical activity tracks the envelope of ongoing speech at frequencies ≤10 Hz that correspond to the occurrence of syllables, words and phrases (Vander Ghinst et al., 2019; Fuglsang et al., 2020). Cortical speech tracking is enhanced by attention, and enhanced tracking is associated with better speech comprehension, even as subjects age (Mesgarani and Chang, 2012; Decruy et al., 2019). Indeed, envelop tracking increases more with comprehension in older subjects than in young adults (Decruy et al., 2019), and with hearing loss in older adults (Fuglsang et al., 2020), suggesting that compensatory brain mechanisms enhance speech tracking when the task is more difficult (e.g., with aging and/or hearing loss). Such results raise the possibility that activation of nAChRs by exogenous agonist, including nicotine itself, could help compensate for auditory deficits by increasing the gain and temporal consistency of cortical responses (Metherate et al., 2012), similarly to the findings of the present study. Indeed, recent psychoacoustic studies show performance enhancement with systemic nicotine (polacrilex gum) in normal-hearing

young adults, especially in more difficult listening conditions (Pham et al., 2020). Future studies will explore this in human subjects with auditory processing deficits associated with aging or communication disorders.

DATA AVAILABILITY STATEMENT

The original contributions presented in the study are included in the article/supplementary material, further inquiries can be directed to the corresponding author/s.

ETHICS STATEMENT

The animal study was reviewed and approved by University of California, Irvine, IACUC.

AUTHOR CONTRIBUTIONS

II and RM contributed to the conception and design of the study. II collected and analyzed the data. Both authors prepared the manuscript and approved the submitted version.

FUNDING

This work was supported by the National Institute on Deafness and Other Communication Disorders R01 DC013200 and R01 DC017687.

ACKNOWLEDGMENTS

We thank Emily Provenzano for assistance with pilot studies.

REFERENCES

Albuquerque, E. X., Pereira, E. F., Alkondon, M., and Rogers, S. W. (2009). Mammalian nicotinic acetylcholine receptors: from structure to function. *Physiol. Rev.* 89, 73–120. doi: 10.1152/physrev.00015.2008

Askew, C., Intskirveli, I., and Metherate, R. (2017). Systemic nicotine increases gain and narrows receptive fields in A1 via integrated cortical and subcortical actions. *eNeuro* 4:ENEURO.0192-17.2017.

Askew, C. E., Lopez, A. J., Wood, M. A., and Metherate, R. (2019). Nicotine excites VIP interneurons to disinhibit pyramidal neurons in auditory cortex. *Synapse* 73:e22116.

Baschnagel, J. S., and Hawk, L. W. Jr. (2008). The effects of nicotine on the attentional modification of the acoustic startle response in nonsmokers. *Psychopharmacology* 198, 93–101. doi: 10.1007/s00213-008-1094-y

Behler, O., Breckel, T. P., and Thiel, C. M. (2015). Nicotine reduces distraction under low perceptual load. *Psychopharmacology* 232, 1269–1277. doi: 10.1007/s00213-014-3761-5

Celesia, G. G., and Jasper, H. H. (1966). Acetylcholine released from cerebral cortex in relation to state of activation. *Neurology* 16, 1053–1070. doi: 10.1212/wnl.16.11.1053

Creutzfeldt, O., Hellweg, F. C., and Schreiner, C. (1980). Thalamocortical transformation of responses to complex auditory stimuli. *Exp. Brain Res.* 39, 87–104.

Cruikshank, S. J., Rose, H. J., and Metherate, R. (2002). Auditory thalamocortical synaptic transmission in vitro. *J. Neurophysiol.* 87, 361–384. doi: 10.1152/jn.00549.2001

Dani, J. A., and Bertrand, D. (2007). Nicotinic acetylcholine receptors and nicotinic cholinergic mechanisms of the central nervous system. *Annu. Rev. Pharmacol. Toxicol.* 47, 699–729. doi: 10.1146/annurev.pharmtox.47.120505.105214

Decruy, L., Vanthornhout, J., and Francart, T. (2019). Evidence for enhanced neural tracking of the speech envelope underlying age-related speech-in-noise difficulties. *J. Neurophysiol.* 122, 601–615. doi: 10.1152/jn.00687.2018

Fuglsang, S. A., Marcher-Rorsted, J., Dau, T., and Hjortkjaer, J. (2020). Effects of sensorineural hearing loss on cortical synchronization to competing speech during selective attention. *J. Neurosci.* 40, 2562–2572. doi: 10.1523/jneurosci.1936-19.2020

Hara, K., and Harris, R. A. (2002). The anesthetic mechanism of urethane: the effects on neurotransmitter-gated ion channels. *Anesth. Analg.* 94, 313–318. doi: 10.1097/00000539-200202000-00015

Harkrider, A. W., and Champlin, C. A. (2001). Acute effect of nicotine on non-smokers: III. LLRs and EEGs. *Hear. Res.* 160, 99–110. doi: 10.1016/s0378-5955(01)00347-1

Harkrider, A. W., Champlin, C. A., and McFadden, D. (2001). Acute effect of nicotine on non-smokers: I. OAEs and ABRs. *Hear. Res.* 160, 73–88. doi: 10.1016/s0378-5955(01)00345-8

Harkrider, A. W., and Hedrick, M. S. (2005). Acute effect of nicotine on auditory gating in smokers and non-smokers. *Hear. Res.* 202, 114–128. doi: 10.1016/j.heares.2004.11.009

Intskirveli, I., Joshi, A., Vizcarra-Chacon, B. J., and Metherate, R. (2016). Spectral breadth and laminar distribution of thalamocortical inputs to A1. *J. Neurophysiol.* 115, 2083–2094. doi: 10.1152/jn.00887.2015

Intskirveli, I., and Metherate, R. (2012). Nicotinic neuromodulation in auditory cortex requires MAPK activation in thalamocortical and intracortical circuits. *J. Neurophysiol.* 107, 2782–2793. doi: 10.1152/jn.01129.2011

Kawai, H., Lazar, R., and Metherate, R. (2007). Nicotinic control of axon excitability regulates thalamocortical transmission. *Nat. Neurosci.* 10, 1168–1175. doi: 10.1038/nn1956

Knott, V., Choueiry, J., Dort, H., Smith, D., Impey, D., de la Salle, S., et al. (2014a). Baseline-dependent modulating effects of nicotine on voluntary and involuntary attention measured with brain event-related P3 potentials. *Pharmacol. Biochem. Behav.* 122, 107–117. doi: 10.1016/j.pbb.2014.03.020

Knott, V., Impey, D., Philippe, T., Smith, D., Choueiry, J., de la Salle, S., et al. (2014b). Modulation of auditory deviance detection by acute nicotine is baseline and deviant dependent in healthy nonsmokers: a mismatch negativity study. *Hum. Psychopharmacol.* 29, 446–458. doi: 10.1002/hup.2418

Mesgarani, N., and Chang, E. F. (2012). Selective cortical representation of attended speaker in multi-talker speech perception. *Nature* 485, 233–236. doi: 10.1038/nature11020

Metherate, R., and Ashe, J. H. (1995). GABAergic suppression prevents the appearance and subsequent fatigue of an NMDA receptor-mediated potential in neocortex. *Brain Res.* 699, 221–230. doi: 10.1016/0006-8993(95)00909-a

Metherate, R., Intskirveli, I., and Kawai, H. D. (2012). Nicotinic filtering of sensory processing in auditory cortex. *Front. Behav. Neurosci.* 6:44.

Morley, B. J., and Happe, H. K. (2000). Cholinergic receptors: dual roles in transduction and plasticity. *Hear. Res.* 147, 104–112. doi: 10.1016/s0378-5955(00)00124-6

Muller-Preuss, P., and Mitzdorf, U. (1984). Functional anatomy of the inferior colliculus and the auditory cortex: current source density analyses of click-evoked potentials. *Hear. Res.* 16, 133–142. doi: 10.1016/0378-5955(84)90003-0

Noftz, W. A., Beebe, N. L., Mellott, J. G., and Schofield, B. R. (2020). Cholinergic projections from the pedunculopontine tegmental nucleus contact excitatory and inhibitory neurons in the inferior colliculus. *Front. Neural Circuits* 14:43. doi: 10.3389/fncir.2020.00043

Parikh, V., Kozak, R., Martinez, V., and Sarter, M. (2007). Prefrontal acetylcholine release controls cue detection on multiple timescales. *Neuron* 56, 141–154. doi: 10.1016/j.neuron.2007.08.025

Pham, C. Q., Kapolowicz, M. R., Metherate, R., and Zeng, F. G. (2020). Nicotine enhances auditory processing in healthy and normal-hearing young adult nonsmokers. *Psychopharmacology* 237, 833–840. doi: 10.1007/s00213-019-05421-x

Phillips, E. A. K., Schreiner, C. E., and Hasenstaub, A. R. (2017). Diverse effects of stimulus history in waking mouse auditory cortex. *J. Neurophysiol.* 118, 1376–1393. doi: 10.1152/jn.00094.2017

Poorthuis, R. B., Bloem, B., Verhoog, M. B., and Mansvelder, H. D. (2013). Layer-specific interference with cholinergic signaling in the prefrontal cortex by smoking concentrations of nicotine. *J. Neurosci.* 33, 4843–4853. doi: 10.1523/jneurosci.5012-12.2013

Sceniak, M. P., and Maciver, M. B. (2006). Cellular actions of urethane on rat visual cortical neurons in vitro. *J. Neurophysiol.* 95, 3865–3874. doi: 10.1152/jn.01196.2005

Sottile, S. Y., Ling, L., Cox, B. C., and Caspary, D. M. (2017). Impact of ageing on postsynaptic neuronal nicotinic neurotransmission in auditory thalamus. *J. Physiol.* 595, 5375–5385. doi: 10.1113/jp274467

Stiebler, I., Neulist, R., Fichtel, I., and Ehret, G. (1997). The auditory cortex of the house mouse: left-right differences, tonotopic organization and quantitative analysis of frequency representation. *J. Comp. Physiol. A* 181, 559–571. doi: 10.1007/s003590050140

Todorovic, A., van Ede, F., Maris, E., and de Lange, F. P. (2011). Prior expectation mediates neural adaptation to repeated sounds in the auditory cortex: an MEG study. *J. Neurosci.* 31, 9118–9123. doi: 10.1523/jneurosci.1425-11.2011

Ulanovsky, N., Las, L., Farkas, D., and Nelken, I. (2004). Multiple time scales of adaptation in auditory cortex neurons. *J. Neurosci.* 24, 10440–10453. doi: 10.1523/jneurosci.1905-04.2004

Vander Ghinst, M., Bourguignon, M., Niesen, M., Wens, V., Hassid, S., Choufani, G., et al. (2019). Cortical tracking of speech-in-noise develops from childhood to adulthood. *J. Neurosci.* 39, 2938–2950. doi: 10.1523/jneurosci.1732-18.2019

Wang, X., Lu, T., Bendor, D., and Bartlett, E. (2008). Neural coding of temporal information in auditory thalamus and cortex. *Neuroscience* 154, 294–303. doi: 10.1016/j.neuroscience.2008.03.065

Yao, J. D., Bremen, P., and Middlebrooks, J. C. (2015). Emergence of spatial stream segregation in the ascending auditory pathway. *J. Neurosci.* 35, 16199–16212. doi: 10.1523/jneurosci.3116-15.2015

Zhou, Y., Liu, B. H., Wu, G. K., Kim, Y. J., Xiao, Z., Tao, H. W., et al. (2010). Preceding inhibition silences layer 6 neurons in auditory cortex. *Neuron* 65, 706–717. doi: 10.1016/j.neuron.2010.02.021

Conflict of Interest: The authors declare that the research was conducted in the absence of any commercial or financial relationships that could be construed as a potential conflict of interest.

frontiers in Neural Circuits

ORIGINAL RESEARCH
published: 15 July 2021
doi: 10.3389/fncir.2021.715369

Multiple Sources of Cholinergic Input to the Superior Olivary Complex

Nichole L. Beebe[1,2†], *Chao Zhang*[3†], *R. Michael Burger*[3] *and Brett R. Schofield*[1,2*]

[1]Department of Anatomy and Neurobiology, Hearing Research Focus Group, Northeast Ohio Medical University, Rootstown, OH, United States, [2]Brain Health Research Institute, Kent State University, Kent, OH, United States, [3]Department of Biological Sciences, Lehigh University, Bethlehem, PA, United States

The superior olivary complex (SOC) is a major computation center in the brainstem auditory system. Despite previous reports of high expression levels of cholinergic receptors in the SOC, few studies have addressed the functional role of acetylcholine in the region. The source of the cholinergic innervation is unknown for all but one of the nuclei of the SOC, limiting our understanding of cholinergic modulation. The medial nucleus of the trapezoid body, a key inhibitory link in monaural and binaural circuits, receives cholinergic input from other SOC nuclei and also from the pontomesencephalic tegmentum. Here, we investigate whether these same regions are sources of cholinergic input to other SOC nuclei. We also investigate whether individual cholinergic cells can send collateral projections bilaterally (i.e., into both SOCs), as has been shown at other levels of the subcortical auditory system. We injected retrograde tract tracers into the SOC in gerbils, then identified retrogradely-labeled cells that were also immunolabeled for choline acetyltransferase, a marker for cholinergic cells. We found that both the SOC and the pontomesencephalic tegmentum (PMT) send cholinergic projections into the SOC, and these projections appear to innervate all major SOC nuclei. We also observed a small cholinergic projection into the SOC from the lateral paragigantocellular nucleus of the reticular formation. These various sources likely serve different functions; e.g., the PMT has been associated with things such as arousal and sensory gating whereas the SOC may provide feedback more closely tuned to specific auditory stimuli. Further, individual cholinergic neurons in each of these regions can send branching projections into both SOCs. Such projections present an opportunity for cholinergic modulation to be coordinated across the auditory brainstem.

Keywords: acetylcholine, gerbil, pontomesencephalic tegmentum, modulation, arousal, plasticity, hearing, collateral

OPEN ACCESS

Edited by:
Catherine Carr, University of Maryland, College Park, United States

Reviewed by:
Randy J. Kulesza, Lake Erie College of Osteopathic Medicine, United States
Laura M. Hurley, Indiana University Bloomington, United States

***Correspondence:**
Brett R. Schofield
bschofie@neomed.edu

†These authors have contributed equally to this work and share first authorship

Received: *26 May 2021*
Accepted: *24 June 2021*
Published: *15 July 2021*

Citation:
Beebe NL, Zhang C, Burger RM and Schofield BR (2021) Multiple Sources of Cholinergic Input to the Superior Olivary Complex. Front. Neural Circuits 15:715369. doi: 10.3389/fncir.2021.715369

INTRODUCTION

The superior olivary complex (SOC) serves as a major computation center in the brainstem auditory system. It participates in a variety of brainstem auditory circuits and is a hub for many ascending and descending auditory pathways. Among the many functions SOC serves in hearing, its roles in sound localization are well known (Harrison and Feldman, 1970; Grothe et al., 2010). Ascending auditory inputs to SOC emerge from the cochlear nucleus (CN; Cant and Casseday, 1986; Kuwabara et al., 1991; Thompson and Schofield, 2000). In turn, ascending projections from the SOC

project primarily to nuclei of the lateral lemniscus and the inferior colliculus (IC), with smaller projections to the superior colliculus and auditory thalamus (Schofield et al., 2014; Mellott et al., 2018; Mansour et al., 2021). The SOC neurons that are responsible for computing the location of sound sources in the azimuth plane include medial superior olive (MSO) and lateral superior olive (LSO) neurons (Helfert and Aschoff, 1996). To ensure computational stability and accuracy, these neurons establish a complex and precise neural circuitry (Adams and Mugnaini, 1990; Schofield and Cant, 1991; Smith et al., 1998). In this network, the role of excitation and inhibition in shaping sound-evoked responses are well studied using simple acoustic stimuli (Brugge and Geisler, 1978; Albrecht et al., 2014; Grothe and Pecka, 2014). However, in response to more complex stimuli, the ability to maintain computational stability and accuracy may be challenged. Elevated input intensity or complicated input components causes synaptic depression, and weakened synapses affect the timing and strength of signal transmission among these SOC neurons (Banks and Smith, 1992; Grothe and Sanes, 1993; Song et al., 2005; Kopp-Scheinpflug et al., 2008). In addition to the known excitatory and inhibitory inputs, neuromodulatory mechanisms may be available to modify the SOC network dynamically for optimized performance. Numerous studies have suggested that SOC neurons employ local neuromodulation to regulate synaptic transmission to accommodate the complexity of acoustic inputs. In the MNTB, a number of ion channels and/or receptors are involved in regulating the signal transmission at its large and highly reliable synapse from the calyx of Held (Kopp-Scheinpflug et al., 2011). In the MSO, $GABA_B$ receptors modulate binaural synaptic inputs to ensure the precision of neural computation (Pecka et al., 2008; Hassfurth et al., 2010; Fischl et al., 2012). In the LSO, serotonergic modulation induces synaptic suppression of both excitatory and inhibitory inputs (Fitzgerald and Sanes, 1999).

The role of broad neuromodulatory systems that pervade most regions of the brain has received little attention at the level of the SOC. ACh regulates neural activity at several levels of auditory processing including the cochlea (Taranda et al., 2009; Ciuman, 2010), cochlear nucleus (e. g, Fujino and Oertel, 2001; Goyer et al., 2016; Kuenzel, 2019), inferior colliculus (Farley et al., 1983; Habbicht and Vater, 1996), thalamus (Sottile et al., 2017a,b) and cortex (Metherate, 2011; reviewed by Schofield and Hurley, 2018). Numerous reports suggest acetylcholine (ACh) is a neuromodulator of computational importance in the SOC. Receptor binding indicates that SOC nuclei have high levels of cholinergic receptors (Morley and Happe, 2000; Gahring et al., 2004; Happe and Morley, 2004). Developmental knock-out of alpha-7 nicotinic receptors suggests that ACh may contribute to temporal processing in the superior paraolivary nucleus (Felix et al., 2019). We have shown previously that, in the MNTB, ACh affects suprathreshold response magnitude, enhances near-threshold level discrimination, and enhances coding for signal in noise (Zhang et al., 2021).

Subcortical auditory centers derive their cholinergic input from two primary sources, the pontomesencephalic tegmentum (PMT) and the SOC. The PMT comprises the pedunculopontine tegmental nucleus (PPT) and the laterodorsal tegmental nucleus (LDT), both of which contain cholinergic and non-cholinergic neurons. The SOC contains multiple groups of cholinergic cells, including the well-known olivocochlear cells as well as lesser-known cholinergic cells that project to the cochlear nucleus or the MNTB (Sherriff and Henderson, 1994; Zhang et al., 2021). Cholinergic neurons in the PMT project broadly to CN, IC, and auditory thalamus (Schofield et al., 2011). We previously showed that the MNTB receives input from cholinergic cells of the SOC and the PMT (Zhang et al., 2021). In that report, we showed a tracer deposit restricted to the MNTB resulted in labeled cholinergic cells in the PMT and SOC. Larger tracer deposits that encroached on adjacent nuclei in the medial SOC produced similar results, but because none of those deposits excluded the MNTB, the sources of ACh input to other SOC nuclei were ambiguous. Here, we investigate cholinergic inputs to the SOC more broadly and we investigate the possibility of bilaterally branching projections from cholinergic cells of the SOC and the PMT into the SOC.

To identify the sources of cholinergic input to the SOC, we employed *in vivo* extracellular recordings to physiologically identify major nuclei in the SOC in the adult gerbil. Recordings were followed by injections of retrograde tracers (RetroBeads) to label innervating neurons. Among retrogradely labeled neurons, cholinergic cells were identified with an antibody to choline acetyltransferase (ChAT). Subsequent analysis revealed that both PMT and SOC provide cholinergic innervation of the ipsilateral and contralateral SOC. In addition, a small number of cholinergic cells in the lateral paragigantocellular nucleus (LPGi) project to at least some SOC nuclei. Individual cholinergic cells in each of these areas can send branching axons to innervate the SOC bilaterally. The results suggest a widespread cholinergic innervation of the SOC, with many SOC nuclei receiving cholinergic input from multiple sources, including cells that project bilaterally to the SOC.

MATERIALS AND METHODS

Surgery and Perfusion

All procedures were conducted in compliance with Public Health Service and Institutional Animal Care and Use Committee (IACUC) guidelines. Adult Mongolian gerbils (*Meriones unguiculatus*) aged at least 3 months of either sex were used in all experiments. Tract tracer injections were made using methods described previously (Zhang et al., 2021). Initial anesthesia was administered with an intraperitoneal injection (5 ml/kg body weight) of a mixture consisting of 20% ketamine (100 mg/ml) and 2% xylazine (100 mg/ml) in 0.9% NaCl solution, yielding a final dose of 100 mg/kg body weight for ketamine and 10 mg/kg body weight for xylazine. The anesthetic depth was constantly monitored by assessing muscle tone and respiration rate. To maintain appropriate anesthesia, supplemental doses of anesthetic (0.05–0.10 ml) were injected subcutaneously every 30 min or whenever necessary. Subjects were transferred to a sound-attenuation booth (Industrial Acoustics) and mounted in a custom-made stereotaxic instrument. Body temperature was maintained at 37°C to 39°C by a heating pad through a homeothermic controller. One to three small craniotomies were

performed on the interparietal bone caudal to the transverse sinus. The number of craniotomies depended on the number of injection targets. The dura was opened to expose the brain tissue.

Acoustic stimuli were digitally generated using TDT system III (Tucker-Davis Technologies) commanded through SPIKE, a custom-made software was used to collect spike times as well as analog chart recordings. The stimuli were attenuated (PA4/PA5; Tucker-Davis Technologies) and delivered to E.A.R. 3A earphones that are coupled to the external auditory meatus with tubes and calibrated using a $\frac{1}{4}$-inch free-field microphone and a microphone preamp (model 2221, Larson Davis). A low impedance glass search electrode (<1 MΩ) filled with 1M NaCl was first advanced using a remotely driven actuator into the brain stem to map the approximate borders of SOC nuclei. Major SOC subdivisions were identified based on differential noise-burst evoked responses. LSO neuron responses are evoked by ipsilateral sound stimulation and suppressed by contralateral sound (Boudreau and & Tsuchitani, 1968; Tollin and Yin, 2002). MSO neuron clusters are driven by either ipsilateral or contralateral sound (Goldberg and & Brown, 1969; Yin and Chan, 1990). Monaural MNTB neurons only respond to contralateral ear stimulation (Guinan and Li, 1990; Koka and Tollin, 2014). Because the MNTB is adjacent to VNTB and SPN, two other contralaterally driven SOC nuclei, the low-impedance search electrode was then replaced by a high impedance electrode (>5 MΩ) to record single-unit responses for a more precise identification of the MNTB population. Neurons with sustained sound-evoked responses that phase lock to low frequency stimulation were considered MNTB neurons. To ensure precise targeting, each population was demarcated from stereotaxic coordinates obtained from multiple search penetrations. Once the location was confirmed, the search electrode was withdrawn from the brain and replaced by a micropipette that was first backfilled with mineral oil and then front loaded with green or red RetroBeads (Lumafluor Inc.) diluted tenfold in 0.9% saline. Retrobeads were used because they are highly sensitive and are taken up minimally or not at all by fibers of passage unless the fibers are damaged (Katz et al., 1984; Schofield, 2008). To minimize damage to surrounding tracts, small deposits of diluted Retrobeads were made using a glass micropipette. Areas of tracer deposit showed minimal tissue damage under microscopic inspection, so we are confident that the vast majority of retrogradely-labeled cells had axon terminals in the tracer deposit site. For deposits directed at medial SOC, the electrode was lowered to the same coordinates identified for the MNTB whereas more lateral deposits were directed toward the coordinates identified for the LSO. Once the electrode was lowered to the desired depth, 100–200 nL of tracer was injected using a Nanoliter injector (World Precision Instruments). In a few cases, the same tracer was deposited *via* both medial and lateral locations to encompass a larger area of the SOC. In some animals, red beads were injected into the SOC on one side of the brain and green beads were injected on the opposite side. For this goal, separate micropipettes were used for each tracer to avoid cross-contamination.

After the retrograde tracers were deposited, the micropipette was removed and the craniotomy was covered with aseptic silicone gel and the incision was closed with Vetbond glue (3M). The animals then recovered on a heating pad under frequent monitoring for 24 h. Additional analgesic measures were applied during this period if necessary. After 48–72 h, the animals were injected with 0.2 ml/kg body weight Somnasol euthanasia solution (Henry Schein) intraperitoneally (yielding a final dose of 78 mg/kg body weight for pentobarbital sodium and 10 mg/kg body weight for phenytoin sodium) and perfused intracardially with 0.9% NaCl in 0.01 M phosphate buffer (PBS) followed by 4% paraformaldehyde in PBS. The brains were harvested and post-fixed in the latter solution at 4°C overnight. The brains were maintained in 30% sucrose PBS until processing for immunostaining.

Immunohistochemistry

After removal of the cerebral cortex, the brain was frozen and cut on a sliding microtome into 40–50 μm sections in the transverse plane. Sections were treated in 0.4% Triton X-100 in PBS for 30 min (all steps at room temperature unless noted). After three 5-min washes in PBS, the tissue was treated with 20% normal rabbit serum (NRS) with 0.1% Triton X-100 in PBS for 1 h. Goat anti-ChAT polyclonal antibody (Chemicon AB 144P) was applied with 0.1% Triton X-100 and 1% NRS in PBS for 24–72 h at 4°C. The concentration of the primary antibody varied from 1:100–1:400. Following three 5-min washes in PBS, the tissue was incubated for 1 h with a secondary antibody (biotinylated rabbit anti-goat IgG, BA-5000, Vector Lab), at a 1:100 concentration with 1% NRS in PBS. Following three additional 5-min washes, tissue was incubated with an AlexaFluor 647-labeled streptavidin (1:100; Molecular Probes S- 21374) for 1 h at room temperature. The sections were rinsed in PBS then mounted on gelatin-coated slides and allowed to dry, then coverslipped with DPX (Aldrich Chemical Co., St. Louis, MO).

The anti-ChAT antibody recognizes choline acetyltransferase, the synthetic enzyme for acetylcholine found in cholinergic neurons. In guinea pig tissue, pre-adsorption with the ChAT peptide eliminated staining, and the antibody recognized a single band on a Western blot of guinea pig brainstem tissue (Motts et al., 2008). The pattern and appearance of ChAT staining reported here matched that seen in previous studies and in other species.

Photography and Data Analysis

Photomicrographs of RetroBeads and ChAT-labeled cells were taken with a Zeiss AxioImager.Z2 microscope with an attached Apotome 2 to provide optical sectioning at 0.5 μm depth intervals. Low magnification images were taken using a 5× objective without the Apotome, while high magnification images were taken using a 63× oil-immersion objective (NA=1.4) with the Apotome. High magnification images shown are maximum intensity projections of image stacks. Adobe Photoshop was used to colorize and crop images and for global adjustment of levels. Plots of RetroBead- and ChAT-labeled cells were created with a Neurolucida system (MBF Biosciences) attached to a Zeiss AxioImager.Z1 microscope. Results from 14 tracer deposits in nine gerbils were used for analysis. We used anti-ChAT immunostaining to identify the Ch5 and

Ch6 cholinergic groups, which mark the PPT and LDT, respectively (Mesulam et al., 1983). The LDT is located largely within the periaqueductal gray whereas the PPT extends through the pontomesencephalic tegmentum from a dorso-caudal location surrounding the superior cerebellar peduncle to a rostroventral location approaching the substantia nigra (Woolf and Butcher, 1986). The nuclei of the SOC are similar to those in guinea pigs and can be distinguished readily based on differences in background fluorescence of the cells and neuropil (Schofield and Cant, 1991). We are not aware of descriptions of the LPGi in gerbils, but we were able to identify the nucleus based on descriptions in other species (Andrezik et al., 1981; Kamiya et al., 1988; Stornetta et al., 2013). Every third section through the rostro-caudal extent of each area of interest was examined for ChAT+ cells, RetroBead-labeled cells, and cells labeled with multiple markers. The location of each labeled cell was plotted with a symbol indicating the labels present in the cell. After all the sections were plotted, the numbers of labeled cells were exported using Neurolucida Explorer, and were further analyzed in Microsoft Excel. Plots to show the distribution of labeled cells were exported from Neurolucida Explorer and figures were prepared with Adobe Illustrator CC.

RESULTS

Injection Sites

Each of the cases described here had deposits of RetroBeads that included various parts of the SOC. The large size of RetroBeads (on a molecular scale) often leads to irregular diffusion patterns and an irregular border of the deposit site (Schofield, 2008). In fact, a single injection can appear as multiple deposits in a single tissue section. As described in Methods, we frequently deposited RetroBeads at multiple sites in order to include a larger portion of the SOC, so it was essential to evaluate the entire SOC to identify the nuclei that were included in each experiment. **Figure 1A** shows an example of a large deposit of red RetroBeads. For this experiment, the beads were deposited *via* two penetrations at different medial-lateral locations. **Figure 1B** illustrates the spread of these deposits as seen in three different rostro-caudal levels through the SOC, showing that all major nuclei of the SOC were involved as were many periolivary nuclei. In other experiments, the deposits involved primarily medial SOC nuclei (**Figure 1C**) or lateral SOC nuclei (**Figure 1D**); the distributions are summarized in **Table 1**. In many cases, RetroBeads spread into the reticular formation just dorsal to the SOC, but the results in these cases did not differ from those with deposits restricted to the SOC.

Results were similar for red RetroBeads and green RetroBeads. Deposits of either tracer resulted in retrogradely-labeled cells in many auditory nuclei, including the cochlear nucleus and inferior colliculus, matching previous reports of inputs to the SOC (reviewed in Thompson and Schofield, 2000). Here, we focus on two questions regarding cholinergic inputs to the SOC. Our first goal was to identify the locations of cholinergic cells that project to the SOC, which we identified as cells that contained RetroBeads and were also immunopositive for choline acetyltransferase (ChAT), a selective marker of cholinergic cells. We focused on cholinergic cells in the PMT and the SOC, the primary sources of cholinergic input to the brainstem auditory nuclei (reviewed by Schofield and Hurley, 2018), and identified in our previous study of cholinergic inputs to the MNTB (Zhang et al., 2021). We also describe a small projection from the lateral paragigantocellular nucleus (LPGi) that projects to at least some of the SOC nuclei. Our second goal was to determine whether individual cholinergic cells send branching axonal projections (i.e., collateral projections) to both left and right SOC. For both goals, the presence of deposit sites within the SOC limited our ability to fully assess projections from within the injected SOC. Nonetheless, the results indicate that many of the SOC nuclei receive cholinergic inputs from multiple sources.

The SOC Receives Cholinergic Input From Multiple Regions

Our previous report described cholinergic projections to the medial SOC, concentrating on the MNTB. Here, we expanded our study to include the entire SOC. In every case, the retrogradely labeled cells included both ChAT+ and ChAT-negative cells. In general, more cells were labeled after larger tracer deposits. While our goal was to assess inputs to the SOC overall, a few tracer deposits were limited to just one or two SOC nuclei; observations from these cases are described where relevant. Retrogradely-labeled cells in the PMT were quantified. Retrogradely-labeled cells are also described in the SOC and in the LPGi, however, cells in these areas were not quantified due to limited overall numbers of retrogradely-labeled/ChAT+ cells and because of proximity to the injection site.

Projections From the Pontomesencephalic Tegmentum

Figure 2 shows cells in the PMT that were retrogradely labeled with red RetroBeads ("red beads", RB) or green RetroBeads ("green beads", GB). Many of these cells were ChAT immunopositive (ChAT+), suggesting they are cholinergic (**Figures 2A–G**). Other retrogradely labeled cells were clearly ChAT-immunonegative ("ChAT-negative", **Figure 2H**). The presence of nearby cells with strong ChAT staining suggests that the lack of immunostaining in these retrograde cells was not due to failure of the immunostain (e.g., from lack of tissue penetration by the reagents). In addition to cholinergic cells, both the PPT and the LDT contain glutamatergic and GABAergic neurons, each of which could contribute to the ChAT-negative population (Wang and Morales, 2009; Boucetta et al., 2014; Kroeger et al., 2017). Similar results were produced by smaller tracer deposits, including deposits limited to the MNTB (G18-2007 RB; Zhang et al., 2021) as well as deposits restricted to the LSO/LNTB (G18 3033 RB) or the SPN (G18-2010 RB). Regardless of deposit size, ChAT-negative cells were among the tracer-labeled population, indicating that both cholinergic and non-cholinergic PMT cells project to the SOC nuclei.

For quantitative assessment of projections from the PMT nuclei, we chose eight deposits with the most substantial retrograde labeling along with robust immunostaining (**Table 1**). On average, 19–32% of retrogradely labeled cells

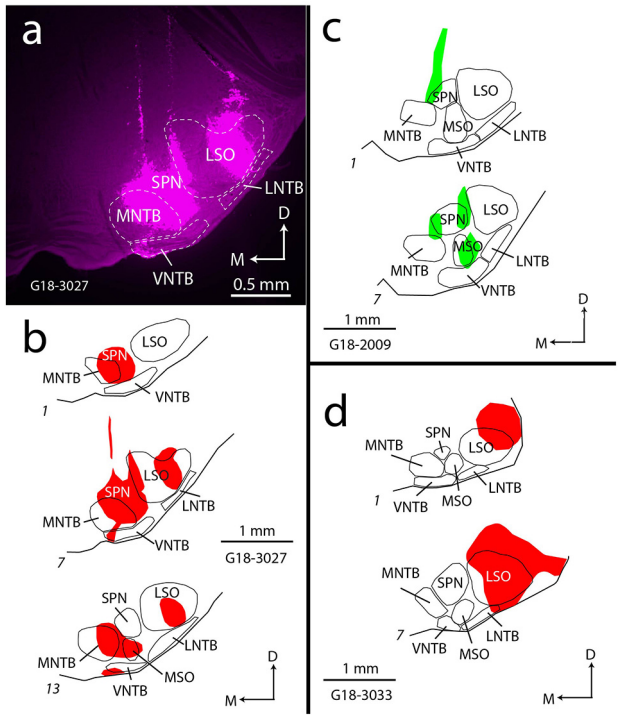

FIGURE 1 | Examples of RetroBead injections in the SOC. **(A)** Photograph showing multiple deposits of red RetroBeads (magenta) in the SOC of case G18-3027. **(B)** Drawings depicting the rostro-caudal extent of the red RetroBead injection in case G18-3027. Section 7 corresponds to the photograph in panel **(A)**. This injection included most major SOC nuclei. In this and subsequent panels, sections are arranged from caudal (section 1) to rostral. **(C)** Drawings depicting the extent of the green RetroBead injection in case G18-2009. The deposits, in this case, were located in central parts of the SOC. **(D)** Drawings depicting the extent of the green RetroBead injection in case G18-3033. This deposit included only lateral parts of the SOC. Abbreviations: D, dorsal; LNTB, lateral nucleus of the trapezoid body; LSO, lateral superior olivary nucleus; M, medial; MNTB, medial nucleus of the trapezoid body; MSO, medial superior olivary nucleus; SOC, superior olivary complex; SPN, superior paraolivary nucleus; VNTB, ventral nucleus of the trapezoid body.

were ChAT+ (**Table 2**). We conclude that both cholinergic and non-cholinergic cells in the PPT and LDT project to the SOC.

Despite variation in tracer deposit size or involvement of different nuclei, the distribution of labeled cells in the PMT nuclei was qualitatively similar across cases. **Figure 3** illustrates the distribution of ChAT+, RB-labeled cells (magenta triangles) in the PPT and LDT after a large injection (Case G18-3027; deposit site shown in **Figures 1A,B**). ChAT+ tracer-labeled cells were present bilaterally in PPT and LDT, with more cells ipsilateral than contralateral and, on each side, more cells in PPT than in LDT (**Table 3**).

Projections From the Superior Olivary Complex

Even though the tracer deposits obscured some of the SOC, it was possible to identify retrogradely labeled cells in parts of the SOC separated from the deposit sites. Such cells were numerous, reflecting well-known intra-olivary connections (reviewed by Thompson and Schofield, 2000). **Figure 4** shows examples of

TABLE 1 | Summary of tracer deposits.

Case	MNTB	SPN	VNTB	MSO	LSO	LNTB
G18-2007 GB	XX	XX	XX			
G18-2007 RB	XX					
G18-2008 GB*	XX	XX	XX	XX		
G18-2009 GB*	X	XX		XX		
G18-2010 RB		XX				
G18-2010 GB	XX	XX				
G18-2011 RB	XX	XX		X		
G18-2011 GB	XX	XX				
G18-2012 RB*	XX	XX				
G18-2012 GB*	XXX	X				
G18-3027 RB*	XXX	XXX	XX	XX	XX	
G18-3030 RB*	XX	X		X	X	
G18-3030 GB	XX	X			XX	
G18-3033 RB*					XXX	X
G18-3033 GB*					XX	

*For each tracer deposit, the extent of involvement of each SOC nucleus is indicated. Lack of markings indicates no involvement of a given nucleus, an "X" marking indicates minimal involvement of a nucleus, an "XX" marking indicates moderate involvement of a nucleus, and an "XXX" marking indicates extensive involvement of a nucleus. GB—green RetroBeads, LNTB—lateral nucleus of the trapezoid body, LSO—lateral superior olivary nucleus, MNTB—medial nucleus of the trapezoid body, MSO—medial superior olivary nucleus, RB—red RetroBeads, SPN—superior paraolivary nucleus, VNTB—ventral nucleus of the trapezoid body. *Indicates cases used for quantitative analysis.*

tracer-labeled cells in the SOC ipsilateral or contralateral to a tracer deposit. Both ChAT+ (**Figures 4A–E**) and ChAT-negative (**Figure 4F**) tracer-labeled cells were observed. ChAT+ cells were scattered across the SOC, located among nearly all periolivary nuclei as well as within the LSO and around its borders (in the peri-LSO region). Similar results were observed after smaller tracer deposits. Deposits in the lateral SOC (LSO and LNTB) labeled ChAT+ cells in the ipsilateral and contralateral SOC (**Figures 4C,D**). A deposit restricted to the SPN also labeled ChAT+ cells bilaterally in the SOC. In all cases, tracer-labeled cells included ChAT-negative as well as ChAT+ cells. **Figure 5** shows the distribution of ChAT+ and ChAT-negative retrograde cells (magenta and green, respectively) in the SOC after a deposit of green RetroBeads in the right SOC. Variation between cases was common; e.g., the VNTB often contained more ChAT+ retrograde cells than depicted in **Figure 5**. Such cells could also be clustered in an undefined region lateral to the MNTB, along the medial border of the MSO (a region noted to contain olivocochlear cells in gerbils; Aschoff et al., 1988). Across our cases, the only nucleus that never contained a ChAT+ retrograde cell was the lateral nucleus of the trapezoid body. It is likely that different cholinergic cells have different targets within the SOC, but further experiments will be needed to address this issue.

Small tracer deposits again provide additional information about cholinergic targets. Deposits in the lateral SOC (LSO and LNTB) labeled ChAT+ cells in the ipsilateral and contralateral SOC (**Figures 4C,D**). A deposit restricted to the SPN also labeled ChAT+ cells bilaterally in the SOC. In both cases, the labeled cells included ChAT-negative as well as ChAT+ cells. These cells were scattered among the olivary nuclei, similar to that seen after larger injections (i.e., in VNTB and LSO as well as other periolivary regions).

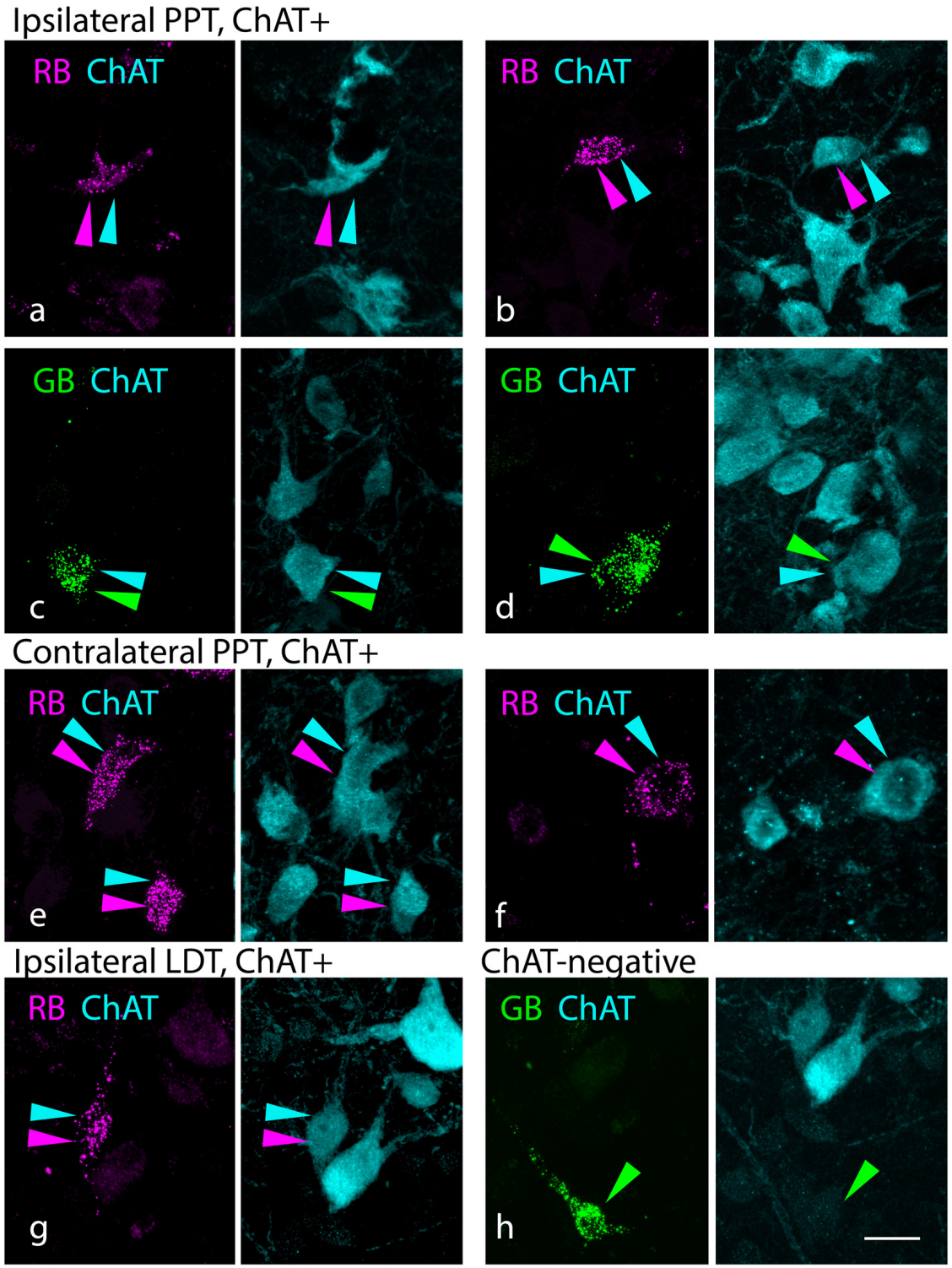

FIGURE 2 | Cholinergic and non-cholinergic PMT cells project to the SOC. **(A–D)** Paired photographs show tracer-labeled cells (left panel, magenta or green) in the PPT ipsilateral to the injected SOC. The right panel in each pair shows the ChAT immunostain (cyan) from the same area, demonstrating that the tracer-labeled cells were also ChAT-immunopositive. Examples were seen with both red beads ["RB", in **(A** and **B)**] and green beads ["GB" in **(C,D)**]. **(E,F)** ChAT+ cells labeled with RB in the PPT contralateral to the injected SOC. **(G)** Example of a ChAT+ RB-labeled cell in the ipsilateral LDT. **(H)** Example of a ChAT-negative, GB-labeled cell in the LDT contralateral to a GB injection. Panels **(A)** and **(F)** are from deposit G18-3033 RB (lateral SOC); the remaining panels are from deposit G18-2012 (medial SOC deposits). Scale bar = 20 μm. Abbreviations: LDT, laterodorsal tegmental nucleus; PMT, pontomesencephalic tegmentum.

TABLE 2 | Percentage of retrograde cells in each nucleus that were ChAT+.

Nucleus	Average	st dev	Maximum
Ipsilateral PPT	32%	20%	62%
Ipsilateral LDT	21%	17%	50%
Contralateral PPT	29%	18%	57%
Contralateral LDT	19%	13%	37%

*Summary of the percentage of retrogradely labeled PMT cells that were ChAT+. On average, 25–40% of retrogradely labeled cells were ChAT+. Data from eight tracer deposits (see asterisks in **Table 1**). The maximum column indicates the highest percentage of cells that were ChAT+ across all cases for each area. Total number of retrograde cells = 2,478. Total number of ChAT+/retrograde cells = 673.*

TABLE 3 | Distribution of tracer-labeled, ChAT+ cells in the PMT nuclei.

Nucleus	% of cells	st dev
Ipsilateral PPT	42%	13%
Ipsilateral LDT	17%	8%
Contralateral PPT	31%	18%
Contralateral LDT	10%	5%

*Summary of the distribution of ChAT+ retrogradely labeled cells in the four nuclei of the PMT. Data from eight tracer deposits (see asterisks in **Table 1**). Total number of retrograde cells = 2,478. Total number of ChAT+/retrograde cells = 673.*

Projections From the Lateral Paragigantocellular Nucleus (LPGi)

As described above, our tracer deposits routinely labeled ChAT+ PMT and SOC cells. Given the spread of tracer deposits across cases, these results are consistent with cholinergic projections from these sources that terminate broadly throughout the SOC. Another area, the LPGi, has been reported in mice to project to several auditory brainstem areas, including parts of the SOC (Stornetta et al., 2013). The LPGi, a nucleus of the reticular formation also known as the medial rostral ventrolateral medulla, is located caudal to the SOC, just lateral to the medullary pyramid. This nucleus has been closely tied to autonomic and respiratory functions and has numerous connections with auditory structures (Andrezik et al., 1981; Kamiya et al., 1988; Bellintani-Guardia et al., 1996). In the

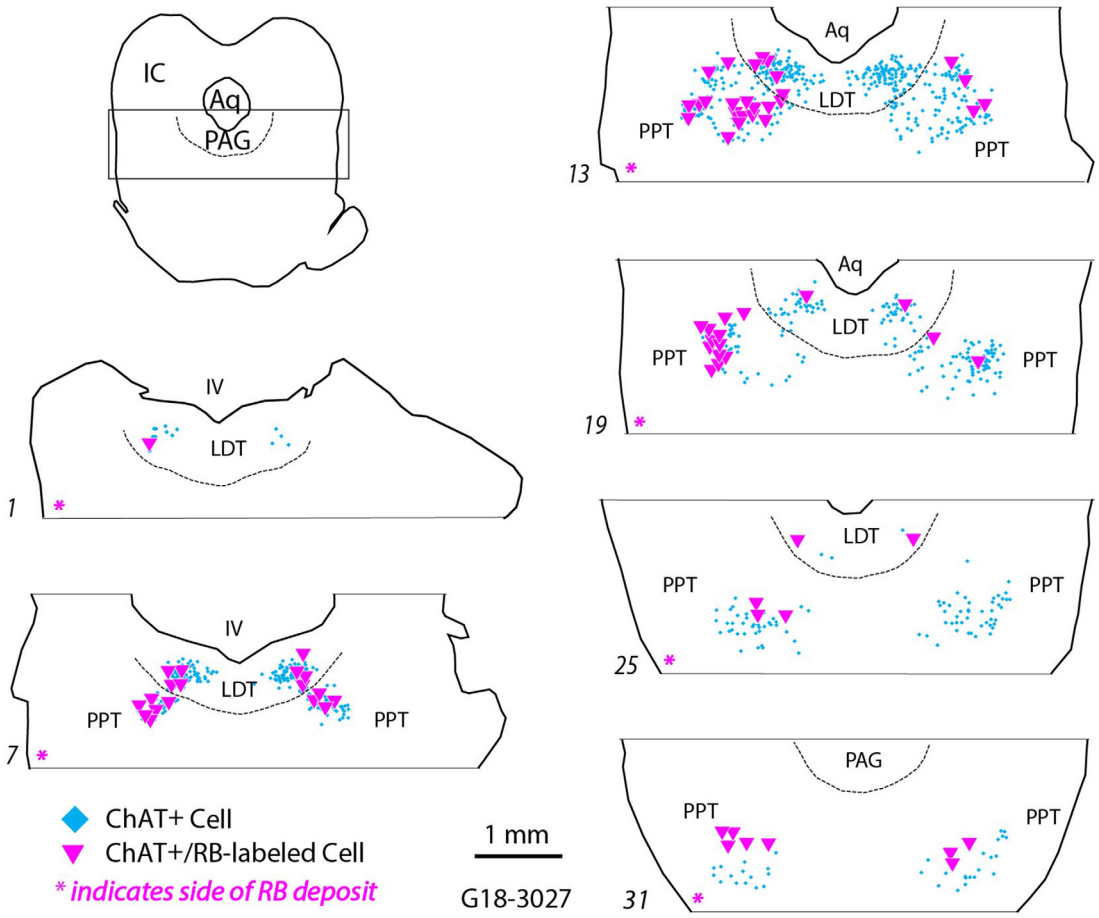

FIGURE 3 | Retrogradely labeled cholinergic cells (magenta triangles) were located in the pontomesencephalic nuclei ipsilateral and contralateral to an injection of red RetroBeads in the left SOC. Each symbol represents a single labeled cell. ChAT+ cells that did not contain RetroBeads are illustrated (cyan diamonds) to indicate the extent of the pedunculopontine and laterodorsal tegmental nuclei (PPT and LDT, respectively). Numbered sections are arranged from caudal to rostral and represent the dorsal tegmental region (indicated by the rectangle in the orientation section). The dashed line indicates the ventral border of the periaqueductal gray (PAG). The magenta asterisk at the bottom of each section outline indicates the side ipsilateral to the RB deposit in the SOC. Aq, cerebral aqueduct; IC, inferior colliculus, IV, fourth ventricle.

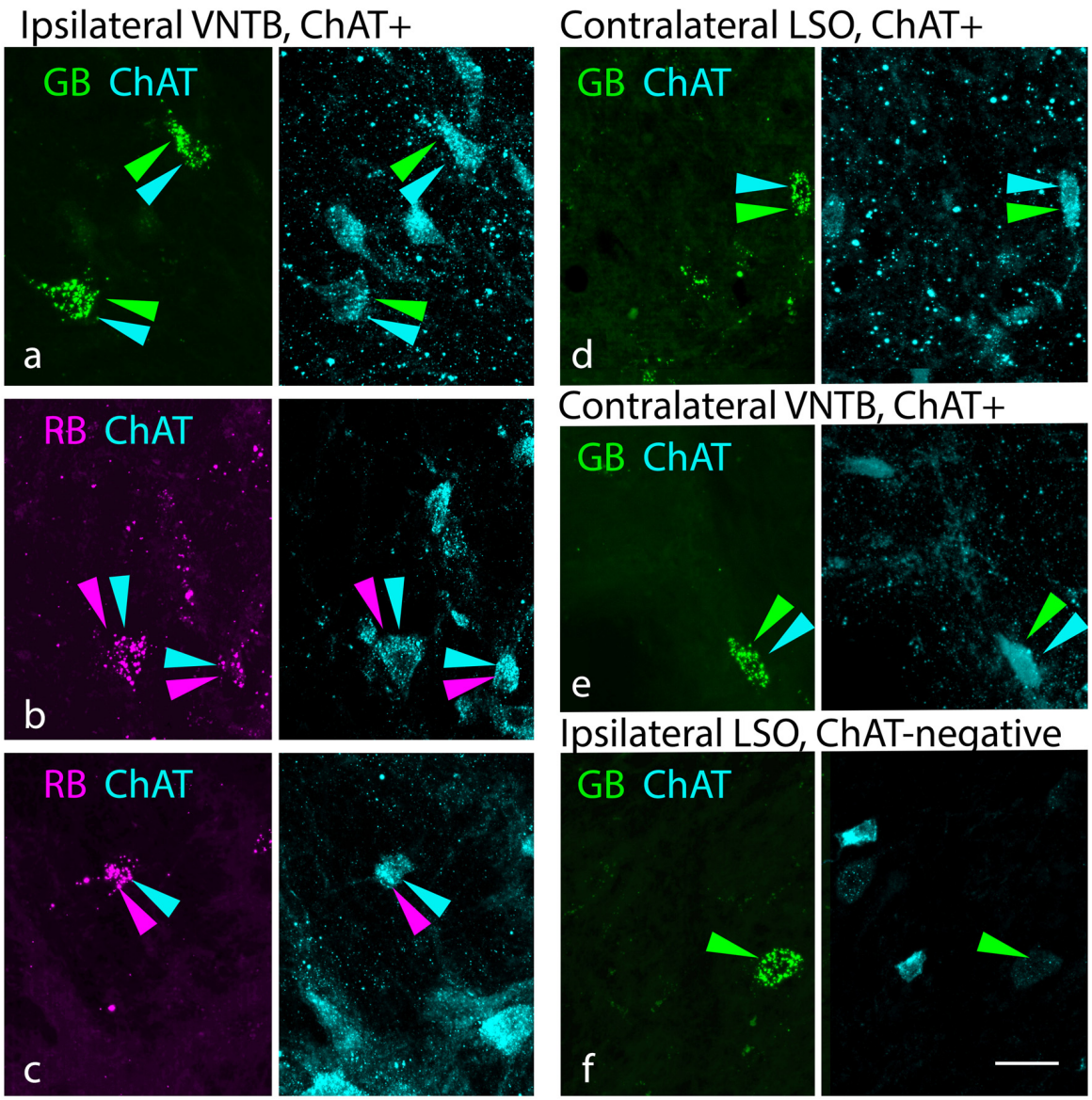

FIGURE 4 | Cholinergic and non-cholinergic SOC cells were labeled by retrograde transport from the SOC. **(A–C)** Examples of ChAT+ tracer-labeled cells in the VNTB ipsilateral to the tracer deposit. Paired photographs show tracer-labeled cells (magenta or green, left panel) and ChAT immunostain (cyan, right panel), demonstrating that the tracer-labeled cells could be ChAT-immunopositive. Examples included cells labeled with green beads (GB) or red beads (RB). **(D,E)** Examples of ChAT+ tracer-labeled cells in the contralateral lateral superior olivary nucleus [LSO, panel **(D)** or contralateral VNTB (panel **E**)]. **(F)** Example of a GB-labeled ChAT-negative neuron in the LSO ipsilateral to a tracer deposit. LSO, lateral superior olivary nucleus; VNTB, ventral nucleus of the trapezoid body. Panels (**A,E,** and **F**) are from deposit G18-2012 GB (medial SOC deposit), panel **(B)** is from deposit G18-2011 RB (medial SOC deposit), and panels **(C)** and **(D)** are from G18-3033 (lateral SOC deposits). Scale bar = 20 μm.

present study, we found retrogradely labeled cells in the LPGi in some but not all cases. The LPGi is small (typically present in just one section in a one-in-six series). A single section generally contained just a few retrograde labeled cells. Like the PMT and SOC, the LPGi contains a variety of neurotransmitter phenotypes, and the retrogradely labeled cells included both ChAT+ and ChAT-negative examples (**Figure 6**). Such cells were observed ipsilateral and contralateral to the tracer deposit.

The presence of ChAT+ retrograde cells in LPGi did not appear to be related simply to the size of the tracer deposits. The small number of cholinergic cells in the LPGi may explain some of the variability, but another possibility is that the LPGi projections do not terminate throughout the SOC. The limited evidence available from mice suggests that LPGi projections to SOC terminate most densely in the LSO and along the dorsal margin of the SOC, with smaller projections to some of the other SOC nuclei (Stornetta et al., 2013). In the present study, we

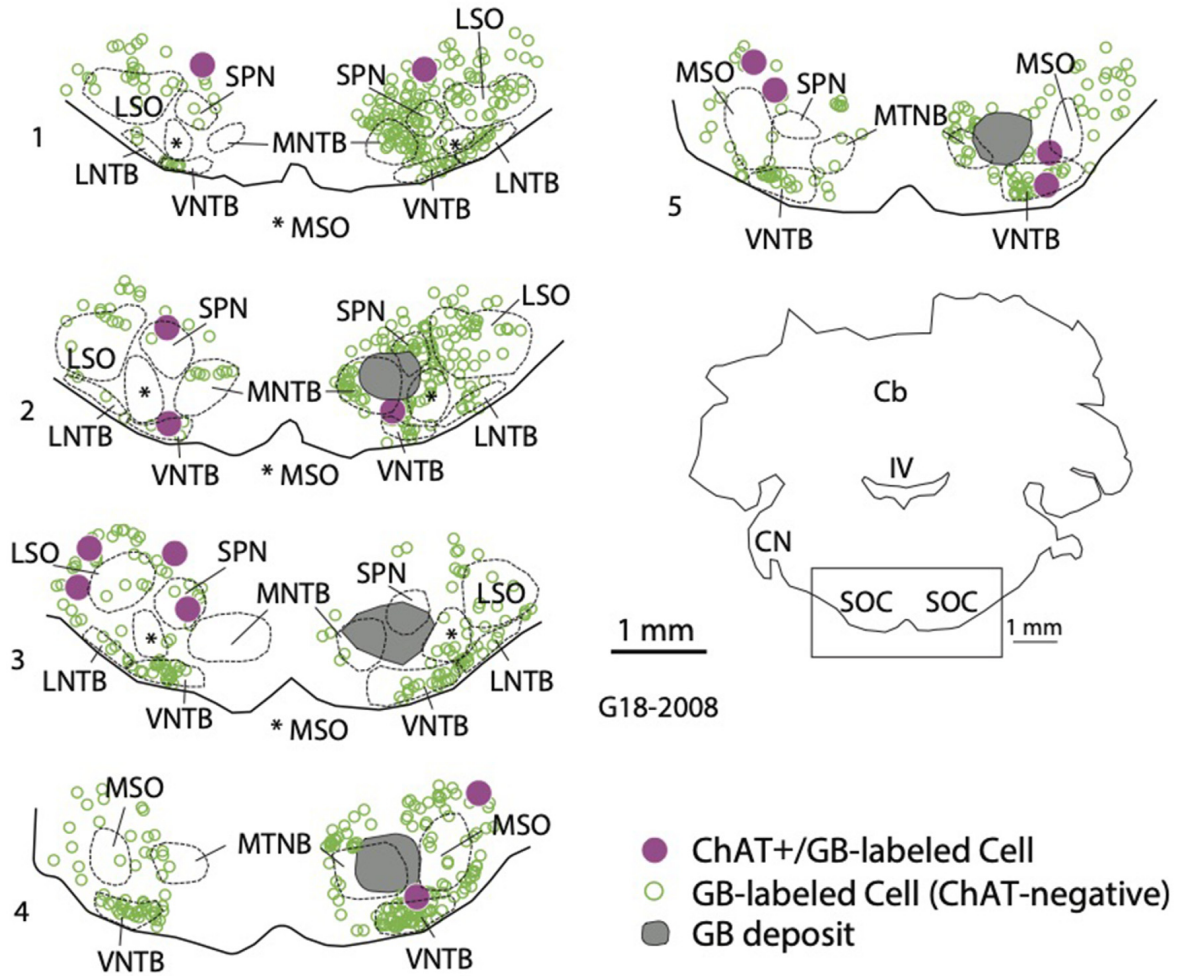

FIGURE 5 | Retrogradely labeled cholinergic cells were located in the SOC both ipsilateral and contralateral to a tracer deposit. The plot shows a deposit of green beads (GB, deposit shown in gray) in the right SOC. GB-labeled cells that were ChAT+ (magenta circles) were scattered among SOC nuclei on both sides. In addition, a large number of GB-labeled cells that were ChAT-negative were also labeled (open green circles). Numbered sections are arranged from caudal to rostral and represent the ventral portion of each section to show the SOC (indicated by the rectangle in the orientation section). IV, fourth ventricle; Cb, cerebellum; CN, cochlear nucleus; LNTB, lateral nucleus of the trapezoid body; LSO, lateral superior olivary nucleus; MNTB, medial nucleus of the trapezoid body; MSO, medial superior olivary nucleus; SOC, superior olivary complex; SPN, superior paraolivary nucleus; VNTB, ventral nucleus of the trapezoid body.

observed ChAT+ retrograde cells in the LPGi after large deposits restricted to medial or lateral SOC as well as a smaller deposit restricted to the SPN (case G18-2010 RB). The small injection in the MNTB (case G18-2007 RB) labeled cells in the LPGi, but none were ChAT+.

Axonal Branching Allows Individual Cholinergic Cells to Innervate Left and Right SOC

Six of our experimental animals received bilateral injections, with RB in one SOC and GB in the opposite SOC. If an individual cholinergic neuron has an axon that branches to innervate both left and right SOC, we could expect to find such cells triple-labeled with the two tracers and the ChAT immunostain. We observed numerous cells in the PMT nuclei that contained both retrograde tracers; many, but not all, of these cells, were ChAT+. **Figure 7** shows ChAT+, double-retrograde-labeled cells in the PPT (**Figures 7A,B**) and the LDT (**Figure 7C**). Triple-labeled cells were observed more often in the PPT than in the LDT, reflecting the pattern seen with single retrograde labeling. **Figure 7D** shows a double-retrograde cell in the LDT that was ChAT-negative. Such cells were observed in the PMT in all our cases with bilateral tracer deposits, suggesting that noncholinergic PMT cells also project bilaterally to the SOC.

Double-retrograde cells were also observed in the SOC. While the presence of the tracer deposits hindered full analysis of labeled SOC cells, there were clear examples of ChAT+, double-retrograde labeled cells in numerous SOC nuclei (**Figures 8A–E**). ChAT-negative double retrograde cells were also labeled (**Figure 8D**, cell on right); we focus here on the cholinergic (ChAT+) cells. Across cases, these cells

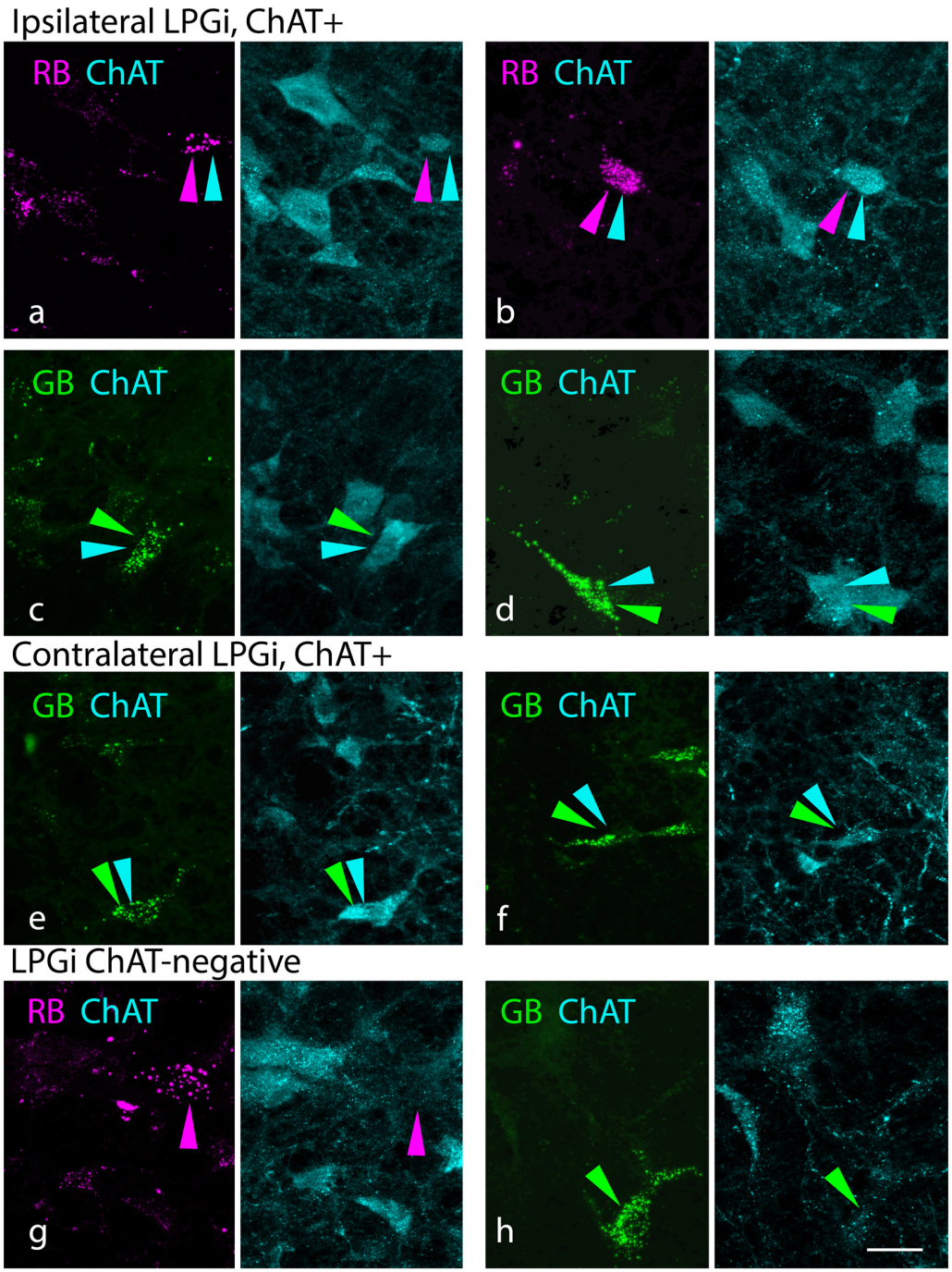

FIGURE 6 | The lateral paragigantocellular nucleus (LPGi) contains cholinergic cells that project to the SOC. Paired photographs show tracer-labeled cells (magenta or green, left panel) and ChAT immunostain (cyan, right panel), demonstrating that the tracer-labeled cells could be ChAT-immunopositive. **(A–D)** ChAT+ cells labeled with red RetroBeads (RB; **A,B**) or green Retrobeads (GB, **C,D**) in the LPGi ipsilateral to a tracer deposit. **(E,F)** GB-labeled ChAT+ cells in the LPGi contralateral to the tracer deposit. **(G,H)** Tracer-labeled ChAT-negative cells in the LPGi. Panel **(B)** is from deposit G18-3033 RB (lateral SOC deposit); panel **(H)** is from deposit G18-3030 GB (medial SOC deposit); remaining panels are from deposit G18-2012 (medial SOC deposits). Scale bar = 20 μm.

were scattered across many of the SOC nuclei, including the LSO and various periolivary regions. Several of the examples shown in **Figures 8C–E** are from G18-3033, which had tracer deposits limited to the lateral SOC. In contrast, the examples in **Figures 7A,B** are from a case in which the tracer deposits focused on medial SOC nuclei (G18-2012; see **Table 1**). These results suggest that bilateral cholinergic projections can terminate in both the lateral and the medial SOC.

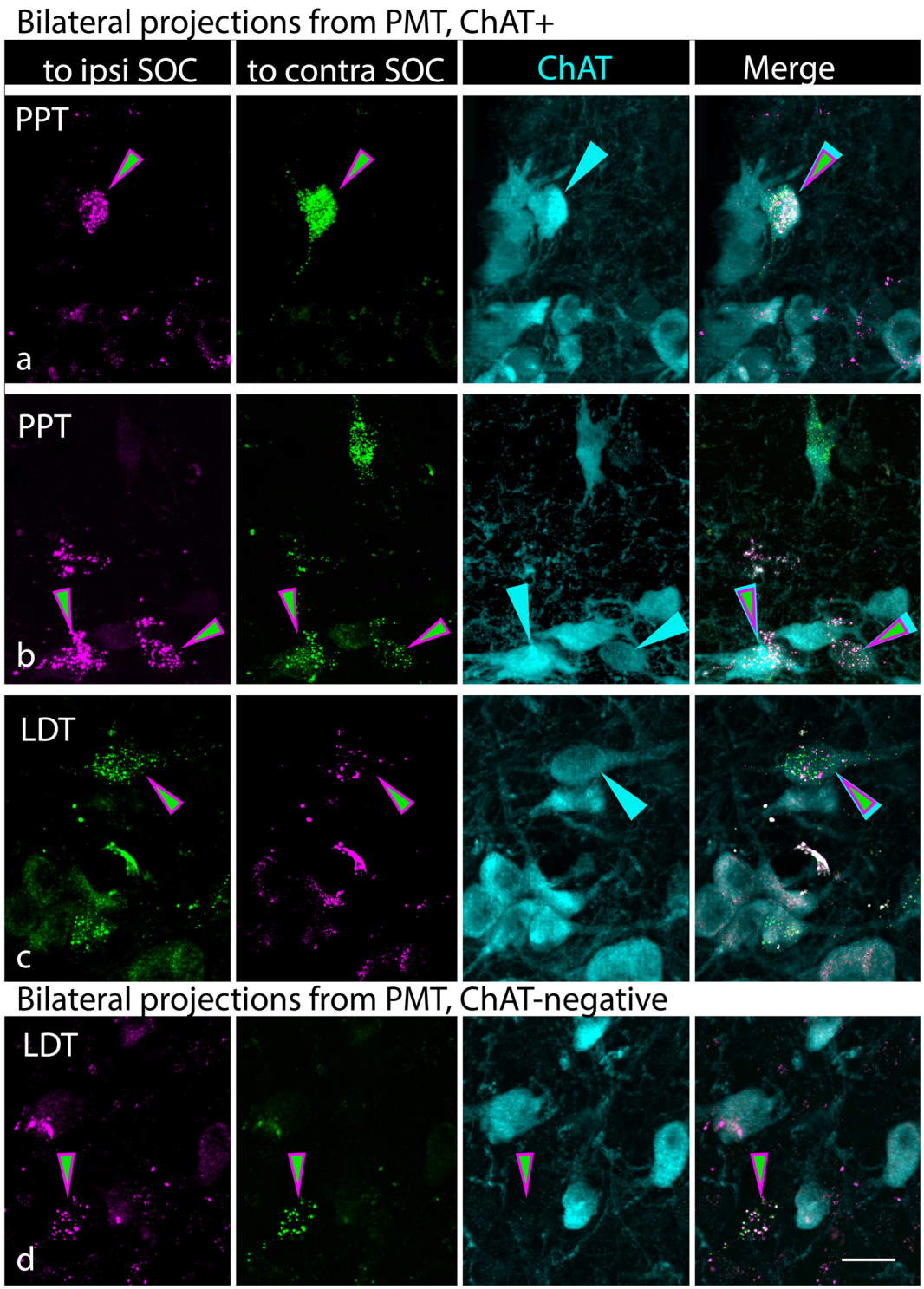

FIGURE 7 | Cholinergic and non-cholinergic cells in the PMT send branching axonal projections to innervate the SOC bilaterally. **(A–C)** Each row of photographs shows a single field of view. The first two columns show the tracer label (RB in magenta; GB in green), with the first column showing the tracer injected into the ipsilateral SOC and the second column showing the tracer injected into the contralateral SOC (relative to the labeled cells). Magenta/green arrows identify cells that contain both retrograde tracers. Column 3 shows the ChAT staining, with arrows pointing to the same cells as in the first two columns. Column 4 shows the images merged, highlighting the triple-labeled cells. Examples are from the PPT **(A,B)** and LDT **(C)**. **(D)** A single cell in the LDT that contains both retrograde tracers, indicating a bilateral projection to the SOC, but is ChAT-negative (column 3), indicating it is unlikely to be cholinergic. All panels from case G18-2012. Scale bar = 20 μm.

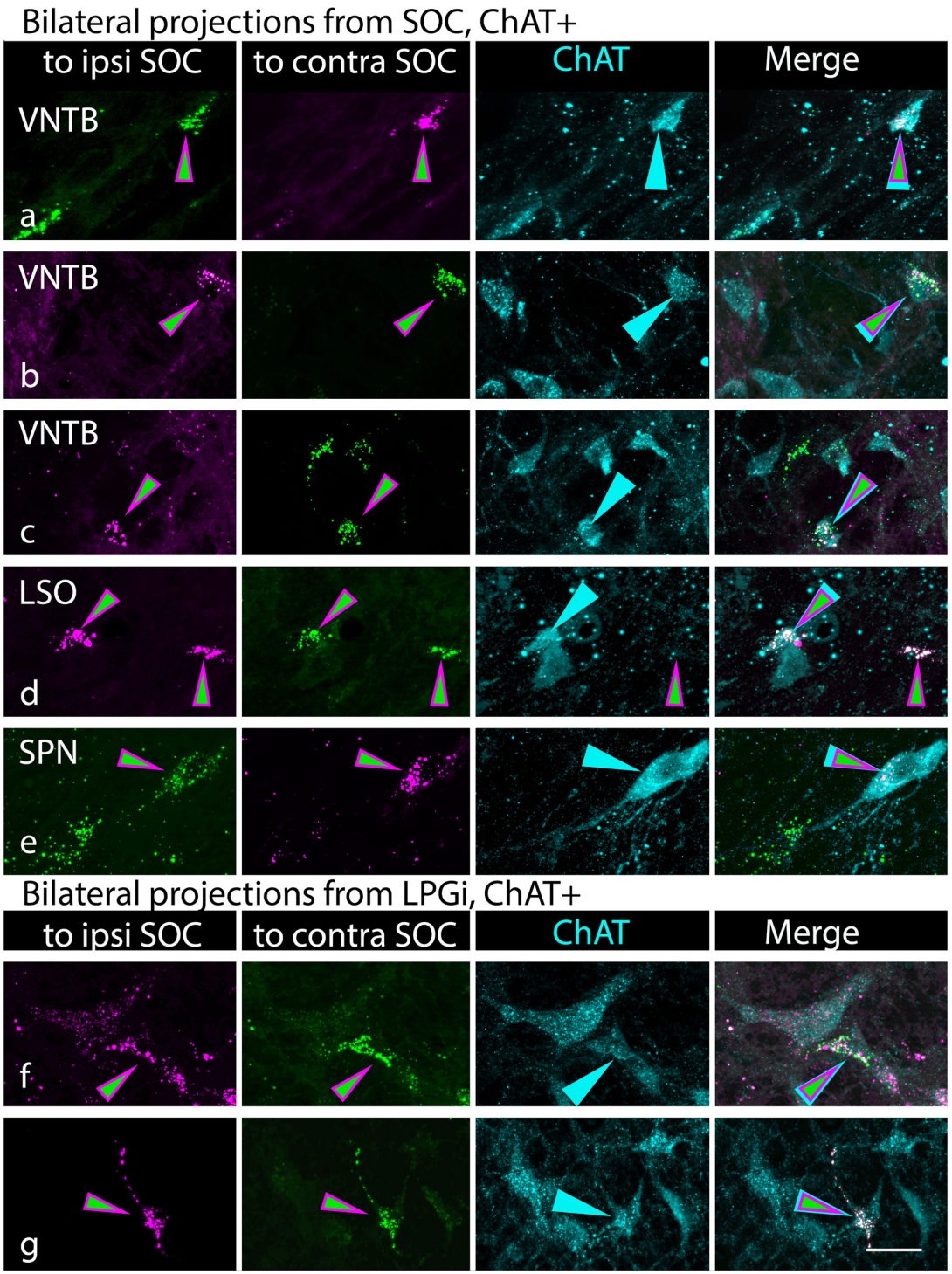

FIGURE 8 | Cholinergic cells in the superior olivary complex (SOC) and lateral paragigantocellular nucleus (LPGi) send branching axonal projections to innervate the SOC bilaterally. Each row of photographs shows a single field of view. The first two columns show the tracer label (RB in magenta; GB in green), with the first column showing the tracer injected into the ipsilateral SOC and the second column showing the tracer injected into the contralateral SOC (relative to the labeled cells). Magenta/green arrows identify cells that contain both retrograde tracers. Column 3 shows the ChAT staining, with cyan arrows pointing to the same cells as in the first two columns. Column 4 shows the merged image, highlighting the triple-labeled cells. **(A–E)** Triple-labeled cells were found in numerous SOC nuclei, indicated by the labels in column 1. VNTB, ventral nucleus of the trapezoid body; LSO, lateral superior olivary nucleus, SPN, superior paraolivary nucleus. ChAT-negative cells could also be labeled with both retrograde tracers (panel **D**, cell on the right). **(F,G)** Triple-labeled cells in the LPGi. Panels **(A,B,** and **F)** are from G18-2012 (medial SOC deposits); panels **(C,D,** and **E)** are from G18-3033 (lateral SOC deposits); panel **(G)** is from case G18-3030 (medial SOC deposits). Scale bar = 20 μm.

As described above, the LPGi contained retrogradely labeled, ChAT+ cells both ipsilateral and contralateral to the tracer deposit in several of our cases. Despite the small number of labeled cells in LPGi, we observed triple-labeled cells in cases with bilateral tracer deposits (**Figures 8F,G**), indicating that individual LPGi cholinergic cells can project bilaterally to the SOC. The number of cells was too small for quantitative analysis, but the fact that we observed triple labeled cells with a method that underestimates such projections (Schofield et al., 2007) suggests that bilateral projections may be a particularly common pattern for LPGi cholinergic cells.

DISCUSSION

Here, we've shown that the SOC receives cholinergic input from within the ipsilateral SOC, from the contralateral SOC, and bilaterally from the PMT (**Figure 9**). Projections from the PMT arise from both the PPT and the LDT, with ipsilateral projections more prominent and, on each side, PPT projections outnumbering LDT projections. Non-cholinergic PMT cells also appear to project to the SOC. Both cholinergic and non-cholinergic SOC cells also appear to project to many SOC nuclei. While non-cholinergic projections are especially numerous within the SOC, cholinergic SOC cells appear to innervate many of the SOC nuclei. Finally, a portion of the cholinergic cells that project to the SOC appear to have midline crossing axonal collaterals, allowing them to innervate both left and right SOC nuclei, presumably to provide a coordinated bilateral modulation of auditory processing in the SOC. In addition to the substantial cholinergic projections from the PMT and SOC, we document a smaller bilateral projection from the LPGi, a small nucleus of the reticular formation with connections to numerous auditory nuclei. Each of these regions, the PMT, the SOC, and the LPGi, provide cholinergic input to the SOC that likely serves a wide range of functions.

Technical Considerations

The tracers and immunostains used here have been validated in previous studies and are unlikely to exhibit serious difficulties for interpretation (e.g., Motts and Schofield, 2010; Zhang et al., 2021). The main factor for consideration is the possibility of the retrograde tracer labeling axons of passage, i.e., axons that traverse but do not terminate in the area of the tracer deposit. As described in "Materials and Methods" section (Section "Surgery and Perfusion"), Retrobeads show little if any labeling of axons of passage unless those axons are damaged. We used fine glass micropipettes to limit such damage. Nonetheless, some axons may have been damaged during physiological recording or by the tracer micropipette. This concern was greatest for cells within the SOC that were injected, so we chose to report the presence and distribution of the labeled cells but not to quantify the labeled cells within the SOC. PMT cells are located a significant distance away from the SOC, so we had fewer concerns about quantifying the cells within these nuclei. The LPGi is located caudal to the SOC, so there is less chance that its axons were damaged unless they terminate in the SOC. Ultimately, confirmation of these findings will be from experiments based on chemically selective anterograde tracing of cholinergic axons from an identified source. Of the three sources of cholinergic input that we describe, the LPGi is the only one so far confirmed by anterograde transport methods (Stornetta et al., 2013). Similar confirmation will be needed for the cholinergic projections to the SOC from cells in the PMT and in the SOC itself. Such experiments will also provide important information about the

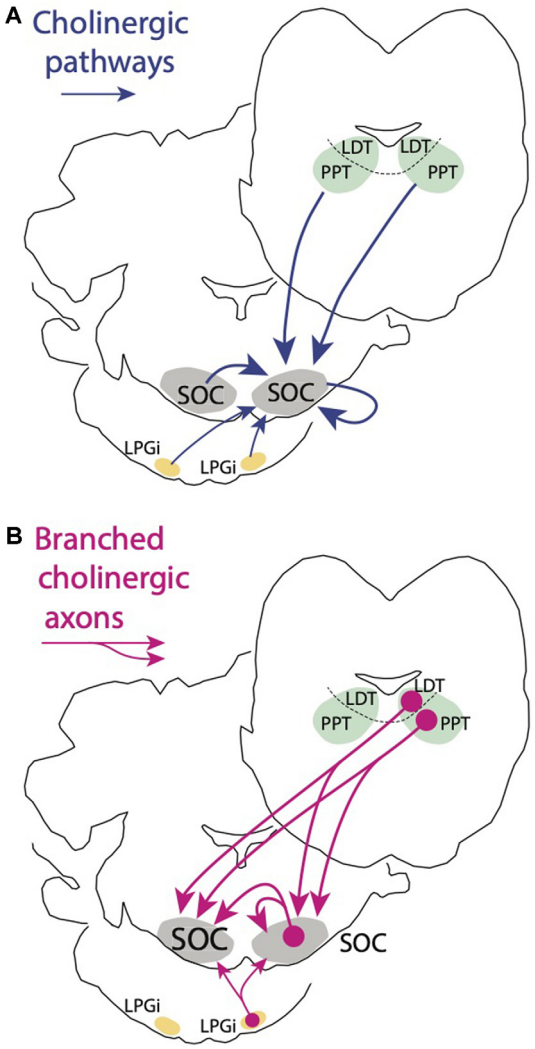

FIGURE 9 | Schematic summarizing major findings from the present study. **(A)** Cholinergic inputs to each SOC originate from three areas. One area is the pontomesencephalic tegmentum (PMT), comprising the pedunculopontine tegmental nucleus (PPT) and the laterodorsal tegmental nucleus (LDT). Each SOC receives cholinergic input from both ipsilateral and contralateral PPT and LDT. The second source of cholinergic input to the SOC is from SOC cells themselves. Each SOC receives cholinergic input from neurons within the same SOC as well as from neurons in the contralateral SOC. A third, smaller source is the lateral paragigantocellular nucleus (LPGi). Both ipsilateral and contralateral LPGi project to the SOC. **(B)** A second finding is that individual cholinergic neurons can send branching axons to innervate the SOC bilaterally. Such collateral projections can arise from cholinergic cells in each of the regions that supply cholinergic innervation to the SOC (for simplicity, projections are shown only from one side).

density and distribution of cholinergic projections from each of these sources.

Effects of ACh in the SOC

Our previous work suggested multiple roles for ACh in the MNTB, including effects on suprathreshold response magnitude, enhancement of near-threshold level discrimination, and enhanced coding of signal in the noise, with evidence that the MNTB receives cholinergic inputs from both the SOC and the PMT (Zhang et al., 2021). In the nearby SPN, mice lacking the cholinergic α7 nicotinic receptor show delayed sound-evoked responses and degraded spike precision (Felix et al., 2019). Aside from these studies, there is little direct information about the effects of ACh in SOC nuclei. In the cochlear nucleus (CN), which sends auditory information into the SOC, the roles of ACh have been studied more extensively. The effects ACh has in the CN vary by both CN region and cell type. For example, in the dorsal CN (DCN), ACh can alter neuronal sensitivity, affect spontaneous firing rates, and affect synaptic plasticity (Chen et al., 1998; Zhang and Kaltenbach, 2000; Zhao and Tzounopoulos, 2011). Blocking muscarinic signaling in the fusiform cell layer of the DCN affects spontaneous activity and alters stimulus timing-dependent plasticity; given the ties between these processes and evidence of tinnitus, cholinergic signaling in the DCN may be altered in tinnitus (Stefanescu and Shore, 2017). In T-stellate cells of the ventral CN (VCN), ACh contributes to sound-evoked excitation and may play a role in the encoding of spectral peaks in noise (Fujino and Oertel, 2001; Oertel et al., 2011). In spherical bushy cells, a different VCN cell type, cholinergic signaling plays a role in setting resting membrane potential, increases dynamic range and increases temporal precision (Goyer et al., 2016). The roles of ACh in the SOC likely vary based on the nucleus and cell type.

The effects of ACh are dependent on the subtypes of ACh receptors expressed by SOC cells. Many authors have described moderate or high expression of the nicotinic α7 subunit in the SOC (Morley et al., 1977; Hunt and Schmidt, 1978; Clarke et al., 1985). As described above, mice lacking the α7 subunit have delayed evoked responses and decreased spike timing precision in several auditory nuclei, including the SPN (Felix et al., 2019). The β4 nicotinic subunit is also highly expressed in the SOC (Gahring et al., 2004), and the relatively rare α5 nicotinic subunit is highly enriched in the SOC, especially in the SPN, compared to other brain regions (Wada et al., 1989). This all points to a variety of nicotinic acetylcholine receptors (nAChRs) being especially dense in the SOC. Muscarinic acetylcholine receptors (mAChRs) are also present in the SOC (Glendenning and Baker, 1988). There is less information about which subtypes of mAChRs are present, although both M2 and M3 receptors seem to be expressed in SOC nuclei (Safieddine et al., 1996; Yao and Godfrey, 1997). Activation of nAChRs (cation channels) typically elicits fast depolarization. Calcium permeability, ligand affinity, and channel kinetics can all differ based on subunit makeup for nAChRs (Gharpure et al., 2020). In contrast, mAChRs are G-protein coupled receptors and their activation typically elicits slower responses. Activation of mAChRs can lead to depolarization or hyperpolarization depending on the associated G proteins. mAChRs have been shown to regulate synaptic plasticity and circuit activity throughout the brain (Fernández de Sevilla et al., 2020). Despite their "slow" kinetics (compared to nAChRs), mAChRs may also contribute significantly to temporal processing, even in temporally demanding auditory cell types (Kuenzel, 2019). Based on receptor expression profiles, we would expect both nicotinic and muscarinic effects throughout the SOC.

Functional Diversity of Sources of Cholinergic Projections to the SOC

A key finding in the present study is the identification of multiple sources of cholinergic input to the SOC: the PMT, cholinergic cells in the SOC itself, and for at least some SOC nuclei, inputs from cholinergic cells in the LPGi. It is likely that projections from each of these regions serve different functions.

Cholinergic Sources From Within the SOC

The present study identified cholinergic cells scattered throughout the SOC that innervate SOC nuclei on both sides of the brain. These cholinergic SOC cells clearly overlap in distribution with olivocochlear cells, but to the best of our knowledge, there is no evidence for olivocochlear cells to send axonal branches to any SOC nucleus. Medial olivocochlear cells (MOCs) situated in medial parts of the SOC send projections into the cochlea that synapse on outer hair cells to affect the cochlear amplifier (Schofield and Beebe, 2020). MOCs also send branches into the CN (Benson and Brown, 1990; Brown et al., 1991), and may be the source of cholinergic inputs onto T-stellate cell dendrites. As discussed above, cholinergic inputs to T-stellate cells have been shown to enhance the encoding of signal in noise (Fujino and Oertel, 2001), much like cholinergic inputs to the MNTB (Zhang et al., 2021). MOC branches in the CN may also serve to convey information about cochlear gain (Brown et al., 1988). If cholinergic innervation of the SOC comes in part from MOC branches, we would expect it to serve similar purposes, either enhancing signal in noise or conveying information about outer hair cell activation. Given the role of MOCs in modulating the cochlear amplifier, an intra-olivary projection might serve to modulate the SOC neuron threshold or gain to compensate for alterations in input from the ear.

Lateral olivocochlear cells (LOCs) are situated in lateral parts of the SOC and synapse in the cochlea on the afferent terminals of spiral ganglion neurons, where they meet inner hair cells (Schofield and Beebe, 2020). LOCs are more heterogeneous and less well-understood than MOCs, however, there is some evidence that they might send axon branches into the CN, and specifically to different regions of the CN than MOCs (Ryan et al., 1990). Even at the level of the cochlea where they have been most studied, the functions of LOCs are not well-understood (Frank and Goodrich, 2018).

The SOC also contains a group of small cholinergic cells in the VNTB that project to the CN and lack the characteristic morphology of MOCs (Sherriff and Henderson, 1994). Targets of these cells appear to include cells of the acoustic nerve nucleus,

suggesting a role in early (and rapid) responses to startling stimuli (Gómez-Nieto et al., 2008). Here, we demonstrate that the SOC receives cholinergic input from within the ipsilateral SOC and from the contralateral SOC, however, it is unclear which cholinergic groups (MOCs, LOCs, or non-olivocochlear) participate in these projections. Based on the wide mediolateral distribution of cholinergic SOC cells that make SOC projections, we hypothesize that multiple cholinergic groups in the SOC may be involved.

Cholinergic Cells in the PMT

Cholinergic cells of the PMT are implicated in a variety of processes. As part of the ascending reticular activating system, they are active during waking and REM sleep and less active during slow-wave sleep (Boucetta and Jones, 2009). PMT cells also function in motor control, sensory gating, reward association, and attention (Garcia-Rill, 1991; Winn, 2006; Yeomans et al., 2006). Activation of cholinergic PMT cells enhances the startle response, in keeping with its wider roles in arousal (Azzopardi et al., 2018). PMT projections to auditory nuclei might serve to generally increase auditory responses during periods of increased arousal or may have a more selective response, perhaps enhancing neuronal responses only to certain salient sounds.

Cholinergic PMT cells project to many auditory nuclei, including the medial geniculate body, the inferior colliculus, and the CN (Steriade et al., 1988; Motts and Schofield, 2010; Mellott et al., 2011). Many PMT cells respond to auditory stimuli, but in contrast to SOC neurons, the PMT neurons tend to be broadly tuned for frequency and often adapt quickly to a repeated stimulus (Reese et al., 1995a,b). Some PMT neurons show a longer latency response to auditory stimuli, perhaps related to descending inputs from the auditory cortex (Reese et al., 1995a,b; Schofield and Motts, 2009). Projections from the auditory cortex have been implicated in cortically-driven plasticity of subcortical auditory neurons, including neurons in the CN, IC, and MG (reviewed in Schofield and Beebe, 2019). The present results raise the question of cortically-driven cholinergic effects in the SOC.

Cholinergic Cells in the Lateral Paragigantocellular Nucleus (LPGi)

The LPGi is well connected to other auditory nuclei: it receives input from the CN, IC, and the auditory cortex, and it projects to the CN and the IC (Andrezik et al., 1981; Kandler and Herbert, 1991; Van Bockstaele et al., 1993; Bellintani-Guardia et al., 1996). However, none of these studies marked the cholinergic cells in the LPGi, so it is unclear to what extent they are involved in the auditory circuits. The LPGi contains other neurotransmitter phenotypes (e.g., serotonin, GABA) and some of these cells may correspond to the ChAT-negative LPGi cells labeled by the tracer in the present study, but again it is impossible to relate these projections to the physiology of the cells. Complicating speculation is the unclear relationship of the auditory components in LPGi vs. autonomic components (e.g., Carrive and Gorissen, 2008; Koganezawa et al., 2008; Dergacheva et al., 2010). Auditory functions may be focused in the rostral LPGi and autonomic functions more caudally, but this remains to be confirmed physiologically (Andrezik et al., 1981). Further insight into the functions of the cholinergic LPGi cells will require more data on the response properties of these cells and their specific targets in the SOC and other auditory nuclei.

Functions of Bilateral Innervation *via* Branching Cholinergic Axons

At its simplest level, a branching axon allows an individual neuron to influence two (or more) distant targets. Widespread axonal branching can allow for a relatively small population of neurons to exert effects across a large portion of a pathway, supporting global adjustments of neuronal sensitivity, for example, in response to an arousing stimulus. Such branching is common among modulatory systems, including cholinergic projections from the PMT (Descarries and Mechawar, 2008). Within the subcortical auditory system, cholinergic PMT cells can send collateral projections to targets on the two sides of the brain (e.g., left and right IC), to targets at different hierarchical levels of the auditory pathway (e.g., to IC and auditory thalamus), or to a combination (bilateral and multilevel; Schofield et al., 2011). Bilateral projections from individual PMT cholinergic cells to left and right SOC demonstrated in the present study, provide another example of widespread cholinergic projections. It will be interesting in future studies to determine whether these cholinergic cells also innervate other auditory structures, extending the span of PMT cholinergic projections from the SOC to, perhaps, the thalamus.

We also observed bilateral projections from SOC and LPGi cholinergic neurons. For further insight into their function, more information is needed about the cells giving rise to these projections. Under what conditions are these cells active? How broad are their projections within the SOC? Do they project to additional targets outside the SOC? While collateral branching could provide an opportunity for widespread effects, restricted projections may indicate highly specific effects on the target cells.

Conclusions

A key issue from the discussions above is that cholinergic projections from different sources are likely to serve different functions. Projections from the PMT are likely to be activated in association with arousal and top-down modulation, perhaps contributing to plasticity driven by higher functions. Projections from the SOC are more likely to be narrowly tuned for auditory stimulus parameters and to serve as a feedback function for the earliest stages of auditory processing, from the cochlea to CN and SOC. Some cholinergic functions may be similar across SOC nuclei (e.g., the need to adjust neuronal sensitivity in response to reduced afferent input), but other functions may be more narrow, associated with individual nuclei and especially with individual cell types. The plethora of ACh receptor types could allow for varied functions within and across nuclei. A key step for future studies will be to identify the receptor types associated with specific cell types and with specific auditory circuits. Another important step will be to

trace cholinergic pathways into the SOC with anterograde tracing methods. The retrograde tracing experiments here suggest widespread projections from each cholinergic area. Visualizing the terminations of each pathway will provide valuable information about the nuclei and cell types targeted by each source of cholinergic input.

DATA AVAILABILITY STATEMENT

The original contributions presented in the study are included in the article, further inquiries can be directed to the corresponding author.

ETHICS STATEMENT

The animal study was reviewed and approved by IACUC Lehigh University.

AUTHOR CONTRIBUTIONS

NB, CZ, RB, and BS performed the research. NB, CZ, RB, and BS wrote the manuscript. All authors contributed to the article and approved the submitted version.

FUNDING

This work was funded from grants NIH R15 DC016461 to RB and NIH R01 DC004391 to BS, and from a CAS graduate student research grant and Gordon C. Thorne Fellowship awarded to CZ from Lehigh University.

ACKNOWLEDGMENTS

We thank Nina Lenkey and Colleen Sowick for expert technical assistance.

REFERENCES

Adams, J. C., and Mugnaini, E. (1990). Immunocytochemical evidence for inhibitory and disinhibitory circuits in the superior olive. *Hear. Res.* 49, 281–298. doi: 10.1016/0378-5955(90)90109-3

Albrecht, O., Dondzillo, A., Mayer, F., Thompson, J. A., and Klug, A. (2014). Inhibitory projections from the ventral nucleus of the trapezoid body to the medial nucleus of the trapezoid body in the mouse. *Front. Neural Circuits* 8:83. doi: 10.3389/fncir.2014.00083

Andrezik, J. A., Chan-Palay, V., and Palay, S. L. (1981). The nucleus paragigantocellularis lateralis in the rat. Demonstration of afferents by the retrograde transport of horseradish peroxidase. *Anat. Embryol. (Berl)* 161, 373–390. doi: 10.1007/BF00316049

Aschoff, A., Muller, M., and Ott, H. (1988). Origin of cochlea efferents in some gerbil species. A comparative anatomical study with fluorescent tracers. *Exp. Brain. Res.* 71, 252–261. doi: 10.1007/BF00247485

Azzopardi, E., Louttit, A. G., DeOliveira, C., Laviolette, S. R., and Schmid, S. (2018). The role of cholinergic midbrain neurons in startle and prepulse inhibition. *J. Neurosci.* 38, 8798–8808. doi: 10.1523/JNEUROSCI.0984-18.2018

Banks, M. I., and Smith, P. H. (1992). Intracellular recordings from neurobiotin-labeled cells in brain slices of the rat medial nucleus of the trapezoid body. *J. Neurosci.* 12, 2819–2837. doi: 10.1523/JNEUROSCI.12-07-02819.1992

Bellintani-Guardia, B., Schweizer, M., and Herbert, H. (1996). Analysis of projections from the cochlear nucleus to the lateral paragigantocellular reticular nucleus in the rat. *Cell Tissue Res.* 283, 493–505. doi: 10.1007/s004410050560

Benson, T. E., and Brown, M. C. (1990). Synapses formed by olivocochlear axon branches in the mouse cochlear nucleus. *J. Comp. Neurol.* 295, 52–70. doi: 10.1002/cne.902950106

Boucetta, S., Cisse, Y., Mainville, L., Morales, M., and Jones, B. E. (2014). Discharge profiles across the sleep-waking cycle of identified cholinergic, GABAergic and glutamatergic neurons in the pontomesencephalic tegmentum of the rat. *J. Neurosci.* 34, 4708–4727. doi: 10.1523/JNEUROSCI.2617-13.2014

Boucetta, S., and Jones, B. E. (2009). Activity profiles of cholinergic and intermingled GABAergic and putative glutamatergic neurons in the pontomesencephalic tegmentum of urethane-anesthetized rats. *J. Neurosci.* 29, 4664–4674. doi: 10.1523/JNEUROSCI.5502-08.2009

Boudreau, J. C., and & Tsuchitani, C. (1968). Binaural interaction in the cat superior olive S segment. *J Neurophysiol* 31, 442–454. doi: 10.1152/jn.1968.31.3.442

Brown, M. C., Liberman, M. C., Benson, T. E., and Ryugo, D. K. (1988). Brainstem branches from olivocochlear axons in cats and rodents. *J. Comp. Neurol.* 278, 591–603. doi: 10.1002/cne.902780410

Brown, M. C., Pierce, S., and Berglund, A. M. (1991). Cochlear-nucleus branches of thick (medial) olivocochlear fibers in the mouse: a cochleotopic projection. *J. Comp. Neurol.* 303, 300–315. doi: 10.1002/cne.903030211

Brugge, J. F., and Geisler, C. D. (1978). Auditory mechanisms of the lower brainstem. *Annu. Rev. Neurosci.* 1, 363–394. doi: 10.1146/annurev.ne.01.030178.002051

Cant, N. B., and Casseday, J. H. (1986). Projections from the anteroventral cochlear nucleus to the lateral and medial superior olivary nuclei. *J. Comp. Neurol.* 247, 457–476. doi: 10.1002/cne.902470406

Carrive, P., and Gorissen, M. (2008). Premotor sympathetic neurons of conditioned fear in the rat. *Eur. J. Neurosci.* 28, 428–446. doi: 10.1111/j.1460-9568.2008.06351.x

Chen, K., Waller, H. J., and Godfrey, D. A. (1998). Effects of endogenous acetylcholine on spontaneous activity in rat dorsal cochlear nucleus slices. *Brain Res.* 783, 219–226. doi: 10.1016/s0006-8993(97)01348-6

Ciuman, R. R. (2010). The efferent system or olivocochlear function bundle - fine regulator and protector of hearing perception. *Int. J. Biomed. Sci.* 6, 276–288.

Clarke, P. B., Schwartz, R. D., Paul, S. M., Pert, C. B., and Pert, A. (1985). Nicotinic binding in rat brain: autoradiographic comparison of [3H]acetylcholine, [3H]nicotine and [125I]-alpha-bungarotoxin. *J. Neurosci.* 5, 1307–1315. doi: 10.1523/JNEUROSCI.05-05-01307.1985

Dergacheva, O., Wang, X., Lovett-Barr, M. R., Jameson, H., and Mendelowitz, D. (2010). The lateral paragigantocellular nucleus modulates parasympathetic cardiac neurons: a mechanism for rapid eye movement sleep-dependent changes in heart rate. *J. Neurophysiol.* 104, 685–694. doi: 10.1152/jn.00228.2010

Descarries, L., and Mechawar, N. (2008). "Structural organization of monoamine and acetylcholine neuron systems in the rat CNS," in *Handbook of Neurochemistry and Molecular Neurobiology*, eds A. Lajtha and E. S. Vizi (New York: Springer), 1–20.

Farley, G. R., Morley, B. J., Javel, E., and Gorga, M. P. (1983). Single-unit responses to cholinergic agents in the rat inferior colliculus. *Hear. Res.* 11, 73–91. doi: 10.1016/0378-5955(83)90046-1

Felix, R. A., Chavez, V. A., Novicio, D. M., Morley, B. J., and Portfors, C. V. (2019). Nicotinic acetylcholine receptor subunit α_7-knockout mice exhibit degraded auditory temporal processing. *J. Neurophysiol.* 122, 451–465. doi: 10.1152/jn.00170.2019

Fernández de Sevilla, D., Núñez, A., and Buño, W. (2020). Muscarinic receptors, from synaptic plasticity to its role in network activity. *Neuroscience* 456, 60–70. doi: 10.1590/1519-6984.245386

Fischl, M. J., Combs, T. D., Klug, A., Grothe, B., and Burger, R. M. (2012). Modulation of synaptic input by $GABA_B$ receptors improves coincidence detection for computation of sound location: $GABA_B$-dependent modulation improves coincidence detection. *J. Physiol.* 590, 3047–3066. doi: 10.1113/jphysiol.2011.226233

Fitzgerald, K. K., and Sanes, D. H. (1999). Serotonergic modulation of synapses in the developing gerbil lateral superior olive. *J. Neurophysiol.* 81, 2743–2752. doi: 10.1152/jn.1999.81.6.2743

Frank, M. M., and Goodrich, L. V. (2018). Talking back: development of the olivocochlear efferent system. *Wiley Interdiscip. Rev. Dev. Biol.* 7:e324. doi: 10.1002/wdev.324

Fujino, K., and Oertel, D. (2001). Cholinergic modulation of stellate cells in the mammalian ventral cochlear nucleus. *J. Neurosci.* 21, 7372–7383. doi: 10.1523/JNEUROSCI.21-18-07372.2001

Gahring, L. C., Persiyanov, K., and Rogers, S. W. (2004). Neuronal and astrocyte expression of nicotinic receptor subunit beta4 in the adult mouse brain. *J. Comp. Neurol.* 468, 322–333. doi: 10.1002/cne.10942

Garcia-Rill, E. (1991). The pedunculopontine nucleus. *Prog. Neurobiol.* 36, 363–389. doi: 10.1016/0301-0082(91)90016-t

Gharpure, A., Noviello, C. M., and Hibbs, R. E. (2020). Progress in nicotinic receptor structural biology. *Neuropharmacology* 171:108086. doi: 10.1016/j.neuropharm.2020.108086

Glendenning, K. K., and Baker, B. N. (1988). Neuroanatomical distribution of receptors for three potential inhibitory neurotransmitters in the brainstem auditory nuclei of the cat. *J. Comp. Neurol.* 275, 288–308. doi: 10.1002/cne.902750210

Goldberg, J. M., and & Brown, P. B. (1969). Response of binaural neurons of dog superior olivary complex to dichotic tonal stimuli: some physiological mechanisms of sound localization. *J. Neurophysiol.* 32, 613–636. doi: 10.1152/jn.1969.32.4.613

Gómez-Nieto, R., Horta-Junior, J. A., Castellano, O., Herrero-Turrion, M. J., Rubio, M. E., and Lopez, D. E. (2008). Neurochemistry of the afferents to the rat cochlear root nucleus: possible synaptic modulation of the acoustic startle. *Neuroscience* 154, 51–64. doi: 10.1016/j.neuroscience.2008.01.079

Goyer, D., Kurth, S., Gillet, C., Keine, C., Rübsamen, R., and Kuenzel, T. (2016). Slow cholinergic modulation of spike probability in ultra-fast time-coding sensory neurons. *Eneuro* 3:ENEURO.0186-16.2016. doi: 10.1523/ENEURO.0186-16.2016

Grothe, B., and Pecka, M. (2014). The natural history of sound localization in mammals–a story of neuronal inhibition. *Front. Neural Circuits* 8:116. doi: 10.3389/fncir.2014.00116

Grothe, B., Pecka, M., and McAlpine, D. (2010). Mechanisms of sound localization in mammals. *Physiol. Rev.* 90, 983–1012. doi: 10.1152/physrev.00026.2009

Grothe, B., and Sanes, D. H. (1993). Bilateral inhibition by glycinergic afferents in the medial superior olive. *J. Neurophysiol.* 69, 1192–1196. doi: 10.1152/jn.1993.69.4.1192

Guinan, J. J. Jr., and Li, R. Y. (1990). Signal processing in brainstem auditory neurons which receive giant endings (calyces of Held) in the medial nucleus of the trapezoid body of the cat. *Hear Res.* 49, 321–334. doi: 10.1016/0378-5955(90)90111-2

Habbicht, H., and Vater, M. (1996). A microiontophoretic study of acetylcholine effects in the inferior colliculus of horseshoe bats: implications for a modulatory role. *Brain Res.* 724, 169–179. doi: 10.1016/0006-8993(96)00224-7

Happe, H. K., and Morley, B. J. (2004). Distribution and postnatal development of alpha 7 nicotinic acetylcholine receptors in the rodent lower auditory brainstem. *Brain Res. Dev. Brain Res.* 153, 29–37. doi: 10.1016/j.devbrainres.2004.07.004

Harrison, J. M., and Feldman, M. L. (1970). "Anatomical aspects of the cochlear nucleus and superior olivary complex," in *Contributions to Sensory Physiology Volume 4*, ed W. D. Neff (New York: Academic Press), 95–142.

Hassfurth, B., Grothe, B., and & Koch, U. (2010). The mammalian interaural time difference detection circuit is differentially controlled by GABAB receptors during development. *J. Neurosci.* 30, 9715–9727. doi: 10.1523/JNEUROSCI.1552-10.2010

Helfert, R. H., and Aschoff, A. (1996). "Superior Olivary Complex and Nuclei of the Lateral Lemniscus," in *The Central Auditory Brain*, eds G. Ehret and R. Romand (Oxford: Oxford University Press), 193–258.

Hunt, S., and Schmidt, J. (1978). Some observations on the binding patterns of alpha-bungarotoxin in the central nervous system of the rat. *Brain Res.* 157, 213–232. doi: 10.1016/0006-8993(78)90025-2

Kamiya, H., Itoh, K., Yasui, Y., Ino, T., and Mizuno, N. (1988). Somatosensory and auditory relay nucleus in the rostral part of the ventrolateral medulla: a morphological study in the cat. *J. Comp. Neurol.* 273, 421–435. doi: 10.1002/cne.902730311

Kandler, K., and Herbert, H. (1991). Auditory projections from the cochlear nucleus to pontine and mesencephalic reticular nuclei in the rat. *Brain Res.* 562, 230–242. doi: 10.1016/0006-8993(91)90626-7

Katz, L. C., Burkhalter, A., and Dreyer, W. J. (1984). Fluorescent latex microspheres as a retrograde neuronal marker for *in vivo* and *in vitro* studies of visual cortex. *Nature* 310, 498–500. doi: 10.1038/310498a0

Koganezawa, T., Shimomura, Y., and Terui, N. (2008). The role of the RVLM neurons in the viscero-sympathetic reflex: a mini review. *Auton. Neurosci.* 142, 17–19. doi: 10.1016/j.autneu.2008.03.007

Koka, K., and Tollin, D. J. (2014). Linear coding of complex sound spectra by discharge rate in neurons of the medial nucleus of the trapezoid body (MNTB) and its inputs. *Front. Neural Circuits* 8:144. doi: 10.3389/fncir.2014.00144

Kopp-Scheinpflug, C., Tolnai, S., Malmierca, M. S., and Rubsamen, R. (2008). The medial nucleus of the trapezoid body: comparative physiology. *Neuroscience* 154, 160–170. doi: 10.1016/j.neuroscience.2008.01.088

Kopp-Scheinpflug, C., Tozer, A. J., Robinson, S. W., Tempel, B. L., Hennig, M. H., and Forsythe, I. D. (2011). The sound of silence: ionic mechanisms encoding sound termination. *Neuron* 71, 911–925. doi: 10.1016/j.neuron.2011.06.028

Kroeger, D., Ferrari, L. L., Petit, G., Mahoney, C. E., Fuller, P. M., Arrigoni, E., et al. (2017). Cholinergic, glutamatergic and GABAergic neurons of the pedunculopontine tegmental nucleus have distinct effects on sleep/wake behavior in mice. *J. Neurosci.* 37, 1352–1366. doi: 10.1523/JNEUROSCI.1405-16.2016

Kuenzel, T. (2019). Modulatory influences on time-coding neurons in the ventral cochlear nucleus. *Hear. Res.* 384:107824. doi: 10.1016/j.heares.2019.107824

Kuwabara, N., DiCaprio, R. A., and Zook, J. M. (1991). Afferents to the medial nucleus of the trapezoid body and their collateral projections. *J. Comp. Neurol.* 314, 684–706. doi: 10.1002/cne.903140405

Mansour, Y., Ahmed, S. N., and Kulesza, R. (2021). Abnormal morphology and subcortical projections to the medial geniculate in an animal model of autism. *Exp. Brain Res.* 239, 381–400. doi: 10.1007/s00221-020-05982-w

Mellott, J. G., Beebe, N. L., and Schofield, B. R. (2018). GABAergic and non-GABAergic projections to the superior colliculus from the auditory brainstem. *Brain Struct. Funct.* 223, 1923–1936. doi: 10.1007/s00429-017-1599-4

Mellott, J. G., Motts, S. D., and Schofield, B. R. (2011). Multiple origins of cholinergic innervation of the cochlear nucleus. *Neuroscience* 180, 138–147. doi: 10.1016/j.neuroscience.2011.02.010

Mesulam, M. M., Mufson, E. J., Wainer, B. H., and Levey, A. I. (1983). Central cholinergic pathways in the rat:an overview based on an alternative nomenclature (Ch1–Ch6). *Neuroscience* 10, 1185–1201. doi: 10.1016/0306-4522(83)90108-2

Metherate, R. (2011). Functional connectivity and cholinergic modulation in auditory cortex. *Neurosci. Biobehav. Rev.* 35, 2058–2063. doi: 10.1016/j.neubiorev.2010.11.010

Morley, B. J., and Happe, H. K. (2000). Cholinergic receptors: dual roles in transduction and plasticity. *Hear. Res.* 147, 104–112. doi: 10.1016/s0378-5955(00)00124-6

Morley, B. J., Lorden, J. F., Brown, G. B., Kemp, G. E., and Bradley, R. J. (1977). Regional distribution of nicotinic acetylcholine receptor in rat brain. *Brain. Res.* 134, 161–166. doi: 10.1016/0006-8993(77)90935-0

Motts, S. D., and Schofield, B. R. (2010). Cholinergic and non-cholinergic projections from the pedunculopontine and laterodorsal tegmental nuclei to the medial geniculate body in guinea pigs. *Front. Neuroanat.* 4:137. doi: 10.3389/fnana.2010.00137

Motts, S. D., Slusarczyk, A. S., Sowick, C. S., and Schofield, B. R. (2008). Distribution of cholinergic cells in guinea pig brainstem. *Neuroscience* 154, 186–195. doi: 10.1016/j.neuroscience.2007.12.017

Oertel, D., Wright, S., Cao, X. J., Ferragamo, M., and Bal, R. (2011). The multiple functions of T stellate/multipolar/chopper cells in the ventral cochlear nucleus. *Hear. Res.* 276, 61–69. doi: 10.1016/j.heares.2010.10.018

Pecka, M., Brand, A., Behrend, O., and Grothe, B. (2008). Interaural time difference processing in the mammalian medial superior olive: the role of glycinergic inhibition. *J. Neurosci.* 28, 6914–6925. doi: 10.1523/JNEUROSCI.1660-08.2008

Reese, N. B., Garcia-Rill, E., and Skinner, R. D. (1995a). Auditory input to the pedunculopontine nucleus: I. Evoked potentials. *Brain. Res. Bull.* 37, 257–264. doi: 10.1016/0361-9230(95)00002-v

Reese, N. B., Garcia-Rill, E., and Skinner, R. D. (1995b). Auditory input to the pedunculopontine nucleus: II. Unit responses. *Brain. Res. Bull.* 37, 265–273. doi: 10.1016/0361-9230(95)00001-u

Ryan, A. F., Keithley, E. M., Wang, Z.-X., and Schwartz, I. R. (1990). Collaterals from lateral and medial olivocochlear efferent neurons innervate different regions of the cochlear nucleus and adjacent brainstem. *J. Comp. Neurol.* 300, 572–582. doi: 10.1002/cne.903000410

Safieddine, S., Bartolami, S., Wenthold, R. J., and Eybalin, M. (1996). Pre- and postsynaptic M3 muscarinic receptor mRNAs in the rodent peripheral auditory system. *Mol. Brain Res.* 40, 127–135. doi: 10.1016/0169-328x(96)00047-2

Schofield, B. R. (2008). Retrograde axonal tracing with fluorescent markers. *Curr. Protoc. Neurosci.* 43:117. doi: 10.1002/0471142301.ns0117s43

Schofield, B. R., Mellott, J. G., and Motts, S. D. (2014). Subcollicular projections to the auditory thalamus and collateral projections to the inferior colliculus. *Front. Neuroanat.* 8:70. doi: 10.3389/fnana.2014.00070

Schofield, B. R., and Beebe, N. L. (2019). "Descending auditory pathways and plasticity," in *The Oxford Handbook of the Auditory Brainstem*, ed K. Kandler (Oxford: Oxford University Press), 610–638.

Schofield, B. R., and Beebe, N. L. (2020). "The efferent auditory system: central pathways that modulate peripheral input," in *Reference Module in Neuroscience and Biobehavioral Psychology* (Amsterdam, Netherlands: Elsevier).

Schofield, B. R., and Cant, N. B. (1991). Organization of the superior olivary complex in the guinea pig. I. Cytoarchitecture, cytochrome oxidase histochemistry and dendritic morphology. *J. Comp. Neurol.* 314, 645–670. doi: 10.1002/cne.903140403

Schofield, B. R., and Hurley, L. (2018). "Circuits for modulation of auditory function," in *Springer Handbook of Auditory Research: The Mammalian Auditory Pathways*, eds D. L. Oliver, N. B. Cant, R. R. Fay, and A. N. Popper (New York: Springer International Publishing), 235–267.

Schofield, B. R., and Motts, S. D. (2009). Projections from auditory cortex to cholinergic cells in the midbrain tegmentum of guinea pigs. *Brain Res. Bull.* 80, 163–170. doi: 10.1016/j.brainresbull.2009.06.015

Schofield, B. R., Motts, S. D., and Mellott, J. G. (2011). Cholinergic cells of the pontomesencephalic tegmentum: connections with auditory structures from cochlear nucleus to cortex. *Hear. Res.* 279, 85–95. doi: 10.1016/j.heares.2010.12.019

Schofield, B. R., Schofield, R. M., Sorensen, K. A., and Motts, S. D. (2007). On the use of retrograde tracers for identification of axon collaterals with multiple fluorescent retrograde tracers. *Neuroscience* 146, 773–783. doi: 10.1016/j.neuroscience.2007.02.026

Sherriff, F. E., and Henderson, Z. (1994). Cholinergic neurons in the ventral trapezoid nucleus project to the cochlear nuclei in the rat. *Neuroscience* 58, 627–633. doi: 10.1016/0306-4522(94)90086-8

Smith, P. H., Joris, P. X., and Yin, T. C. (1998). Anatomy and physiology of principal cells of the medial nucleus of the trapezoid body (MNTB) of the cat. *J. Neurophysiol.* 79, 3127–3142. doi: 10.1152/jn.1998.79.6.3127

Song, P., Yang, Y., Barnes-Davies, M., Bhattacharjee, A., Hamann, M., Forsythe, I. D., et al. (2005). Acoustic environment determines phosphorylation state of the Kv3.1 potassium channel in auditory neurons. *Nat. Neurosci.* 8, 1335–1342. doi: 10.1038/nn1533

Sottile, S. Y., Hackett, T. A., Cai, R., Ling, L., Llano, D. A., Caspary, D. M., et al. (2017a). Presynaptic neuronal nicotinic receptors differentially shape select inputs to auditory thalamus and are negatively impacted by aging. *J. Neurosci.* 37, 11377–11389. doi: 10.1523/JNEUROSCI.1795-17.2017

Sottile, S. Y., Ling, L., Cox, B. C., and Caspary, D. M. (2017b). Impact of ageing on postsynaptic neuronal nicotinic neurotransmission in auditory thalamus. *J. Physiol.* 595, 5375–5385. doi: 10.1113/JP274467

Stefanescu, R. A., and Shore, S. E. (2017). Muscarinic acetylcholine receptors control baseline activity and Hebbian stimulus timing-dependent plasticity in fusiform cells of the dorsal cochlear nucleus. *J. Neurophysiol.* 117, 1229–1238. doi: 10.1152/jn.00270.2016

Steriade, M., Paré, D., Parent, A., and Smith, Y. (1988). Projections of cholinergic and non-cholinergic neurons of the brainstem core to relay and associational thalamic nuclei in the cat and macaque monkey. *Neuroscience* 25, 47–67. doi: 10.1016/0306-4522(88)90006-1

Stornetta, R. L., Macon, C. J., Nguyen, T. M., Coates, M. B., and Guyenet, P. G. (2013). Cholinergic neurons in the mouse rostral ventrolateral medulla target sensory afferent areas. *Brain Struct. Funct.* 218, 455–475. doi: 10.1007/s00429-012-0408-3

Taranda, J., Maison, S. F., Ballestero, J. A., Katz, E., Savino, J., Vetter, D. E., et al. (2009). A point mutation in the hair cell nicotinic cholinergic receptor prolongs cochlear inhibition and enhances noise protection. *PLoS Biol.* 7:e18. doi: 10.1371/journal.pbio.1000018

Thompson, A. M., and Schofield, B. R. (2000). Afferent projections of the superior olivary complex. *Microsc. Res. Tech.* 51, 330–354. doi: 10.1002/1097-0029(20001115)51:4<330::AID-JEMT4>3.0.CO;2-X

Tollin, D. J., and Yin, T. C. (2002). The coding of spatial location by single units in the lateral superior olive of the cat. I. Spatial receptive fields in azimuth. *J Neurosci.* 22, 1454–1467. doi: 10.1523/JNEUROSCI.22-04-01454.2002

Van Bockstaele, E. J., Akaoka, H., and Aston-Jones, G. (1993). Brainstem afferents to the rostral (juxtafacial) nucleus paragigantocellularis: integration of exteroceptive and interoceptive sensory inputs in the ventral tegmentum. *Brain Res.* 603, 1–18. doi: 10.1016/0006-8993(93)91293-2

Wada, E., Wada, K., Boulter, J., Deneris, E., Heinemann, S., Patrick, J., et al. (1989). Distribution of alpha2, alpha3, alpha4 and beta2 neuronal nicotinic receptor subunit mRNAs in the central nervous system: a hybridization histochemical study in the rat. *J. Comp. Neurol.* 284, 314–335. doi: 10.1002/cne.902840212

Wang, H. L., and Morales, M. (2009). Pedunculopontine and laterodorsal tegmental nuclei contain distinct populations of cholinergic, glutamatergic and GABAergic neurons in the rat. *Eur. J. Neurosci.* 29, 340–358. doi: 10.1111/j.1460-9568.2008.06576.x

Winn, P. (2006). How best to consider the structure and function of the pedunculopontine tegmental nucleus: Evidence from animal studies. *J. Neurol. Sci.* 248, 234–250. doi: 10.1016/j.jns.2006.05.036

Woolf, N. J., and Butcher, L. L. (1986). Cholinergic systems in the rat brain: III. Projections from the pontomesencephalic tegmentum to the thalamus, tectum, basal ganglia and basal forebrain. *Brain Res. Bull.* 16, 603–637. doi: 10.1016/0361-9230(86)90134-6

Yao, W., and Godfrey, D. A. (1997). Densitometric evaluation of markers for cholinergic transmission in rat superior olivary complex. *Neurosci. Lett.* 229, 21–24. doi: 10.1016/s0304-3940(97)00400-x

Yeomans, J. S., Lee, J., Yeomans, M. H., Steidl, S., and Li, L. (2006). Midbrain pathways for prepulse inhibition and startle activation in rat. *Neuroscience* 142, 921–929. doi: 10.1016/j.neuroscience.2006.06.025

Yin, T. C., and Chan, J. C. (1990). Interaural time sensitivity in medial superior olive of cat. *J Neurophysiol.* 64, 465–488. doi: 10.1152/jn.1990.64.2.465

Zhang, C., Beebe, N. L., Schofield, B. R., Pecka, M., and Burger, R. M. (2021). Endogenous cholinergic signaling modulates sound-evoked responses of the medial nucleus of the trapezoid body. *J. Neurosci.* 41, 674–688. doi: 10.1523/JNEUROSCI.1633-20.2020

Zhang, J. S., and Kaltenbach, J. A. (2000). Modulation of spontaneous activity by acetylcholine receptors in the rat dorsal cochlear nucleus *in vivo*. *Hear. Res.* 140, 7–17. doi: 10.1016/s0378-5955(99)00181-1

Zhao, Y., and Tzounopoulos, T. (2011). Physiological activation of cholinergic inputs controls associative synaptic plasticity *via* modulation of endocannabinoid signaling. *J. Neurosci.* 31, 3158–3168. doi: 10.1523/JNEUROSCI.5303-10.2011

Conflict of Interest: The authors declare that the research was conducted in the absence of any commercial or financial relationships that could be construed as a potential conflict of interest.

frontiers in Neural Circuits

ORIGINAL RESEARCH
published: 09 August 2021
doi: 10.3389/fncir.2021.709387

$\alpha_3\beta_4$* Nicotinic Acetylcholine Receptors Strongly Modulate the Excitability of VIP Neurons in the Mouse Inferior Colliculus

*Luis M. Rivera-Perez, Julia T. Kwapiszewski and Michael T. Roberts**

Kresge Hearing Research Institute, Department of Otolaryngology – Head and Neck Surgery, University of Michigan, Ann Arbor, MI, United States

The inferior colliculus (IC), the midbrain hub of the central auditory system, receives extensive cholinergic input from the pontomesencephalic tegmentum. Activation of nicotinic acetylcholine receptors (nAChRs) in the IC can alter acoustic processing and enhance auditory task performance. However, how nAChRs affect the excitability of specific classes of IC neurons remains unknown. Recently, we identified vasoactive intestinal peptide (VIP) neurons as a distinct class of glutamatergic principal neurons in the IC. Here, in experiments using male and female mice, we show that cholinergic terminals are routinely located adjacent to the somas and dendrites of VIP neurons. Using whole-cell electrophysiology in brain slices, we found that acetylcholine drives surprisingly strong and long-lasting excitation and inward currents in VIP neurons. This excitation was unaffected by the muscarinic receptor antagonist atropine. Application of nAChR antagonists revealed that acetylcholine excites VIP neurons mainly via activation of $\alpha_3\beta_4$* nAChRs, a nAChR subtype that is rare in the brain. Furthermore, we show that acetylcholine excites VIP neurons directly and does not require intermediate activation of presynaptic inputs that might express nAChRs. Lastly, we found that low frequency trains of acetylcholine puffs elicited temporal summation in VIP neurons, suggesting that *in vivo*-like patterns of cholinergic input can reshape activity for prolonged periods. These results reveal the first cellular mechanisms of nAChR regulation in the IC, identify a functional role for $\alpha_3\beta_4$* nAChRs in the auditory system, and suggest that cholinergic input can potently influence auditory processing by increasing excitability in VIP neurons and their postsynaptic targets.

Keywords: inferior colliculus, neuromodulation, acetylcholine, nicotinic acetylcholine receptors, auditory system, VIP neurons, pharmacology

OPEN ACCESS

Edited by:
Conny Kopp-Scheinpflug, Ludwig Maximilian University of Munich, Germany

Reviewed by:
Michael Pecka, Ludwig Maximilian University of Munich, Germany
Gunsoo Kim, Korea Brain Research Institute, South Korea

***Correspondence:**
Michael T. Roberts
microb@umich.edu

Received: *13 May 2021*
Accepted: *19 July 2021*
Published: *09 August 2021*

Citation:
Rivera-Perez LM, Kwapiszewski JT and Roberts MT (2021) $\alpha_3\beta_4$ Nicotinic Acetylcholine Receptors Strongly Modulate the Excitability of VIP Neurons in the Mouse Inferior Colliculus. Front. Neural Circuits 15:709387. doi: 10.3389/fncir.2021.709387*

INTRODUCTION

Growing evidence indicates that cholinergic signaling through nicotinic acetylcholine receptors (nAChRs) critically shapes sound processing in the central auditory system (Goyer et al., 2016; Askew et al., 2017; Felix et al., 2019; Zhang et al., 2021). The inferior colliculus (IC), the midbrain hub of the central auditory system, receives extensive input from cholinergic neurons in the pontomesencephalic tegmentum (PMT; Motts and Schofield, 2009), and expresses several nAChR

subunits, including α_3, α_4, α_7, β_2, β_3, and β_4 (Clarke et al., 1985; Wada et al., 1989; Morley and Happe, 2000; Whiteaker et al., 2002; Salas et al., 2003; Gahring et al., 2004; Happe and Morley, 2004; Bieszczad et al., 2012; Sottile et al., 2017). Because activity in the PMT is influenced by the sleep-wake cycle, attention, rewards, and sensory novelty, it is hypothesized that PMT neurons regulate auditory processing in the IC as a function of behavioral state (Jones, 1991; Kozak et al., 2005; Schofield et al., 2011; Boucetta et al., 2014). Consistent with this, *in vivo* studies have shown that nicotinic drugs alter the gain of input-output functions in IC neurons (Farley et al., 1983; Habbicht and Vater, 1996), and human psychophysics studies indicate that nicotine improves performance in auditory attention and discrimination tasks (Knott et al., 2012; Smucny et al., 2016; Pham et al., 2020), an effect partly attributable to alterations in the IC (Askew et al., 2017). In addition, temporal coding of auditory stimuli is degraded in the IC of α_7 knockout mice (Felix et al., 2019). However, despite the importance of nAChRs to auditory processing, the cellular mechanisms by which nAChRs influence the excitability IC neurons remain largely unknown.

This gap in knowledge has eluded the field mostly due to the complexity of the neuronal populations in the IC, where it has proven difficult to identify and study specific neuron classes using conventional approaches. We recently overcame this obstacle, identifying vasoactive intestinal peptide (VIP) neurons as the first molecularly identifiable neuron class in the IC (Goyer et al., 2019). Vasoactive intestinal peptide neurons are found throughout the major IC subdivisions, they are glutamatergic, and they have a stellate morphology with spiny dendrites that, within the central nucleus of the IC (ICc), typically extend across two or more isofrequency laminae. Vasoactive intestinal peptide neurons project to several auditory regions, including the auditory thalamus, superior olivary complex, and the contralateral IC, and they receive input from the dorsal cochlear nucleus, the contralateral IC, and likely from other sources. By using the VIP-IRES-Cre mouse model, we can selectively target VIP neurons for electrophysiological and anatomical experiments. Thus, we are in a position for the first time to determine the cellular mechanisms of cholinergic signaling in a defined class of IC neurons.

Here, we hypothesized that the excitability of VIP neurons in the IC is modulated by cholinergic signaling. Using immunofluorescence, we showed that cholinergic terminals are frequently located in close proximity to VIP neurons, suggesting that VIP neurons receive direct cholinergic input. We then found that brief applications of ACh elicited surprisingly long periods of depolarization and spiking in VIP neurons. These responses were not affected by atropine, a muscarinic acetylcholine receptor (mAChR) antagonist, but were largely blocked by mecamylamine, an antagonist partially selective for β_4-containing receptors, and by SR16584, an antagonist selective for $\alpha_3\beta_4$* receptors (* *indicates that the identity of the fifth subunit in the receptor pentamer is unknown*). Consistent with this, voltage clamp recordings showed that ACh puffs led to prolonged inward currents that were largely blocked by mecamylamine and by SR16584. Moreover, cholinergic responses were resistant to manipulations affecting synaptic transmission, indicating that the nAChRs mediating these responses are expressed by VIP neurons. Finally, we showed that 10 and 30 Hz trains of lower concentration ACh puffs elicited temporal summation in VIP neurons, suggesting that the *in vivo* firing patterns of cholinergic PMT neurons are likely to drive prolonged excitation of VIP neurons. We thus provide the first evidence that $\alpha_3\beta_4$* nAChRs, a subtype with limited distribution in the brain, elicit direct and potent excitation of IC VIP neurons. Combined, our data reveal that cholinergic modulation exerts a surprisingly potent and long-lasting increase in the excitability of an important class of IC principal neurons.

MATERIALS AND METHODS

Animals

All experiments were approved by the University of Michigan Institutional Animal Care and Use Committee and were in accordance with NIH guidelines for the care and use of laboratory animals. Animals were kept on a 12-h day/night cycle with *ad libitum* access to food and water. VIP-IRES-Cre mice (*Vip*$^{TM1(cre)Zjh}$/J, Jackson Laboratory, stock # 010908) (Taniguchi et al., 2011) were crossed with Ai14 reporter mice (B6.Cg-*Gt(ROSA)26Sor*$^{TM14(CAG-tdTomato)Hze}$/J, Jackson Laboratory, stock #007914) (Madisen et al., 2010) to yield F1 offspring that expressed the fluorescent protein tdTomato in VIP neurons. Because mice on the C57BL/6J background undergo age-related hearing loss, experiments were restricted to mice aged P30 – P85, an age range where hearing loss should be minimal or not present (Zheng et al., 1999).

Immunofluorescence

Mice aged P53 – P85 were deeply anesthetized with isoflurane and perfused transcardially with 0.1 M phosphate-buffered saline (PBS), pH 7.4, for 1 min and then with a 10% buffered formalin solution (Millipore Sigma, cat# HT501128) for 15 min. Brains were collected and post-fixed in the same formalin solution and cryoprotected overnight at 4°C in 0.1 M PBS containing 20% sucrose. Brains were cut into 40 μm sections on a vibratome. Sections were rinsed in 0.1 M PBS, and then treated with 10% normal donkey serum (Jackson ImmunoResearch Laboratories, West Grove, PA) and 0.3% TritonX-100 for 2 h. Slices were incubated overnight at 4°C in rabbit anti-VAChT (3:500, Synaptic Systems, cat# 139103, RRID:AB_887864). This antibody was previously validated by Western blot and has been successfully used to identify cholinergic terminals in the cochlear nucleus and hippocampus (Goyer et al., 2016; Gillet et al., 2018; Zhang et al., 2019). The next day, sections were rinsed in 0.1 M PBS and incubated in Alexa Fluor 647-tagged donkey anti-rabbit IgG (1:500, ThermoFisher, cat# A-31573) for 2 h at room temperature. Sections were then mounted on slides (SouthernBiotech, cat# SLD01-BX) and coverslipped using Fluoromount-G (SouthernBiotech, cat# 0100–01). Images were collected using a 1.40 NA 63x oil-immersion objective and 0.1 μm Z-steps on a Leica TCS SP8 laser scanning confocal microscope.

Analysis of Cholinergic Terminals Adjacent to VIP Neurons

After immunofluorescence was performed, we used Neurolucida 360 software (MBF Bioscience) to reconstruct VIP neurons and assess the distribution of cholinergic terminals on reconstructed neurons. Terminals that were <2 μm from the dendrites or soma of the reconstructed cell were counted as synapses onto that neuron.

Brain Slice Preparation

Whole-cell patch-clamp recordings were performed in acutely prepared brain slices from VIP-IRES-Cre x Ai14 mice. Both males (n = 40) and females (n = 31) aged P30-P50 were used. No differences were observed between animals of different sexes. Mice were deeply anesthetized with isoflurane and then rapidly decapitated. The brain was removed, and a tissue block containing the IC was dissected in 34°C ACSF containing the following (in mM): 125 NaCl, 12.5 glucose, 25 $NaHCO_3$, 3 KCl, 1.25 NaH_2PO_4, 1.5 $CaCl_2$ and 1 $MgSO_4$, bubbled to a pH of 7.4 with 5% CO_2 in 95% O_2. Coronal sections of the IC (200 μm) were cut in 34°C ACSF with a vibrating microtome (VT1200S, Leica Biosystems) and incubated at 34°C for 30 min in ACSF bubbled with 5% CO_2 in 95% O_2. Slices were then incubated at room temperature for at least 30 min before being transferred to the recording chamber. All recordings were targeted at VIP neurons located in the central nucleus of the IC. Because the borders of IC subdivisions are not well-defined in acutely prepared slices, it is possible that a small number of VIP neurons were recorded from just outside the central nucleus, in the dorsal or lateral cortices of the IC.

Current-Clamp Electrophysiology

Slices were placed in a recording chamber under a fixed stage upright microscope (BX51WI, Olympus Life Sciences) and were constantly perfused with 34°C ACSF at ∼2 ml/min. All recordings were conducted near physiological temperature (34°C). Inferior colliculus neurons were patched under visual control using epifluorescence and Dodt gradient-contrast imaging. Current-clamp recordings were performed with a BVC-700A patch clamp amplifier (Dagan Corporation). Data were low pass filtered at 10 kHz, sampled at 50 kHz with a National Instruments PCIe-6343 data acquisition board, and acquired using custom written algorithms in Igor Pro. Electrodes were pulled from borosilicate glass (outer diameter 1.5 mm, inner diameter 0.86 mm, Sutter Instrument) to a resistance of 3.5 – 5.0 MΩ using a P-1000 microelectrode puller (Sutter Instrument). The electrode internal solution contained (in mM): 115 Kgluconate, 7.73 KCl, 0.5 EGTA, 10 HEPES, 10 Na_2 phosphocreatine, 4 MgATP, 0.3 NaGTP, supplemented with 0.1% biocytin (w/v), pH adjusted to 7.4 with KOH and osmolality to 290 mmol/kg with sucrose. Data were corrected for an 11 mV liquid junction potential.

To test the effect of ACh on the excitability of VIP neurons, acetylcholine chloride (Sigma cat # A6625), was freshly dissolved each day in a vehicle solution containing (in mM): 125 NaCl, 3 KCl, 12.5 Glucose and 3 HEPES. The solution was balanced to a pH of 7.40 with NaOH. The working concentration of ACh was 1 mM unless stated otherwise. To apply ACh puffs on brain slices, ACh solution was placed in pipettes pulled from borosilicate glass (outer diameter 1.5 mm, inner diameter 0.86 mm, Sutter Instrument) with a resistance of 3.5 – 5.0 MΩ using a P-1000 microelectrode puller (Sutter Instrument) connected to a pressure ejection system built based on the OpenSpritzer design (Forman et al., 2017). The puffer pipette was placed ∼ 20 μm from the soma of the patched cell, and five 10 ms puff applications at 10 psi and 1 min apart were presented per condition. To isolate the receptors mediating the effects of ACh on VIP neurons, we bath applied the following drugs individually or in combination: 1 μM atropine (mAChR antagonist, Sigma), 5 μM mecamylamine (Mec, relatively non-selective antagonist with higher affinity for β_4 containing receptors, Sigma), 10 μM DHβE ($\alpha_4\beta_2$* nAChR antagonist, Tocris), 50 μM SR16584 ($\alpha_3\beta_4$* nAChR antagonist, Tocris), and 5 nM methyllycaconitine (MLA, α_7 nAChR antagonist, Sigma). All drugs were washed-in for 10 min before testing how the drugs affected the responses of the recorded neurons to ACh puffs. In one experiment, antagonists for $GABA_A$, glycine, AMPA, and NMDA receptors were bath applied to isolate direct effects of ACh on VIP neurons from possible ACh-induced changes in release from terminals synapsing onto VIP neurons. The following drug concentrations were used: 5 μM SR95531 (gabazine, $GABA_A$ receptor antagonist, Hello Bio), 1 μM strychnine hydrochloride (glycine receptor antagonist, Millipore Sigma), 10 μM NBQX disodium salt (AMPA receptor antagonist, Hello Bio), 50 μM D-AP5 (NMDA receptor antagonist, Hello Bio). All drugs were washed-in for 10 min before testing how the drugs affected the responses of the recorded neurons to ACh puffs. Except for when the effects of atropine alone were directly tested, 1 μM atropine was included in the ACSF under all conditions.

Effect of Repeated ACh Applications

ACh puffs were applied as described above except at lower concentrations (30 μM and 100 μM). Trials containing trains of 1, 2, 3, 5, or 10 puffs at 10 Hz were delivered with a 1-min intertrial period. Five trials were presented per condition.

Voltage-Clamp Recordings of nAChR Currents

For voltage-clamp experiments, the recording setup was the same as above except that recordings were performed using an Axopatch 200A amplifier. During the recordings, series resistance compensation was performed using 90% prediction and 90% correction. The series resistance of the electrode was never greater than 10 MΩ. The electrode internal solution contained (in mM): 115 CsOH, 115 D-gluconic acid, 7.76 CsCl, 0.5 EGTA, 10 HEPES, 10 Na_2 phosphocreatine, 4 MgATP, 0.3 NaGTP, supplemented with 0.1% biocytin (w/v), pH adjusted to 7.4 with CsOH and osmolality to 290 mmol/kg with sucrose. As detailed above, the ACh puffer was placed approximately 20 μm from the soma of the patched cell, and five 10 ms puff applications at 10 psi were presented per condition, waiting 1 min between puffs. Receptor antagonists were applied as described above for the current clamp

experiments. 1 μM atropine was included in the ACSF under all conditions. Voltage-clamp holding potentials were not corrected for the liquid junction potential.

Analysis of Electrophysiological Recordings

Action potential counts and measurements of the area under current clamp depolarizations and voltage clamp currents were made using custom written algorithms in Igor Pro 8 (Wavemetrics). Action potential counts were made with a threshold-crossing algorithm and were verified by eye. To determine the area under current clamp depolarizations, data were first median filtered using a 4000 sample (80 ms) smoothing window to remove action potentials while leaving the waveform of the underlying slow depolarization intact. The area under the median-filtered depolarization was then calculated using the "Area" function. The area under voltage clamp currents was determined by applying the "Area" function to traces that were first median filtered using the same parameters as above. Responses to the five ACh puffs delivered per neuron per treatment condition were averaged, and these average values were used for the summary analyses.

Statistical Analyses

Data were analyzed and are presented following the estimation statistics approach, which emphasizes effect sizes and their confidence intervals over p values (Bernard, 2019; Calin-Jageman and Cumming, 2019). Results from null hypothesis significance tests are also provided, but a focus on the estimation statistics is encouraged. Data analysis and significance tests were performed using custom algorithms combined with the statistical functions available in Igor Pro 8 (Wavemetrics), MATLAB R2021a (MathWorks), and R 4.1.0 (The R Project for Statistical Computing).

In **Figures 2–6**, comparisons of results are shown using Gardner-Altman estimation plots (two groups) or Cumming estimation plots (three or more groups). The design of these plots was heavily influenced by the DABEST package (Ho et al., 2019), although the plots shown here were made using our own algorithms in MATLAB. Since our data involved repeated measures from individual cells, our estimation plots use parallel coordinates plots to show the measured responses for each cell, with each line representing data from one cell. The parallel coordinates plots are accompanied by paired mean difference plots that show the pairwise differences between control responses and treatment responses. Paired mean differences are presented with bias-corrected and accelerated 95% bootstrap confidence intervals, which were generated using the "boot" package in R using 10,000 resampling iterations (Davison and Hinkley, 1997; Canty and Ripley, 2021). Bootstrap sampling distributions are plotted alongside the mean differences as histograms that were smoothed with the normal kernel function using the MATLAB "fitdist" command.

Statistical tests for differences between two groups were made using the "independence_test" function in the "coin" package in R (Hothorn et al., 2006; Hothorn et al., 2008). The "independence_test" is a non-parametric permutation test based on the theoretical framework of Strasser and Weber (Strasser and Weber, 1999). The "independence_test" was set to use a block design to represent the paired measurements in our data, to perform a two-sided test where the null hypothesis was zero Pearson correlation, and to generate the conditional null distribution using Monte Carlo resampling with 10,000 iterations. Statistical testing for differences between the control group and two or more treatment groups were made using linear mixed models (LMMs) implemented through the "lme4" and "lmerTest" packages in R (Bates et al., 2015; Kuznetsova et al., 2017). Drug treatments were the fixed effects and individual cells were the random effects. F statistics, t statistics, and p values for LMMs were generated using Satterthwaite's degrees of freedom method as implemented in the "lmerTest" package. In **Figure 7**, summary data for the responses to trains of acetylcholine puffs are presented as mean ± SD, and the summary data were fit with a linear regression performed in Igor Pro. Test statistics for all significance tests are reported in the figure legends. Effects were considered significant when $p < 0.05$.

RESULTS

Cholinergic Synapses Are Found Adjacent to the Somas and Dendrites of VIP Neurons

The IC receives cholinergic input from the two nuclei that comprise the PMT: the pedunculopontine tegmental nucleus and the laterodorsal tegmental nucleus. Together, these nuclei distribute cholinergic axons and synapses throughout the IC, contacting both GABAergic and glutamatergic neurons (Motts and Schofield, 2009; Schofield et al., 2011; Noftz et al., 2020; Beebe and Schofield, 2021). However, the specific neuronal populations that cholinergic terminals synapse onto in the IC remain unclear. To test whether VIP neurons receive cholinergic input, we performed immunofluorescence on brain slices from VIP-IRES-Cre x Ai14 mice, in which VIP neurons express the fluorescent protein tdTomato, using an antibody against the vesicular acetylcholine transporter (VAChT). High resolution images were collected using a laser-scanning confocal microscope with a 1.40 NA 63x oil-immersion objective and 0.1 μm Z-steps. Analysis of these images showed that $VAChT^+$ boutons and terminals were routinely located <2 μm from the somas, dendrites, or both of VIP neurons (**Figure 1**). Similar results were observed in IC sections from five mice. These results suggest that VIP neurons receive cholinergic input (Rees et al., 2017). We therefore hypothesized that cholinergic signaling modulates the excitability of VIP neurons.

Brief Puffs of ACh Drive Prolonged Firing in VIP Neurons *Via* Non-α_7 nAChRs

To test whether acetylcholine alters the excitability of VIP neurons, we targeted current clamp recordings to fluorescent VIP neurons in acute IC slices from VIP-IRES-Cre x Ai14 mice and used a puffer pipette to provide brief puffs of ACh near

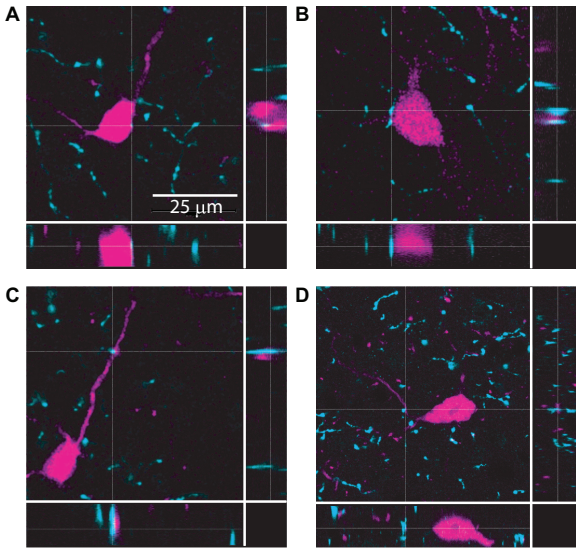

FIGURE 1 | Cholinergic terminals are routinely found in close proximity to VIP neuron somas and dendrites. Confocal images from IC sections show examples of cholinergic terminals (identified by dashed crosshairs) labeled by anti-VAChT (cyan) located <2 µm from the somas (top row, **A,B**) or dendrites (bottom row, **C,D**) of VIP neurons (magenta). The three panels in each image provide a top view and two side views centered on the cholinergic terminal identified by the crosshairs. Images are from 3 mice.

the recorded cell. We found that 10 ms puffs of 1 mM ACh delivered approximately 20 µm from the VIP cell soma drove depolarization and firing in 116 out of 126 VIP neurons. These effects were surprisingly strong and long-lasting, suggesting that cholinergic signaling can potently increase the excitability of VIP neurons (**Figure 2**).

Since ACh depolarized VIP neurons for up to 1 s, we first hypothesized that this effect was mediated by a slow metabotropic mechanism involving mAChRs. However, we found that ACh-mediated excitation of VIP neurons was not altered by 1 µM atropine, a mAChR antagonist, indicating that mAChRs are not involved in this phenomenon (**Figures 2A–C**). For the remainder of this study, all recordings were conducted in the presence of 1 µM atropine, allowing us to isolate effects on nAChRs.

Next, we used mecamylamine (Mec), a broad-spectrum nAChR antagonist partially selective for β4-containing nAChRs (Papke et al., 2008, 2010), and methyllycaconitine (MLA), an antagonist selective for α_7 nAChRs, to assess the contributions of nAChRs to the cholinergic excitation of VIP neurons. We found that bath application of 5 µM Mec nearly abolished the firing and strongly reduced the depolarization elicited by ACh puffs on VIP neurons. When both 5 µM Mec and 5 nM MLA were applied, the remaining depolarization was nearly eliminated (**Figures 2D–F**). When 5 nM MLA was applied first, ACh-elicited firing and depolarization in VIP neurons were not significantly altered. Subsequent addition of 5 µM Mec to the bath abolished the ACh effect (**Figures 2G–I**). Combined, these results suggest that cholinergic modulation of VIP neurons is predominately driven by non-α_7, Mec-sensitive nAChRs.

Brief ACh Puffs Elicit a Long-Lasting Inward Current in VIP Neurons

nAChRs are commonly associated with fast, short-lasting depolarizations, but our data suggest that activation of nAChRs elicits prolonged depolarization in VIP neurons. To analyze the currents generated by activation of nAChRs in VIP neurons, we used voltage-clamp recordings with the holding potential at –60 mV. We found that a 10 ms puff of 1 mM ACh elicited an inward current in VIP neurons that lasted hundreds of milliseconds (mean decay τ = 438 ± 173 ms, mean ± SD, based on exponential fit; n = 5 neurons; **Figure 3A**). The peak of the ACh-evoked inward current was –329 ± 154 pA, and the 10 – 90% rise time was 89 ± 31 ms (mean ± SD, n = 5 neurons). Furthermore, similar to the depolarizations observed in our current-clamp experiments, 5 µM Mec abolished most of the current elicited by ACh, and the combination of 5 µM Mec and 5 nM MLA abolished the elicited current completely (**Figure 3B**). Therefore, our results suggest that the nAChRs mediating the effect of ACh on VIP neurons remain activated for extended periods, presumably due to slow kinetics and/or limited desensitization. Since α_7 nAChRs have fast kinetics and rapid desensitization (Castro and Albuquerque, 1993; Anand et al., 1998; Papke et al., 2000; Mike et al., 2000), both the pharmacology and kinetics of the inward currents observed here are consistent with a mechanism mediated by non-α_7 nAChRs.

ACh-Driven Firing in VIP Neurons Does Not Require Activation of Presynaptic nAChRs

Many glutamatergic and GABAergic neurons in the IC express nAChRs (Sottile et al., 2017). In addition, nAChRs are often located on presynaptic terminals where their activation can directly promote neurotransmitter release (Dani and Bertrand, 2007). Therefore, it is possible that the ACh-elicited excitation of VIP neurons requires activation of an intermediate population of neurons or terminals that in turn excite VIP neurons through the release of a different, non-cholinergic neurotransmitter. We therefore tested if cholinergic modulation of VIP neurons requires activation of receptors for glutamate, GABA, and/or glycine, the main neurotransmitters in the IC. By using pharmacology to block these receptors (10 µM NBQX to block AMPA receptors, 50 µM D-APV to block NMDA receptors, 5 µM gabazine to block $GABA_A$ receptors, and 1 µM strychnine to block glycine receptors), we isolated the effects of ACh puffs on VIP neurons from most other potential inputs. After bath application of the synaptic blockers, we observed that the spiking and depolarization elicited by ACh persisted and was not significantly altered (**Figures 4A,B**).

Next, we globally reduced synaptic release probability by decreasing the concentration of Ca^{2+} in the ACSF from 1.5 mM to 0.5 mM. Since the relationship between release probability and extracellular Ca^{2+} is described by a power law (Dodge and Rahamimoff, 1967), this reduction in ACSF Ca^{2+} should

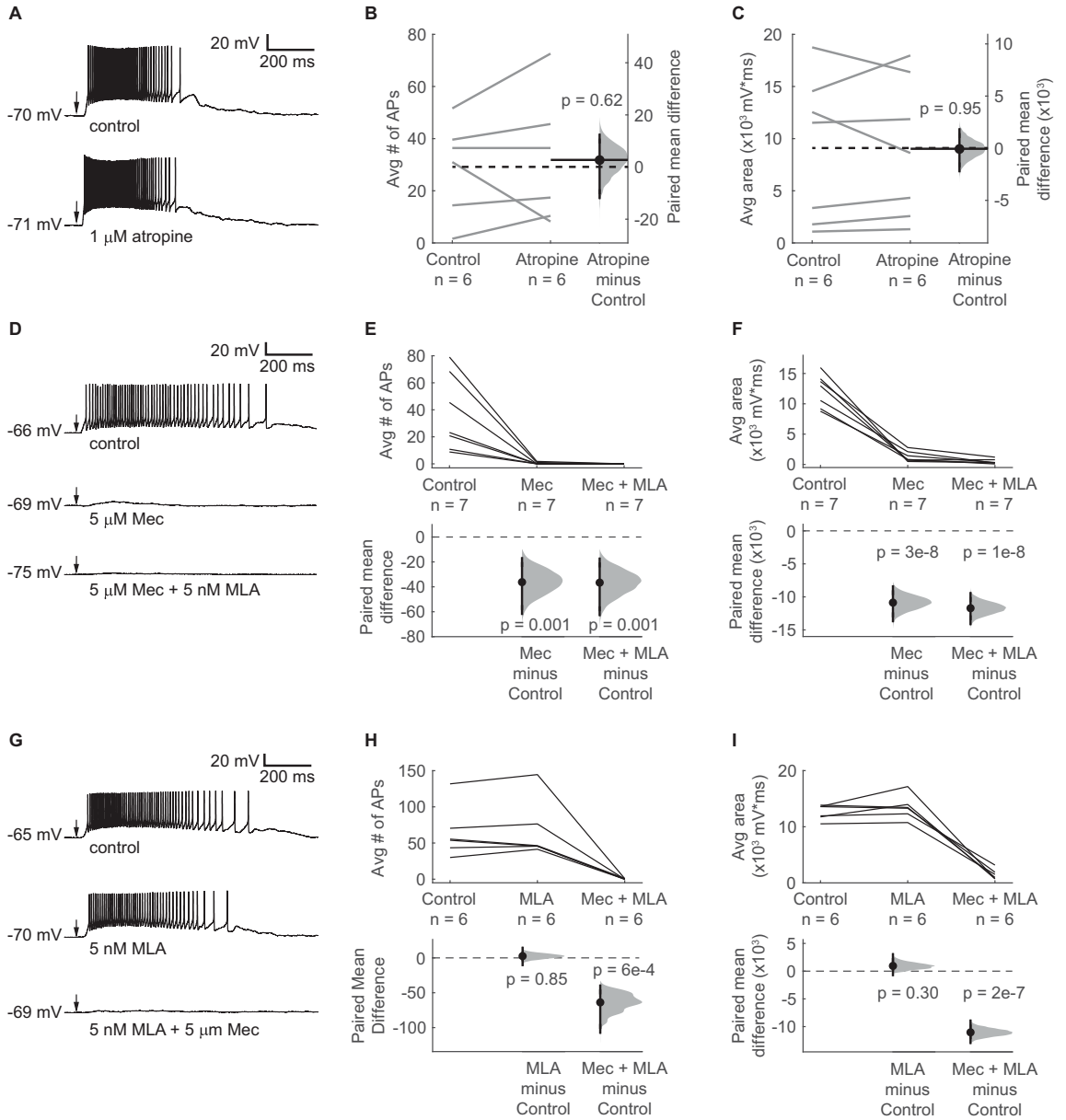

FIGURE 2 | ACh-induced depolarization of VIP neurons is mediated by non-α_7 nAChRs**. (A)** A 10 ms puff of 1 mM ACh elicited a long-lasting depolarization and spiking in a representative VIP neuron under control conditions (top). 1 μM atropine did not alter the ACh response (bottom). **(B,C)** Atropine did not change the average number of action potentials elicited by ACh or the average area under the median-filtered curve (spikes: paired independence test, $Z = -0.486$, $p = 0.62$, $n = 6$; area: paired independence test, $Z = 0.086$, $p = 0.95$, $n = 6$). Dashed horizontal lines show the mean of the control responses. Solid horizontal lines show the mean difference between the control and atropine conditions. Note that in all remaining experiments, 1 μM atropine was always present in the ACSF. **(D)** Example traces show ACh-elicited depolarization in a VIP neuron in control ACSF (top), 5 μM Mec (middle), and 5 μM Mec + 5 nM MLA (bottom). **(E)** Mec reduced the average number of action potentials elicited by ACh puffs from 36.6 ± 28.2 to 0.4 ± 0.7 (mean ± SD; LMM: treatment effect, $F_{2,12} = 11.99$, $p = 0.001$, $n = 7$; control vs. Mec, $t_{12} = -4.22$, $p = 0.001$; control vs. Mec + MLA, $t_{12} = -4.26$, $p = 0.001$). **(F)** The total depolarization elicited by ACh puffs, measured as the area under the median filtered curve, was significantly decreased by Mec and further decreased by MLA (LMM: treatment effect $F_{2,12} = 111.6$, $p = 2e\text{-}8$, $n = 7$; control vs. Mec, $t_{12} = -12.43$, $p = 3e\text{-}8$; control vs. Mec + MLA, $t_{12} = -13.39$, $p = 1e\text{-}8$). **(G)** When MLA was applied before Mec, MLA alone did not have a clear effect on ACh responses. From top to bottom: control, 5 nM MLA, and 5 μM Mec + 5 nM MLA. **(H)** The average number of action potentials elicited by ACh was not significantly affected by MLA, while subsequent application of Mec + MLA eliminated firing (LMM: treatment effect, $F_{2,10} = 17.23$, $p = 6e\text{-}4$, $n = 6$; control vs. MLA, $t_{10} = 0.20$, $p = 0.85$; control vs. Mec + MLA, $t_{10} = -4.98$, $p = 6e\text{-}4$). **(I)** MLA alone did not significantly alter the depolarization elicited by ACh, while subsequent application of Mec + MLA caused an 89% reduction in the average depolarization (LMM: treatment effect, $F_{2,10} = 120.4$, $p = 1e\text{-}7$, $n = 6$; control vs. MLA, $t_{10} = 1.10$, $p = 0.30$; control vs. Mec + MLA, $t_{10} = -12.85$, $p = 2e\text{-}7$). In **(A,D,G)** arrows indicate the time of the ACh puffs, and voltages indicate resting membrane potential. In **(E,F,H,I)**, horizontal dashed lines indicate the level of zero mean difference, and vertical lines on the paired mean difference points indicate 95% bootstrap confidence intervals.

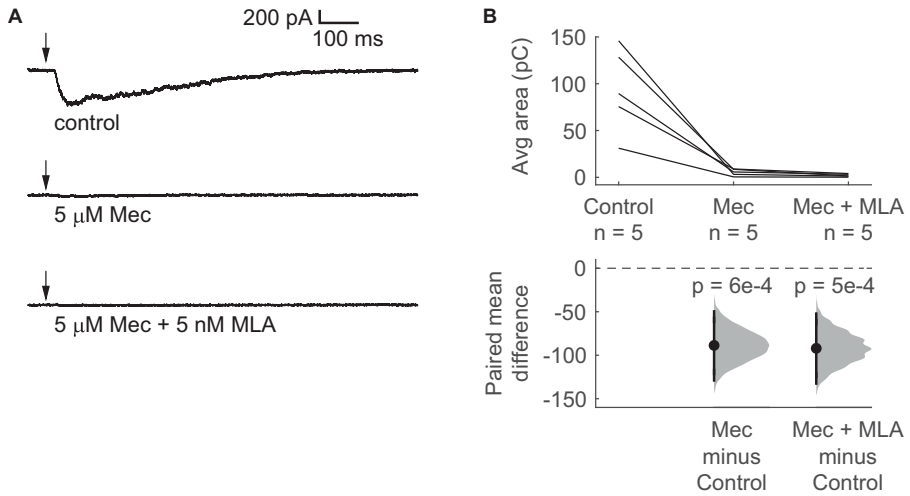

FIGURE 3 | Brief ACh puffs elicit long-lasting inward currents in VIP neurons. **(A)** Example traces of currents elicited by ACh puffs in control ACSF (top), 5 μM Mec (middle), and 5 μM Mec + 5 nM MLA (bottom). Arrows indicate the time of the ACh puffs. **(B)** The total charge flux elicited by ACh, measured by the average area under the median-filtered curve, significantly decreased after bath application of Mec. Subsequent application of MLA did not cause a further reduction (LMM: treatment effect, $F_{2,8}$ = 20.52, p = 7e-4, n = 5; control vs. Mec, t_8 = –5.44, p = 6e-4; control vs. Mec + MLA, t_8 = –5.65, p = 5e-4). Horizontal dashed line indicates the level of zero mean difference. Vertical lines on the paired mean difference points indicate 95% bootstrap confidence intervals.

dramatically decrease neurotransmitter release. We observed that decreasing extracellular Ca^{2+} did not significantly alter the spiking or depolarization elicited by ACh puffs on VIP neurons (**Figures 4C,D**). These results suggest that ACh acts on nAChRs present on VIP neurons themselves, and not via activation of presynaptic nAChRs.

$\alpha_4\beta_2$* nAChRs Do Not Mediate the Effect of ACh on VIP Neurons

Our results thus far indicate that Mec-sensitive nAChRs mediate most of the effect of ACh on VIP neurons. However, Mec is a relatively broad-spectrum antagonist of non-homomeric nAChRs, with subtype selectivity depending on the concentration used (Papke et al., 2001, 2008, 2010). Since $\alpha_4\beta_2$* nAChRs are widely expressed in the IC and are the most common subtype of nAChR found in the brain (Millar and Gotti, 2009), we performed current-clamp recordings to assess how DHβE, a selective antagonist for $\alpha_4\beta_2$* nAChRs, affected the response of VIP neurons to ACh puffs. After bath-applying 10 μM DHβE for 10 min, our results showed that blocking $\alpha_4\beta_2$* nAChRs did not significantly alter the spiking or depolarization elicited by ACh application (**Figure 5**). Therefore, our data suggest that cholinergic modulation of VIP neurons involves little or no contribution from $\alpha_4\beta_2$* or α_7 nAChRs, the most common nAChRs in the brain.

ACh-Driven Excitation of VIP Neurons Is Mediated by $\alpha_3\beta_4$* nAChRs

Although $\alpha_3\beta_4$* nAChRs are relatively rare in the brain, previous studies indicate that α_3 and β_4 nAChR subunits are expressed in the IC (Wada et al., 1989; Marks et al., 2002, 2006; Whiteaker et al., 2002; Salas et al., 2003; Gahring et al., 2004). In addition, Mec strongly antagonizes $\alpha_3\beta_4$* nAChRs at a concentration of 5 μM (Papke et al., 2008, 2010), which we used in our current-clamp and voltage-clamp recordings. We therefore hypothesized that $\alpha_3\beta_4$* nAChRs mediate the excitatory effect of ACh on VIP neurons. To test this, we used SR16584, a selective $\alpha_3\beta_4$* nAChR antagonist (Zaveri et al., 2010). Because SR16584 is dissolved in DMSO, we first established that a vehicle control (1:1000 DMSO:ACSF) did not affect the ability of 10 ms puffs of 1 mM ACh to excite VIP neurons (**Figures 6A–C**). Next, we bath applied 50 μM SR16584 and found that it nearly abolished the spiking and strongly reduced the depolarization elicited by ACh (**Figures 6A–C**), similar to our results with Mec applications. Furthermore, after only a 10-min washout of SR16584, the excitatory effect of ACh partially recovered.

ACh-Induced Inward Currents in VIP Neurons Are Predominately Mediated by $\alpha_3\beta_4$* nAChRs

Based on our current-clamp results, we hypothesized that bath application of SR16584 would abolish most of the inward current elicited by ACh in VIP neurons. To test this, we performed voltage-clamp recordings as described above. As before, ACh elicited large and sustained inward currents that were not altered by the vehicle control (**Figure 6D**). Application of 50 μM SR16584 abolished 93 ± 6% of the inward current on average (mean ± SD), revealing a much smaller and faster current in 6 of 7 recorded cells, similar to that observed during application of Mec. This remaining current was blocked by application of 5 nM MLA plus 50 μM SR16584, suggesting that it was mediated by α_7 nAChRs (**Figures 6D,E**). Together with our current clamp results, these results demonstrate that ACh-induced excitation of

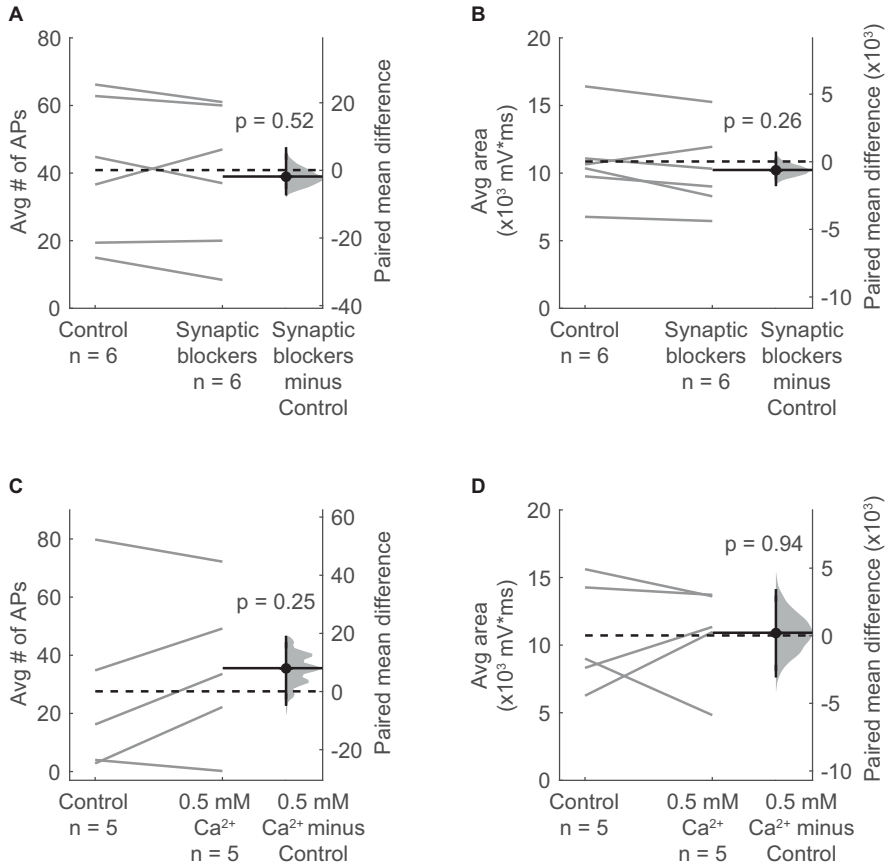

FIGURE 4 | Depolarization of VIP neurons by ACh is consistent with an intrinsic mechanism and not presynaptic effects. **(A,B)** The average number of action potentials **(A)** and depolarization **(B)** elicited by an ACh puff were not affected by bath application of antagonists against AMPA, NMDA, $GABA_A$, and glycine receptors (10 μM NBQX, 50 μM D-AP5, 5 μM SR95537, and 1 μM strychnine; action potentials: paired independence test, $Z = 0.724$, $p = 0.52$, $n = 6$; area: paired independence test, $Z = 1.28$, $p = 0.26$, $n = 6$). **(C,D)** The average number of action potentials **(C)** and depolarization **(D)** elicited by an ACh puff were unaffected by decreasing the ACSF Ca^{2+} concentration from 1.5 to 0.5 mM (action potentials: paired independence test, $Z = -1.29$, $p = 0.25$, $n = 5$; area: paired independence test, $Z = -0.137$, $p = 0.94$, $n = 5$). **(A–D)** Dashed horizontal lines show the mean of the control responses. Solid horizontal lines show the mean difference between the control and treatment conditions.

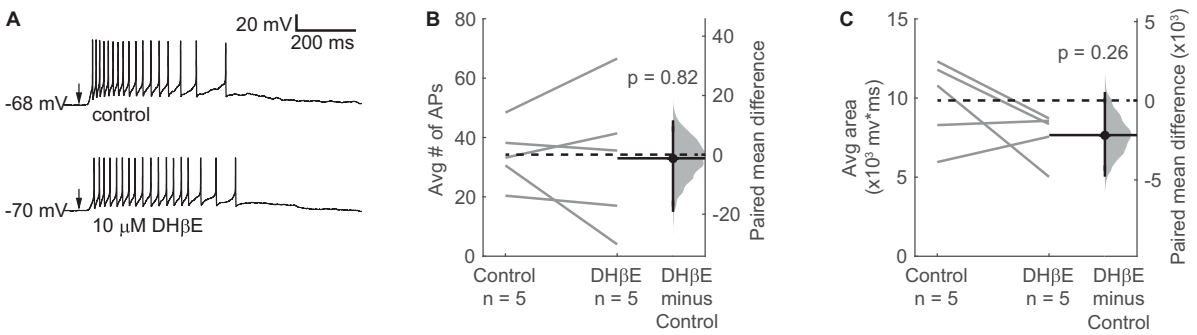

FIGURE 5 | $\alpha_4\beta_2$* nAChRs do not mediate the ACh-induced depolarization of VIP neurons. **(A)** Example traces show that a spike train elicited by a 10 ms puff of 1 mM ACh (top) was not blocked by 10 μM DHβE (bottom), an $\alpha_4\beta_2$* nAChR antagonist. Arrows indicate the time of the ACh puffs, and voltages indicate resting membrane potential. **(B,C)** DHβE did not significantly affect the average number of action potentials **(B)** or the total depolarization **(C)** elicited by ACh puffs (action potentials: paired independence test, $Z = 0.185$, $p = 0.82$, $n = 5$; area: paired independence test, $Z = 1.40$, $p = 0.26$, $n = 5$). Dashed horizontal lines show the mean of the control responses. Solid horizontal lines show the mean difference between the control and DHβE conditions.

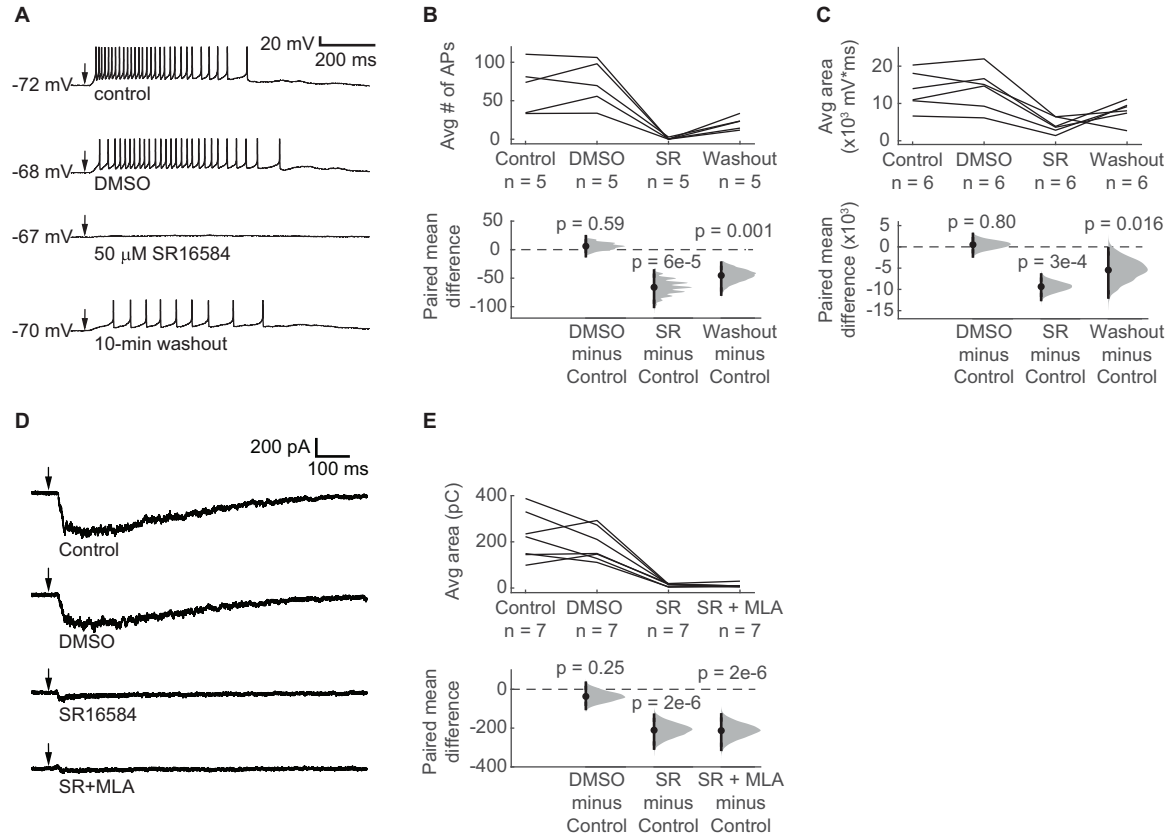

FIGURE 6 | ACh-induced depolarization of VIP neurons is predominately mediated by $\alpha_3\beta_4$* nAChRs. **(A)** Example traces show that 50 μM SR16584, an $\alpha_3\beta_4$* nAChR antagonist, blocked action potential firing and most of the depolarization elicited by 1 mM ACh puffs. Conditions from top to bottom: control, vehicle (1:1000 DMSO:ACSF), 50 μM SR16584, and 10-min washout (control ACSF). Arrows indicate the time of the ACh puffs, and voltages indicate resting membrane potential. **(B)** The average number of action potentials elicited by ACh was reduced to 0.64 ± 1.22 (mean ± SD) after bath application of SR16584 (LMM: treatment effect, $F_{3,12}$ = 20.33, p = 5e-5, n = 5; control vs. DMSO, t_{12} = 0.55, p = 0.59; control vs. SR, t_{12} = –6.01, p = 6e-5; control vs. washout, t_{12} = –4.13, p = 0.001). **(C)** The average total depolarization was also significantly decreased by application of SR16584 (LMM: treatment effect, $F_{3,15}$ = 10.90, p = 5e-4, n = 6; control vs. DMSO, t_{15} = 0.26, p = 0.80, control vs. SR, t_{15} = –4.64, p = 3e-4; control vs. washout, t_{15} = –2.71, p = 0.016). **(D)** Example traces show that 50 μM SR16584 blocked nearly all of the inward current elicited by 1 mM ACh puffs. Conditions from top to bottom: control, vehicle (1:1000 DMSO:ACSF), 50 μM SR16584, 50 μM SR16584 + 5 nM MLA. Arrows indicate the time of the ACh puffs. Holding potential was –60 mV. **(E)** Inward current elicited by ACh was decreased to 7.4 ± 6.2% (mean ± SD) of control by SR16584 (LMM: treatment effect, $F_{3,18}$ = 27.5, p = 6e-7, n = 7; control vs. DMSO, t_{18} = –1.20, p = 0.25; control vs. SR, t_{18} = –6.93, p = 2e-6; control vs. SR + MLA, t_{18} = –7.01, p = 2e-6). **(B,C,E)** Horizontal dashed lines indicate the level of zero mean difference. Vertical lines on the paired mean difference points indicate 95% bootstrap confidence intervals.

VIP neurons is mediated mainly by $\alpha_3\beta_4$* nAChRs and provide the first evidence for a functional role of $\alpha_3\beta_4$* nAChRs in the IC.

Repeated ACh Pulses Elicit Temporal Summation in VIP Neurons

Thus far we have examined how isolated puffs of 1 mM ACh affected the excitability of VIP neurons. However, the time course and concentration of ACh released from cholinergic synapses onto VIP neurons *in vivo* is unknown. Previous studies show that the average firing rates of cholinergic PMT neurons *in vivo* tend to be rather low, typically less than a few Hz (Boucetta et al., 2014), but arousing sensory stimuli elicit brief bursts of firing that can reach 100 – 200 Hz (Reese et al., 1995a,b; Sakai, 2012). In addition, our immunofluorescence data suggest that VIP neurons often receive multiple cholinergic inputs, which may reflect convergence from multiple PMT neurons. We therefore decided to test the effects of 10 and 30 Hz trains of ACh puffs, reasoning that VIP neurons would likely encounter these frequencies of input *in vivo*. Based on the slow kinetics and limited desensitization of $\alpha_3\beta_4$* nAChRs (David et al., 2010), we hypothesized that lower concentrations of ACh delivered in trains would elicit long-lasting excitation of VIP neurons due to temporal summation of cholinergic EPSPs. To test this, we made current-clamp recordings from VIP neurons while delivering trains of 1 – 10 puffs of 30 μM or 100 μM ACh at 10 Hz (**Figures 7A,E**) or 30 μM ACh at 30 Hz (**Figure 7I**). We observed that as the number of puffs increased, VIP neurons increasingly depolarized and could transition from firing no spikes in response to a single ACh puff to firing trains of spikes in response multiple ACh puffs (**Figures 7B,F,J**). The amount of depolarization elicited by increasing numbers of ACh puffs, as measured by the average

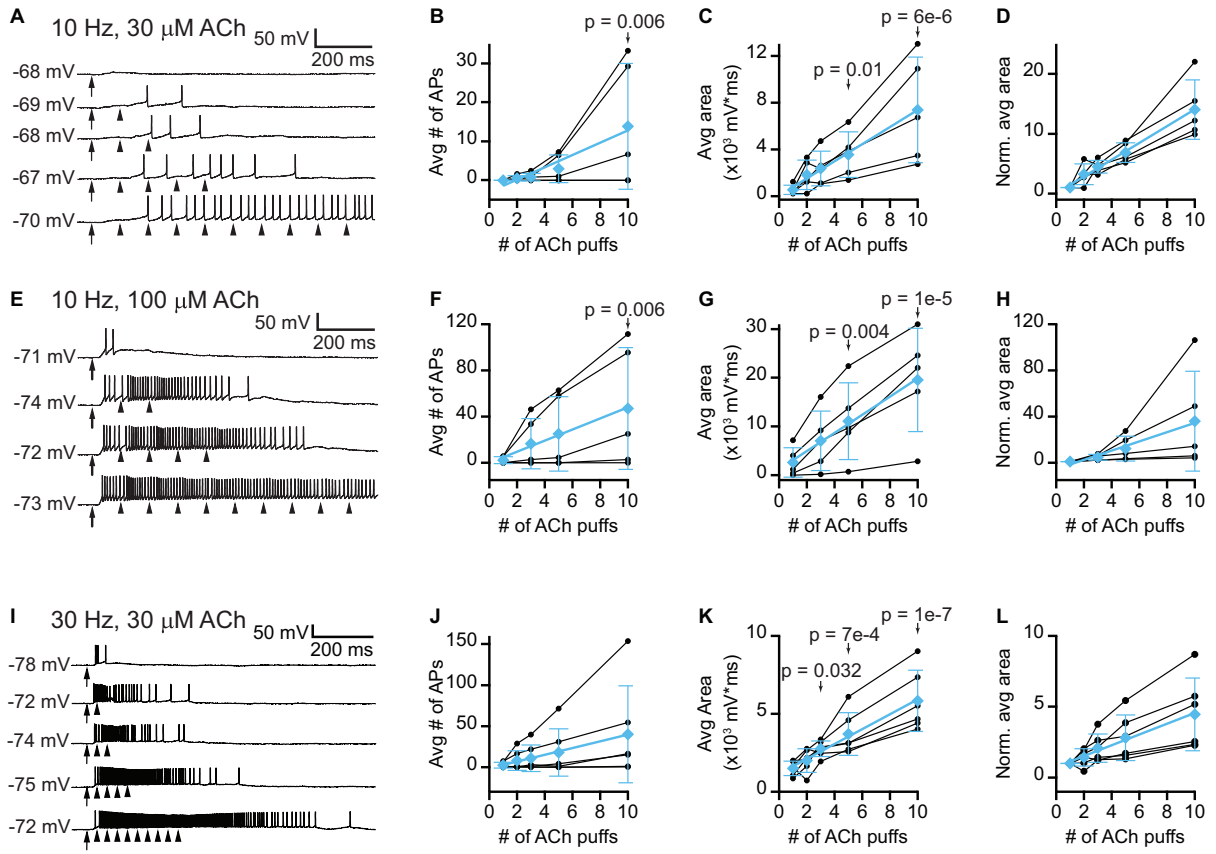

FIGURE 7 | Trains of lower concentration ACh puffs elicit temporal summation and spiking in VIP neurons. **(A)** Example traces show that 10 Hz trains of 10 ms, 30 μM ACh puffs elicited increased depolarization and probability of firing as the train duration increased from 1 to 10 puffs (top to bottom, respectively). **(B)** In 3 out of 5 neurons, increasing the number of 30 μM ACh puffs led to spiking. LMM analysis of the responses of all 5 neurons revealed a significant difference in response between 10 puffs and 1 puff (LMM: treatment effect, $F_{4,16} = 3.61$, $p = 0.028$, $n = 5$; 1 puff vs. 2 puffs, $t_{16} = 0.11$, $p = 0.91$; 1 puff vs. 3 puffs, $t_{16} = 0.19$, $p = 0.86$; 1 puff vs. 5 puffs, $t_{16} = 0.68$, $p = 0.51$; 1 puff vs. 10 puffs, $t_{16} = 3.19$, $p = 0.006$). **(C,D)** In 5 out of 5 neurons, increasing the number of 30 μM ACh puffs progressively increased the absolute **(C)** or normalized **(D)** total depolarization, measured as the area under the median-filtered curve, indicating that temporal summation occurred (LMM of absolute values: treatment effect, $F_{4,16} = 12.8$, $p = 7e\text{-}5$, $n = 5$; 1 puff vs. 2 puffs, $t_{16} = 1.23$, $p = 0.24$, 1 puff vs. 3 puffs, $t_{16} = 1.77$, $p = 0.10$; 1 puff vs. 5 puffs, $t_{16} = 2.92$, $p = 0.01$; 1 puff vs. 10 puffs, $t_{16} = 6.63$, $p = 6e\text{-}6$). Cyan data in **(B–D)** show mean ± SD responses and linear fits to these means [**(B)**, slope = 1.6 APs/puff, $r = 0.97$; **(C)**, slope = 730 mV*ms/puff, $r = 0.99$; **(D)**, slope = 1.4 normalized units/puff, $r = 0.99$]. **(E)** Example traces show that 10 Hz trains of 10 ms, 100 μM ACh puffs elicited increased depolarization and probability of firing as the train duration increased from 1 to 10 puffs (top to bottom, respectively). **(F)** In 4 out of 5 neurons, increasing the number of 100 μM ACh puffs led to spiking. LMM analysis of the responses of all 5 neurons revealed a significant difference between 10 puffs and 1 puff (LMM: treatment effect, $F_{3,12} = 3.99$, $p = 0.03$, $n = 5$; 1 puff vs. 3 puffs, $t_{12} = 1.08$, $p = 0.30$; 1 puff vs. 5 puffs, $t_{12} = 1.72$, $p = 0.11$; 1 puff vs. 10 puffs, $t_{12} = 3.38$, $p = 0.006$). **(G,H)** In 5 out of 5 neurons, increasing the number of 100 μM ACh puffs progressively increased the absolute **(G)** or normalized **(H)** total depolarization, measured as the area under the median-filtered curve, indicating that temporal summation occurred (LMM of absolute values: treatment effect, $F_{3,12} = 18.0$, $p = 9.7e\text{-}5$, $n = 5$; 1 puff vs. 3 puffs, $t_{12} = 1.87$, $p = 0.09$; 1 puff vs. 5 puffs, $t_{12} = 3.54$, $p = 0.004$; 1 puff vs. 10 puffs, $t_{12} = 7.07$, $p = 1e\text{-}5$). Cyan data in **(F–H)** show mean ± SD responses and linear fits to these means [**(F)**, slope = 4.8 APs/puff, $r = 0.99$; **(G)**, slope = 1860 mV*ms/puff, $r = 0.99$; **(H)**, slope = 4.0 normalized units/puff, $r = 0.99$]. **(I)** Example traces show that 30 Hz trains of 10 ms, 30 μM ACh puffs elicited increased depolarization and probability of firing as the train duration increased from 1 to 10 puffs (top to bottom, respectively). **(J)** In 4 out of 6 neurons, increasing the number of 30 μM ACh puffs led to increased spiking. However, LMM analysis did not reveal a significant effect of puff number (LMM: treatment effect, $F_{4,20} = 2.70$, $p = 0.06$, $n = 6$). **(K,L)** In 6 out of 6 neurons, increasing the number of 30 μM ACh puffs progressively increased the absolute **(K)** or normalized **(L)** total depolarization, measured as the area under the median-filtered curve, indicating that temporal summation occurred (LMM of absolute values: treatment effect, $F_{4,20} = 19.5$, $p = 1e\text{-}6$, $n = 6$; 1 puff vs. 2 puffs, $t_{20} = 0.92$, $p = 0.37$; 1 puff vs. 3 puffs, $t_{20} = 2.31$, $p = 0.032$; 1 puff vs. 5 puffs, $t_{20} = 4.02$, $p = 7e\text{-}4$; 1 puff vs. 10 puffs, $t_{20} = 7.91$, $p = 1e\text{-}7$). Cyan data in **(J–L)** show mean ± SD responses and linear fits to these means [**(J)**, slope = 4.1 APs/puff, $r = 0.99$; **(K)**, slope = 480 mV*ms/puff, $r = 0.99$; **(L)**, slope = 0.38 normalized units/puff, $r = 0.99$]. In **(A,E,I)** arrows and arrowheads indicate the times of ACh puffs, and voltages indicate resting membrane potential. LMM analysis was not run for the normalized data in **(D,H,L)** since LMM results for the non-normalized data are provided in **(C,G,K)**.

area under the median-filtered trace, produced rising input-output functions (**Figures 7C,G,K**). Linear fits to the means of the normalized responses for 10 Hz trains had slopes of 1.4 and 4.0 normalized units/puff, indicating that temporal summation was supralinear on average for both 30 μM and 100 μM puff trains, respectively (cyan data, **Figures 7D,H**). The 30 Hz trains of 30 μM ACh puffs resulted in sublinear integration, with a linear fit to the means of the normalized responses having a slope of

0.38 normalized units/puff (cyan data, **Figure 7L**). Although this relationship was sublinear, the slope was positive, and temporal summation still occurred, with the total depolarization after 10 puffs being 3.8x that elicited by a single puff.

Together, these results suggest that even if cholinergic synapses *in vivo* elicit smaller and/or briefer EPSPs, these EPSPs will be subject to temporal summation during periods of heightened PMT activity, thereby driving excitation of VIP neurons more effectively than isolated inputs. In addition, our results point to a potentially complicated relationship between the frequency of cholinergic input trains and the extent of temporal summation, suggesting that different patterns of cholinergic input may support diverse computations in VIP neurons. A more comprehensive analysis of the relationship between cholinergic input frequency and temporal summation in VIP neurons awaits a future study when cholinergic inputs to VIP neurons can be directly stimulated, most likely with optogenetics, over a wider range of frequencies. The present results suggest that specific patterns of cholinergic excitation can combine in diverse ways with the ascending and local auditory inputs that VIP neurons receive (Goyer et al., 2019) to critically reshape auditory processing in VIP neurons and their postsynaptic targets.

DISCUSSION

Here, we report the first cellular-level mechanism for cholinergic modulation in the auditory midbrain. Our data show that cholinergic terminals are routinely found in close proximity to the dendrites and somas of VIP neurons in the IC. In whole-cell recordings, brief applications of ACh to VIP neurons elicited surprisingly strong, long-lasting depolarizations and sustained inward currents. Despite the prolonged nature of these responses, they were not altered by blocking muscarinic receptors. Instead, using several nAChR antagonists, we determined that ACh excites VIP neurons mainly by activating $\alpha_3\beta_4$* nAChRs, with a small contribution from α_7 nAChRs. $\alpha_3\beta_4$* nAChRs are rare in the brain and have mainly been studied in the medial habenula and interpeduncular nucleus, where they play an important role in nicotine addiction (Sheffield et al., 2000; Grady et al., 2009; Scholze et al., 2012; Beiranvand et al., 2014). Our results uncover a novel role for $\alpha_3\beta_4$* receptors in the central auditory pathway, revealing a potent neuromodulatory mechanism in which ACh can drive a sustained increase in the excitability of VIP neurons. Since VIP neurons project locally, to the auditory thalamus, and to several other auditory and non-auditory brain regions, cholinergic modulation of VIP neurons has the potential to exert widespread influence on auditory processing and its downstream effects.

$\alpha_3\beta_4$* nAChRs Mediate Prolonged Depolarization of VIP Neurons

Although nAChRs are often noted for driving fast and brief responses to cholinergic inputs, these effects are generally attributable to α_7 nAChRs, which have fast kinetics and rapid desensitization (Christophe et al., 2002; Arroyo et al., 2012; Bennett et al., 2012). A growing number of studies have documented instances in which non-α_7 nAChRs mediate longer-lasting changes in neuronal excitability. For example, in VIP interneurons in the auditory cortex, nicotine induces firing for up to several minutes, and this effect was blocked by DHβE, an $\alpha_4\beta_2$* nAChR antagonist (Askew et al., 2019). In layer 1 of cerebral cortex, α_7 nAChRs mediate an early, fast response to ACh, while non-α_7 nAChRs mediate a later, slower response (Christophe et al., 2002; Arroyo et al., 2012; Bennett et al., 2012). Likewise, at the motoneuron-Renshaw cell synapse in the spinal cord, in combination with glutamatergic signaling, homomeric α_7 nAChRs mediate an early, fast response to ACh, while $\alpha_4\beta_2$* nAChRs mediate a slower, longer-lasting response (Lamotte d'Incamps and Ascher, 2008; d'Incamps et al., 2012; Lamotte d'Incamps et al., 2018).

While previous studies show that mRNA for α_7, α_4, and β_2 nAChR subunits is common in the IC (Clarke et al., 1985; Wada et al., 1989; Morley and Happe, 2000; Happe and Morley, 2004; Bieszczad et al., 2012; Sottile et al., 2017), our data point to a limited role for α_7 and no functional role for $\alpha_4\beta_2$* nAChRs in VIP neurons. Instead, we found that $\alpha_3\beta_4$* nAChRs are the dominant nAChRs in VIP neurons, mediating a strong, long-lasting depolarization in response to ACh application. Consistent with our observations, $\alpha_3\beta_4$* nAChRs are capable of mediating sustained currents due to their slow desensitization, with time constants on the order of seconds, and relatively long single-channel open times and burst durations (David et al., 2010). In addition, *in situ* hybridization studies and binding studies have consistently shown that the IC is one of the few places in the brain where α_3 and β_4 nAChRs are expressed (Wada et al., 1989; Marks et al., 2002, 2006; Whiteaker et al., 2002; Salas et al., 2003; Gahring et al., 2004), and β_4 knockout mice exhibit decreased α_3 mRNA levels in the IC, supporting the hypothesis that α_3 and β_4 subunits interact in the IC (Salas et al., 2004). Our findings confirm and extend these results by providing the first evidence of a functional role for $\alpha_3\beta_4$* nAChRs in the IC. Moreover, the widespread expression of α_3 and β_4 mRNA observed in past *in situ* hybridization studies suggests that other IC neuron types, in addition to VIP neurons, are likely to express $\alpha_3\beta_4$* nAChRs. Application of the pharmacological approach used here to additional neuron types will help expand our understanding of the functional roles of $\alpha_3\beta_4$* nAChRs in the IC.

It is important to note that $\alpha_3\beta_4$* nAChRs can have two stoichiometries, $(\alpha_3\beta_4)_2\alpha_3$ or $(\alpha_3\beta_4)_2\beta_4$, and can also combine with a different fifth subunit, $(\alpha_3\beta_4)_2$X, where the fifth subunit can be α_2, α_5, α_6, or β_3 (Scholze and Huck, 2020). Previous studies indicate that the exact subunit composition of an $\alpha_3\beta_4$* nAChR has some effect on Ca^{2+} permeability and desensitization rate, but generally little or no effect on the potency and efficacy of ACh (Wang et al., 1996; Gerzanich et al., 1998; Groot-Kormelink et al., 2001; Papke et al., 2010; Stokes and Papke, 2012). It will be important for future studies to determine which type or types of $\alpha_3\beta_4$* nAChRs are expressed in VIP neurons.

Trains of Cholinergic Inputs May Drive Long-Lasting Modulatory Effects

To mimic more *in vivo*-like patterns of cholinergic input, we tested how VIP neurons responded to trains of ACh puffs. Our

results show that, even at a relatively low application rate of 10 Hz, cholinergic EPSPs underwent substantial temporal summation in VIP neurons. This temporal summation allowed 10 and 30 Hz trains of 30 μM ACh puffs to transition from eliciting no spikes with 1 or 3 puffs to multiple spikes with 5 or 10 puffs. Trains of 100 μM ACh puffs elicited an even more pronounced increase in firing. Although ACh puffs probably do not match the concentration and time course of synaptically released ACh *in vivo*, our results show that ACh strongly excited VIP neurons under a range of conditions, uncovering a cellular mechanism that likely drives similar effects *in vivo* and highlighting the need for future experiments to build on these results.

It is well established that cholinergic PMT neurons, the source of cholinergic input to the IC, alter their firing rate as a function of behavioral state. For example, Boucetta et al. found that cholinergic PMT neurons fired maximally during the active wake and paradoxical sleep states (mean firing rates of 2.3 Hz and 3.7 Hz, respectively) and nearly ceased firing during slow wave sleep (0.04 Hz) (Boucetta et al., 2014). Sakai found similar changes across the sleep-wake cycle, but also found that arousing stimuli (a hand clap or an air puff) drove cholinergic PMT neurons to fire bursts of 2 – 5 spikes with instantaneous frequencies of 100 – 200 Hz (Sakai, 2012). Many PMT neurons also respond to sensory stimuli. For example, almost half of PMT neurons fire in response to auditory click stimuli, with half of these neurons firing short latency bursts (Reese et al., 1995a,b). Such responses might be driven by the primary auditory cortex, which projects to the PMT (Schofield and Motts, 2009; Schofield, 2010). Furthermore, our immunofluorescence data suggest that VIP neurons often integrate multiple cholinergic inputs. It therefore seems likely that certain behavioral states and sensory stimuli drive cholinergic input to VIP neurons at rates sufficient to elicit the temporal summation we observed. Thus, our data support the hypothesis that cholinergic input from the PMT drives prolonged increases in the excitability in VIP neurons as a function of behavioral state and sensory input. Since VIP neurons project broadly within and beyond the IC, changes that alter cholinergic input to VIP neurons have the potential to drive wide-ranging changes in the excitability of the auditory and non-auditory circuits that VIP neurons target.

Functional Implications for Auditory Processing

Previous studies have identified clear roles for muscarinic signaling in the IC, including roles in cortically driven plasticity (Ji et al., 2001; Ji and Suga, 2009) and stimulus specific adaptation (Ayala and Malmierca, 2015), but the roles of nicotinic signaling in the IC are less clear. Psychophysical studies indicate that systemic nicotine exposure in non-smokers can enhance performance in auditory tasks (Harkrider and Hedrick, 2005; Knott et al., 2009; Pham et al., 2020). Intriguingly, recent work from Askew and colleagues suggests that systemic nicotine sharpens frequency tuning in the IC, which likely contributes to sharper tuning in auditory cortex and improved discrimination in behavioral tasks (Askew et al., 2017). However, the authors found that nicotine mainly suppressed activity in the IC. Since we found that activation of nAChRs increases VIP neuron excitability, this raises the interesting possibility that the local projections of VIP neurons might mainly target inhibitory neurons. Alternatively, a more complicated circuit interaction might occur. We plan to test how cholinergic modulation of VIP neurons shapes the auditory response properties of VIP neurons and their postsynaptic targets in future studies.

Finally, it is unknown how cholinergic signaling shapes the excitability of other IC neuron classes. The IC contains a rich diversity of neurons, but these have long proved difficult to reliably classify, making it difficult to investigate cholinergic modulation in a systematic way. Fortunately, in addition to VIP neurons, recent studies have identified GABAergic NPY neurons (Silveira et al., 2020) and glutamatergic CCK neurons (Kreeger et al., 2021) as distinct IC neuron classes. To gain a fuller understanding of how cholinergic modulation shapes auditory processing in the IC, it will be important to determine the diverse effects cholinergic modulation exerts on these and other, yet to be identified, neuron classes.

DATA AVAILABILITY STATEMENT

The raw data supporting the conclusions of this article will be made available by the authors, without undue reservation.

ETHICS STATEMENT

The animal study was reviewed and approved by the University of Michigan Institutional Animal Care and Use Committee.

AUTHOR CONTRIBUTIONS

LR-P and MR conceived of the study, obtained funding, and prepared the initial draft of the manuscript. LR-P and JK performed experiments. MR supervised the study. All authors designed experiments, analyzed data, prepared figures, revised the manuscript, and approved the submitted version.

FUNDING

This work was supported by a Rackham Graduate Student Research Grant (University of Michigan) and National Institutes of Health grants T32 DC005356 (LR-P, PI: Gabriel Corfas), F31 DC019292 (LR-P), and R01 DC018284 (MR).

ACKNOWLEDGMENTS

We thank Pierre Apostolides, Don Caspary and Brett Schofield for discussions and helpful advice on this work, Corey Powell for advice on the statistical approach, and Kevin Cruz-Colón for his help establishing the protocol for the immunohistochemistry experiments.

REFERENCES

Anand, R., Nelson, M. E., Gerzanich, V., Wells, G. B., and Lindstrom, J. (1998). Determinants of Channel Gating Located in the N-Terminal Extracellular Domain of Nicotinic α7 Receptor. *J. Pharmacol. Exp. Ther.* 287, 469–479.

Arroyo, S., Bennett, C., Aziz, D., Brown, S. P., and Hestrin, S. (2012). Prolonged Disynaptic Inhibition in the Cortex Mediated by Slow, Non-α7 Nicotinic Excitation of a Specific Subset of Cortical Interneurons. *J. Neurosci.* 32, 3859–3864. doi: 10.1523/jneurosci.0115-12.2012

Askew, C., Intskirveli, I., and Metherate, R. (2017). Systemic Nicotine Increases Gain and Narrows Receptive Fields in A1 via Integrated Cortical and Subcortical Actions. *Eneuro* 4, ENEURO.0192–17.2017. doi: 10.1523/ENEURO.0192-17.2017

Askew, C. E., Lopez, A. J., Wood, M. A., and Metherate, R. (2019). Nicotine excites VIP interneurons to disinhibit pyramidal neurons in auditory cortex. *Synase* 73:e22116.

Ayala, Y. A., and Malmierca, M. S. (2015). Cholinergic Modulation of Stimulus-Specific Adaptation in the Inferior Colliculus. *J. Neurosci.* 35, 12261–12272. doi: 10.1523/jneurosci.0909-15.2015

Bates, D., Mächler, M., Bolker, B., and Walker, S. (2015). Fitting Linear Mixed-Effects Models Using lme4. *J. Stat. Soft.* 67, 1–48.

Beebe, N. L., and Schofield, B. R. (2021). Cholinergic boutons are closely associated with excitatory cells and four subtypes of inhibitory cells in the inferior colliculus. *J. Chem. Neuroanat.* 116:101998. doi: 10.1016/j.jchemneu.2021.101998

Beiranvand, F., Zlabinger, C., Orr-Urtreger, A., Ristl, R., Huck, S., and Scholze, P. (2014). Nicotinic acetylcholine receptors control acetylcholine and noradrenaline release in the rodent habenulo-interpeduncular complex. *Br. J. Pharmacol.* 171, 5209–5224. doi: 10.1111/bph.12841

Bennett, C., Arroyo, S., Berns, D., and Hestrin, S. (2012). Mechanisms Generating Dual-Component Nicotinic EPSCs in Cortical Interneurons. *J. Neurosci.* 32, 17287–17296. doi: 10.1523/jneurosci.3565-12.2012

Bernard, C. (2019). Changing the Way We Report, Interpret, and Discuss Our Results to Rebuild Trust in Our Research. *Eneuro* 6, ENEURO.0259–19.2019. doi: 10.1523/ENEURO.0259-19.2019

Bieszczad, K. M., Kant, R., Constantinescu, C. C., Pandey, S. K., Kawai, H. D., Metherate, R., et al. (2012). Nicotinic acetylcholine receptors in rat forebrain that bind 18F-nifene: relating PET imaging, autoradiography and behavior. *Synapse* 66, 418–434. doi: 10.1002/syn.21530

Boucetta, S., Cissé, Y., Mainville, L., Morales, M., and Jones, B. E. (2014). Discharge Profiles across the Sleep–Waking Cycle of Identified Cholinergic, GABAergic, and Glutamatergic Neurons in the Pontomesencephalic Tegmentum of the Rat. *J. Neurosci.* 34, 4708–4727. doi: 10.1523/jneurosci.2617-13.2014

Calin-Jageman, R. J., and Cumming, G. (2019). Estimation for Better Inference in Neuroscience. *Eneuro* 6, ENEURO.0205–19.2019. doi: 10.1523/ENEURO.0205-19.2019

Canty, A., and Ripley, B. D. (2021). *boot: Bootstrap R (S-Plus) Functions*. R package version 1.3–28. Available online at: https://cran.r-project.org/web/packages/boot/citation.html

Castro, N. G., and Albuquerque, E. X. (1993). Brief-lifetime, fast-inactivating ion channels account for the α-bungarotoxin-sensitive nicotinic response in hippocampal neurons. *Neurosci. Lett.* 164, 137–140. doi: 10.1016/0304-3940(93)90876-m

Christophe, E., Roebuck, A., Staiger, J. F., Lavery, D. J., Charpak, S., and Audinat, E. (2002). Two Types of Nicotinic Receptors Mediate an Excitation of Neocortical Layer I Interneurons. *J. Neurophysiol.* 88, 1318–1327. doi: 10.1152/jn.2002.88.3.1318

Clarke, P., Schwartz, R., Paul, S., Pert, C., and Pert, A. (1985). Nicotinic binding in rat brain: autoradiographic comparison of [3H]acetylcholine, [3H]nicotine, and [125I]-alpha-bungarotoxin. *J. Neurosci.* 5, 1307–1315. doi: 10.1523/jneurosci.05-05-01307.1985

Dani, J. A., and Bertrand, D. (2007). Nicotinic acetylcholine receptors and nicotinic cholinergic mechanisms of the central nervous system. *Annu. Rev. Pharmacol. Toxicol.* 47, 699–729. doi: 10.1146/annurev.pharmtox.47.120505.105214

David, R., Ciuraszkiewicz, A., Simeone, X., Orr-Urtreger, A., Papke, R. L., McIntosh, J. M., et al. (2010). Biochemical and functional properties of distinct nicotinic acetylcholine receptors in the superior cervical ganglion of mice with targeted deletions of nAChR subunit genes. *Eur. J. Neurosci.* 31, 978–993. doi: 10.1111/j.1460-9568.2010.07133.x

Davison, A., and Hinkley, D. (1997). *Bootstrap Methods and their Application (Cambridge Series in Statistical and Probabilistic Mathematics)*. Cambridge: Cambridge University Press. doi: 10.1017/CBO9780511802843

d'Incamps, B. L., Krejci, E., and Ascher, P. (2012). Mechanisms Shaping the Slow Nicotinic Synaptic Current at the Motoneuron–Renshaw Cell Synapse. *J. Neurosci.* 32, 8413–8423. doi: 10.1523/jneurosci.0181-12.2012

Dodge, F. A., and Rahamimoff, R. (1967). Co-operative action of calcium ions in transmitter release at the neuromuscular junction. *J. Physiol.* 193, 419–432. doi: 10.1113/jphysiol.1967.sp008367

Farley, G. R., Morley, B. J., Javel, E., and Gorga, M. P. (1983). Single-unit responses to cholinergic agents in the rat inferior colliculus. *Hear. Res.* 11, 73–91. doi: 10.1016/0378-5955(83)90046-1

Felix, R. A., Chavez, V. A., Novicio, D. M., Morley, B. J., and Portfors, C. V. (2019). Nicotinic acetylcholine receptor subunit α 7 -knockout mice exhibit degraded auditory temporal processing. *J. Neurophysiol.* 122, 451–465. doi: 10.1152/jn.00170.2019

Forman, C. J., Tomes, H., Mbobo, B., Burman, R. J., Jacobs, M., Baden, T., et al. (2017). Openspritzer: an open hardware pressure ejection system for reliably delivering picolitre volumes. *Sci. Rep.* 7:2188.

Gahring, L. C., Persiyanov, K., and Rogers, S. W. (2004). Neuronal and astrocyte expression of nicotinic receptor subunit β4 in the adult mouse brain. *J. Compar. Neurol.* 468, 322–333. doi: 10.1002/cne.10942

Gerzanich, V., Wang, F., Kuryatov, A., and Lindstrom, J. (1998). alpha 5 Subunit alters desensitization, pharmacology, Ca++ permeability and Ca++ modulation of human neuronal alpha 3 nicotinic receptors. *J. Pharmacol. Exp. Ther.* 286, 311–320.

Gillet, C., Goyer, D., Kurth, S., Griebel, H., and Kuenzel, T. (2018). Cholinergic innervation of principal neurons in the cochlear nucleus of the Mongolian gerbil. *J. Comp. Neurol.* 526, 1647–1661. doi: 10.1002/cne.24433

Goyer, D., Kurth, S., Gillet, C., Keine, C., Rübsamen, R., and Kuenzel, T. (2016). Slow Cholinergic Modulation of Spike Probability in Ultra-Fast Time-Coding Sensory Neurons. *Eneuro* 3, ENEURO.0186–16.2016. doi: 10.1523/ENEURO.0186-16.2016

Goyer, D., Silveira, M. A., George, A. P., Beebe, N. L., Edelbrock, R. M., Malinski, P. T., et al. (2019). A novel class of inferior colliculus principal neurons labeled in vasoactive intestinal peptide-Cre mice. *Elife* 8:e43770.

Grady, S. R., Moretti, M., Zoli, M., Marks, M. J., Zanardi, A., Pucci, L., et al. (2009). Rodent Habenulo–Interpeduncular Pathway Expresses a Large Variety of Uncommon nAChR Subtypes, But Only the α3β4 and α3β3β4 Subtypes Mediate Acetylcholine Release. *J. Neurosci.* 29, 2272–2282. doi: 10.1523/jneurosci.5121-08.2009

Groot-Kormelink, P. J., Boorman, J. P., and Sivilotti, L. G. (2001). Formation of functional α3β4α5 human neuronal nicotinic receptors in Xenopus oocytes: a reporter mutation approach. *Br. J. Pharmacol.* 134, 789–796. doi: 10.1038/sj.bjp.0704313

Habbicht, H., and Vater, M. (1996). A microiontophoretic study of acetylcholine effects in the inferior colliculus of horseshoe bats: implications for a modulatory role. *Brain Res.* 724, 169–179. doi: 10.1016/0006-8993(96)00224-7

Happe, H. K., and Morley, B. J. (2004). Distribution and postnatal development of α7 nicotinic acetylcholine receptors in the rodent lower auditory brainstem. *Dev. Brain Res.* 153, 29–37. doi: 10.1016/j.devbrainres.2004.07.004

Harkrider, A. W., and Hedrick, M. S. (2005). Acute effect of nicotine on auditory gating in smokers and non-smokers. *Hear. Res.* 202, 114–128. doi: 10.1016/j.heares.2004.11.009

Ho, J., Tumkaya, T., Aryal, S., Choi, H., and Claridge-Chang, A. (2019). Moving beyond P values: data analysis with estimation graphics. *Nat. Methods* 16, 565–566. doi: 10.1038/s41592-019-0470-3

Hothorn, T., Hornik, K., Wiel, M. A. V. D., and Zeileis, A. (2006). A Lego System for Conditional Inference. *Am. Stat.* 60, 257–263. doi: 10.1198/000313006x118430

Hothorn, T., Hornik, K., Wiel, M. A. V. D., and Zeileis, A. (2008). Implementing a Class of Permutation Tests: The coin Package. *J. Stat. Softw.* 28, 1–23.

Ji, W., Gao, E., and Suga, N. (2001). Effects of Acetylcholine and Atropine on Plasticity of Central Auditory Neurons Caused by Conditioning in Bats. *J. Neurophysiol.* 86, 211–225. doi: 10.1152/jn.2001.86.1.211

Ji, W., and Suga, N. (2009). Tone-Specific and Nonspecific Plasticity of Inferior Colliculus Elicited by Pseudo-Conditioning: Role of Acetylcholine and Auditory and Somatosensory Cortices. *J. Neurophysiol.* 102, 941–952. doi: 10.1152/jn.00222.2009

Jones, B. E. (1991). Paradoxical sleep and its chemical/structural substrates in the brain. *Neuroscience* 40, 637–656. doi: 10.1016/0306-4522(91)90002-6

Knott, V., Shah, D., Millar, A., McIntosh, J., Fisher, D., Blais, C., et al. (2012). Nicotine, Auditory Sensory Memory, and sustained Attention in a Human Ketamine Model of Schizophrenia: Moderating Influence of a Hallucinatory Trait. *Front. Pharmacol.* 3:172. doi: 10.3389/fphar.2012.00172

Knott, V. J., Bolton, K., Heenan, A., Shah, D., Fisher, D. J., and Villeneuve, C. (2009). Effects of acute nicotine on event-related potential and performance indices of auditory distraction in nonsmokers. *Nicotine Tob. Res.* 11, 519–530. doi: 10.1093/ntr/ntp044

Kozak, R., Bowman, E. M., Latimer, M. P., Rostron, C. L., and Winn, P. (2005). Excitotoxic lesions of the pedunculopontine tegmental nucleus in rats impair performance on a test of sustained attention. *Exp. Brain Res.* 162, 257–264. doi: 10.1007/s00221-004-2143-3

Kreeger, L. J., Connelly, C. J., Mehta, P., Zemelman, B. V., and Golding, N. L. (2021). Excitatory cholecystokinin neurons of the midbrain integrate diverse temporal responses and drive auditory thalamic subdomains. *Proc. Natl. Acad. Sci. U. S. A.* 118, e2007724118. doi: 10.1073/pnas.2007724118

Kuznetsova, A., Brockhoff, P. B., and Christensen, R. H. B. (2017). lmerTest Package: Tests in Linear Mixed Effects Models. *J. Stat. Softw.* 82, 1–26.

Lamotte d'Incamps, B., and Ascher, P. (2008). Four Excitatory Postsynaptic Ionotropic Receptors Coactivated at the Motoneuron–Renshaw Cell Synapse. *J. Neurosci.* 28, 14121–14131. doi: 10.1523/jneurosci.3311-08.2008

Lamotte d'Incamps, B., Zorbaz, T., Dingova, D., Krejci, E., and Ascher, P. (2018). Stoichiometry of the Heteromeric Nicotinic Receptors of the Renshaw Cell. *J. Neurosci.* 38, 4943–4956. doi: 10.1523/jneurosci.0070-18.2018

Madisen, L., Zwingman, T. A., Sunkin, S. M., Oh, S. W., Zariwala, H. A., Gu, H., et al. (2010). A robust and high-throughput Cre reporting and characterization system for the whole mouse brain. *Nat. Neurosci.* 13, 133–140. doi: 10.1038/nn.2467

Marks, M. J., Whiteaker, P., and Collins, A. C. (2006). Deletion of the α7, β2, or β4 Nicotinic Receptor Subunit Genes Identifies Highly Expressed Subtypes with Relatively Low Affinity for [3H]Epibatidine. *Mol. Pharmacol.* 70, 947–959. doi: 10.1124/mol.106.025338

Marks, M. J., Whiteaker, P., Grady, S. R., Picciotto, M. R., McIntosh, J. M., and Collins, A. C. (2002). Characterization of [125I]epibatidine binding and nicotinic agonist-mediated 86Rb+ efflux in interpeduncular nucleus and inferior colliculus of β2 null mutant mice. *J. Neurochem.* 81, 1102–1115. doi: 10.1046/j.1471-4159.2002.00910.x

Mike, A., Castro, N. G., and Albuquerque, E. X. (2000). Choline and acetylcholine have similar kinetic properties of activation and desensitization on the α7 nicotinic receptors in rat hippocampal neurons. *Brain Res.* 882, 155–168. doi: 10.1016/s0006-8993(00)02863-8

Millar, N. S., and Gotti, C. (2009). Diversity of vertebrate nicotinic acetylcholine receptors. *Neuropharmacology* 56, 237–246. doi: 10.1016/j.neuropharm.2008.07.041

Morley, B. J., and Happe, H. K. (2000). Cholinergic receptors: dual roles in transduction and plasticity. *Hear. Res.* 147, 104–112. doi: 10.1016/s0378-5955(00)00124-6

Motts, S. D., and Schofield, B. R. (2009). Sources of cholinergic input to the inferior colliculus. *Neuroscience* 160, 103–114. doi: 10.1016/j.neuroscience.2009.02.036

Noftz, W. A., Beebe, N. L., Mellott, J. G., and Schofield, B. R. (2020). Cholinergic Projections From the Pedunculopontine Tegmental Nucleus Contact Excitatory and Inhibitory Neurons in the Inferior Colliculus. *Front. Neural. Circuits* 14:43. doi: 10.3389/fncir.2020.00043

Papke, R. L., Dwoskin, L. P., Crooks, P. A., Zheng, G., Zhang, Z., McIntosh, J. M., et al. (2008). Extending the analysis of nicotinic receptor antagonists with the study of alpha6 nicotinic receptor subunit chimeras. *Neuropharmacology* 54, 1189–1200. doi: 10.1016/j.neuropharm.2008.03.010

Papke, R. L., Meyer, E., Nutter, T., and Uteshev, V. V. (2000). α7 Receptor-selective agonists and modes of α7 receptor activation. *Eur. J. Pharmacol.* 393, 179–195. doi: 10.1016/s0014-2999(00)00009-1

Papke, R. L., Sanberg, P. R., and Shytle, R. D. (2001). Analysis of Mecamylamine Stereoisomers on Human Nicotinic Receptor Subtypes. *J. Pharmacol. Exp. Ther.* 297, 646–656.

Papke, R. L., Wecker, L., and Stitzel, J. A. (2010). Activation and Inhibition of Mouse Muscle and Neuronal Nicotinic Acetylcholine Receptors Expressed in Xenopus Oocytes. *J. Pharmacol. Exp. Ther.* 333, 501–518. doi: 10.1124/jpet.109.164566

Pham, C. Q., Kapolowicz, M. R., Metherate, R., and Zeng, F.-G. (2020). Nicotine enhances auditory processing in healthy and normal-hearing young adult nonsmokers. *Psychopharmacology* 237, 833–840. doi: 10.1007/s00213-019-05421-x

Rees, C. L., Moradi, K., and Ascoli, G. A. (2017). Weighing the Evidence in Peters' Rule: Does Neuronal Morphology Predict Connectivity? *Trends Neurosci.* 40, 63–71. doi: 10.1016/j.tins.2016.11.007

Reese, N. B., Garcia-Rill, E., and Skinner, R. D. (1995a). Auditory input to the pedunculopontine nucleus: I. Evoked potentials. *Brain Res. Bull.* 37, 257–264. doi: 10.1016/0361-9230(95)00002-v

Reese, N. B., Garcia-Rill, E., and Skinner, R. D. (1995b). Auditory input to the pedunculopontine nucleus: II. Unit responses. *Brain Res. Bull.* 37, 265–273. doi: 10.1016/0361-9230(95)00001-u

Sakai, K. (2012). Discharge properties of presumed cholinergic and noncholinergic laterodorsal tegmental neurons related to cortical activation in non-anesthetized mice. *Neuroscience* 224, 172–190. doi: 10.1016/j.neuroscience.2012.08.032

Salas, R., Cook, K. D., Bassetto, L., and De Biasi, M. (2004). The α3 and β4 nicotinic acetylcholine receptor subunits are necessary for nicotine-induced seizures and hypolocomotion in mice. *Neuropharmacology* 47, 401–407. doi: 10.1016/j.neuropharm.2004.05.002

Salas, R., Pieri, F., Fung, B., Dani, J. A., and De Biasi, M. (2003). Altered Anxiety-Related Responses in Mutant Mice Lacking the β4 Subunit of the Nicotinic Receptor. *J. Neurosci.* 23, 6255–6263. doi: 10.1523/jneurosci.23-15-06255.2003

Schofield, B. R. (2010). Projections from auditory cortex to midbrain cholinergic neurons that project to the inferior colliculus. *Neuroscience* 166:231. doi: 10.1016/j.neuroscience.2009.12.008

Schofield, B. R., and Motts, S. D. (2009). Projections from auditory cortex to cholinergic cells in the midbrain tegmentum of guinea pigs. *Brain Res. Bull.* 80, 163–170. doi: 10.1016/j.brainresbull.2009.06.015

Schofield, B. R., Motts, S. D., and Mellott, J. G. (2011). Cholinergic Cells of the Pontomesencephalic Tegmentum: Connections with Auditory Structures from Cochlear Nucleus to Cortex. *Hear. Res.* 279, 85–95. doi: 10.1016/j.heares.2010.12.019

Scholze, P., and Huck, S. (2020). The α5 Nicotinic Acetylcholine Receptor Subunit Differentially Modulates α4β2* and α3β4* Receptors. *Front. Synaptic. Neurosci.* 12:607959. doi: 10.3389/fnsyn.2020.607959

Scholze, P., Koth, G., Orr-Urtreger, A., and Huck, S. (2012). Subunit composition of α5-containing nicotinic receptors in the rodent habenula. *J. Neurochem.* 121, 551–560. doi: 10.1111/j.1471-4159.2012.07714.x

Sheffield, E. B., Quick, M. W., and Lester, R. A. J. (2000). Nicotinic acetylcholine receptor subunit mRNA expression and channel function in medial habenula neurons. *Neuropharmacology* 39, 2591–2603. doi: 10.1016/s0028-3908(00)00138-6

Silveira, M. A., Anair, J. D., Beebe, N. L., Mirjalili, P., Schofield, B. R., and Roberts, M. T. (2020). Neuropeptide Y Expression Defines a Novel Class of GABAergic Projection Neuron in the Inferior Colliculus. *J. Neurosci.* 40, 4685–4699. doi: 10.1523/jneurosci.0420-20.2020

Smucny, J., Olincy, A., Rojas, D. C., and Tregellas, J. R. (2016). Neuronal effects of nicotine during auditory selective attention in schizophrenia. *Hum. Brain Mapp.* 37, 410–421. doi: 10.1002/hbm.23040

Sottile, S. Y., Hackett, T. A., Cai, R., Ling, L., Llano, D. A., and Caspary, D. M. (2017). Presynaptic Neuronal Nicotinic Receptors Differentially Shape Select Inputs to Auditory Thalamus and Are Negatively Impacted by Aging. *J. Neurosci.* 37, 11377–11389. doi: 10.1523/jneurosci.1795-17.2017

Stokes, C., and Papke, R. L. (2012). Use of an α3-β4 nicotinic acetylcholine receptor subunit concatamer to characterize ganglionic receptor subtypes with specific subunit composition reveals species-specific pharmacologic properties. *Neuropharmacology* 63, 538–546. doi: 10.1016/j.neuropharm.2012.04.035

Strasser, H., and Weber, C. U. (1999). *On the Asymptotic Theory of Permutation Statistics. Report Series SFB "Adaptive Information Systems and Modelling in*

Economics and Management Science". Vienna: University of Economics and Business.

Taniguchi, H., He, M., Wu, P., Kim, S., Paik, R., Sugino, K., et al. (2011). A resource of Cre driver lines for genetic targeting of GABAergic neurons in cerebral cortex. *Neuron* 71, 995–1013. doi: 10.1016/j.neuron.2011.07.026

Wada, E., Wada, K., Boulter, J., Deneris, E., Heinemann, S., Patrick, J., et al. (1989). Distribution of alpha 2, alpha 3, alpha 4, and beta 2 neuronal nicotinic receptor subunit mRNAs in the central nervous system: a hybridization histochemical study in the rat. *J. Comp. Neurol.* 284, 314–335. doi: 10.1002/cne.902840212

Wang, F., Gerzanich, V., Wells, G. B., Anand, R., Peng, X., Keyser, K., et al. (1996). Assembly of Human Neuronal Nicotinic Receptor α5 Subunits with α3, β2, and β4 Subunits. *J. Biol. Chem.* 271, 17656–17665. doi: 10.1074/jbc.271.30.17656

Whiteaker, P., Peterson, C. G., Xu, W., McIntosh, J. M., Paylor, R., Beaudet, A. L., et al. (2002). Involvement of the α3 Subunit in Central Nicotinic Binding Populations. *J. Neurosci.* 22, 2522–2529. doi: 10.1523/jneurosci.22-07-02522.2002

Zaveri, N., Jiang, F., Olsen, C., Polgar, W., and Toll, L. (2010). Novel alpha3beta4 nicotinic acetylcholine receptor-selective ligands. Discovery, structure-activity studies and pharmacological evaluation. *J. Med. Chem.* 53, 8187–8191. doi: 10.1021/jm1006148

Zhang, C., Beebe, N. L., Schofield, B. R., Pecka, M., and Burger, R. M. (2021). Endogenous Cholinergic Signaling Modulates Sound-Evoked Responses of the Medial Nucleus of the Trapezoid Body. *J. Neurosci.* 41, 674–688. doi: 10.1523/jneurosci.1633-20.2020

Zhang, L., Wu, C., Martel, D. T., West, M., Sutton, M. A., and Shore, S. E. (2019). Remodeling of cholinergic input to the hippocampus after noise exposure and tinnitus induction in Guinea pigs. *Hippocampus* 29, 669–682.

Zheng, Q. Y., Johnson, K. R., and Erway, L. C. (1999). Assessment of hearing in 80 inbred strains of mice by ABR threshold analyses. *Hear. Res.* 130, 94–107. doi: 10.1016/s0378-5955(99)00003-9

Conflict of Interest: The authors declare that the research was conducted in the absence of any commercial or financial relationships that could be construed as a potential conflict of interest.

Publisher's Note: All claims expressed in this article are solely those of the authors and do not necessarily represent those of their affiliated organizations, or those of the publisher, the editors and the reviewers. Any product that may be evaluated in this article, or claim that may be made by its manufacturer, is not guaranteed or endorsed by the publisher.

frontiers in Neural Circuits

ORIGINAL RESEARCH
published: 27 August 2021
doi: 10.3389/fncir.2021.718348

5-HT1A Receptors Alter Temporal Responses to Broadband Vocalizations in the Mouse Inferior Colliculus Through Response Suppression

*Arianna Gentile Polese[1,2], Sunny Nigam[3,4] and Laura M. Hurley[3]**

[1] Department of Cell and Developmental Biology, University of Colorado Anschutz Medical Campus, Aurora, CO, United States, [2] Department of Biology, Program in Neuroscience, Indiana University Bloomington, Bloomington, IN, United States, [3] Department of Neurobiology and Anatomy, McGovern Medical School, The University of Texas Health Science Center at Houston, Houston, TX, United States, [4] Department of Physics, Indiana University Bloomington, Bloomington, IN, United States

Neuromodulatory systems may provide information on social context to auditory brain regions, but relatively few studies have assessed the effects of neuromodulation on auditory responses to acoustic social signals. To address this issue, we measured the influence of the serotonergic system on the responses of neurons in a mouse auditory midbrain nucleus, the inferior colliculus (IC), to vocal signals. Broadband vocalizations (BBVs) are human-audible signals produced by mice in distress as well as by female mice in opposite-sex interactions. The production of BBVs is context-dependent in that they are produced both at early stages of interactions as females physically reject males and at later stages as males mount females. Serotonin in the IC of males corresponds to these events, and is elevated more in males that experience less female rejection. We measured the responses of single IC neurons to five recorded examples of BBVs in anesthetized mice. We then locally activated the 5-HT1A receptor through iontophoretic application of 8-OH-DPAT. IC neurons showed little selectivity for different BBVs, but spike trains were characterized by local regions of high spike probability, which we called "response features." Response features varied across neurons and also across calls for individual neurons, ranging from 1 to 7 response features for responses of single neurons to single calls. 8-OH-DPAT suppressed spikes and also reduced the numbers of response features. The weakest response features were the most likely to disappear, suggestive of an "iceberg"-like effect in which activation of the 5-HT1A receptor suppressed weakly suprathreshold response features below the spiking threshold. Because serotonin in the IC is more likely to be elevated for mounting-associated BBVs than for rejection-associated BBVs, these effects of the 5-HT1A receptor could contribute to the differential auditory processing of BBVs in different behavioral subcontexts.

Keywords: serotonin receptor, 5-HT1A, inferior colliculus, auditory, vocalization

OPEN ACCESS

Edited by:
Conny Kopp-Scheinpflug, Ludwig Maximilian University of Munich, Germany

Reviewed by:
Daniel Llano, University of Illinois Urbana-Champaign, United States
Gunsoo Kim, Korea Brain Research Institute, South Korea

***Correspondence:**
Laura M. Hurley
lhurley@indiana.edu

Received: *31 May 2021*
Accepted: *19 July 2021*
Published: *27 August 2021*

Citation:
Gentile Polese A, Nigam S and Hurley LM (2021) 5-HT1A Receptors Alter Temporal Responses to Broadband Vocalizations in the Mouse Inferior Colliculus Through Response Suppression. Front. Neural Circuits 15:718348. doi: 10.3389/fncir.2021.718348

INTRODUCTION

Neuromodulatory neurons that arise outside of the auditory system and synthesize monoamines such as catecholamines and serotonin (Klepper and Herbert, 1991; Forlano et al., 2015; Nevue et al., 2016; Barr and Woolley, 2018; Ghahramani et al., 2018; Schofield and Hurley, 2018; Hurley, 2019; Petersen et al., 2020) can reconfigure auditory circuitry to modify the magnitude and timing of responses to acoustic stimuli (Hurley et al., 2004; Gittelman et al., 2013; Jacob and Nienborg, 2018; Hoyt et al., 2019; Sizemore et al., 2020). However, with some exceptions (e.g., Hurley and Pollak, 2005; Ikeda et al., 2015; Lee et al., 2018), studies of neuromodulatory effects on auditory responses have not examined how neuromodulators affect responses to the types of natural vocal signals that occur in conjunction with neuromodulatory release.

To explore this issue, we assessed the effects of manipulating the serotonergic system on the responses of mouse midbrain auditory neurons in the inferior colliculus (IC) to a type of vocalization with an established relationship to social behavior, and also to serotonin release. The vocalization type is an audible call made by mice in several different contexts. Most commonly known as "squeaks," they have also been called low-frequency harmonic calls or broadband vocalizations (BBVs); the latter designations refer to the presence of prominent low-frequency harmonics that extend into the ultrasonic range (Grimsley et al., 2013; Lupanova and Egorova, 2015; Finton et al., 2017). During opposite-sex interactions, BBVs are predominantly produced by females (Wang et al., 2008a). Even within the opposite-sex context, females produce BBVs in different sub-contexts. During the initial investigative stages of opposite-sex interaction, females produce BBVs that correspond in number and time with kicks or lunges at males (Sugimoto et al., 2011; Finton et al., 2017). BBVs produced in this stage correspond to a smaller number of ultrasonic vocalizations (USVs) produced by males, and predict less male mounting of females in later stages of the interaction. When mounting does occur, however, BBVs are often produced as females are being mounted, and these BBVs may overlap in time with USVs (White et al., 1998; Finton et al., 2017). Males may respond to BBVs with relative attraction (Grimsley et al., 2013), or as if they constitute a signal of rejection (Hood et al., 2020), depending on the behavioral context.

Broadband vocalizations also correlate with activation of the serotonergic system within the IC, which is a hub for ascending and descending auditory pathways (Schofield and Cant, 1999; Coomes and Schofield, 2004; Loftus et al., 2010; Bartlett, 2013; Lesicko et al., 2016; Patel et al., 2017). In the IC of males interacting with females, serotonin measured voltametrically through carbon fiber electrodes is inversely correlated with the number of BBVs produced by their female social partners (Keesom and Hurley, 2016). Serotonin in the IC of males is thus higher when they experience a lack of rejection from females. The sources of serotonin to the IC are two distinct subpopulations of neurons within the dorsal raphe nucleus (DRN; Petersen et al., 2020). These subpopulations are involved in social aggression (Niederkofler et al., 2016), and show distinct responses to social context (Petersen et al., 2020). All of these findings suggest that BBVs are heard by males in different contexts, and that some of these contexts correspond to heightened serotonergic modulation. However, there is no understanding of how IC neurons respond to BBVs, or how serotonin influences the responses of IC neurons to BBVs.

Further complicating the situation is the fact that there are multiple types of serotonin receptor within the IC. Simply increasing serotonin in the IC typically causes a range of effects on the responses of IC neurons that vary across neurons, types of sound, and over time (Hurley and Pollak, 1999, 2005; Bohorquez and Hurley, 2009). In the current study, we therefore took the approach of looking at the effect of one type of receptor, the 5-HT1A receptor. This receptor type is commonly expressed across brain regions, and is prominently expressed in the IC (Thompson et al., 1994; Peruzzi and Dut, 2004; Smith et al., 2014). Many IC neurons respond to activation of the 5-HT1A receptor with suppression of sound-evoked responses (Hurley, 2006, 2007; Castellan Baldan Ramsey et al., 2010). With these points in mind, we took an experimental approach allowing the local pharmacological manipulation of 5-HT1A receptors in the IC of intact mice through iontophoresis of a 5-HT1A agonist and antagonist. This was accomplished in anesthetized mice, allowing for the stable recording of single neurons during iontophoresis. Anesthetized mice also show low endogenous levels of serotonin release (Hall et al., 2010). We found that BBVs evoke responses that are not selective at the level of individual IC neurons, but which show distinct patterns of spikes over time that vary across call types and neuron identities. Activation of 5-HT1A receptors suppresses responses to BBVs, and results in the loss of some response features but not others, altering BBV encoding.

MATERIALS AND METHODS

Animals and Surgical Procedures

All procedures followed the NIH guidelines for the proper care and use of laboratory animals, and were approved by the Bloomington Institutional Animal Care and Use Committee. 77 single units were recorded from 15 adult male CBA/J mice (The Jackson Laboratory, Bar Harbor, ME, United States). Mice were anesthetized via brief exposure to isoflurane fumes, immediately followed by intraperitoneal injection of a drug mixture consisting of 120 mg/kg ketamine and 5 mg/kg xylazine. Ophthalmic ointment was applied to prevent the eyes from drying, and a depilatory cream was used to remove the hair on top of the head. The skin on the head was incised along the midline and reflected to each side, and adherent tissue was cleared from the surface of the skull. After steadying the head with a bite bar and ear bars, a hole was drilled in the skull over each IC. The dura was incised and cleared with a tungsten probe, and each hole was filled with silicon gel. A layer of glass beads was applied to the skull anterior to lambda with cyanoacrylate glue. The mouse was transferred to a custom stereotaxic device in a sound-attenuated chamber, and a post was affixed to the skull anterior to the drilled holes using dental cement. Body temperature was maintained between 36 and 37°C with a temperature regulation system (FHC, Bowdoinham, ME, United States). Throughout the experiment, supplemental

doses of either the presurgical anesthetic mixture or ketamine alone were used to maintain the level of anesthesia.

Electrodes and Recording Procedures

Responses of single cells were recorded extracellularly using high-resistance glass micropipettes (A-M Systems, Carlsborg, WA, United States), connected to a Dagan 2400 amplifier (Minneapolis, MN, United States) by a silver-silver chloride wire. Iontophoresis of drugs was done via a three-barreled pipette attached to the single-barreled recording pipette (single electrode blanks: 6010, three-barreled blanks: 6090; A-M Systems, Carlsborg, WA, United States). After three-barreled pipettes were pulled (A-M Systems; Stoelting 51210; Wood Dale, IL, United States), the tip was broken back to a diameter of 10–15 μm. The single-barrel recording pipettes were attached to the three-barrel pipette so that the recording pipette tip protruded 10–20 μm from the tip of the three-barrel pipette. Recording electrodes had a resistance of 8–20 MΩ under recording conditions. A dissecting microscope was used to visually position the assembled combination electrodes above the IC. The electrode was then lowered using a piezoelectric microdrive (Burleigh/EXFO Inchworm, Mississauga, ON, Canada) in increments of 1 μm. Search stimuli were tones corresponding to the approximate tonotopic location of the electrode (frequencies increase with increasing recording depth), and narrowband noise (NBN) with a bandwidth of 10 kHz, and a center frequency corresponding to the approximate tonotopic location. Electrodes were lowered until well-isolated action potentials (signal:noise ratio >10) responding to one of the search stimuli could be observed. Most neurons showed low levels of spontaneous activity, as previously reported for recording single neurons through glass micropipettes (Hurley and Pollak, 1999, 2005). Data collection for all stimuli began 10 ms prior to stimulus presentation. The responses of neurons to experimental stimuli were recorded before, during, and when possible after the iontophoresis of drugs or vehicle. Following data collection on a single neuron, current was ejected from the electrode to "kill" it; this was done to eliminate the possibility of recording from the same cell twice. After recording from a cell, the electrode was lowered until the next responsive cell was encountered. This was repeated until the electrode reached a depth at which cells did not respond to our vocal stimuli; at this point the electrode was raised out of the IC and repositioned to record from a new site. Spikes were passed through a spike signal enhancer (FHC, Bowdoinham, ME, United States) before being digitized through a data acquisition processor board (Microstar DAP5216A/626; Bellevue, WA, United States). Data was collected and stored for later analysis by the software package Batlab (Dr. Donald Gans, Kent State University).

Recordings were concentrated in the caudal and medial 2/3 of the IC based on landmarks including lambda and blood vessels (Hage and Ehret, 2003; Franklin and Paxinos, 2008). Electrode penetrations were centered approximately 1 mm caudal and medial to lambda and ranged up to 0.5 mm from this central point, targeting the central subdivision of the IC. Most neurons showed well-defined tuning curves. Additionally, most neurons were part of a clear tonotopic progression, with characteristic frequencies (CFs) extending from as low as 3 kHz at more dorsal electrode locations to as high as 55 kHz at more ventral locations. The location of the recording sites was confirmed in eight cases by iontophoretic deposition of neurobiotin (1% in 1M NaCl; Vector Laboratories, Burlingame, CA, United States) during the recording session using a dedicated single-barreled electrode, followed by intracardiac perfusion at the end of the experiment. After brain tissue was extracted, fixed in 4% formaldehyde and sectioned at 50 μm, sections of IC were incubated in fluorescein streptavidin (Vector Laboratories, Burlingame, CA, United States) and visualized under a fluorescence microscope (Nikon Ni-E, Nikon Instruments) at 515 nm. Neurobiotin-labeled cell bodies were observed in the central subdivision of the IC in all cases. However, since experiments consisted of multiple electrode penetrations, we cannot exclude the possibility that some neurons were located in the external nucleus as well.

Drugs and Iontophoresis

Two drugs targeting the 5-HT1A receptor were used in this study: the agonist (±)-8-hydroxy-2-dipropylaminotetralin hydrobromide (8-OH-DPAT), and (3*R*)-3-(Dicyclobutylamino)-8-fluoro-3,4-dihydro-2*H*-1-benzopyran -5-carboxamide hydrochloride (NAD-299). All drugs were obtained from Tocris Bioscience (Ellisville, MO, United States). Drugs were dissolved in 10 mM NaCl at pH 4.5. Drugs were retained in two of the three iontophoresis barrels with a current between −10 and −25 nA, and ejected using a range of currents up to +75 nA. The third barrel was filled with 1 M NaCl and balanced the currents ejected through the drug barrels. The three barrels were connected to iontophoresis pump modules [Dagan ION-100 or Medical Systems NeuroPhore (Harvard Apparatus, Holliston, MA, United States)] via silver-silver chloride wires. Control solutions consisted of the vehicle of 1 M NaCl at pH 4.5, or of 1 M NaCl with 10 mM NaBr. The same sets of stimuli were presented during the pre-drug period, during drug treatment beginning 3–5 min after the onset of drug iontophoresis, and, when neural recordings could be held for long enough, 5–10 min after drug application ceased and retention current was re-applied. 5-HT1A receptors were iontophoretically manipulated for 59 neurons. In some cases multiple drugs were iontophoresed alone and/or in combination. In total, NAD-299 was applied to 40 neurons (alone: n = 35; +8-OH-DPAT: n = 25), and 8-OH-DPAT was applied to 46 neurons (alone: n = 46; +NAD-299: n = 25). For experiments assessing the selectivity of 8-OH-DPAT by comparing it to the effects of NAD-299 in the same neurons, we used the acoustic stimuli generating the most robust responses. For the 34 neurons in the specific experiments on pharmacological selectivity (n = 20 for DPAT versus NAD and 14 for vehicle), responses to Call 5 (see below) were used for 16 neurons, responses to other calls for two neurons, and responses to tones at best frequency for 16 neurons.

Auditory Stimuli

Tone stimuli were generated by BATLAB software and were routed through a PA5 attenuator and FT-6 antialias filter (TDT, Alachua, FL, United States). Stimuli were played through a Vifa speaker, with an operational range from 1 to 120 kHz (Avisoft

Bioacoustics, Glienicke/Nordbahn, Germany). Frequency tuning was measured by presenting tones of 20 ms in duration with rise and fall times of 0.5 ms across the range of frequencies that single cells were responsive to, from 10 dB below threshold to 30–50 dB above threshold at the CF. Depending on the bandwidth of the cell, the frequency intervals of the tones presented varied from 1 to 5 kHz. For neurons that did not respond to tones, narrowband noise (NBN) was used to estimate the CF, as the center frequency of a NBN with a 10 kHz bandwidth that evoked the most robust neural response.

Five different audible broadband vocalizations (BBVs, also "squeaks") were used as stimuli. The BBVs were recorded from females during opposite-sex encounters with 16- bit resolution using a condenser microphone (CM16/CMPA; Avisoft Bioacoustics, Berlin, Germany; 200 kHz maximum range) and sound card (250 kHz sample rate, UltraSoundGate 116 Hb, Avisoft Bioacoustics). Calls were resampled using a custom Matlab script to match the output of the Microstar board. BBVs were chosen to represent a range of structural features characteristic of these call types (**Figure 1**; Lupanova and Egorova, 2015; Finton et al., 2017). BBVs varied in duration ranged in duration from 104.6 ms (Call 1) to 187.9 ms (Call 5). Calls also varied in their amplitude envelopes, spectrotemporal structure, and the presence and duration of deterministic chaos (DC: structured noise due to non-linear vocal fold vibration) versus harmonic structure. For example, Calls 3, 4, and 5 each contained a period of DC in the terminal portion of the call, with these segments being longer for Calls 4 and 5. Although BBVs have not been categorized in the same way that mouse USVs have been, variation in total duration and the relative duration of DC segments correspond to multiple behaviorally relevant characteristics (Finton et al., 2017). DC varies consistently and significantly across individual females, and females produce calls with a higher percent duration of DC when they are in estrus relative to diestrus. Relatively longer BBVs and BBVs with a higher relative DC duration are also more likely to occur when females are being mounted relative to when females are showing rejection of males. Measurements of responses to calls were made at 10–30 dB above the threshold for the lowest intensity evoking a response from any call.

Data Analysis

Spike trains were recorded in BATLAB and exported in ASCII format for further analysis. Spike counts represent the number of spikes per 32 repetitions of the stimulus. For a small number of neurons, 64 or 75 stimulus repetitions were presented. The selectivity index across calls was calculated as $(n_0 /(n_t -1))^*100$, where n_0 is the number of calls not evoking a response, and n_t is the total number of presented calls (Hurley and Pollak, 2005; similar index in Mayko et al., 2012). Responses across calls based on spike rate were compared using the formula: $(\sum_{i=1}^{n}(1-\text{min/max}))/n)^*100$, where n = number of pairwise comparisons of the minimum versus maximum values for the two among calls (excluding comparisons with zero as denominator). With this measure, a score of 100% would still represent the response to a single call, while a score of 0% would represent an identical spike number in the response to all five calls. We also compared responses across calls based on spike number in a preference index, using the formula: $((\sum_{i=1}^{n}(1-\text{min/max}))/n)^*100$, where n = number of pairwise ratios of the minimum versus maximum values for the two among calls, (excluding pairs in which both values were zero). With this measure, a score of 100% would still represent the response to a single call, while a score of 0% would represent an identical spike number in the responses to all five calls.

Statistical comparisons were made using Statistica software (TIBCO, Palo Alto, CA, United States). Comparisons of spike count and peak numbers across calls were performed with repeated measures ANOVAs to control for different baseline firing rates in different neurons. Effects of 8-OH-DPAT were assessed using baseline and drug values for the same calls in the same neurons before and during drug application, with call type as a categorical factor. Pearson's correlations were used to assess the similarities of responses to different pairs of calls across neurons. A repeated measures ANOVA was used to compare the effects of 8-OH-DPAT against a background of no drug application versus NAD-299 application. To do this, the change in spikes in 8-OH-DPAT relative to the preceding baseline condition were compared to the change in spikes during the combination of 8-OH-DPAT and NAD-299 relative to the preceding application of NAD-299 alone. This comparison was made only for neurons in which recordings were made in the baseline, 8-OH-DPAT, NAD-299, and NAD-299 + 8-OH-DPAT conditions. A factorial ANOVA was used to assess whether response features that remained or disappeared in 8-OH-DPAT differed in peak spike density. Only neurons that showed more than one response peak were used in this analysis, and peak spike density values normalized to the largest peak for a given neuron were used. Otherwise, every response feature was treated as an independent value. Tukey's honestly significant different (HSD) was used as a *post hoc* test of differences within significant statistical models. The standard error of the mean (s.e.m.) was used to report variation in statistical groups in the text and figures.

Spike density functions were generated following the algorithm of Shimazaki and Shinomoto (2010). This approach allows kernel size to be optimized over time in order to achieve the best fit to local spikes. Spike density functions were generated by a custom script in Matlab by author SN (MathWorks, Natick, MA, United States). Spike density functions were constructed for set of 30 neurons which showed robust responses to calls, low levels of spontaneous activity, and which were recorded in both baseline conditions and in the presence of 8-OH-DPAT.

RESULTS

IC Neurons Respond Broadly to Female BBVs

We presented a set of five recorded female broadband vocalizations (BBVs) that varied in duration, amplitude envelope, and spectrotemporal structure to 15 anesthetized adult male CBA/J mice (**Figure 1**). High-resistance glass micropipette electrodes were used to extracellularly record sound-evoked

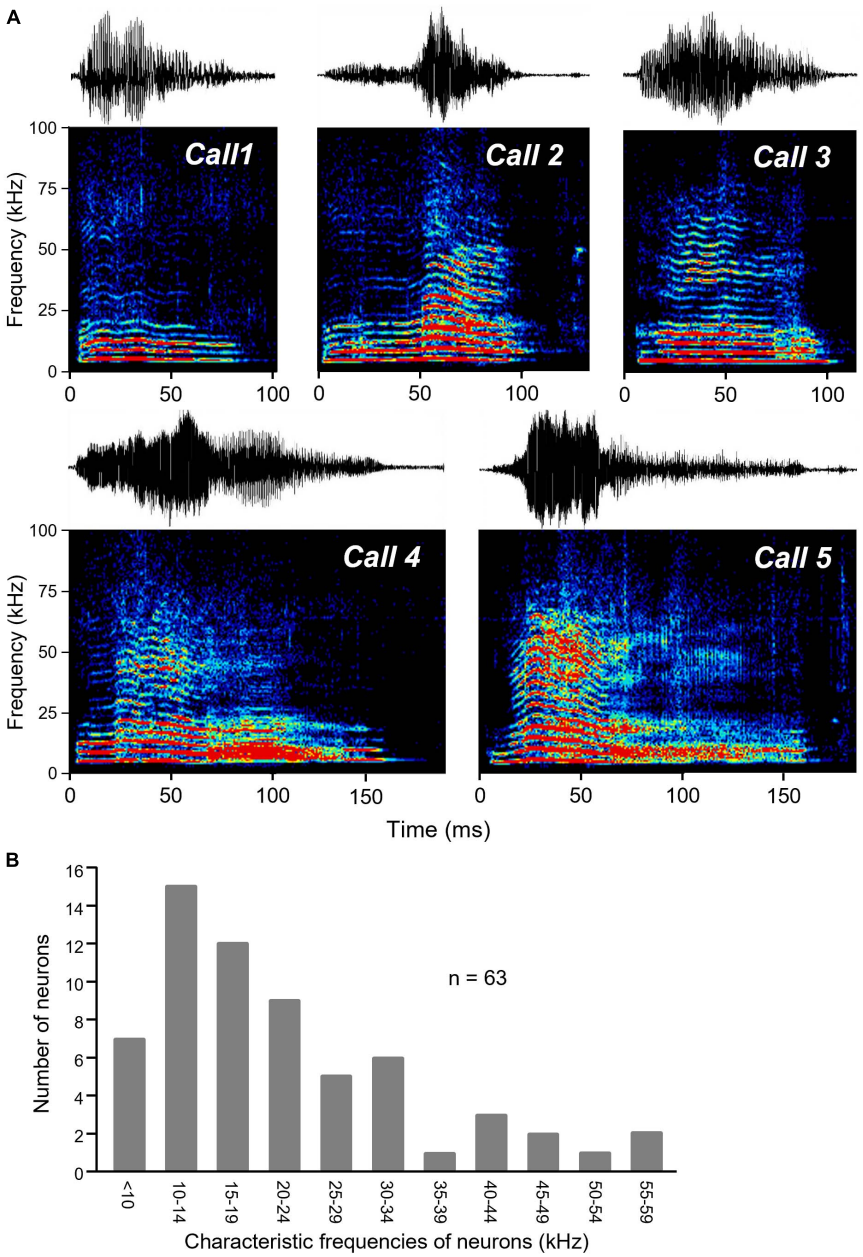

FIGURE 1 | BBVs played to mice. **(A)** Oscillograms (top part of each panel) and spectrograms (lower part of each panel) of the five recorded BBVs used as stimuli for IC neurons. Calls varied in amplitude envelope as well as in duration, spectrotemporal structure, and whether deterministic chaos was present (in the latter portions of calls 3, 4, and 5). Colors represent relative intensity of specific call components. **(B)** Histogram of the characteristic frequencies (CF) of neurons responding to BBVs, which also responded to tones for estimation of CF.

responses from 77 single neurons in the inferior colliculus. Responses to tones at a range of frequencies and intensities were also recorded in the same neurons. BBVs have a power spectrum biased toward low frequencies, although some harmonics extend into higher frequencies (**Figure 1**). Data were collected from neurons that showed a response to at least one of the BBVs. Because of this, the population of neurons responding to calls was biased toward lower frequencies. Neurons with response to tones (n = 64), had CFs in the range 6–55 Hz (mean: 21.3 ± 2.5 KHz).

We used a selectivity index to quantify how broadly neurons responded above a threshold value to the five calls. The selectivity index is $(n_0 /(n_t - 1))*100$, where n_0 is the number of calls not evoking a response, and n_t is the total number of presented calls (Hurley and Pollak, 2005; similar index in Mayko et al., 2012). With this index, the response of a neuron to a single call out of five would create a selectivity of 100%, while a response to all five calls would create a selectivity of 0%. The threshold value that we used to identify a response was a count of 20 spikes over 32 stimulus

repetitions, or a response rate of 0.625 spikes/stimulus. This index was calculated for 69 neurons that showed a response to at least one call. **Figure 2** shows neurons with different selectivity index values; one that responded strongly to all five calls and had a selectivity index of zero (**Figure 2A**) and one that responded only to one of the five calls and had a selectivity index of 100% (**Figure 2B**). Across the population of neurons, 55.1% of neurons showed a selectivity index of zero, 31.9% of neurons had a selectivity index of 25–50%, and the remaining 13% of neurons had a selectivity of 75–100% (**Figure 2C**). Thus, most neurons responded above a threshold value to most of the five BBVs.

Even for neurons that responded to multiple calls, there was variation in the numbers of spikes in responses to different calls (**Figure 2A**). We also compared responses across calls based on the total spike number in response to BBVs using a preference index with the formula: $(\sum_{i=1}^{n}(1-\text{min}/\text{max}))/n)^*100$, where n = number of pairwise comparisons of the minimum versus maximum values for the two among calls. With this measure, a score of 100% would still represent the response to a single call, while a score of 0% would represent an identical spike number in the responses to all five calls. The majority of neurons showed a preference index of 60% or less (**Figure 2D**), with an average preference index of 42.3 ± 2.0%. This value indicates that there was considerable variation in the intensity of the responses to different calls, even when a neuron responded to all of them.

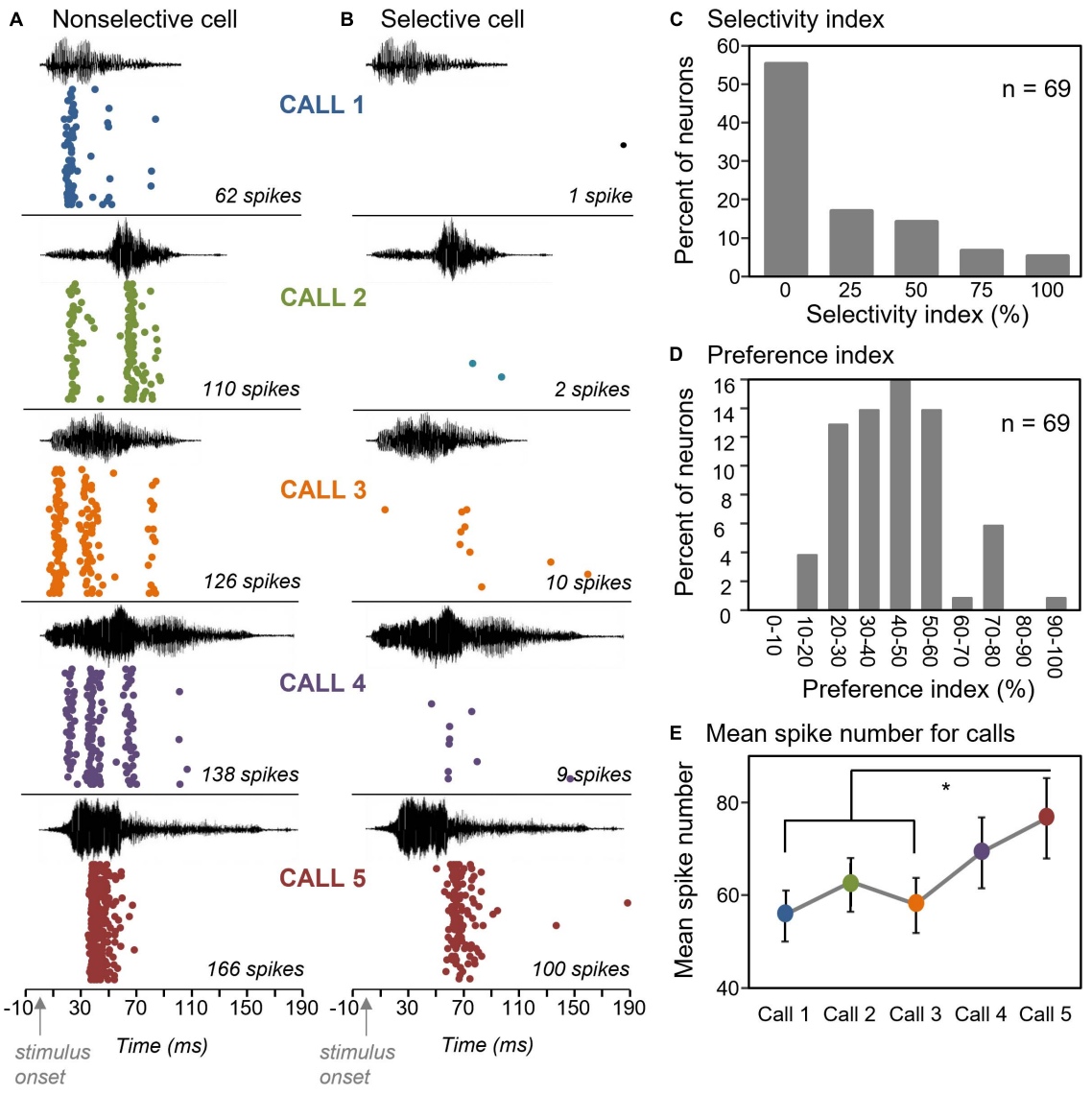

FIGURE 2 | Selectivity of IC neurons for the five BBVs. **(A)** Raster plots of a neuron that responded to all five BBVs. **(B)** Raster plot of a neuron that responded robustly only to Call 5. **(C)** Selectivity index across a group of 69 neurons illustrating a low degree of selectivity, with most neurons responding to all calls. **(D)** Preference index, showing the mean per cent difference in spiking among pairs of calls across a group of 69 neurons. **(E)** Mean spike counts for responses across calls show significant differences, with Calls 1 and 3 evoking fewer spikes than Call 5. *$p < 0.05$.

To assess the sources of heterogeneity in spike numbers, we examined variation in spike number both across neurons, and across calls. Unsurprisingly, different neurons showed significantly different spike numbers, when responses to all five calls were considered [one-way ANOVA on spike counts with cell identity as a categorical factor, $F_{(68,276)} = 11.36$, $p < 0.001$]. Emphasizing the differences among neurons, the response to one call significantly correlated with the responses to the remaining four calls across the neural population (Pearson's correlations, $p < 0.00001$ for all pairwise correlations among calls; **Table 1**). That is, the response of a neuron to a given call predicted it's response to other calls. However, when we accounted for the strong effect of neuron identity by using a repeated measures approach, we found that different calls also evoked significantly different neural responses [repeated measures ANOVA with call type as a within-subjects factor; $F_{(4,272)} = 5.19$, $p < 0.001$]. Call 5 evoked the largest mean response, which significantly differed from responses evoked by both call 1 and call 3 (**Figure 2E**, Tukey's HSD *post hoc* test; $p < 0.001$ for call 1 versus call 5 and $p = 0.004$ for call 3 versus call 5). Although the cause of the higher spike count is not clear, features of Call 5 such as the relatively high-intensity and sharp risetime of the first portion of the call, or its prolonged duration, could have contributed to high spike counts. These results show that spike number was influenced by both the identities of neurons and by call type.

Response Features Characterize Spiking Patterns Over Time

Although neurons showed little difference in whether they responded to most calls, they differed in the patterns of response over time. The spike trains of most neurons were not evenly distributed over the timecourse of the BBV playback. Spike trains were often characterized by distinct time bins that had high spike probabilities (see **Figure 2A**). We called these localized peaks "response features." Response features were quantified in a subset of 30 neurons with robust spike trains by generating smoothed spike density functions from raster plots of responses to BBVs (**Figures 3A,B**; Shimazaki and Shinomoto, 2010). Response features were identified based on the first derivative of the spike density function (slope) as null crossings with preceding accelerations and following decelerations of at least 1 unit in the first derivative function (**Figure 3C**). This ensured a uniform classification of response features. Numbers of response peaks ranged from as few as one to as many as seven for responses to single calls, with a mean of 2.37 ± 0.10 response features across all cells and all calls. Different calls also evoked significantly different numbers of response features [repeated measures ANOVA, $F_{(4,88)} = 4.55$, $p = 0.002$], with Call 4 evoking significantly more response features than either Call 1 or Call 3 (Tukey's HSD, $p = 0.002$ for Call 1 versus Call 4, and $p = 0.046$ for Call 3 versus Call 4).

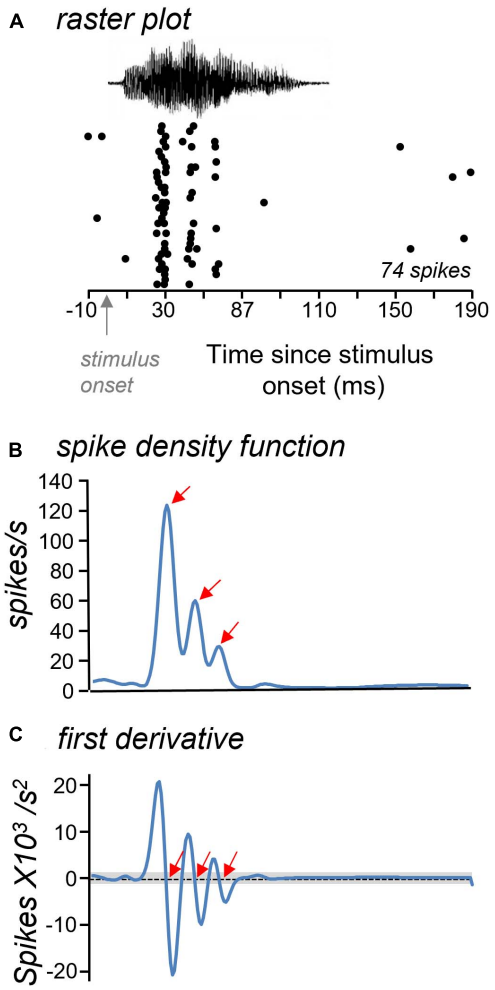

FIGURE 3 | Approach for measuring response features. **(A)** Raster plots were used to generate spike density functions. **(B)** Spike density function with three clear peaks (arrows) illustrating periods of high spike probability. **(C)** Response features were identified from the first derivative of the spike density functions as null crossings that were higher and lower than the threshold criterion (gray bar). Red arrows mark identified response features. The time axis is the same in all plots.

The color map of **Figure 4A** illustrates the numbers of response features in the responses to each call (columns) by the group of 30 neurons (rows). Blue indicates a single response feature for the response of a given neuron to a given call, while white through dark pink indicate increasing numbers of response features (see color key). The color map illustrates a range of patterns across neurons. Some neurons showed similar numbers of response features across all five calls; for example, neuron #4 showed single response features to Calls 1, 2, 3, and 5, and two response features to Call 4 (**Figure 4Bi**). In contrast, neuron #10

TABLE 1 | Pairwise r^2 values for Pearson's correlations between spike numbers for different call types across neurons.

	Call 2	Call 3	Call 4	Call 5
Call 1	0.46	0.62	0.52	0.44
Call 2		0.53	0.47	0.30
Call 3			0.75	0.55
Call 4				0.57

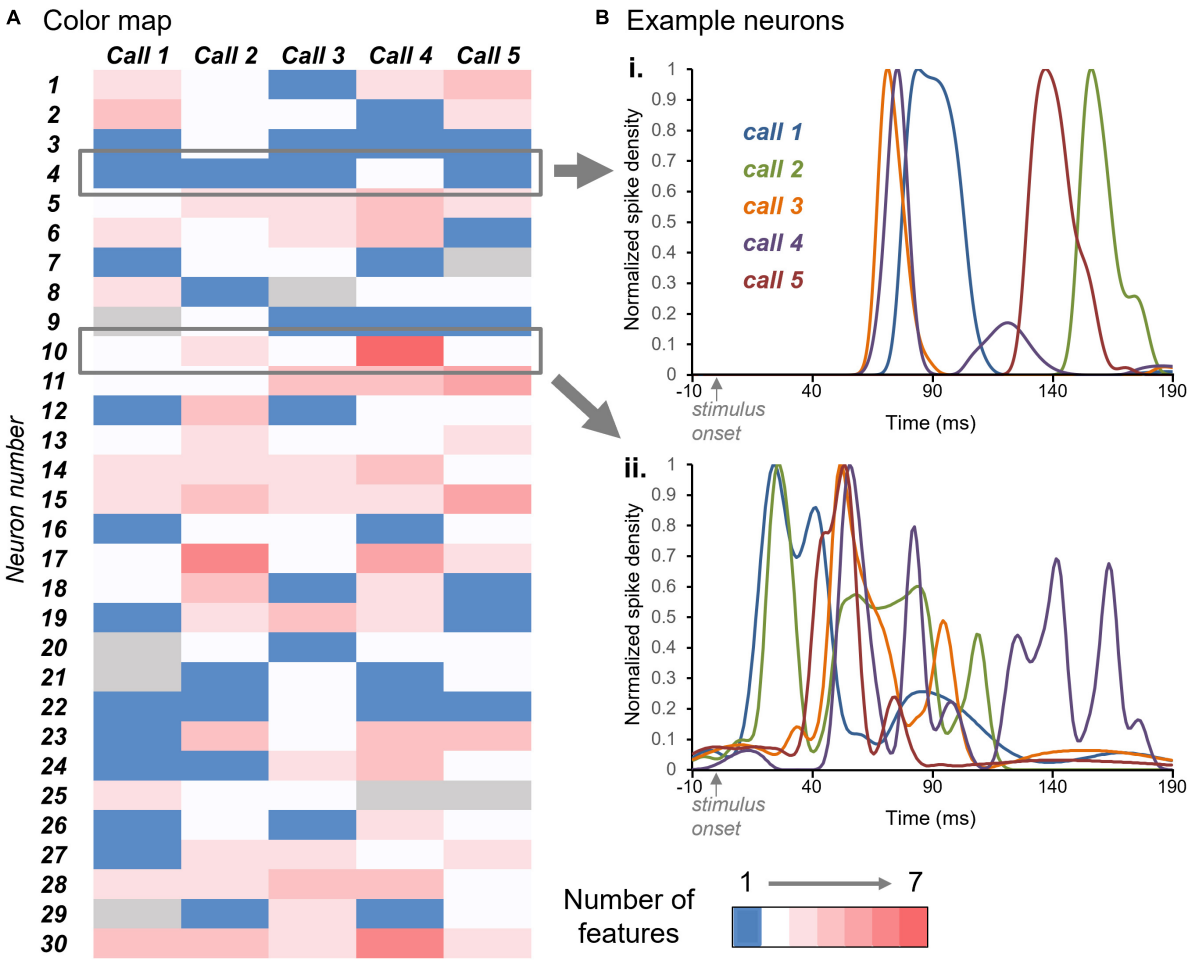

FIGURE 4 | (A) Color map of numbers of response features for the responses of 30 neurons (*y*-axis) across the five BBVs (*x*-axis). Blue indicates single response features and white through red indicate increasing numbers of features, up to seven. Gray indicates the lack of response to a specific call. **(B)** Normalized spike density functions for two neurons indicated by the gray boxes in **(A)**. Spike density functions for the responses to all five calls are plotted together. For the neuron in **(i)**, the number of response features was one for four of the calls, and two for one of the calls. For the neuron in **(ii)**, the numbers of response peaks across calls ranged from two to seven.

showed a range of response features across calls, from two for Calls 1,3, and 5 to seven for Call 4 (**Figure 4Bii**).

The number and timing of response features varied across neurons and also within neurons, across calls. These patterns are both illustrated in **Figure 5**, showing normalized spike density functions for each individual neuron, to facilitate a visual comparison among neurons. Four selected neurons are depicted as colored traces, with the same color representing the responses of the same neurons across calls. Gray traces represent the spike density functions of the remainder of the sample of 30 neurons. Across calls, the largest response features for single neurons occurred at different times. This is illustrated by the varying timing of the spike density functions of the color-labeled neurons across Calls 1–5. Single neurons may show some consistency in the location of their peaks across calls. For example: the neuron indicated in purple tended to respond relatively soon after the onset of calls, while the neuron indicated in green tended to respond relatively late in the spike train. Even so, all four example neurons showed responses that varied in timing and in the numbers of response features across the five calls. Some neurons even responded after calls had ended, as for some of the gray response peaks seen for Call 2. This pattern is consistent with the rebound from inhibition exhibited by some IC neurons.

Pharmacological Manipulation of 5-HT1A Receptors

We assessed the effect of pharmacological manipulation of the 5-HT1A receptor, which is expressed in the IC (Thompson et al., 1994; Peruzzi and Dut, 2004; Smith et al., 2014), on responses to BBVs in 59 neurons. Neural responses were recorded before, during, and when possible after the iontophoresis of the 5-HT1A agonist 8-OH-DPAT. The suppressive effects of 8-OH-DPAT on stimulus-evoked responses in the IC have been reported previously in several studies (Hurley, 2006, 2007; Castellan Baldan Ramsey et al., 2010). Although 8-OH-DPAT

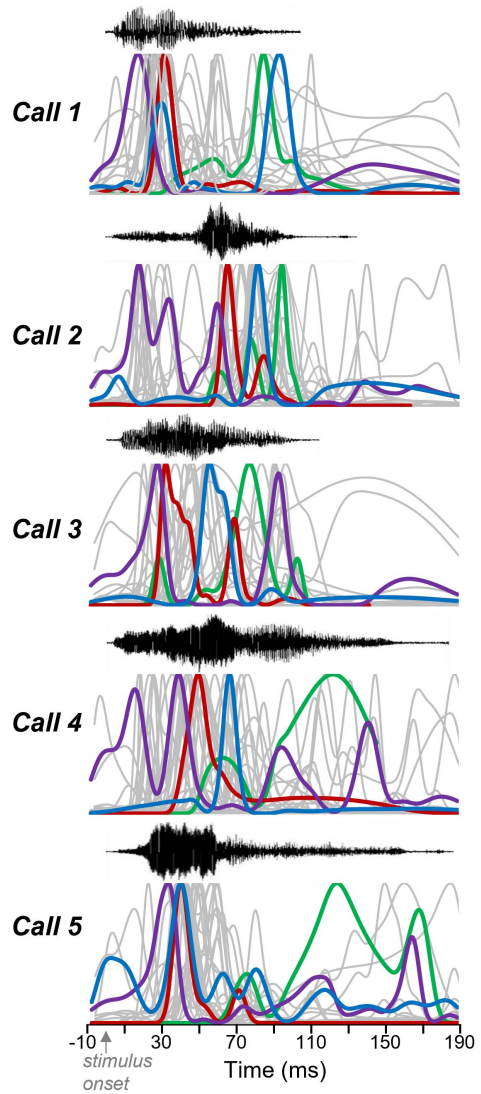

FIGURE 5 | Response features vary among neurons and calls. Oscillograms (top) and normalized spike density functions for 30 neurons across five calls. Specific colors represent spike density functions of single neurons with a range of peak response times. A given color represents responses of the same neuron across calls. Gray spike density functions are from the remaining 26 neurons.

is a commonly used agonist for the 5-HT1A receptor, it also activates the 5-HT7 receptor, which is functionally expressed in the auditory system (e.g., Tang and Trussell, 2015, 2017). To assess the selectivity of 8-OH-DPAT, we therefore combined the application of 8-OH-DPAT with the iontophoresis of NAD-299, a 5-HT1A antagonist. Because the effects of NAD-299 on IC neurons have not to our knowledge been reported, we iontophoresed this drug both alone and in combination with 8-OH DPAT. Our objectives were to (1) measure the effects of NAD-299 at increasing iontophoretic currents, as has previously been accomplished for 8-OH-DPAT, and (2) assess whether NAD-299 counteracted the suppressive effects of 8-OH-DPAT. Due to the difficulty of holding single cells for extended periods of time, not all of these objectives were achieved in the same neurons. In total, NAD-299 was applied to 40 neurons (alone: $n = 35$; +8-OH-DPAT: $n = 25$), and 8-OH-DPAT was applied to 46 neurons (alone: $n = 46$; +NAD-299: $n = 25$).

In contrast to 8-OH-DPAT, the effects of NAD-299 iontophoresis did not correspond linearly to increasing iontophoretic current. NAD-299 sometimes had a bimodal effect on firing rates, such that spike counts increased relative to control at low iontophoretic currents (the opposite of the effect of 8-OH-DPAT), but decreased at higher currents. An inverted U-shaped dosage function has previously been reported for this drug, with lower doses acting more selectively on 5-HT1A receptors, and higher doses activating α1 and β adrenoceptors (Johansson et al., 1997; Martin et al., 1999; Ross et al., 1999). To account for the possibility that NAD-299 affected multiple targets, we compared the effects of 8-OH-DPAT relative to a baseline of no drug application and relative to a baseline of NAD-299. In this way, even if NAD-299 affected additional targets, as long as it also blocked the 5-HT1A receptor, we reasoned that it should reduce the suppressive effects of 8-OH-DPAT. For this approach to work, it was important to compare the effects of 8-OH-DPAT on a baseline of no drug application versus a baseline NAD-299 iontophoresis in the same neurons. We accomplished the entirety of these sequential conditions in a group of 20 neurons. Because this pharmacological goal did not require responses to BBVs, we quantified this comparison for responses to the stimulus producing the largest effect for a given neuron, whether this was a BBV, a tone at the BF, or NBN.

This outcome of this strategy is illustrated in **Figure 6A**, which shows raster plots of a single neuron to Call 5 in the baseline condition and during iontophoresis of 8-OH-DPAT, during a recovery, and during iontophoresis of NAD-299 and a combination of NAD-299 and 8-OH-DPAT (five conditions in total). For this neuron, 8-OH-DPAT showed a typical suppressive effect and recovery. NAD-299 did not alter the neuron's response alone, but precluded the suppressive effect of 8-OH-DPAT when the two drugs were iontophoresed simultaneously. Across the group of 20 neurons that were treated with these drug combinations, 8-OH-DPAT decreased spike counts significantly less in the presence of NAD-299, [**Figure 6B** left panel; repeated measures ANOVA, $F_{(1,19)} = 5.08$, $p = 0.036$]. That is, the suppressive effect of 8-OH-DPAT was greater when compared to a baseline of no iontophoresis versus a baseline of NAD-299 iontophoresis. This finding is consistent with NAD-299 precluding the effect of 8-OH-DPAT. In contrast to the effects of iontophoresed drugs, controls consisting of the iontophoresis of control solutions (1 M NaCl: $n = 8$; 10 mM NaBr in 1 M NaCl: $n = 6$) did not significantly alter spike counts [**Figure 6B** right panel; repeated measures ANOVA, $F_{(1,13)} = 1.19$, $p = 0.294$].

8-OH-DPAT Suppresses Spiking and Reduces Response Features

As previously reported for other types of auditory stimuli, the iontophoresis of 8-OH-DPAT decreased the number of spikes in response to BBV playback. These effects were highly significant

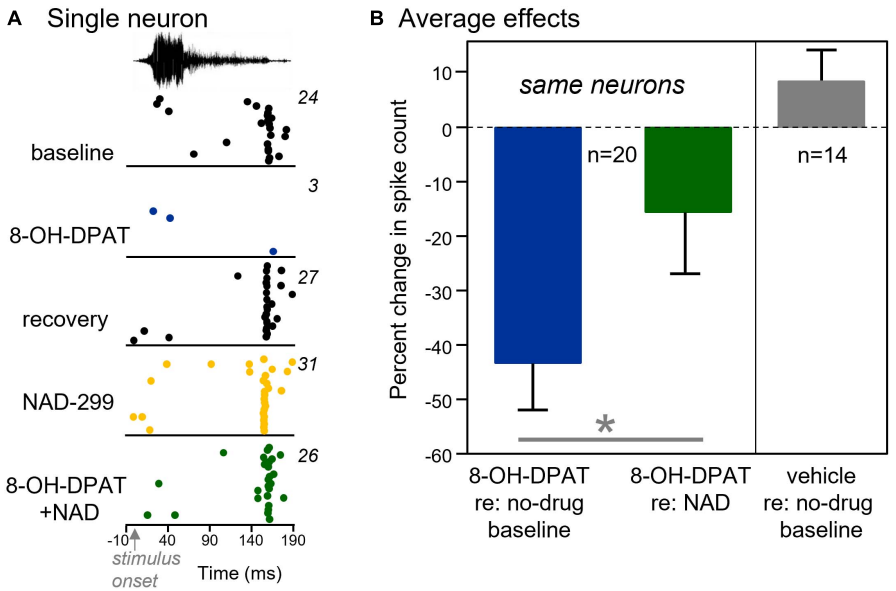

FIGURE 6 | Activation of the 5-HT1A receptor reduces the numbers of sound-evoked spikes. **(A)** For a single neuron, the 5-HT1A agonist 8-OH-DPAT abolishes the response to a BBV. Iontophoresis of the 5-HT1A antagonist NAD-299 precluded the reduction in the number of spikes when it was iontophoresed before 8-OH-DPAT. The BBV was call 5 (see **Figure 1**), played at 10 dB above threshold. **(B)** *Left panel:* 8-OH-DPAT reduced the numbers of spikes significantly less on average when applied in the presence of NAD-299. *Right panel*: Application of vehicle solutions slightly increases but does not significantly alter the numbers of sound-evoked spikes relative to a no-drug baseline. *$p < 0.05$.

[repeated measures ANOVA with call type as a within-subjects variable; for drug effect $F_{(1,89)} = 116.57$, $p < 0.001$; for call type $F_{(4,189)} = 0.65$, $p = 0.63$; for drug × call interaction, $F_{(4,189)} = 0.26$, $p = 0.90$]. Suppressive effects were additionally not different across call types (Tukey's HSD, $p < 0.01$ for baseline versus 8-OH-DPAT comparisons for each call type).

Figure 7A illustrates spike counts in the no-drug baseline versus during iontophoresis of 8-OH-DPAT, for all calls in 41 neurons with robust call responses for which 8-OH-DPAT was successfully applied. The line with a slope of one marks where points would fall if spike numbers were identical in each condition; points below this line indicate decreased spike numbers during 8-OH-DPAT application. Although spike counts increased slightly for some neurons, the effects of 8-OH-DPAT were almost exclusively suppressive. Along with the decrease in spike numbers, 8-OH-DPAT shifted the population distribution for both the selectivity index and the preference index, in the subset of 41 neurons exposed to 8-OH-DPAT (**Figure 7B**). The population became more selective for calls (selectivity index of 13.6 ± 4.3% in baseline versus 24.3 ± 5.2% in 8-OH-DPAT), and showed a higher preference index (preference index of 37.7 ± 2.2% in baseline versus 43.0 ± 3.1% in 8-OH-DPAT). However, only the increase in call selectivity was significant [repeated measures ANOVA for baseline versus 8-OH-DPAT selectivity index, with a category for responses to no calls, $F_{(1,40)} = 7.90$, $p = 0.008$; repeated measures ANOVA for baseline versus 8-OH-DPAT preference index $F_{(1,40)} = 3.47$, $p = 0.07$].

We next assessed the effect of 8-OH-DPAT on the patterns of response features. In parallel with its suppressive effects on spike count, 8-OH-DPAT reduced the numbers of response features in the 30 neurons in which response features were assessed [repeated measures ANOVA with call type as a categorical factor, for drug effect $F_{(1,137)} = 57.39$, $p < 0.001$; for call type $F_{(4,137)} = 1.92$, $p = 0.11$; for drug × call interaction, $F_{(4,187)} = 0.40$, $p = 0.81$]. In contrast to the effects of 8-OH-DPAT on spike counts, the significant reduction in response features did not occur for all call types (Tukey's HSD, $p = 0.32$ for Call 1, $p = 0.003$ for Call 2, $p = 0.08$ for Call 3, $p = 0.01$ for Call 4, $p = 0.002$ for Call 5). The lack of significant reduction in response features for Calls 1 and 3 corresponds to the lower numbers of baseline features for these calls (see above).

We further explored which types of response features were most likely to disappear. **Figure 8** shows three general patterns of the effect of 8-OH-DPAT on response features: proportionate, disproportionate, and reorganizing. The most common of these was a proportionally consistent decrease in the sizes of response features, with the loss of some features. This response pattern was defined as having response features during the application of 8-OH-DPAT that had the same rank order of peak size as in the baseline. Neurons for which all response features except for the largest disappeared, and for which all response peaks including the largest disappeared, were counted in this category. For example, 8-OH-DPAT caused a proportional decrease in the sizes of the three largest of the response features of the neuron in **Figure 8A**, and the disappearance of the smallest response feature. A second type of pattern was the selective loss of some response features but the maintenance of others, to create a disproportionate effect. This type of effect was defined as a reversal in the rank order of peak size in the presence of 8-OH-DPAT relative to baseline. However, even if relative peak

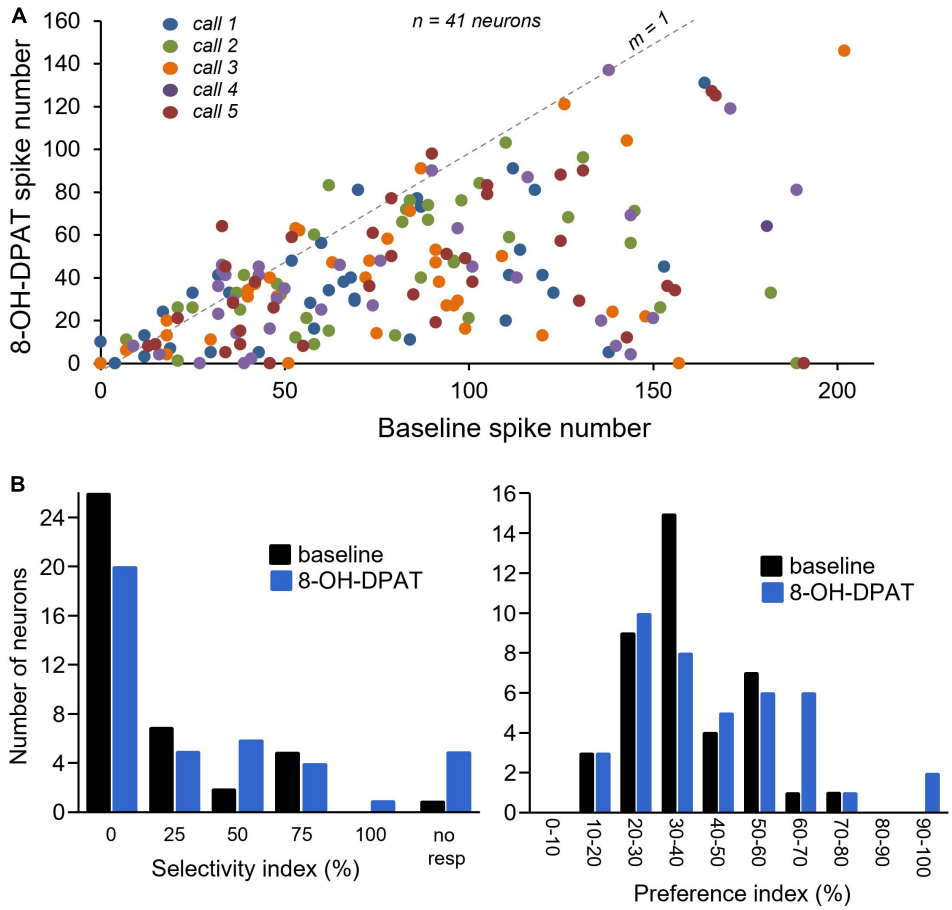

FIGURE 7 | (A) Comparison of numbers of spikes in response to specific calls in the baseline (no drug application) versus during 8-OH-DPAT application. Symbols below the line with a slope of 1 represent a suppression of spikes during drug application. Different colors represent responses to different calls. **(B)** Selectivity index and preference index in a subset of 41 neurons in baseline and during exposure to 8-OH-DPAT.

sizes reversed, if the proportional effect of 8-OH-DPAT (peak sizes in 8-OH-DPAT relative to baseline) were within 20% of each other, responses were not included in this category. For the neuron in **Figure 8B**, 8-OH-DPAT caused a strong suppression of response features in the middle of the spike train, but relatively lesser effects on the response features at the end and particularly the start. Finally, a pattern seen in only a few neurons was the reorganization of the spike train so that response features occurred at different times (**Figure 8C**). This effect was defined as the appearance in 8-OH-DPAT of new peaks with peak latencies more than 10 ms from peaks in the no-drug baseline, as long as the new peaks did not occur within rising or falling time ranges of peaks in the baseline. Out of a total of 103 responses that had more than one peak in the baseline in response to all five calls, 74 (71.8%) showed proportionate effects of 8-OH-DPAT, 19 (18.4%) showed disproportionate effects, and 10 (9.7%) showed reorganizations. Out of the 30 neurons, 14 showed only proportionate effects, although responses to many individual calls in this group had only one response peak, or showed no response peaks during 8-OH-DPAT iontophoresis. Of the 16 neurons that showed non-proportionate effect of 8-OH-DPAT on response peaks (disproportionate or reorganization), eight neurons only had one call with non-proportionate effects, three neurons had two calls with disproportionate effects, and five neurons had three calls with disproportionate effects. Thus, although most neurons showed mixed proportionate and disproportionate effects of 8-OH-DPAT across calls, a minority of neurons had a relatively high number of call responses that were disproportionate.

Of these patterns, the most common proportionate effect (**Figure 8A**) suggests that the smallest response features are the most likely to disappear. To test this hypothesis, we compared the spike densities of response features that were lost during 8-OH-DPAT versus those that were maintained. To account for the variation in spike rates, we normalized the spike densities for each response feature to the spike density for the largest response feature in the spike train. Across the population of neurons, response features that disappeared were significantly smaller than their neighbors [factorial ANOVA for normalized peak height, with status (whether peaks were lost in 8-OH-DPAT or not) and call type as categorical factors: for status $F_{(1,209)} = 97.3407$, $p < 0.001$; for call type $F_{(4,209)} = 0.6214$, $p = 0.65$; for status × call type $F_{(4,209)} = 1.84$, $p = 0.12$]. Average proportional sizes for all

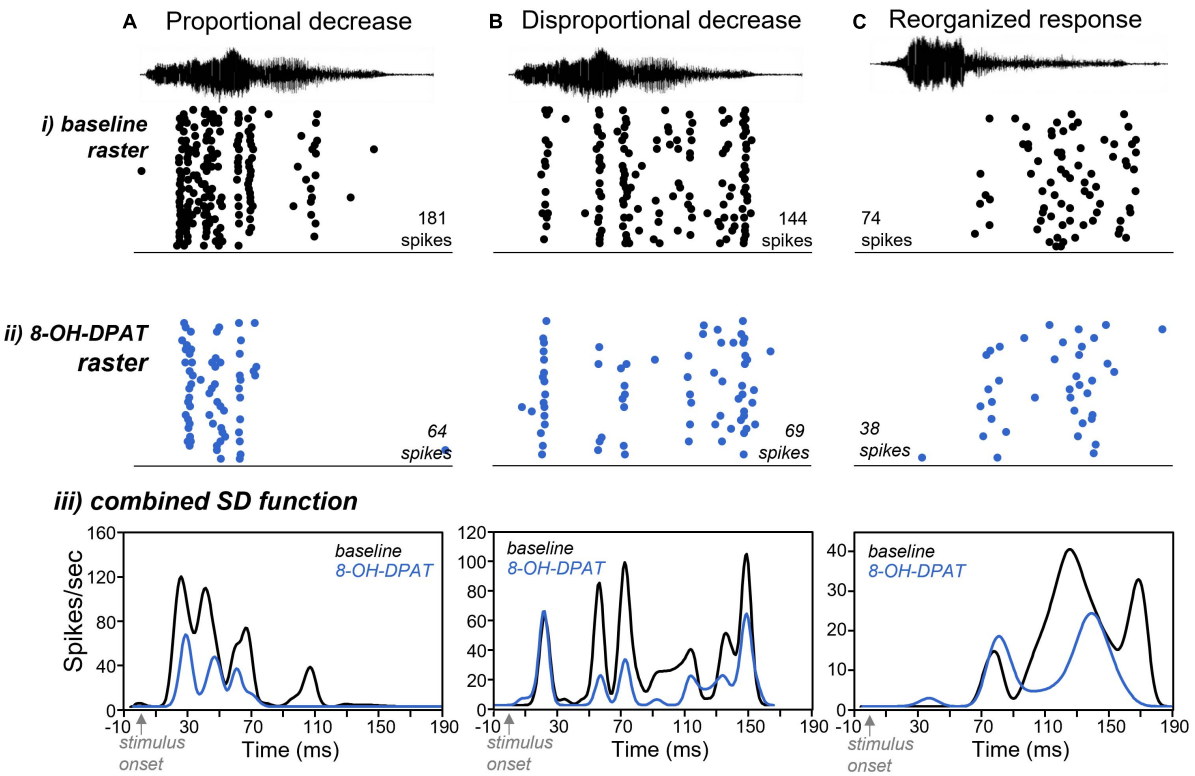

FIGURE 8 | Effects of 8-OH-DPAT on response features. **(A)** Raster plots of the responses of a neuron in **(i)** the baseline condition and **(ii)** during iontophoresis of 8-OH-DPAT. **(iii)** Spike density functions derived from the rater plots in **(i)** and **(ii)**. The neuron in **(A)** showed proportionally similar suppressions of all response features, with the loss of the smallest feature. Call 4 evoked this response. **(B)** Neuron showing selective decreases of response features in the middle of its spike train. Call 4 evoked this response. **(C)** Neuron showing a reorganization of its spike train in the presence of 8-OH-DPAT. Call 5 evoked this response. Time scale is the same for all panels.

peaks that were lost in 8-OH-DPAT versus not lost are shown in **Figure 9**.

DISCUSSION

Serotonin is a neuromodulator that conveys information on social context to auditory regions and modulates auditory processing (Wang et al., 2008b; Hall et al., 2011; Hurley and Sullivan, 2012; Hanson and Hurley, 2014; Keesom and Hurley, 2016). Although serotonin influences the responses to ultrasonic acoustic signals in the auditory system (Hurley and Pollak, 2005), whether these effects extend to audible vocal signals, and the roles of specific receptor pathways in these effects, have not been explored. In the current study, we measured how neurons in the IC respond to five exemplars of a type of audible mouse vocalization, BBVs, and how the 5-HT1A receptor pathway alters responses to this type of call. We found that IC neurons respond to BBVs with characteristic local periods of high spike probability that we called "response features." Local activation of the 5-HT1A receptor within the IC had suppressive effects on BBV-evoked spike numbers that were similar to previously reported effects on responses to tones (Hurley, 2006, 2007; Castellan Baldan Ramsey et al., 2010). However, 5-HT1A-gated suppression interacted with response features to change the temporal patterns of neural responses to BBVs. In the following discussion, we compare the BBV responses we measured to previous reports of responses to acoustic signals in the IC, speculate on the mechanisms of the effects of 5-HT1A receptors, and frame the influence of 5-HT1A receptors in the context of additional serotonin receptor types and of the behavioral conditions that cause elevated serotonin in the IC.

How IC Neurons Respond to BBVs

Most work on the behavioral and neural responses to acoustic signals in mice has focused on USVs, an ultrasonic signal type produced by males and females in both same-sex and opposite-sex interactions (e.g., Nyby, 1983; Holy and Guo, 2005; Holmstrom et al., 2010; Hanson and Hurley, 2012; Grimsley et al., 2013; Neunuebel et al., 2015; Warren et al., 2018). Similar to USVs, BBVs, which contain human-audible harmonics (Lupanova and Egorova, 2015; Finton et al., 2017), are produced across a range of behavioral contexts. BBVs are made by both sexes during non-social distress and same-sex aggression (Irwin et al., 1971; Matthews et al., 2008; Lupanova and Egorova, 2015; Finton et al., 2017). During opposite-sex interactions, BBVs are produced largely by females as they direct kicks and lunges at males, but are also produced as females allow males

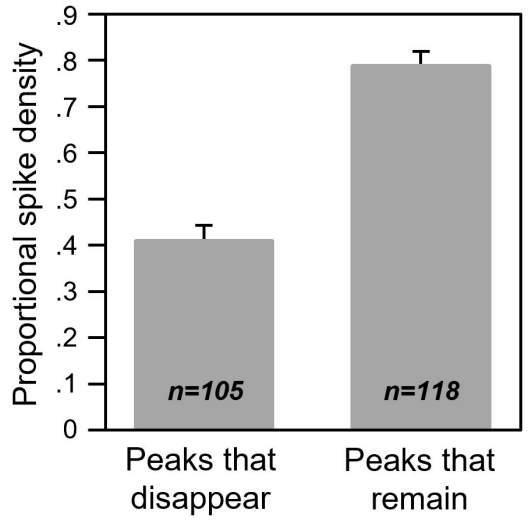

FIGURE 9 | Proportional spike densities for response features that disappeared or remained during iontophoresis of 8-OH-DPAT. The peak spike densities of response features were normalized to the largest response feature in their respective spike trains.

to mount (Wang et al., 2008a; Sugimoto et al., 2011; Finton et al., 2017). From the perspective of a male listener, BBVs might therefore have different behavioral salience at different phases of an opposite-sex interaction. Male perception of BBVs also depends on context. Males approach speakers broadcasting BBVs less when they are paired with the odor of a predator than with female urine (Grimsley et al., 2013).

Since USV responses have been more often recorded than BBV responses, it is useful to compare the two. Given the extreme differences in the structures of BBVs and USVs, one might predict a segregation in the responses to USVs versus BBVs to neurons with low and high CFs, respectively. However, this may not be the case. Although IC neurons that respond to calls with low frequency harmonics often have at least one harmonic that falls within the frequency tuning curve, this is not always true for USVs (Portfors et al., 2009). CFs of IC neurons responding to USVs are often lower than predicted, suggesting that there may be substantial overlap in the CFs of neurons responding to BBVs and USVs. A second comparison is in the selectivity of neural responses for USVs and BBVs. Responses to USVs in the IC have from high to moderate levels of selectivity across studies in bats and mice (Hurley and Pollak, 2005; Portfors et al., 2009). In the current study, BBV responses were strikingly non-selective, with over 72% of neurons responding to four or five BBVs. The fact that mice in the current study were anesthetized could have contributed to this extreme lack of selectivity, but the different structures of BBVs and USVs could also potentially contribute to differences in the selectivity of responses to these two signals. USVs typically consist of single or at most two widely separated harmonics (Holy and Guo, 2005; Hanson and Hurley, 2012). In contrast, BBVs are composed of many harmonics that can extend into the ultrasonic range (**Figure 1**). This broadband structure makes it more likely that BBVs will evoke responses from neurons across a broad range of CFs, and that single neurons will respond to different BBVs. This possibility is supported by the auditory responses of IC neurons in another rodent species, guinea pigs, in which responses to human-audible vocalizations have been recorded. Guinea pigs produce multiple low-frequency harmonic calls that differ significantly in temporal structure (Šuta et al., 2003). Remarkably similar to the current study, 55% of neurons respond to every stimulus type presented in the guinea pig IC (in comparison to 55.1% of neurons in the current study).

Although IC neurons were not selective for BBVs at the level of responses to whole calls, temporal patterns in response to the same calls appeared to be relatively more selective, in that they varied across neurons and across calls (**Figures 2**, **5**). We characterized these patterns by defining "response features," as temporal regions of high spike probability surrounded by areas of lower probability. In the current study, response features were likely to be driven by both the specific spectrotemporal characteristics of calls and the intrinsic properties of neurons. For example, some of the neurons in **Figure 5** responded near the start of calls with pronounced onsets, such as Calls 1 and 5. Likewise, some neurons responded in regions of calls characterized by deterministic chaos, which is structured noise driven by non-linear vocal fold vibration (**Figure 8C**; Fitch et al., 2002; Lupanova and Egorova, 2015). The burst of spikes observed shortly after the end of BBVs in some neurons is consistent with rebound firing, an intrinsic property of some IC neurons (**Figure 5**). With a playback sample of five calls, it is not possible to definitively state which characteristics of calls triggered specific response features. However, the general observation that IC neurons are selective for specific spectrotemporal aspects of stimuli has been observed in multiple studies using systematically varying stimuli to generate spectrotemporal receptive fields (Andoni et al., 2007; Rodríguez et al., 2010; Chen et al., 2012; Park et al., 2021). In relation to the current study, the response features that vary across neurons and across calls suggest that the neural coding of BBVs is more selective when considering response features than responses to whole calls.

5-HT1A Receptor

For most IC neurons, activation of the 5-HT1A receptor by 8-OH-DPAT exerted a suppressive gain control. This effect is similar to previous work in the IC using synthesized stimuli such as tones and FM sweeps (Hurley, 2006, 2007). Spike suppression by 8-OH-DPAT is also consistent with the effects of 5-HT1A receptors in other brain regions, where these receptors also mediate response suppression (Albert and Vahid-Ansari, 2019). The 5-HT1A receptor is generally expressed somatodendritically or in axon hillocks, and acts via G-protein coupled inward rectifier potassium (GIRK) channels to suppress firing in a number of neuron types (Albert and Vahid-Ansari, 2019). In the medial superior olive (MSO), an auditory brainstem nucleus, 5-HT1A receptors are expressed in the axon initial segment, and regulate neural output by affecting spike probability (Ko et al., 2016). In the IC, the subcellular location of the 5-HT1A receptor has not been assessed, but the fact that most neurons showed roughly uniform effects of 8-OH-DPAT for different response features is consistent with expression by the IC neurons being

recorded. The differential effects of 5-HT1A activation on specific response features in some neurons (**Figure 8B**) also suggest the possibility that 5-HT1A receptors could influence the activity of presynaptic IC neurons with response profiles different from those of the neurons being recorded.

Even for neurons with proportionally similar effects of 8-OH-DPAT on different response features, some response features were maintained while others disappeared. The smallest peaks were the most likely to disappear during 5-HT1A activation, consistent with an "iceberg"-like effect, in which suprathreshold responses are more selective than subthreshold responses (Rose and Blakemore, 1974). Neurochemical regulation of the strength of responses relative to threshold is an established mechanism for regulating the selectivity of IC neurons. For example, the manipulation of inhibition can alter primary response characteristics such as frequency tuning (Fuzessery and Hall, 1996; Xie et al., 2007; Wu and Jen, 2009), as well as more complex response characteristics including duration sensitivity (Alluri et al., 2016) or sensitivity to the velocity of frequency modulation (Gittelman and Li, 2011). For the neurons in the current study, the outcome of 5-HT1A-induced spike suppression was to alter the response profile at the level of single neurons, as they showed fewer response features. The disappearance of peaks could also potentially translate to a sparser and more selective population response, with fewer neurons responding to specific spectrotemporal call features.

Other Serotonin Receptors

Because there are multiple types of serotonin receptor, the effects of 5-HT1A activation during serotonin release would depend on the context of other activated receptors. Members of five of the seven main families of serotonin receptor are expressed in the IC, and some of these families have more than one subtype (Hurley and Sullivan, 2012). Serotonin receptors have a wide range of effects on neural excitability and neurotransmission in the IC. In addition to spike suppression by the 5-HT1A receptor, the 5-HT2 receptor reduces the frequency and amplitude of GABAergic and glycinergic IPSCs (Wang et al., 2008b). Activation of the 5-HT1B receptor also has facilitatory effects that are consistent with the inhibition of GABAergic transmission, an effect precluded by prior activation of $GABA_A$ receptors (Hurley et al., 2008).

There are several excellent examples of how other types of serotonin receptors interact with the 5-HT1A receptor in the auditory system. In the dorsal cochlear nucleus, activation of the 5-HT2A receptor increases the excitability of principal neurons (Tang and Trussell, 2015), while increasing the recruitment of feed-forward inhibitory inputs (Tang and Trussell, 2017). At the same time, 5-HT1A receptors decrease excitatory inputs to the principal neurons evoked by auditory nerve fiber stimulation (Tang and Trussell, 2017). Since inputs from multisensory pathways do not show these presynaptic changes, this suite of effects increases responses from multisensory pathways relative to auditory-specific pathways, gating these different sources of information. In pyramidal neurons from Layers II/III of the auditory cortex, 5-HT1A and 5-HT2A receptors reduce GABAergic transmission presynaptically and postsynaptically, respectively (García-Oscos et al., 2015). At the same time, 5-HT1A activation postsynaptically reduces the amplitudes of EPSCs (Cervantes-Ramírez et al., 2019).

In the IC, two receptor types in the 5-HT1 family, the 5-HT1A and 5-HT1B receptors, overlap in their effects on single IC neurons. Activation of these receptors have opposite and additive effects on the firing rates of IC neurons, but 5-HT1A activation has effects on spike timing that are dominant to those of the 5-HT1B receptor (Castellan Baldan Ramsey et al., 2010). These findings suggest that the two receptor types may interact in non-linear ways to influence patterns of neural responses. Although the interaction of serotonin receptor types at the microcircuit level has not been described in the IC, a working hypothesis is that the 5-HT1A receptor could suppress responses to inputs closest to threshold, and increase contrast with the selective disinhibition of presynaptic inputs by other types of serotonin receptor. Because most ascending auditory pathways make synaptic connections in the IC, these effects could filter information on BBVs en route to the auditory thalamus.

An important caveat to our findings is that they were generated in anesthetized subjects. Mice would typically be awake and interacting socially when perceiving calls from other mice, with a physiological state that is different from that of an anesthetized mouse. An alternative to the approach used in this study could have been working with awake restrained mice (e.g., Gourévitch et al., 2020). Although this would differ from an anesthetized state, this model would still not fully capture the physiology of a socially interacting brain. Recording multiunit responses in behaving mice would address this issue and allow for comparison between neural responses and behavior. However, the type of recording in the current study in which well-isolated single neurons are exposed to highly localized manipulation of specific receptor types, is difficult to achieve in moving subjects. Furthermore, recording in anesthetized mice does have some advantages, one of which is the relatively low level of endogenous serotonin release in the IC (Hall et al., 2010). In awake and behaving mice, serotonin levels fluctuate in different social contexts (Hall et al., 2011; Hanson and Hurley, 2014; Keesom and Hurley, 2016), so that the availability of 5-HT1A receptors could also fluctuate, potentially leading to different effects exogenous 5-HT1A activation across contexts. Anesthesia is also unlikely to change the basic suppressive effect of the 5-HT1A receptor, since suppressive effects of this receptor have also been reported in the IC in an awake bat model (Hurley, 2007). All in all, although the use of anesthetized mice may not fully represent the responses of auditory neurons to social signals, this approach can provide a view of the potential repertoire of specific receptor types on a local scale in influencing call responses, particularly if combined with additional studies in awake animals.

Behavioral Context

In different vertebrate species, different neuromodulatory systems modify the responses to acoustic social signals in accordance with behavioral context. In auditory forebrain regions in female zebra finches, local introduction of norepinephrine or an α2 adrenergic agonist increases the signal-to-noise ratio for a range of stimuli including conspecific and heterospecific songs, in

large part by decreasing spontaneous activity (Ikeda et al., 2015). These changes improve the accuracy of a stimulus classification algorithm, demonstrating improved encoding of stimuli during adrenergic activation.

A sensory region in which a feedback loop has been established between enhanced serotonin release triggered by a social signal and the effects of serotonin on signal processing is the electrosensory lobe (ELL) of brown ghost knifefish. This and other weakly electric fish species use self-generated electric organ discharges to navigate and communicate, via their electrosensory systems (Lissmann, 1951; Hopkins, 1988). Simulated conspecific electric signals cause rapid increases in serotonin in the ELL (Fotowat et al., 2016). Increased serotonin in turn selectively increases the excitability of the principal neurons in the ELL to simulated same-sex electric signals (Deemyad et al., 2013). Serotonin increases burst firing and sensitivity to fluctuations in the stimulus envelope, a change that is further reflected in enhanced behavioral responsiveness (Marquez and Chacron, 2020).

In mice, previous work describing serotonin release in the IC during opposite-sex interaction is helpful in framing the effects of serotonin on BBVs within this context. Serotonin levels in the IC of males interacting with female partners is inversely correlated with rejection, measured by the numbers of BBVs, made by female social partners (Keesom and Hurley, 2016). Although this finding alone would suggest that BBVs are not produced when serotonin levels are elevated (when females do not reject males), copious BBVs are also produced when females allow males to mount (Wang et al., 2008a; Finton et al., 2017). Furthermore, Calls 4 and 5, with longer durations and longer relative segments of DC, are similar to calls more likely to be produced during mounting behavior than during female rejection (Finton et al., 2017). Neural responses to BBVs, particularly those similar to Calls 4 and 5, in this behavioral subcontext might therefore be most subject to serotonergic modulation, with BBVs produced in the process of female rejection relatively unmodulated by serotonin. The serotonergic modulatory system could therefore contribute to the differential auditory processing of BBVs in different behavioral subcontexts. Whether these events in the IC can influence the perception of BBVs by males in these subcontexts is currently unknown.

DATA AVAILABILITY STATEMENT

The raw data supporting the conclusions of this article will be made available by the authors, without undue reservation.

ETHICS STATEMENT

The animal study was reviewed and approved by the Bloomington Institutional Animal Care and Use Committee, Indiana University Bloomington, United States.

AUTHOR CONTRIBUTIONS

AG and LH performed the experiments and data analysis, and contributed to writing the manuscript. SN performed the data analysis and contributed to writing the manuscript. All authors contributed to the article and approved the submitted version.

FUNDING

This work was funded by the NIDCD award # R01 DC008963.

ACKNOWLEDGMENTS

The authors would like to thank Dr. Donald Gans for consulting on Batlab software and Dr. Megan Sullivan for writing a Matlab script to resample calls.

REFERENCES

Albert, P. R., and Vahid-Ansari, F. (2019). The 5-HT1A receptor: signaling to behavior. *Biochimie* 161, 34–45. doi: 10.1016/j.biochi.2018.10.015

Alluri, R. K., Rose, G. J., Hanson, J. L., Leary, C. J., Vasquez-Opazo, G. A., Graham, J. A., et al. (2016). Phasic, suprathreshold excitation and sustained inhibition underlie neuronal selectivity for short-duration sounds. *Proc. Natl. Acad. Sci. U.S.A.* 113, E1927–E1935. doi: 10.1073/pnas.1520971113

Andoni, S., Li, N., and Pollak, G. D. (2007). Spectrotemporal receptive fields in the inferior colliculus revealing selectivity for spectral motion in conspecific vocalizations. *J. Neurosci.* 27, 4882–4893. doi: 10.1523/JNEUROSCI.4342-06.2007

Barr, H. J., and Woolley, S. C. (2018). Developmental auditory exposure shapes responses of catecholaminergic neurons to socially-modulated song. *Sci. Rep.* 8:11717. doi: 10.1038/s41598-018-30039-y

Bartlett, E. L. (2013). The organization and physiology of the auditory thalamus and its role in processing acoustic features important for speech perception. *Brain Language* 126, 29–48. doi: 10.1016/j.bandl.2013.03.003

Bohorquez, A., and Hurley, L. M. (2009). Activation of serotonin 3 receptors changes in vivo auditory responses in the mouse inferior colliculus. *Hearing Res.* 251, 29–38. doi: 10.1016/j.heares.2009.02.006

Castellan Baldan Ramsey, L., Sinha, S. R., and Hurley, L. M. (2010). 5-HT1A and 5-HT1B receptors differentially modulate rate and timing of auditory responses in the mouse inferior colliculus: 5-HT receptors change rate and timing in IC. *Eur. J. Neurosci.* 32, 368–379. doi: 10.1111/j.1460-9568.2010.07299.x

Cervantes-Ramírez, V., Canto-Bustos, M., Aguilar-Magaña, D., Pérez-Padilla, E. A., Góngora-Alfaro, J. L., Pineda, J. C., et al. (2019). Citalopram reduces glutamatergic synaptic transmission in the auditory cortex via activation of 5-HT1A receptors. *NeuroReport* 30, 1316–1322. doi: 10.1097/WNR.0000000000001366

Chen, C., Read, H. L., and Escabi, M. A. (2012). Precise feature based time scales and frequency decorrelation lead to a sparse auditory code. *J. Neurosci.* 32, 8454–8468. doi: 10.1523/JNEUROSCI.6506-11.2012

Coomes, D. L., and Schofield, B. R. (2004). Separate projections from the inferior colliculus to the cochlear nucleus and thalamus in guinea pigs. *Hearing Res.* 191, 67–78. doi: 10.1016/j.heares.2004.01.009

Deemyad, T., Metzen, M. G., Pan, Y., and Chacron, M. J. (2013). Serotonin selectively enhances perception and sensory neural responses to stimuli generated by same-sex conspecifics. *Proc. Natl. Acad. Sci. U.S.A.* 110, 19609–19614. doi: 10.1073/pnas.1314008110

Finton, C. J., Keesom, S. M., Hood, K. E., and Hurley, L. M. (2017). What's in a squeak? Female vocal signals predict the sexual behaviour of male house mice

during courtship. *Animal Behav.* 126, 163–175. doi: 10.1016/j.anbehav.2017.01.021

Fitch, W. T., Neubauer, J., and Herzel, H. (2002). Calls out of chaos: the adaptive significance of nonlinear phenomena in mammalian vocal production. *Animal Behav.* 63, 407–418. doi: 10.1006/anbe.2001.1912

Forlano, P. M., Ghahramani, Z. N., Monestime, C. M., Kurochkin, P., Chernenko, A., and Milkis, D. (2015). Catecholaminergic innervation of central and peripheral auditory circuitry varies with reproductive state in female midshipman fish, Porichthys notatus. *PLoS One* 10:e0121914. doi: 10.1371/journal.pone.0121914

Fotowat, H., Harvey-Girard, E., Cheer, J. F., Krahe, R., and Maler, L. (2016). Subsecond sensory modulation of serotonin levels in a primary sensory area and its relation to ongoing communication behavior in a weakly electric fish. *eneuro* 3:ENEURO.115–ENEURO.116. doi: 10.1523/ENEURO.0115-16.2016

Franklin, K. B. J., and Paxinos, G. (2008). *The Mouse Brain in Stereotaxic Coordinates. Compact*, 3. Edn. Amsterdam: Elsevier, Academic Press.

Fuzessery, Z. M., and Hall, J. C. (1996). Role of GABA in shaping frequency tuning and creating FM sweep selectivity in the inferior colliculus. *J. Neurophysiol.* 76, 1059–1073. doi: 10.1152/jn.1996.76.2.1059

García-Oscos, F., Torres-Ramírez, O., Dinh, L., Galindo-Charles, L., Pérez Padilla, E. A., Pineda, J. C., et al. (2015). Activation of 5-HT receptors inhibits GABAergic transmission by pre-and post-synaptic mechanisms in layer II/III of the juvenile rat auditory cortex: synaptic mechanisms in rat auditory cortex. *Synapse* 69, 115–127. doi: 10.1002/syn.21794

Ghahramani, Z. N., Timothy, M., Varughese, J., Sisneros, J. A., and Forlano, P. M. (2018). Dopaminergic neurons are preferentially responsive to advertisement calls and co-active with social behavior network nuclei in sneaker male midshipman fish. *Brain Res.* 1701, 177–188. doi: 10.1016/j.brainres.2018.09.014

Gittelman, J. X., and Li, N. (2011). FM velocity selectivity in the inferior colliculus is inherited from velocity-selective inputs and enhanced by spike threshold. *J. Neurophysiol.* 106, 2399–2414. doi: 10.1152/jn.00250.2011

Gittelman, J. X., Perkel, D. J., and Portfors, C. V. (2013). Dopamine modulates auditory responses in the inferior colliculus in a heterogeneous manner. *JARO* 14, 719–729. doi: 10.1007/s10162-013-0405-0

Gourévitch, B., Mahrt, E. J., Bakay, W., Elde, C., and Portfors, C. V. (2020). GABA(A) receptors contribute more to rate than temporal coding in the IC of awake mice. *J. Neurophysiol.* 123, 134–148. doi: 10.1152/jn.00377.2019

Grimsley, J. M. S., Hazlett, E. G., and Wenstrup, J. J. (2013). Coding the meaning of sounds: contextual modulation of auditory responses in the basolateral amygdala. *J. Neurosci.* 33, 17538–17548. doi: 10.1523/JNEUROSCI.2205-13.2013

Hage, S. R., and Ehret, G. (2003). Mapping responses to frequency sweeps and tones in the inferior colliculus of house mice. *Eur. J. Neurosci.* 18, 2301–2312. doi: 10.1046/j.1460-9568.2003.02945.x

Hall, I. C., Rebec, G. V., and Hurley, L. M. (2010). Serotonin in the inferior colliculus fluctuates with behavioral state and environmental stimuli. *J. Exp. Biol.* 213, 1009–1017. doi: 10.1242/jeb.035956

Hall, I. C., Sell, G. L., and Hurley, L. M. (2011). Social regulation of serotonin in the auditory midbrain. *Behav. Neurosci.* 125, 501–511. doi: 10.1037/a0024426

Hanson, J. L., and Hurley, L. M. (2012). Female presence and estrous state influence mouse ultrasonic courtship vocalizations. *PLoS One* 7:e40782. doi: 10.1371/journal.pone.0040782

Hanson, J. L., and Hurley, L. M. (2014). Context-dependent fluctuation of serotonin in the auditory midbrain: the influence of sex, reproductive state and experience. *J. Exp. Biol.* 217, 526–535. doi: 10.1242/jeb.087627

Holmstrom, L. A., Eeuwes, L. B. M., Roberts, P. D., and Portfors, C. V. (2010). Efficient encoding of vocalizations in the auditory midbrain. *J. Neurosci.* 30, 802–819. doi: 10.1523/JNEUROSCI.1964-09.2010

Holy, T. E., and Guo, Z. (2005). Ultrasonic songs of male mice. *PLoS Biol.* 3:e386. doi: 10.1371/journal.pbio.0030386

Hood, K. E., Navarro, E., and Hurley, L. M. (2020). Playback of female house mouse (*Mus musculus*) rejection vocalizations modifies male behavior. *Soc. Integrat. Com. Biol.* 14:45.

Hopkins, C. D. (1988). Neuroethology of electric communication. *Annu. Rev. Neurosci.* 11, 497–535. doi: 10.1146/annurev.ne.11.030188.002433

Hoyt, J. M., Perkel, D. J., and Portfors, C. V. (2019). Dopamine Acts via D2-Like receptors to modulate auditory responses in the inferior colliculus. *eNeuro* 6:ENEURO.350–ENEURO.319. doi: 10.1523/ENEURO.0350-19.2019

Hurley, L. (2019). "Neuromodulatory feedback to the inferior colliculus," in *The Oxford Handbook of the Auditory Brainstem*, ed. K. Kandler (Oxford: : Oxford University Press), 576–610. doi: 10.1093/oxfordhb/9780190849061.013.15

Hurley, L., Devilbiss, D., and Waterhouse, B. (2004). A matter of focus: monoaminergic modulation of stimulus coding in mammalian sensory networks. *Curr. Opin. Neurobiol.* 14, 488–495. doi: 10.1016/j.conb.2004.06.007

Hurley, L. M. (2006). Different serotonin receptor agonists have distinct effects on sound-evoked responses in inferior colliculus. *J. Neurophysiol.* 96, 2177–2188. doi: 10.1152/jn.00046.2006

Hurley, L. M. (2007). Activation of the serotonin 1A receptor alters the temporal characteristics of auditory responses in the inferior colliculus. *Brain Res.* 1181, 21–29. doi: 10.1016/j.brainres.2007.08.053

Hurley, L. M., and Pollak, G. D. (1999). Serotonin differentially modulates responses to tones and frequency-modulated sweeps in the inferior colliculus. *J. Neurosci.* 19, 8071–8082. doi: 10.1523/JNEUROSCI.19-18-08071.1999

Hurley, L. M., and Pollak, G. D. (2005). Serotonin modulates responses to species-specific vocalizations in the inferior colliculus. *J. Comp. Physiol. A* 191, 535–546. doi: 10.1007/s00359-005-0623-y

Hurley, L. M., and Sullivan, M. R. (2012). From behavioral context to receptors: serotonergic modulatory pathways in the IC. *Front. Neural Circuits* 6:58. doi: 10.3389/fncir.2012.00058

Hurley, L. M., Tracy, J. A., and Bohorquez, A. (2008). Serotonin 1B receptor modulates frequency response curves and spectral integration in the inferior colliculus by reducing GABAergic inhibition. *J. Neurophysiol.* 100, 1656–1667. doi: 10.1152/jn.90536.2008

Ikeda, M. Z., Jeon, S. D., Cowell, R. A., and Remage-Healey, L. (2015). Norepinephrine modulates coding of complex vocalizations in the songbird auditory cortex independent of local neuroestrogen synthesis. *J. Neurosci.* 35, 9356–9368. doi: 10.1523/JNEUROSCI.4445-14.2015

Irwin, S., Kinohi, R., Van Sloten, M., and Workman, M. P. (1971). Drug effects on distress-evoked behavior in mice: methodology and drug class comparisons. *Psychopharmacologia* 20, 172–185. doi: 10.1007/BF00404371

Jacob, S. N., and Nienborg, H. (2018). Monoaminergic neuromodulation of sensory processing. *Front. Neural Circuits* 12:51. doi: 10.3389/fncir.2018.00051

Johansson, L., Sohn, D., Thorberg, S. O., Jackson, D. M., Kelder, D., Larsson, L. G., et al. (1997). The pharmacological characterization of a novel selective 5-hydroxytryptamine1A receptor antagonist, NAD-299. *J. Pharmacol. Exp. Ther.* 283, 216–225.

Keesom, S. M., and Hurley, L. M. (2016). Socially induced serotonergic fluctuations in the male auditory midbrain correlate with female behavior during courtship. *J. Neurophysiol.* 115, 1786–1796. doi: 10.1152/jn.00742.2015

Klepper, A., and Herbert, H. (1991). Distribution and origin of noradrenergic and serotonergic fibers in the cochlear nucleus and inferior colliculus of the rat. *Brain Res.* 557, 190–201. doi: 10.1016/0006-8993(91)90134-H

Ko, K. W., Rasband, M. N., Meseguer, V., Kramer, R. H., and Golding, N. L. (2016). Serotonin modulates spike probability in the axon initial segment through HCN channels. *Nat. Neurosci.* 19, 826–834. doi: 10.1038/nn.4293

Lee, V., Pawlisch, B. A., Macedo-Lima, M., and Remage-Healey, L. (2018). Norepinephrine enhances song responsiveness and encoding in the auditory forebrain of male zebra finches. *J. Neurophysiol.* 119, 209–220. doi: 10.1152/jn.00251.2017

Lesicko, A. M. H., Hristova, T. S., Maigler, K. C., and Llano, D. A. (2016). Connectional modularity of top-down and bottom-up multimodal inputs to the lateral cortex of the mouse inferior colliculus. *J. Neurosci.* 36, 11037–11050. doi: 10.1523/JNEUROSCI.4134-15.2016

Lissmann, H. W. (1951). Continuous electrical signals from the Tail of a Fish, Gymnarchus niloticus Cuv. *Nature* 167, 201–202. doi: 10.1038/167201a0

Loftus, W. C., Bishop, D. C., and Oliver, D. L. (2010). Differential patterns of inputs create functional zones in central nucleus of inferior *Colliculus*. *J. Neurosci.* 30, 13396–13408. doi: 10.1523/JNEUROSCI.0338-10.2010

Lupanova, A. S., and Egorova, M. A. (2015). [Vocalizations of sex partners in the house mouse (MUS MUSCULUS)]. *Zh Evol. Biokhim. Fiziol.* 51, 283–289.

Marquez, M. M., and Chacron, M. J. (2020). Serotonergic modulation of sensory neuron activity and behavior in apteronotus albifrons. *Front. Integr. Neurosci.* 14:38. doi: 10.3389/fnint.2020.00038

Martin, L. P., Jackson, D. M., Wallsten, C., and Waszczak, B. L. (1999). Electrophysiological comparison of 5-Hydroxytryptamine1A receptor antagonists on dorsal raphe cell firing. *J. Pharmacol. Exp. Ther.* 288, 820–826.

Matthews, D. B., Chesler, E. J., Cook, M. N., Cockroft, J., Philip, V. M., and Goldowitz, D. (2008). Genetic mapping of vocalization to a series of increasing acute footshocks using B6.A Consomic and B6.D2 congenic mouse strains. *Behav. Genet.* 38, 417–423. doi: 10.1007/s10519-008-9210-7

Mayko, Z. M., Roberts, P. D., and Portfors, C. V. (2012). Inhibition shapes selectivity to vocalizations in the inferior colliculus of awake mice. *Front. Neural Circuits* 6:73. doi: 10.3389/fncir.2012.00073

Neunuebel, J. P., Taylor, A. L., Arthur, B. J., and Egnor, S. R. (2015). Female mice ultrasonically interact with males during courtship displays. *eLife* 4:e06203. doi: 10.7554/eLife.06203

Nevue, A. A., Elde, C. J., Perkel, D. J., and Portfors, C. V. (2016). Dopaminergic input to the inferior colliculus in mice. *Front. Neuroanat.* 9:168. doi: 10.3389/fnana.2015.00168

Niederkofler, V., Asher, T. E., Okaty, B. W., Rood, B. D., Narayan, A., Hwa, L. S., et al. (2016). Identification of serotonergic neuronal modules that affect aggressive behavior. *Cell Rep.* 17, 1934–1949. doi: 10.1016/j.celrep.2016.10.063

Nyby, J. (1983). Ultrasonic vocalizations during sex behavior of male house mice (*Mus musculus*): a description. *Behav. Neural Biol.* 39, 128–134. doi: 10.1016/S0163-1047(83)90722-7

Park, S., Salles, A., Allen, K., Moss, C. F., and Elhilali, M. (2021). Natural statistics as inference principles of auditory tuning in biological and artificial midbrain networks. *eNeuro* 8:ENEURO.525–ENEURO.520. doi: 10.1523/ENEURO.0525-20.2021

Patel, M. B., Sons, S., Yudintsev, G., Lesicko, A. M. H., Yang, L., Taha, G. A., et al. (2017). Anatomical characterization of subcortical descending projections to the inferior colliculus in mouse: subcortical descending projections to IC. *J. Comp. Neurol.* 525, 885–900. doi: 10.1002/cne.24106

Peruzzi, D., and Dut, A. (2004). GABA, serotonin and serotonin receptors in the rat inferior *colliculus*. *Brain Res.* 998, 247–250. doi: 10.1016/j.brainres.2003.10.059

Petersen, C. L., Koo, A., Patel, B., and Hurley, L. M. (2020). Serotonergic innervation of the auditory midbrain: dorsal raphe subregions differentially project to the auditory midbrain in male and female mice. *Brain Struct. Funct.* 225, 1855–1871. doi: 10.1007/s00429-020-02098-3

Portfors, C. V., Roberts, P. D., and Jonson, K. (2009). Over-representation of species-specific vocalizations in the awake mouse inferior colliculus. *Neuroscience* 162, 486–500. doi: 10.1016/j.neuroscience.2009.04.056

Rodríguez, F. A., Read, H. L., and Escabí, M. A. (2010). Spectral and temporal modulation tradeoff in the inferior colliculus. *J. Neurophysiol.* 103, 887–903. doi: 10.1152/jn.00813.2009

Rose, D., and Blakemore, C. (1974). Effects of bicuculline on functions of inhibition in visual cortex. *Nature* 249, 375–377. doi: 10.1038/249375a0

Ross, S. B., Thoorberg, S. O., Jerning, E., Mohell, N., Stenfors, C., Wallsten, C., et al. (1999). Robalzotan (NAD-299), a novel selective 5-HT 1A receptor antagonist. *CNS Drug Rev.* 5, 213–232.

Schofield, B. R., and Cant, N. B. (1999). Descending auditory pathways: projections from the inferior colliculus contact superior olivary cells that project bilaterally to the cochlear nuclei. *J. Comp. Neurol.* 409, 210–223. doi: 10.1002/(sici)1096-9861(19990628)409:2<210::aid-cne3<3.0.co;2-a

Schofield, B. R., and Hurley, L. (2018). "Circuits for modulation of auditory function," in *The Mammalian Auditory Pathways Springer Handbook of Auditory Research*, eds D. L. Oliver, N. B. Cant, R. R. Fay, and A. N. Popper (Cham: Springer International Publishing), 235–267. doi: 10.1007/978-3-319-71798-2_9

Shimazaki, H., and Shinomoto, S. (2010). Kernel bandwidth optimization in spike rate estimation. *J. Comput. Neurosci.* 29, 171–182. doi: 10.1007/s10827-009-0180-4

Sizemore, T. R., Hurley, L. M., and Dacks, A. M. (2020). Serotonergic modulation across sensory modalities. *J. Neurophysiol.* 123, 2406–2425. doi: 10.1152/jn.00034.2020

Smith, A. R., Kwon, J. H., Navarro, M., and Hurley, L. M. (2014). Acoustic trauma triggers upregulation of serotonin receptor genes. *Hear. Res.* 315, 40–48. doi: 10.1016/j.heares.2014.06.004

Sugimoto, H., Okabe, S., Kato, M., Koshida, N., Shiroishi, T., Mogi, K., et al. (2011). A role for strain differences in waveforms of ultrasonic vocalizations during male–female interaction. *PLoS One* 6:e22093. doi: 10.1371/journal.pone.0022093

Šuta, D., Kvašòák, E., Popeláø, J., and Syka, J. (2003). Representation of species-specific vocalizations in the inferior colliculus of the guinea pig. *J. Neurophysiol.* 90, 3794–3808. doi: 10.1152/jn.01175.2002

Tang, Z.-Q., and Trussell, L. O. (2015). Serotonergic regulation of excitability of principal cells of the dorsal cochlear nucleus. *J. Neurosci.* 35, 4540–4551. doi: 10.1523/JNEUROSCI.4825-14.2015

Tang, Z.-Q., and Trussell, L. O. (2017). Serotonergic modulation of sensory representation in a central multisensory circuit is pathway specific. *Cell Rep.* 20, 1844–1854. doi: 10.1016/j.celrep.2017.07.079

Thompson, G. C., Thompson, A. M., Garrett, K. M., and Britton, B. H. (1994). Serotonin and serotonin receptors in the central auditory system. *Otolaryngol. Head Neck Surg.* 110, 93–102. doi: 10.1177/019459989411000111

Wang, H., Liang, S., Burgdorf, J., Wess, J., and Yeomans, J. (2008a). Ultrasonic vocalizations induced by sex and amphetamine in M2, M4, M5 Muscarinic and D2 dopamine receptor knockout mice. *PLoS One* 3:e1893. doi: 10.1371/journal.pone.0001893

Wang, H.-T., Luo, B., Huang, Y.-N., Zhou, K.-Q., and Chen, L. (2008b). Sodium salicylate suppresses serotonin-induced enhancement of GABAergic spontaneous inhibitory postsynaptic currents in rat inferior *colliculus* in vitro. *Hear. Res.* 236, 42–51. doi: 10.1016/j.heares.2007.11.015

Warren, M. R., Spurrier, M. S., Roth, E. D., and Neunuebel, J. P. (2018). Sex differences in vocal communication of freely interacting adult mice depend upon behavioral context. *PLoS One* 13:e0204527. doi: 10.1371/journal.pone.0204527

White, N. R., Prasad, M., Barfield, R. J., and Nyby, J. G. (1998). 40- and 70-kHz vocalizations of mice (*Mus musculus*) during Copulation. *Physiol. Behav.* 63, 467–473. doi: 10.1016/S0031-9384(97)00484-8

Wu, F.-J., and Jen, P. H.-S. (2009). Involvement of GABA-mediated inhibition in shaping the frequency selectivity of neurons in the inferior colliculus of the big brown bat, eptesicus fuscus. *Chinese J. Physiol.* 52, 38–46. doi: 10.4077/CJP.2009.AMH002

Xie, R., Gittelman, J. X., and Pollak, G. D. (2007). Rethinking tuning: *In Vivo* whole-cell recordings of the inferior colliculus in awake bats. *J. Neurosci.* 27, 9469–9481. doi: 10.1523/JNEUROSCI.2865-07.2007

Conflict of Interest: The authors declare that the research was conducted in the absence of any commercial or financial relationships that could be construed as a potential conflict of interest.

Publisher's Note: All claims expressed in this article are solely those of the authors and do not necessarily represent those of their affiliated organizations, or those of the publisher, the editors and the reviewers. Any product that may be evaluated in this article, or claim that may be made by its manufacturer, is not guaranteed or endorsed by the publisher.

frontiers in Neural Circuits

MINI REVIEW
published: 12 October 2021
doi: 10.3389/fncir.2021.759342

Nitric Oxide Signaling in the Auditory Pathway

*Conny Kopp-Scheinpflug[1] and Ian D. Forsythe[2]**

[1] Neurobiology Laboratory, Division of Neurobiology, Faculty of Biology, Ludwig Maximilian University of Munich, Munich, Germany, [2] Auditory Neurophysiology Laboratory, Department of Neuroscience, Psychology and Behaviour, College of Life Sciences, University of Leicester, Leicester, United Kingdom

Nitric oxide (NO) is of fundamental importance in regulating immune, cardiovascular, reproductive, neuromuscular, and nervous system function. It is rapidly synthesized and cannot be confined, it is highly reactive, so its lifetime is measured in seconds. These distinctive properties (contrasting with classical neurotransmitters and neuromodulators) give rise to the concept of NO as a "volume transmitter," where it is generated from an active source, diffuses to interact with proteins and receptors within a sphere of influence or volume, but limited in distance and time by its short half-life. In the auditory system, the neuronal NO-synthetizing enzyme, nNOS, is highly expressed and tightly coupled to postsynaptic calcium influx at excitatory synapses. This provides a powerful activity-dependent control of postsynaptic intrinsic excitability via cGMP generation, protein kinase G activation and modulation of voltage-gated conductances. NO may also regulate vesicle mobility via retrograde signaling. This Mini Review focuses on the auditory system, but highlights general mechanisms by which NO mediates neuronal intrinsic plasticity and synaptic transmission. The dependence of NO generation on synaptic and sound-evoked activity has important local modulatory actions and NO serves as a "volume transmitter" in the auditory brainstem. It also has potentially destructive consequences during intense activity or on spill-over from other NO sources during pathological conditions, when aberrant signaling may interfere with the precisely timed and tonotopically organized auditory system.

Keywords: auditory processing, neuronal excitability and ion channel regulation, hearing loss, neuronal nitric oxide synthase (nNOS), volume transmission, synaptic plasticity

OPEN ACCESS

Edited by:
Manuel S. Malmierca, University of Salamanca, Spain

Reviewed by:
Maria Eulalia Rubio, University of Pittsburgh, United States
Adrian Rees, Newcastle University, United Kingdom

***Correspondence:**
Ian D. Forsythe
idf@leicester.ac.uk

Received: *16 August 2021*
Accepted: *23 September 2021*
Published: *12 October 2021*

Citation:
Kopp-Scheinpflug C and Forsythe ID (2021) Nitric Oxide Signaling in the Auditory Pathway. Front. Neural Circuits 15:759342. doi: 10.3389/fncir.2021.759342

INTRODUCTION

Nitric oxide (NO) is a small molecule, highly mobile, highly reactive and soluble in water and lipid membranes, so that once synthesized it cannot be contained. While its lifetime in biological tissues may be short, its mobility permits unimpeded diffusion over significant cellular distances. The discovery of the action of "Endothelium-Derived Relaxing Factor" on vascular smooth muscle and

Abbreviations: cGMP, cyclic guanosine monophosphate; EPSC, excitatory postsynaptic current; GABA, gamma-aminobutyric acid; $GABA_AR$, gamma-aminobutyric acid ionotropic receptor; GTP, guanosine triphosphate; HCN, hyperpolarization-activated cyclic nucleotide gated cation channel; HCN1, hyperpolarization-activated cyclic nucleotide gated cation channel type 1; HCN2, hyperpolarization-activated cyclic nucleotide gated cation channel type 2; KCC2, potassium-chloride cotransporter type 2; LSO, lateral superior olive; MNTB, medial nucleus of the trapezoid body; MSO, medial superior olive; N, number of synaptic release sites; NADPH, nicotinamide adenine dinucleotide phosphate; NMDAR, N-methyl-D-aspartic acid or N-methyl-D-aspartate receptor; nNOS, neuronal nitric oxide synthase; NO, nitric oxide; P, release probability; PKG, protein kinase G; PSD95, postsynaptic density 95; sGC, soluble guanylate cyclase; SPN, superior paraolivary nucleus; SR, spontaneous rate.

its identification as nitric oxide earned Furchgott, Murad and Ignarro, a Nobel Prize in 1998. NO action in the brain was first linked with NMDAR-mediated increases in cGMP in the cerebellum (Garthwaite et al., 1988) and its general signaling mechanisms in the brain have been widely reviewed (Garthwaite, 2008; Friebe and Koesling, 2009; Steinert et al., 2010).

Even the NO "receptor" is unconventional, in being a cytoplasmic hemoprotein ("soluble" guanylyl cyclase, sGC) generating cGMP from GTP. Although a misnomer, we have stuck with the term "soluble" and use of "sGC" to abbreviate guanylyl cyclase. It has been shown elsewhere in the brain, including in the inferior colliculus, that the GC is actually not soluble, but anchored to PSD-95 at the synapse (Russwurm et al., 2001; Olthof et al., 2019). Indeed, the signaling cascade exhibits extreme amplification, so that physiological signaling is thought to be achieved by NO in the nanomolar concentrations (Hall and Garthwaite, 2009; Bradley and Steinert, 2015).

Nitric oxide is synthetized from L-arginine and oxygen using NADPH and co-factors. This reaction is mediated by neuronal nitric oxide synthase (nNOS) in the brain. In the postsynaptic density of glutamatergic synapses, nNOS is activity-dependent and coupled through calmodulin to calcium influx at NMDARs. The canonical nNOS signaling pathway is shown in **Figure 1**, with examples of pharmacological agents (competitive antagonists, NO donors, sGC activators, and NO-chelating agents). The concentration of cGMP in any one cellular compartment is not only determined by the rate of production, but also by degradation through local phosphodiesterases, which further modulate signaling (**Figure 1**). Although cGMP may exert direct action on cyclic nucleotide-gated channels (Kaupp and Seifert, 2002) the majority of the signaling is via activation of protein kinase G (PKG) extending NO signaling capabilities, with different sGC isoforms providing important tissue-specific control (Friebe and Koesling, 2009). Facilitation of this signaling pathway is achieved by spatial proximity using cytoskeletal scaffolding proteins to bind sequential enzymes in the pathway, so nNOS is located in the postsynaptic density through PSD-95, which also binds NMDAR (Brenman et al., 1996; Christopherson et al., 1999).

Beyond the proven link to calcium influx through NMDAR, nNOS can be activated by calcium influx through calcium-permeable AMPA receptors (Haj-Dahmane et al., 2017) and L-type voltage-gated calcium channels (Pigott and Garthwaite, 2016; see **Figure 1**). NO signaling also modulates neuronal intrinsic excitability by acting on voltage-gated calcium, sodium, and potassium channels (Tozer et al., 2012).

Nitric oxide modulates neuronal excitability very broadly and yet nNOS knockout mice survive, as if NO is "part" of a massively redundant system (and perhaps compensated by the remaining eNOS and iNOS genes). NO signaling is highly ubiquitous in the animal kingdom (Moroz et al., 2020) and its breadth and diversity means we have yet to build consensus about its physiological roles in the nervous system. The literature has myriad observations (including those of the authors) that have yet to be consolidated into their full physiological context. The hypothesis of **retrograde NO transmission** has particularly fascinated neuroscientists, for which the evidence is reviewed elsewhere (Garthwaite, 2008). However, a presynaptic focus may have biased investigations away from other NO signaling roles: consequently, less attention has focused on **NO-mediated cGMP signaling beyond the synapse**, on kinase regulation of ion channels, and non-cGMP signaling via nitrosylation, control of gene expression or as a free radical. The auditory pathway provides a system in which many of these issues can be explored. In fact, the generation of cGMP, NO-induced intrinsic plasticity, synaptic plasticity and changes in *in vivo* firing rates have been clearly demonstrated in the auditory brainstem: cochlear nucleus: (Cao et al., 2019; Hockley et al., 2019, 2020), Superior Olivary Complex: (Steinert et al., 2008, 2011; Tozer et al., 2012; Yassin et al., 2014; Kopp-Scheinpflug et al., 2015), and Inferior Colliculus: (Olthof et al., 2019) and in an animal model of tinnitus (Coomber et al., 2014, 2015).

NITRIC OXIDE SIGNALING PATHWAYS IN AUDITORY NEURONS

There are **multiple elements to understanding NO signaling in the auditory system:** evidence for the presence of key signaling molecules in the pathway (nNOS/sGC/NADPH, see **Table 1**), identification of the target proteins and ion channels modulated, and observation of physiological/behavioral change on pharmacological intervention or genetic manipulation. This evidence must be weighed against physiological data and normal behavior since there is the potential for spill-over from other NO-generating systems and pathology, for example associated with iNOS activation during inflammatory processes. An important caveat in studying NO signaling is the extent to which an *in vitro* experimental system supports NO signaling (e.g., possessing an arginine source, NO donor validation, etc.) and whether an *in vivo* system is achieving NO activation (or inactivation) within a physiological or pathological context.

Adenosine 5′-triphosphate (ATP) is a major neurotransmitter and neuromodulator in the cochlea causing an increase in intracellular calcium. NO inhibits this ATP-induced calcium response via a negative feedback mechanism in inner hair cells, while at the same time enhancing the ATP-induced calcium response in outer hair cells and spiral ganglion neurons (Shen et al., 2003, 2006; Yukawa et al., 2005). Noise exposure increases nNOS expression in cochlear nucleus neurons (Coomber et al., 2014) and in spiral ganglion neurons, causing the NO concentration in the cochlea to rise from about 300 to 600 nM (Shi et al., 2002; Alvarado et al., 2016). The interaction of nNOS with activity-dependent calcium increases might be a component of the feedback in protecting inner hair cells from noise over-exposure (Shen et al., 2003; Mohrle et al., 2017). Application of nNOS inhibitors or NO donors *in vivo*, differentially affected spontaneous and sound-evoked firing rates in different cell types, which may contribute to increased gain during tinnitus (Coomber et al., 2015; Hockley et al., 2019, 2020).

There have been many studies of short-term plasticity at the giant calyx of Held synapse in the auditory brainstem (Taschenberger and von Gersdorff, 2000; Schneggenburger and Forsythe, 2006), but activity-dependent

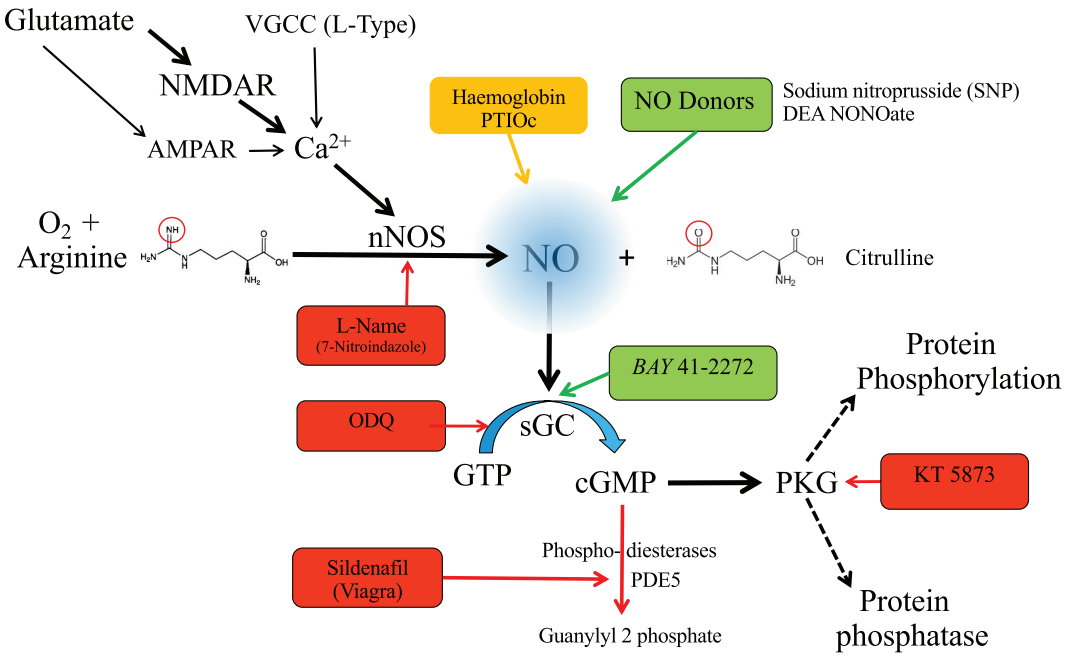

FIGURE 1 | Pharmacology of nitric oxide signaling. NO is generated by glutamatergic stimulation of NMDARs, but other sources of calcium from Calcium permeable AMPAR or L-type calcium channels are also recognized. Calcium influx activates nNOS (via calmodulin) which catalyzes the conversion of the amino-acid arginine to citrulline, releasing NO. nNOS activity may be blocked by competitive antagonists such as L-NAME (NG-Nitro-L-arginine methyl ester HCl), absorbed by chelating agents, or generated independently of nNOS by perfusion of NO donors. NO diffuses across cytoplasm, membranes and between cells to bind to its intracellular receptor – soluble guanylyl cyclase (sGC) which catalyzes GTP to cGMP – a cyclic nucleotide which activates protein kinase G (PKG). ODQ (1*H*-[1,2,4]Oxadiazolo[4,3-*a*]quinoxalin-1-one) is a competitive blocker of sGC, while BAY 41-2272 is a positive modulator. KT 5873 is an antagonist of PKG. cGMP signaling may in turn be suppressed with phosphodiesterases, such as PDE5, which can be blocked by sildenafil. Blockers or antagonists are shown in red, chelating agents in orange, and positive modulators in green. The canonical pathway is indicated by the thick black arrows, with links from other sources by fine arrows, and the spectrum of PKG actions via dashed arrows.

long-term plasticity has never been reported at this giant synapse. However, it is not always appreciated that NO reduces EPSC amplitudes at the calyx of Held through postsynaptic AMPAR modulation rather than a presynaptic mechanism (Steinert et al., 2008). Such a postsynaptic NO-action is corroborated by the lack of NO-modulation of presynaptic potassium currents, which would have changed transmitter release via the action potential (Wang and Kaczmarek, 1998; Yang et al., 2014). Nevertheless, other studies have demonstrated PKG-mediated modulation of synaptic vesicle endocytosis using capacitance measurements, although no change in transmitter release was reported (Eguchi et al., 2012). It is important to recognize that the probability of transmitter release, the number of release sites and rates of exocytosis and vesicle recycling are in a complex equilibrium (Hennig et al., 2008). Increased release probability (P) is "offset" by a reduced number of release sites (N) possessing fusion competent vesicles; hence after modulation the synapse may be in a different state (higher P, lower N; or lower P, higher N) even though there may be little evidence of a change in EPSC amplitude (Billups et al., 2005). Nevertheless, NO-signaling does cause an increase in spontaneous EPSCs in VCN T-stellate cells (Cao et al., 2019).

Direct effects of NO on evoked transmitter release have yet to be reported in the auditory pathway, so it is reasonable to postulate that **NO-modulation of postsynaptic neuronal excitability** (rather than synaptic mechanisms) is its primary mechanism of action. These actions may be mediated by the canonical cGMP second messenger and/or PKG-mediated phosphorylation of ion channels, for which there is direct evidence; or NO actions could be mediated by peroxynitrite formation or protein modification, such as nitrosylation (Steinert et al., 2010).

In neurons of the medial nucleus of the trapezoid body (MNTB), synaptic stimulation of the calyx of Held synapse (or perfusion of NO donors) raised cGMP and increased action potential duration, due to modulation of postsynaptic Kv3 and Kv2 potassium channels (Steinert et al., 2008, 2011). This is due to local activity-dependent generation of NO, and reciprocal modulation of potassium channel activity: so that Kv3 takes a lesser role and Kv2 takes a greater role in postsynaptic action potential repolarization, following NO signaling. This shift in intrinsic excitability reveals the hallmark of volume transmission, in that active synapses influence local quiescent neurons (having no synaptic input). This has implications for ion channel expression that follows a tonotopic gradient, such as HCN or Kv3 channels, which might be opposed (or amplified) by gradients of NO signaling, and hence ion channel activity will reflect the sum of channel expression and channel modulation (Steinert et al., 2008).

TABLE 1 | Sites of NO signaling in the auditory pathway.

Brain area	Region/cell type	Evidence for NO-signaling	References
Cochlea	Inner hair cells (IHC)	Histology/physiology	Reuss and Riemann, 2000; Shen et al., 2003
	Outer hair cells (OHC)	Physiology	Shen et al., 2006
	Supporting cells	Histology	Heinrich et al., 2004
	Spiral ganglion neurons (SGN)	Histology	Fessenden et al., 1999; Vyas et al., 2019
Cochlear nucleus	Bushy cells of the anteroventral cochlear nucleus (AVCN)	Histology/physiology	Fessenden et al., 1999; Coomber et al., 2014, 2015; Hockley et al., 2019
	Stellate cells of the AVCN	Histology/physiology	Coomber et al., 2014; Cao et al., 2019
	Octopus cells of the posteroventral cochlear nucleus (PVCN)	Histology	Coomber et al., 2015
	Deep layers of the dorsal cochlear nucleus (DCN)	Histology/physiology	Rodrigo et al., 1994; Coomber et al., 2014
	Granule cell domain (GCD)	Histology/physiology	Coomber et al., 2015
Superior olivary complex	Medial nucleus of the trapezoid body (MNTB)	Histology/physiology	Rodrigo et al., 1994; Fessenden et al., 1999; Reuss and Riemann, 2000; Schaeffer et al., 2003; Steinert et al., 2008, 2011; Yassin et al., 2014; Kopp-Scheinpflug et al., 2015
	Ventral nucleus of the trapezoid body (VNTB)	Histology/physiology	Fessenden et al., 1999; Reuss and Riemann, 2000; Steinert et al., 2008
	Superior paraolivary nucleus (SPN)	Histology/physiology	Fessenden et al., 1999; Reuss and Riemann, 2000; Schaeffer et al., 2003; Steinert et al., 2008; Yassin et al., 2014; Kopp-Scheinpflug et al., 2015
	Lateral superior olive (LSO)	Histology/physiology	Rodrigo et al., 1994; Fessenden et al., 1999; Reuss and Riemann, 2000; Kopp-Scheinpflug et al., 2015
	Medial superior olive (MSO)	Histology/physiology	Reuss and Riemann, 2000; Kopp-Scheinpflug et al., 2015
Nuclei of the lateral lemniscus	Ventral nucleus of the lateral lemniscus (VNLL)	Histology	Rodrigo et al., 1994
	Intermediate nucleus of the lateral lemniscus (INLL)	Histology	Rodrigo et al., 1994
	Dorsal nucleus of the lateral lemniscus (DNLL)	Histology	Rodrigo et al., 1994
Inferior colliculus	Central nucleus of the inferior colliculus (ICc)	Histology/physiology	Olthof et al., 2019
	External cortex of the inferior colliculus (ICe)	Histology	Herbert et al., 1991; Vincent and Kimura, 1992; Coote and Rees, 2008; Keesom et al., 2018
	Dorsal cortex of the inferior colliculus (ICd)	Histology	Herbert et al., 1991; Vincent and Kimura, 1992; Coote and Rees, 2008; Keesom et al., 2018
Medial geniculate body	Ventral division of the medial geniculate body (MGBv)	Histology	Olucha-Bordonau et al., 2004
	Medial division of the medial geniculate body (MGBm)	Histology	Druga and Syka, 1993; Bertini and Bentivoglio, 1997
	Dorsal division of the medial geniculate body (MGBd)	Histology	Rodrigo et al., 1994; Bertini and Bentivoglio, 1997
Auditory cortex	Primary auditory cortex (Au1)	Histology/physiology	Wakatsuki et al., 1998; Lee et al., 2008

Nitric oxide also modulates HCN1 and HCN2 channels, which are differentially expressed across the superior olivary complex (Koch et al., 2004). The MNTB expresses HCN2, which has slow kinetics, while in the medial and lateral superior olive (MSO, LSO) and in the superior paraolivary nucleus (SPN), HCN channels are dominated by HCN1 subunits, which have fast kinetics. NO had distinct actions on these two channels: it facilitated HCN2 in a cGMP-dependent manner and inhibited and slowed HCN1 kinetics in a cGMP-independent manner (Kopp-Scheinpflug et al., 2015). Regulation of HCN currents is a

key means of setting and regulating resting membrane potentials and the neuron membrane time-constant, since the higher Na^+ permeability of HCN channels will drive the equilibrium to more positive potentials. In turn, a higher resting conductance generates a faster membrane time-constant, thereby modulating integration of synaptic inputs.

Another important homeostatic process is the control of intracellular chloride concentrations. A developmental shift in the chloride equilibrium potential in young animals is documented across many areas of the CNS, including the auditory brainstem. "Inhibitory" neurotransmitters such as GABA and glycine mediate depolarizing synaptic responses in neonatal animals, which become hyperpolarizing around the time of hearing onset, due to an upregulation of the potassium-chloride cotransporter 2 (KCC2; Kandler and Friauf, 1995; Lee et al., 2016). Very high levels of KCC2 (driving the chloride equilibrium to around −100 mV) are expressed in the SPN and in combination with large glycinergic inputs (from the MNTB) and high levels of HCN1 currents, enable the ionic computation of the end of a sound (Kopp-Scheinpflug et al., 2011). Activity-dependent regulation of KCC2 has been widely documented in the hippocampus and neocortex where changes in chloride gradients impact the strength of $GABA_A$R-mediated inhibition (Chamma et al., 2013). In the SPN the strength of glycinergic inhibition is suppressed via a cGMP-dependent NO signaling at KCC2; creating a shift in the chloride equilibrium by +15 mV. This action is specific to those neurons that are expressing KCC2, which allows differential modulation of chloride reversal potentials in different neuronal populations (Yassin et al., 2014), all of which may be receiving the same inhibitory projection (for example from the MNTB).

DISCUSSION AND OPEN QUESTIONS

Nitric oxide signaling is widespread, with diverse sites and convoluted actions in the nervous system. Consequently, it is often difficult to identify the source of NO signaling for a specific physiological or behavioral output, and difficult to separate physiological roles from pathological consequences, with the potential for spill-over from one synthase into the signaling system of another, e.g., iNOS to nNOS (Hopper and Garthwaite, 2006). NO is an important mediator of inflammation and pathology via up-regulation of iNOS in microglia (generating micromolar concentrations of NO). Microglia are present in the auditory brainstem, where they are involved in developmental pruning of the calyx of Held synapse (Milinkeviciute et al., 2019) and in regulating inflammation. Inflammation is associated with noise-induced hearing loss (Fuentes-Santamaria et al., 2017) and mediated by pro-inflammatory cytokines. Hearing loss and inflammation can also be caused by severe hyperbilirubinemia (Schiavon et al., 2018), where subsequent degeneration of the calyx of Held synapse is mitigated by blocking NO signaling (Haustein et al., 2010). It is worth speculating that these links between hearing loss, inflammation and NO signaling could be associated with pathological actions of microglia. The wide actions of nitric oxide, nitrosylation, nitrergic stress, and inflammation are associated with multiple neurodegenerative disease mechanisms (Bourgognon et al., 2021) and perhaps underlies broader NO mediated pathology (Steinert et al., 2010).

Nitric Oxide has a broad impact on auditory neurons and signaling. It increases evoked firing rates by enhancing intrinsic excitability, by reducing inhibitory strength and by potentiating excitatory inputs via positive feedback (Wakatsuki et al., 1998; Steinert et al., 2008; Lee, 2009; Cao et al., 2019; Hockley et al., 2019). An interesting facet of auditory signaling are high rates of spontaneous AP firing; these spontaneous rates (SRs) arise from a combination of transmitter release at inner hair cells and the intrinsic excitability of all neurons along the pathway. There is a progressive decrease in SRs from the cochlea to the cortex (Eggermont, 2015), that seems to be mirrored by higher nNOS expression in the brainstem and midbrain compared to lower nNOS expression in MGB and cortex (Druga and Syka, 1993; Olucha-Bordonau et al., 2004; Lee et al., 2008). High SRs are advantageous for temporal processing tasks in the brainstem, but are less important at higher auditory centers (such as the MGB and cortex) where auditory processing has evolved from a temporal code toward a rate code. The idea that auditory brainstem SRs carry information has been comprehensively discussed elsewhere (Litvak et al., 2003; Eggermont, 2015). While synchronization and phase-locking of AP firing are important properties of sound-evoked activity, non-sound-evoked, spontaneous firing is synchronized only during development (Babola et al., 2018) or possibly during pathological auditory signaling (Herbert et al., 1991). SRs in the healthy, mature auditory system are not synchronized. This is important because incoming sound-evoked activity defines a time window within which an action potential could be generated, intrinsic excitability permitting. So when SR is high, there is a high probability that a neuron is refractory when a sound-evoked stimulus arrives, but the stochastic distribution and desynchronization of SR between neurons maximizes the number of short latency action potentials across the population. NO-mediated modulation of SR could maintain a desynchronized SR, ensuring temporally precise and faithful transmission of responses to sound. The lower SR in higher auditory brain areas would render NO-mediated desynchronization of SR redundant, in contrast to the developing auditory system (Sonntag et al., 2009; Babola et al., 2018). An open question for the future is the extent to which activity-dependent NO signaling controls basal activity rates: a low SR before hearing onset requires little NO, and high SR on maturation needs more NO, while a stressed auditory system following noise exposure would demand even higher NO concentrations. Recruitment of NO has been shown following noise exposure (Shi et al., 2002; Zheng et al., 2006; Coomber et al., 2014, 2015; Alvarado et al., 2016) and could be involved in the development of tinnitus. The question of whether NO signaling is a cause of tinnitus or a response to correct aberrant excitability and desynchronized SR, will require future studies (Sedley, 2019).

The proposed role in desynchronizing SR might explain why NO-volume transmission does not necessarily interfere with the precise tonotopically dominated sound evoked processing. A common theme of NO action in the auditory system

is the homeostatic control of excitability, be that synaptic excitation/inhibition (Wakatsuki et al., 1998; Yassin et al., 2014; Cao et al., 2019), spontaneous firing rates or neuronal intrinsic excitability. The contribution of NO to synaptic plasticity and memory formation is widely accepted in higher brain centers. Recent studies in the fruit fly have proposed that NO is more associated with active forgetting and updating of memories (Aso et al., 2019; Green and Lin, 2020). Such mechanisms might underlie auditory re-mapping following temporary hearing loss (Keating and King, 2015; Resnik and Polley, 2017). Failure to update memories in the absence of NO might also explain impaired auditory fear conditioning in nNOS knockout mice (Kelley et al., 2009).

There is strong evidence for the presence of NO signaling within the auditory brainstem. There are also broad observations of NO-mediated modulation of neuronal excitability and synaptic transmission. However, a consensus on the roles of NO in the auditory pathway has yet to be reached. Elsewhere there is ample evidence for NO involvement in synaptic plasticity, but less agreement about common downstream mechanisms. This no doubt reflects the broad signaling capabilities of cGMP and PKG (and alternate signaling by direct reactions of NO with proteins). Perhaps we need to integrate our investigations of NO signaling over a much broader range of targets (genetic, ion channel, cell signaling, metabolism/growth) in homeostasis, synaptic transmission and intrinsic excitability, and include (or control for) the potential for spill-over from pathological to physiological signaling. The superior olivary complex may lack the complexity of higher centers, but it has a well-characterized anatomy and physiology in which these complex interacting systems can be carefully explored.

KEY CONCEPTS

- NO generation is activity-dependent and through NMDAR activation at excitatory synapses.
- Signaling involves both cGMP -dependent and -independent signaling cascades.
- NO acts by diffusion through a process of Volume Transmission to regulate excitability of neurons (including those that are active and inactive within a sphere of influence).
- NO modulates postsynaptic neuronal excitability via modulation of voltage-gated ion channels.
- Aberrant signaling underlies impaired auditory processing via changes in excitability and spontaneous firing rates.

AUTHOR CONTRIBUTIONS

Both authors contributed to the conception, design, and writing of the review, and have read and approved the submitted version.

FUNDING

This research was funded by the DFG (SFB870 A-10) and BBSRC (United Kingdom).

REFERENCES

Alvarado, J. C., Fuentes-Santamaria, V., Gabaldon-Ull, M. C., Jareno-Flores, T., Miller, J. M., and Juiz, J. M. (2016). Noise-Induced "Toughening" Effect in Wistar Rats: Enhanced Auditory Brainstem Responses Are Related to Calretinin and Nitric Oxide Synthase Upregulation. *Front. Neuroanat.* 10:19. doi: 10.3389/fnana.2016.00019

Aso, Y., Ray, R. P., Long, X., Bushey, D., Cichewicz, K., Ngo, T. T., et al. (2019). Nitric oxide acts as a cotransmitter in a subset of dopaminergic neurons to diversify memory dynamics. *Elife* 8:e49257. doi: 10.7554/eLife.49257

Babola, T. A., Li, S., Gribizis, A., Lee, B. J., Issa, J. B., Wang, H. C., et al. (2018). Homeostatic Control of Spontaneous Activity in the Developing Auditory System. *Neuron* 99:511–524 e515. doi: 10.1016/j.neuron.2018.07.004

Bertini, G., and Bentivoglio, M. (1997). Nitric oxide synthase in the adult and developing thalamus: histochemical and immunohistochemical study in the rat. *J. Comp. Neurol.* 388, 89–105. doi: 10.1002/(sici)1096-9861(19971110)388:1

Billups, B., Graham, B. P., Wong, A. Y., and Forsythe, I. D. (2005). Unmasking group III metabotropic glutamate autoreceptor function at excitatory synapses in the rat CNS. *J. Physiol.* 565, 885–896. doi: 10.1113/jphysiol.2005.086736

Bourgognon, J. M., Spiers, J. G., Robinson, S. W., Scheiblich, H., Glynn, P., Ortori, C., et al. (2021). Inhibition of neuroinflammatory nitric oxide signaling suppresses glycation and prevents neuronal dysfunction in mouse prion disease. *Proc. Natl. Acad. Sci. U.S.A.* 79:118. doi: 10.1073/pnas.2009579118

Bradley, S. A., and Steinert, J. R. (2015). Characterisation and comparison of temporal release profiles of nitric oxide generating donors. *J. Neurosci. Methods* 245, 116–124. doi: 10.1016/j.jneumeth.2015.02.024

Brenman, J. E., Chao, D. S., Gee, S. H., McGee, A. W., Craven, S. E., Santillano, D. R., et al. (1996). Interaction of nitric oxide synthase with the postsynaptic density protein PSD-95 and alpha1-syntrophin mediated by PDZ domains. *Cell* 84, 757–767. doi: 10.1016/s0092-8674(00)81053-3

Cao, X. J., Lin, L., Sugden, A. U., Connors, B. W., and Oertel, D. (2019). Nitric oxide-mediated plasticity of interconnections between t-stellate cells of the ventral cochlear nucleus generate positive feedback and constitute a central gain control in the auditory system. *J. Neurosci.* 39, 6095–6107. doi: 10.1523/JNEUROSCI.0177-19.2019

Chamma, I., Heubl, M., Chevy, Q., Renner, M., Moutkine, I., Eugene, E., et al. (2013). Activity-dependent regulation of the K/Cl transporter KCC2 membrane diffusion, clustering, and function in hippocampal neurons. *J. Neurosci.* 33, 15488–15503. doi: 10.1523/JNEUROSCI.5889-12.2013

Christopherson, K. S., Hillier, B. J., Lim, W. A., and Bredt, D. S. (1999). PSD-95 assembles a ternary complex with the N-methyl-D-aspartic acid receptor and a bivalent neuronal NO synthase PDZ domain. *J. Biol. Chem.* 274, 27467–27473. doi: 10.1074/jbc.274.39.27467

Coomber, B., Berger, J. I., Kowalkowski, V. L., Shackleton, T. M., Palmer, A. R., and Wallace, M. N. (2014). Neural changes accompanying tinnitus following unilateral acoustic trauma in the guinea pig. *Eur. J. Neurosci.* 40, 2427–2441. doi: 10.1111/ejn.12580

Coomber, B., Kowalkowski, V. L., Berger, J. I., Palmer, A. R., and Wallace, M. N. (2015). Modulating central gain in tinnitus: changes in nitric oxide synthase in the ventral cochlear nucleus. *Front. Neurol.* 6:53. doi: 10.3389/fneur.2015.00053

Coote, E. J., and Rees, A. (2008). The distribution of nitric oxide synthase in the inferior colliculus of guinea pig. *Neuroscience* 154, 218–225. doi: 10.1016/j.neuroscience.2008.02.030

Druga, R., and Syka, J. (1993). NADPH-diaphorase activity in the central auditory structures of the rat. *Neuroreport* 4, 999–1002. doi: 10.1097/00001756-199308000-00001

Eggermont, J. J. (2015). Animal models of spontaneous activity in the healthy and impaired auditory system. *Front. Neural. Circuits* 9:19. doi: 10.3389/fncir.2015.00019

Eguchi, K., Nakanishi, S., Takagi, H., Taoufiq, Z., and Takahashi, T. (2012). Maturation of a PKG-dependent retrograde mechanism for exoendocytic coupling of synaptic vesicles. *Neuron* 74, 517–529. doi: 10.1016/j.neuron.2012.03.028

Fessenden, J. D., Altschuler, R. A., Seasholtz, A. F., and Schacht, J. (1999). Nitric oxide/cyclic guanosine monophosphate pathway in the peripheral and central auditory system of the rat. *J. Comp. Neurol.* 404, 52–63.

Friebe, A., and Koesling, D. (2009). The function of NO-sensitive guanylyl cyclase: what we can learn from genetic mouse models. *Nitric Oxide* 21, 149–156. doi: 10.1016/j.niox.2009.07.004

Fuentes-Santamaria, V., Alvarado, J. C., Melgar-Rojas, P., Gabaldon-Ull, M. C., Miller, J. M., and Juiz, J. M. (2017). The Role of Glia in the Peripheral and Central Auditory System Following Noise Overexposure: Contribution of TNF-alpha and IL-1beta to the Pathogenesis of Hearing Loss. *Front. Neuroanat.* 11:9. doi: 10.3389/fnana.2017.00009

Garthwaite, J. (2008). Concepts of neural nitric oxide-mediated transmission. *Eur. J. Neurosci.* 27, 2783–2802. doi: 10.1111/j.1460-9568.2008.06285.x

Garthwaite, J., Charles, S. L., and Chess-Williams, R. (1988). Endothelium-derived relaxing factor release on activation of NMDA receptors suggests role as intercellular messenger in the brain. *Nature* 336, 385–388. doi: 10.1038/336385a0

Green, D. J., and Lin, A. C. (2020). How nitric oxide helps update memories. *Elife* 9:e53832. doi: 10.7554/eLife.53832

Haj-Dahmane, S., Beique, J. C., and Shen, R. Y. (2017). GluA2-Lacking AMPA Receptors and Nitric Oxide Signaling Gate Spike-Timing-Dependent Potentiation of Glutamate Synapses in the Dorsal Raphe Nucleus. *eNeuro* 4, ENEURO.116–117. doi: 10.1523/ENEURO.0116-17.2017

Hall, C. N., and Garthwaite, J. (2009). What is the real physiological NO concentration in vivo? *Nitric Oxide* 21, 92–103. doi: 10.1016/j.niox.2009.07.002

Haustein, M. D., Read, D. J., Steinert, J. R., Pilati, N., Dinsdale, D., and Forsythe, I. D. (2010). Acute hyperbilirubinaemia induces presynaptic neurodegeneration at a central glutamatergic synapse. *J. Physiol.* 588, 4683–4693. doi: 10.1113/jphysiol.2010.199778

Heinrich, U. R., Maurer, J., and Mann, W. (2004). Evidence for a possible NOS back-up system in the organ of Corti of the guinea pig. *Eur. Arch. Otorhinolaryngol.* 261, 121–128. doi: 10.1007/s00405-003-0648-1

Hennig, M. H., Postlethwaite, M., Forsythe, I. D., and Graham, B. P. (2008). Interactions between multiple sources of short-term plasticity during evoked and spontaneous activity at the rat calyx of Held. *J. Physiol.* 586, 3129–3146. doi: 10.1113/jphysiol.2008.152124

Herbert, H., Aschoff, A., and Ostwald, J. (1991). Topography of projections from the auditory cortex to the inferior colliculus in the rat. *J. Comp. Neurol.* 304, 103–122. doi: 10.1002/cne.903040108

Hockley, A., Berger, J. I., Palmer, A. R., and Wallace, M. N. (2020). Nitric oxide increases gain in the ventral cochlear nucleus of guinea pigs with tinnitus. *Eur. J. Neurosci.* 52, 4057–4080. doi: 10.1111/ejn.14913

Hockley, A., Berger, J. I., Smith, P. A., Palmer, A. R., and Wallace, M. N. (2019). Nitric oxide regulates the firing rate of neuronal subtypes in the guinea pig ventral cochlear nucleus. *Eur. J. Neurosci.* 51, 963–983. doi: 10.1111/ejn.14572

Hopper, R. A., and Garthwaite, J. (2006). Tonic and phasic nitric oxide signals in hippocampal long-term potentiation. *J. Neurosci.* 26, 11513–11521. doi: 10.1523/JNEUROSCI.2259-06.2006

Kandler, K., and Friauf, E. (1995). Development of glycinergic and glutamatergic synaptic transmission in the auditory brainstem of perinatal rats. *J. Neurosci.* 15, 6890–6904.

Kaupp, U. B., and Seifert, R. (2002). Cyclic nucleotide-gated ion channels. *Physiol. Rev.* 82, 769–824. doi: 10.1152/physrev.00008.2002

Keating, P., and King, A. J. (2015). Sound localization in a changing world. *Curr. Opin. Neurobiol.* 35, 35–43. doi: 10.1016/j.conb.2015.06.005

Keesom, S. M., Morningstar, M. D., Sandlain, R., Wise, B. M., and Hurley, L. M. (2018). Social isolation reduces serotonergic fiber density in the inferior colliculus of female, but not male, mice. *Brain Res.* 1694, 94–103. doi: 10.1016/j.brainres.2018.05.010

Kelley, J. B., Balda, M. A., Anderson, K. L., and Itzhak, Y. (2009). Impairments in fear conditioning in mice lacking the nNOS gene. *Learn. Mem.* 16, 371–378. doi: 10.1101/lm.1329209

Koch, U., Braun, M., Kapfer, C., and Grothe, B. (2004). Distribution of HCN1 and HCN2 in rat auditory brainstem nuclei. *Eur. J. Neurosci.* 20, 79–91. doi: 10.1111/j.0953-816X.2004.03456.x

Kopp-Scheinpflug, C., Pigott, B. M., and Forsythe, I. D. (2015). Nitric oxide selectively suppresses I_H currents mediated by HCN1-containing channels. *J. Physiol.* 593, 1685–1700. doi: 10.1113/jphysiol.2014.282194

Kopp-Scheinpflug, C., Tozer, A. J., Robinson, S. W., Tempel, B. L., Hennig, M. H., and Forsythe, I. D. (2011). The sound of silence: ionic mechanisms encoding sound termination. *Neuron* 71, 911–925. doi: 10.1016/j.neuron.2011.06.028

Lee, H., Bach, E., Noh, J., Delpire, E., and Kandler, K. (2016). Hyperpolarization-independent maturation and refinement of GABA/glycinergic connections in the auditory brain stem. *J. Neurophysiol.* 115, 1170–1182. doi: 10.1152/jn.00926.2015

Lee, J. J. (2009). Nitric oxide modulation of GABAergic synaptic transmission in mechanically isolated rat auditory cortical neurons. *Korean J. Physiol. Pharmacol.* 13, 461–467. doi: 10.4196/kjpp.2009.13.6.461

Lee, J. J., Cho, Y. W., Huh, Y., Cha, C. I., and Yeo, S. G. (2008). Effect of nitric oxide on auditory cortical neurons of aged rats. *Neurosci. Lett.* 447, 37–41. doi: 10.1016/j.neulet.2008.09.074

Litvak, L. M., Delgutte, B., and Eddington, D. K. (2003). Improved temporal coding of sinusoids in electric stimulation of the auditory nerve using desynchronizing pulse trains. *J. Acoust. Soc. Am.* 114, 2079–2098. doi: 10.1121/1.1612493

Milinkeviciute, G., Henningfield, C. M., Muniak, M. A., Chokr, S. M., Green, K. N., and Cramer, K. S. (2019). Microglia regulate pruning of specialized synapses in the auditory brainstem. *Front. Neural. Circuits* 13:55. doi: 10.3389/fncir.2019.00055

Mohrle, D., Reimann, K., Wolter, S., Wolters, M., Varakina, K., Mergia, E., et al. (2017). NO-sensitive guanylate cyclase isoforms no-gc1 and no-gc2 contribute to noise-induced inner hair cell synaptopathy. *Mol. Pharmacol.* 92, 375–388. doi: 10.1124/mol.117.108548

Moroz, L. L., Romanova, D. Y., Nikitin, M. A., Sohn, D., Kohn, A. B., Neveu, E., et al. (2020). The diversification and lineage-specific expansion of nitric oxide signaling in Placozoa: insights in the evolution of gaseous transmission. *Sci. Rep.* 10:13020. doi: 10.1038/s41598-020-69851-w

Olthof, B. M. J., Gartside, S. E., and Rees, A. (2019). Puncta of neuronal nitric oxide synthase (nnos) mediate NMDA receptor signaling in the auditory midbrain. *J. Neurosci.* 39, 876–887. doi: 10.1523/JNEUROSCI.1918-18.2018

Olucha-Bordonau, F. E., Perez-Villalba, A., Teruel-Marti, V., and Ruiz-Torner, A. (2004). Chemical divisions in the medial geniculate body and surrounding paralaminar nuclei of the rat: quantitative comparison of cell density, NADPH diaphorase, acetyl cholin esterase and basal expression of c-fos. *J. Chem. Neuroanat.* 28, 147–162. doi: 10.1016/j.jchemneu.2004.05.010

Pigott, B. M., and Garthwaite, J. (2016). Nitric oxide is required for L-Type Ca^{2+} channel-dependent long-term potentiation in the hippocampus. *Front. Synaptic Neurosci.* 8:17. doi: 10.3389/fnsyn.2016.00017

Resnik, J., and Polley, D. B. (2017). Fast-spiking GABA circuit dynamics in the auditory cortex predict recovery of sensory processing following peripheral nerve damage. *Elife* 6:e21452. doi: 10.7554/eLife.21452

Reuss, S., and Riemann, R. (2000). Distribution and projections of nitric oxide synthase neurons in the rodent superior olivary complex. *Microsc. Res. Tech.* 51, 318–329. doi: 10.1002/1097-0029(20001115)51:4

Rodrigo, J., Springall, D. R., Uttenthal, O., Bentura, M. L., Abadia-Molina, F., Riveros-Moreno, V., et al. (1994). Localization of nitric oxide synthase in the adult rat brain. *Philos. Trans. R. Soc. Lond B. Biol. Sci.* 345, 175–221. doi: 10.1098/rstb.1994.0096

Russwurm, M., Wittau, N., and Koesling, D. (2001). Guanylyl cyclase/PSD-95 interaction: targeting of the nitric oxide-sensitive alpha2beta1 guanylyl cyclase to synaptic membranes. *J. Biol. Chem.* 276, 44647–44652. doi: 10.1074/jbc.M105587200

Schaeffer, D. F., Reuss, M. H., Riemann, R., and Reuss, S. (2003). A nitrergic projection from the superior olivary complex to the inferior colliculus of the rat. *Hear. Res.* 183, 67–72. doi: 10.1016/s0378-5955(03)00219-3

Schiavon, E., Smalley, J. L., Newton, S., Greig, N. H., and Forsythe, I. D. (2018). Neuro-inflammation and ER-stress are key mechanisms of acute bilirubin toxicity and hearing loss in a mouse model. *PLoS One* 13:e0201022. doi: 10.1371/journal.pone.0201022

Schneggenburger, R., and Forsythe, I. D. (2006). The calyx of Held. *Cell Tissue Res.* 326, 311–337. doi: 10.1007/s00441-006-0272-7

Sedley, W. (2019). Tinnitus: Does Gain Explain? *Neuroscience* 407, 213–228. doi: 10.1016/j.neuroscience.2019.01.027

Shen, J., Harada, N., Nakazawa, H., Kaneko, T., Izumikawa, M., and Yamashita, T. (2006). Role of nitric oxide on ATP-induced Ca^{2+} signaling in outer hair cells of the guinea pig cochlea. *Brain Res.* 1081, 101–112. doi: 10.1016/j.brainres.2005.12.129

Shen, J., Harada, N., and Yamashita, T. (2003). Nitric oxide inhibits adenosine 5'-triphosphate-induced Ca^{2+} response in inner hair cells of the guinea pig cochlea. *Neurosci. Lett.* 337, 135–138. doi: 10.1016/s0304-3940(02)01320-4

Shi, X., Ren, T., and Nuttall, A. L. (2002). The electrochemical and fluorescence detection of nitric oxide in the cochlea and its increase following loud sound. *Hear. Res.* 164, 49–58. doi: 10.1016/s0378-5955(01)00409-9

Sonntag, M., Englitz, B., Kopp-Scheinpflug, C., and Rubsamen, R. (2009). Early postnatal development of spontaneous and acoustically evoked discharge activity of principal cells of the medial nucleus of the trapezoid body: an in vivo study in mice. *J. Neurosci.* 29, 9510–9520. doi: 10.1523/JNEUROSCI.1377-09.2009

Steinert, J. R., Chernova, T., and Forsythe, I. D. (2010). Nitric oxide signaling in brain function, dysfunction, and dementia. *Neuroscientist* 16, 435–452. doi: 10.1177/1073858410366481

Steinert, J. R., Kopp-Scheinpflug, C., Baker, C., Challiss, R. A., Mistry, R., Haustein, M. D., et al. (2008). Nitric oxide is a volume transmitter regulating postsynaptic excitability at a glutamatergic synapse. *Neuron* 60, 642–656. doi: 10.1016/j.neuron.2008.08.025

Steinert, J. R., Robinson, S. W., Tong, H., Haustein, M. D., Kopp-Scheinpflug, C., and Forsythe, I. D. (2011). Nitric oxide is an activity-dependent regulator of target neuron intrinsic excitability. *Neuron* 71, 291–305. doi: 10.1016/j.neuron.2011.05.037

Taschenberger, H., and von Gersdorff, H. (2000). Fine-tuning an auditory synapse for speed and fidelity: developmental changes in presynaptic waveform, EPSC kinetics, and synaptic plasticity. *J. Neurosci.* 20, 9162–9173.

Tozer, A. J., Forsythe, I. D., and Steinert, J. R. (2012). Nitric oxide signalling augments neuronal voltage-gated L-type (Cav1) and P/q-type (Cav2.1) channels in the mouse medial nucleus of the trapezoid body. *PLoS One* 7:e32256. doi: 10.1371/journal.pone.0032256

Vincent, S. R., and Kimura, H. (1992). Histochemical mapping of nitric oxide synthase in the rat brain. *Neuroscience* 46, 755–784. doi: 10.1016/0306-4522(92)90184-4

Vyas, P., Wu, J. S., Jimenez, A., Glowatzki, E., and Fuchs, P. A. (2019). Characterization of transgenic mouse lines for labeling type I and type II afferent neurons in the cochlea. *Sci. Rep.* 9:5549. doi: 10.1038/s41598-019-41770-5

Wakatsuki, H., Gomi, H., Kudoh, M., Kimura, S., Takahashi, K., Takeda, M., et al. (1998). Layer-specific NO dependence of long-term potentiation and biased NO release in layer V in the rat auditory cortex. *J. Physiol.* 513, 71–81. doi: 10.1111/j.1469-7793.1998.071by.x

Wang, L. Y., and Kaczmarek, L. K. (1998). High-frequency firing helps replenish the readily releasable pool of synaptic vesicles. *Nature* 394, 384–388. doi: 10.1038/28645

Yang, Y. M., Wang, W., Fedchyshyn, M. J., Zhou, Z., Ding, J., and Wang, L. Y. (2014). Enhancing the fidelity of neurotransmission by activity-dependent facilitation of presynaptic potassium currents. *Nat. Commun.* 5:4564. doi: 10.1038/ncomms5564

Yassin, L., Radtke-Schuller, S., Asraf, H., Grothe, B., Hershfinkel, M., Forsythe, I. D., et al. (2014). Nitric oxide signaling modulates synaptic inhibition in the superior paraolivary nucleus (SPN) via cGMP-dependent suppression of KCC2. *Front. Neural. Circuits* 8:65. doi: 10.3389/fncir.2014.00065

Yukawa, H., Shen, J., Harada, N., Cho-Tamaoka, H., and Yamashita, T. (2005). Acute effects of glucocorticoids on ATP-induced Ca^{2+} mobilization and nitric oxide production in cochlear spiral ganglion neurons. *Neuroscience* 130, 485–496. doi: 10.1016/j.neuroscience.2004.09.037

Zheng, Y., Seung Lee, H., Smith, P. F., and Darlington, C. L. (2006). Neuronal nitric oxide synthase expression in the cochlear nucleus in a salicylate model of tinnitus. *Brain Res.* 1123, 201–206. doi: 10.1016/j.brainres.2006.09.045

Conflict of Interest: The authors declare that the research was conducted in the absence of any commercial or financial relationships that could be construed as a potential conflict of interest.

Publisher's Note: All claims expressed in this article are solely those of the authors and do not necessarily represent those of their affiliated organizations, or those of the publisher, the editors and the reviewers. Any product that may be evaluated in this article, or claim that may be made by its manufacturer, is not guaranteed or endorsed by the publisher.

frontiers in Neural Circuits

ORIGINAL RESEARCH
published: 12 November 2021
doi: 10.3389/fncir.2021.747472

Expression Patterns of the Neuropeptide Urocortin 3 and Its Receptor CRFR2 in the Mouse Central Auditory System

*Sara Pagella[1], Jan M. Deussing[2] and Conny Kopp-Scheinpflug[1]**

[1] Division of Neurobiology, Faculty of Biology, Ludwig-Maximilians-University Munich, Munich, Germany, [2] Research Group Molecular Neurogenetics, Max Planck Institute of Psychiatry, Munich, Germany

Sensory systems have to be malleable to context-dependent modulations occurring over different time scales, in order to serve their evolutionary function of informing about the external world while also eliciting survival-promoting behaviors. Stress is a major context-dependent signal that can have fast and delayed effects on sensory systems, especially on the auditory system. Urocortin 3 (UCN3) is a member of the corticotropin-releasing factor family. As a neuropeptide, UCN3 regulates synaptic activity much faster than the classic steroid hormones of the hypothalamic-pituitary-adrenal axis. Moreover, due to the lack of synaptic re-uptake mechanisms, UCN3 can have more long-lasting and far-reaching effects. To date, a modest number of studies have reported the presence of UCN3 or its receptor CRFR2 in the auditory system, particularly in the cochlea and the superior olivary complex, and have highlighted the importance of this stress neuropeptide for protecting auditory function. However, a comprehensive map of all neurons synthesizing UCN3 or CRFR2 within the auditory pathway is lacking. Here, we utilize two reporter mouse lines to elucidate the expression patterns of UCN3 and CRFR2 in the auditory system. Additional immunolabelling enables further characterization of the neurons that synthesize UCN3 or CRFR2. Surprisingly, our results indicate that within the auditory system, UCN3 is expressed predominantly in principal cells, whereas CRFR2 expression is strongest in non-principal, presumably multisensory, cell types. Based on the presence or absence of overlap between UCN3 and CRFR2 labeling, our data suggest unusual modes of neuromodulation by UCN3, involving volume transmission and autocrine signaling.

Keywords: urocortin, CRFR2, auditory, stress signaling, multimodal, volume transmission, calyx of Held synapse

OPEN ACCESS

Edited by:
Catherine Carr, University of Maryland, College Park, United States

Reviewed by:
Douglas E. Vetter, University of Mississippi Medical Center, United States
Max Anstötz, Northwestern University, United States
Laura M. Hurley, Indiana University Bloomington, United States

****Correspondence:***
Conny Kopp-Scheinpflug
cks@bio.lmu.de

Received: *26 July 2021*
Accepted: *18 October 2021*
Published: *12 November 2021*

Citation:
Pagella S, Deussing JM and Kopp-Scheinpflug C (2021) Expression Patterns of the Neuropeptide Urocortin 3 and Its Receptor CRFR2 in the Mouse Central Auditory System. Front. Neural Circuits 15:747472. doi: 10.3389/fncir.2021.747472

INTRODUCTION

Temporary changes in hearing during stressful situations or episodes of anxiety or sadness are commonly experienced by humans and animals (Neuser and Knoop, 1986; Schmitt et al., 2000; Horner, 2003; Kadner et al., 2006; Mazurek et al., 2010; Pacheco-Unguetti and Parmentier, 2014; Lin et al., 2016; Szczepek et al., 2018). Such changes can range from decreased attention to sincere auditory hallucinations (Hoskin et al., 2014). More profound and chronic stress system

dysregulation such as with post-traumatic stress disorder (PTSD) can come with a plethora of associated auditory abnormalities (Shalev et al., 2000; Guthrie and Bryant, 2005; Karl et al., 2006; Clifford et al., 2018). Conversely, specific acoustic qualities of sound can trigger stress-like sensations or even fear in both humans and animals, with the acoustic startle response being the most prominent example (Davis, 1984; Trost et al., 2012; Koelsch et al., 2013; Koelsch, 2014; Behler and Uppenkamp, 2020; Hegewald et al., 2020).

There is a clear reciprocity between stress and sensory systems. On one hand, the stress response relies on incoming information from the external environment provided by sensory systems to execute its function of maintaining allostasis, while on the other hand, sensory systems have to adapt constantly to changes in external conditions that are potentially threatening to the animal's current state. Since ears, unlike eyes, are open and sensing for 24 h a day, the auditory system plays a pivotal role in survival and has to be protected not only from noise trauma, but also from degenerative damage resulting from non-auditory stressors such as infections and head trauma. Hence, strong two-way interactions between stress signaling and the auditory system are warranted.

In the auditory system, the medial subdivision of the medial geniculate body (MGBm), the external cortex of the inferior colliculus (ICe) and the auditory cortex (Au) are well-known areas of connection to stress pathways. In particular, the MGBm-amygdala-pathway is known to be involved in auditory fear conditioning and in attributing emotional salience to sounds (LeDoux et al., 1984). The ICe receives hypothalamic input (Sakanaka et al., 1987) which might be involved in circadian regulation of stress, since both areas contain independent clocks (Park et al., 2016). The primary auditory cortex (Au1) sends direct projections to the lateral amygdala, which in turn projects to the auditory association cortex (Romanski and LeDoux, 1993; McDonald, 1998; Phelps and LeDoux, 2005). On top of these discrete connections, a wide network of mostly serotoninergic and cholinergic projections coming from the reticular formation innervate the auditory system throughout its extent from cochlea to cortex (Klepper and Herbert, 1991; Hurley and Hall, 2011; Schofield et al., 2011). Noradrenergic inputs, which mostly target the dorsal (DCN) and the granule cell domain (GCD) of the cochlear nucleus (CN), the ICe, the superior olivary complex (SOC), and the Au are even less understood (Levitt and Moore, 1978; Klepper and Herbert, 1991; Mulders and Robertson, 2001).

Non-auditory areas are crucial in shaping auditory responses by stressors coming from other sensory modalities. For example, olfactory stimulation with predator odor has been shown to trigger changes in neuronal firing rates of the locus coeruleus, a brainstem nucleus that receives auditory input and releases norepinephrine (Curtis et al., 2012). There, presentation of a stressor such as corticotropin-releasing factor (CRF) or a predator odor increases spontaneous tonic firing and decreases sound-evoked phasic firing of the neurons. Such a shift from tonic to phasic firing in locus coeruleus neurons is suggested to facilitate different behavioral reactions (Aston-Jones and Cohen, 2005).

The activation of the hypothalamic-pituitary-adrenal axis (HPA) is commonly regarded as the cornerstone of the stress response. Briefly, this entails release of CRF from hypothalamic paraventricular nucleus' neurons into the anterior pituitary gland, which in turn secretes adrenocorticotropic hormone (ACTH) that, upon reaching the adrenal glands, stimulates cortisol synthesis and release. Cortisol targets specific cell groups throughout the body *via* blood circulation (Charmandari et al., 2005). In its target cells, cortisol binds to its nuclear receptor and elicits the transcriptional modifications to adapt cellular function. It takes about 30 min to reach sufficient ACTH concentrations in the blood for cortisol to be synthetized (Sapolsky et al., 2000), a delay that could impede the timeliness of the response.

Thanks to the pioneering work of the Vetter-lab, a much faster, HPA axis-independent stress axis has been discovered in the cochlea, that not only involves all the constituents for cortisol production, but also a local CRF system (Basappa et al., 2012). The CRF system consists of two receptors CRFR1 and CRFR2, four ligands and the non-membrane-bound CRF-binding-protein. The four ligands, CRF, urocortin 1 (UCN1), 2 (UCN2), and 3 (UCN3) display different affinities for the two receptor types. CRF and UCN1 are most affine to CRFR1 but may also at bind to CRFR2 at very high concentrations (Chang et al., 1993; Chen et al., 1993; Vita et al., 1993; Perrin et al., 1995; Deussing and Chen, 2018). In contrast, UCN2 and UCN3 bind exclusively to CRFR2 (Lewis et al., 2001; Reyes et al., 2001; Deussing et al., 2010).

The most abundant stress peptide in the auditory system is CRF, which is expressed in the cochlea (Basappa et al., 2012), the principal neurons of the lateral superior olive (LSO), the ventral nucleus of the lateral lemniscus (VNLL), the inferior colliculus (IC), and the medial geniculate body (MGB) (including the peripeduncular and posterior intralaminar nuclei), the Brodman areas 20, 39, 40, and 41 and, although much weaker, in the deep layers of the DCN and lateral part of the medial nucleus of the trapezoid body (MNTB) (Imaki et al., 1991). UCN1 expression in the auditory system is much more distinct and has been reported only in a small subset of lateral olivocochlear bundle cells (LOC) with high characteristic frequencies (CF) as well as in the neuropil of the DCN deep layers and IC (Kozicz et al., 1998; Kaiser et al., 2011).

To date, no data are available that suggest UCN2 expression in the auditory system (Lewis et al., 2001). That makes UCN3 the primary ligand for CRFR2. So far, UCN3 expression in the auditory system was reported in the cochlea and SOC (Lewis et al., 2001; Li et al., 2002; Fischl et al., 2019). However, the physiological importance of UCN3 and its receptor CRFR2 for auditory function has been emphasized by knockout models of UCN3 and CRFR2, both showing enhanced vulnerability to noise trauma (Graham et al., 2010; Fischl et al., 2019). Although noise trauma and systemic stress are two major causes of hearing loss in humans (Masuda et al., 2012), our knowledge of the UCN3–CRFR2 contribution to auditory signal processing is rather limited.

In the present study, we take advantage of two reporter mouse lines, one for UCN3 and the other for its receptor CRFR2 to provide an extensive description of UCN3 and CRFR2 expression

in the central auditory system. Immunocytochemistry was used for co-labeling the neurons highlighted by the reporter to allow the best possible identification of specific areas and cell types.

Characteristic expression patterns throughout this study showed UCN3 expression in principal auditory neurons and CRFR2 expression in non-principal/multimodal neurons of the same nucleus. Fewer areas revealed neurons that express both the ligand as well as the receptor. Together, both types of expression suggest that volume transmission as well as autocrine regulation are possible signaling mechanisms for UCN3.

MATERIALS AND METHODS

All experimental procedures were reviewed and approved by the Bavarian district government (ROB-55.2-2532.Vet_02-18-1183) and were done according to the European Communities Council Directive (2010/63/EU). Mice were housed in a vivarium with a normal light–dark cycle (12 h light/12 h dark) and food and water *ad libitum*.

Mouse Models

Experiments were conducted on four UCN3 reporter mice (UCN3 tdTom) and three CRFR2 reporter mice (CRFR2 tdTom) of both sexes (five males and two females). After weaning, mice were separated by sex and group housed with same sex littermates until used in the experiment. In this absence of deliberate stressors, no differences in expression patterns were observed between males and females.

Reporter mice were generated by breeding UCN3-Cre mice [Tg(UCN3-Cre)KF31Gsat; The Gene Expression Nervous System Atlas (GENSAT) Project; Mutant Mouse Resource & Research Centers (MMRC) stock no: 033033-UCD] or CRFR2-Cre mice (Henckens et al., 2017) with $R26^{CAG-LSL-tdTomato}$ mice (Ai9, The Jackson Laboratory, Bar Harbor, ME, United States; stock no: 007905) as previously described (Shemesh et al., 2016).

Immunohistochemistry

Mice received an overdose of pentobarbital (400 mg kg^{-1} body weight; I.P.) and were perfusion-fixed with 4% paraformaldehyde (PFA) intracardially. Following overnight postfixation in 4% PFA, brainstems were sectioned coronally at 50 μm using a vibrating blade microtome (V1200S, Leica, Wetzlar, Germany). After rinsing in phosphate-buffered saline (PBS), sections were transferred to a blocking solution containing 1% bovine serum albumin, 0.5% Triton X-100, and 0.1% saponin in PBS. The floating sections were then incubated for 48 h at 4°C in blocking solution containing primary antibodies, which were used in different combinations as specified in the figures. Sections were washed three times in PBS for 15 min and were then incubated with secondary antibodies overnight at 4°C. Antibodies against calbindin D28K (SWANT, #07F Burgdorf, Switzerland, 1:300) were combined with secondary antibodies Alexa 488 (Dianova anti-rabbit, #115-545-206, Hamburg, Germany, 1:200). Antibodies against parvalbumin PV-28 (SWANT, Burgdorf, Switzerland, 1:500) were combined with secondary antibodies AMCA (Dianova, anti-mouse, Hamburg, Germany, #715-156-150, 1:100). Antibodies against VGluT1 (Synaptic Systems #135304, Göttingen, Germany, 1:500) were combined with secondary antibodies Alexa 647 (Dianova, anti-guinea pig, Hamburg, Germany, #706-605-148). Antibodies against vesicular glutamate transporter type 2 (VGluT2) (Synaptic Systems, Göttingen, Germany, #135402, 1:500) were combined with secondary antibodies Alexa 488 (Dianova anti-rabbit, #115-545-206, Hamburg, Germany, 1:200). Antibodies against glycine transporter type 2 (GlyT2; Millipore #1773, 1:1000) were combined with secondary antibodies Alexa 647 (Dianova, anti-guinea pig, Hamburg, Germany, #706-605-148). Antibodies against VChat (Synaptic System #139105, Göttingen, Germany, 1:200) were combined with secondary antibodies Alexa 647 (Dianova, anti-guinea pig, Hamburg, Germany, #706-605-148). Sections were washed in PBS, mounted on slides and coverslipped with vectashield mounting medium (Vector Laboratories, Burlingame, CA, United States).

Confocal Microscopy and Image Analysis

Confocal optical sections were acquired with a confocal laser-scanning microscope equipped with HCX PL APO CS 20×/NA0.7 and HCX PL APO Lambda Blue 63×/NA1.4 immersion oil objectives (Leica). Fluorochromes were visualized with excitation wavelengths of 405 nm (emission filter 410–430 nm) for amino-methylcoumarin (AMCA), 488 nm (emission filter 510–540 nm) for Alexa 488, 561 nm (emission filter 565–585 nm) for Cy3, and 647 nm (emission filter 663–738 nm) for Alexa 647. For each optical section, the images were collected sequentially for the different fluorochromes. Stacks of 8-bit grayscale images were obtained with axial distances of 290 nm between optical sections and pixel sizes of 120–1520 nm depending on the selected zoom factor and objective. To improve the signal-to-noise ratio, images were averaged from three successive scans. RGB stacks, montages of RGB optical sections and maximum-intensity projections were assembled using the ImageJ StackGroom plugin. Color schemes were adjusted to C-M-Y-W.

RESULTS

Expression patterns of UCN3 and CRFR2 in the cochlea and spiral ganglion neurons were reported in detail before (Graham et al., 2010; Fischl et al., 2019), so that here, we start with the description of UCN3 and CRFR2 expression in the CN. From there we proceed to the SOC, the LL, the IC, and the MGB. The auditory cortex exhibited hardly any UCN3 or CRFR2 expression so that we focused on subcortical auditory areas.

Cochlear Nucleus

The mouse CN (**Figure 1A**) is divided into four main areas: anteroventral (AVCN), posteroventral (PVCN), and dorsal (DCN) CN as well as the granule cell domain (GCD) (Harrison and Irving, 1965; Mugnaini et al., 1980; Willard and Ryugo, 1983). AVCN and PVCN contain similar neuronal cell types such as globular (GBCs) and spherical bushy cells (SBCs), stellate cells

(T-stellate and D-stellate), and little cells (LCs), all of which are regarded as principal auditory neurons (Cant, 1993; Oertel et al., 2011; Ngodup et al., 2020). In addition, the PVCN also contains octopus cells (OCs) which inhabit their own domain near the auditory nerve root region (Oertel et al., 2000). Location, morphology and co-labeling with recognized markers were used to identify these neurons.

The UCN3 tdTom reporter mouse showed an abundance of UCN3-positive neuronal cell bodies in the magnocellular domain (MCD) of AVCN and PVCN (**Figures 1B–G**). Auditory nerve terminals innervate the VCN tonotopically, with ventro-lateral neurons receiving inputs originating from the apex of the cochlea and therefore being responsive to low-frequency sounds. Neurons located more dorso-medially receive input from the base of the cochlea, which is sensitive to higher sound frequencies (Liberman, 1991, 1993). UCN3-positive neurons are found predominantly in the ventro-lateral, low-frequency part of the AVCN and progress to occupy more intermediate areas in the PVCN. No UCN3 expression was observed in the octopus cell domain (OCD), which is visualized by the empty space visible in **Figure 1D**. Only some of the UCN3-positive neurons in the MCD of the VCN co-localize with the Ca^{2+} binding protein calbindin (**Figures 1E–G**). Therefore we used size measures to assess if these UCN3-positive neurons qualify as canonical principal auditory neurons, which in the MCD are quite large in diameter (Oertel et al., 2000; Bazwinsky et al., 2008; Lauer et al., 2013). In addition to the large soma size (mean ± SD: 19.59 ± 2.17 μm; $n = 44$ neurons; 3 mice; **Figures 1N,Q**), morphological characteristics such as a round soma, typical bush-like dendrites, and projections to the contralateral MNTB and ipsilateral LSO allowed us to identify some UCN3-positive neurons as bushy cells (**Figure 1N**; Webster and Trune, 1982). However, a large number of UCN3-positive neurons in the VCN seem to be stellate cells based on their distinct multipolar (stellate) shape (**Figure 1N**) and by prominent ascending fibers originating from these cells and profusely innervating the ipsilateral DCN (**Figures 1H,I**). The observation of many UCN3-positive axons leaving the VCN, crossing in the trapezoid body, but not terminating in a calyx of Held suggest a T-stellate cell origin, as the "T" in T-stellate was, indeed, given to underline the fact that very often these neurons send axons across to the other side through the trapezoid (tz) body (Oertel et al., 1990). Other UCN3-positive stellate cell axons connect the VCN to the DCN. These fibers could be of D- or T-stellate cell origin and the neuronal somata of these cell types are found rostrocaudally in the VCN. The innervation pattern of this bundle is similar to that of metabotropic acetylcholine receptor type 2 (AChR M2) recently described (Malfatti et al., 2021). Using an AChR M2 reporter mouse, this bundle was interpreted as originating from VCN T-stellate cells. After entering the DCN, the UCN3-positive fibers span the whole of the deep layers, but without entering the molecular domain, which is characterized by an abundance of cholinergic inputs (**Figures 1G,H**; Fujino and Oertel, 2001). In conclusion, the UCN3 tdTom reporter shows that in the VCN, a small number of globular bushy cells and a larger number of stellate cells express UCN3. Both, bushy cells and T-stellate cells are found in the MCD of the nucleus and are involved in the faithful transmission of sound information from the cochlear nerve. In contrast to the MCD, the granular cell domain (GCD) does not exhibit any UCN3-positive cells or fibers (**Figures 1C,D**). Instead, UCN3-positive projections originating from the VCN innervate large parts of the DCN, spanning the deep (polymorphic) and the fusiform layers up to the molecular layer but not trespassing into the GCD nor the molecular layer. The GCD forms a more or less defined area between the magnocellular core of the VCN and the DCN (Mugnaini et al., 1980). The GCD consists mainly of granule cells as well as some other less frequent cell types (unipolar brush cells, chestnut cells, and Golgi cells) (Floris et al., 1994; Weedman et al., 1996; Yaeger and Trussell, 2015). Cells in the GCD are considered non-principal neurons. Although they respond to sound stimulation, especially at high intensities, they mainly integrate sound information with multisensory inputs, rather than to encode straightforward sound properties (Yang et al., 2005; Flores et al., 2015). Much of this multisensory, integrative processing takes place in the molecular layer. The axons of the granule cells populate the molecular layer of the DCN as parallel fibers where they interact with the dendrites of fusiform cells and cartwheel cells. Inputs from non-auditory areas such as the pontine nuclei, the nucleus cuneatus, the vestibular nucleus or the spinal trigeminal nucleus (Zhao et al., 1995; Wright and Ryugo, 1996; Ohlrogge et al., 2001; Ryugo et al., 2003; Zhou and Shore, 2004; Zhan et al., 2006; Zhan and Ryugo, 2007) tend to be positive for the VGluT2, whereas primary auditory inputs are predominantly VGluT1 positive (Zhan and Ryugo, 2007; Zeng et al., 2011).

The expression pattern of CRFR2, differs considerably from the UCN3 expression patterns. In the CN, CRFR2 is expressed almost exclusively in neurons and axonal tracts of the GCD (**Figures 1J–M**). Cell bodies and axons span the entire rostrocaudal extent of the GCD, including the lamina between VCN and DCN (**Figures 1J–M**). The morphology of these cells suggests them to be granule cells (**Figure 1O**). They exhibit the characteristic small size with a mean (±SD) diameter of 9.51 ± 1.02 μm ($n = 31$ neurons; 3 mice; **Figure 1Q**). This size is significantly smaller then neurons of the MCD (ANOVA: $p \leq 0.001$; **Figures 1O,Q**). Another prominent feature of granule cells are their axons, which take the characteristic parallel course with respect to the nucleus borders. The CRFR2-positive fibers inhabit the DCN molecular layer, which is also VGluT2-positive and predestines them as granule cells' parallel fibers (**Figures 1J–M**; Rubio et al., 2008). In addition to CRFR2 labeling of granule cells and parallel fibers, another population of slightly bigger CRFR2-positive cells were observed at the dorsolateral edge of the DCN (**Figures 1J–L,P**). These neurons are slightly larger in diameter (mean ± SD: 10.45 ± 0.88 μm; $n = 39$ neurons; 3 mice) than granule cells (ANOVA: $p = 0.036$; **Figures 1O–Q**), but clearly smaller than magnocellular cells (ANOVA: $p \leq 0.001$; **Figures 1N,Q**). Their size and the fact that they are not entirely embedded in the parallel fiber mesh, but rather somewhat underneath suggests them to be small cap cells (Osen, 1969; Cant, 1993; Ryugo, 2008). Small cap cells receive input from medial olivocochlear complex (MOC) neurons in the ventral nucleus of the trapezoid body (VNTB) and project back to the VNTB and

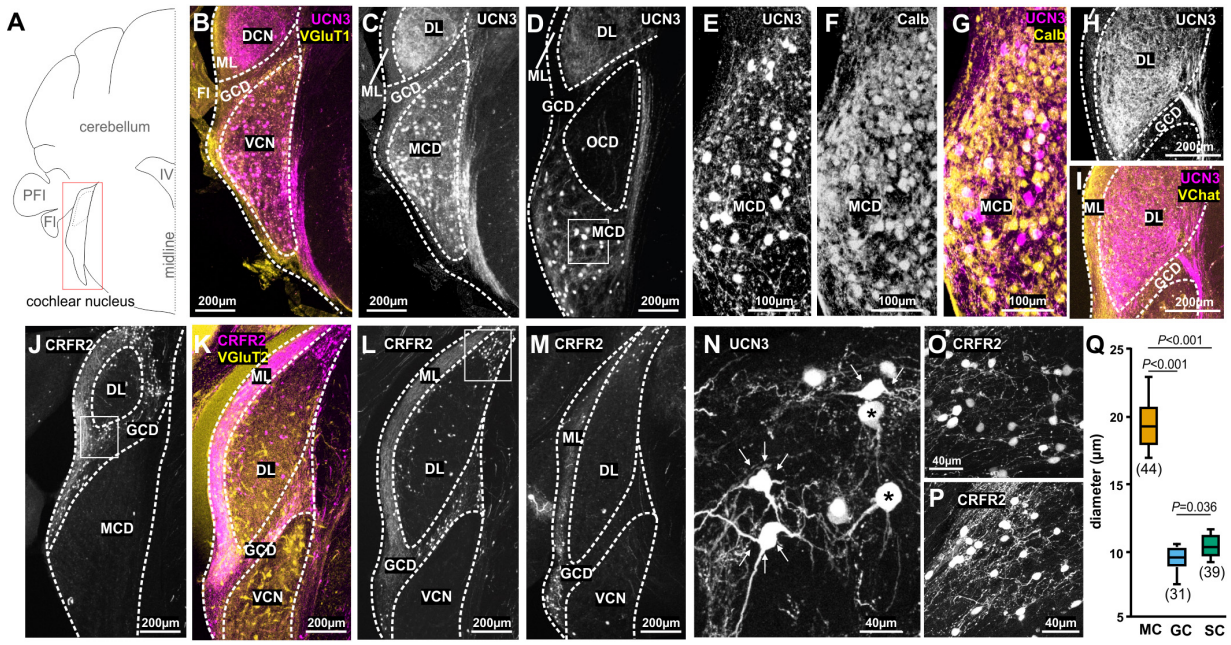

FIGURE 1 | Spatial segregation of UCN3 and CRFR2 expression in the cochlear nucleus. **(A)** Schematic coronal section showing the cochlear nucleus as the region of interest. PFl, paraflocculus; Fl, flocculus; IV, fourth ventricle. **(B)** UCN3 expression (magenta) in the VCN and in the DCN VGluT1 (yellow) labeling dominates in the molecular layer (ML) of the DCN and the granule cell domain (GDC). **(C)** Same image as in **(B)**. UCN-expression in neuronal cell bodies of the VCN magnocellular domain (MCD) and in dense fiber networks in the deep layer (DL) of DCN. **(D)** More caudal coronal section highlighting the lack of UCN3 expression in the octopus cell domain (OCD). Square in the MCD indicates UCN3-positive cell bodies in the MCD, shown in higher magnification in **(M)**. **(E–H)** Co-staining of UCN3-positive neurons in the MCD **(E)** with calbindin **(F)**. Neurons co-labeled for UCN3 (magenta) and calbindin (yellow) appear white. **(H,I)** UCN3-expressing fibers in the DCN deep layer (DL) do not enter the molecular layer (ML), which is characterized by yellow VChat labeling in **(I)**. **(J–L)** Coronal sections in **(J–L)** show CRFR2 expression in different rostro-caudal positions along the cochlear nucleus. **(J)** CRFR2 expression in the parallel fibers of the DCN molecular layer (ML), in granule cells of the granule cell domain (GCD), but not in the MCD of the VCN. Square in the GCD indicates UCN3-positive cell bodies shown in higher magnification in **(O)**. **(K)** Co-staining of CRFR2 (magenta) and VGluT2 (yellow) in a more caudal image compared to **(J)**. White color in the GCD and the ML suggest co-labeling. **(L)** Same image as in **(K)**. CRFR2 expression in ML parallel fibers, in GCD granule cells and in neurons of the small cell cap (white square), which are shown in higher magnification in **(P)**. **(M)** CRFR2 expression in a more caudal section compared to **(J,K)**, depicting again parallel fibers, granule cells, and small cells. **(N)** Higher magnification of UCN3-positive MCD neurons reveal a globular (asterisk) or multipolar shape (white arrows). **(O)** Higher magnification of CRFR2-expressing granule cells. **(P)** Higher magnification of CRFR2-expressing small cap cells. **(Q)** Quantification of cell diameters of magnocellular cells of the VCN (MC), granule cells (GC), and small cells (SC). ANOVA was used to test for statistical differences.

also to the MGB (Benson and Brown, 1990; Ryan et al., 1990; Brown et al., 1991; Thompson and Thompson, 1991; Ye et al., 2000; Malmierca et al., 2002; de Venecia et al., 2005; Darrow et al., 2012; Hockley et al., 2021). Both areas, the GCD and the small cap cell location contain CRFR2 positive fibers. In contrast to the UCN3 expression, only a few cells in the magnocellular cores of DCN and VCN were CRFR2 positive. CRFR2-positive cells in in the AVCN are most likely GBCs that form calyces of Held in the lateral part of the MNTB as we will describe in the next paragraph.

Superior Olivary Complex

The mouse SOC is a cluster of interacting nuclei serving essential functions of auditory processing which require both temporal precision and binaural integration. Roughly, the SOC nuclei can be sorted into those involved in sound source localization in the horizontal plane like the medial and lateral nucleus of the trapezoid body (LNTB and MNTB) and the medial superior olive (MSO) and LSO and those that are not involved in sound localization (Grothe and Pecka, 2014). The latter include the periolivary nuclei like the VNTB, the superior paraolivary nucleus (SPN), and the dorsal periolivary nucleus (DPO), whose function seems to vary between species and ranges from efferent feedback to encoding communication sounds (Frank and Goodrich, 2018; Kopp-Scheinpflug et al., 2018).

We previously reported the expression of UCN3 in the auditory brainstem nuclei with respect to the protection of the auditory system from sound over-exposure (Fischl et al., 2019). Surprisingly, this protective function was not accompanied by high numbers of UCN3-positive neuronal cell bodies in the SOC, but rather with an abundance of UCN3 expressing axons and synaptic terminals in this area (**Figures 2A,B**). A few UCN3-positive somata are found at the dorsomedial edge of the SPN, the VNTB and in a poorly defined area around the dorsolateral edge of LSO possibly corresponding to the DPO (**Figures 2B,C**). Cells in the VNTB and the DPO areas are part of the MOC system. Distinct UCN3 expression was observed at the calyces of Held (**Figures 2B,D**). This calyceal UCN3 expression was confined to the calyces contacting MNTB neurons in the lateral subdivision of the MNTB (**Figure 2B**). According to the tonotopic organization of the MNTB, the

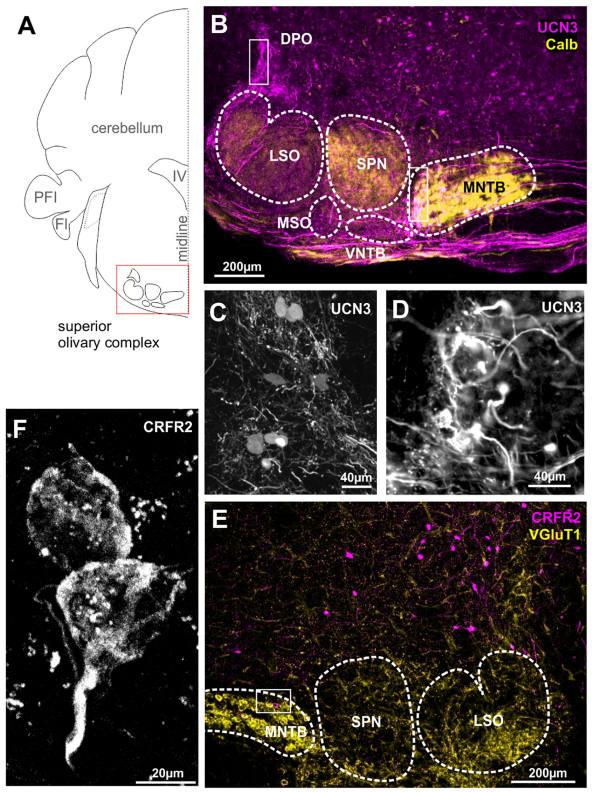

FIGURE 2 | Urocortin 3-positive neurons and fibers dominate over sparse CRFR2 expression in the SOC. **(A)** Schematic coronal section showing the superior olivary complex (SOC) as the region of interest. PFI, parafloccullus; Fl, flocculus; IV, fourth ventricle. **(B)** Dense UCN3-positive fiber bundles (magenta) enter the SOC from the contralateral side of the brain and innervate the MNTB, SPN, and LSO. Calbindin (yellow) is used as counter stain for SOC nuclei. UCN3-positive neuronal cell bodies are present in the VNTB and in the DPO (white square). Calyces of Held in the lateral, low-frequency MNTB are UCN3-positive (white square in MNTB). The data shown in **(A–C)** corroborate previously published findings (Fischl et al., 2019), but are shown here for direct comparison with the data on the UCN3 receptor CRFR2. **(C)** Higher magnification of UCN3-positive DPO neurons and fibers. **(D)** Higher magnification of UCN3-positive calyx synapses in the lateral MNTB. **(E)** Sparse CRFR2 expression (magenta) in the SOC. Instead, CRFR2-positive neurons are found in the reticular formation dorsal to the SOC. VGluT1 (yellow) is used a counterstain. **(F)** CRFR2 expression in the calyces of Held.

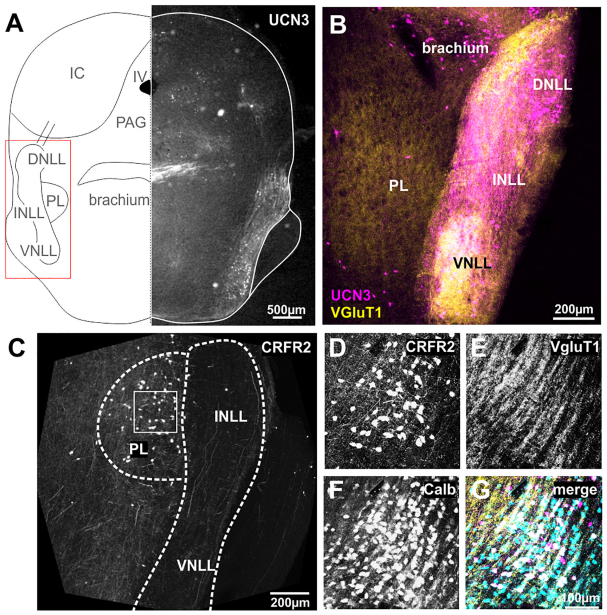

FIGURE 3 | Neurons and fibers of the lateral lemniscus express UCN3 but not CRFR2. **(A)** Schematic coronal section showing the nuclei of the lateral lemniscus (NLL) as the region of interest. IV, fourth ventricle; PL, paralemniscal nucleus; PAG, periaqueductal gray; IC, inferior colliculus. Left side shows UCN3 expression in the brachium, the intermediate (INLL), and the ventral (VNLL) nuclei of the lateral lemniscus. **(B)** Higher magnification of the NLL shows UCN3 expression (magenta) in the brachium and all three NLLs. White color in the VNLL suggests co-labeling of UCN3 (magenta) and VGluT1 terminals. The paralemniscal (PL) areas are medial to the INLL are positive for VGluT1, but show no UCN3 expression. **(C)** Instead the PL shows strong CRFR2 labeling. **(D)** CRFR2-positive neural cell bodies in the PL. **(E)** Dense network of VGluT1-positive fibers surrounding PL neurons. **(F)** PL neurons are calbindin-positive. **(G)** Co-labeling of CRFR2 (magenta), VGluT1 (yellow), and calbindin (turquoise) suggests that a subpopulation of calbindin-positive neurons also express CRFR2 (white color).

neurons that receive the UCN3-positive input are low-CF cells. The UCN3 expression in the calyces of Held corroborate the UCN3-positive AVCN neurons to be identified and GBCs (Felmy and Schneggenburger, 2004). Other, contralaterally originating, ascending fibers terminate in the MSO and VNTB area. In addition, we observed ipsilateral ascending fibers, which contact lateral, low-frequency LSO neurons. The origin of these UCN3-positive axons is most likely in the AVCN bushy cells. Another distinctive bundle of UCN3-expressing fibers terminates at the level of the DPO (**Figures 2B,C**). Overall, compared to the CN, UCN3 expression in the SOC neurons is scarce. This is reflected by equally sparse CRFR2 expression in the SOC. However, the expression of CRFR2 in lateral calyces of the MNTB (**Figure 2F**) as well as in fibers in the lateral limb of the LSO (**Figure 2E**) should be highlighted, because they mirror the UCN3 expression in these nuclei and suggest a possible autocrine regulation of CRFR2 (**Figures 2B,E**).

Lateral Lemnisci

The cochlear nuclei and the SOC connect to the IC *via* a fiber bundle that passes along the lateral edge of the brainstem and is termed lateral lemniscus (**Figure 3A**). Within these fibers, there are three distinct neuronal populations, the dorsal, the intermediate and the ventral nucleus of the lateral lemniscus, DNLL, INLL, and VNLL, respectively (Merchán et al., 1997; Oertel and Wickesberg, 2002; Ito et al., 2011). The nuclei of the LL receive their input predominantly from the contralateral VCN and the ipsilateral SOC (Glendenning et al., 1981). Additionally, the DNLL exchanges reciprocal projections with the contralateral DNLL (Oliver and Shneiderman, 1989). Although there is still much to learn about the LL's role in auditory processing, a main function seems to be to send a fast feed-forward inhibition as well as a long-lasting inhibition into the IC (Ammer et al., 2015). The INLL receives additional input from the contralateral

paralemniscal nucleus (Kelly et al., 2009). The nuclei of the lateral lemniscus (NLLs) seem to provide a major link between the auditory and the stress system. UCN3 is strongly expressed in both, neuronal cell bodies as well as fibers in all three nuclei, the VNLL, the INLL, and the DNLL (**Figure 3B**). UCN3 expression in VNLL seems to colabel with VGluT1, but less so in the INLL and DNLL (**Figure 3B**). A group of UCN3-positive neurons medial from the DNLL most likely belong to the brachium (**Figures 3A,B**).

Despite the strong UCN3 expression, the NLLs seem to be devoid of CRFR2 expression. Only very few CRFR2-positive fibers pass through the NLLs (**Figure 3C**). Instead, CRFR2 is strongly expressed in the paraleminscal nucleus (PL) located medial to the INLL (**Figure 3C**). The PL is not a principal auditory nucleus, but it receives auditory input and is potentially involved in audio-vocal feedback (Covey, 1993; Metzner, 1993; Feliciano et al., 1995; Hage et al., 2006; Varga et al., 2008). CRFR2-positive PL neurons are embedded in a dense network of VGluT1-positive fibers (**Figures 3D,E**). Almost all of the UCN3-positive PL neurons are also expressing calbindin (**Figures 3F,G**).

Inferior Colliculus

The IC is an auditory midbrain structure that receives ascending input from nearly all auditory brainstem nuclei, processes this information into new coding strategies and passes it on to the auditory thalamus. The IC is divided into the central core region (ICc) which harbors principal auditory neurons and into the external shell or cortex region (ICe) which receives multimodal inputs (Winer and Schreiner, 2005). Here, we report an extensive innervation of the ICc by UCN3-positive fibers (**Figures 4A,B,D**). More specifically, a long-range projection originating from the ipsilateral lateral lemniscus innervates the most lateral and ventral locations in the ICc. These again, as in case of the lateral calyces in the MNTB and the inputs to the lateral limb of the LSO, are areas containing low sound frequency-tuned cells. Strong GlyT2 labeling in the UCN3-positive areas of the ICc (**Figure 4C**), suggest that the UCN3-positive fibers may originate from the glycinergic VNLL neurons, rather than from the GABAergic DNLL neurons. Because GlyT2 antibodies only label the vesicular transporters in the glycinergic terminals but not along the axons, the UCN3-positive fibers appear purely magenta before entering the IC, but look more whitish upon entering the ICc, suggesting co-labeling with GlyT2 (**Figures 4C,D**). In contrast to the abundance of UCN3-positive fibers, neuronal cells bodies expressing UCN3 were only rarely observed in the ICc and in the dorsal IC (ICd; **Figure 4B**).

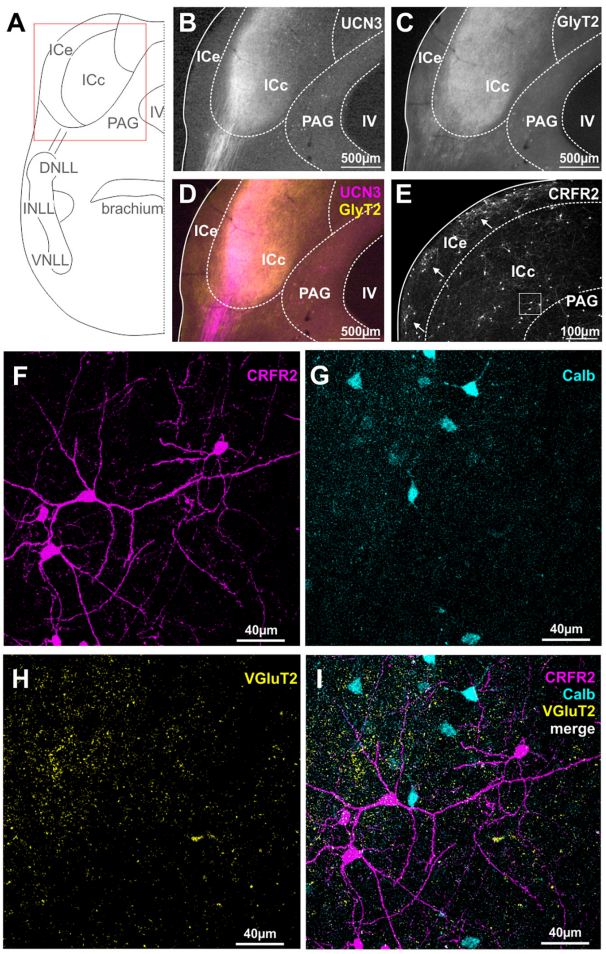

FIGURE 4 | Spatial segregation of UCN3 and CRFR2 expression in the IC. **(A)** Schematic coronal section showing the inferior colliculus (IC) as the region of interest. IV, fourth ventricle; PAG, periaqueductal gray; NLLs, nuclei of the lateral lemniscus. **(B)** UCN3-positive fibers innervate the lateral part of the central nucleus of the IC (ICc). **(C)** GlyT2 expression in the IC. **(D)** Co-staining of UCN3 (magenta) and GlyT2 (yellow) shows a change in color of UCN3-positive fibers being magenta before entering the IC and appearing more whitish within the IC. UCN3 expression was not observed in the external (ICe) and dorsal (ICd) cortex of the IC. **(E)** Clusters of CRFR2-positive neuronal cell bodies in the ICe (white arrows). CRFR2-positive cells in ICc (white square) will be shown in higher magnification in **(F–I)**. **(F)** Higher magnification of CRFR2-positive cell bodies in ICc. **(G)** Calbindin-positive neurons in ICc. **(H)** VGluT2 labeling in ICc. **(I)** Merged image reveals no overlap between CRFR2 (magenta) and calbindin (turquoise) expression.

Similar to our observations on the DCN, the expression patterns of CRFR2 seems to be spatially segregated from the UCN3 expression. CRFR2 is predominantly expressed in cell bodies of ICe and to a much lesser extent in neuronal cell bodies of the ICd and ICc. Interestingly, within the ICe, CRFR2 expression is clustered in circular patches of tissue (**Figure 4E**) that have been previously described as expressing GAD67 and being the targets of somatosensory and other multisensory inputs to this area (Lesicko et al., 2016). The ICe is known to be an integrative-modulatory area, and the sources of this modulation also include descending projections from principal neurons in higher auditory centers (Adams, 1980). These descending projections, however, tend to segregate neatly outside of the aforementioned patches (Lesicko et al., 2016).

In the ICc and the ICd only few neurons are CRFR2-positive. These are scattered throughout the two subdivisions do not follow a clear pattern of distribution. The CRFR2-positive ICc neurons are characterized by a stellate morphology without a strong cellular orientation axis (**Figure 4F**). This suggest that these neurons are of the non-flat/disc-shape type that span

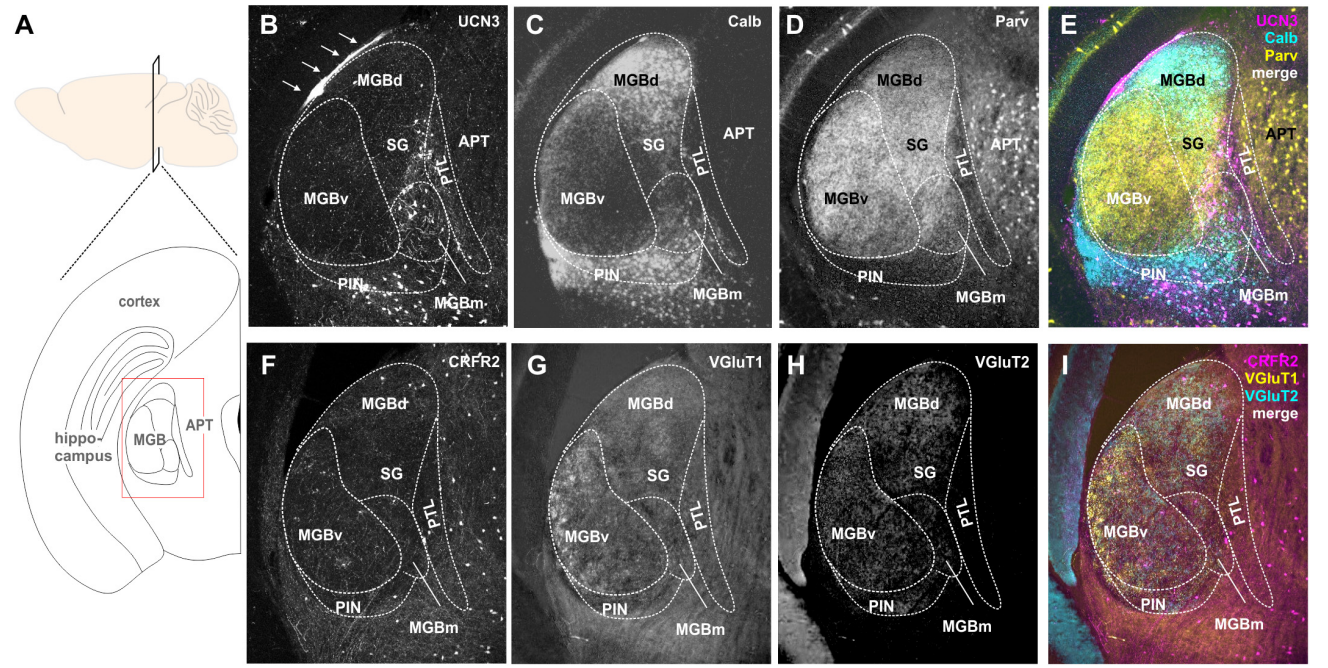

FIGURE 5 | Expression of UCN3 and CRFR2 in the medial geniculate body (MGB) and the pretectal thalamic transition zones. **(A)** Sagital view of the brain indicating the level of the schematic coronal section (below) showing the medial geniculate body (MGB) as the region of interest. APT. anterior pretectal nucleus. **(B)** UCN3-expression in the medial subdivision of the MGB (MGBm), in the posterior intralaminar thalamic nucleus (PIN), and in the pretectal thalamic lamina (PTL). The thin layer of UCN3-positive fibers might occur in the marginal zone of the medial geniculate (white arrows). Calbindin **(C)** and parvalbumin **(D)** expression in the MGB were used as counterstain to identify substructures of the MGB. **(E)** Merge shows parvalbumin (yellow) expression in ventral MGB (MGBv), the suprageniculate thalamic nucleus (SG), and APT. Calbindin is mainly expressed in dorsal MGB (MGBd) and PIN. Neither parvalbumin nor calbindin show strong expression in the UCN3-positive neurons in MGBm and PIN. **(F)** Few CRFR2-positive neuronal cell bodies are present in the MGBm and the PTL. A network of CRFR2-positive fibers seems to surround the MGB without entering its core. **(G–I)** VGlutT1 **(G)** and VGluT2 **(H)** were used as counterstain.

multiple isofrequency laminae (Meininger et al., 1986). These CRFR2-positive ICc neurons are embedded in a dense network of VGluT2-positive fibers (**Figures 4F,H,I**). The CRFR2-positive neurons are also distinct from those which express calbindin (**Figures 4F,G,I**). Both of these observations indicate that CRFR2-positive ICc neurons are different from those ICc neurons that receive the main auditory input mediating sound localization information from the lower brainstem (Takahashi et al., 1987).

The expression patterns of UCN3 and CRFR2 in the IC lack obvious synaptic contacts between the ligand- and the receptor-expressing neurons, strengthening the hypothesis of non-synaptic means of volume transmission in this system.

Medial Geniculate Body

The MGB is the auditory part of the thalamus and is composed of three main subdivisions, dorsal (MGBd), ventral (MGBv), and MGBm (Anderson et al., 2009). These subdivisions give rise to two major information streams to the cortex: the lemniscal stream (through MGBv) conveying ascending auditory information from the IC to Au1 (Winer, 1992; Anderson and Linden, 2011), and the non-lemniscal (through MGBd and MGBm) stream, conveying multimodal, more context-dependent information to secondary auditory cortex areas (Winer and Schreiner, 2005; Anderson et al., 2009). In addition, there are other parageniculate nuclei: the suprageniculate thalamic nucleus (SG), the posterior intralaminar thalamic nucleus (PIN), and the posterior limitans thalamic nucleus, which is also known as pretectothalamic lamina (PTL) (Anderson and Linden, 2011; Marquez-Legorreta et al., 2016).

Many UCN3-positive neuronal cell bodies were observed in the non-principal auditory areas like the MGBm, PIN, and PTL (**Figures 5A,B**). In addition, there are UCN3-positive fibers in the MGBm as well as a thin layer, which might be the marginal zone of the medial geniculate (**Figures 5A,B**). Counterstaining with parvalbumin, which in the brainstem is generally considered as an indicator for principal auditory neurons, showed only little overlap with UCN3-positive neurons in the MGBm (**Figures 5B,D,E**). However, in the MGB, many of the neurons in the MGBd and PIN are calbindin positive (**Figures 5B,C,E**), even though these areas are not considered to contain auditory principal neurons (Cruikshank et al., 2001; Lu et al., 2009; Marquez-Legorreta et al., 2016). This suggests that calbindin and parvalbumin might characterize different neurons in the thalamus compared to auditory brainstem and midbrain.

CRFR2-expression in the MGB was observed mostly in fibers and terminals (**Figures 5F–I**). These seemed to extent over several areas, but were especially prominent in the MGBm, PIN, and PTL. The origins of these CRFR2-positive fibers are most likely the multimodal domains of the IC, the ICe, and ICd. Additionally, a few CRFR2-positive neuronal cell bodies were

present in the area of the PTL. However, even though the PTL also contained UCN3-positive neurons, at this point it is unclear if UCN3 and CRFR2 are expressed in the same cells. The lack of strong CRFR2 expression suggests that the receptor is expressed at a distant location like the amygdala where the UCN3-positive MGBm neurons project to. This would complete the pathway for auditory fear conditioning, hence providing an interesting link between auditory and stress system (Linke et al., 2000).

DISCUSSION

In this study, we characterized the expression patterns of the stress peptide UCN3 and its receptor CRFR2 in the mouse auditory pathway and found a strong presence in most subcortical structures. The combination of ligand and receptor expression allowed forming hypotheses about possible signaling mechanisms, which can be tested in future physiological experiments. In most auditory areas, a spatial segregation between UCN3-expression in auditory structures containing auditory principal neurons and CRFR2-expression in multisensory areas was observed (**Table 1**). This study introduces stress peptides as potential modulators of central auditory function.

Benefits and Shortcomings of Using Reporter Mouse Lines to Study Protein Expression

The expression of the fluorescent protein starts whenever the gene of interest turns on. It then produces the fluorescent protein, which will stay in the neurons. Therefore, the most common criticism of reporter mouse lines is the question of when in the lifetime of the animal the protein of interest is expressed. Consequently, UCN3 might not be expressed constitutively in all the auditory nuclei that we described in this study and it is possible that some of these expression patterns are developmentally regulated or are subject to specific stressful events. Nevertheless, utilizing these reporter models allowed us to observe the entire expression patterns that could occur for example in different behaviorally relevant situations or at different time points in an animal's life. Since the influence of systemic stressors on auditory processing is not yet understood, knowing the auditory areas or cell types that can potentially be modulated by stress signaling is an important first step.

A major advantage of using reporter mouse lines for stress peptide signaling is that the expression can be visualized even when the target protein is very small and is expressed at very low concentrations. This aspect is crucial because neuropeptides are notoriously produced in very small quantities, mainly because they bind to G-protein coupled receptors (GPCRs), which have nanomolar sensitivities. This is in stark contrast to most ionotropic receptors, which have micromolar sensitivities (van den Pol, 2012). The small quantity and the small size of the peptide itself (38 amino acids for UCN3) makes detection with conventional immunohistochemistry particularly challenging. In addition, CRFR2 has some quite unusual characteristics that make it also difficult to detect *via* antibody binding. Specifically, CRFR2 contains a non-cleavable pseudosignaling peptide (PSP) attached to its N-terminal (Schulz et al., 2010; Teichmann et al., 2012). The PSP is absent from the other receptor type, CRFR1, and it confers some unique physiological traits of CRFR2 expression. In fact, PSP has been shown to anchor CRFR2 to the endoplasmatic reticulum and prevent its expression at the level of the membrane. This could potentially also impede the detection through receptor-mediated autoradiography, because the receptor might be inaccessible for radio ligand binding if the proper physiological triggers for membrane expression have not taken place. Tethering of the receptor intracellularly might also mask antigens for immunohistochemistry and hence much information could be lost by this technique. Besides, binding of the radiolabeled ligand has to compete with the endogenous ligand binding which might already be occupying the site.

Fluorescent *in situ* hybridization (FISH) and other genetic-based methods are also inferior to the use of reporter mice, because they can provide only a snapshot in time of the target's expression that portrays only the genetic material actively being translated and therefore is highly dependent on any stress-related conditions of the animal prior to the sacrifice. Initial reports utilized FISH to study the general expression patterns of UCN3 and CRFR2 in the mammalian brain included information on the auditory system (Lewis et al., 2001; Li et al., 2002).

Receptor-Ligand Mismatch

For decades, neuroscientists have reported a rather unexpected phenomenon regarding neurotransmitters and, even more so, neuropeptides: an apparent lack of direct synaptic contact between neurons expressing a receptor and those expressing its high-affinity ligand in certain brain areas and cell types (Herkenham, 1987). An observation that seems to contradict the dogma of synaptic transmission. Even if acknowledged, this phenomenon has not spurred extensive investigation, with a few notable exceptions (Agnati et al., 1995; Ludwig and Leng, 2006). Very often, this intriguing finding has been attributed to technical limitations as explained in the previous paragraph. However, other possible solutions to this mystery have been explored and even proved for some neuropeptides (Liu et al., 1994; Liu and Sandkuhler, 1995; Brown et al., 2008; Ha et al., 2013). First of all, one has to consider that neuropeptides, in contrast to classical neurotransmitters, could reach their target receptor over very long distances through blood circulation. That is the case for example for leptin, ghrelin, and insulin, which are released at the level of the gastrointestinal system, but also affect the central nervous system (Rhea et al., 2018; Stengel and Tache, 2018). Not all neuropeptides can cross the blood–brain barrier; however, experimental evidence shows generalized effects of UCN3 after central injections, supporting a neuroendocrine option for UCN3 (Sharpe and Phillips, 2009; Yeh et al., 2016).

Besides the long-range endocrine signaling, some neuropeptides such as galanin (Freund-Mercier and Stoeckel, 1995) and oxytocin can also be released by dendrites and neuronal somata (Vila-Porcile et al., 2009). In invertebrates,

TABLE 1 | Distribution of UCN3- and CRFR2-positive neuronal cell bodies, fibers, and terminals in the auditory pathway.

Brain area	Region/cell type	UCN3		CRFR2		References
		Cells	Fibers	Cells	Fibers	
Cochlea	Inner hair cells (IHC)	–	+	–	+	Fischl et al., 2019
	Outer hair cells (OHC)	–	–	–	–	Basappa et al., 2012; Fischl et al., 2019
	Supporting cells			++	–	Basappa et al., 2012
	Spiral ganglion neurons (SGN)			+++	+	Graham et al., 2010
Cochlear nucleus	Bushy cells of the anteroventral cochlear nucleus (AVCN)	+	+			Fischl et al., 2019, This study
	Stellate cells of the anteroventral cochlear nucleus (AVCN)	++	+			This study
	Octopus cells of the posteroventral cochlear nucleus (PVCN)	–	–			This study
	Deep layers of the dorsal cochlear nucleus (DCN)	–	+++	–	–	This study
	Granule cell domain (GCD)	–	–	+++	+++	This study
	Small cells	–	–	++	–	This study
Superior olivary complex	MNTB	–	++	–	+	Fischl et al., 2019, This study
	VNTB	+	+	–	–	Fischl et al., 2019, This study
	SPN	++	+	–	+	Lewis et al., 2001; Li et al., 2002; Deussing et al., 2010; Fischl et al., 2019, This study
	LSO	+	+	–	+	Fischl et al., 2019, This study
	DPO	+++	+++	–	+	Fischl et al., 2019, This study
Nuclei of the lateral lemniscus	VNLL	++	++	–	–	This study
	INLL	++	++	–	–	This study
	DNLL	++	++	–	–	This study
	PL	–	–	++	–	This study
Inferior colliculus	ICc	–	+++	+	–	This study
	ICe	–	–	++	–	This study
	ICd	–	–	+	–	This study
Medial geniculate body	MGBv	–	–	–	–	This study
	MGBm	++	++	+	+	This study
	MGBd	–	–	–	–	This study
	SG	–	+	+	–	This study
	PIN	++	++	–	+	This study
	PTL	++	++	–	+	This study
	MZMG	–	+	–	+	This study

The number of plus signs symbolizes the relative strength and a minus sign the lack of expression (Lewis et al., 2001; Li et al., 2002; Deussing et al., 2010; Graham et al., 2010; Basappa et al., 2012; Fischl et al., 2019).

where mechanisms of neuropeptide release have been studied more intensely, it has been shown that neuropeptides are shuffled anterogradely and retrogradely within the same neuron using different molecular motors (Barkus et al., 2008; Wong et al., 2012).

Finally, the lack of synaptic re-uptake mechanisms and the presence of extracellular peptidases are strong indicators that volume transmission plays a major role in many instances. However, due to the presence of the extracellular peptidases, most of the effects remain local and limited in time (Defea et al., 2000). This is emphasized by the fact that neuropeptides and their receptors have an overall discrete expression in certain areas. A more widespread diffusion would defeat the purpose of this specialization.

Possible Binding of CRFR2 by Other Ligands

The possibility, that in some areas UCN3 might not be the only ligand for CRFR2 has to be taken into account when making functional considerations. UCN2 can also bind to CRFR2 with high affinity, UCN1 can bind with moderate and CRF with low affinity. To date, there is no report about the presence of UCN2 in the auditory system. However, CRF positive neuronal cell bodies are present in the DCN, lateral MTNB, ICe, DNLL, VNLL, and

MGB (Imaki et al., 1991). Although CRF has a very low affinity for CRFR2 and would have to be released at extremely high concentrations to sufficiently occupy the receptor, it cannot be excluded that CRF might also act on CRFR2 receptors in the auditory pathway. Despite possible binding of CRFR2 by UCN2 or CRF, UCN3 is still the most likely ligand (Li et al., 2002). In contrast to the other ligands, UCN3 binds exclusively to CRFR2, and so its sole purpose is to be released and to bind this receptor. Hence, the spatial segregation between presynaptic UCN3 and postsynaptic CRFR2 expression that we observed in multiple auditory areas, could not simply be explained by postulating that in these areas CRF rather than UCN3 might be the main ligand. Moreover, it suggests that if UCN3 is expressed it has to bind to its exclusive receptor CRFR2 to have a functional effect even if it involves volume transmission.

Volume transmission might be corroborated by the fact that another ligand-receptor pairs of stress peptides also shows a segregation of ligand and receptor. In the IC, the ligand CRF is expressed in the integrative cells of the external cortex (Imaki et al., 1991), whereas its receptor, CRFR1 is expressed in principal auditory neurons of the central nucleus (Justice et al., 2008). A note of caution has to be given though, that the latter publication was not specifically focused on the auditory system and the identity of the cell types expressing CRFR1 was not clearly established.

Nevertheless, the general presence of other ligands gives an interesting perspective on how this system could be extremely well refined for balanced modulation. For example, certain stressors might be too mild to release a large enough quantity of CRF to compete with UCN3 for CRFR2 binding, which would make the modulation modality- and/or intensity-dependent. Alternatively, CRF might be released by a different population of neurons than UCN3, which is mostly released by neurons tuned to low sound frequencies.

Functional Implications of Urocortin 3 and CRFR2 Expression in the Auditory System

The most intriguing finding of our study is that the neuromodulatory ligand UCN3 tends to be expressed in auditory principal neurons, whereas CRFR2 labeling is mostly found in non-principal, multimodal neurons. Such a distribution is unusual, because typically the auditory principal neurons are the target of neuromodulatory inputs rather than being their source (Schofield et al., 2011; Sizemore et al., 2020). An obvious example is the CN where UCN3 is expressed in the magnocellular core of both VCN and DCN while CRFR2 is mostly found in the granular cell domain and the parallel fibers. Similarly, in the IC, UCN3 positive fibers are found within the central nucleus, while CRFR2 is expressed in the external cortex of the IC.

Normally, we would consider modulation as coming from other systems, that are either cross-modal or are devoted to modulation itself like the reticular formation, both of which would then alter the incoming auditory information. Indeed, the presence and function of modulatory inputs to auditory structures have been described in many studies (Ryugo et al., 2003). For example, a large body of work on the DCN revealed how somatosensory inputs from head and neck can suppress self-generated sound perception (Shore, 2005; Koehler and Shore, 2013; Singla et al., 2017). A lot of clarification came from identifying the anatomical origin of these modulatory fibers and in-depth mechanistic explanations (Trussell and Oertel, 2018). More so, clinical evidence from the treatment of certain types of tinnitus utilizing cranio-cervical manipulations provided additional strength to these data (Levine, 1999).

However, the occurrence of reverse patterns of modulation as we describe here for the UCN3–CRFR2 system is novel and its functional significance is up for discovery. Although a few cross-modal feedback projections from auditory structures might form part of the UCN3–CRFR2 system, to our knowledge, the finding of an on-site modulation of stressful situations has not yet been explored in the central auditory pathway.

The interesting scenario here is that sound-driven release of the ligand might affect the cells responsible for receiving external modulation and set them up for specific types of firing. For instance, release of UCN3 from fibers reaching the central nucleus of the IC might bypass the principal auditory cells in ICc and instead directly modulate the activity of the multimodal cells in the ICe *via* volume transmission. The timescale of volume transmission is certainly an interesting aspect with regard to the fast signal processing of primary ascending auditory information. Non-gaseous neuromodulators including UCN3 are long-lived and their lifetime is typically determined by the tissue-specific degradation processes (for review see, Russo, 2017). Although, to our knowledge, the lifetime of UCN3 in the brain is not yet known, the lifetime of other neuropeptides such as oxytocin and vasopressin in the cerebrospinal fluid is reported to be up to 20 min. These 20 min together with the downstream G-protein coupled signaling cascade of UCN3 and most other neuropeptides suggest the action of UCN3 to be slow compared to the primary auditory signal processing. However, since processing of auditory information takes place at different time scales from microseconds to many seconds or even hours, UCN3 signaling is just in time to modulate processes involved in temporal abstraction rather than temporal resolution or temporal integration (Kopp-Scheinpflug and Linden, 2021). Such a setting could maintain faithfulness of direct ascending auditory transmission on one hand, while at the same time interfering with the modulatory effects of the ICe cells and their inputs to non-auditory areas.

Another interesting finding is that CRFR2 expression in the SOC seems less abundant than that of UCN3. Instead, CRFR2 expression in surrounding non-auditory areas of the cranial nerve and nuclei of the reticular formation is very strong, suggesting that one purpose of UCN3-release by SOC neurons might be to affect surrounding non-auditory structures rather than afferent auditory principal neurons. With respect to the SOC as an evolutionary highly conserved collection of nuclei that are essential for the execution of precise and survival-promoting encoding of sound information, too much modulatory impact could even be detrimental in the SOC.

An exception of the UCN3 positive structures in the SOC are the calyces of Held innervating lateral, low-frequency tuned MNTB neurons. Here, we found an area in which an autocrine modulation could take place, since these lateral calyces of Held express both the receptor and the ligand. It is still unknown, whether the same calyces express both ligand and receptor; a question that will have to be answered by single cell physiology or through the generation of a double reporter mouse line. In this case, the autocrine route seems to be the prevalent one, even if it does not exclude that volume transmission is also happening. In fact, it is known that neuropeptides can travel up to hundreds of micrometers to reach their receptor (Fuxe et al., 2010); yet the concentration that actually reaches the furthest targets declines linearly with the amount to extracellular peptidases being expressed along the way. To date, information on the presence and localization of extracellular peptidases is still lacking in these auditory areas. Hence, it seems most reasonable that the CRFR2 expressing calyces in the lateral MNTB would receive the majority of UCN3 released within the same area compared to other CRFR2 expressing cells more at a distance. Similar possible combinations of autocrine and paracrine signaling has been suggested for CRF-CRFR1 signaling between cochlear supporting cells (Graham et al., 2011).

The strong expression of UCN3 in VNTB neurons is most likely due to its contribution in the efferent feedback system of the medial olivocochlear complex (MOC). MOC neurons project to the outer hair cells of the cochlea and protect these during damaging sound intensities. However, prior research on the contribution of UCN3 during sound over exposure did not show an effect on cochlear outer hair cells (Fischl et al., 2019). Efferent projections of MOC neurons also send collaterals into the CN targeting the small cell cap. Here, we showed that the small cells express CRFR2 and therefore qualify as the MOC-UCN3-target. Indeed, a very recent study investigating the physiology of CN small cells suggest a special role for these cells in processing communication sounds, a function that is most certainly subject to stress and emotional modulation (Hockley et al., 2021).

CONCLUSION

With this work, we aim to highlight the presence of the UCN3–CRFR2 system as so far unexplored neuromodulators in the central auditory pathway. First, the expression of both factors is widespread in subcortical auditory nuclei. Second, the ligand-receptor expression patterns suggest unusual forms of neurotransmission such as local or long distance volume transmission and possibly even autocrine regulation. Third, an interesting pattern of segregation between the ligand being expressed in auditory principal cells and the receptor being expressed in non-principal neurons implies a stress-dependent modulation of the canonical modulators. These results open up a new field of research, investigating which stressors could be activated under what circumstances and how these stressors influence central auditory processing.

DATA AVAILABILITY STATEMENT

The raw data supporting the conclusions of this article will be made available by the authors, without undue reservation.

ETHICS STATEMENT

The animal study was reviewed and approved by the Bavarian district government.

AUTHOR CONTRIBUTIONS

All authors contributed to the conception and design of the study and data collection. SP performed experiments and wrote the first draft of the manuscript. All authors contributed to manuscript revision, and read and approved the submitted version.

FUNDING

This research was funded by the DFG (SFB870 A-10 and GS-82 Graduate School of Systemic Neurosciences GSN^{LMU}), by the German Ministry of Science and Education (IMADAPT, FKZ: 01KU1901), and by the Marie Skłodowska-Curie innovative training network PurinesDX.

ACKNOWLEDGMENTS

The authors gratefully acknowledge Benedikt Grothe for constant support, Lucy Anderson for helpful comments on the manuscript, and Olga Alexandrova and Hilde Wohlfrom for expert technical support throughout the process.

REFERENCES

Adams, J. C. (1980). Crossed and descending projections to the inferior colliculus. *Neurosci. Lett.* 19, 1–5. doi: 10.1016/0304-3940(80)90246-3

Agnati, L. F., Zoli, M., Stromberg, I., and Fuxe, K. (1995). Intercellular communication in the brain: wiring versus volume transmission. *Neuroscience* 69, 711–726. doi: 10.1016/0306-4522(95)00308-6

Ammer, J. J., Siveke, I., and Felmy, F. (2015). Activity-dependent transmission and integration control the timescales of auditory processing at an inhibitory synapse. *Curr. Biol.* 25, 1562–1572. doi: 10.1016/j.cub.2015.04.026

Anderson, L. A., Christianson, G. B., and Linden, J. F. (2009). Stimulus-specific adaptation occurs in the auditory thalamus. *J. Neurosci.* 29, 7359–7363. doi: 10.1523/JNEUROSCI.0793-09.2009

Anderson, L. A., and Linden, J. F. (2011). Physiological differences between histologically defined subdivisions in the mouse auditory thalamus. *Hear. Res.* 274, 48–60. doi: 10.1016/j.heares.2010.12.016

Aston-Jones, G., and Cohen, J. D. (2005). An integrative theory of locus coeruleus-norepinephrine function: adaptive gain and optimal performance. *Annu. Rev. Neurosci.* 28, 403–450. doi: 10.1146/annurev.neuro.28.061604.135709

Barkus, R. V., Klyachko, O., Horiuchi, D., Dickson, B. J., and Saxton, W. M. (2008). Identification of an axonal kinesin-3 motor for fast anterograde vesicle transport that facilitates retrograde transport of neuropeptides. *Mol. Biol. Cell* 19, 274–283. doi: 10.1091/mbc.e07-03-0261

Basappa, J., Graham, C. E., Turcan, S., and Vetter, D. E. (2012). The cochlea as an independent neuroendocrine organ: expression and possible roles of a local hypothalamic-pituitary-adrenal axis-equivalent signaling system. *Hear. Res.* 288, 3–18. doi: 10.1016/j.heares.2012.03.007

Bazwinsky, I., Hartig, W., and Rubsamen, R. (2008). Characterization of cochlear nucleus principal cells of Meriones unguiculatus and Monodelphis domestica by use of calcium-binding protein immunolabeling. *J. Chem. Neuroanat.* 35, 158–174. doi: 10.1016/j.jchemneu.2007.10.003

Behler, O., and Uppenkamp, S. (2020). Activation in human auditory cortex in relation to the loudness and unpleasantness of low-frequency and infrasound stimuli. *PLoS One* 15:e0229088. doi: 10.1371/journal.pone.0229088

Benson, T. E., and Brown, M. C. (1990). Synapses formed by olivocochlear axon branches in the mouse cochlear nucleus. *J. Comp. Neurol.* 295, 52–70. doi: 10.1002/cne.902950106

Brown, C. H., Ruan, M., Scott, V., Tobin, V. A., and Ludwig, M. (2008). Multifactorial somato-dendritic regulation of phasic spike discharge in vasopressin neurons. *Prog. Brain Res.* 170, 219–228. doi: 10.1016/S0079-6123(08)00419-6

Brown, M. C., Pierce, S., and Berglund, A. M. (1991). Cochlear-nucleus branches of thick (medial) olivocochlear fibers in the mouse: a cochleotopic projection. *J. Comp. Neurol.* 303, 300–315. doi: 10.1002/cne.903030211

Cant, N. (1993). "The synaptic organization of the ventral cochlear nucleus of the cat: the peripheral cap of small cells," in *The Mammalian Cochlear Nuclei*, eds M. A. Merchàn, J. M. Juiz, D. A. Godfrey, and E. Mugnaini (Boston: Springer), 91–105.

Chang, C. P., Pearse, R. V. II, O'Connell, S., and Rosenfeld, M. G. (1993). Identification of a seven transmembrane helix receptor for corticotropin-releasing factor and sauvagine in mammalian brain. *Neuron* 11, 1187–1195. doi: 10.1016/0896-6273(93)90230-o

Charmandari, E., Tsigos, C., and Chrousos, G. (2005). Endocrinology of the stress response. *Annu. Rev. Physiol.* 67, 259–284. doi: 10.1146/annurev.physiol.67.040403.120816

Chen, R., Lewis, K. A., Perrin, M. H., and Vale, W. W. (1993). Expression cloning of a human corticotropin-releasing-factor receptor. *Proc. Natl. Acad. Sci. USA* 90, 8967–8971. doi: 10.1073/pnas.90.19.8967

Clifford, G., Dalgleish, T., and Hitchcock, C. (2018). Prevalence of auditory pseudohallucinations in adult survivors of physical and sexual trauma with chronic post-traumatic stress disorder (PTSD). *Behav. Res. Ther.* 111, 113–118. doi: 10.1016/j.brat.2018.10.015

Covey, E. (1993). Response properties of single units in the dorsal nucleus of the lateral lemniscus and paralemniscal zone of an echolocating bat. *J. Neurophysiol.* 69, 842–859. doi: 10.1152/jn.1993.69.3.842

Cruikshank, S. J., Killackey, H. P., and Metherate, R. (2001). Parvalbumin and calbindin are differentially distributed within primary and secondary subregions of the mouse auditory forebrain. *Neuroscience* 105, 553–569. doi: 10.1016/s0306-4522(01)00226-3

Curtis, A. L., Leiser, S. C., Snyder, K., and Valentino, R. J. (2012). Predator stress engages corticotropin-releasing factor and opioid systems to alter the operating mode of locus coeruleus norepinephrine neurons. *Neuropharmacology* 62, 1737–1745. doi: 10.1016/j.neuropharm.2011.11.020

Darrow, K. N., Benson, T. E., and Brown, M. C. (2012). Planar multipolar cells in the cochlear nucleus project to medial olivocochlear neurons in mouse. *J. Comp. Neurol.* 520, 1365–1375. doi: 10.1002/cne.22797

Davis, M. (1984). "The mammalian startle response," in *Neural mechanisms of startle behavior*, ed. R. C. Eaton (New York, NY: Plenum Press), 287–351.

de Venecia, R. K., Liberman, M. C., Guinan, J. J. Jr., and Brown, M. C. (2005). Medial olivocochlear reflex interneurons are located in the posteroventral cochlear nucleus: a kainic acid lesion study in guinea pigs. *J. Comp. Neurol.* 487, 345–360. doi: 10.1002/cne.20550

Defea, K., Schmidlin, F., Dery, O., Grady, E. F., and Bunnett, N. W. (2000). Mechanisms of initiation and termination of signalling by neuropeptide receptors: a comparison with the proteinase-activated receptors. *Biochem. Soc. Trans.* 28, 419–426.

Deussing, J. M., Breu, J., Kuhne, C., Kallnik, M., Bunck, M., Glasl, L., et al. (2010). Urocortin 3 modulates social discrimination abilities via corticotropin-releasing hormone receptor type 2. *J. Neurosci.* 30, 9103–9116. doi: 10.1523/JNEUROSCI.1049-10.2010

Deussing, J. M., and Chen, A. (2018). The Corticotropin-Releasing Factor Family: Physiology of the Stress Response. *Physiol. Rev.* 98, 2225–2286. doi: 10.1152/physrev.00042.2017

Feliciano, M., Saldana, E., and Mugnaini, D. (1995). Direct projections from the rat primary auditory neocortex to nucleus sagulum, paralemniscal regions, superior olivary complex and cochlear nuclei. *Aud. Neurosci.* 1995, 287–308.

Felmy, F., and Schneggenburger, R. (2004). Developmental expression of the Ca2+-binding proteins calretinin and parvalbumin at the calyx of Held of rats and mice. *Eur. J. Neurosci.* 20, 1473–1482. doi: 10.1111/j.1460-9568.2004.03604.x

Fischl, M. J., Ueberfuhr, M. A., Drexl, M., Pagella, S., Sinclair, J. L., Alexandrova, O., et al. (2019). Urocortin 3 signalling in the auditory brainstem aids recovery of hearing after reversible noise-induced threshold shift. *J. Physiol.* 597, 4341–4355. doi: 10.1113/JP278132

Flores, E. N., Duggan, A., Madathany, T., Hogan, A. K., Marquez, F. G., Kumar, G., et al. (2015). A non-canonical pathway from cochlea to brain signals tissue-damaging noise. *Curr. Biol.* 25, 606–612. doi: 10.1016/j.cub.2015.01.009

Floris, A., Dino, M., Jacobowitz, D. M., and Mugnaini, E. (1994). The unipolar brush cells of the rat cerebellar cortex and cochlear nucleus are calretinin-positive: a study by light and electron microscopic immunocytochemistry. *Anat. Embryol.* 189, 495–520. doi: 10.1007/BF00186824

Frank, M. M., and Goodrich, L. V. (2018). Talking back: Development of the olivocochlear efferent system. *Wiley Interdiscip. Rev. Dev. Biol.* 7:e324. doi: 10.1002/wdev.324

Freund-Mercier, M. J., and Stoeckel, M. E. (1995). Somatodendritic autoreceptors on oxytocin neurones. *Adv. Exp. Med. Biol.* 395, 185–194.

Fujino, K., and Oertel, D. (2001). Cholinergic modulation of stellate cells in the mammalian ventral cochlear nucleus. *J. Neurosci.* 21, 7372–7383.

Fuxe, K., Dahlstrom, A. B., Jonsson, G., Marcellino, D., Guescini, M., Dam, M., et al. (2010). The discovery of central monoamine neurons gave volume transmission to the wired brain. *Prog. Neurobiol.* 90, 82–100. doi: 10.1016/j.pneurobio.2009.10.012

Glendenning, K. K., Brunso-Bechtold, J. K., Thompson, G. C., and Masterton, R. B. (1981). Ascending auditory afferents to the nuclei of the lateral lemniscus. *J. Comp. Neurol.* 197, 673–703. doi: 10.1002/cne.901970409

Graham, C. E., Basappa, J., Turcan, S., and Vetter, D. E. (2011). The cochlear CRF signaling systems and their mechanisms of action in modulating cochlear sensitivity and protection against trauma. *Mol. Neurobiol.* 44, 383–406. doi: 10.1007/s12035-011-8203-3

Graham, C. E., Basappa, J., and Vetter, D. E. (2010). A corticotropin-releasing factor system expressed in the cochlea modulates hearing sensitivity and protects against noise-induced hearing loss. *Neurobiol. Dis.* 38, 246–258. doi: 10.1016/j.nbd.2010.01.014

Grothe, B., and Pecka, M. (2014). The natural history of sound localization in mammals–a story of neuronal inhibition. *Front. Neural. Circuits* 8:116. doi: 10.3389/fncir.2014.00116

Guthrie, R. M., and Bryant, R. A. (2005). Auditory startle response in firefighters before and after trauma exposure. *Am. J. Psychiatry* 162, 283–290. doi: 10.1176/appi.ajp.162.2.283

Ha, S., Baver, S., Huo, L., Gata, A., Hairston, J., Huntoon, N., et al. (2013). Somato-dendritic localization and signaling by leptin receptors in hypothalamic POMC and AgRP neurons. *PLoS One* 8:e77622. doi: 10.1371/journal.pone.0077622

Hage, S. R., Jurgens, U., and Ehret, G. (2006). Audio-vocal interaction in the pontine brainstem during self-initiated vocalization in the squirrel monkey. *Eur. J. Neurosci.* 23, 3297–3308. doi: 10.1111/j.1460-9568.2006.04835.x

Harrison, J. M., and Irving, R. (1965). The Anterior Ventral Cochlear Nucleus. *J. Comp. Neurol.* 124, 15–41. doi: 10.1002/cne.901240103

Hegewald, J., Schubert, M., Freiberg, A., Romero Starke, K., Augustin, F., Riedel-Heller, S. G., et al. (2020). Traffic noise and mental health: a systematic review and meta-analysis. *Int. J. Environ. Res. Public Health* 17, 17176175. doi: 10.3390/ijerph17176175

Henckens, M., Printz, Y., Shamgar, U., Dine, J., Lebow, M., Drori, Y., et al. (2017). CRF receptor type 2 neurons in the posterior bed nucleus of the stria terminalis

critically contribute to stress recovery. *Mol. Psychiatry* 22, 1691–1700. doi: 10.1038/mp.2016.133

Herkenham, M. (1987). Mismatches between neurotransmitter and receptor localizations in brain: observations and implications. *Neuroscience* 23, 1–38. doi: 10.1016/0306-4522(87)90268-5

Hockley, A., Wu, C., and Shore, S. (2021). Cochlear nucleus small cells use olivocochlear collaterals to encode sounds in noise. *bioRxiv* 2021:444983.

Horner, K. C. (2003). The emotional ear in stress. *Neurosci. Biobehav. Rev.* 27, 437–446. doi: 10.1016/s0149-7634(03)00071-x

Hoskin, R., Hunter, M. D., and Woodruff, P. W. (2014). The effect of psychological stress and expectation on auditory perception: A signal detection analysis. *Br. J. Psychol.* 105, 524–546. doi: 10.1111/bjop.12048

Hurley, L. M., and Hall, I. C. (2011). Context-dependent modulation of auditory processing by serotonin. *Hear. Res.* 279, 74–84. doi: 10.1016/j.heares.2010.12.015

Imaki, J., Imaki, T., Vale, W., and Sawchenko, P. E. (1991). Distribution of corticotropin-releasing factor mRNA and immunoreactivity in the central auditory system of the rat. *Brain Res.* 547, 28–36. doi: 10.1016/0006-8993(91)90571-c

Ito, T., Bishop, D. C., and Oliver, D. L. (2011). Expression of glutamate and inhibitory amino acid vesicular transporters in the rodent auditory brainstem. *J. Comp. Neurol.* 519, 316–340. doi: 10.1002/cne.22521

Justice, N. J., Yuan, Z. F., Sawchenko, P. E., and Vale, W. (2008). Type 1 corticotropin-releasing factor receptor expression reported in BAC transgenic mice: implications for reconciling ligand-receptor mismatch in the central corticotropin-releasing factor system. *J. Comp. Neurol.* 511, 479–496. doi: 10.1002/cne.21848

Kadner, A., Pressimone, V. J., Lally, B. E., Salm, A. K., and Berrebi, A. S. (2006). Low-frequency hearing loss in prenatally stressed rats. *Neuroreport* 17, 635–638. doi: 10.1097/00001756-200604240-00015

Kaiser, A., Alexandrova, O., and Grothe, B. (2011). Urocortin-expressing olivocochlear neurons exhibit tonotopic and developmental changes in the auditory brainstem and in the innervation of the cochlea. *J. Comp. Neurol.* 519, 2758–2778. doi: 10.1002/cne.22650

Karl, A., Malta, L. S., and Maercker, A. (2006). Meta-analytic review of event-related potential studies in post-traumatic stress disorder. *Biol. Psychol.* 71, 123–147. doi: 10.1016/j.biopsycho.2005.03.004

Kelly, J. B., van Adel, B. A., and Ito, M. (2009). Anatomical projections of the nuclei of the lateral lemniscus in the albino rat (Rattus norvegicus). *J. Comp. Neurol.* 512, 573–593. doi: 10.1002/cne.21929

Klepper, A., and Herbert, H. (1991). Distribution and origin of noradrenergic and serotonergic fibers in the cochlear nucleus and inferior colliculus of the rat. *Brain Res.* 557, 190–201. doi: 10.1016/0006-8993(91)90134-h

Koehler, S. D., and Shore, S. E. (2013). Stimulus-timing dependent multisensory plasticity in the guinea pig dorsal cochlear nucleus. *PLoS One* 8:e59828. doi: 10.1371/journal.pone.0059828

Koelsch, S. (2014). Brain correlates of music-evoked emotions. *Nat. Rev. Neurosci.* 15, 170–180. doi: 10.1038/nrn3666

Koelsch, S., Skouras, S., Fritz, T., Herrera, P., Bonhage, C., Kussner, M. B., et al. (2013). The roles of superficial amygdala and auditory cortex in music-evoked fear and joy. *Neuroimage* 81, 49–60. doi: 10.1016/j.neuroimage.2013.05.008

Kopp-Scheinpflug, C., and Linden, J. F. (2021). "Coding of Temporal Information," in *The Senses: A Comprehensive Reference*, ed. B. Fritzsch (Cambridge: Academic Press), 691–712.

Kopp-Scheinpflug, C., Sinclair, J. L., and Linden, J. F. (2018). When Sound Stops: Offset Responses in the Auditory System. *Trends Neurosci.* 41, 712–728. doi: 10.1016/j.tins.2018.08.009

Kozicz, T., Yanaihara, H., and Arimura, A. (1998). Distribution of urocortin-like immunoreactivity in the central nervous system of the rat. *J. Comp. Neurol.* 391, 1–10. doi: 10.1002/(sici)1096-9861(19980202)391

Lauer, A. M., Connelly, C. J., Graham, H., and Ryugo, D. K. (2013). Morphological characterization of bushy cells and their inputs in the laboratory mouse (Mus musculus) anteroventral cochlear nucleus. *PLoS One* 8:e73308. doi: 10.1371/journal.pone.0073308

LeDoux, J. E., Sakaguchi, A., and Reis, D. J. (1984). Subcortical efferent projections of the medial geniculate nucleus mediate emotional responses conditioned to acoustic stimuli. *J. Neurosci.* 4, 683–698.

Lesicko, A. M., Hristova, T. S., Maigler, K. C., and Llano, D. A. (2016). Connectional Modularity of Top-Down and Bottom-Up Multimodal Inputs to the Lateral Cortex of the Mouse Inferior Colliculus. *J. Neurosci.* 36, 11037–11050. doi: 10.1523/JNEUROSCI.4134-15.2016

Levine, R. A. (1999). Somatic (craniocervical) tinnitus and the dorsal cochlear nucleus hypothesis. *Am. J. Otolaryngol.* 20, 351–362. doi: 10.1016/s0196-0709(99)90074-1

Levitt, P., and Moore, R. Y. (1978). Noradrenaline neuron innervation of the neocortex in the rat. *Brain Res.* 139, 219–231. doi: 10.1016/0006-8993(78)90925-3

Lewis, K., Li, C., Perrin, M. H., Blount, A., Kunitake, K., Donaldson, C., et al. (2001). Identification of urocortin III, an additional member of the corticotropin-releasing factor (CRF) family with high affinity for the CRF2 receptor. *Proc. Natl. Acad. Sci. USA* 98, 7570–7575. doi: 10.1073/pnas.121165198

Li, C., Vaughan, J., Sawchenko, P. E., and Vale, W. W. (2002). Urocortin III-immunoreactive projections in rat brain: partial overlap with sites of type 2 corticotrophin-releasing factor receptor expression. *J. Neurosci.* 22, 991–1001.

Liberman, M. C. (1991). Central projections of auditory-nerve fibers of differing spontaneous rate. I. Anteroventral cochlear nucleus. *J. Comp. Neurol.* 313, 240–258. doi: 10.1002/cne.903130205

Liberman, M. C. (1993). Central projections of auditory nerve fibers of differing spontaneous rate, II: Posteroventral and dorsal cochlear nuclei. *J. Comp. Neurol.* 327, 17–36. doi: 10.1002/cne.903270103

Lin, C. S., Lin, Y. S., Liu, C. F., Weng, S. F., Lin, C., and Lin, B. S. (2016). Increased risk of sudden sensorineural hearing loss in patients with depressive disorders: population-based cohort study. *J. Laryngol. Otol.* 130, 42–49. doi: 10.1017/S0022215115002960

Linke, R., Braune, G., and Schwegler, H. (2000). Differential projection of the posterior paralaminar thalamic nuclei to the amygdaloid complex in the rat. *Exp. Brain Res.* 134, 520–532. doi: 10.1007/s002210000475

Liu, H., Brown, J. L., Jasmin, L., Maggio, J. E., Vigna, S. R., Mantyh, P. W., et al. (1994). Synaptic relationship between substance P and the substance P receptor: light and electron microscopic characterization of the mismatch between neuropeptides and their receptors. *Proc. Natl. Acad. Sci. USA* 91, 1009–1013. doi: 10.1073/pnas.91.3.1009

Liu, X. G., and Sandkuhler, J. (1995). The effects of extrasynaptic substance P on nociceptive neurons in laminae I and II in rat lumbar spinal dorsal horn. *Neuroscience* 68, 1207–1218. doi: 10.1016/0306-4522(95)00187-n

Lu, E., Llano, D. A., and Sherman, S. M. (2009). Different distributions of calbindin and calretinin immunostaining across the medial and dorsal divisions of the mouse medial geniculate body. *Hear. Res.* 257, 16–23. doi: 10.1016/j.heares.2009.07.009

Ludwig, M., and Leng, G. (2006). Dendritic peptide release and peptide-dependent behaviours. *Nat. Rev. Neurosci.* 7, 126–136. doi: 10.1038/nrn1845

Malfatti, T., Ciralli, B., Hilscher, M. M., Edwards, S. J., Kullander, K., Leao, R. N., et al. (2021). Using Cortical neuron markers to target cells in the dorsal cochlear nucleus. *eNeuro* 8:2020. doi: 10.1523/ENEURO.0413-20.2020

Malmierca, M. S., Merchan, M. A., Henkel, C. K., and Oliver, D. L. (2002). Direct projections from cochlear nuclear complex to auditory thalamus in the rat. *J. Neurosci.* 22, 10891–10897.

Marquez-Legorreta, E., Horta-Junior Jde, A., Berrebi, A. S., and Saldana, E. (2016). Organization of the Zone of Transition between the Pretectum and the Thalamus, with Emphasis on the Pretectothalamic Lamina. *Front. Neuroanat.* 10:82. doi: 10.3389/fnana.2016.00082

Masuda, M., Kanzaki, S., Minami, S., Kikuchi, J., Kanzaki, J., Sato, H., et al. (2012). Correlations of inflammatory biomarkers with the onset and prognosis of idiopathic sudden sensorineural hearing loss. *Otol. Neurotol.* 33, 1142–1150. doi: 10.1097/MAO.0b013e3182635417

Mazurek, B., Haupt, H., Joachim, R., Klapp, B. F., Stover, T., and Szczepek, A. J. (2010). Stress induces transient auditory hypersensitivity in rats. *Hear. Res.* 259, 55–63. doi: 10.1016/j.heares.2009.10.006

McDonald, A. J. (1998). Cortical pathways to the mammalian amygdala. *Prog. Neurobiol.* 55, 257–332. doi: 10.1016/s0301-0082(98)00003-3

Meininger, V., Pol, D., and Derer, P. (1986). The inferior colliculus of the mouse. A Nissl and Golgi study. *Neuroscience* 17, 1159–1179. doi: 10.1016/0306-4522(86)90085-0

Merchán, M. A., Malmierca, M. S., Bajo, V. M., and Bjaalie, J. G. (1997). "The nuclei of the lateral lemniscus," in *Acoustical signal processing in the central auditory system*, ed. J. Syka. Berlin: Springer. 211–226.

Metzner, W. (1993). An audio-vocal interface in echolocating horseshoe bats. *J. Neurosci.* 13, 1899–1915.

Mugnaini, E., Warr, W. B., and Osen, K. K. (1980). Distribution and light microscopic features of granule cells in the cochlear nuclei of cat, rat, and mouse. *J. Comp. Neurol.* 191, 581–606. doi: 10.1002/cne.901910406

Mulders, W. H., and Robertson, D. (2001). Origin of the noradrenergic innervation of the superior olivary complex in the rat. *J. Chem. Neuroanat.* 21, 313–322. doi: 10.1016/s0891-0618(01)00118-1

Neuser, J., and Knoop, T. (1986). Sudden idiopathic hearing loss: psychopathology and antecedent stressful life-events. *Br. J. Med. Psychol.* 59, 245–251. doi: 10.1111/j.2044-8341.1986.tb02690.x

Ngodup, T., Romero, G. E., and Trussell, L. O. (2020). Identification of an inhibitory neuron subtype, the L-stellate cell of the cochlear nucleus. *Elife* 9:54350. doi: 10.7554/eLife.54350

Oertel, D., Bal, R., Gardner, S. M., Smith, P. H., and Joris, P. X. (2000). Detection of synchrony in the activity of auditory nerve fibers by octopus cells of the mammalian cochlear nucleus. *Proc. Natl. Acad. Sci. USA* 97, 11773–11779. doi: 10.1073/pnas.97.22.11773

Oertel, D., and Wickesberg, R. E. (2002). "Ascending pathways through ventral nuclei of the lateral lemniscus and their possible role in pattern recognition in natural sounds," in *Integrative functions in the mammalian auditory pathway*, eds D. Oertel and R. Fay (Berlin: Springer), 207–237.

Oertel, D., Wright, S., Cao, X. J., Ferragamo, M., and Bal, R. (2011). The multiple functions of T stellate/multipolar/chopper cells in the ventral cochlear nucleus. *Hear. Res.* 276, 61–69. doi: 10.1016/j.heares.2010.10.018

Oertel, D., Wu, S. H., Garb, M. W., and Dizack, C. (1990). Morphology and physiology of cells in slice preparations of the posteroventral cochlear nucleus of mice. *J. Comp. Neurol.* 295, 136–154. doi: 10.1002/cne.902950112

Ohlrogge, M., Doucet, J. R., and Ryugo, D. K. (2001). Projections of the pontine nuclei to the cochlear nucleus in rats. *J. Comp. Neurol.* 436, 290–303.

Oliver, D. L., and Shneiderman, A. (1989). An EM study of the dorsal nucleus of the lateral lemniscus: inhibitory, commissural, synaptic connections between ascending auditory pathways. *J. Neurosci.* 9, 967–982.

Osen, K. K. (1969). Cytoarchitecture of the cochlear nuclei in the cat. *J. Comp. Neurol.* 136, 453–484. doi: 10.1002/cne.901360407

Pacheco-Unguetti, A. P., and Parmentier, F. B. (2014). Sadness increases distraction by auditory deviant stimuli. *Emotion* 14, 203–213. doi: 10.1037/a0034289

Park, J. S., Cederroth, C. R., Basinou, V., Meltser, I., Lundkvist, G., and Canlon, B. (2016). Identification of a circadian clock in the inferior colliculus and its dysregulation by noise exposure. *J. Neurosci.* 36, 5509–5519. doi: 10.1523/JNEUROSCI.3616-15.2016

Perrin, M., Donaldson, C., Chen, R., Blount, A., Berggren, T., Bilezikjian, L., et al. (1995). Identification of a second corticotropin-releasing factor receptor gene and characterization of a cDNA expressed in heart. *Proc. Natl. Acad. Sci. USA* 92, 2969–2973. doi: 10.1073/pnas.92.7.2969

Phelps, E. A., and LeDoux, J. E. (2005). Contributions of the amygdala to emotion processing: from animal models to human behavior. *Neuron* 48, 175–187. doi: 10.1016/j.neuron.2005.09.025

Reyes, T. M., Lewis, K., Perrin, M. H., Kunitake, K. S., Vaughan, J., Arias, C. A., et al. (2001). Urocortin II: a member of the corticotropin-releasing factor (CRF) neuropeptide family that is selectively bound by type 2 CRF receptors. *Proc. Natl. Acad. Sci. USA* 98, 2843–2848. doi: 10.1073/pnas.051626398

Rhea, E. M., Rask-Madsen, C., and Banks, W. A. (2018). Insulin transport across the blood-brain barrier can occur independently of the insulin receptor. *J. Physiol.* 596, 4753–4765. doi: 10.1113/JP276149

Romanski, L. M., and LeDoux, J. E. (1993). Information cascade from primary auditory cortex to the amygdala: corticocortical and corticoamygdaloid projections of temporal cortex in the rat. *Cereb. Cortex* 3, 515–532. doi: 10.1093/cercor/3.6.515

Rubio, M. E., Gudsnuk, K. A., Smith, Y., and Ryugo, D. K. (2008). Revealing the molecular layer of the primate dorsal cochlear nucleus. *Neuroscience* 154, 99–113. doi: 10.1016/j.neuroscience.2007.12.016

Russo, A. F. (2017). Overview of neuropeptides: awakening the senses? *Headache* 57(Suppl. 2), 37–46. doi: 10.1111/head.13084

Ryan, A. F., Keithley, E. M., Wang, Z. X., and Schwartz, I. R. (1990). Collaterals from lateral and medial olivocochlear efferent neurons innervate different regions of the cochlear nucleus and adjacent brainstem. *J. Comp. Neurol.* 300, 572–582. doi: 10.1002/cne.903000410

Ryugo, D. K. (2008). Projections of low spontaneous rate, high threshold auditory nerve fibers to the small cell cap of the cochlear nucleus in cats. *Neuroscience* 154, 114–126. doi: 10.1016/j.neuroscience.2007.10.052

Ryugo, D. K., Haenggeli, C. A., and Doucet, J. R. (2003). Multimodal inputs to the granule cell domain of the cochlear nucleus. *Exp. Brain Res.* 153, 477–485. doi: 10.1007/s00221-003-1605-3

Sakanaka, M., Shibasaki, T., and Lederis, K. (1987). Corticotropin-releasing factor-containing afferents to the inferior colliculus of the rat brain. *Brain Res.* 414, 68–76. doi: 10.1016/0006-8993(87)91326-6

Sapolsky, R. M., Romero, L. M., and Munck, A. U. (2000). How do glucocorticoids influence stress responses? Integrating permissive, suppressive, stimulatory, and preparative actions. *Endocr. Rev.* 21, 55–89. doi: 10.1210/edrv.21.1.0389

Schmitt, C., Patak, M., and Kroner-Herwig, B. (2000). Stress and the onset of sudden hearing loss and tinnitus. *Int. Tinnitus J.* 6, 41–49.

Schofield, B. R., Motts, S. D., and Mellott, J. G. (2011). Cholinergic cells of the pontomesencephalic tegmentum: connections with auditory structures from cochlear nucleus to cortex. *Hear. Res.* 279, 85–95. doi: 10.1016/j.heares.2010.12.019

Schulz, K., Rutz, C., Westendorf, C., Ridelis, I., Vogelbein, S., Furkert, J., et al. (2010). The pseudo signal peptide of the corticotropin-releasing factor receptor type 2a decreases receptor expression and prevents Gi-mediated inhibition of adenylyl cyclase activity. *J. Biol. Chem.* 285, 32878–32887. doi: 10.1074/jbc.M110.129627

Shalev, A. Y., Peri, T., Brandes, D., Freedman, S., Orr, S. P., and Pitman, R. K. (2000). Auditory startle response in trauma survivors with posttraumatic stress disorder: a prospective study. *Am. J. Psychiatry* 157, 255–261. doi: 10.1176/appi.ajp.157.2.255

Sharpe, A. L., and Phillips, T. J. (2009). Central urocortin 3 administration decreases limited-access ethanol intake in nondependent mice. *Behav. Pharmacol.* 20, 346–351. doi: 10.1097/FBP.0b013e32832f01ba

Shemesh, Y., Forkosh, O., Mahn, M., Anpilov, S., Sztainberg, Y., Manashirov, S., et al. (2016). Ucn3 and CRF-R2 in the medial amygdala regulate complex social dynamics. *Nat. Neurosci.* 19, 1489–1496. doi: 10.1038/nn.4346

Shore, S. E. (2005). Multisensory integration in the dorsal cochlear nucleus: unit responses to acoustic and trigeminal ganglion stimulation. *Eur. J. Neurosci.* 21, 3334–3348. doi: 10.1111/j.1460-9568.2005.04142.x

Singla, S., Dempsey, C., Warren, R., Enikolopov, A. G., and Sawtell, N. B. (2017). A cerebellum-like circuit in the auditory system cancels responses to self-generated sounds. *Nat. Neurosci.* 20, 943–950. doi: 10.1038/nn.4567

Sizemore, T. R., Hurley, L. M., and Dacks, A. M. (2020). Serotonergic modulation across sensory modalities. *J. Neurophysiol.* 123, 2406–2425. doi: 10.1152/jn.00034.2020

Stengel, A., and Tache, Y. (2018). Gut-Brain neuroendocrine signaling under conditions of stress-focus on food intake-regulatory mediators. *Front. Endocrinol.* 9:498. doi: 10.3389/fendo.2018.00498

Szczepek, A. J., Dietz, G. P. H., Reich, U., Hegend, O., Olze, H., and Mazurek, B. (2018). Differences in stress-induced modulation of the auditory system between wistar and lewis rats. *Front. Neurosci.* 12:828. doi: 10.3389/fnins.2018.00828

Takahashi, T. T., Carr, C. E., Brecha, N., and Konishi, M. (1987). Calcium binding protein-like immunoreactivity labels the terminal field of nucleus laminaris of the barn owl. *J. Neurosci.* 7, 1843–1856.

Teichmann, A., Rutz, C., Kreuchwig, A., Krause, G., Wiesner, B., and Schulein, R. (2012). The Pseudo signal peptide of the corticotropin-releasing factor receptor type 2A prevents receptor oligomerization. *J. Biol. Chem.* 287, 27265–27274. doi: 10.1074/jbc.M112.360594

Thompson, A. M., and Thompson, G. C. (1991). Posteroventral cochlear nucleus projections to olivocochlear neurons. *J. Comp. Neurol.* 303, 267–285. doi: 10.1002/cne.903030209

Trost, W., Ethofer, T., Zentner, M., and Vuilleumier, P. (2012). Mapping aesthetic musical emotions in the brain. *Cereb. Cortex* 22, 2769–2783. doi: 10.1093/cercor/bhr353

Trussell, L. O., and Oertel, D. (2018). "Microcircuits of the dorsal cochlear nucleus," in *The Mammalian Auditory Pathways*, eds D. L. Oliver, N. Cant, R. R. Fay, and A. N. Popper (New York: Springer), 73–99.

van den Pol, A. N. (2012). Neuropeptide transmission in brain circuits. *Neuron* 76, 98–115. doi: 10.1016/j.neuron.2012.09.014

Varga, T., Palkovits, M., Usdin, T. B., and Dobolyi, A. (2008). The medial paralemniscal nucleus and its afferent neuronal connections in rat. *J. Comp. Neurol.* 511, 221–237. doi: 10.1002/cne.21829

Vila-Porcile, E., Xu, Z. Q., Mailly, P., Nagy, F., Calas, A., Hokfelt, T., et al. (2009). Dendritic synthesis and release of the neuropeptide galanin: morphological evidence from studies on rat locus coeruleus neurons. *J. Comp. Neurol.* 516, 199–212. doi: 10.1002/cne.22105

Vita, N., Laurent, P., Lefort, S., Chalon, P., Lelias, J. M., Kaghad, M., et al. (1993). Primary structure and functional expression of mouse pituitary and human brain corticotrophin releasing factor receptors. *FEBS Lett.* 335, 1–5. doi: 10.1016/0014-5793(93)80427-v

Webster, D. B., and Trune, D. R. (1982). Cochlear nuclear complex of mice. *Am. J. Anat.* 163, 103–130. doi: 10.1002/aja.1001630202

Weedman, D. L., Pongstaporn, T., and Ryugo, D. K. (1996). Ultrastructural study of the granule cell domain of the cochlear nucleus in rats: mossy fiber endings and their targets. *J. Comp. Neurol.* 369, 345–360.

Willard, F. H., and Ryugo, D. K. (1983). *Anatomy of the central auditory system in The auditory psychobiology of the Mouse*, (Springfield, IL: Charles C Thomas Publisher), 201–304.

Winer, J. A. (1992). "The functional architecture of the medial geniculate body and the primary auditory cortex," in *The mammalian auditory pathway: Neuroanatomy*, eds D. B. Webster and R. R. Fay New York, NY: Springer 222–409.

Winer, J. A., and Schreiner, C. E. (2005). "The central auditory system: a functional analysis," in *The Inferior Colliculus*, eds J. A. Winer and C. E. Schreiner (New York, NY: Springer), 1–68.

Wong, M. Y., Zhou, C., Shakiryanova, D., Lloyd, T. E., Deitcher, D. L., and Levitan, E. S. (2012). Neuropeptide delivery to synapses by long-range vesicle circulation and sporadic capture. *Cell* 148, 1029–1038. doi: 10.1016/j.cell.2011.12.036

Wright, D. D., and Ryugo, D. K. (1996). Mossy fiber projections from the cuneate nucleus to the cochlear nucleus in the rat. *J. Comp. Neurol.* 365, 159–172.

Yaeger, D. B., and Trussell, L. O. (2015). Single granule cells excite Golgi cells and evoke feedback inhibition in the cochlear nucleus. *J. Neurosci.* 35, 4741–4750. doi: 10.1523/JNEUROSCI.3665-14.2015

Yang, Y., Saint Marie, R. L., and Oliver, D. L. (2005). Granule cells in the cochlear nucleus sensitive to sound activation detected by Fos protein expression. *Neuroscience* 136, 865–882. doi: 10.1016/j.neuroscience.2005.02.007

Ye, Y., Machado, D. G., and Kim, D. O. (2000). Projection of the marginal shell of the anteroventral cochlear nucleus to olivocochlear neurons in the cat. *J. Comp. Neurol.* 420, 127–138.

Yeh, C., Ting, C. H., Doong, M. L., Chi, C. W., Lee, S. D., and Chen, C. Y. (2016). Intracerebroventricular urocortin 3 counteracts central acyl ghrelin-induced hyperphagic and gastroprokinetic effects via CRF receptor 2 in rats. *Drug Des. Devel. Ther.* 10, 3281–3290. doi: 10.2147/DDDT.S113195

Zeng, C., Shroff, H., and Shore, S. E. (2011). Cuneate and spinal trigeminal nucleus projections to the cochlear nucleus are differentially associated with vesicular glutamate transporter-2. *Neuroscience* 176, 142–151. doi: 10.1016/j.neuroscience.2010.12.010

Zhan, X., Pongstaporn, T., and Ryugo, D. K. (2006). Projections of the second cervical dorsal root ganglion to the cochlear nucleus in rats. *J. Comp. Neurol.* 496, 335–348. doi: 10.1002/cne.20917

Zhan, X., and Ryugo, D. K. (2007). Projections of the lateral reticular nucleus to the cochlear nucleus in rats. *J. Comp. Neurol.* 504, 583–598. doi: 10.1002/cne.21463

Zhao, H. B., Parham, K., Ghoshal, S., and Kim, D. O. (1995). Small neurons in the vestibular nerve root project to the marginal shell of the anteroventral cochlear nucleus in the cat. *Brain Res.* 700, 295–298. doi: 10.1016/0006-8993(95)01078-a

Zhou, J., and Shore, S. (2004). Projections from the trigeminal nuclear complex to the cochlear nuclei: a retrograde and anterograde tracing study in the guinea pig. *J. Neurosci. Res.* 78, 901–907. doi: 10.1002/jnr.20343

Conflict of Interest: The authors declare that the research was conducted in the absence of any commercial or financial relationships that could be construed as a potential conflict of interest.

Publisher's Note: All claims expressed in this article are solely those of the authors and do not necessarily represent those of their affiliated organizations, or those of the publisher, the editors and the reviewers. Any product that may be evaluated in this article, or claim that may be made by its manufacturer, is not guaranteed or endorsed by the publisher.

frontiers in Neural Circuits

HYPOTHESIS AND THEORY
published: 06 January 2022
doi: 10.3389/fncir.2021.785603

Disturbed Balance of Inhibitory Signaling Links Hearing Loss and Cognition

Marlies Knipper[1], Wibke Singer[1], Kerstin Schwabe[2], Gisela E. Hagberg[3,4], Yiwen Li Hegner[5,6], Lukas Rüttiger[1], Christoph Braun[5,6] and Rüdiger Land[7]*

[1] Department of Otolaryngology, Head and Neck Surgery, Tübingen Hearing Research Center (THRC), Molecular Physiology of Hearing, University of Tübingen, Tübingen, Germany, [2] Experimental Neurosurgery, Department of Neurosurgery, Hannover Medical School, Hanover, Germany, [3] Department of Biomedical Magnetic Resonance, University Hospital Tübingen (UKT), Tübingen, Germany, [4] High-Field Magnetic Resonance, Max Planck Institute for Biological Cybernetics, Tübingen, Germany, [5] MEG Center, University of Tübingen, Tübingen, Germany, [6] Center of Neurology, Hertie-Institute for Clinical Brain Research, University of Tübingen, Tübingen, Germany, [7] Department of Experimental Otology, Institute for Audioneurotechnology, Hannover Medical School, Hanover, Germany

Neuronal hyperexcitability in the central auditory pathway linked to reduced inhibitory activity is associated with numerous forms of hearing loss, including noise damage, age-dependent hearing loss, and deafness, as well as tinnitus or auditory processing deficits in autism spectrum disorder (ASD). In most cases, the reduced central inhibitory activity and the accompanying hyperexcitability are interpreted as an active compensatory response to the absence of synaptic activity, linked to increased central neural gain control (increased output activity relative to reduced input). We here suggest that hyperexcitability also could be related to an immaturity or impairment of tonic inhibitory strength that typically develops in an activity-dependent process in the ascending auditory pathway with auditory experience. In these cases, high-SR auditory nerve fibers, which are critical for the shortest latencies and lowest sound thresholds, may have either not matured (possibly in congenital deafness or autism) or are dysfunctional (possibly after sudden, stressful auditory trauma or age-dependent hearing loss linked with cognitive decline). Fast auditory processing deficits can occur despite maintained basal hearing. In that case, tonic inhibitory strength is reduced in ascending auditory nuclei, and fast inhibitory parvalbumin positive interneuron (PV-IN) dendrites are diminished in auditory and frontal brain regions. This leads to deficits in central neural gain control linked to hippocampal LTP/LTD deficiencies, cognitive deficits, and unbalanced extra-hypothalamic stress control. Under these conditions, a diminished inhibitory strength may weaken local neuronal coupling to homeostatic vascular responses required for the metabolic support of auditory adjustment processes. We emphasize the need to distinguish these two states of excitatory/inhibitory imbalance in hearing disorders: (i) Under conditions of preserved fast auditory processing and sustained tonic inhibitory strength, an excitatory/inhibitory imbalance following auditory deprivation can maintain precise hearing through a memory linked, transient disinhibition that leads to enhanced spiking fidelity (central neural gain↑) (ii) Under conditions of critically diminished fast auditory processing and reduced tonic inhibitory strength,

OPEN ACCESS

Edited by:
R. Michael Burger,
Lehigh University, United States

Reviewed by:
Hiroshi Kuba,
Nagoya University, Japan
Christian Keine,
University of Oldenburg, Germany
Shaowen Bao,
University of Arizona, United States

****Correspondence:***
Marlies Knipper
Marlies.Knipper@uni-tuebingen.de

Received: *29 September 2021*
Accepted: *08 December 2021*
Published: *06 January 2022*

Citation:
Knipper M, Singer W, Schwabe K, Hagberg GE, Li Hegner Y, Rüttiger L, Braun C and Land R (2022) Disturbed Balance of Inhibitory Signaling Links Hearing Loss and Cognition. Front. Neural Circuits 15:785603. doi: 10.3389/fncir.2021.785603

hyperexcitability can be part of an increased synchronization over a broader frequency range, linked to reduced spiking reliability (central neural gain⇓). This latter stage mutually reinforces diminished metabolic support for auditory adjustment processes, increasing the risks for canonical dementia syndromes.

Keywords: inhibitory strength, fast auditory processing, PV interneurons, dementia, tinnitus, deafness, BDNF, hearing loss

INTRODUCTION

Hearing loss is a very common problem in the aging population of industrial societies. Globally, an estimated 1.57 billion people had hearing loss in 2019, accounting for one in five people (20.3%) (Goman and Lin, 2016; Collaborators, 2021). The problem is even worse among the elderly; more than 25% of people over 60 suffer from hearing loss. Hearing loss not only impairs communication, social interaction, and quality of life, but has also been identified as a common risk factor for cognitive decline and Alzheimer's disease (Lin F. R. et al., 2011; Livingston et al., 2017; Montero-Odasso et al., 2020). However, at the moment there has been no confirmation of a direct link between hearing loss and cognitive decline, which is, instead, currently assumed to be based on differences in myelination (Lin H. W. et al., 2011), auditory cognitive dysfunctions, or neurodegenerative processes (Fortunato et al., 2016; Uchida et al., 2019; Johnson et al., 2021).

Here, we review how impaired auditory input can affect the excitatory/inhibitory balance within the central auditory system and suggest that hearing loss and cognitive decline may be linked through changes in the excitatory/inhibitory balance associated with the functional attenuation of distinct auditory fiber types. We further suggest that these changes in the excitatory/inhibitory balance may, in turn, influence neurovascular coupling, possibly further affecting cognitive function in aging.

In the following, we lay out this idea in more detail. First, we provide an overview of the development of inhibitory GABAergic circuits (see Section "Maturation of GABA-Responsive Neurons Prior to Hearing Onset"). Second, we describe the role that different auditory nerve-fiber types might play during development and in regulating the excitatory/inhibitory balance in the auditory system (see Section "Activity-Dependent Maturation of GABAergic Inhibitory Circuits After Hearing Onset: The Potential Role of Auditory Nerve Fibers"). We then discuss the role of fast auditory processing (see **Box 1**) may play for maintaining the excitatory/inhibitory balance and sustaining or improving stimulus resolution and discrimination above noise after, e.g., mild acoustic trauma or hearing deficits. We hypothesize that fast auditory processing is a prerequisite for an increased central neural gain process (see **Box 2**). Within this multi-level reinforcing framework, activity dependent brain-derived neurotrophic factor (BDNF) and fast spiking PV-IN contribute to improving central auditory plasticity (see Section "Altered Excitation and Inhibition After Acoustic Trauma and Age-Related Hearing Loss Are Linked to Increased Central Neural Gain"). In other auditory impairments such as acute acoustic trauma, deafness, or tinnitus, hyperexcitability may be the result of reduced (tonic) inhibitory strength (see **Box 3**) following less-developed or impaired fast auditory processing and subsequent failure to recruit BDNF and PV-IN dependent increased central neural gain (see Section "Altered Excitation and Inhibition in Acute Acoustic Trauma, Deafness, and Tinnitus: Lost Fast Auditory Processing"). Further, we discuss how a decline in fast auditory nerve processing, when critically reducing tonic inhibitory strength in auditory nuclei, might be linked to cognitive deficits or autism (see Section "Altered Excitation and Inhibition Following Diminished Fast Auditory Processing Linked to 'Central' Hearing Loss"). Finally, we point to a possible role for inhibitory circuits in regulating neurovascular hemodynamic responses as a stress-sensitive process. Ultimately, under these conditions, deficits in central processing and auditory cognitive brain dysfunctions are expected. Sustained fast auditory processing and tonic inhibitory strength may be a key signature that bridge hearing and cognition (see Section "Coupling of Inhibitory/Excitatory Circuit Activation to Cerebral Blood Flow").

This article should not be understood to be all-encompassing, but a reference to the respective research interests of the authors, in order to increase awareness that the brain's hyperexcitability can have different origins, dependent on whether the inhibitory strength generated in microcircuits with auditory experience is maintained or not. We finally deliberately propose this view as a "general concept." In the best case, we hope to inspire an interdisciplinary effort to examine the suggested hypothesis in the context of various auditory diseases. Only then can personalized intervention strategies be successfully implemented to overcome such devastating disorders as dementia, to which auditory cognitive deficits may contribute.

MATURATION OF BALANCED INHIBITORY/EXCITATORY CIRCUITS IN THE AUDITORY SYSTEM

Maturation of GABA-Responsive Neurons Prior to Hearing Onset

A balance between excitation and inhibition is crucial for the precise encoding of complex sounds. In this context, it is important to consider that balanced excitatory/inhibitory neuronal activity develops only after hearing onset. Early in neonatal development, radially migrating neurons that originate in the ventricular zone of the pallium (cortex) give rise to glutamatergic pyramidal neurons, while a second population of tangentially migrating neurons, originating

BOX 1 | Fast auditory processing.

We define fast auditory processing as the increase in auditory acuity that is linked to lowering of hearing thresholds, increased suprathreshold ABR waves I and IV, the shortening of first spike latencies, and widening of response dynamic range with auditory experience, all shown in DCN neurons (Eckert et al., 2021), IC neurons (Chumak et al., 2016), and auditory cortex neurons (de Villers-Sidani et al., 2007; Xu et al., 2010). Because high-SR auditory fibers determine the threshold of the auditory-nerve response measured by the compound action potential (CAP) (Bourien et al., 2014), and these highly active fibers enable the shortest-latency auditory responses whatever the characteristic frequency (Meddis, 2006; Heil et al., 2008), we hypothesize that fast (high-SR) auditory fibers are also responsible for lowering of thresholds and shortening of latency of cortical auditory responses with auditory experience (de Villers-Sidani et al., 2007). This improved auditory acuity occurs after hearing onset in rodents ∼P11 (de Villers-Sidani et al., 2007) and in humans likely between the 27th embryonic week and 6th to 12th months after birth (Neville and Bavelier, 2002). Moreover, fast auditory processing is a likely prerequisite for precise temporal auditory coding, pure tone pitch perception, and frequency discrimination – all characteristics that are required for proper speech intelligibility (Oxenham, 2018) and experience-driven auditory attention (Addleman and Jiang, 2019).

BOX 2 | Increased central neural gain.

We define increased central neural gain as the identifiable network homeostasis that increases stimulus-evoked synchronous neural activity at the level of the inferior colliculus (IC) (ABR wave IV) relative to its input at the level of the auditory nerve (ABR wave I). Increased central neural gain can occur following, e.g., auditory deprivation (age, injury, and trauma) or sound enrichment. As a multi-level framework, central neural gain includes a positive auditory feedforward and positive fronto-striatal feedback cycle that require co-activation. Mechanistically increased central neural gain likely requires a reinforcement process, as it is also known from auditory perception or improved task performance [for a review see Irvine (2018a)]. During improved task performance, for example, PV-IN activity in frontal brain regions contributes to feedforward inhibition that narrows the window for temporal summation of EPSPs and action potential initiation in, e.g., principle neurons (Pouille and Scanziani, 2001). Through feedback inhibition, a sharpening of receptive fields and pattern separation is initiated (Leutgeb et al., 2007). During this process, stimulus resolution and discrimination above noise, as well as neuronal output activity, is facilitated in sensory systems through, e.g., cortical or prefrontal brain inhibitory neurons that specifically suppress the firing of other inhibitory neurons (Caraiscos et al., 2004; Cardin et al., 2009; Pi et al., 2013; Hu et al., 2014; Kim et al., 2016; Chen et al., 2017). This results in enhanced stimulus response reliability, decreased response variability, and increased signal-to-noise ratio (Sohal et al., 2009; Zhu et al., 2015; Espinoza et al., 2018).

in the ventricular zone of the subpallium (subcortical telencephalon), give rise to GABA-producing local-circuit neurons (Marin and Rubenstein, 2001). Tangentially migrating GABAergic neurons, which target either higher-level cortical regions or lower-level brain regions posterior to the midbrain, originate from different brain regions and are characterized by different paired-box (Pax) homeobox genes. The GABAergic interneurons that migrate from the subpallium to cortical regions are thought to express Pax6 (Maricich and Herrup, 1999; Marin and Rubenstein, 2001), while the GABAergic interneurons that migrate from ventricular zones to lower brain levels posterior to midbrain regions express Pax2 (Nornes et al., 1990; Maricich and Herrup, 1999; Rowitch et al., 1999; Fotaki et al., 2008).

In rodents, the radially migrating excitatory neurons, followed by the tangentially migrating GABAergic neurons, reach their final destinations around birth (Marin and Rubenstein, 2001; Markram et al., 2004; Li et al., 2018). At this stage, GABA at the GABA-responsive neurons still acts in excitatory fashion (**Figure 1A**), corresponding with a transient, initial hyperexcitability phase (**Figure 1A**, green arrows and crosses). In the cortex, this occurs after migration of GABAergic neurons to the cortical plate (Marin and Rubenstein, 2001).

The initial hyperexcitability is due to the high intracellular chloride concentration of GABA-responsive neurons, which when activated by GABA favors a chloride efflux and thereby a depolarization of the neuron (Ben-Ari et al., 1989; Marin and Rubenstein, 2001; Ben-Ari, 2002) (**Figure 1A**, inset red arrow Cl^-). In the auditory pathway of rodents, it has been shown that, early in postnatal development and prior to hearing onset, a high intracellular chloride concentration ($[Cl^-]_i$) is maintained in most neurons, ensured by the sodium-potassium-chloride co-transporter type 1 (NKCC1) (**Figure 1A**, inset NKCC1⇑). Hence, Cl^--mediated synaptic activities cause a depolarizing response (Balakrishnan et al., 2003; Cherubini et al., 2011; Friauf et al., 2011). Briefly, prior to hearing onset, around P5-P6 in rodents (Lohrke et al., 2005), or possibly driven by auditory experience, as shown after unilateral or bilateral cochlear ablation (Shibata et al., 2004), a switch of GABA-responsive neurons occurs and the effect of GABA changes from depolarizing to hyperpolarizing (**Figure 1B**). The switch from depolarizing to hyperpolarizing responses of GABA-responsive neurons is linked to an enhanced expression of the neuronal potassium chloride co-transporter type 2 (KCC2), which leads to a low concentration of intracellular chloride and, consequently, to a hyperpolarizing inhibitory postsynaptic potential upon GABA stimulation (Kandler and Gillespie, 2005) (**Figure 1B**, inset GABA KCC2⇑). Accordingly, the levels of the KCC2 transporter in the brainstem and ascending associated hippocampal regions are expectedly low before hearing onset (**Figure 1A**, inset KCC2⇓), and increase from the first postnatal week onward in a region-specific pattern (**Figure 1B**, inset KCC2⇑), as shown for the ascending auditory pathway (Lohrke et al., 2005) and other brain regions (Kandler and Friauf, 1995; Rivera et al., 1999; Friauf et al., 2011; Hirtz et al., 2011; Watanabe and Fukuda, 2015). This is the time when an upregulation of activity-dependent *Bdnf* transcripts is observed in cochlear spiral ganglion neurons (SGN) and at lower auditory brain levels (Singer et al., 2014) (**Figure 1B**, BDNF⇑). BDNF is suggested to modulate GABAergic synapses by postsynaptic regulation of chloride transport (Wardle and Poo, 2003). Since BDNF drives the upregulation of KCC2 expression (Ben-Ari et al., 2012) and both BDNF (Aid et al., 2007) and KCC2 (Fiumelli et al., 2005; Wake et al., 2007) are controlled by neuronal activity (Awad et al., 2018), the switch from depolarizing to hyperpolarizing responses of projecting neurons may start in the ascending auditory pathway and associated limbic frontal

BOX 3 | Tonic inhibitory strength.

We define tonic inhibitory strength as a sustained form of microcircuit network suppression. In the case of loss of inhibitory strength, spontaneous firing rate would increase without increasing a stimulus-evoked spike output. In the cerebellar cortex, such a phenomenon was described after a blockade of tonic inhibition in granule cells (Duguid et al., 2012). It is currently assumed that tonic inhibition suppresses spontaneous activity through a reduction of the neuronal input resistance and membrane time constants, thereby improving stimulus discrimination above noise (Caraiscos et al., 2004). The ability of tonic inhibition to change conductance in many neurons is assumed to require perisynaptic and extrasynaptic δ subunit-containing $GABA_A$ receptors, which are likely activated through fast-spiking, parvalbumin (PV)-expressing and soma-inhibiting interneurons (IN) (Ferando and Mody, 2015). When tonic PV-IN activity is functionally impaired, the rapid increase in bursting reduces the signal-to-noise ratio (Duguid et al., 2012). The pathological hyper-synchronization resembles electrical seizure activity (Rossignol et al., 2013; Fröhlich, 2016; Hsieh et al., 2017), and possibly enhances baseline spontaneous gamma power, reduces evoked gamma power (Mamashli et al., 2017), and can in this way also disturb the signal-to-noise ratio.

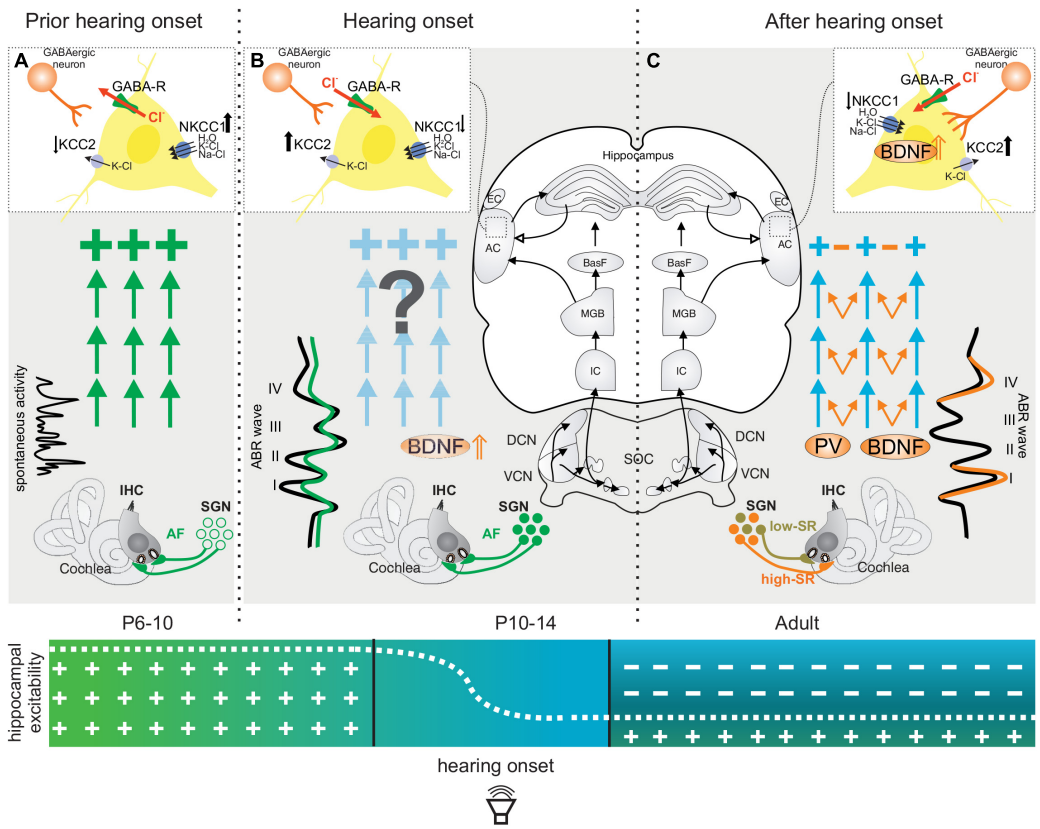

FIGURE 1 | Maturation of neuronal inhibitory circuits in the auditory system prior to **(A)**, during **(B)**, and after **(C)** hearing onset. **(A)** Prior to hearing onset, when GABAergic neurons (inset, light red cell) do not yet contact target cells, GABA-responsive pyramidal neurons favor a chloride efflux (inset, red arrow) and thereby a depolarization of GABA-responsive neurons. A high intracellular chloride concentration in these cells is supported by low levels of neuronal potassium chloride co-transporter type 2 (↓ KCC2) and elevated sodium-potassium-chloride co-transporter type 1 (NKCC1↑). At this time, an initial hyper-excitability dominates (large green crosses) and IHCs show only spontaneous firing. **(B)** Shortly before hearing onset, BDNF is upregulated in the cochlea (Wiechers et al., 1999) and a switch in the effect of GABA from depolarizing to hyperpolarizing occurs (Lohrke et al., 2005) (**B** inset, GABAergic neuron and red inward arrow), accompanied by a reduced NKCC1↓ and an increased KCC2↑ expression (**B**, inset). This may already be driven by auditory input (Shibata et al., 2004) (**B**, green ABR wave on the left). **(C)** A switch of the GABA action from excitatory/depolarizing to inhibitory/hyperpolarizing is initiated in projection neurons after hearing onset, (P10–14). This time period parallels the maturation of the high-SR (**C**, orange fiber) and low-SR auditory nerve fibers (**C**, green fibers). The switch of GABA from excitatory to inhibitory (**B,C**, inset) is initiated by an upregulation of KCC2 ↑ after hearing onset, (P10–14). KCC2 promotes a lower concentration of intracellular chloride in GABA-responsive neurons and consequently promotes hyperpolarizing inhibitory postsynaptic potentials upon GABA stimulation. As up-regulation of KCC2 is driven by BDNF, and BDNF is shown to foster the maturation of parvalbumin networks (**C**, orange arrows), fast (high-SR) auditory fiber processing may trigger the stimulus-evoked release of BDNF from auditory projection neurons and subsequently drive synaptogenesis of complex parvalbumin-expressing GABAergic interneuron networks toward sharply clustered brain circuits that respond precisely to auditory stimuli (**C**, orange arrows, orange ABR wave). ABR, auditory brainstem response; IHC, inner hair cell; SGN, spiral ganglion neuron; VCN, ventral cochlear nucleus; DCN, dorsal cochlear nucleus; SOC, superior olivary complex; IC, inferior colliculus; MGB, medial geniculate body; BasF, basal Forebrain; AC, auditory cortex; EC, entorhinal cortex; PV, parvalbumin.

brain regions in response to an upregulation of activity–driven *Bdnf* transcripts. Activity-driven *Bdnf* transcripts are the result of independently transcribed non-coding exon IV and exon VI that, from a total of eight non-coding exons (I–VIII), are spliced to a common protein-encoding exon (IX) (Timmusk et al., 1993; Aid et al., 2007; Vaghi et al., 2014)

FIGURE 2 | Schematic drawing of the rodent *Bdnf* gene, which is composed of eight non-coding exons (I–VIII) that are individually transcribed and alternatively spliced to the protein-encoding exon IX. *Bdnf* exon IV and VI are directly or indirectly regulated by changes in neuronal activity. In BDNF-Live-Exon-Visualization (BLEV) mice (Matt et al., 2018; Singer et al., 2018b), BDNF exon IV and VI are individually labeled with either cyan (exon IV) or yellow (exon VI) fluorescence protein in regions of activity-dependent translation of BDNF. Modified after (Aid et al., 2007; Singer et al., 2018b).

(**Figure 2**). Both exon IV (**Figure 2**, cyan) and exon VI (**Figure 2**, yellow) comprise promoters directly or indirectly regulated by neuronal activity (Hong et al., 2008; Dieni et al., 2012; West et al., 2014; Chacon-Fernandez et al., 2016; Tuvikene et al., 2016).

In analogy to the visual system, the upregulation of BDNF in the cochlea and ascending pathway prior to hearing onset is suggested to occur in response to the influences of top-down hypothalamic corticotropin-releasing factor (CRF) (Knipper et al., 2015; Vetter, 2015). In response to these changes, spontaneous glutamate release from inner hair cells (IHCs), long predicted to play a crucial role in the maturation of central auditory circuits (Friauf and Lohmann, 1999; Kandler and Gillespie, 2005; Kandler et al., 2009; Hirtz et al., 2011), could activate *Bdnf* promoters in SGN to drive the depolarizing-to-hyperpolarizing switch in a bottom-up direction within the ascending auditory circuits both prior to and following hearing onset (**Figure 1B**, BDNF⇑). This would prepare auditory microcircuits for the subsequently occurring experience-driven synaptogenesis of perisomatic GABAergic contacts with the ascending microcircuits (next section). Taking this into account, differences in the vulnerability of cochlear neurons related to altered cochlear BDNF (Meltser et al., 2014) or CRF levels (Graham and Vetter, 2011) may be reconsidered in future studies in the context of changes in cochlear BDNF or CRF might potentially affect GABAergic inhibitory strength in the auditory pathway.

In summary, prior to the first auditory experience and during hearing onset, an initial period of hyperexcitability exists, with excitatory activity dominating over inhibitory activity. Within this transient time period, GABA-responsive neurons have reached their target regions but still react with depolarizing responses, due to the low level of neuronal KCC2 and high $[Cl^-]_I$ concentrations.

Activity-Dependent Maturation of GABAergic Inhibitory Circuits After Hearing Onset: The Potential Role of Auditory Nerve Fibers

When considering possible events that may be causally linked to inhibitory GABAergic circuit formation in the auditory system, it is interesting to focus on the differential maturation times of different types of auditory nerve fibers. These roughly 30,000 auditory nerve fibers in the mammalian inner ear receive signals from individual IHC *via* ribbon synapses (Spoendlin, 1969; Liberman, 1980; Nadol, 1988), and transmit the signals further to the subsequent structures of the central auditory pathway. Auditory nerve fibers differ in their spontaneous firing rates (SR) and sound level thresholds and can be divided into at least two types. The low-SR, high-threshold auditory fibers, characterized by a low spontaneous firing rate of <18 spikes/s, comprise around 40% of all auditory nerve fibers, and the high-SR low threshold fibers, which have a high spontaneous firing rate >18 spikes/s, comprise the remaining 60% (Sachs and Abbas, 1974; Liberman, 1982; Yates, 1991; Merchan-Perez and Liberman, 1996; Glowatzki and Fuchs, 2002; Grant et al., 2010). SGNs with different SRs form synapses at different modiolar-to-pillar positions along the basolateral surface of IHCs (Liberman, 1982).

The mechanism that leads to maturation and differentiation of the distinct SR characteristics of auditory nerve fiber types is still under debate. A recent study of Shrestha et al. (2018), identified characteristic patterns of genes in SGNs of mature mice (P25), that from their anatomical position across the IHCs were characteristic for SGN fates of high, middle, and low-SR auditory nerve fibers. They showed that prior to hearing onset, representative genes for the SGN fate of low-SR auditory nerve fibers are shaped out of pre-existing SGNs that have the SGN fate typical of high-SR auditory nerve fibers. This happens over time - between P3 and P8 - in an activity-dependent manner (Shrestha et al., 2018). This would mean that prior to hearing onset, the SGN fate of high-SR would precede that of low-SR fibers. In contrast, when auditory nerve activity was recorded at the time of hearing onset —in mice around P11—, their multivesicular excitatory postsynaptic currents (EPSCs) with lower amplitudes preceded and contrasted with monophasic EPSCs with sharp rise times and 10 times larger amplitudes that were recorded after hearing onset at P19–P21 (Grant et al., 2010). It was speculated that low EPSC amplitude distributions may represent fibers with low spontaneous rates (**Figure 1C**, light green fiber), 'as most synaptic events may be insufficiently large to activate APs.' In contrast, fibers with monophasic EPSCs and larger amplitudes may correspond to high-SR ANF (**Figure 1C**, orange fiber), as most excitatory postsynaptic potentials (EPSPs) may activate APs (Glowatzki and Fuchs, 2002; Grant et al., 2010). This suggested a substantial shift in the mode of transmitter release in IHCs, from preferential release of single vesicles in IHCs in immature animals during hearing onset, to preferential and coordinated release of seven to nine vesicles in IHCs from hearing animals (Grant et al., 2010).

In addition, medial efferents that form transient cholinergic synapses with IHCs during the first postnatal week (Glowatzki and Fuchs, 2000) may contribute to the different SR of auditory fibers or SGN fate (Knipper et al., 2015, review), as they alter the precision of spike timing of auditory fibers (Johnson et al., 2011, 2013). In analogy to the visual system, an altered spike timing

precision may initiate, e.g., a hypothalamic top-down feedback signal to cochlear neurons, resulting in BDNF upregulation, here suggested to potentially influence the inhibitory strength of ANF (see Section "Maturation of GABA-Responsive Neurons Prior to Hearing Onset"). This may be analogous to the BDNF- and dopamine-induced improvement of retinal acuity through receptive-field re-organization of retinal ganglion cells (RGCs) (Sinclair et al., 2004; Witkovsky, 2004; Landi et al., 2009). Moreover, lateral dopaminergic feedback to auditory nerve fibers may influence high-SR rate characteristics, as shown by auditory nerve recording under dopaminergic receptor blockade (Ruel et al., 2006), as previously discussed in detail (Knipper et al., 2015). Here, a dopamine-induced modification of $GABA_A$ receptor-mediated tonic inhibition may be considered (Crunelli and Di Giovanni, 2014).

Overall, it can be concluded that several events may contribute to the different physiological functions and firing-rate characteristics of auditory nerve fibers in the mature auditory system (i) IHC-driven synaptic events that mature during hearing onset, (ii) differences in cochlear IHC output activity through differential maturation of efferent feedback to auditory fibers, as well as (iii) differences in the genetic fate of SGNs. After hearing onset, fast auditory processing (**Box 1**) matures with high-SR auditory nerve fiber responses that determine the threshold of compound action potentials of the auditory nerve (Bourien et al., 2014) and are responsible for the shortest latencies seen in auditory responses at any given characteristic frequency, suggesting that they determine the perceptual thresholds (Meddis, 2006; Heil et al., 2008). The process of high-SR auditory nerve fiber maturation is thus likely related to the increased ABR wave amplitudes and their shortened latencies after hearing onset (∼P11) in rodents (e.g., Song et al., 2006) as well as to the sharpening of cortical receptive fields observed in rodents between the 2nd and 3rd postnatal week (Lendvai et al., 2000; de Villers-Sidani et al., 2007; Takesian et al., 2018).

The sharpening of cortical receptive fields, i.e., narrower bandwidth responses, occurs for all sensory cortices, including the auditory cortex (Xu et al., 2010) as a result of the stimulus-evoked release of BDNF from cortical pyramidal neurons (Itami et al., 2007; Hong et al., 2008; Xu et al., 2010; Lehmann et al., 2012; Griffen and Maffei, 2014; Kimura and Itami, 2019) (**Figures 1B,C**, BDNF ⇑). The released BDNF appears to drive the synaptogenesis of a complex network from peri-somatic and dendritic fast-spiking PV-INs that contact cortical pyramidal neurons (Hong et al., 2008; Xu et al., 2010; Lehmann et al., 2012) (**Figure 1C**, blue, orange arrows and inset). In accordance with this, between the 2nd to 3rd postnatal week, PV-IN staining levels increase in ascending auditory circuits and their cortical projections (Lohmann and Friauf, 1996), and inhibitory strength increases in microcircuits, as also observed in other sensory systems (Lohmann and Friauf, 1996; Itami et al., 2007; Xu et al., 2010; Lehmann et al., 2012; Kimura and Itami, 2019) (**Figure 1C**, inset perisomatic GABAergic contacts increase).

Important to mention here is that the overall process of maturation of fast auditory processing appears to be dispensable for basal hearing function. Thus, when BDNF was deleted in GABAergic precursor neurons in the brainstem of mice under the Pax2 promoter, and despite normal hearing thresholds based on measuring outer hair cell function, supra-threshold auditory nerve (ABR wave I) amplitudes remained low and the late ABR wave IV was delayed, indicating that fast auditory processing may have not matured properly (Zuccotti et al., 2012). As a result, profound deficits in precise auditory acuity occurred (Zuccotti et al., 2012; Chumak et al., 2016; Eckert et al., 2021), and was evident in the reduced dynamic range, elevated spontaneous firing rates (SFR), delayed first-spike latency, and reduced inhibitory strength in the dorsal cochlear nucleus and inferior colliculus (IC) (Chumak et al., 2016; Eckert et al., 2021). Under these conditions also, dendritic filopodia extensions of PV-IN positive interneurons were few in the auditory cortex and hippocampus in comparison to wild-type animals, despite PV-IN being normal in numbers (Eckert et al., 2021). This suggested that in rodents during the first postnatal weeks, the maturation of fast auditory processing (**Figure 1C**, high-SR in orange), the maturation of inhibitory strength in the ascending auditory pathway (Zuccotti et al., 2012; Chumak et al., 2016; Eckert et al., 2021) (**Figure 1C**, PV, orange arrows), and the stimulus-evoked release of BDNF from cortical pyramidal neurons (**Figure 1C**, inset, BDNF⇑) that drives the synaptogenesis of fast-spiking PV-IN microcircuits (Xu et al., 2010) are events that depend on experiencing sound.

To obtain an idea when this critical time period of maturation of inhibitory strength occurs in auditory and associated circuits in humans, we have to consider that the fast inhibitory PV-IN activity regulates not only higher cortical microcircuit functions (Griffen and Maffei, 2014; Kimura and Itami, 2019), but also feedforward and feedback inhibition (Hu et al., 2014, 2018) and its functional correlates, i.e., the gamma- and beta frequency oscillations (Cardin et al., 2009; Sohal et al., 2009; Gill and Grace, 2014; Chen et al., 2017). In children, increased gamma oscillations, associated with feedforward inhibition, occur at the age of less than 6 months, and are followed by increased beta oscillations, reflecting feedback inhibition (Sowell et al., 2001; Ortiz-Mantilla et al., 2016). At the same time, the latencies of the sound-induced auditory brainstem response (ABR) become shorter (Neville and Bavelier, 2002; Sharma et al., 2016). In parallel, functional brain connectivity increases from the 6th month of age onwards, when the neural activity becomes more clustered and specific for sensory modalities (Sowell et al., 2001; Neville and Bavelier, 2002; Ortiz-Mantilla et al., 2016) (**Figure 1B**, blue arrow). The clustering of sensory modalities, in turn, is accompanied by an enhanced comprehension of speech in noise (Obleser et al., 2007; Youssofzadeh et al., 2018), all progressing with a gradually improved capacity for auditory discrimination and temporal discrimination (Sowell et al., 2001; Fox et al., 2012; Miller and Buschman, 2013; Ankmnal Veeranna et al., 2019).

We thus conclude that auditory experience-dependent maturation processes of high-SR auditory nerve fibers in the auditory system are critical for the maturation of fast auditory processing, including the formation of activity-driven, fast inhibitory PV-IN microcircuits. Only then is the neuronal network implemented for a fine-grained resolution

of sound discrimination, temporally precise hearing, and fast discrimination of novel auditory information (**Figures 1B,C**).

ALTERED EXCITATION AND INHIBITION AFTER ACOUSTIC TRAUMA AND AGE-RELATED HEARING LOSS ARE LINKED TO INCREASED CENTRAL NEURAL GAIN

Numerous studies have indicated that acoustic trauma and age-dependent hearing loss are linked to reduced inhibition and enhanced excitation in ascending auditory circuits (Gerken, 1996; Milbrandt et al., 2000; Caspary et al., 2008; Wang et al., 2012; Ouda et al., 2015; Recanzone, 2018). Since low-SR auditory nerve fibers are vulnerable to noise damage and aging (**Figure 3**, low-SR in light green) (Heinz and Young, 2004; Heinz et al., 2005; Ruel et al., 2008; Kujawa and Liberman, 2009; Wang et al., 2012; Furman et al., 2013; Sergeyenko et al., 2013; Plack et al., 2014; Wu et al., 2019), deficits in this auditory nerve fiber type have been linked with temporal auditory discrimination deficits that follow acoustic trauma and age-related hearing loss in animals (Kujawa and Liberman, 2009; Plack et al., 2014; Wu et al., 2019) and humans (Liberman and Kujawa, 2017; Wu et al., 2019). Temporal auditory discimination deficits include those in spike timing and the synchronization of neural auditory responses that were shown to be required for following amplitude-modulated stimuli (Kuwada et al., 2002; Johnson et al., 2021). Auditory steady state responses are also an indicator for the proper processing of amplitude-modulated acoustic stimuli in subcortical areas and in the frontocentral cortex (Engelien et al., 2000). Previous studies indicated that during aging or after acoustic trauma, auditory response latencies can be shortened, and temporal coding, as measured through auditory steady state responses, enhanced (Möhrle et al., 2016; Eckert et al., 2021) when ABR wave IV is disproportionally elevated in response to a reduced ABR wave I (**Figure 3**, ABR wave in blue), a feature suggested to be linked to increased central neural gain (**Box 2**) (**Figure 3**, enhanced blue crosses).

In addition to low-SR auditory fiber processing sounds (Bharadwaj et al., 2015; Liberman, 2017), sustained fast (high-SR) auditory processing, is thus also critical for central neural gain and temporal auditory coding (Möhrle et al., 2017; Eckert et al., 2021). In line with this, computational models suggested that in response to deprived auditory input, the generation of sufficiently high discharge rates for centrally compensating homeostatic network changes may only work under conditions of preserved high-SR auditory nerve fibers (Schaette and Kempter, 2009). Diminished auditory input after acoustic trauma (**Figure 3**, crossed low-SR fibers contacting IHCs) has long been reported to possibly lead to a homeostatic network change and to an upregulation of neuronal responsiveness in central circuits (Salvi et al., 2000) (**Figure 3**, enhanced blue crosses). This homeostatic network change can be accompanied by a disproportional elevation of discharge rates as seen in the amplitude ratio of late ABR wave IV to early ABR wave I (**Figure 3**, ABR wave). Enhanced output relative to input in auditory neurons after acoustic trauma is suggested to be the result of disinhibition of neurons in the ventral or dorsal cochlear nucleus (Brigande and Heller, 2009; Cai S. et al., 2009; Schaette and Kempter, 2009; Schaette and McAlpine, 2011; Gu et al., 2012) or neurons of the IC (Gu et al., 2012; Heeringa and van Dijk, 2014). The subsequent hyperexcitability (**Figure 3**, high-SR in orange) spreads to the auditory cortex (Lu et al., 2011). The increased output of, e.g., CN neurons has been linked to steeper rate-level functions and a smaller dynamic range (Cai R. et al., 2009). As described for improved auditory perception, the process of accentuation of auditory stimuli that leads to central neural gain may require the co-activation of the basal forebrain to amplify stimulus-induced responses at subcortical and cortical levels (**Figure 3**, BasF blue downward arrow and cross) (Kilgard et al., 2002; Bajo et al., 2014; Kraus and White-Schwoch, 2015; Irvine, 2018a). Also, the activation of the inferior frontal gyrus (IFG), as part of the prefrontal cortex (PFC) (**Figure 3**, IFG), is crucial to retaining temporal and spatial associations of auditory events during auditory perception (Schonwiesner et al., 2007; Malmierca et al., 2014; Jafarpour et al., 2019). In general, the activation of PFC brain regions during perception is crucial to memorizing behaviorally relevant signals and increasing synaptic strength (Kraus and White-Schwoch, 2015; Weinberger, 2015; Irvine, 2018b). Particular and distinct medial (mPFC) and dorsolateral PFC (dlPFC) regions display crucial functions for basal inhibition of the hypothalamic-pituitary-adrenal (HPA) axis reactivity during central adjustment processes [review in Sullivan and Gratton (2002); Meltser and Canlon (2011), Canlon et al. (2013); de Kloet et al. (2014)de Kloet et al. (2019); Irvine (2018a), and Viho et al. (2019)]. Finally, in the auditory cortex, central neural gain control has been linked to feedforward inhibition, driven by the PV-IN, that spreads from the thalamus to the auditory cortex, eliciting amplified sound responses (Rabinowitz et al., 2012; Ji et al., 2016; Lohse et al., 2020; Pennington and David, 2020). The crucial role of PV-IN activation for central neural gain is emphasized through PV-IN potentiating drugs, which in the auditory cortex can trigger an enhanced signal-to-noise ratio (Deng et al., 2020). Optogenetic activation of PV-neurons, moreover, reduced spiking in the auditory cortex in general while enhancing functional connectivity (Hamilton et al., 2013). In the somatosensory and visual systems, an activation of PV-IN neurons is linked to enhanced stimulus-induced performance (Kim et al., 2016; Chen et al., 2017) that leads to enhanced response reliability, decreased signal variability, and improved reliability of signal information processing through an improved signal-to-noise ratio (Cardin et al., 2009; Sohal et al., 2009; Zhu et al., 2015) (**Figure 3**, Cortical resolution ⇑).

Evidence that the activity-dependent BDNF recruitment may be part of this homeostatic central neural gain process (**Figure 3**, BDNF ⇑) came from experiments using BDNF-Live-Exon-Visualization (BLEV) reporter mice, generated to monitor the activity-dependent usage of BDNF from exon IV and exon VI. In these mice, stimulus-induced changes in *Bdnf* transcripts can be seen in nerve endings, glia cells, and capillaries (Matt et al., 2018; Singer et al., 2018b). This is in line with observations of activity-driven *Bdnf* transcripts shown for

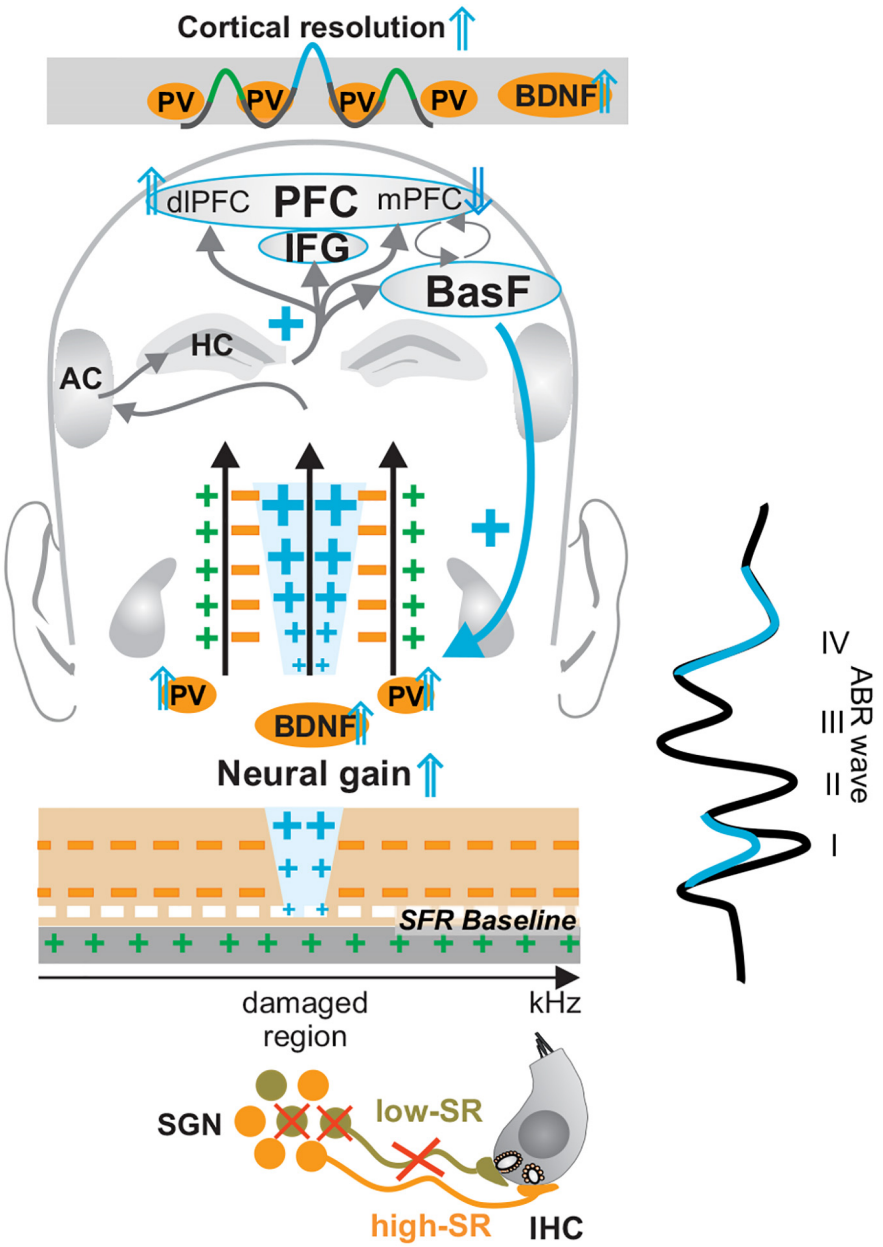

FIGURE 3 | Central neural gain mechanism following mild acoustic trauma and aging. When the numbers of low-SR auditory fibers (in light green) decline during aging or following auditory damage, a significantly enhanced output of central circuits (central compensation and enhanced blue crosses) may critically depend on the maintained activity of high-SR auditory fibers (in orange), to assure the generation of high discharge rates and central compensation of deprived auditory input (ABR wave in blue). During this process of central neural gain (blue crosses), a BDNF- and memory–dependent amplification process requires the activation of hippocampal circuits (upper blue cross), the activation of the basal forebrain (BasF), the balancing activation of dorsolateral, medial prefrontal cortex (dlPFC and mPFC) and specific PFC regions, such as the inferior frontal gyrus (IFG), to enhance auditory signals above noise levels (feedback mechanism, blue downward arrow and cross on the right side). Modified after Knipper et al. (2020). IHC, inner hair cell; SGN, spiral ganglion neuron; SFR, spontaneous firing rate; HC, hippocampus; IFG, inferior frontal gyrus; BasF, basal Forebrain; PFC, prefrontal cortex; dlPFC, dorsolateral PFC; mPFC, medial PFC; AC, auditory cortex; PV, parvalbumin.

platelets (Chacon-Fernandez et al., 2016), capillary endothelial cells (Donovan et al., 2000), microglia, and astrocytes (Ferrini and De Koninck, 2013; Parkhurst et al., 2013). In BLEV mice 2 weeks after 80 dB SPL exposure, both wave I (**Figure 4A**) and wave IV (Matt et al., 2018) were elevated (=sustained elevation), whereas through mild acoustic trauma using 100 dB SPL exposure, wave I (**Figure 4A**) was reduced and wave IV (Matt et al., 2018) was unchanged (=centrally compensated) [see differences in **Figures 4A,B**, in control, 80 and 100 dB, (Matt et al., 2018)]. This was linked to elevated *Bdnf* exon IV/VI transcript levels both in the brainstem (Matt et al., 2018) and hippocampal CA3 region (Matt et al., 2018) (**Figure 4C, yellow** and **cyan**),

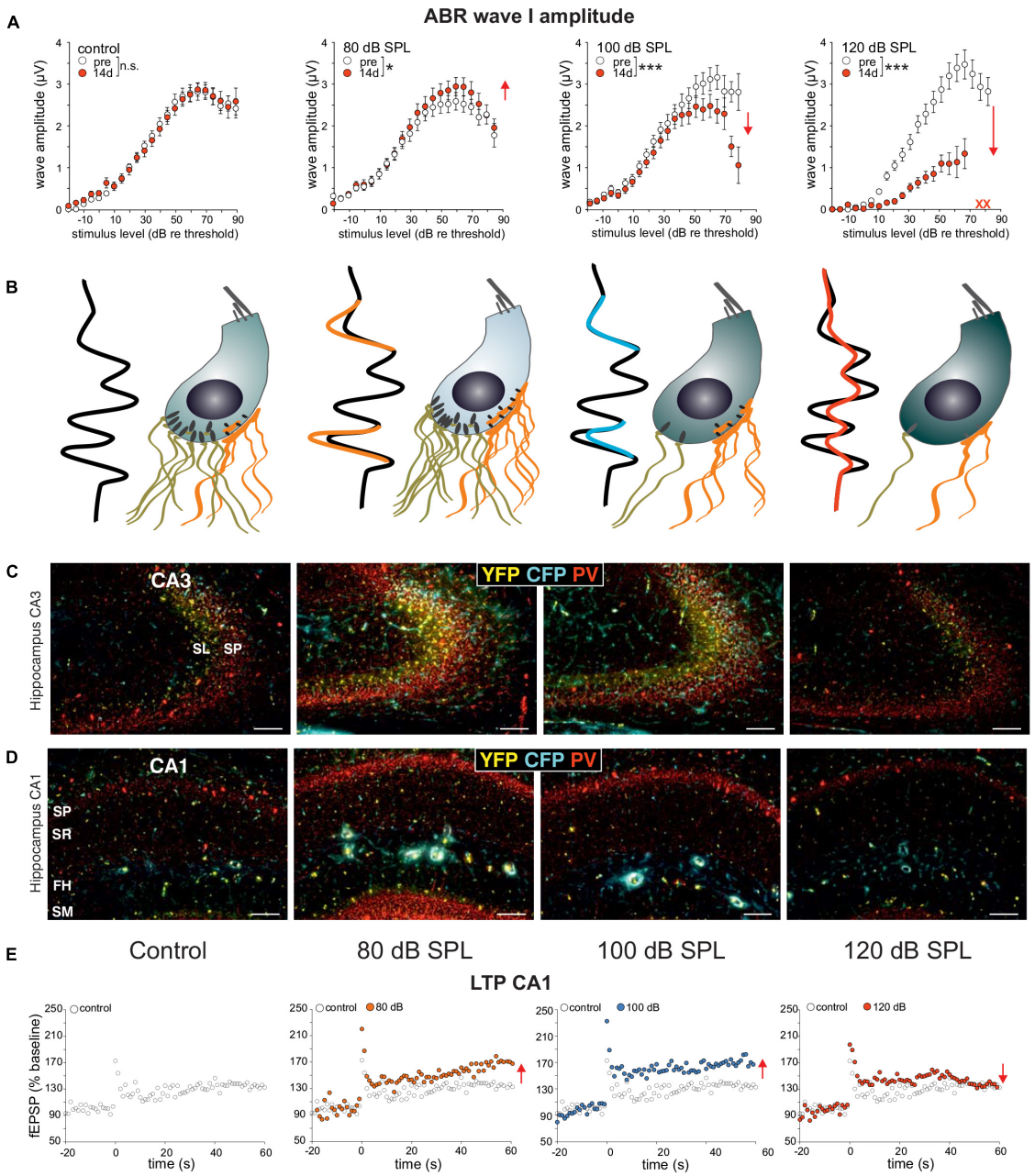

FIGURE 4 | (A) ABR wave I responses are enhanced after sound exposure of 80 dB SPL and reduced after 100 dB SPL stimulation which can be compensated on the level of the ABR wave IV (see **B**), while ABR wave I amplitudes decrease after 120 dB SPL exposure. **(B)** ABR wave I amplitude changes are linked to changes in IHC ribbons that are mostly preserved after sound enrichment (80 dB SPL), but decline following mild acoustic trauma (100 dB SPL). In contrast, following severe stressful acoustic trauma (120 dB SPL), ribbon loss exceeds 50%, pointing to a loss of high-SR auditory fibers. **(C,D)** This goes along with marked increases in PV (red), *Bdnf* exon IV transcripts in capillaries (cyan), and exon VI transcripts in nerve endings (yellow), as can be observed in hippocampal CA3 **(C)** and CA1 **(D)** regions following 80 and 100 dB SPL, but not following 120 dB SPL exposure (Matt et al., 2018). **(E)** Significantly increased LTP observed after 80 dB SPL and 100 dB SPL, but not after 120 dB SPL sound exposure compared to that of the controls. Scale bars in **(B,C)** indicate 100 µm. Modified after Matt et al. (2018). SP, stratum pyramidale; SR, stratum radiatum; FH, fissura hippocampi; SM, stratum moleculare; SL, stratum lucidum.

associated with enhanced *Bdnf* exon IV transcripts in capillaries in the stratum lucidum (**Figure 4C**, cyan in SL). Also, PV-IN levels in perisomatic localization in the CA1 region were enhanced (**Figure 4D**, red) and linked with reduced PV-IN levels in dendritic localization [not shown, (Matt et al., 2018)], which together led to elevated hippocampal LTP (**Figure 4E**). When BLEV mice were exposed to stressful acoustic trauma of 120 dB SPL, however, that led to critically diminished numbers of high-SR auditory nerve fibers (judged from IHCs ribbon loss exceeding >50%), persistently reduced ABR wave IV amplitudes

(Matt et al., 2018), failed recruitment of activity-dependent *Bdnf* transcripts, lowered hippocampal perisomatic PV-IN levels, and lower LTP levels were observed (**Figures 4C–E**, right panels) (Matt et al., 2018). This suggested that maintained fast (high-SR) auditory fiber processing is critical for central activity-dependent BDNF recruitment during homeostatic increased central neural gain. Particularly stressful acoustic trauma had, in previous studies, already been shown to lead to failed central neural gain that was linked to changes in hippocampal plasticity gene expression (Rüttiger et al., 2013; Singer et al., 2013; Matt et al., 2018).

Previous studies linked impaired *Bdnf* exon IV or VI transcripts with deficits in cognition and memory (Sakata et al., 2010; Vaghi et al., 2014; Mallei et al., 2015; Hill et al., 2016), together with deficits in cortical inhibition (Hong et al., 2008; Knipper et al., 2021), but this needs to be reconsidered in future studies with regard to deficiencies in the specific driving force for activating BDNF and inhibitory PV-IN activity.

ALTERED EXCITATION AND INHIBITION IN ACUTE ACOUSTIC TRAUMA, DEAFNESS, AND TINNITUS: LOST FAST AUDITORY PROCESSING

Hyperexcitability linked to reduced inhibition has also been observed in acquired deafness, congenital deafness, and tinnitus. The imbalance in excitation and inhibition in these auditory impairments is often interpreted as a compensatory response to auditory deprivation linked to increased central neural gain or an adaptive rewiring process. Here, we reconsider the imbalances of excitation/inhibition in these cases in the context of a loss of tonic inhibitory strength (**Box 3**), which can contribute to hearing disorders through decreased discharge population synchrony (enhanced variability) and a diminished signal-to-noise ratio following less developed or reduced fast (high-SR) auditory nerve fiber processing.

Lost Fast Auditory Processing Following Acquired Deafness, Acoustic Trauma, or Tinnitus

Imbalances in excitation and inhibition are observed in acquired deafness, which can be caused by cochlear damage, middle-ear ossicle removal, acoustic trauma, or drug-induced deafness (Kotak et al., 2013; Mowery et al., 2019). In previous studies, it was shown that acquired deafness in mature animals led to hyperexcitability that coincided with a decrease in GABA and glutamic acid decarboxylase (GAD65) (Bledsoe et al., 1995; Abbott et al., 1999). Acquired deafness was linked with enhanced glutamatergic transmission, as shown in the superior olivocochlear complex or the midbrain (Potashner et al., 1997), with reduced glycinergic inhibition (Suneja et al., 1998; Potashner et al., 2000) or with decreases in GAD65 (Milbrandt et al., 2000). For the adult gerbil IC, it was shown that after monaural deafening, increased excitation occurred very quickly (McAlpine et al., 1997), even within a few minutes of deafening of the contralateral ear (Mossop et al., 2000). This fast time scale argues against a rewiring process or compensating refinement as causes of the enhanced excitability (Mossop et al., 2000). The rapid occurrence of increased excitation after deafening (Mossop et al., 2000) pointed rather to faster events, such as an acute switch of the GABAergic responsiveness from inhibitory to depolarizing activity (see also Section "Maturation of GABA-Responsive Neurons Prior to Hearing Onset"). Not yet analyzed in the short-term, a re-emergence of depolarizing GABAergic signaling and decline of KCC2 has been observed 3–30 days after auditory nerve transection (Tighilet et al., 2016). In addition, a rapid decline of KCC2 and a re-emergence of depolarizing GABAergic signaling has been observed within minutes during pathological epileptic firing (Khirug et al., 2010; Lee et al., 2011; Nardou et al., 2011), a feature that may be noted in future studies in the context of sudden deafness. Previous studies reported that a majority of subjects with acquired, single-sided sudden deafness experienced tinnitus on the affected side (Lee et al., 2017). Also, in patients with normal maturation of the auditory pathway who experienced acquired sudden sensorineural hearing loss, tinnitus regularly occurs, with a prevalence of 60–90%, often on the deaf side (Van de Heyning et al., 2008; Chadha et al., 2009; Eggermont and Kral, 2016). Not surprising in this context, tinnitus-inducing acoustic trauma has been linked with hyper-excitability and disinhibition, as observed in the cochlear nucleus (Dehmel et al., 2012; Koehler and Shore, 2013; Auerbach et al., 2014; Gao et al., 2016), in the IC (Chen and Jastreboff, 1995; Bauer et al., 2008), in the medial geniculate body (MGB) (Kalappa et al., 2014), or in the auditory cortex (Norena and Farley, 2013; Eggermont and Tass, 2015). In the majority of tinnitus studies, the elevated spontaneous activity, or hyperexcitability and reduced inhibition, was discussed in the context of an increased central neural gain [see reviews: (Schaette and Kempter, 2006, 2012; Norena, 2011; Schaette and McAlpine, 2011; Auerbach et al., 2014; Sedley et al., 2016; Shore et al., 2016; Roberts, 2018; Roberts and Salvi, 2019].

Other studies showed that tinnitus is more linked to impaired homeostatic adjustment processes (Zeng, 2013; Knipper et al., 2015; Auerbach et al., 2019; Möhrle et al., 2019; Sedley, 2019) than to an increase in central neural gain [see for a review (Knipper et al., 2013, 2020, 2021; Zeng, 2020)]. This was first observed in rodent models of tinnitus (Rüttiger et al., 2013; Singer et al., 2013) and confirmed in patients (Hofmeier et al., 2018, 2021; Möhrle et al., 2019; Refat et al., 2021). In tinnitus patients, the delayed and reduced ABR wave V was shown to be accompanied by reduced blood-oxygen-level-dependent (BOLD) fMRI (functional Magnet Resonance Imaging) responses in the MGB, and in the primary auditory cortex and hippocampal regions (Hofmeier et al., 2018, 2021). It was speculated that a loss of fast auditory processing in the tinnitus frequency channels (**Figure 5**, crossed high-SR in orange) contributes through diminished tonic inhibitory strength (**Box 3**) of PV-IN (**Figure 5**, enhanced green crosses, reduced orange minus) to elevated response variability, reduced spike reliability and reduced signal-to-noise ratio (Zeng, 2020) in affected frequency regions (**Figure 5**, elevated SRF baseline red dashed line, enhanced green crosses). The relation of lost tonic inhibitory strength to reduced signal-to-noise ratio was, meanwhile, confirmed in numerous

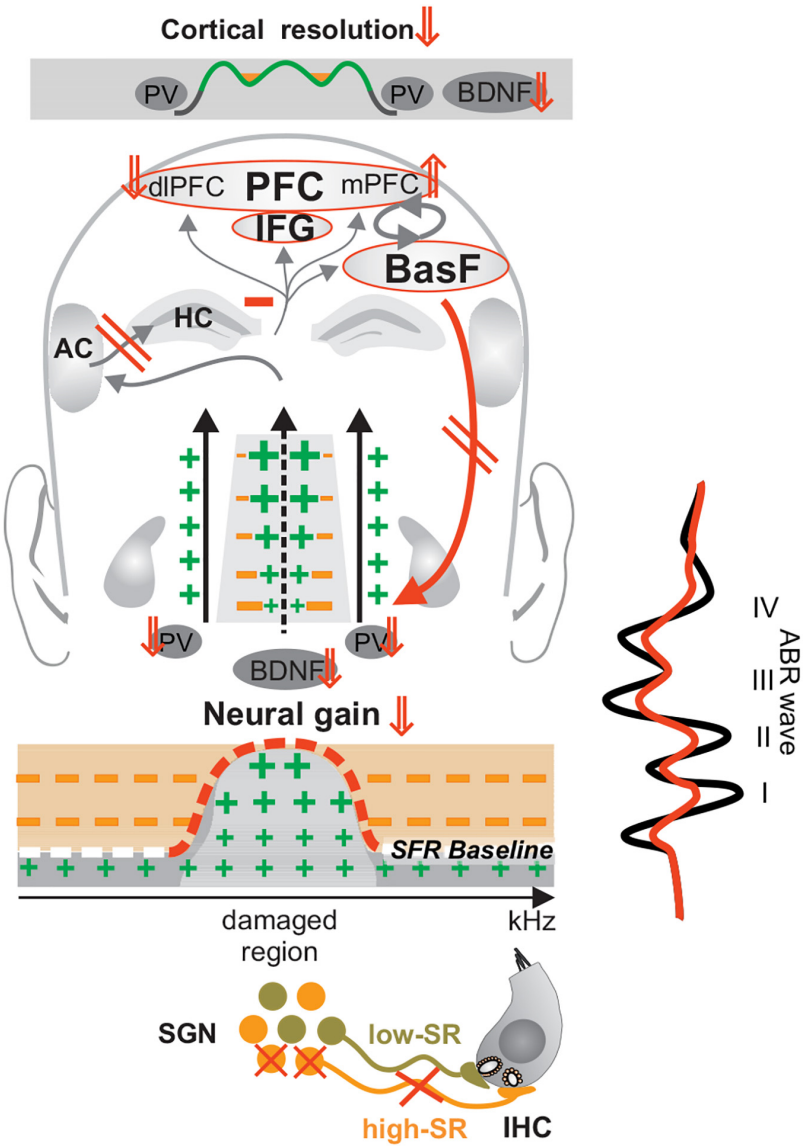

FIGURE 5 | Lost fast auditory processing following acquired deafness, trauma or tinnitus. A critical loss of high-SR fiber (orange fibers) firing may promote the re-emergence of hyperexcitability (enhanced green crosses) in affected frequency regions through the loss of tonic inhibitory PV-IN activity (reduced orange minus) subsequent to a decrease of recruitment of activity-dependent BDNF. The subsequent elevation of basal spontaneous firing rates suggests an unbalanced prefrontal stress control (mPFC⇑, dlPFC⇓, negative feedback mechanism, and red downward arrow), which may contribute to a lack of compensation of altered auditory input (red ABR wave), further alertness and distress to, e.g., manifestations of phantom noise. Modified after Knipper et al. (2020). IHC, inner hair cell; SGN, spiral ganglion neuron; SFR, spontaneous firing rate; HC, hippocampus; IFG, inferior frontal gyrus; BasF, basal Forebrain; PFC, prefrontal cortex; dlPFC, dorsolateral PFC; mPFC, medial PFC; AC, auditory cortex; PV, parvalbumin.

studies. Thus, e.g., optogenetic suppression of PV-IN activity, led to reduced task performance and reduced signal-to-noise ratio linked to increased baseline spontaneous gamma power and occlusion of changes in evoked gamma power (Chen et al., 2017). Also, a pharmacological PV-IN activation was previously shown to have the potential to diminish noise-induced tinnitus in animal studies (Deng et al., 2020). Moreover, reduced PV-density, but not somatostatin-positive interneurons density, in the primary auditory cortex was reported in tinnitus-perceiving animals (Masri et al., 2021). Regarding the tight correlation of BOLD to high-frequency gamma oscillations (Zumer et al., 2010; Butler et al., 2017), we thus speculate that the reduced and delayed ABR wave V and reduced BOLD fMRI responses in the auditory cortex observed in tinnitus patients (Hofmeier et al., 2018, 2021) may be the result of diminished tonic PV-IN strength, which through diminished discharge population synchrony, reduced spike reliability and enhanced spike variability (Cardin et al., 2009; Pi et al., 2013; Kim et al., 2016; Chen et al., 2017) may have contributed to an enhanced perception of internal noise (Knipper et al., 2020; Zeng, 2020).

If we question how, in the case of tinnitus, the internal noise can be heard as a disturbing sound, the observation becomes crucial that the tinnitus group exhibited not only reduced evoked fBOLD in the auditory cortex, but also elevated positive resting state connectivity (r-fcMRI) of default mode network activity, including the prefrontal cortex regions (PFC) (Hofmeier et al., 2018). In the tinnitus group, elevated r-fcMRI correlations were observed in the medial PFC (Hofmeier et al., 2018), a brain region said to be linked to stress excitation (McKlveen et al., 2013, 2016; Utevsky and Platt, 2014). This elevated r-fcMRI connectivity in mPFC correlated with the reduced sound-induced BOLD fMRI activity in the MGB (Hofmeier et al., 2018) and this reduced activity, in turn, correlated with increased latencies of the ABR wave V responses (Hofmeier et al., 2018) (**Figure 5**, mPFC⇑). Together, this points to an unbalanced extra-hypothalamic prefrontal (PFC) and hippocampal stress control (Sullivan and Gratton, 2002; Meltser and Canlon, 2011; Canlon et al., 2013; de Kloet, 2014; Irvine, 2018b; Viho et al., 2019). This unbalanced HPA stress control is suggested to contribute to further alertness and distress due to the phantom noise (Knipper et al., 2020, 2021).

Interesting in this context is that lower BDNF activation was previously associated with enhanced distress levels in tinnitus patients that suffered from BDNF Val^{66}Met polymorphism (Vanneste et al., 2018). Also, reduced activity-dependent BDNF recruitment, linked with impaired *glucocorticoid receptor* phosphorylation was shown to lead to impaired long-term memory retention and to deficits in forming postsynaptic dendritic spines, for example after motor-skill training (Arango-Lievano et al., 2019). This means that diminished fast auditory processing (**Figure 5**, crossed high-SR fibers in orange) in distinct affected frequency regions could, through reduced activity-dependent BDNF (**Figure 5**, BDNF ⇓), lead to diminished PV-IN inhibitory strength (**Figure 4**, PV ⇓) and subsequent elevated SFR (**Figure 5**, SFR ⇑, red dashed line). The reduced activity-dependent BDNF recruitment in frontal brain regions would further diminish hippocampal responsiveness and diminish extra-hypothalamic prefrontal (PFC)/hippocampal stress control, and thus enhance alertness to the 'brain noise.' A previously suggested negative feedback of stress-receptor activation particular to fast auditory nerve response vulnerability (Singer et al., 2013, 2018a) (**Figure 4**) would accelerate the self-reinforcing downward spiral towards the increased stress and anxiety of tinnitus patients. Distress is, meanwhile, the best predictor of tinnitus severity, and a stronger predictor for tinnitus than any demographic factors (Crönlein et al., 2016; Beukes et al., 2021).

Failed Maturation of Fast Auditory Processing Following Congenital Deafness

Numerous studies have analyzed hearing loss prior to hearing onset induced by kainate injection or ossicle destruction. Inhibitory neuronal markers were significantly diminished (Milbrandt et al., 2000; Mossop et al., 2000), whereas the excitability of various ascending central auditory neurons was significantly increased (Nordeen et al., 1983; Kitzes, 1984; Kitzes and Semple, 1985; Popelar et al., 1994). Also, cochlear ablation prior to hearing onset (Sanes et al., 1992) or deafness in the *deafness* (*dn/dn*) mutant mouse (Oleskevich and Walmsley, 2002) led to larger EPSP amplitudes and lower inhibitory synaptic strength. This phenomenon was observed in the cochlear nucleus (Oleskevich and Walmsley, 2002), in the lateral lemniscus, and in IC neurons (Sanes et al., 1992), as well as in thalamocortical and intracortical primary auditory cortex neurons (Kotak et al., 2005, 2013; Mowery et al., 2019). It was suggested that the larger EPSP amplitudes in congenital deafness may result from an increase in AMPA- and non-NMDA receptors and a decrease in inhibitory postsynaptic potential conductance. In another deaf *Vglut3*$^{-/-}$ animal model, where glutamate release from IHCs is abolished due to deletion of vesicular glutamate transporter 3 (VGlut3) (Seal et al., 2008), elevated spontaneous activity, with longer bursts and smaller spikes, was recorded from cochlear (Babola et al., 2018; Sun et al., 2018) and from IC neurons (Babola et al., 2018). Since an enhanced excitability was seen in the IC neurons of VGlut3$^{-/-}$ mice, even when the auditory cortex neurons were ablated, a top-down modulatory effect as the source for the enhanced central excitability could be excluded (Babola et al., 2018). In general, in these different cases of congenital deafness, the enhanced excitability in the ascending pathway were interpreted as an adaptive response to auditory deprivation (Babola et al., 2018) as a result of central rewiring (Nordeen et al., 1983; Moore, 1994), or as a compensatory response to the absence of synaptic activity (Davis and Bezprozvanny, 2001; Oleskevich and Walmsley, 2002) due to maladaptive central synaptic refinement (Ortmann et al., 2011). We propose that the enhanced excitability in the ascending auditory pathway in congenital deafness is neither the result of a long-term wiring process nor a compensatory response to the absence of central synaptic refinement, but rather may reflect inappropriate inhibitory shaping of auditory nerve fibers through efferent feedback control, possibly contributing to a failed switching of GABA-responsive neurons from depolarizing to hyperpolarizing activity prior to the onset of hearing (Lohrke et al., 2005) (**Figure 6**, see also Section "Maturation of GABA-Responsive Neurons Prior to Hearing Onset"). It may also indicate a failure of a proper maturation of fast (high-SR) auditory processing in the absence of auditory experience.

For congenital deafness in humans, this would inspire the question about a critical time period for the restoration of hearing through cochlear implants (CI); i.e., if not restored early enough, do the relevant auditory brain circuits remain in a stage of insufficient inhibitory strengths that hampers precise sharpening of receptive fields and proper inhibitory strength in the fine-grained microcircuits required for speech discrimination and temporal coding (Oxenham, 2018; Kral et al., 2019; Thompson et al., 2021)? The immediate onset of tinnitus that occurred in 60–90% of cases in children with cochlear implants when the implants were not in use (Van de Heyning et al., 2008; Chadha et al., 2009), may indicate that constant electrical stimulation through CIs is required to suppress 'internal noise' and to 'silence' phantom noise (Knipper et al., 2020). Recalling, moreover, that CIs in children are implanted on average at the age of 1–2 years (Peterson and Bergeson, 2015; Easwar et al., 2017), postponing

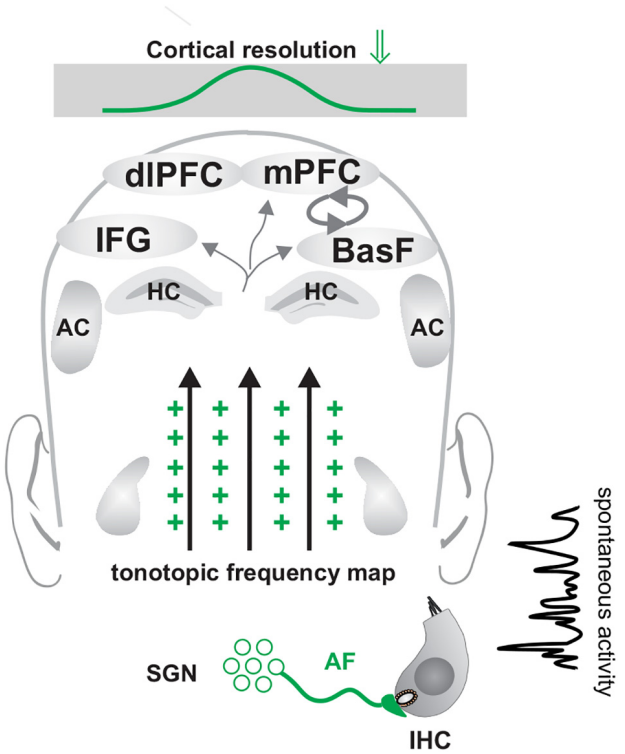

FIGURE 6 | Enhanced excitability in the ascending auditory pathway (green crosses) in congenital deafness may reflect the maturational stage of the initial hyperexcitability (green crosses) in the ascending auditory pathway, when spontaneous firing dominates and fast (high-SR) auditory processing has not yet matured. During that time period, GABA-responsive neurons respond with depolarizing instead of hyperpolarizing activity. Modified after Knipper et al. (2020). IHC, inner hair cell; SGN, spiral ganglion neuron; HC, hippocampus; IFG, inferior frontal gyrus; BasF, basal Forebrain; PFC, prefrontal cortex; dlPFC, dorsolateral PFC; mPFC, medial PFC; AC, auditory cortex.

the first auditory experience in these CI-carriers by 1–1.5 years (Sharma et al., 2002; Petersen et al., 2015) might induce a delay that is too long for some maturation steps. A judgment about a critical delay of auditory experience for proper implementation of distinct developmental steps may be assessed by looking at the prevailing deficits described in congenitally deaf CI-carriers. Deficits in CI-carriers include a reduction in binaural sound localization (Hamalainen et al., 2011; Lazard et al., 2012; Petersen et al., 2013; Slugocki and Trainor, 2014), missing left-hemisphere dominance (Petersen et al., 2013; Peterson and Bergeson, 2015; Easwar et al., 2017), weaker pitch sensitivity (Houtsma and Smurzynski, 1990; Kaernbach and Bering, 2001), lower dynamic range and higher thresholds (Sharma et al., 2002; Deroche et al., 2014), as well as lower mismatch negativity amplitudes, and prolonged CI-evoked cortical auditory evoked potential latencies (Ponton and Eggermont, 2001; Sharma et al., 2002).

To date, the latency of the auditory cortical component P_1, which is used as an objective measure of developmental hearing experience (Sharma et al., 2005a,b), were reported to be shorter in early-implanted deaf children as compared to late-implanted children (Sharma et al., 2005a). This already points to a critical time window of CI implantation to achieve temporal precise hearing. The less variable performance, the reduced expansion of activated areas at the primary auditory cortex, and less exuberant connections between the visual cortex and auditory cortex in early- versus late-implanted congenitally deaf cats (Lomber et al., 2010; Land et al., 2016; Kral et al., 2019) point to critical time windows for CI implantation. In such cases, a possibly immature stage of cortical inhibitory shaping with incompletely accomplished clustering and pattern segregation of auditory-specific modalities may be considered.

It is likely that documented deficits in CI-carriers, such as in latency shift, sound localization, or pitch sensitivity, may critically depend on fast auditory processing and possibly on proper high-SR auditory fiber processing. Even missing left hemisphere dominance (Petersen et al., 2013; Peterson and Bergeson, 2015; Easwar et al., 2017) may be related to the strong impact that neuronal activity and sensory experience is predicted to have on the proliferation and differentiation of oligodendrocytes during myelination (Xin and Chan, 2020). Keeping this in mind, there is a distinct need for the influence of fast (high-SR) auditory processing on myelination progress to be urgently tested in future studies. In the course of hearing restoration through successful implementation of CIs or hearing aids, attempts should be made to monitor the implementation of proper inhibitory strength.

ALTERED EXCITATION AND INHIBITION FOLLOWING DIMINISHED FAST AUDITORY PROCESSING LINKED TO 'CENTRAL' HEARING LOSS

Failed Fast Auditory Processing in Autism Spectrum Disorders

An excitation/inhibition imbalance is also considered to be a characteristic feature of ASD, which is accompanied by reduced PV-IN labeling (Takano and Matsui, 2015; Pirone et al., 2018; Goel et al., 2019), elevated levels of the activity-related gene Arg3.1/Arc (Korb and Finkbeiner, 2011; Goel et al., 2019; Eckert et al., 2021), or by increased fEPSPs (Mohn et al., 2014). A reduced inhibition linked with reduced levels of GABA-synthetisising enzymes and GABA receptors was observed in the brain of patients with ASD (Fatemi et al., 2002, 2009, 2010; Reynell and Harris, 2013; Schur et al., 2016; Cukier et al., 2020). In autism patients and animal models, the reduced inhibition is said to reduce reliability (increasing variability) of signal transformation and the signal-to-noise ratio (Dinstein et al., 2012; Haigh et al., 2016). Interestingly, deficits in fast auditory processing are also reported in nearly normal-hearing children that have ASD (Fitch et al., 2013; Foss-Feig et al., 2017), and here, deficits in fast auditory processing are linked to markedly delayed and displaced auditory steady-state responses (Stroganova et al., 2020), or with rapid spectral-ripple discrimination deficits (Ankmnal Veeranna et al., 2019).

A previous study in a mouse model with a cell-specific deletion of *Bdnf* in Pax2 positive GABAergic precursor cells

(*Bdnf*^{Pax2}KOs mice) showed an autism-like phenotype (Eckert et al., 2021). These mice exhibited normal basal hearing function, but with reduced and delayed ABR wave IV, diminished PV-IN labeling in the auditory cortex and hippocampus, and with reduced tonic inhibitory strength and elevated spontaneous firing rates in dorsal cochlear nucleus (Eckert et al., 2021) and IC neurons (Chumak et al., 2016). These features were associated with a reduced (sound)-induced LTP/LTD adjustment, impaired learning, deficits in social behavior, and enhanced anxiety and stress levels (Eckert et al., 2021). This phenotype thus pointed to a diminished extra-hypothalamic stress control (de Kloet et al., 2019). Impaired PV-IN mediated inhibitory shaping of auditory and hippocampal circuits, as observed in *Bdnf*^{Pax2}KOs, was moreover suggested to lead to impaired central neural gain after sound enrichment, deficits in LTD, and pathologically increased activity-related gene Arc expression (Eckert et al., 2021). Proper LTD and balanced Arc expression levels are crucial for the control of fast changes in AMPA receptor trafficking during novelty discrimination (Derkach et al., 2007; Waung et al., 2008; Blair et al., 2019; Penrod et al., 2019; Roth et al., 2020).

This finding emphasizes that deficits in fast auditory processing, leading to diminished tonic inhibitory strength, can impair central neural gain and affect not only temporal coding but also cognitive functions, including novelty discrimination tasks and learning.

Deficits in fast auditory processing may be uniquely critical in the auditory system, which in comparison to other senses relies particularly on narrow time windows and a high speed of information flow (Zajac and Nettelbeck, 2018). To further validate a causal relationship between failed maturation of fast auditory processing and the autism phenotype, it will be necessary to explore in more detail the fine-structure of ABR and auditory steady-state responses, in combination with functional electroencephalography (EEG), and fMRI in animal models and children with autism-spectrum disorders.

Failed Fast Auditory Processing During Age-Dependent 'Central' Hearing Loss

A link between deficits in fast auditory processing and age-related deficits in cognition has previously been proposed. Thus, studies analyzing aging animals showed that, independently of age or hearing thresholds, animals fell into two groups regarding central auditory responses to cochlear synaptopathy: The 'high-compensating' group was able to respond to cochlear synaptopathy with an enhanced input/output function (elevated ABR wave IV/I ratio), linked with enhanced LTP and maintained temporal processing (Eckert et al., 2021) (**Figure 7A**, left panel). The other, the 'low-compensating' group, exhibited weakened compensatory capacity (lower ABR wave IV/I ratio), linked with lower LTP, and weakened temporal coding (Marchetta et al., 2020) (**Figure 7B**, right panel). The reduced capacity to centrally compensate age-dependent cochlear synaptopathy, and the lower hippocampal LTP with attenuated temporal coding, was associated with a prolonged latency of the auditory nerve response (ABR wave I) in comparison to the high-compensating group (Marchetta et al., 2020), suggesting that fast (high-SR) auditory processing was mitigated in this group. In the 'low-compensating group,' moreover, lower levels of *Bdnf* IV and VI transcripts were seen in hippocampal nerve terminals and capillaries in comparison to the high-compensating group, (**Figures 7C,D**, compare yellow and cyan staining). Although differences in auditory response latencies, auditory neural responses to modulated tones, and LTP may point to differences in inhibitory strength following differential impairment of fast auditory fiber processing (Marchetta et al., 2020), experimental evidence for this is currently missing. Reduced GABAergic activity was, however, previously observed in ascending auditory circuits, e.g., during aging, a phenomenon that was hypothesized to be linked to cognitive decline (Ibrahim and Llano, 2019; Pal et al., 2019; Rogalla and Hildebrandt, 2020). In these cases also, it may be useful to consider deficits in fast auditory processing as being causally related to age-dependent hearing loss that is associated with cognitive deficits.

COUPLING OF INHIBITORY/EXCITATORY CIRCUIT ACTIVATION TO CEREBRAL BLOOD FLOW

The Role of GABAergic Activity for Neurovascular Coupling

In questioning whether reduced tonic inhibitory strength following fast auditory processing may be particularly critical for cognition, as predicted from autism animal models (see Section "Failed Fast Auditory Processing in Autism Spectrum Disorders"), the critical time period of maturation of fast auditory processing and inhibitory strength in auditory and associated limbic circuits - between the 2nd and 3rd postnatal week in rodents (Itami et al., 2007; Eckert et al., 2021) needs to be reconsidered. In rodents, this time period overlaps with the time of progressively faster BOLD signals, in which brain regions manifest an increased intensity in response to sensory stimulation (Colonnese et al., 2008). Thus, before P11 in rodents (prior to hearing onset), brain activation is not associated with sustained increases of the cerebral blood flow (CBF), which would result in none or a negative BOLD signal (Colonnese et al., 2008; Kozberg et al., 2013; Iadecola, 2017). Only in the 2nd and 3rd week does neural activity lead to increasingly faster and more intense hemodynamic responses, as shown by BOLD fMRI (Colonnese et al., 2008; Iadecola, 2017). The increased hemodynamic BOLD fMRI response during this critical time period is linked with pronounced neurovascular and systemic changes, including increases in vascular density, synaptogenesis, energy metabolism, and sensitivity of the cerebral microcirculation to vasoactive stimuli (Nehlig et al., 1989; Colonnese et al., 2008; Goyal et al., 2014; Engl et al., 2017; Iadecola, 2017). The time of increased hemodynamic BOLD fMRI responses is also the time when in rodents, long-term potentiation in the hippocampus gradually matures (Ostrovskaya et al., 2020).

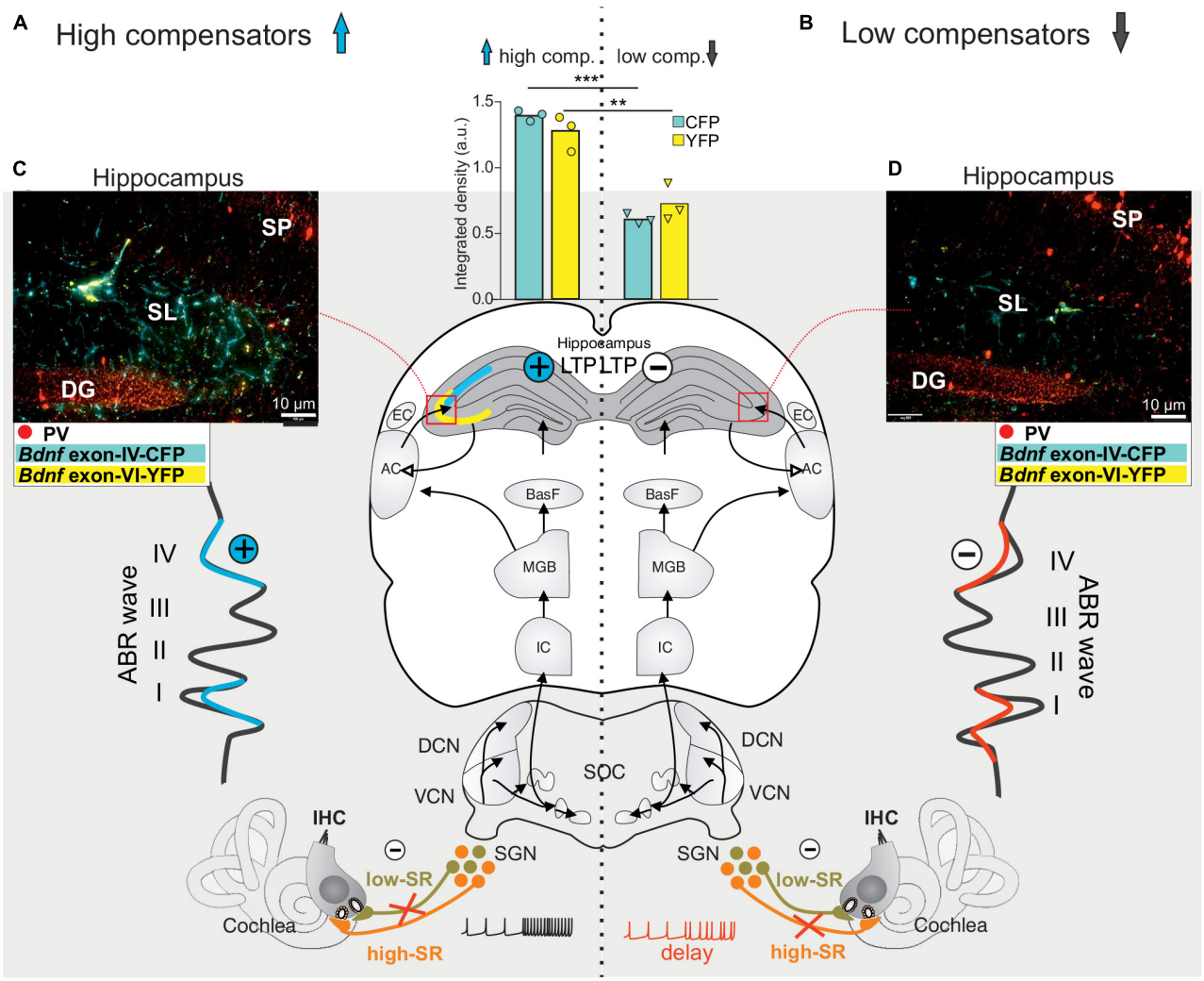

FIGURE 7 | Schematic presentation of high and low central compensatory mechanisms in the aging auditory system. **(A)** Independent of aging or differences in hearing thresholds, cochlear synaptopathy can differ, depending on whether de-afferentation due to low-SR auditory nerve fiber loss dominates (**A**, low-SR in light green) or high-SR auditory nerve fiber loss dominates (**B**, high-SR in orange). In the first case, an ABR wave I reduction is associated with disproportionally increased ABR wave IV amplitude (**A**, left blue amplitude, plus in blue circle), with elevated *Bdnf* exon IV (cyan) and exon VI (yellow) expression in hippocampal circuits (**C**, left panel and bar graph) and higher hippocampal LTP (plus in blue circle). In the case of a critical loss of fast (high-SR) auditory nerve fiber processing (**B**, high-SR in orange), an attenuated temporal resolution capacity of auditory nerve fibers (**B**, delay) is associated with permanently decreased ABR wave IV amplitude (**B**, red amplitude, minus in white circle), decreased recruitment of hippocampal *Bdnf* exon IV and exon VI transcripts (**D**, right panel and bar graph) and significantly lower LTP mobilization (minus in white circle). ABR, auditory brainstem response; IHC, inner hair cell; VCN, ventral cochlear nucleus; DCN, dorsal cochlear nucleus; SOC, superior olivary complex; IC, inferior colliculus; MGB, medial geniculate body; BasF, basal Forebrain; AC, auditory cortex; EC, entorhinal cortex; PV, parvalbumin.

We questioned whether the maturation of fast (high-SR) auditory processing, of inhibitory PV-IN microcircuits, of hemodynamic BOLD fMRI responses, and of LTP may not only be correlated in time, but also functionally. More precisely, we asked whether the imbalances in excitation and inhibition in hearing disorders that correlated with reduced tonic inhibitory strength, as predicted in the case of impaired fast auditory nerve fiber responses (Chumak et al., 2016; Eckert et al., 2021), might also have implications for hemodynamic responses.

This hypothesis is based on new insights into the mechanism of hemodynamic responses: Previously, glutamatergic neuronal activity was assumed to mainly trigger hemodynamic responses and vasodilation during a bilateral homeostatic response: Glutamatergic neuronal activity, such as neural feedforward signaling, includes neuronal-derived nitric oxide (NO) release from the glutamatergic synapses that causes a metabolic feedback signal in smooth muscle cells of parenchymal arterioles, finally leading to vasodilation [for a review see Attwell et al. (2010); Kisler et al. (2017); Ledo et al. (2021)]. Newer findings, however, suggest that arteriole vasodilation may possibly occur independently of NO (Chow et al., 2020). In line with this, neurovascular coupling is preserved in mice lacking endothelial NO synthase (Girouard et al., 2007). Also, a release of NO from GABAergic interneurons was shown to affect the hemodynamic

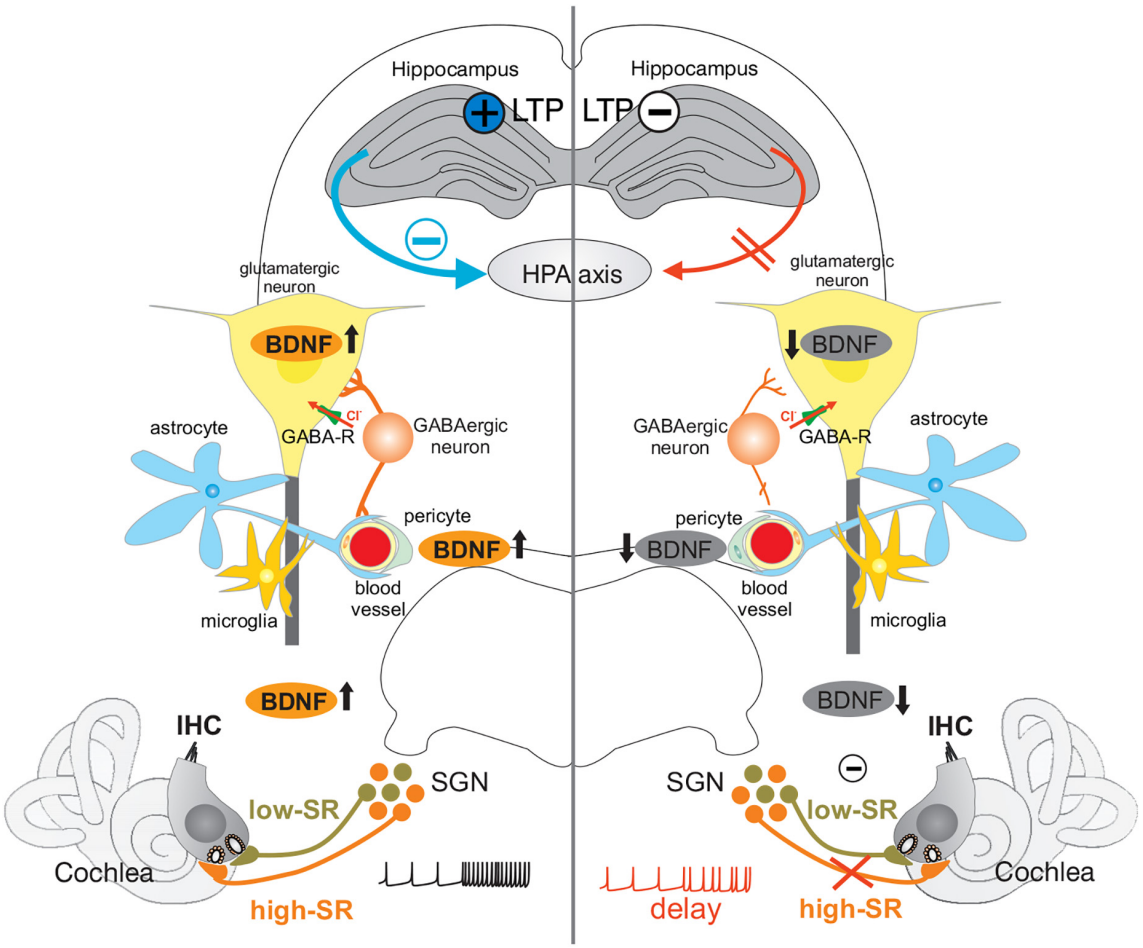

FIGURE 8 | Under healthy conditions **(Left)**, fast auditory processing (high-SR in orange) enables context-specific information processing in auditory and associated circuits (hippocampus, HPA axis) through upregulation of activity-dependent BDNF (↑). Increased central neural gain, represented by increased hippocampal LTP (black cross in blue circle), allows the facilitation of BDNF/PV-IN circuits by BDNF ↑ in glutamatergic neurons, and an increase in perisomatic inhibitory strength (GABAergic neuron contacting glutamatergic neuron) dependent on increased stimulus responses. These in turn provide a balanced HPA axis control (blue arrow and minus) and local hemodynamic supply (blood vessels) for a long-lasting improved signal-to-noise ratio and stimulus discrimination above noise (black spike train). During aging, or following acoustic trauma, acute, or congenital deafness **(Right)**, a critical loss of high-SR auditory nerve fibers (orange) occurs, leading to reduced auditory driving force and BDNF expression (↓). This is associated with reduced hippocampal LTP (black minus in white circle), reduced tonic-PV-IN strength (reduced synaptic contacts of GABAergic neurons on glutamatergic neurons), altered extra-hypothalamic stress control (red arrow to HPA axis), and possibly disturbed coupling of inhibitory neuronal activity to hemodynamic responses, leading to altered sound processing (red spike train). IHC, inner hair cell; SGN, spiral ganglion neuron; GABA-R, GABA receptor; HPA axis, hypothalamic-pituitary-adrenal axis; LTP, long-term potentiation; BDNF, brain-derived neurotrophic factor.

responses through the nitric-oxide sensitive guanylyl cyclase (NOsGC) pathway (Cauli et al., 2004; Kocharyan et al., 2008; Lee et al., 2020). These observations were corroborated by experiments employing an optogenetic activation of GABAergic interneurons, which provoked a significant increase in the CBF (Uhlirova et al., 2016; Iadecola, 2017; Vazquez et al., 2018). Also, optogenetic activation of GABAergic interneurons increased CBF even when glutamatergic GABAergic activity was pharmacologically blocked (Anenberg et al., 2015). Fast PV-IN are decisive in generating gamma-oscillations, as measured with EEG in combination with optogenetic techniques to stimulate PV-INs (Cardin et al., 2009; Sohal et al., 2009; Chen et al., 2017). Thus previous studies that found a significantly reduced gamma activity following stress events that lead to impaired neurovascular coupling (Sohal et al., 2009; Lee et al., 2015; Chen et al., 2017; Han et al., 2019) would also support the involvement of PV-IN GABAergic signaling on CBF. Interestingly, in this case, reduced GABAergic activity after stress occurred in nNOS-positive interneurons (Czeh et al., 2015, 2018; Csabai et al., 2018; Han et al., 2019), underscoring PV-IN activity as possibly contributing to NO-induced vasodilation.

The contradicting assumptions, that on the one hand NO-release from GABA-IN may influence endothelia cells of blood vessels, and thereby change their diameter (Lee et al., 2020), while on the other hand arteriole vasodilation is suggested to occur independently of NO (Chow et al., 2020), may moreover find a rational solution through suggestions that put capillary dilation in the focus of hemodynamic responses, rather than

smooth-muscle-cell arteriole dilation. Thus, capillary flow was recently suggested not to be a passive consequence of the flow in upstream smooth muscle-unsheathed arterioles, but vice versa; capillary dilation may be a primary event preceding arteriole dilatation (Kisler et al., 2017). In this scenario, capillary dilation would occur as a result of the relaxation of pericytes, and this local dilation would spread from capillaries toward larger arterioles in a secondary step (Hall et al., 2014; Lendahl et al., 2019; Han et al., 2020). A crucial role of pericytes for capillary vasodilation during hemodynamic responses has been shown in numerous previous studies (Lourenco et al., 2014; Sweeney-Reed et al., 2016; Caporarello et al., 2019; Alarcon-Martinez et al., 2020), although others failed to demonstrate this (Fernandez-Klett et al., 2010; Hill et al., 2015; Wei et al., 2016; Cudmore et al., 2017; Iadecola, 2017). On the other hand, pericytes have been shown to express NO-responsive enzymes (Friebe et al., 2018). Also, a pericyte-induced role for vasodilation through capillaries would become feasible, since the large surface area of capillaries and minimal changes in their diameter would produce a large change in blood flow (Han et al., 2020).

It is thus challenging to consider that the increase in PV-IN mediated inhibitory strength between the 2nd and 3rd postnatal week (Itami et al., 2007; Eckert et al., 2021) and the coinciding progressive changes in shape and intensity of BOLD signals (Colonnese et al., 2008) are functionally related events. While all these findings may support the notion that PV-IN have a potential to modulate CBF, evidence for their participation in neurovascular coupling to physiological stimuli is still limited. We may, however, conclude that, in addition to glutamatergic neuronal activity influences on vasodilation (Attwell et al., 2010; Kisler et al., 2017; Ledo et al., 2021), PV-IN GABAergic activity may play a role in hemodynamic responses.

CONCLUSION

During aging or following acoustic trauma, acute or congenital deafness, a critical diminution of fast (high-SR) auditory driving force diminishes activity-dependent BDNF activities and tonic-PV-IN strength, hippocampal LTP, extra-hypothalamic stress control and possibly proper coupling of inhibitory neuronal activity to hemodynamic responses, accelerating a negative feedback cycle (**Figure 8**, right side). Under healthy conditions (**Figure 8**, left side), when critical fast auditory processing is maintained, context-specific information through specific activation of BDNF signaling in auditory and associated circuits, allow, through increased central neural gain, the facilitation of BDNF/PV-IN dependent increase stimulus responses that in turn guarantee a balanced HPA axis control and local hemodynamic supply for a long-lasting improved signal–to-noise ratio and stimulus discrimination above noise.

In view of the increasing evidence of a link between hearing loss and dementia, a better understanding of this possible relationship is an important challenge (Livingston et al., 2017; Griffiths et al., 2020; Montero-Odasso et al., 2020). We suggest here that a differential role of auditory fiber processing for specific imbalances in excitation/inhibition can be regarded as a key signature of hearing disorders with or without cognitive decline.

AUTHOR CONTRIBUTIONS

MK designed, wrote, and revised the manuscript. WS wrote the manuscript and made the figures. KS, GEH, LR, CB, and RL wrote and revised the manuscript. YLH wrote the figure legends and helped writing the manuscript. All authors contributed to the article and approved the submitted version.

FUNDING

This work was funded by the Deutsche Forschungsgemeinschaft (DFG, German Research Foundation) – Project number 335549539/GRK2381, FOR 2060 project RU 713/3-2 (WS and LR), SPP 1608 RU 316/12-1 (LR), KN 316/12-1 (MK). MK and LR are members of the Research Training Group [grant number 335549539/GRK 2381] "cGMP: From Bedside to Bench". This work was also supported by the Deutsche Forschungsgemeinschaft (Cluster of Excellence 2177 "Hearing4all" Project number 390895286) (RL and KS), EU-LACH Grant #16/T01-0118 and "Computational Neuroimaging of the human Brainstem at 9.4 Tesla" (BMBF #01GQ1805B) (GEH).

ACKNOWLEDGMENTS

English language services were provided by stels-ol.de.

REFERENCES

Abbott, S. D., Hughes, L. F., Bauer, C. A., Salvi, R., and Caspary, D. M. (1999). Detection of glutamate decarboxylase isoforms in rat inferior colliculus following acoustic exposure. *Neuroscience* 93, 1375–1381. doi: 10.1016/s0306-4522(99)00300-0

Addleman, D. A., and Jiang, Y. V. (2019). Experience-Driven Auditory Attention. *Trends Cognit. Sci.* 23, 927–937. doi: 10.1016/j.tics.2019.08.002

Aid, T., Kazantseva, A., Piirsoo, M., Palm, K., and Timmusk, T. (2007). Mouse and rat BDNF gene structure and expression revisited. *J. Neurosci. Res.* 85, 525–535. doi: 10.1002/jnr.21139

Alarcon-Martinez, L., Villafranca-Baughman, D., Quintero, H., Kacerovsky, J. B., Dotigny, F., Murai, K. K., et al. (2020). Interpericyte tunnelling nanotubes regulate neurovascular coupling. *Nature* 585, 91–95. doi: 10.1038/s41586-020-2589-x

Anenberg, E., Chan, A. W., Xie, Y., LeDue, J. M., and Murphy, T. H. (2015). Optogenetic stimulation of GABA neurons can decrease local neuronal activity while increasing cortical blood flow. *J. Cereb. Blood Flow Metab.* 35, 1579–1586. doi: 10.1038/jcbfm.2015.140

Ankmnal Veeranna, S., Allan, C., Macpherson, E., and Allen, P. (2019). Spectral ripple discrimination in children with auditory processing disorder. *Int. J. Audiol.* 58, 733–737. doi: 10.1080/14992027.2019.1627007

Arango-Lievano, M., Borie, A. M., Dromard, Y., Murat, M., Desarmenien, M. G., Garabedian, M. J., et al. (2019). Persistence of learning-induced synapses depends on neurotrophic priming of glucocorticoid receptors. *Proc. Natl. Acad. Sci. U S A.* 116, 13097–13106. doi: 10.1073/pnas.1903203116

Attwell, D., Buchan, A. M., Charpak, S., Lauritzen, M., Macvicar, B. A., and Newman, E. A. (2010). Glial and neuronal control of brain blood flow. *Nature* 468, 232–243. doi: 10.1038/nature09613

Auerbach, B. D., Radziwon, K., and Salvi, R. (2019). Testing the Central Gain Model: Loudness Growth Correlates with Central Auditory Gain Enhancement in a Rodent Model of Hyperacusis. *Neuroscience* 407, 93–107. doi: 10.1016/j.neuroscience.2018.09.036

Auerbach, B. D., Rodrigues, P. V., and Salvi, R. J. (2014). Central gain control in tinnitus and hyperacusis. *Front. Neurol.* 5:206. doi: 10.3389/fneur.2014.00206

Awad, P. N., Amegandjin, C. A., Szczurkowska, J., Carrico, J. N., Fernandes, do Nascimento, A. S., et al. (2018). KCC2 Regulates Dendritic Spine Formation in a Brain-Region Specific and BDNF Dependent Manner. *Cereb. Cortex* 28, 4049–4062. doi: 10.1093/cercor/bhy198

Babola, T. A., Li, S., Gribizis, A., Lee, B. J., Issa, J. B., Wang, H. C., et al. (2018). Homeostatic Control of Spontaneous Activity in the Developing Auditory System. *Neuron* 99, 511–524e515. doi: 10.1016/j.neuron.2018.07.004

Bajo, V. M., Leach, N. D., Cordery, P. M., Nodal, F. R., and King, A. J. (2014). The cholinergic basal forebrain in the ferret and its inputs to the auditory cortex. *Eur. J. Neurosci.* 40, 2922–2940. doi: 10.1111/ejn.12653

Balakrishnan, V., Becker, M., Lohrke, S., Nothwang, H. G., Guresir, E., and Friauf, E. (2003). Expression and function of chloride transporters during development of inhibitory neurotransmission in the auditory brainstem. *J. Neurosci.* 23, 4134–4145. doi: 10.1523/JNEUROSCI.23-10-04134.2003

Bauer, C. A., Turner, J. G., Caspary, D. M., Myers, K. S., and Brozoski, T. J. (2008). Tinnitus and inferior colliculus activity in chinchillas related to three distinct patterns of cochlear trauma. *J. Neurosci. Res.* 86, 2564–2578. doi: 10.1002/jnr.21699

Ben-Ari, Y. (2002). Excitatory actions of gaba during development: the nature of the nurture. *Nat. Rev. Neurosci.* 3, 728–739. doi: 10.1038/nrn920

Ben-Ari, Y., Cherubini, E., Corradetti, R., and Gaiarsa, J. L. (1989). Giant synaptic potentials in immature rat CA3 hippocampal neurones. *J. Physiol.* 416, 303–325. doi: 10.1113/jphysiol.1989.sp017762

Ben-Ari, Y., Khalilov, I., Kahle, K. T., and Cherubini, E. (2012). The GABA excitatory/inhibitory shift in brain maturation and neurological disorders. *Neuroscientist* 18, 467–486. doi: 10.1177/1073858412438697

Beukes, E. W., Manchaiah, V., Allen, P. M., Andersson, G., and Baguley, D. M. (2021). Exploring tinnitus heterogeneity. *Prog. Brain Res.* 260, 79–99. doi: 10.1016/bs.pbr.2020.05.022

Bharadwaj, H. M., Masud, S., Mehraei, G., Verhulst, S., and Shinn-Cunningham, B. G. (2015). Individual differences reveal correlates of hidden hearing deficits. *J. Neurosci.* 35, 2161–2172. doi: 10.1523/JNEUROSCI.3915-14.2015

Blair, L. J., Criado-Marrero, M., Zheng, D., Wang, X., Kamath, S., Nordhues, B. A., et al. (2019). The Disease-Associated Chaperone FKBP51 Impairs Cognitive Function by Accelerating AMPA Receptor Recycling. *eNeuro* 6, ENEURO.242–ENEURO.218. doi: 10.1523/ENEURO.0242-18.2019

Bledsoe, S. C. Jr., Nagase, S., Miller, J. M., and Altschuler, R. A. (1995). Deafness-induced plasticity in the mature central auditory system. *Neuroreport* 7, 225–229. doi: 10.1097/00001756-199512290-00054

Bourien, J., Tang, Y., Batrel, C., Huet, A., Lenoir, M., Ladrech, S., et al. (2014). Contribution of auditory nerve fibers to compound action potential of the auditory nerve. *J. Neurophysiol.* 112, 1025–1039. doi: 10.1152/jn.00738.2013

Brigande, J. V., and Heller, S. (2009). Quo vadis, hair cell regeneration? *Nat. Neurosci.* 12, 679–685. doi: 10.1038/nn.2311

Butler, R., Bernier, P. M., Lefebvre, J., Gilbert, G., and Whittingstall, K. (2017). Decorrelated Input Dissociates Narrow Band gamma Power and BOLD in Human Visual Cortex. *J. Neurosci.* 37, 5408–5418. doi: 10.1523/JNEUROSCI.3938-16.2017

Cai, R., Guo, F., Zhang, J., Xu, J., Cui, Y., and Sun, X. (2009). Environmental enrichment improves behavioral performance and auditory spatial representation of primary auditory cortical neurons in rat. *Neurobiol. Learn. Mem.* 91, 366–376. doi: 10.1016/j.nlm.2009.01.005

Cai, S., Ma, W. L., and Young, E. D. (2009). Encoding intensity in ventral cochlear nucleus following acoustic trauma: implications for loudness recruitment. *J. Assoc. Res. Otolaryngol.* 10, 5–22. doi: 10.1007/s10162-008-0142-y

Canlon, B., Theorell, T., and Hasson, D. (2013). Associations between stress and hearing problems in humans. *Hearing Res.* 295, 9–15. doi: 10.1016/j.heares.2012.08.015

Caporarello, N., D'Angeli, F., Cambria, M. T., Candido, S., Giallongo, C., Salmeri, M., et al. (2019). Pericytes in Microvessels: From "Mural" Function to Brain and Retina Regeneration. *Int. J. Mol. Sci.* 20:6351. doi: 10.3390/ijms20246351

Caraiscos, V. B., Elliott, E. M., You-Ten, K. E., Cheng, V. Y., Belelli, D., Newell, J. G., et al. (2004). Tonic inhibition in mouse hippocampal CA1 pyramidal neurons is mediated by a5 subunit-containing gamma-aminobutyric acid type A receptors. *Proc. Natl. Acad. Sci. USA* 101, 3662–3667. doi: 10.1073/pnas.0307231101

Cardin, J. A., Carlen, M., Meletis, K., Knoblich, U., Zhang, F., Deisseroth, K., et al. (2009). Driving fast-spiking cells induces gamma rhythm and controls sensory responses. *Nature* 459, 663–667. doi: 10.1038/nature08002

Caspary, D. M., Ling, L., Turner, J. G., and Hughes, L. F. (2008). Inhibitory neurotransmission, plasticity and aging in the mammalian central auditory system. *J. Exp. Biol.* 211, 1781–1791. doi: 10.1242/jeb.013581

Cauli, B., Tong, X. K., Rancillac, A., Serluca, N., Lambolez, B., Rossier, J., et al. (2004). Cortical GABA interneurons in neurovascular coupling: relays for subcortical vasoactive pathways. *J. Neurosci.* 24, 8940–8949. doi: 10.1523/JNEUROSCI.3065-04.2004

Chacon-Fernandez, P., Sauberli, K., Colzani, M., Moreau, T., Ghevaert, C., and Barde, Y. A. (2016). Brain-derived Neurotrophic Factor in Megakaryocytes. *J. Biol. Chem.* 291, 9872–9881. doi: 10.1074/jbc.M116.720029

Chadha, N. K., Gordon, K. A., James, A. L., and Papsin, B. C. (2009). Tinnitus is prevalent in children with cochlear implants. *Int. J. Pediatric Otorhinolaryngol.* 73, 671–675. doi: 10.1016/j.ijporl.2008.12.032

Chen, G. D., and Jastreboff, P. J. (1995). Salicylate-induced abnormal activity in the inferior colliculus of rats. *Hearing Res.* 82, 158–178. doi: 10.1016/0378-5955(94)00174-o

Chen, G., Zhang, Y., Li, X., Zhao, X., Ye, Q., Lin, Y., et al. (2017). Distinct Inhibitory Circuits Orchestrate Cortical beta and gamma Band Oscillations. *Neuron* 96, 1403–1418e1406. doi: 10.1016/j.neuron.2017.11.033

Cherubini, E., Griguoli, M., Safiulina, V., and Lagostena, L. (2011). The depolarizing action of GABA controls early network activity in the developing hippocampus. *Mol. Neurobiol.* 43, 97–106. doi: 10.1007/s12035-010-8147-z

Chow, B. W., Nunez, V., Kaplan, L., Granger, A. J., Bistrong, K., Zucker, H. L., et al. (2020). Caveolae in CNS arterioles mediate neurovascular coupling. *Nature* 579, 106–110. doi: 10.1038/s41586-020-2026-1

Chumak, T., Rüttiger, L., Lee, S. C., Campanelli, D., Zuccotti, A., Singer, W., et al. (2016). BDNF in Lower Brain Parts Modifies Auditory Fiber Activity to Gain Fidelity but Increases the Risk for Generation of Central Noise After Injury. *Mol. Neurobiol.* 53, 5607–5627. doi: 10.1007/s12035-015-9474-x

Collaborators, G. H. L. (2021). Hearing loss prevalence and years lived with disability, 1990-2019: findings from the Global Burden of Disease Study 2019. *Lancet* 397, 996–1009. doi: 10.1016/S0140-6736(21)00516-X

Colonnese, M. T., Phillips, M. A., Constantine-Paton, M., Kaila, K., and Jasanoff, A. (2008). Development of hemodynamic responses and functional connectivity in rat somatosensory cortex. *Nat. Neurosci.* 11, 72–79. doi: 10.1038/nn2017

Crönlein, T., Langguth, B., Pregler, M., Kreuzer, P. M., Wetter, T. C., and Schecklmann, M. (2016). Insomnia in patients with chronic tinnitus: Cognitive and emotional distress as moderator variables. *J. Psychosom. Res.* 83, 65–68. doi: 10.1016/j.jpsychores.2016.03.001

Crunelli, V., and Di Giovanni, G. (2014). Monoamine modulation of tonic GABAA inhibition. *Rev. Neurosci.* 25, 195–206. doi: 10.1515/revneuro-2013-0059

Csabai, D., Wiborg, O., and Czeh, B. (2018). Reduced Synapse and Axon Numbers in the Prefrontal Cortex of Rats Subjected to a Chronic Stress Model for Depression. *Front. Cell. Neurosci.* 12:24. doi: 10.3389/fncel.2018.00024

Cudmore, R. H., Dougherty, S. E., and Linden, D. J. (2017). Cerebral vascular structure in the motor cortex of adult mice is stable and is not altered by voluntary exercise. *J. Cereb. Blood Flow Metab.* 37, 3725–3743. doi: 10.1177/0271678X16682508

Cukier, H. N., Griswold, A. J., Hofmann, N. K., Gomez, L., Whitehead, P. L., Abramson, R. K., et al. (2020). Three Brothers With Autism Carry a Stop-Gain Mutation in the HPA-Axis Gene NR3C2. *Autism Res.* 13, 523–531. doi: 10.1002/aur.2269

Czeh, B., Vardya, I., Varga, Z., Febbraro, F., Csabai, D., Martis, L. S., et al. (2018). Long-Term Stress Disrupts the Structural and Functional Integrity of GABAergic Neuronal Networks in the Medial Prefrontal Cortex of Rats. *Front. Cell. Neurosci.* 12:148. doi: 10.3389/fncel.2018.00148

Czeh, B., Varga, Z. K., Henningsen, K., Kovacs, G. L., Miseta, A., and Wiborg, O. (2015). Chronic stress reduces the number of GABAergic interneurons in the adult rat hippocampus, dorsal-ventral and region-specific differences. *Hippocampus* 25, 393–405. doi: 10.1002/hipo.22382

Davis, G. W., and Bezprozvanny, I. (2001). Maintaining the stability of neural function: a homeostatic hypothesis. *Annu. Rev. Physiol.* 63, 847–869. doi: 10.1146/annurev.physiol.63.1.847

de Kloet, E. R. (2014). From receptor balance to rational glucocorticoid therapy. *Endocrinology* 155, 2754–2769. doi: 10.1210/en.2014-1048

de Kloet, E. R., Claessens, S. E., and Kentrop, J. (2014). Context modulates outcome of perinatal glucocorticoid action in the brain. *Front. Endocrinol.* 5:100. doi: 10.3389/fendo.2014.00100

de Kloet, E. R., de Kloet, S. F., de Kloet, C. S., and de Kloet, A. D. (2019). Top-down and bottom-up control of stress-coping. *J. Neuroendocrinol.* 31:e12675. doi: 10.1111/jne.12675

de Villers-Sidani, E., Chang, E. F., Bao, S., and Merzenich, M. M. (2007). Critical period window for spectral tuning defined in the primary auditory cortex (A1) in the rat. *J. Neurosci.* 27, 180–189. doi: 10.1523/JNEUROSCI.3227-06.2007

Dehmel, S., Pradhan, S., Koehler, S., Bledsoe, S., and Shore, S. (2012). Noise overexposure alters long-term somatosensory-auditory processing in the dorsal cochlear nucleus–possible basis for tinnitus-related hyperactivity? *J. Neurosci.* 32, 1660–1671. doi: 10.1523/JNEUROSCI.4608-11.2012

Deng, D., Masri, S., Yao, L., Ma, X., Cao, X., Yang, S., et al. (2020). Increasing endogenous activity of NMDARs on GABAergic neurons increases inhibition, alters sensory processing and prevents noise-induced tinnitus. *Sci. Rep.* 10:11969. doi: 10.1038/s41598-020-68652-5

Derkach, V. A., Oh, M. C., Guire, E. S., and Soderling, T. R. (2007). Regulatory mechanisms of AMPA receptors in synaptic plasticity. *Nat. Rev. Neurosci.* 8, 101–113. doi: 10.1038/nrn2055

Deroche, M. L., Culling, J. F., Chatterjee, M., and Limb, C. J. (2014). Roles of the target and masker fundamental frequencies in voice segregation. *J. Acoust. Soc. Am.* 136:1225. doi: 10.1121/1.4890649

Dieni, S., Matsumoto, T., Dekkers, M., Rauskolb, S., Ionescu, M. S., Deogracias, R., et al. (2012). BDNF and its pro-peptide are stored in presynaptic dense core vesicles in brain neurons. *J. Cell Biol.* 196, 775–788. doi: 10.1083/jcb.201201038

Dinstein, I., Heeger, D. J., Lorenzi, L., Minshew, N. J., Malach, R., and Behrmann, M. (2012). Unreliable evoked responses in autism. *Neuron* 75, 981–991. doi: 10.1016/j.neuron.2012.07.026

Donovan, M. J., Lin, M. I., Wiegn, P., Ringstedt, T., Kraemer, R., Hahn, R., et al. (2000). Brain derived neurotrophic factor is an endothelial cell survival factor required for intramyocardial vessel stabilization. *Development* 127, 4531–4540.

Duguid, I., Branco, T., London, M., Chadderton, P., and Hausser, M. (2012). Tonic inhibition enhances fidelity of sensory information transmission in the cerebellar cortex. *J. Neurosci.* 32, 11132–11143. doi: 10.1523/JNEUROSCI.0460-12.2012

Easwar, V., Yamazaki, H., Deighton, M., Papsin, B., and Gordon, K. (2017). Simultaneous bilateral cochlear implants: Developmental advances do not yet achieve normal cortical processing. *Brain Behav.* 7:e00638. doi: 10.1002/brb3.638

Eckert, P., Marchetta, P., Manthey, M. K., Walter, M. H., Jovanovic, S., Savitska, D., et al. (2021). Deletion of BDNF in Pax2 Lineage-Derived Interneuron Precursors in the Hindbrain Hampers the Proportion of Excitation/Inhibition, Learning, and Behavior. *Front. Mol. Neurosci.* 14:642679. doi: 10.3389/fnmol.2021.642679

Eggermont, J. J., and Kral, A. (2016). Somatic memory and gain increase as preconditions for tinnitus: Insights from congenital deafness. *Hearing Res.* 333, 37–48. doi: 10.1016/j.heares.2015.12.018

Eggermont, J. J., and Tass, P. A. (2015). Maladaptive neural synchrony in tinnitus: origin and restoration. *Front. Neurol.* 6:29. doi: 10.3389/fneur.2015.00029

Engelien, A., Huber, W., Silbersweig, D., Stern, E., Frith, C. D., Doring, W., et al. (2000). The neural correlates of 'deaf-hearing' in man: conscious sensory awareness enabled by attentional modulation. *Brain J. Neurol.* 123(Pt 3), 532–545. doi: 10.1093/brain/123.3.532

Engl, E., Jolivet, R., Hall, C. N., and Attwell, D. (2017). Non-signalling energy use in the developing rat brain. *J. Cereb. Blood Flow Metab.* 37, 951–966. doi: 10.1177/0271678X16648710

Espinoza, C., Guzman, S. J., Zhang, X., and Jonas, P. (2018). Parvalbumin(+) interneurons obey unique connectivity rules and establish a powerful lateral-inhibition microcircuit in dentate gyrus. *Nat. Commun.* 9:4605. doi: 10.1038/s41467-018-06899-3

Fatemi, S. H., Halt, A. R., Stary, J. M., Kanodia, R., Schulz, S. C., and Realmuto, G. R. (2002). Glutamic acid decarboxylase 65 and 67 kDa proteins are reduced in autistic parietal and cerebellar cortices. *Biol. Psychiatry* 52, 805–810. doi: 10.1016/s0006-3223(02)01430-0

Fatemi, S. H., Reutiman, T. J., Folsom, T. D., and Thuras, P. D. (2009). GABA(A) receptor downregulation in brains of subjects with autism. *J. Autism Dev. Disord.* 39, 223–230. doi: 10.1007/s10803-008-0646-7

Fatemi, S. H., Reutiman, T. J., Folsom, T. D., Rooney, R. J., Patel, D. H., and Thuras, P. D. (2010). mRNA and protein levels for GABAAalpha4, alpha5, beta1 and GABABR1 receptors are altered in brains from subjects with autism. *J. Autism Dev. Disord.* 40, 743–750. doi: 10.1007/s10803-009-0924-z

Ferando, I., and Mody, I. (2015). *In vitro* gamma oscillations following partial and complete ablation of d subunit-containing $GABA_A$ receptors from parvalbumin interneurons. *Neuropharmacology* 88, 91–98. doi: 10.1016/j.neuropharm.2014.09.010

Fernandez-Klett, F., Offenhauser, N., Dirnagl, U., Priller, J., and Lindauer, U. (2010). Pericytes in capillaries are contractile *in vivo*, but arterioles mediate functional hyperemia in the mouse brain. *Proc. Natl. Acad. Sci. U S A.* 107, 22290–22295. doi: 10.1073/pnas.1011321108

Ferrini, F., and De Koninck, Y. (2013). Microglia control neuronal network excitability *via* BDNF signalling. *Neural Plast.* 2013:429815. doi: 10.1155/2013/429815

Fitch, R. H., Alexander, M. L., and Threlkeld, S. W. (2013). Early neural disruption and auditory processing outcomes in rodent models: implications for developmental language disability. *Front. Syst. Neurosci.* 7:58. doi: 10.3389/fnsys.2013.00058

Fiumelli, H., Cancedda, L., and Poo, M. M. (2005). Modulation of GABAergic transmission by activity *via* postsynaptic Ca2+-dependent regulation of KCC2 function. *Neuron* 48, 773–786. doi: 10.1016/j.neuron.2005.10.025

Fortunato, S., Forli, F., Guglielmi, V., De Corso, E., Paludetti, G., Berrettini, S., et al. (2016). A review of new insights on the association between hearing loss and cognitive decline in ageing. *Acta Otorhinolaryngol. Ital.* 36, 155–166. doi: 10.14639/0392-100X-993

Foss-Feig, J. H., Schauder, K. B., Key, A. P., Wallace, M. T., and Stone, W. L. (2017). Audition-specific temporal processing deficits associated with language function in children with autism spectrum disorder. *Autism Res.* 10, 1845–1856. doi: 10.1002/aur.1820

Fotaki, V., Price, D. J., and Mason, J. O. (2008). Newly identified patterns of Pax2 expression in the developing mouse forebrain. *BMC Dev. Biol.* 8:79. doi: 10.1186/1471-213X-8-79

Fox, A. M., Reid, C. L., Anderson, M., Richardson, C., and Bishop, D. V. (2012). Maturation of rapid auditory temporal processing and subsequent nonword repetition performance in children. *Dev. Sci.* 15, 204–211. doi: 10.1111/j.1467-7687.2011.01117.x

Friauf, E., and Lohmann, C. (1999). Development of auditory brainstem circuitry. Activity-dependent and activity-independent processes. *Cell Tissue Res.* 297, 187–195. doi: 10.1007/s004410051346

Friauf, E., Rust, M. B., Schulenborg, T., and Hirtz, J. J. (2011). Chloride cotransporters, chloride homeostasis, and synaptic inhibition in the developing auditory system. *Hearing Res.* 279, 96–110. doi: 10.1016/j.heares.2011.05.012

Friebe, A., Voussen, B., and Groneberg, D. (2018). NO-GC in cells 'off the beaten track'. *Nitric Oxide* 77, 12–18. doi: 10.1016/j.niox.2018.03.020

Fröhlich, F. (2016). *Network Neuroscience*. Amsterdam: Elsevier.

Furman, A. C., Kujawa, S. G., and Liberman, M. C. (2013). Noise-induced cochlear neuropathy is selective for fibers with low spontaneous rates. *J. Neurophysiol.* 110, 577–586. doi: 10.1152/jn.00164.2013

Gao, Y., Manzoor, N., and Kaltenbach, J. A. (2016). Evidence of activity-dependent plasticity in the dorsal cochlear nucleus, *in vivo*, induced by brief sound exposure. *Hearing Res.* 341, 31–42. doi: 10.1016/j.heares.2016.07.011

Gerken, G. M. (1996). Central tinnitus and lateral inhibition: an auditory brainstem model. *Hearing Res.* 97, 75–83. doi: 10.1016/s0378-5955(96)80009-8

Gill, K. M., and Grace, A. A. (2014). The role of a5 $GABA_A$ receptor agonists in the treatment of cognitive deficits in schizophrenia. *Curr. Pharm. Des.* 20, 5069–5076. doi: 10.1016/j.bbr.2014.02.013

Girouard, H., Park, L., Anrather, J., Zhou, P., and Iadecola, C. (2007). Cerebrovascular nitrosative stress mediates neurovascular and endothelial

dysfunction induced by angiotensin II. *Arterioscler. Thromb. Vasc. Biol.* 27, 303–309. doi: 10.1161/01.ATV.0000253885.41509.25

Glowatzki, E., and Fuchs, P. A. (2000). Cholinergic synaptic inhibition of inner hair cells in the neonatal mammalian cochlea. *Science* 288, 2366–2368. doi: 10.1126/science.288.5475.2366

Glowatzki, E., and Fuchs, P. A. (2002). Transmitter release at the hair cell ribbon synapse. *Nat. Neurosci.* 5, 147–154. doi: 10.1038/nn796

Goel, A., Cantu, D. A., Guilfoyle, J., Chaudhari, G. R., Newadkar, A., Todisco, B., et al. (2019). Author Correction: Impaired perceptual learning in a mouse model of Fragile X syndrome is mediated by parvalbumin neuron dysfunction and is reversible. *Nat. Neurosci.* 22:143. doi: 10.1038/s41593-018-0273-3

Goman, A. M., and Lin, F. R. (2016). Prevalence of Hearing Loss by Severity in the United States. *Am. J. Public Health* 106, 1820–1822. doi: 10.2105/AJPH.2016.303299

Goyal, M. S., Hawrylycz, M., Miller, J. A., Snyder, A. Z., and Raichle, M. E. (2014). Aerobic glycolysis in the human brain is associated with development and neotenous gene expression. *Cell Metabol.* 19, 49–57. doi: 10.1016/j.cmet.2013.11.020

Graham, C. E., and Vetter, D. E. (2011). The mouse cochlea expresses a local hypothalamic-pituitary-adrenal equivalent signaling system and requires corticotropin-releasing factor receptor 1 to establish normal hair cell innervation and cochlear sensitivity. *J. Neurosci.* 31, 1267–1278. doi: 10.1523/JNEUROSCI.4545-10.2011

Grant, L., Yi, E., and Glowatzki, E. (2010). Two modes of release shape the postsynaptic response at the inner hair cell ribbon synapse. *J. Neurosci.* 30, 4210–4220. doi: 10.1523/JNEUROSCI.4439-09.2010

Griffen, T. C., and Maffei, A. (2014). GABAergic synapses: their plasticity and role in sensory cortex. *Front. Cell. Neurosci.* 8:91. doi: 10.3389/fncel.2014.00091

Griffiths, T. D., Lad, M., Kumar, S., Holmes, E., McMurray, B., Maguire, E. A., et al. (2020). How Can Hearing Loss Cause Dementia? *Neuron* 108, 401–412. doi: 10.1016/j.neuron.2020.08.003

Gu, J. W., Herrmann, B. S., Levine, R. A., and Melcher, J. R. (2012). Brainstem auditory evoked potentials suggest a role for the ventral cochlear nucleus in tinnitus. *J. Assoc. Res. Otolaryngol.* 13, 819–833. doi: 10.1007/s10162-012-0344-1

Haigh, S. M., Coffman, B. A., Murphy, T. K., Butera, C. D., and Salisbury, D. F. (2016). Abnormal auditory pattern perception in schizophrenia. *Schizophr. Res.* 176, 473–479. doi: 10.1016/j.schres.2016.07.007

Hall, C. N., Reynell, C., Gesslein, B., Hamilton, N. B., Mishra, A., Sutherland, B. A., et al. (2014). Capillary pericytes regulate cerebral blood flow in health and disease. *Nature* 508, 55–60. doi: 10.1038/nature13165

Hamalainen, J. A., Ortiz-Mantilla, S., and Benasich, A. A. (2011). Source localization of event-related potentials to pitch change mapped onto age-appropriate MRIs at 6 months of age. *NeuroImage* 54, 1910–1918. doi: 10.1016/j.neuroimage.2010.10.016

Hamilton, L. S., Sohl-Dickstein, J., Huth, A. G., Carels, V. M., Deisseroth, K., and Bao, S. (2013). Optogenetic activation of an inhibitory network enhances feedforward functional connectivity in auditory cortex. *Neuron* 80, 1066–1076. doi: 10.1016/j.neuron.2013.08.017

Han, K., Lee, M., Lim, H. K., Jang, M. W., Kwon, J., Lee, C. J., et al. (2020). Excitation-Inhibition Imbalance Leads to Alteration of Neuronal Coherence and Neurovascular Coupling under Acute Stress. *J. Neurosci.* 40, 9148–9162. doi: 10.1523/JNEUROSCI.1553-20.2020

Han, K., Min, J., Lee, M., Kang, B. M., Park, T., Hahn, J., et al. (2019). Neurovascular Coupling under Chronic Stress Is Modified by Altered GABAergic Interneuron Activity. *J. Neurosci.* 39, 10081–10095. doi: 10.1523/JNEUROSCI.1357-19.2019

Heeringa, A. N., and van Dijk, P. (2014). The dissimilar time course of temporary threshold shifts and reduction of inhibition in the inferior colliculus following intense sound exposure. *Hear. Res.* 312, 38–47. doi: 10.1016/j.heares.2014.03.004

Heil, P., Neubauer, H., Brown, M., and Irvine, D. R. (2008). Towards a unifying basis of auditory thresholds: distributions of the first-spike latencies of auditory-nerve fibers. *Hearing Res.* 238, 25–38. doi: 10.1016/j.heares.2007.09.014

Heinz, M. G., and Young, E. D. (2004). Response growth with sound level in auditory-nerve fibers after noise-induced hearing loss. *J. Neurophysiol.* 91, 784–795. doi: 10.1152/jn.00776.2003

Heinz, M. G., Issa, J. B., and Young, E. D. (2005). Auditory-nerve rate responses are inconsistent with common hypotheses for the neural correlates of loudness recruitment. *J. Assoc. Res. Otolaryngol. JARO* 6, 91–105. doi: 10.1007/s10162-004-5043-0

Hill, J. L., Hardy, N. F., Jimenez, D. V., Maynard, K. R., Kardian, A. S., Pollock, C. J., et al. (2016). Loss of promoter IV-driven BDNF expression impacts oscillatory activity during sleep, sensory information processing and fear regulation. *Transl. Psychiatry* 6:e873. doi: 10.1038/tp.2016.153

Hill, R. A., Tong, L., Yuan, P., Murikinati, S., Gupta, S., and Grutzendler, J. (2015). Regional Blood Flow in the Normal and Ischemic Brain Is Controlled by Arteriolar Smooth Muscle Cell Contractility and Not by Capillary Pericytes. *Neuron* 87, 95–110. doi: 10.1016/j.neuron.2015.06.001

Hirtz, J. J., Boesen, M., Braun, N., Deitmer, J. W., Kramer, F., Lohr, C., et al. (2011). Cav1.3 calcium channels are required for normal development of the auditory brainstem. *J. Neurosci.* 31, 8280–8294. doi: 10.1523/JNEUROSCI.5098-10.2011

Hofmeier, B., Wertz, J., Refat, F., Hinrichs, P., Saemisch, J., Singer, W., et al. (2021). Functional biomarkers that distinguish between tinnitus with and without hyperacusis. *Clin. Transl. Med.* 11:e378. doi: 10.1002/ctm2.378

Hofmeier, B., Wolpert, S., Aldamer, E. S., Walter, M., Thiericke, J., Braun, C., et al. (2018). Reduced sound-evoked and resting-state BOLD fMRI connectivity in tinnitus. *NeuroImage Clin.* 20, 637–649. doi: 10.1016/j.nicl.2018.08.029

Hong, E. J., McCord, A. E., and Greenberg, M. E. (2008). A biological function for the neuronal activity-dependent component of Bdnf transcription in the development of cortical inhibition. *Neuron* 60, 610–624. doi: 10.1016/j.neuron.2008.09.024

Houtsma, A. J. M., and Smurzynski, J. (1990). Pitch identification and discrimination for complex tones with many harmonics. *J. Acoust. Soc. Am.* 87, 304–310.

Hsieh, T. H., Lee, H. H. C., Hameed, M. Q., Pascual-Leone, A., Hensch, T. K., and Rotenberg, A. (2017). Trajectory of Parvalbumin Cell Impairment and Loss of Cortical Inhibition in Traumatic Brain Injury. *Cereb. Cortex* 27, 5509–5524. doi: 10.1093/cercor/bhw318

Hu, H., Gan, J., and Jonas, P. (2014). Interneurons. Fast-spiking, parvalbumin(+) GABAergic interneurons: from cellular design to microcircuit function. *Science* 345:1255263. doi: 10.1126/science.1255263

Hu, H., Roth, F. C., Vandael, D., and Jonas, P. (2018). Complementary Tuning of Na(+) and K(+) Channel Gating Underlies Fast and Energy-Efficient Action Potentials in GABAergic Interneuron Axons. *Neuron* 98, 156–165e156. doi: 10.1016/j.neuron.2018.02.024

Iadecola, C. (2017). The Neurovascular Unit Coming of Age: A Journey through Neurovascular Coupling in Health and Disease. *Neuron* 96, 17–42. doi: 10.1016/j.neuron.2017.07.030

Ibrahim, B. A., and Llano, D. A. (2019). Aging and Central Auditory Disinhibition: Is It a Reflection of Homeostatic Downregulation or Metabolic Vulnerability? *Brain Sci.* 9:351. doi: 10.3390/brainsci9120351

Irvine, D. R. F. (2018a). Auditory perceptual learning and changes in the conceptualization of auditory cortex. *Hearing Res.* 366, 3–16. doi: 10.1016/j.heares.2018.03.011

Irvine, D. R. F. (2018b). Plasticity in the auditory system. *Hearing Res.* 362, 61–73.

Itami, C., Kimura, F., and Nakamura, S. (2007). Brain-derived neurotrophic factor regulates the maturation of layer 4 fast-spiking cells after the second postnatal week in the developing barrel cortex. *J. Neurosci.* 27, 2241–2252. doi: 10.1523/JNEUROSCI.3345-06.2007

Jafarpour, A., Griffin, S., Lin, J. J., and Knight, R. T. (2019). Medial Orbitofrontal Cortex, Dorsolateral Prefrontal Cortex, and Hippocampus Differentially Represent the Event Saliency. *J. Cogn. Neurosci.* 31, 874–884. doi: 10.1162/jocn_a_01392

Ji, X. Y., Zingg, B., Mesik, L., Xiao, Z., Zhang, L. I., and Tao, H. W. (2016). Thalamocortical Innervation Pattern in Mouse Auditory and Visual Cortex: Laminar and Cell-Type Specificity. *Cereb. Cortex* 26, 2612–2625. doi: 10.1093/cercor/bhv099

Johnson, J. C. S., Marshall, C. R., Weil, R. S., Bamiou, D. E., Hardy, C. J. D., and Warren, J. D. (2021). Hearing and dementia: from ears to brain. *Brain J. Neurol.* 144, 391–401. doi: 10.1093/brain/awaa429

Johnson, S. L., Eckrich, T., Kuhn, S., Zampini, V., Franz, C., Ranatunga, K. M., et al. (2011). Position-dependent patterning of spontaneous action potentials in immature cochlear inner hair cells. *Nat. Neurosci.* 14, 711–717. doi: 10.1038/nn.2803

Johnson, S. L., Kuhn, S., Franz, C., Ingham, N., Furness, D. N., Knipper, M., et al. (2013). Presynaptic maturation in auditory hair cells requires a critical

period of sensory-independent spiking activity. *Proc. Natl. Acad. Sci. U S A.* 110, 8720–8725. doi: 10.1073/pnas.1219578110

Kaernbach, C., and Bering, C. (2001). Exploring the temporal mechanism involved in the pitch of unresolved harmonics. *J. Acoust. Soc. Am.* 110, 1039–1048. doi: 10.1121/1.1381535

Kalappa, B. I., Brozoski, T. J., Turner, J. G., and Caspary, D. M. (2014). Single unit hyperactivity and bursting in the auditory thalamus of awake rats directly correlates with behavioural evidence of tinnitus. *J. Physiol.* 592, 5065–5078. doi: 10.1113/jphysiol.2014.278572

Kandler, K., and Friauf, E. (1995). Development of glycinergic and glutamatergic synaptic transmission in the auditory brainstem of perinatal rats. *J. Neurosci.* 15, 6890–6904. doi: 10.1523/JNEUROSCI.15-10-06890.1995

Kandler, K., and Gillespie, D. C. (2005). Developmental refinement of inhibitory sound-localization circuits. *Trends Neurosci.* 28, 290–296. doi: 10.1016/j.tins.2005.04.007

Kandler, K., Clause, A., and Noh, J. (2009). Tonotopic reorganization of developing auditory brainstem circuits. *Nat. Neurosci.* 12, 711–717. doi: 10.1038/nn.2332

Khirug, S., Ahmad, F., Puskarjov, M., Afzalov, R., Kaila, K., and Blaesse, P. (2010). A single seizure episode leads to rapid functional activation of KCC2 in the neonatal rat hippocampus. *J. Neurosci.* 30, 12028–12035. doi: 10.1523/JNEUROSCI.3154-10.2010

Kilgard, M. P., Pandya, P. K., Engineer, N. D., and Moucha, R. (2002). Cortical network reorganization guided by sensory input features. *Biol. Cybernet.* 87, 333–343. doi: 10.1007/s00422-002-0352-z

Kim, H., Ahrlund-Richter, S., Wang, X., Deisseroth, K., and Carlen, M. (2016). Prefrontal Parvalbumin Neurons in Control of Attention. *Cell* 164, 208–218. doi: 10.1016/j.cell.2015.11.038

Kimura, F., and Itami, C. (2019). A hypothetical model concerning how spike-timing-dependent plasticity contributes to neural circuit formation and initiation of the critical period in barrel cortex. *J. Neurosci.* 39, 3784–3791. doi: 10.1523/JNEUROSCI.1684-18.2019

Kisler, K., Nelson, A. R., Montagne, A., and Zlokovic, B. V. (2017). Cerebral blood flow regulation and neurovascular dysfunction in Alzheimer disease. *Nat. Rev. Neurosci.* 18, 419–434. doi: 10.1038/nrn.2017.48

Kitzes, L. M. (1984). Some physiological consequences of neonatal cochlear destruction in the inferior colliculus of the gerbil. *Meriones Unguiculatus Brain Res.* 306, 171–178. doi: 10.1016/0006-8993(84)90366-4

Kitzes, L. M., and Semple, M. N. (1985). Single-unit responses in the inferior colliculus: effects of neonatal unilateral cochlear ablation. *J. Neurophysiol.* 53, 1483–1500. doi: 10.1152/jn.1985.53.6.1483

Knipper, M., Mazurek, B., van Dijk, P., and Schulz, H. (2021). Too blind to see the elephant? Why neuroscientists ought to be interested in tinnitus. *JARO* 22, 609–621. doi: 10.1007/s10162-021-00815-1

Knipper, M., Panford-Walsh, R., Singer, W., Rüttiger, L., and Zimmermann, U. (2015). Specific synaptopathies diversify brain responses and hearing disorders: you lose the gain from early life. *Cell Tissue Res.* 361, 77–93. doi: 10.1007/s00441-015-2168-x

Knipper, M., Van Dijk, P., Nunes, I., Rüttiger, L., and Zimmermann, U. (2013). Advances in the neurobiology of hearing disorders: recent developments regarding the basis of tinnitus and hyperacusis. *Prog. Neurobiol.* 111, 17–33. doi: 10.1016/j.pneurobio.2013.08.002

Knipper, M., van Dijk, P., Schulze, H., Mazurek, B., Krauss, P., Scheper, V., et al. (2020). The Neural Bases of Tinnitus: Lessons from Deafness and Cochlear Implants. *J. Neurosci.* 40, 7190–7202. doi: 10.1523/JNEUROSCI.1314-19.2020

Kocharyan, A., Fernandes, P., Tong, X. K., Vaucher, E., and Hamel, E. (2008). Specific subtypes of cortical GABA interneurons contribute to the neurovascular coupling response to basal forebrain stimulation. *J. Cereb. Blood Flow Metab.* 28, 221–231. doi: 10.1038/sj.jcbfm.9600558

Koehler, S. D., and Shore, S. E. (2013). Stimulus timing-dependent plasticity in dorsal cochlear nucleus is altered in tinnitus. *J. Neurosci.* 33, 19647–19656. doi: 10.1523/JNEUROSCI.2788-13.2013

Korb, E., and Finkbeiner, S. (2011). Arc in synaptic plasticity: from gene to behavior. *Trends Neurosci.* 34, 591–598. doi: 10.1016/j.tins.2011.08.007

Kotak, V. C., Fujisawa, S., Lee, F. A., Karthikeyan, O., Aoki, C., and Sanes, D. H. (2005). Hearing loss raises excitability in the auditory cortex. *J. Neurosci.* 25, 3908–3918. doi: 10.1523/JNEUROSCI.5169-04.2005

Kotak, V. C., Takesian, A. E., MacKenzie, P. C., and Sanes, D. H. (2013). Rescue of inhibitory synapse strength following developmental hearing loss. *PLoS One* 8:e53438. doi: 10.1371/journal.pone.0053438

Kozberg, M. G., Chen, B. R., DeLeo, S. E., Bouchard, M. B., and Hillman, E. M. (2013). Resolving the transition from negative to positive blood oxygen level-dependent responses in the developing brain. *Proc. Natl. Acad. Sci. U S A.* 110, 4380–4385. doi: 10.1073/pnas.1212785110

Kral, A., Dorman, M. F., and Wilson, B. S. (2019). Neuronal Development of Hearing and Language: Cochlear Implants and Critical Periods. *Annu. Rev. Neurosci.* 42, 47–65. doi: 10.1146/annurev-neuro-080317-061513

Kraus, N., and White-Schwoch, T. (2015). Unraveling the Biology of Auditory Learning: A Cognitive-Sensorimotor-Reward Framework. *Trends Cognit. Sci.* 19, 642–654. doi: 10.1016/j.tics.2015.08.017

Kujawa, S. G., and Liberman, M. C. (2009). Adding insult to injury: cochlear nerve degeneration after "temporary" noise-induced hearing loss. *J. Neurosci.* 29, 14077–14085. doi: 10.1523/JNEUROSCI.2845-09.2009

Kuwada, S., Anderson, J. S., Batra, R., Fitzpatrick, D. C., Teissier, N., and D'Angelo, W. R. (2002). Sources of the scalp-recorded amplitude-modulation following response. *J. Am. Acad. Audiol.* 13, 188–204.

Land, R., Baumhoff, P., Tillein, J., Lomber, S. G., Hubka, P., and Kral, A. (2016). Cross-Modal Plasticity in Higher-Order Auditory Cortex of Congenitally Deaf Cats Does Not Limit Auditory Responsiveness to Cochlear Implants. *J. Neurosci.* 36, 6175–6185. doi: 10.1523/JNEUROSCI.0046-16.2016

Landi, S., Ciucci, F., Maffei, L., Berardi, N., and Cenni, M. C. (2009). Setting the pace for retinal development: environmental enrichment acts through insulin-like growth factor 1 and brain-derived neurotrophic factor. *J. Neurosci.* 29, 10809–10819. doi: 10.1523/JNEUROSCI.1857-09.2009

Lazard, D. S., Giraud, A. L., Gnansia, D., Meyer, B., and Sterkers, O. (2012). Understanding the deafened brain: implications for cochlear implant rehabilitation. *Eur. Ann. Otorhinolaryngol. Head Neck Dis.* 129, 98–103. doi: 10.1016/j.anorl.2011.06.001

Ledo, A., Lourenco, C. F., Cadenas, E., Barbosa, R. M., and Laranjinha, J. (2021). The bioactivity of neuronal-derived nitric oxide in aging and neurodegeneration: Switching signaling to degeneration. *Free Radic. Biol. Med.* 162, 500–513. doi: 10.1016/j.freeradbiomed.2020.11.005

Lee, H. H., Deeb, T. Z., Walker, J. A., Davies, P. A., and Moss, S. J. (2011). NMDA receptor activity downregulates KCC2 resulting in depolarizing GABAA receptor-mediated currents. *Nat. Neurosci.* 14, 736–743. doi: 10.1038/nn.2806

Lee, L., Boorman, L., Glendenning, E., Christmas, C., Sharp, P., Redgrave, P., et al. (2020). Key Aspects of Neurovascular Control Mediated by Specific Populations of Inhibitory Cortical Interneurons. *Cereb. Cortex* 30, 2452–2464. doi: 10.1093/cercor/bhz251

Lee, S. Y., Nam, D. W., Koo, J. W., De Ridder, D., Vanneste, S., and Song, J. J. (2017). No auditory experience, no tinnitus: Lessons from subjects with congenital- and acquired single-sided deafness. *Hearing Res.* 354, 9–15. doi: 10.1016/j.heares.2017.08.002

Lee, S., Kang, B. M., Shin, M. K., Min, J., Heo, C., Lee, Y., et al. (2015). Chronic Stress Decreases Cerebrovascular Responses During Rat Hindlimb Electrical Stimulation. *Front. Neurosci.* 9:462. doi: 10.3389/fnins.2015.00462

Lehmann, K., Steinecke, A., and Bolz, J. (2012). GABA through the ages: regulation of cortical function and plasticity by inhibitory interneurons. *Neural Plast.* 2012:892784. doi: 10.1155/2012/892784

Lendahl, U., Nilsson, P., and Betsholtz, C. (2019). Emerging links between cerebrovascular and neurodegenerative diseases-a special role for pericytes. *EMBO Rep.* 20:e48070. doi: 10.15252/embr.201948070

Lendvai, B., Stern, E. A., Chen, B., and Svoboda, K. (2000). Experience-dependent plasticity of dendritic spines in the developing rat barrel cortex *in vivo*. *Nature* 404, 876–881. doi: 10.1038/35009107

Leutgeb, J. K., Leutgeb, S., Moser, M. B., and Moser, E. I. (2007). Pattern separation in the dentate gyrus and CA3 of the hippocampus. *Science* 315, 961–966. doi: 10.1126/science.1135801

Li, S., Kumar, T. P., Joshee, S., Kirschstein, T., Subburaju, S., Khalili, J. S., et al. (2018). Endothelial cell-derived GABA signaling modulates neuronal migration and postnatal behavior. *Cell Res.* 28, 221–248. doi: 10.1038/cr.2017.135

Liberman, M. C. (1980). Efferent synapses in the inner hair cell area of the cat cochlea: an electron microscopic study of serial sections. *Hear. Res.* 3, 189–204. doi: 10.1016/0378-5955(80)90046-5

Liberman, M. C. (1982). Single-neuron labeling in the cat auditory nerve. *Science* 216, 1239–1241. doi: 10.1126/science.7079757

Liberman, M. C. (2017). Noise-induced and age-related hearing loss: new perspectives and potential therapies. *F1000Research* 6:927. doi: 10.12688/f1000research.11310.1

Liberman, M. C., and Kujawa, S. G. (2017). Cochlear synaptopathy in acquired sensorineural hearing loss: Manifestations and mechanisms. *Hearing Res.* 349, 138–147. doi: 10.1016/j.heares.2017.01.003

Lin, F. R., Niparko, J. K., and Ferrucci, L. (2011). Hearing loss prevalence in the United States. *Arch. Internal Med.* 171, 1851–1852.

Lin, H. W., Furman, A. C., Kujawa, S. G., and Liberman, M. C. (2011). Primary neural degeneration in the Guinea pig cochlea after reversible noise-induced threshold shift. *J. Assoc. Res. Otolaryngol.* 12, 605–616. doi: 10.1007/s10162-011-0277-0

Livingston, G., Sommerlad, A., Orgeta, V., Costafreda, S. G., Huntley, J., Ames, D., et al. (2017). Dementia prevention, intervention, and care. *Lancet* 390, 2673–2734.

Lohmann, C., and Friauf, E. (1996). Distribution of the calcium-binding proteins parvalbumin and calretinin in the auditory brainstem of adult and developing rats. *J. Comparat. Neurol.* 367, 90–109.

Lohrke, S., Srinivasan, G., Oberhofer, M., Doncheva, E., and Friauf, E. (2005). Shift from depolarizing to hyperpolarizing glycine action occurs at different perinatal ages in superior olivary complex nuclei. *Eur. J. Neurosci.* 22, 2708–2722. doi: 10.1111/j.1460-9568.2005.04465.x

Lohse, M., Bajo, V. M., King, A. J., and Willmore, B. D. B. (2020). Neural circuits underlying auditory contrast gain control and their perceptual implications. *Nat. Commun.* 11:324. doi: 10.1038/s41467-019-14163-5

Lomber, S. G., Meredith, M. A., and Kral, A. (2010). Cross-modal plasticity in specific auditory cortices underlies visual compensations in the deaf. *Nat. Neurosci.* 13, 1421–1427. doi: 10.1038/nn.2653

Lourenco, C. F., Santos, R. M., Barbosa, R. M., Cadenas, E., Radi, R., and Laranjinha, J. (2014). Neurovascular coupling in hippocampus is mediated *via* diffusion by neuronal-derived nitric oxide. *Free Radic. Biol. Med.* 73, 421–429. doi: 10.1016/j.freeradbiomed.2014.05.021

Lu, J., Lobarinas, E., Deng, A., Goodey, R., Stolzberg, D., Salvi, R. J., et al. (2011). GABAergic neural activity involved in salicylate-induced auditory cortex gain enhancement. *Neuroscience* 189, 187–198. doi: 10.1016/j.neuroscience.2011.04.073

Mallei, A., Baj, G., Ieraci, A., Corna, S., Musazzi, L., Lee, F. S., et al. (2015). Expression and Dendritic Trafficking of BDNF-6 Splice Variant are Impaired in Knock-In Mice Carrying Human BDNF Val66Met Polymorphism. *Int. J. Neuropsychopharmacol.* 18:yv069. doi: 10.1093/ijnp/pyv069

Malmierca, M. S., Sanchez-Vives, M. V., Escera, C., and Bendixen, A. (2014). Neuronal adaptation, novelty detection and regularity encoding in audition. *Front. Syst. Neurosci.* 8:111. doi: 10.3389/fnsys.2014.00111

Mamashli, F., Khan, S., Bharadwaj, H., Michmizos, K., Ganesan, S., Garel, K. A., et al. (2017). Auditory processing in noise is associated with complex patterns of disrupted functional connectivity in autism spectrum disorder. *Autism Res.* 10, 631–647. doi: 10.1002/aur.1714

Marchetta, P., Savitska, D., Kubler, A., Asola, G., Manthey, M., Mohrle, D., et al. (2020). Age-Dependent Auditory Processing Deficits after Cochlear Synaptopathy Depend on Auditory Nerve Latency and the Ability of the Brain to Recruit LTP/BDNF. *Brain Sci.* 10:710. doi: 10.3390/brainsci10100710

Maricich, S. M., and Herrup, K. (1999). Pax-2 expression defines a subset of GABAergic interneurons and their precursors in the developing murine cerebellum. *J. Neurobiol.* 41, 281–294.

Marin, O., and Rubenstein, J. L. (2001). A long, remarkable journey: tangential migration in the telencephalon. *Nat. Rev. Neurosci.* 2, 780–790. doi: 10.1038/35097509

Markram, H., Toledo-Rodriguez, M., Wang, Y., Gupta, A., Silberberg, G., and Wu, C. (2004). Interneurons of the neocortical inhibitory system. *Nat. Rev. Neurosci.* 5, 793–807. doi: 10.1038/nrn1519

Masri, S., Chan, N., Marsh, T., Zinsmaier, A., Schaub, D., Zhang, L., et al. (2021). Chemogenetic Activation of Cortical Parvalbumin-Positive Interneurons Reverses Noise-Induced Impairments in Gap Detection. *J. Neurosci.* 41, 8848–8857. doi: 10.1523/JNEUROSCI.2687-19.2021

Matt, L., Eckert, P., Panford-Walsh, R., Geisler, H. S., Bausch, A. E., Manthey, M., et al. (2018). Visualizing BDNF Transcript Usage During Sound-Induced Memory Linked Plasticity. *Front. Mol. Neurosci.* 11:260. doi: 10.3389/fnmol.2018.00260

McAlpine, D., Martin, R. L., Mossop, J. E., and Moore, D. R. (1997). Response properties of neurons in the inferior colliculus of the monaurally deafened ferret to acoustic stimulation of the intact ear. *J. Neurophysiol.* 78, 767–779. doi: 10.1152/jn.1997.78.2.767

McKlveen, J. M., Morano, R. L., Fitzgerald, M., Zoubovsky, S., Cassella, S. N., Scheimann, J. R., et al. (2016). Chronic Stress Increases Prefrontal Inhibition: A Mechanism for Stress-Induced Prefrontal Dysfunction. *Biol. Psychiatry* 80, 754–764. doi: 10.1016/j.biopsych.2016.03.2101

McKlveen, J. M., Myers, B., Flak, J. N., Bundzikova, J., Solomon, M. B., Seroogy, K. B., et al. (2013). Role of prefrontal cortex glucocorticoid receptors in stress and emotion. *Biol. Psychiatry* 74, 672–679. doi: 10.1016/j.biopsych.2013.03.024

Meddis, R. (2006). Auditory-nerve first-spike latency and auditory absolute threshold: a computer model. *J. Acoust. Soc. Am.* 119, 406–417.

Meltser, I., and Canlon, B. (2011). Protecting the auditory system with glucocorticoids. *Hearing Res.* 281, 47–55. doi: 10.1016/j.heares.2011.06.003

Meltser, I., Cederroth, C. R., Basinou, V., Savelyev, S., Lundkvist, G. S., and Canlon, B. (2014). TrkB-mediated protection against circadian sensitivity to noise trauma in the murine cochlea. *Curr. Biol. CB* 24, 658–663.

Merchan-Perez, A., and Liberman, M. C. (1996). Ultrastructural differences among afferent synapses on cochlear hair cells: correlations with spontaneous discharge rate. *J. Comp. Neurol.* 371, 208–221.

Milbrandt, J. C., Holder, T. M., Wilson, M. C., Salvi, R. J., and Caspary, D. M. (2000). GAD levels and muscimol binding in rat inferior colliculus following acoustic trauma. *Hear. Res.* 147, 251–260. doi: 10.1016/s0378-5955(00)00135-0

Miller, E. K., and Buschman, T. J. (2013). Cortical circuits for the control of attention. *Curr. Opin. Neurobiol.* 23, 216–222. doi: 10.1016/j.conb.2012.11.011

Mohn, J. L., Alexander, J., Pirone, A., Palka, C. D., Lee, S. Y., Mebane, L., et al. (2014). New molecular insights into cognitive and autistic-like disabilities. *Mol. Psychiatry* 19:1053. doi: 10.1038/mp.2014.129

Möhrle, D., Hofmeier, B., Amend, M., Wolpert, S., Ni, K., Bing, D., et al. (2019). Enhanced Central Neural Gain Compensates Acoustic Trauma-induced Cochlear Impairment, but Unlikely Correlates with Tinnitus and Hyperacusis. *Neuroscience* 407, 146–169. doi: 10.1016/j.neuroscience.2018.12.038

Möhrle, D., Ni, K., Varakina, K., Bing, D., Lee, S. C., Zimmermann, U., et al. (2016). Loss of auditory sensitivity from inner hair cell synaptopathy can be centrally compensated in the young but not old brain. *Neurobiol. Aging* 44, 173–184. doi: 10.1016/j.neurobiolaging.2016.05.001

Möhrle, D., Reimann, K., Wolter, S., Wolters, M., Varakina, K., Mergia, E., et al. (2017). NO-sensitive guanylate cyclase isoforms NO-GC1 and NO-GC2 contribute to noise-induced inner hair cell synaptopathy. *Mol. Pharmacol.* 92, 375–388. doi: 10.1124/mol.117.108548

Montero-Odasso, M., Ismail, Z., and Livingston, G. (2020). One third of dementia cases can be prevented within the next 25 years by tackling risk factors. The case "for" and "against". *Alzheimers Res. Ther.* 12:81. doi: 10.1186/s13195-020-00646-x

Moore, D. R. (1994). Auditory brainstem of the ferret: long survival following cochlear removal progressively changes projections from the cochlear nucleus to the inferior colliculus. *J. Comparat. Neurol.* 339, 301–310. doi: 10.1002/cne.903390209

Mossop, J. E., Wilson, M. J., Caspary, D. M., and Moore, D. R. (2000). Down-regulation of inhibition following unilateral deafening. *Hearing Res.* 147, 183–187. doi: 10.1016/s0378-5955(00)00054-x

Mowery, T. M., Caras, M. L., Hassan, S. I., Wang, D. J., Dimidschstein, J., Fishell, G., et al. (2019). Preserving Inhibition during Developmental Hearing Loss Rescues Auditory Learning and Perception. *J. Neurosci.* 39, 8347–8361. doi: 10.1523/JNEUROSCI.0749-19.2019

Nadol, J. B. Jr. (1988). Innervation densities of inner and outer hair cells of the human organ of Corti. Evidence for auditory neural degeneration in a case of Usher's syndrome. *ORL J. Oto-rhino-laryngol. Related Specialties* 50, 363–370. doi: 10.1159/000276014

Nardou, R., Yamamoto, S., Chazal, G., Bhar, A., Ferrand, N., Dulac, O., et al. (2011). Neuronal chloride accumulation and excitatory GABA underlie aggravation of neonatal epileptiform activities by phenobarbital. *Brain J. Neurol.* 134, 987–1002. doi: 10.1093/brain/awr041

Nehlig, A., Pereira, de Vasconcelos, A., and Boyet, S. (1989). Postnatal changes in local cerebral blood flow measured by the quantitative autoradiographic

[14C]iodoantipyrine technique in freely moving rats. *J. Cereb. Blood Flow Metab.* 9, 579–588. doi: 10.1038/jcbfm.1989.83

Neville, H., and Bavelier, D. (2002). Human brain plasticity: evidence from sensory deprivation and altered language experience. *Prog. Brain Res.* 138, 177–188. doi: 10.1016/S0079-6123(02)38078-6

Nordeen, K. W., Killackey, H. P., and Kitzes, L. M. (1983). Ascending projections to the inferior colliculus following unilateral cochlear ablation in the neonatal gerbil, Meriones unguiculatus. *J. Comparat. Neurol.* 214, 144–153. doi: 10.1002/cne.902140204

Norena, A. J. (2011). An integrative model of tinnitus based on a central gain controlling neural sensitivity. *Neurosci. Biobehav. Rev.* 35, 1089–1109. doi: 10.1016/j.neubiorev.2010.11.003

Norena, A. J., and Farley, B. J. (2013). Tinnitus-related neural activity: theories of generation, propagation, and centralization. *Hearing Res.* 295, 161–171. doi: 10.1016/j.heares.2012.09.010

Nornes, H. O., Dressler, G. R., Knapik, E. W., Deutsch, U., and Gruss, P. (1990). Spatially and temporally restricted expression of Pax2 during murine neurogenesis. *Development* 109, 797–809.

Obleser, J., Wise, R. J., Dresner, M. A., and Scott, S. K. (2007). Functional integration across brain regions improves speech perception under adverse listening conditions. *J. Neurosci.* 27, 2283–2289. doi: 10.1523/JNEUROSCI.4663-06.2007

Oleskevich, S., and Walmsley, B. (2002). Synaptic transmission in the auditory brainstem of normal and congenitally deaf mice. *J. Physiol.* 540, 447–455. doi: 10.1113/jphysiol.2001.013821

Ortiz-Mantilla, S., Hamalainen, J. A., Realpe-Bonilla, T., and Benasich, A. A. (2016). Oscillatory Dynamics Underlying Perceptual Narrowing of Native Phoneme Mapping from 6 to 12 Months of Age. *J. Neurosci.* 36, 12095–12105. doi: 10.1523/JNEUROSCI.1162-16.2016

Ortmann, M., Muller, N., Schlee, W., and Weisz, N. (2011). Rapid increases of gamma power in the auditory cortex following noise trauma in humans. *Eur. J. Neurosci.* 33, 568–575. doi: 10.1111/j.1460-9568.2010.07542.x

Ostrovskaya, O. I., Cao, G., Eroglu, C., and Harris, K. M. (2020). Developmental onset of enduring long-term potentiation in mouse hippocampus. *Hippocampus* 30, 1298–1312. doi: 10.1002/hipo.23257

Ouda, L., Profant, O., and Syka, J. (2015). Age-related changes in the central auditory system. *Cell Tissue Res.* 361, 337–358.

Oxenham, A. J. (2018). How We Hear: The Perception and Neural Coding of Sound. *Annu. Rev. Psychol.* 69, 27–50. doi: 10.1146/annurev-psych-122216-011635

Pal, I., Paltati, C. R. B., Kaur, C., Shubhi, S., Kumar, P., Jacob, T. G., et al. (2019). Morphological and neurochemical changes in GABAergic neurons of the aging human inferior colliculus. *Hearing Res.* 377, 318–329. doi: 10.1016/j.heares.2019.02.005

Parkhurst, C. N., Yang, G., Ninan, I., Savas, J. N., Yates, J. R. III, Lafaille, J. J., et al. (2013). Microglia promote learning-dependent synapse formation through brain-derived neurotrophic factor. *Cell* 155, 1596–1609. doi: 10.1016/j.cell.2013.11.030

Pennington, J. R., and David, S. V. (2020). Complementary Effects of Adaptation and Gain Control on Sound Encoding in Primary Auditory Cortex. *eNeuro* 7, ENEURO.205–ENEURO.220. doi: 10.1523/ENEURO.0205-20.2020

Penrod, R. D., Kumar, J., Smith, L. N., McCalley, D., Nentwig, T. B., Hughes, B. W., et al. (2019). Activity-regulated cytoskeleton-associated protein (Arc/Arg3.1) regulates anxiety- and novelty-related behaviors. *Genes Brain Behav.* 18:e12561. doi: 10.1111/gbb.12561

Petersen, B., Gjedde, A., Wallentin, M., and Vuust, P. (2013). Cortical plasticity after cochlear implantation. *Neural Plastic.* 2013:318521.

Petersen, B., Weed, E., Sandmann, P., Brattico, E., Hansen, M., Sorensen, S. D., et al. (2015). Brain responses to musical feature changes in adolescent cochlear implant users. *Front. Hum. Neurosci.* 9:7. doi: 10.3389/fnhum.2015.00007

Peterson, N., and Bergeson, T. R. (2015). Contribution of hearing aids to music perception by cochlear implant users. *Cochlear Implants Int.* 16(Suppl. 3), S71–S78. doi: 10.1179/1467010015Z.000000000268

Pi, H. J., Hangya, B., Kvitsiani, D., Sanders, J. I., Huang, Z. J., and Kepecs, A. (2013). Cortical interneurons that specialize in disinhibitory control. *Nature* 503, 521–524. doi: 10.1038/nature12676

Pirone, A., Alexander, J. M., Koenig, J. B., Cook-Snyder, D. R., Palnati, M., Wickham, R. J., et al. (2018). Social Stimulus Causes Aberrant Activation of the Medial Prefrontal Cortex in a Mouse Model With Autism-Like Behaviors. *Front. Synaptic Neurosci.* 10:35. doi: 10.3389/fnsyn.2018.00035

Plack, C. J., Barker, D., and Prendergast, G. (2014). Perceptual consequences of "hidden" hearing loss. *Trends Hear.* 18:2331216514550621.

Ponton, C. W., and Eggermont, J. J. (2001). Of kittens and kids: altered cortical maturation following profound deafness and cochlear implant use. *Audiol. Neuro-otol.* 6, 363–380. doi: 10.1159/000046846

Popelar, J., Erre, J. P., Aran, J. M., and Cazals, Y. (1994). Plastic changes in ipsi-contralateral differences of auditory cortex and inferior colliculus evoked potentials after injury to one ear in the adult guinea pig. *Hear. Res.* 72, 125–134. doi: 10.1016/0378-5955(94)90212-7

Potashner, S. J., Suneja, S. K., and Benson, C. G. (1997). Regulation of D-aspartate release and uptake in adult brain stem auditory nuclei after unilateral middle ear ossicle removal and cochlear ablation. *Exp. Neurol.* 148, 222–235. doi: 10.1006/exnr.1997.6641

Potashner, S. J., Suneja, S. K., and Benson, C. G. (2000). Altered glycinergic synaptic activities in guinea pig brain stem auditory nuclei after unilateral cochlear ablation. *Hear. Res.* 147, 125–136. doi: 10.1016/s0378-5955(00)00126-x

Pouille, F., and Scanziani, M. (2001). Enforcement of temporal fidelity in pyramidal cells by somatic feed-forward inhibition. *Science* 293, 1159–1163. doi: 10.1126/science.1060342

Rabinowitz, N. C., Willmore, B. D., Schnupp, J. W., and King, A. J. (2012). Spectrotemporal contrast kernels for neurons in primary auditory cortex. *J. Neurosci.* 32, 11271–11284. doi: 10.1523/JNEUROSCI.1715-12.2012

Recanzone, G. (2018). The effects of aging on auditory cortical function. *Hear. Res.* 366, 99–105. doi: 10.1016/j.heares.2018.05.013

Refat, F., Wertz, J., Hinrichs, P., Klose, U., Samy, H., Abdelkader, R. M., et al. (2021). Co-occurrence of Hyperacusis Accelerates With Tinnitus Burden Over Time and Requires Medical Care. *Front. Neurol.* 12:627522. doi: 10.3389/fneur.2021.627522

Reynell, C., and Harris, J. J. (2013). The BOLD signal and neurovascular coupling in autism. *Dev. Cognit. Neurosci.* 6, 72–79. doi: 10.1016/j.dcn.2013.07.003

Rivera, C., Voipio, J., Payne, J. A., Ruusuvuori, E., Lahtinen, H., Lamsa, K., et al. (1999). The K+/Cl- co-transporter KCC2 renders GABA hyperpolarizing during neuronal maturation. *Nature* 397, 251–255. doi: 10.1038/16697

Roberts, L. E. (2018). Neural plasticity and its initiating conditions in tinnitus. *HNO* 66, 172–178. doi: 10.1007/s00106-017-0449-2

Roberts, L. E., and Salvi, R. (2019). Overview: Hearing loss, tinnitus, hyperacusis, and the role of central gain. *Neuroscience* 407, 1–7. doi: 10.1016/j.neuroscience.2019.03.021

Rogalla, M. M., and Hildebrandt, K. J. (2020). Aging But Not Age-Related Hearing Loss Dominates the Decrease of Parvalbumin Immunoreactivity in the Primary Auditory Cortex of Mice. *eNeuro* 7, ENEURO.511–ENEURO.519. doi: 10.1523/ENEURO.0511-19.2020

Rossignol, E., Kruglikov, I., van den Maagdenberg, A. M., Rudy, B., and Fishell, G. (2013). CaV 2.1 ablation in cortical interneurons selectively impairs fast-spiking basket cells and causes generalized seizures. *Ann. Neurol.* 74, 209–222. doi: 10.1002/ana.23913

Roth, R. H., Cudmore, R. H., Tan, H. L., Hong, I., Zhang, Y., and Huganir, R. L. (2020). Cortical Synaptic AMPA Receptor Plasticity during Motor Learning. *Neuron* 105, 895–908e895. doi: 10.1016/j.neuron.2019.12.005

Rowitch, D. H., Kispert, A., and McMahon, A. P. (1999). Pax-2 regulatory sequences that direct transgene expression in the developing neural plate and external granule cell layer of the cerebellum. *Brain Res. Dev. Brain Res.* 117, 99–108. doi: 10.1016/s0165-3806(99)00104-2

Ruel, J., Chabbert, C., Nouvian, R., Bendris, R., Eybalin, M., Leger, C. L., et al. (2008). Salicylate enables cochlear arachidonic-acid-sensitive NMDA receptor responses. *J. Neurosci.* 28, 7313–7323. doi: 10.1523/JNEUROSCI.5335-07.V2008

Ruel, J., Wang, J., Dememes, D., Gobaille, S., Puel, J. L., and Rebillard, G. (2006). Dopamine transporter is essential for the maintenance of spontaneous activity of auditory nerve neurones and their responsiveness to sound stimulation. *J. Neurochem.* 97, 190–200. doi: 10.1111/j.1471-4159.2006.03722.x

Rüttiger, L., Singer, W., Panford-Walsh, R., Matsumoto, M., Lee, S. C., Zuccotti, A., et al. (2013). The reduced cochlear output and the failure to adapt the central auditory response causes tinnitus in noise exposed rats. *PLoS One* 8:e57247. doi: 10.1371/journal.pone.0057247

Sachs, M. B., and Abbas, P. J. (1974). Rate versus level functions for auditory-nerve fibers in cats: tone-burst stimuli. *J. Acoust. Soc. Am.* 56, 1835–1847. doi: 10.1121/1.1903521

Sakata, K., Jin, L., and Jha, S. (2010). Lack of promoter IV-driven BDNF transcription results in depression-like behavior. *Genes Brain Behav.* 9, 712–721. doi: 10.1111/j.1601-183X.2010.00605.x

Salvi, R. J., Wang, J., and Ding, D. (2000). Auditory plasticity and hyperactivity following cochlear damage. *Hear. Res.* 147, 261–274. doi: 10.1016/s0378-5955(00)00136-2

Sanes, D. H., Song, J., and Tyson, J. (1992). Refinement of dendritic arbors along the tonotopic axis of the gerbil lateral superior olive. *Brain Res. Dev. Brain Res.* 67, 47–55. doi: 10.1016/0165-3806(92)90024-q

Schaette, R., and Kempter, R. (2006). Development of tinnitus-related neuronal hyperactivity through homeostatic plasticity after hearing loss: a computational model. *Eur. J. Neurosci.* 23, 3124–3138. doi: 10.1111/j.1460-9568.2006.04774.x

Schaette, R., and Kempter, R. (2009). Predicting tinnitus pitch from patients' audiograms with a computational model for the development of neuronal hyperactivity. *J. Neurophysiol.* 101, 3042–3052. doi: 10.1152/jn.91256.2008

Schaette, R., and Kempter, R. (2012). Computational models of neurophysiological correlates of tinnitus. *Front. Syst. Neurosci.* 6:34. doi: 10.3389/fnsys.2012.00034

Schaette, R., and McAlpine, D. (2011). Tinnitus with a normal audiogram: physiological evidence for hidden hearing loss and computational model. *J. Neurosci.* 31, 13452–13457. doi: 10.1523/JNEUROSCI.2156-11.2011

Schonwiesner, M., Novitski, N., Pakarinen, S., Carlson, S., Tervaniemi, M., and Naatanen, R. (2007). Heschl's gyrus, posterior superior temporal gyrus, and mid-ventrolateral prefrontal cortex have different roles in the detection of acoustic changes. *J. Neurophysiol.* 97, 2075–2082. doi: 10.1152/jn.01083.2006

Schur, R. R., Draisma, L. W., Wijnen, J. P., Boks, M. P., Koevoets, M. G., Joels, M., et al. (2016). Brain GABA levels across psychiatric disorders: A systematic literature review and meta-analysis of (1) H-MRS studies. *Hum. Brain Mapp.* 37, 3337–3352. doi: 10.1002/hbm.23244

Seal, R. P., Akil, O., Yi, E., Weber, C. M., Grant, L., Yoo, J., et al. (2008). Sensorineural deafness and seizures in mice lacking vesicular glutamate transporter 3. *Neuron* 57, 263–275. doi: 10.1016/j.neuron.2007.11.032

Sedley, W. (2019). Tinnitus: Does gain explain? *Neuroscience* 407, 213–228. doi: 10.1016/j.neuroscience.2019.01.027

Sedley, W., Friston, K. J., Gander, P. E., Kumar, S., and Griffiths, T. D. (2016). An Integrative Tinnitus Model Based on Sensory Precision. *Trends Neurosci.* 39, 799–812. doi: 10.1016/j.tins.2016.10.004

Sergeyenko, Y., Lall, K., Liberman, M. C., and Kujawa, S. G. (2013). Age-related cochlear synaptopathy: an early-onset contributor to auditory functional decline. *J. Neurosci.* 33, 13686–13694. doi: 10.1523/JNEUROSCI.1783-13.2013

Sharma, A., Dorman, M. F., and Kral, A. (2005a). The influence of a sensitive period on central auditory development in children with unilateral and bilateral cochlear implants. *Hear. Res.* 203, 134–143. doi: 10.1016/j.heares.2004.12.010

Sharma, A., Dorman, M. F., and Spahr, A. J. (2002). A sensitive period for the development of the central auditory system in children with cochlear implants: implications for age of implantation. *Ear Hear.* 23, 532–539. doi: 10.1097/00003446-200212000-00004

Sharma, A., Martin, K., Roland, P., Bauer, P., Sweeney, M. H., Gilley, P., et al. (2005b). P1 latency as a biomarker for central auditory development in children with hearing impairment. *J. Am. Acad. Audiol.* 16, 564–573. doi: 10.3766/jaaa.16.8.5

Sharma, M., Bist, S. S., and Kumar, S. (2016). Age-Related Maturation of Wave V Latency of Auditory Brainstem Response in Children. *J. Audiol. Otol.* 20, 97–101. doi: 10.7874/jao.2016.20.2.97

Shibata, S., Kakazu, Y., Okabe, A., Fukuda, A., and Nabekura, J. (2004). Experience-dependent changes in intracellular Cl- regulation in developing auditory neurons. *Neurosci. Res.* 48, 211–220. doi: 10.1016/j.neures.2003.10.011

Shore, S. E., Roberts, L. E., and Langguth, B. (2016). Maladaptive plasticity in tinnitus–triggers, mechanisms and treatment. *Nat. Rev. Neurol.* 12, 150–160. doi: 10.1038/nrneurol.2016.12

Shrestha, B. R., Chia, C., Wu, L., Kujawa, S. G., Liberman, M. C., and Goodrich, L. V. (2018). Sensory Neuron Diversity in the Inner Ear Is Shaped by Activity. *Cell* 174, 1229–1246e1217. doi: 10.1016/j.cell.2018.07.007

Sinclair, J. R., Jacobs, A. L., and Nirenberg, S. (2004). Selective ablation of a class of amacrine cells alters spatial processing in the retina. *J. Neurosci.* 24, 1459–1467. doi: 10.1523/JNEUROSCI.3959-03.2004

Singer, W., Kasini, K., Manthey, M., Eckert, P., Armbruster, P., Vogt, M. A., et al. (2018a). The glucocorticoid antagonist mifepristone attenuates sound-induced long-term deficits in auditory nerve response and central auditory processing in female rats. *FASEB J.* 32, 3005–3019. doi: 10.1096/fj.201701041RRR

Singer, W., Manthey, M., Panford-Walsh, R., Matt, L., Geisler, H. S., Passeri, E., et al. (2018b). BDNF-Live-Exon-Visualization (BLEV) Allows Differential Detection of BDNF Transcripts *in vitro* and *in vivo*. *Front. Mol. Neurosci.* 11:325. doi: 10.3389/fnmol.2018.00325

Singer, W., Panford-Walsh, R., and Knipper, M. (2014). The function of BDNF in the adult auditory system. *Neuropharmacology* 76(Pt C), 719–728. doi: 10.1016/j.neuropharm.2013.05.008

Singer, W., Zuccotti, A., Jaumann, M., Lee, S. C., Panford-Walsh, R., Xiong, H., et al. (2013). Noise-induced inner hair cell ribbon loss disturbs central arc mobilization: a novel molecular paradigm for understanding tinnitus. *Mol. Neurobiol.* 47, 261–279. doi: 10.1007/s12035-012-8372-8

Slugocki, C., and Trainor, L. J. (2014). Cortical indices of sound localization mature monotonically in early infancy. *Eur. J. Neurosci.* 40, 3608–3619. doi: 10.1111/ejn.12741

Sohal, V. S., Zhang, F., Yizhar, O., and Deisseroth, K. (2009). Parvalbumin neurons and gamma rhythms enhance cortical circuit performance. *Nature* 459, 698–702. doi: 10.1038/nature07991

Song, L., McGee, J. A., and Walsh, E. J. (2006). Consequences of combined maternal, fetal and persistent postnatal hypothyroidism on the development of auditory function in Tshrhyt mutant mice. *Brain Res.* 1101, 59–72. doi: 10.1016/j.brainres.2006.05.027

Sowell, E. R., Delis, D., Stiles, J., and Jernigan, T. L. (2001). Improved memory functioning and frontal lobe maturation between childhood and adolescence: a structural MRI study. *J. Int. Neuropsychol. Soc. JINS* 7, 312–322. doi: 10.1017/s135561770173305x

Spoendlin, H. (1969). Innervation patterns in the organ of corti of the cat. *Acta Otolaryngol.* 67, 239–254. doi: 10.3109/00016486909125448

Stroganova, T. A., Komarov, K. S., Sysoeva, O. V., Goiaeva, D. E., Obukhova, T. S., Ovsiannikova, T. M., et al. (2020). Left hemispheric deficit in the sustained neuromagnetic response to periodic click trains in children with ASD. *Mol. Autism* 11:100. doi: 10.1186/s13229-020-00408-4

Sullivan, R. M., and Gratton, A. (2002). Prefrontal cortical regulation of hypothalamic-pituitary-adrenal function in the rat and implications for psychopathology: side matters. *Psychoneuroendocrinology* 27, 99–114. doi: 10.1016/s0306-4530(01)00038-5

Sun, S., Babola, T., Pregernig, G., So, K. S., Nguyen, M., Su, S. M., et al. (2018). Hair Cell Mechanotransduction Regulates Spontaneous Activity and Spiral Ganglion Subtype Specification in the Auditory System. *Cell* 174, 1247–1263e1215. doi: 10.1016/j.cell.2018.07.008

Suneja, S. K., Benson, C. G., and Potashner, S. J. (1998). Glycine receptors in adult guinea pig brain stem auditory nuclei: regulation after unilateral cochlear ablation. *Exp. Neurol.* 154, 473–488. doi: 10.1006/exnr.1998.6946

Sweeney-Reed, C. M., Lee, H., Rampp, S., Zaehle, T., Buentjen, L., Voges, J., et al. (2016). Thalamic interictal epileptiform discharges in deep brain stimulated epilepsy patients. *J. Neurol.* 263, 2120–2126. doi: 10.1007/s00415-016-8246-5

Takano, T., and Matsui, K. (2015). Increased expression of GAP43 in interneurons in a rat model of experimental polymicrogyria. *J. Child Neurol.* 30, 716–728. doi: 10.1177/0883073814541476

Takesian, A. E., Bogart, L. J., Lichtman, J. W., and Hensch, T. K. (2018). Inhibitory circuit gating of auditory critical-period plasticity. *Nat. Neurosci.* 21, 218–227. doi: 10.1038/s41593-017-0064-2

Thompson, A. C., Irvine, D. R. F., and Fallon, J. B. (2021). Provision of interaural time difference information in chronic intracochlear electrical stimulation enhances neural sensitivity to these differences in neonatally deafened cats. *Hear. Res.* 406:108253. doi: 10.1016/j.heares.2021.108253

Tighilet, B., Dutheil, S., Siponen, M. I., and Norena, A. J. (2016). Reactive Neurogenesis and Down-Regulation of the Potassium-Chloride Cotransporter KCC2 in the Cochlear Nuclei after Cochlear Deafferentation. *Front. Pharmacol.* 7:281. doi: 10.3389/fphar.2016.00281

Timmusk, T., Palm, K., Metsis, M., Reintam, T., Paalme, V., Saarma, M., et al. (1993). Multiple promoters direct tissue-specific expression of the rat BDNF gene. *Neuron* 10, 475–489. doi: 10.1016/0896-6273(93)90335-o

Tuvikene, J., Pruunsild, P., Orav, E., Esvald, E. E., and Timmusk, T. (2016). AP-1 Transcription Factors Mediate BDNF-Positive Feedback Loop in Cortical

Neurons. *J. Neurosci.* 36, 1290–1305. doi: 10.1523/JNEUROSCI.3360-15.2016

Uchida, Y., Sugiura, S., Nishita, Y., Saji, N., Sone, M., and Ueda, H. (2019). Age-related hearing loss and cognitive decline - The potential mechanisms linking the two. *Auris Nasus Larynx* 46, 1–9. doi: 10.1016/j.anl.2018.08.010

Uhlirova, H., Kilic, K., Tian, P., Thunemann, M., Desjardins, M., Saisan, P. A., et al. (2016). Cell type specificity of neurovascular coupling in cerebral cortex. *eLife* 5:e14315. doi: 10.7554/eLife.14315

Utevsky, A. V., and Platt, M. L. (2014). Status and the brain. *PLoS Biol.* 12:e1001941. doi: 10.1371/journal.pbio.1001941

Vaghi, V., Polacchini, A., Baj, G., Pinheiro, V. L., Vicario, A., and Tongiorgi, E. (2014). Pharmacological profile of brain-derived neurotrophic factor (BDNF) splice variant translation using a novel drug screening assay: a "quantitative code". *J. Biol. Chem.* 289, 27702–27713. doi: 10.1074/jbc.M114.586719

Van de Heyning, P., Vermeire, K., Diebl, M., Nopp, P., Anderson, I., and De Ridder, D. (2008). Incapacitating unilateral tinnitus in single-sided deafness treated by cochlear implantation. *Ann. Otol. Rhinol. Laryngol.* 117, 645–652. doi: 10.1177/000348940811700903

Vanneste, S., Joos, K., Ost, J., and De Ridder, D. (2018). Influencing connectivity and cross-frequency coupling by real-time source localized neurofeedback of the posterior cingulate cortex reduces tinnitus related distress. *Neurobiol. Stress* 8, 211–224. doi: 10.1016/j.ynstr.2016.11.003

Vazquez, A. L., Fukuda, M., and Kim, S. G. (2018). Inhibitory Neuron Activity Contributions to Hemodynamic Responses and Metabolic Load Examined Using an Inhibitory Optogenetic Mouse Model. *Cereb. Cortex* 28, 4105–4119. doi: 10.1093/cercor/bhy225

Vetter, D. E. (2015). Cellular signaling protective against noise-induced hearing loss - A role for novel intrinsic cochlear signaling involving corticotropin-releasing factor? *Biochem. Pharmacol.* 97, 1–15. doi: 10.1016/j.bcp.2015.06.011

Viho, E. M. G., Buurstede, J. C., Mahfouz, A., Koorneef, L. L., van Weert, L., Houtman, R., et al. (2019). Corticosteroid Action in the Brain: The Potential of Selective Receptor Modulation. *Neuroendocrinology* 109, 266–276. doi: 10.1159/000499659

Wake, H., Watanabe, M., Moorhouse, A. J., Kanematsu, T., Horibe, S., Matsukawa, N., et al. (2007). Early changes in KCC2 phosphorylation in response to neuronal stress result in functional downregulation. *J. Neurosci.* 27, 1642–1650. doi: 10.1523/JNEUROSCI.3104-06.2007

Wang, F., Hong, B., Han, D. Y., Zhao, L. Y., Sui, Y. N., Liu, Y. Q., et al. (2012). [Changes of gamma-amino butyric acid and electrophysiology inferior colliculus after noise exposure in guinea pig]. *Zhonghua Yi Xue Za Zhi* 92, 1565–1568.

Wardle, R. A., and Poo, M. M. (2003). Brain-derived neurotrophic factor modulation of GABAergic synapses by postsynaptic regulation of chloride transport. *J. Neurosci.* 23, 8722–8732. doi: 10.1523/JNEUROSCI.23-25-08722.2003

Watanabe, M., and Fukuda, A. (2015). Development and regulation of chloride homeostasis in the central nervous system. *Front. Cell. Neurosci.* 9:371. doi: 10.3389/fncel.2015.00371

Waung, M. W., Pfeiffer, B. E., Nosyreva, E. D., Ronesi, J. A., and Huber, K. M. (2008). Rapid translation of Arc/Arg3.1 selectively mediates mGluR-dependent LTD through persistent increases in AMPAR endocytosis rate. *Neuron* 59, 84–97. doi: 10.1016/j.neuron.2008.05.014

Wei, H. S., Kang, H., Rasheed, I. D., Zhou, S., Lou, N., Gershteyn, A., et al. (2016). Erythrocytes Are Oxygen-Sensing Regulators of the Cerebral Microcirculation. *Neuron* 91, 851–862. doi: 10.1016/j.neuron.2016.07.016

Weinberger, N. M. (2015). New perspectives on the auditory cortex: learning and memory. *Handbook Clin. Neurol.* 129, 117–147. doi: 10.1016/B978-0-444-62630-1.00007-X

West, A. E., Pruunsild, P., and Timmusk, T. (2014). Neurotrophins: transcription and translation. *Handb. Exp. Pharmacol.* 220, 67–100. doi: 10.1007/978-3-642-45106-5_4

Wiechers, B., Gestwa, G., Mack, A., Carroll, P., Zenner, H. P., and Knipper, M. (1999). A changing pattern of brain-derived neurotrophic factor expression correlates with the rearrangement of fibers during cochlear development of rats and mice. *J. Neurosci.* 19, 3033–3042. doi: 10.1523/JNEUROSCI.19-08-03033.1999

Witkovsky, P. (2004). Dopamine and retinal function. *Doc. Ophthalmol. Adv. Ophthalmol.* 108, 17–40. doi: 10.1023/b:doop.0000019487.88486.0a

Wu, P. Z., Liberman, L. D., Bennett, K., de Gruttola, V., O'Malley, J. T., and Liberman, M. C. (2019). Primary Neural Degeneration in the Human Cochlea: Evidence for Hidden Hearing Loss in the Aging Ear. *Neuroscience* 407, 8–20. doi: 10.1016/j.neuroscience.2018.07.053

Xin, W., and Chan, J. R. (2020). Myelin plasticity: sculpting circuits in learning and memory. *Nat. Rev. Neurosci.* 21, 682–694. doi: 10.1038/s41583-020-00379-8

Xu, H., Kotak, V. C., and Sanes, D. H. (2010). Normal hearing is required for the emergence of long-lasting inhibitory potentiation in cortex. *J. Neurosci.* 30, 331–341. doi: 10.1523/JNEUROSCI.4554-09.2010

Yates, G. K. (1991). Auditory-nerve spontaneous rates vary predictably with threshold. *Hear. Res.* 57, 57–62. doi: 10.1016/0378-5955(91)90074-j

Youssofzadeh, V., Vannest, J., and Kadis, D. S. (2018). fMRI connectivity of expressive language in young children and adolescents. *Hum. Brain Mapp.* 39, 3586–3596. doi: 10.1002/hbm.24196

Zajac, I. T., and Nettelbeck, T. (2018). Auditory speed tasks as potential candidates for the study of cognitive ageing. *Neuropsychol. Dev. Cogn. B Aging Neuropsychol. Cogn.* 25, 167–185. doi: 10.1080/13825585.2016.1272671

Zeng, F. G. (2013). An active loudness model suggesting tinnitus as increased central noise and hyperacusis as increased nonlinear gain. *Hear. Res.* 295, 172–179. doi: 10.1016/j.heares.2012.05.009

Zeng, F. G. (2020). Tinnitus and hyperacusis: Central noise, gain and variance. *Curr. Opin. Physiol.* 18, 123–129. doi: 10.1016/j.cophys.2020.10.009

Zhu, Y., Qiao, W., Liu, K., Zhong, H., and Yao, H. (2015). Control of response reliability by parvalbumin-expressing interneurons in visual cortex. *Nat. Commun.* 6:6802. doi: 10.1038/ncomms7802

Zuccotti, A., Kuhn, S., Johnson, S. L., Franz, C., Singer, W., Hecker, D., et al. (2012). Lack of brain-derived neurotrophic factor hampers inner hair cell synapse physiology, but protects against noise-induced hearing loss. *J. Neurosci.* 32, 8545–8553. doi: 10.1523/JNEUROSCI.1247-12.2012

Zumer, J. M., Brookes, M. J., Stevenson, C. M., Francis, S. T., and Morris, P. G. (2010). Relating BOLD fMRI and neural oscillations through convolution and optimal linear weighting. *NeuroImage* 49, 1479–1489. doi: 10.1016/j.neuroimage.2009.09.020

Conflict of Interest: The authors declare that the research was conducted in the absence of any commercial or financial relationships that could be construed as a potential conflict of interest.

Publisher's Note: All claims expressed in this article are solely those of the authors and do not necessarily represent those of their affiliated organizations, or those of the publisher, the editors and the reviewers. Any product that may be evaluated in this article, or claim that may be made by its manufacturer, is not guaranteed or endorsed by the publisher.

frontiers in Neural Circuits

ORIGINAL RESEARCH
published: 03 February 2022
doi: 10.3389/fncir.2022.784396

Brain-Derived Neurotrophic Factor Is Involved in Activity-Dependent Tonotopic Refinement of MNTB Neurons

*Mackenna Wollet and Jun Hee Kim**

Department of Cellular and Integrative Physiology, UT Health San Antonio, San Antonio, TX, United States

In the mammalian brain, auditory brainstem nuclei are arranged topographically according to acoustic frequency responsiveness. During postnatal development, the axon initial segment (AIS) of principal neurons undergoes structural refinement depending on location along the tonotopic axis within the medial nucleus of the trapezoid body (MNTB). However, the molecular mechanisms underlying the structural refinement of the AIS along the tonotopic axis in the auditory brainstem have not been explored. We tested the hypothesis that brain-derived neurotrophic factor (BDNF) is a molecular mediator of the structural development of the MNTB in an activity-dependent manner. Using *BDNF* heterozygous mutant ($BDNF^{+/-}$) mice, we examined the impact of global BDNF reduction on structural and functional development of MNTB neurons by assessing AIS structure and associated intrinsic neuronal properties. BDNF reduction inhibits the structural and functional differentiation of principal neurons along the tonotopic axis in the MNTB. Augmented sound input during the critical period of development has been shown to enhance the structural refinement of the AIS of MNTB neurons. However, in $BDNF^{+/-}$ mice, MNTB neurons did not show this activity-dependent structural modification of the AIS following repeated sound stimulation. In addition, $BDNF^{+/-}$ mice lacked a defined isofrequency band of neuronal activity following exposure to 16 kHz sound, suggesting degradation of tonotopy. Taken together, structural development and functional refinement of auditory brainstem neurons require physiological levels of BDNF to establish proper tonotopic gradients.

Keywords: BDNF, auditory brainstem, MNTB, tonotopy, axon initial segment

OPEN ACCESS

Edited by:
Conny Kopp-Scheinpflug, Ludwig Maximilian University of Munich, Germany

Reviewed by:
Ian D. Forsythe, University of Leicester, United Kingdom
R. Michael Burger, Lehigh University, United States

****Correspondence:***
Jun Hee Kim
kimjh@uthscsa.edu

Received: *27 September 2021*
Accepted: *07 January 2022*
Published: *03 February 2022*

Citation:
Wollet M and Kim JH (2022) Brain-Derived Neurotrophic Factor Is Involved in Activity-Dependent Tonotopic Refinement of MNTB Neurons. Front. Neural Circuits 16:784396. doi: 10.3389/fncir.2022.784396

INTRODUCTION

Along the auditory processing pathway, the topographic organization of neurons is important for determining where sound frequencies are processed within each auditory nucleus. In the MNTB, one of the key sound localization nuclei in the auditory brainstem, neurons are arranged with graded frequency-responsiveness (from high- to low-frequency) along the medio-lateral axis, respectively. Physiological factors including ion channel expression and cell morphology

(e.g., soma size) are graded along the tonotopic axis in brainstem nuclei (Weatherstone et al., 2017; Akter et al., 2018). For example, voltage-gated potassium channel (K_V3) is highly expressed in high-frequency responding neurons, and expression decreases moving toward low-frequency responding neurons in a graded fashion in the mouse and avian brainstem (Li et al., 2001; Parameshwaran et al., 2001; von Hehn et al., 2004; Leao et al., 2006). In contrast to K_V3 channels, K_V1 channels have the opposite expression pattern within the MNTB with the highest K_V1 density laterally (Leao et al., 2006). In terms of cell morphology, the soma size of MNTB neurons is different along the tonotopic axis, where lateral neurons are larger than medial neurons (Weatherstone et al., 2017). In addition, the length and location of the AIS, a key axonal domain responsible for action potential (AP) initiation and neuronal excitability, is also dependent on cell location along the tonotopic axis in the chick and mouse (Kuba et al., 2006, 2014; Kim et al., 2019). Tonotopic refinement of the AIS is impaired in deaf animals- either congenitally or *via* cochlear removal (Kuba et al., 2010; Kim et al., 2019). Oppositely, AIS tonotopic differentiation is enhanced following increased neural activity driven by acoustic enrichment during the critical development period in mice (Kim et al., 2019). The structural refinement of the AIS is dependent on tonotopic location and requires sound-evoked activity in the auditory brainstem. The AIS determines neuronal excitability and modulates neuronal output, thus can control auditory processing along the ascending auditory pathway (Kuba et al., 2006; Grubb and Burrone, 2010). However, the molecular mechanisms driving establishment of the tonotopic gradient of the AIS in the MNTB are unknown.

Previous work in cultured hippocampal neurons showed BDNF signaling regulates AIS location and affects neuronal excitability (Guo et al., 2017). Here, we investigated whether BDNF, an essential molecule for activity-dependent plasticity, is a molecular mediator for establishing tonotopic gradients of the AIS and associated neuronal properties in the auditory brainstem. BDNF expression begins in the inner ear at postnatal day 4 (P4) and the expression pattern follows the ascending pathway during development (Hafidi, 1999; Wiechers et al., 1999). By P14, *BDNF* mRNA expression is arranged tonotopically within the cochlea where expression is highest in the apical and medial turns, opposite of the *NT3* mRNA expression gradient (Schimmang et al., 2003). Acoustic enrichment increases BDNF transcript levels and protein levels in rodent brainstem due to increased neuronal activity (Wang et al., 2011; Matt et al., 2018). Using anti-BDNF antibodies to neutralize BDNF signaling, activity-dependent plasticity of tonotopy following pure tone sound stimulation was prevented in the rat auditory cortex (Anomal et al., 2013). We studied the effects of globally reduced BDNF levels on structural and intrinsic properties of MNTB neurons along the tonotopic axis in $BDNF^{+/-}$ mice. Given the role of BDNF in sound-evoked activity, tonotopic plasticity, and structural differentiation, we found that BDNF is one of the molecular mediators responsible for establishing structural tonotopic gradients and related physiological properties of auditory brainstem neurons during postnatal development.

MATERIALS AND METHODS

Animals

Both sexes of wild-type (WT) mice and $BDNF^{+/-}$ mice with a C57BL/6J background were used under the guidelines approved by the UT Health San Antonio Institutional Animal Care and Use Committee. BDNF heterozygous mice (B6.129S4-*Bdnf*^{tm1Jae}/J) were obtained from Jackson Labs in heterozygous breeding pairs. All experiments were done between postnatal days 9 and 11 (P9-P11; **Figure 3**) and P18-P23 (**Figures 1**, **2**, **4**, **5**) during the animals' light cycle. Animals were housed in a 12-h light/dark cycle.

Sound Stimulation

Mice were exposed to random noise centered at 16 kHz frequency at 80 dB during their light cycle for 3 h per day from P13 to P19 (**Figure 4**). Sixteen kHz pure tone exposure at 80 dB occurred during the light cycle for 90 min preceded by 60 min of silence in the sound attenuation chamber (**Figure 5**; Med Associates, Albans, VT) and the stimuli were generated by Tucker Davis Technologies equipment and software.

Slice Preparation

Mice were anesthetized with isoflurane then rapidly decapitated. The brains were then quickly removed and immersed in ice-cold low-calcium artificial cerebrospinal fluid (aCSF) containing (in mM): 125 NaCl, 2.5 KCl, 3 $MgCl_2$, 0.1 $CaCl_2$, 25 glucose, 25 $NaHCO_3$, 1.25 NaH_2PO_4, pH 7.4 bubbled with carbogen (95% O_2, 5% CO_2; osmolarity 310–320 mOsm. Transverse 200 μm-thick brainstem slices containing the MNTB were collected using a Vibratome (VT1200S, Leica, Germany). Slices were then prepared further for either electrophysiology or immunohistochemistry experiments.

Immunohistochemistry

Brain slices were fixed with 4% paraformaldehyde (PFA) for 10 min then washed with PBS three times. Free-floating slices were blocked in 4% goat serum and 0.3% (w/v) Triton X-100, 0.1% Tween 20 in PBS for 1 h and then were incubated with primary antibody overnight at 4°C. Primary antibodies used: Anti-Ankyrin G (Mouse IgG1, NeuroMab, 1:200), Anti-MAP2 (Rabbit or Mouse IgG1, Millipore, 1:500), Anti-β4-spectrin (Rabbit; Bhat lab, UTHSCSA, 1:500), Anti-c-Fos (Rabbit, Synaptic Systems, 1:500). Slices were washed with PBS three times then incubated with corresponding secondary antibodies for 2 h at room temperature. Secondary antibodies (Invitrogen): Alexa Fluor 555 goat anti-GP, Alexa Fluor 488 goat anti-rabbit, and Alexa Fluor 647 goat anti-mouse IgG1 all at 1:500 dilution. Analysis of Z-stack confocal images was performed in Fiji. Medial neurons are in the most medial 30% of the MNTB, and lateral neurons are located in the most lateral 30% of the MNTB. Identification of neuronal AIS utilized either AnkG or β4-spectrin on $MAP2^+$ cells. A segmented line tool in Fiji was used to measure length and distance from the soma. AIS length

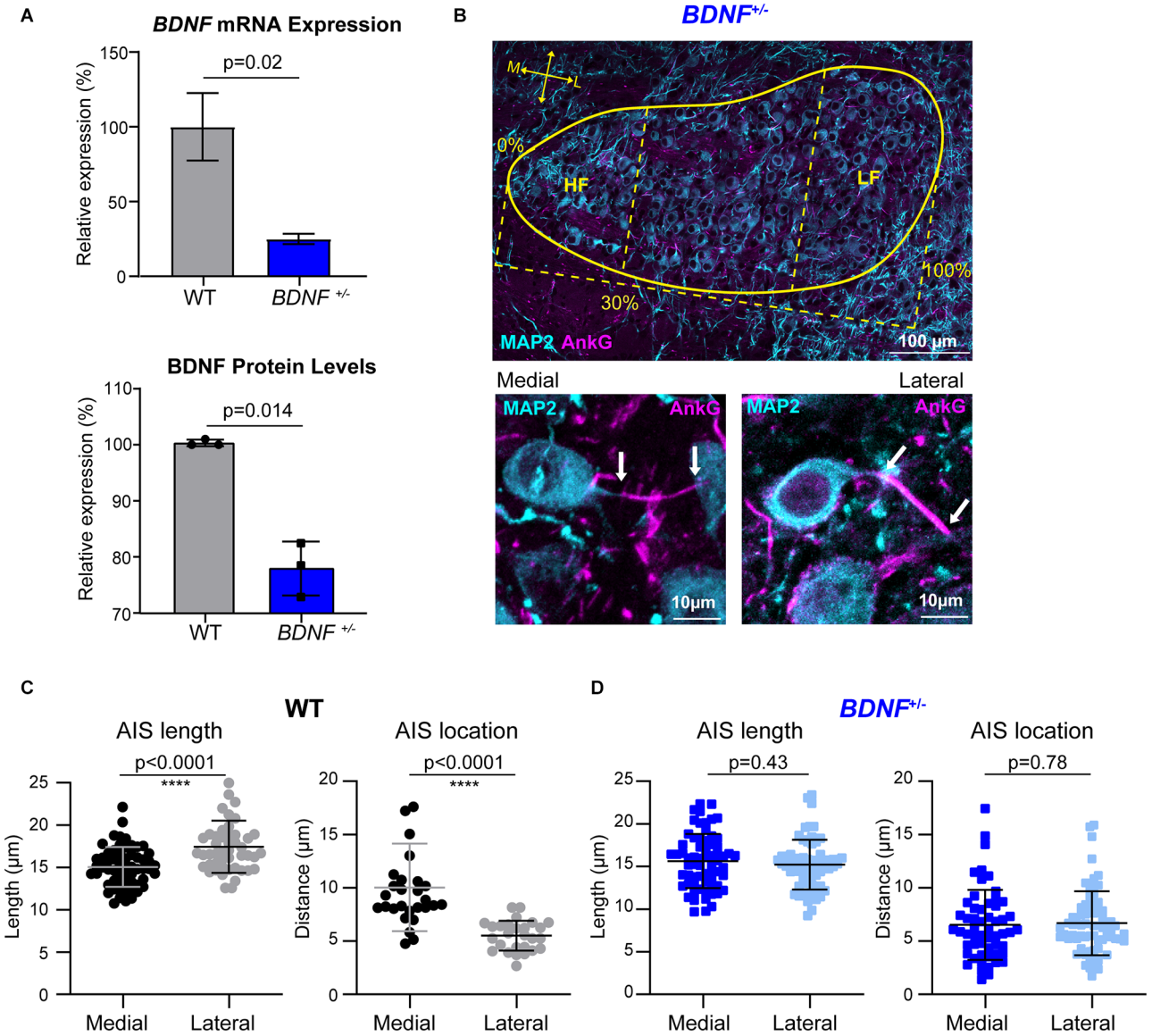

FIGURE 1 | The tonotopic arrangement of the AIS in MNTB neurons is abolished in *BDNF*$^{+/-}$ mice. **(A)** *BDNF* mRNA expression (top) and BDNF protein level (bottom) in the MNTB from WT and *BDNF*$^{+/-}$ mice using qPCR and Western Blot, respectively. *BDNF* mRNA expression and protein level from *BDNF*$^{+/-}$ mice were normalized by those from WT (indicated by Relative expression, %). **(B)** The MNTB (at P20, the yellow line indicates border) was immunostained with MAP2 (cyan) and AnkG (magenta). HF indicates the high-frequency responding region, 30% of the medial (M) MNTB, and LF indicates the low-frequency responding region, 30% of the lateral (L) MNTB. (Bottom) Magnified images of medial and lateral MNTB neurons of *BDNF*$^{+/-}$ mice. Arrows indicate the proximal and distal ends of AIS. **(C)** Summary of length (µm) and location (distance from the soma) of the AIS in WT MNTB neurons. **(D)** AIS length and distance from soma from *BDNF*$^{+/-}$ medial and lateral neurons. Each point represents individual cells from three WT mice and four *BDNF*$^{+/-}$ mice. All error bars represent mean ± SD. **** indicates $p < 0.0001$.

was measured from the proximal end of AnkG$^+$ (or β4-spectrin$^+$) signal to the most distal end, and AIS location was measured from the proximal end of AnkG$^+$ (or β4-spectrin$^+$) signal to edge of cell soma. For c-Fos analysis, the double staining against MAP2 and c-Fos were performed from WT and *BDNF*$^{+/-}$ mice. MAP2- and c-Fos-positive cells (c-Fos$^+$ neurons) were counted using the cell counter plugin of Fiji software. Only the cells with c-Fos$^+$ nuclei were counted and the constant threshold level of fluorescence intensity was used in each slice. The percentage of c-Fos$^+$ cells was calculated by dividing the number of c-Fos$^+$ MAP2$^+$ MNTB neurons by the total number of MAP2$^+$ MNTB neurons in each slice. Details were described in Kim et al. (2019).

Electrophysiology

After vibratome sectioning, slices were incubated in a chamber containing normal aCSF bubbled with carbogen at 35°C for 30 min and then kept at room temperature. The normal aCSF was the same as the low-calcium aCSF, except 3 mM $MgCl_2$ and 0.1 mM $CaCl_2$ were increased to 1 mM $MgCl_2$ and 2 mM $CaCl_2$. Whole-cell patch-clamp recording was carried

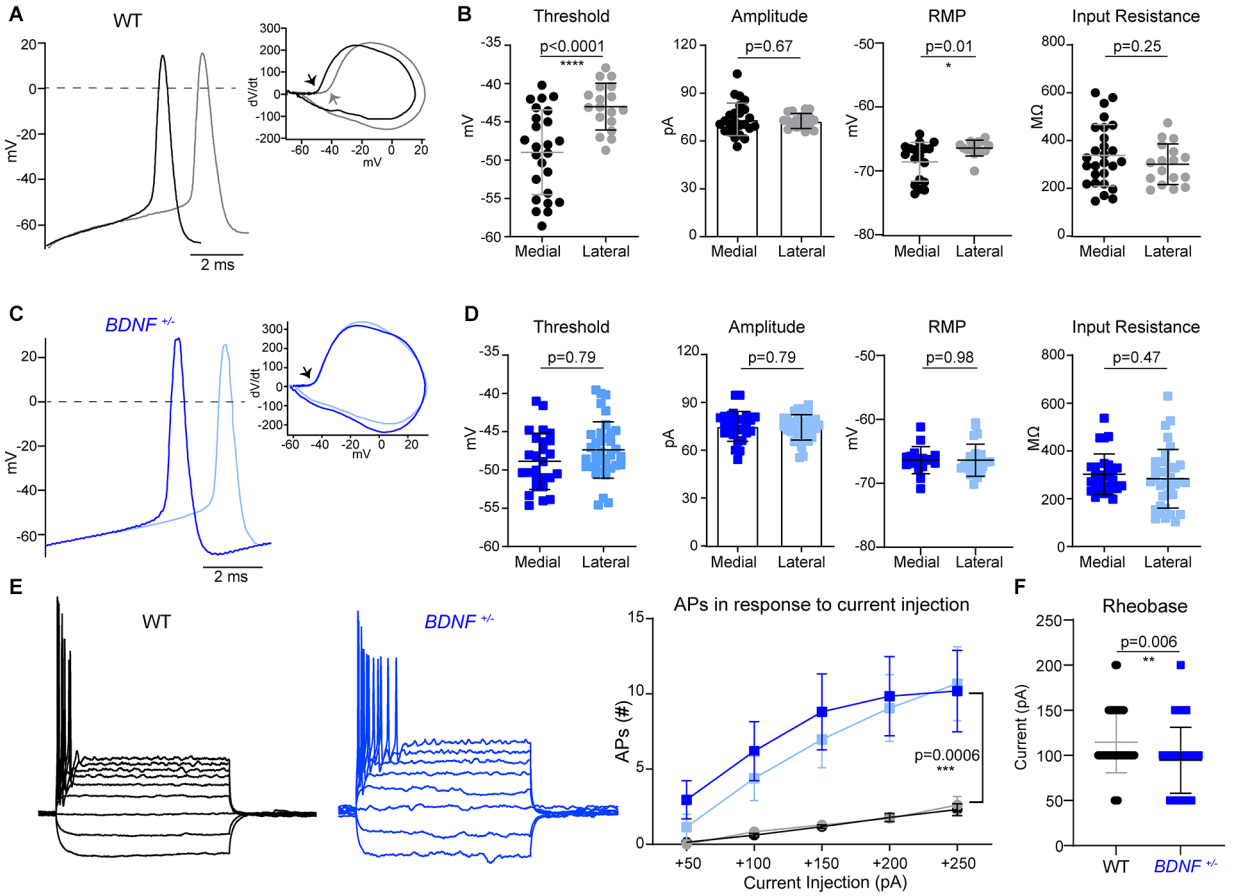

FIGURE 2 | The difference in MNTB neuron intrinsic properties along the tonotopic axis is abolished in *BDNF*$^{+/-}$ mice. **(A)** Representative traces of APs evoked by current injection from medial (black) and lateral (gray) MNTB neurons in WT. Inset, dV/dt phase plot against membrane potential. The arrow points to the AP threshold, which differs between medial and lateral WT neurons. **(B)** Summary of AP threshold; determined as the membrane potential at dV/dt = 10, AP amplitude; determined as the difference between threshold and peak potential of AP, resting membrane potential, and input resistance of WT neurons. Each point represents an individual cell from 13 mice (medial) and seven mice (lateral). * indicates $p < 0.05$ and **** indicates $p < 0.0001$. **(C)** Representative traces of APs from *BDNF*$^{+/-}$ medial (dark blue) and lateral (light blue) neurons. dV/dt phase plot shows no difference in AP threshold between medial and lateral. **(D)** Summary of AP threshold, amplitude, resting membrane potential, and input resistance from *BDNF*$^{+/-}$ MNTB neurons. $n = 10$ mice (medial) and nine mice (lateral). **(E)** Membrane potential changes in WT and *BDNF*$^{+/-}$ neurons in response to step-like current injections from −100 pA to +250 pA in increments of 50 pA (left). The number of spikes in response to depolarizing current injection (right). Repeated measures ANOVA displayed significant difference based on genotype ($F_{(1, 99)} = 12.55$; $p = 0.0006$). *** indicates $p < 0.001$. **(F)** Rheobase current was quantified by genotype in WT and *BDNF*$^{+/-}$ neurons. ** indicates $p < 0.01$.

out on postsynaptic principal neurons in the MNTB at room temperature (∼24°C). Action potentials (APs) were recorded in normal aCSF using the current-clamp mode of the EPC-10 (HEKA Electronik, Lambrecht/Pfalz, Germany). The pipettes were filled with an internal solution containing (in mM) 125 K-gluconate, 20 KCl, 5 Na_2-phosphocreatine, 10 HEPES, 4 Mg-ATP, 0.2 EGTA, and 0.3 GTP, pH adjusted to 7.3 with KOH. The holding potential was −65 mV in the voltage-clamp mode. Current-clamp protocols were 200 ms in duration with current steps from −100 to 250 pA (50 pA increments). Patch electrodes had resistances of 4–5 MΩ. Series resistance was <15 MΩ without compensation. The threshold of AP was determined by the point where dV/dt exceeds 10 V/s and the amplitude of AP from the threshold to the AP peak in the plot of dV/dt and voltage, which were taken from the first AP evoked in depolarizing current injection protocol. Data were analyzed and displayed with Igor Pro (Wavemetrics, Lake Oswego, OR, United States).

Western Blot

Whole tissue lysate of WT and *BDNF*$^{+/-}$ brainstems (at P21) were extracted with RIPA buffer. Equal protein amounts were loaded onto a 4–15% Tris/Glycine precast gel (Bio-Rad) and transferred to a nitrocellulose membrane. Membranes were blotted with anti-BDNF (Rb, 1:200, Abcam) and anti-β-actin (Mouse, 1:1,000; Abcam), which was used for normalization. Fluorescent secondary antibodies used: Mouse-800CW (1:7,500, LI-COR) and Rabbit-680RD (1:7,500, LI-COR). Membranes were imaged on Odyssey CLx (LI-COR), and images analyzed using Fiji software.

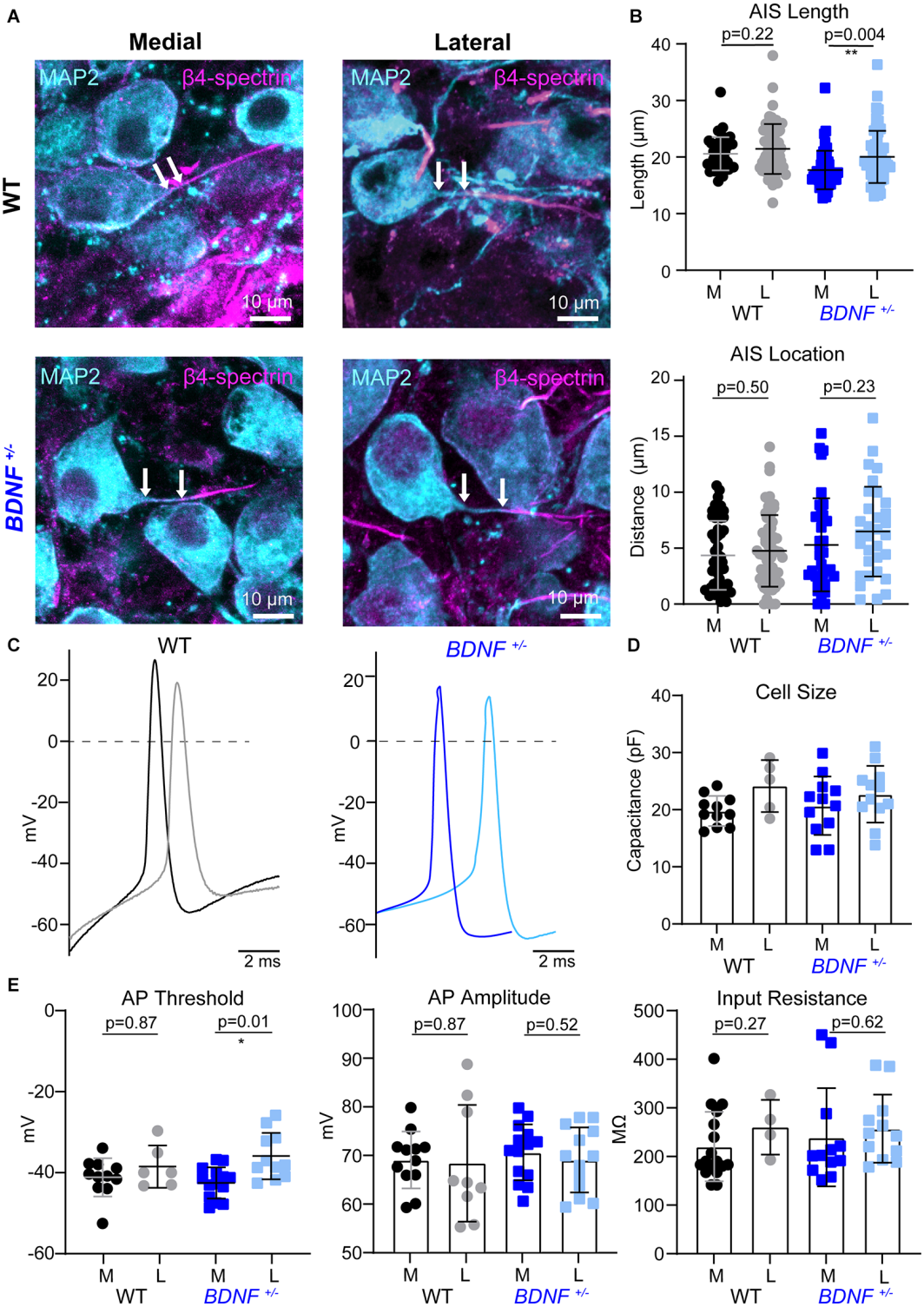

FIGURE 3 | AIS structures and intrinsic properties of MNTB neurons at pre-hearing age. **(A)** MNTB neurons (MAP2, cyan) and corresponding AIS (β4-spectrin, magenta) of WT and *BDNF*$^{+/-}$ mice (at P9). Scale bar represents 10 μm. Arrows point to the edge of the soma and proximal end of the AIS, indicating the distance of the AIS. **(B)** Quantification of AIS location and length according to genotype and tonotopic location. Each point represents an individual cell from three mice/group. ** indicates $p < 0.01$. **(C)** Representative AP traces of medial and lateral neurons from WT and *BDNF*$^{+/-}$mice. **(D)** Individual cell size was quantified by capacitance (pF) measurements during whole-cell recordings. Each point represents an individual cell. **(E)** Summary of AP threshold, amplitude, and input resistance by genotype and tonotopic location from five WT mice and four *BDNF*$^{+/-}$ mice. * indicates $p < 0.05$.

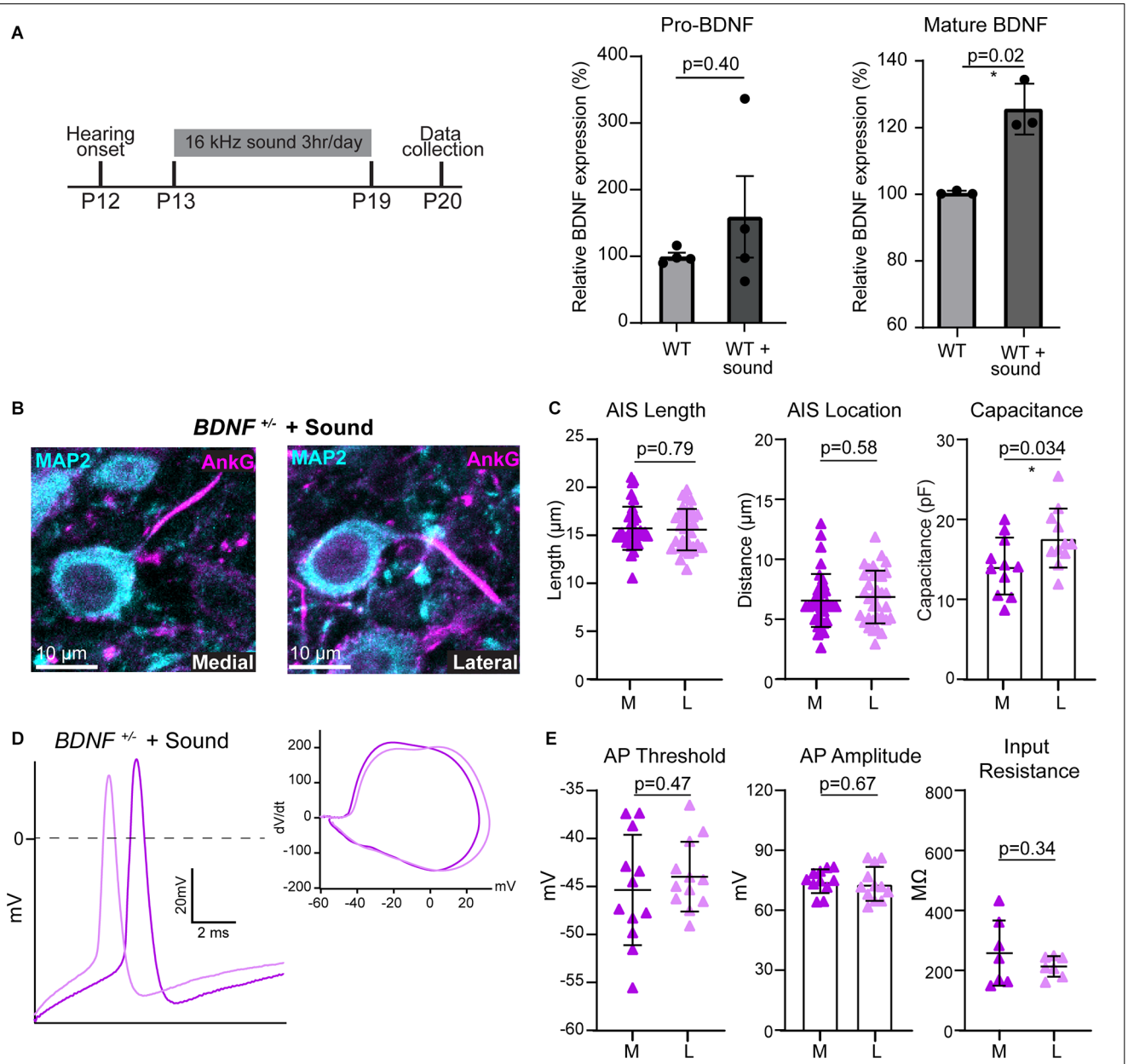

FIGURE 4 | BDNF is necessary for the activity-dependent plasticity of MNTB neurons. **(A)** Sound stimulation paradigm schematic; 16 kHz sound for 3 h/day from P13 to P19 followed by data collection and mature and pro-BDNF protein levels in WT and WT + sound. * indicates $p < 0.05$. **(B)** MNTB neurons of *BDNF*$^{+/-}$ mice following sound stimulation were immunostained with anti-MAP2 (cyan) and anti-AnkG (magenta). **(C)** AIS length and location, and cell size were quantified by condition and tonotopic location. Each point represents individual cells from four mice for *BDNF*$^{+/-}$ and three mice for *BDNF*$^{+/-}$ + sound. **(D)** Representative AP traces from *BDNF*$^{+/-}$ medial (dark purple) and lateral (light purple) neurons after sound stimulation. Inset, dV/dt phase plot against membrane potential. **(E)** Summary of AP threshold, amplitude, and input resistance were quantified for each condition and tonotopic location. Each point represents an individual cell.

Quantitative Polymerase Chain Reaction (qPCR)

RNA isolation and reverse transcription reaction were performed as previously described in Kim et al. (2019). RNA extraction was done from p9 whole brain tissue of WT and *BDNF*$^{+/-}$ mice using RNAqueous kit with no alterations to procedure (AM1931, Thermofisher). qPCR was executed using 7900HT Fast Real-Time PCR system (Applied Biosystems), data were analyzed using SDS v2.4 (Applied Biosystems). *GAPDH* was used as a reference housekeeping gene. Delta (Δ) CT ($Mean_{Gene}$-$Mean_{GAPDH}$) was utilized to calculate ΔΔCT (ΔCT_{Pos}-ΔCT_{Neg}), and data was normalized to WT (100%). Mouse primers used: BDNF Forward: 5'-TCGTTCCTTTCGAGTTAGCC, BDNF Reverse: 5'-TTGGTAAACGGCACAAAAC, GAPDH Forward: 5'-AGTATGACTCCACTCACGGCAA, and GAPDH Reverse: 5'-TCTCGCTCCTGGAAGATGGT.

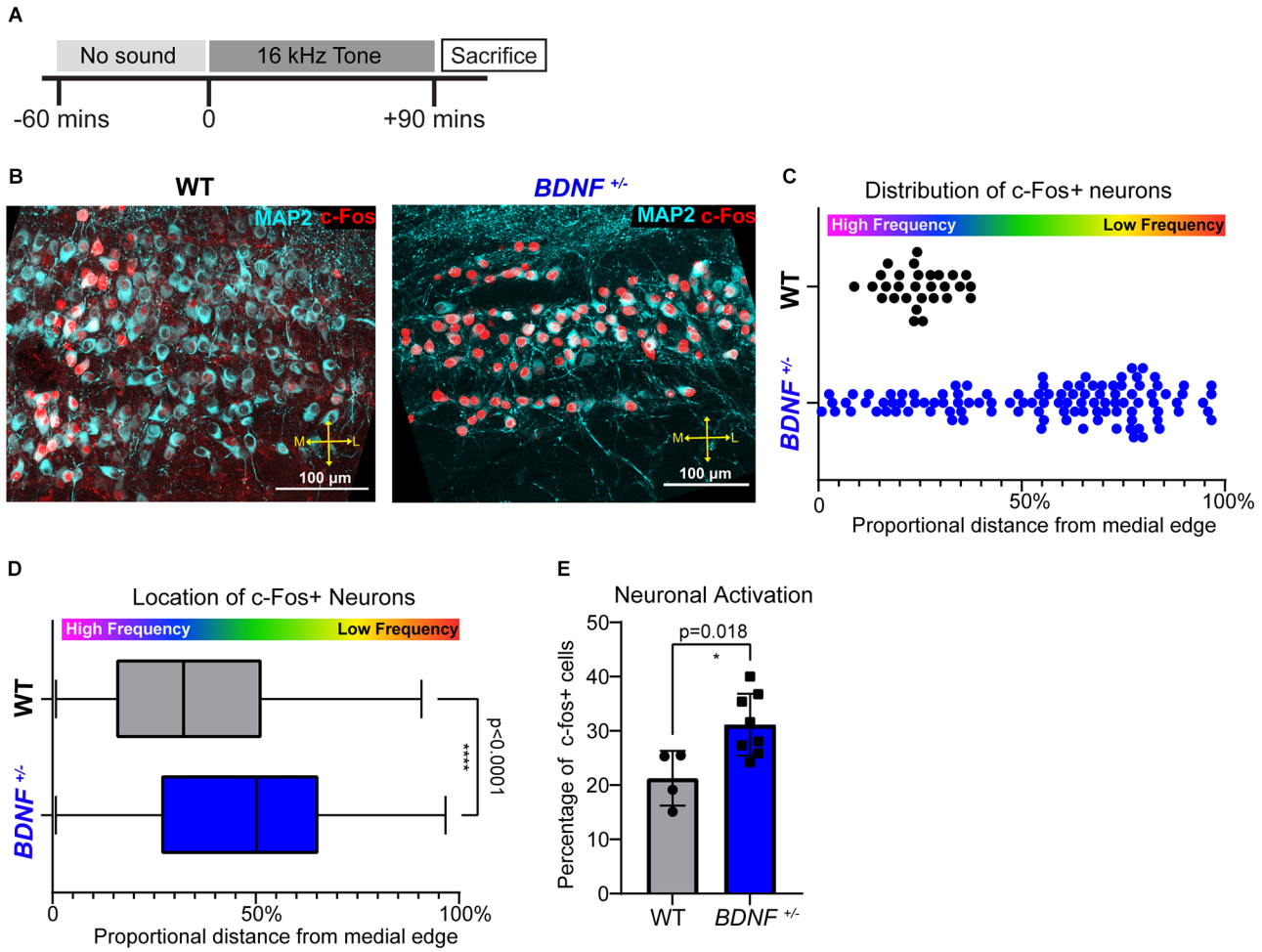

FIGURE 5 | High frequency sound responding neurons is not tonotopically organized in *BDNF*$^{+/-}$ mice. **(A)** Tone exposure paradigm schematic. P21 mice were exposed to a pure 16 kHz tone for 90 min preceded by 60 min of silence in a sound-attenuated chamber. **(B)** Representative image of the MNTB immunostained with MAP2 (cyan) and c-Fos (red). Scale bars represent 100 µm. **(C)** Quantification of the representative image in **(B)** displayed as proportional location of each c-Fos^{+} neuron from the medial edge of MNTB (see the MNTB border and proportional location in **Figure 1B**). Each point represents one cell. Activated MNTB neurons in *BDNF*$^{+/-}$ are more laterally located (median: 24.29% in *BDNF*$^{+/}$ and 61.12% in WT; $p < 0.0001$, Mann-Whitney U test). **(D)** Distribution analysis of c-Fos^{+} neurons displayed as the proportional distance from the medial edge of MNTB where 0% is the medial edge of the MNTB and 100% is the most lateral edge of the MNTB. Activated MNTB neurons in *BDNF*$^{+/-}$ are more laterally located ($p < 0.0001$, Mann-Whitney U test) and widespread compared to WT ($p < 0.0001$, Kolmogorov-Smirnov test). **** indicates $p < 0.0001$. **(E)** Quantification of c-Fos^{+} neurons divided by total MNTB neurons between genotypes. *BDNF*$^{+/-}$ mice ($n = 5$) have larger proportion of c-Fos^{+} MNTB neurons compared to WT ($n = 3$) mice ($p = 0.018$, Wel.ch's *t*-test). * indicates $p < 0.05$.

Statistics

All statistical analyses were performed in GraphPad Prism version 9.2.0 for Windows (GraphPad Software, San Diego, CA, United States). The normality of datasets was analyzed using the Kolmogorov-Smirnov test. Parametric or non-parametric tests were carried out accordingly. To compare the two groups, an unpaired *t*-test with Welch's correction (parametric) or Mann-Whitney U test (non-parametric) was carried out. To compare three or more groups, one-way ANOVA with Turkey's multiple comparison test was used. Values in results are represented as mean ± SD. Error bars in figures are ± SD. In **Figure 5**, Kolmogorov-Smirnov tests are used to evaluate the distribution of c-Fos^{+} cells. **Figure 5** contains a box and whisker plot with the median as the center to display neuron distribution within the MNTB.

RESULTS

Global Reduction of BDNF Impairs Structural Differentiation of the AIS Along the Tonotopic Axis in the MNTB

The AIS of MNTB neurons is differentiated by structure and function along the tonotopic axis during postnatal development (Kim et al., 2019). To determine whether BDNF mediates the structural refinement of the AIS along the tonotopic axis, we examined the effects of globally reduced BDNF on AIS

length and location along the medial-lateral axis in the MNTB using *BDNF*$^{+/-}$ mice. Analysis of *BDNF* mRNA and protein using qPCR and Western Blot respectively showed a significant reduction of *BDNF* mRNA expression and BDNF protein level in *BDNF*$^{+/-}$ mice compared to WT (mRNA: ∼75% reduction in *BDNF*$^{+/-}$, $p = 0.026$, Welch's *t*-test, $n = 2$ and 3; protein: ∼22% reduction in *BDNF*$^{+/-}$, $p = 0.014$, Welch's *t*-test, $n = 3$/group; **Figure 1A**). In WT and *BDNF*$^{+/-}$ mice (at P20 ± 2 days), we quantified the AIS length and location, measured by the distance from principal neuron soma, as described in Kim et al. (2019). The MNTB was proportionally defined by the percent of the total distance from medial to lateral edges of the MNTB, where medial neurons are within 30% of the medial MNTB border and lateral neurons are within 30% of the lateral MNTB border (**Figure 1B**). Using MAP2 and AnkG immunostaining, we examined the effect of reduced BDNF on AIS structural properties of MNTB neurons along the tonotopic axis in *BDNF*$^{+/-}$ mice (**Figure 1C**). In WT mice, the AIS length and location of medial MNTB neurons were significantly different from lateral MNTB neurons. In WT mice, the AIS length was 15.05 ± 2.35 μm ($n = 59$ cells) for medial neurons and 17.43 ± 3.09 μm ($n = 48$ cells) for lateral neurons ($p < 0.0001$; Welch's 2-tailed *t*-test). The AIS distance from the soma was 10.03 ± 4.10 μm (medial) and 5.51 ± 1.40 μm (lateral, $p < 0.0001$, Welch's 2-tailed *t*-test; $n = 27$ and 28 cells respectively; **Figure 1D**). Consistent with our previous work (Kim et al., 2019), AIS length was significantly shorter and more distal from the soma in medial MNTB neurons compared to lateral MNTB neurons. In *BDNF*$^{+/-}$ mice, MNTB neurons did not show this structural differentiation in the AIS length or distance along the tonotopic axis. AIS length was 15.64 ± 3.19 μm in medial neurons and 15.21 ± 2.92 μm in lateral neurons ($p = 0.43$, Student's *t*-test, $n = 66$ and 64 cells respectively). AIS distance from soma was 6.53 ± 3.29 μm in medial neurons and 6.68 ± 2.99 μm in lateral neurons ($p = 0.78$, Student's *t*-test, $n = 56$ and 68 cells respectively; **Figure 1E**). Reduced global BDNF disrupts the tonotopic refinement of AIS properties in the MNTB, indicating that BDNF is associated with the structural development of MNTB neurons. In addition to AIS structural properties, the soma size of MNTB neurons is dependent on location; lateral MNTB neurons are larger than medial neurons (Weatherstone et al., 2017). In the current study, membrane capacitance measurements using whole-cell patch-clamp recordings showed the tonotopic gradient in WT neurons. WT medial neurons had membrane capacitance of 17.02 ± 4.25 pF ($n = 25$), whereas lateral neurons had 20.11 ± 4.65 pF ($n = 32$ neurons, $p = 0.01$, Student's *t*-test; **Table 1**). Similarly, *BDNF*$^{+/-}$ mice maintained the tonotopic differentiation of membrane capacitance: medial neurons had a smaller capacitance (13.72 ± 3.20 pF, $n = 27$) than lateral neurons (17.18 ± 3.16 pF, $n = 37$, $p < 0.0001$, Student's *t*-test; **Table 1**). Notably, regardless of neuron location, MNTB neurons were significantly smaller in *BDNF*$^{+/-}$ mice compared to WT. Taken together, the reduction of BDNF disrupts the tonotopic differentiation of AIS length and location in the MNTB. The result indicates that globally reduced levels of BDNF impair the structural development of MNTB principal neurons along the tonotopic axis.

Tonotopic Organization of MNTB Neuron Intrinsic Properties Is Abolished in *BDNF*$^{+/-}$ Mouse

Next, we investigated how structural alterations of the AIS, caused by BDNF reduction, impact the intrinsic properties and firing pattern of MNTB neurons in *BDNF*$^{+/-}$ mice. APs were recorded from medial and lateral MNTB neurons in response to current injections (from −100 pA to 250 pA, Δ = 50 pA). Phasic plotting the dV/dt of APs from MNTB neurons, evoked by a depolarizing current injection, was analyzed (**Figure 2A**). In WT mice (at P20), medial neurons had a lower AP threshold and resting potential (more hyperpolarized) compared with lateral neurons, indicating there was a difference in intrinsic properties of MNTB neurons along the tonotopic axis (Threshold, medial: −48.98 ± 5.53 mV and lateral: −41.86 ± 3.06 mV, $p < 0.0001$, Welch's test; RMP, medial: −68.58 ± 3.03 mV and lateral: −66.42 ± 1.22 mV, $p = 0.01$, Welch's test). However, there was no difference in AP amplitude, half-width, or input resistance between medial and lateral WT neurons (**Figure 2B**, **Table 1**). In *BDNF*$^{+/-}$ mice, there was no difference in AP threshold or resting membrane potential of MNTB neurons along the tonotopic axis (**Figures 2C,D**). AP threshold was −48.87 ± 3.68 mV ($n = 26$) in medial neurons and −47.38 ± 3.68 mV ($n = 36$) in lateral neurons ($p = 0.12$, Student's *t*-test). RMP was −66.38 ± 2.12 mV ($n = 17$) in medial neurons and −66.40 ± 2.52 mV ($n = 24$) in lateral neurons ($p = 0.98$, Student's *t*-test). There was no difference in AP amplitude, half-width, or input resistance between medial and lateral neurons in *BDNF*$^{+/-}$ mice (**Figure 2D**, **Table 1**). Thus, global BDNF reduction affects tonotopic differentiation in the AIS and intrinsic properties of MNTB neurons during postnatal development.

Regardless of their location along the tonotopic axis, MNTB neurons from *BDNF*$^{+/-}$ mice showed an increased number of AP spikes evoked by depolarizing current injections (50 pA to 250 pA), compared with WT mice ($p = 0.0006$, ANOVA; **Figure 2E**). In response to 200 pA current injection (100 ms), the number of spikes was significantly greater in *BDNF*$^{+/-}$ mice (9.4 ± 13.04 APs, $n = 61$ cells) than WT mice (1.76 ± 1.11 APs, $n = 41$ cells, $p < 0.0001$, Welch's *t*-test), indicating increased excitability in *BDNF*$^{+/-}$ neurons. Rheobase currents were significantly smaller in *BDNF*$^{+/-}$ mice (94.62 ± 36.58 pA) than WT mice (114.6 ± 34 pA, $p = 0.006$, Student's *t*-test; **Figure 2F**). The results indicate that reduced BDNF increases the excitability of MNTB neurons regardless of their location.

At Pre-hearing Age, Reduction of BDNF Does Not Impact Tonotopic Segregation of AIS Structure in the MNTB

BDNF reduction altered structural and physiological development of MNTB neurons that might be dependent on sound-evoked activity after hearing onset at P12. It is possible that BDNF reduction impacts intrinsic properties of MNTB neurons before hearing onset when the auditory processing is dependent on the spontaneous cochlear activity instead of sound-evoked activity. Thus, to test whether a physiological level of BDNF is critical for intrinsic development, which is independent

TABLE 1 | Summary of intrinsic properties of MNTB neurons.

Values represented as Mean ± SD	WT Medial	WT Lateral	BDNF$^{+/-}$ Medial	BDNF$^{+/-}$ Lateral
Rheobase (pA)	112 ± 36.66^{A} n = 19	108.4 ± 32.83^{A} n = 15	92.86 ± 37.07^{A} n = 28	93.42 ± 37.07^{A} n = 38
Input Resistance (MΩ)	338 ± 128.7^{A} n = 27	301 ± 84.74^{A} n = 17	302.6 ± 84.74^{A} n = 28	284 ± 123^{A} n = 36
Resting Membrane (mV)	−68.58 ± 3.03^{A} n = 18	−66.42 ± 1.23^{B} n = 15	−66.38 ± 2.12^{B} n = 17	−66.40 ± 2.52^{B} n = 24
AP Threshold (mV)	−48.98 ± 5.53^{A} n = 25	−43 ± 3.06^{B} n = 18	−48.87 ± 3.68^{AB} n = 26	−47.38 ± 3.68^{A} n = 36
AP Amplitude (pA)	73.53 ± 10.22^{A} n = 25	72.55 ± 4.69^{A} n = 18	75 ± 9.37^{A} n = 26	74.4 ± 7.92^{A} n = 35
AP Half-width (s)	0.57 ± 0.13^{A} n = 18	0.52 ± 0.06^{A} n = 15	0.56 ± 0.12^{A} n = 16	0.56 ± 0.17^{A} n = 20
Capacitance (pF)	17.02 ± 4.25^{A} n = 25	20.11 ± 4.56^{B} n = 32	13.72 ± 3.21^{C} n = 27	17.18 ± 3.16^{A} n = 37

Within rows, means with superscripts containing the same letter are not significantly different. Within the same row, all values with an "A" superscript are not statistically different from each other, and all values with "B" superscript are not statistically different from each other. Within a row, means superscripted with "A" are statistically different from means superscripted with "B".

of sound input, we examined the structural properties of the AIS between pre-hearing *BDNF*$^{+/-}$ and WT mice at P9. Pre-hearing WT mice show no tonotopic segregation of AIS properties between medial and lateral neurons (**Figures 3A,B**), supporting the previous finding that the tonotopic refinement of AIS structures occurs in an activity-dependent manner after hearing onset. However, *BDNF*$^{+/-}$ neurons showed a tonotopic differentiation of AIS length without difference in AIS distance from the soma between medial and lateral neurons. In *BDNF*$^{+/-}$ mice at P9, AIS length was shorter in medial neurons than lateral neurons (17.71 ± 3.39 μm vs. 20.03 ± 4.61 μm, p = 0.004, Welch's two-tailed t-test). There was no difference in AIS location along the tonotopic axis (5.29 ± 4.15 μm, n = 37 medial vs. 6.48 ± 4.01 μm, n = 32 lateral neurons, p = 0.23, Student's t-test; **Figure 3B**).

Next, we examined whether the tonotopic differentiation in the intrinsic properties of MNTB neurons is present in WT and *BDNF*$^{+/-}$ mice at pre-hearing age (**Figure 3C**). In the whole-cell recording, membrane capacitance did not differ between genotypes in the same position along the tonotopic axis at P9 (**Figure 3D**). At P9 before hearing onset, the AP threshold was not tonotopically different in WT neurons. However, in *BDNF*$^{+/-}$, lateral neurons showed a higher threshold than medial neurons (**Figure 3E**). AP threshold was not tonotopically organized in WT mice (p = 0.87), but *BDNF*$^{+/-}$ neurons have a tonotopic difference of AP threshold (p = 0.01, Welch's two-tailed t-test). Similar to WT, there was no significant difference in AP amplitude between lateral and medial neurons in *BDNF*$^{+/-}$ mice (lateral: 68.97 ± 6.69 mV and medial: 70.53 ± 5.75 mV, p = 0.52, Student's t-test). There was no significant difference in AP amplitude between lateral and medial neurons in WT mice (lateral: 68.25 ± 12 mV and medial: 68.98 ± 5.85 mV, p = 0.87, Welch's test). *BDNF*$^{+/-}$ and WT neurons had similar input resistance within the same tonotopic location paralleling the P21 results (**Figure 3E**). Taken together, MNTB neurons from pre-hearing *BDNF*$^{+/-}$ mice showed tonotopic differences in AIS length and AP threshold. As opposed to unlike in WT mice. However, this tonotopic differentiation did not persist through postnatal development and disappeared after hearing onset (at P21). It suggests that BDNF level may contribute to setting intrinsic properties of MNTB neurons before hearing onset when spontaneous cochlear activity is dominant in the immature auditory system.

BDNF Is Necessary for Enhanced Tonotopic Refinement Induced by the Sound Augmented Environment

After hearing onset, sound deprivation and enhancement modify structural properties of MNTB neurons during development, and specifically, sound stimulation enhances the tonotopic differences of AIS structure (Kim et al., 2019). We hypothesized that sound stimulation increases BDNF expression which enhances the structural and physiological plasticity of MNTB neurons. Sound stimulation has been shown to increase BDNF transcript and protein levels in the brainstem (Wang et al., 2011; Matt et al., 2018). In WT mice, sound stimulation (80 dB, 16 kHz, 3 h/day) from P13 to P19 increased mature BDNF protein by 25%, but not pro-BDNF, in the auditory brainstem (mature BDNF: p = 0.02, Welch's t-test, n = 3 per group; pro-BDNF: p = 0.40, Welch's t-test, n = 4/group; **Figure 4A**). We examined whether increased endogenous BDNF by sound stimulation rescues the lack of tonotopic differentiation of AIS structure in *BDNF*$^{+/-}$ mice. In *BDNF*$^{+/-}$ mice, which were exposed to the additional sound stimulation (subsequently named *BDNF*$^{+/-}$ + Sound mice), AIS distance from the soma was 6.51 ± 2.21 μm in medial and 6.8 ± 2.20 μm in lateral neurons (n = 36 and 34 cells respectively, p = 0.58, Student's t-test; **Figures 4B,C**). AIS length of medial neurons was 15.72 ± 2.24 μm and the length of lateral neurons was 15.58 ± 2.15 μm. AIS length did not differ along the tonotopic axis in *BDNF*$^{+/-}$ + Sound mice (n = 35 and 33 cells respectively, p = 0.79, Mann-Whitney U test; **Figure 4C**). The tonotopic difference in soma size was not observed in *BDNF*$^{+/-}$ + Sound mice (**Figure 4C**). The result demonstrated that augmented sound inputs could not rescue the alterations in AIS structural properties of MNTB neurons caused by global BDNF reduction in *BDNF*$^{+/-}$ mice.

Next, we examined the physiological properties of MNTB neurons in *BDNF*$^{+/-}$ mice following sound stimulation. Phasic plotting the dV/dt of APs from MNTB neurons demonstrated no difference in AP threshold or amplitude between medial and lateral neurons in *BDNF*$^{+/-}$ + Sound (**Figures 4D,E**). Increased sound input did not induce tonotopic differentiation

of neuronal properties in $BDNF^{+/-}$ mice. Although exposed to sound stimulation, lack of tonotopic differentiation of AP threshold was maintained in $BDNF^{+/-}$ + Sound mice (medial: -45.37 ± 5.75 mV and lateral: -43.98 ± 3.62 mV, $p = 0.47$, Student's *t*-test; **Figure 4E**). No significant tonotopic difference was found in AP amplitude or input resistance in $BDNF^{+/-}$ + Sound animals ($p = 0.67$, Student's *t*-test; **Figure 4E**) like $BDNF^{+/-}$ animals. $BDNF^{+/-}$ mice were unable to establish MNTB tonotopic gradients of intrinsic or structural properties even when exposed to an augmented sound input during the critical period of development. Mice with BDNF reduction were unable to properly respond to changes in sound-evoked activity, indicating that BDNF is a key molecule for activity-dependent structural and physiological plasticity of auditory brainstem neurons.

$BDNF^{+/-}$ Mice Lack Frequency-Responsiveness of Neurons and Show an Impaired Tonotopy in the MNTB

Tonotopy describes a topographic organization of frequency-responsiveness of neurons within each auditory nucleus. To examine if BDNF reduction and associated structural and physiological alterations affect the tonotopy of MNTB neurons, we assessed neuronal activity of MNTB neurons in response to a high frequency tone sound (16 kHz, 90 min, 80 dB) using *c-fos*, an early response gene, immunostaining (Karmakar et al., 2017; Kim et al., 2019; **Figure 5A**). The expression of c-Fos in the MNTB in response to 16 kHz tone was different between WT and $BDNF^{+/-}$ mice. In WT mice, c-Fos positive neurons (c-Fos$^+$ and MAP2$^+$) were mostly located in the medial MNTB, forming a clear band of 16 kHz sound-sensitive neurons, in concordance with high frequency responding neurons residing in the medial portion of the MNTB (Kandler et al., 2009). However, in $BDNF^{+/-}$ mice, c-Fos$^+$ cells were widely spread out across the MNTB without a distinct band-like expression (**Figures 5B,C**). The distribution analysis for c-Fos$^+$ neurons along the tonotopic axis showed the expression of c-Fos in response to 16 kHz sound was specifically concentrated on the medial MNTB from WT mice, but not in $BDNF^{+/-}$ mice: 0% indicating most medial MNTB position and 100% indicating most lateral MNTB position (WT: 32.36% and $BDNF^{+/-}$: 50.21%; $p < 0.0001$, Mann-Whitney U test; **Figure 5D**). The MNTB from $BDNF^{+/-}$ mice lack frequency-responsiveness of neurons to 16 kHz sound stimulation, indicating an impaired tonotopy of the MNTB within the auditory brainstem.

To examine neuronal activation in response to 16 kHz sound, we quantified the percentage of c-Fos$^+$ neurons (c-Fos$^+$ and MAP2$^+$ cell #/MAP2$^+$ cell # *100) within the MNTB between genotypes. In response to 16 kHz tone, the percentage of c-Fos$^+$ cells was significantly higher in $BDNF^{+/-}$ mice compared to WT ($n = 5$ and 3, respectively; $p = 0.018$, Welch's *t*-test; **Figure 5E**), indicating that more MNTB neurons were responsive to the 16 kHz tone sound regardless of their location. The result paralleled physiological properties showing an increased excitability of MNTB neurons in $BDNF^{+/-}$ mice (**Figure 2E**). Taken together, $BDNF^{+/-}$ mice had hyperexcitable MNTB neurons and disorganized isofrequency bands based on the spatial organization of neural activity in response to high frequency sound.

DISCUSSION

The results demonstrated the role of BDNF in the structural and physiological refinement of MNTB neurons along the mediolateral tonotopic axis using a $BDNF^{+/-}$ mouse. Our study is the first *ex vivo* investigation of AIS plasticity with a global reduction of BDNF, which allows us to maintain circuit connections within a sensory system dependent on peripheral inputs. Tonotopy, a driving organization principle of the auditory system, relies on not only sound input but also BDNF signaling to establish proper gradients within the auditory brainstem and ensure precise binaural processing.

Role of BDNF in the Structural Development of the MNTB

BDNF is an important neurotrophic factor for neural development in an activity-dependent manner, whether that is driven by peripheral inputs or spontaneous activity (Kuczewski et al., 2008; Jiao et al., 2011). We addressed the impact of global BDNF reduction on the structural and physiological refinement of the AIS in a sound input-dependent manner in mature MNTB neurons (at P20) and in a sound input-independent manner in immature neurons in the pre-hearing stage (at P9). Previous works show that tonotopic gradients of K_V channel expression and currents require sound input since pre-hearing and congenitally deaf animals do not possess these gradients (von Hehn et al., 2004; Leao et al., 2006; Kim et al., 2019). BDNF is a molecular mediator of neural activity-dependent plasticity shown in LTP of the hippocampus CA1 synapse (Korte et al., 1995; Patterson et al., 1996) and the visual cortex (Akaneya et al., 1997; Huber et al., 1998), as well as structural plasticity of myelin following increased sound input in humans and rats (Bengtsson et al., 2005; de Villers-Sidani et al., 2010). Within the auditory system, BDNF expression is dependent on sound-evoked activity shown with increased BDNF transcript and protein levels in the brainstem following sound stimulation (Wang et al., 2011; Matt et al., 2018). Here we found that at a pre-hearing age when peripheral sound input is not involved in recruiting BDNF, a global reduction of BDNF alters the AIS location of MNTB neurons and abnormally promotes tonotopic differences of AIS length and AP threshold. As opposite to WT mice, tonotopic gradients are present at P9 in $BDNF^{+/-}$ that are completely abolished by P21. BDNF reduction appears to have disparate effects on tonotopic refinement pre-hearing compared to post-hearing onset, although the underlying mechanism of the disparate effects is not understood. It is known that spontaneous activity driven by supporting cells in the cochlea occurs before hearing onset and allows for intrinsic sound-independent activity throughout the auditory pathway (Sonntag et al., 2009; Babola et al., 2018). Detectable levels of BDNF are present in the brainstem by P6, and spontaneous firing from brainstem neurons drives activity-dependent expression of BDNF before

hearing onset (Hafidi, 1999). Thus, the differences were seen in AIS structure between WT and $BDNF^{+/-}$ mice before hearing onset could be due to the discrepancy of spontaneous activity between genotypes. BDNF effects on spontaneous activity in pre-hearing age and sound-evoked activity in post-hearing age might be different during development. In the condition with reduced BDNF, spontaneous activity may play a compensatory role in setting intrinsic properties of MNTB neurons, but when switching from spontaneous to sound-evoked activity after hearing onset, this compensatory effect may disappear. It would be worthy to test this hypothesis in future studies.

BDNF Modulates the Neuronal Activity of MNTB Neurons

The effects of BDNF on neuronal excitability are variable and there are different acute vs. chronic effects. In $BDNF^{+/-}$ mice, chronically reduced BDNF levels decreased neuronal activity of pyramidal neurons in the entorhinal cortex (Abidin et al., 2019). We found that regardless of tonotopic location, MNTB neurons from $BDNF^{+/-}$ mice showed a hyperexcitability in response to depolarizing current injection and increased neuronal activity in response to high frequency tone exposure compared to WT littermates. Interestingly, an overall increase of neuronal activity was observed, but the tonotopy of the auditory brainstem has been impaired in $BDNF^{+/-}$ mice. *In vitro* administration of BDNF increased cell excitability in cultured hippocampal and sensory neurons (Zhang et al., 2008; Guo et al., 2017), but bath perfusion of BDNF reduced excitability of interneurons in the dentate gyrus (Holm et al., 2009; Nieto-Gonzalez and Jensen, 2013). The variable response to BDNF administration might be due to varied ion channel expression, which is influenced by BDNF signaling, across different brain regions.

Physiological Relevance

How does the disruption of the tonotopic arrangement of neuronal properties impact auditory function? Several genetically modified mice lacking tonotopic gradients of neuronal structure display auditory function abnormalities. CXCR1 mutant mice, which have disrupted microglia-neuron communication, lacked the soma size tonotopic gradient observed in WT mice and had longer peak latencies of the auditory brainstem responses (ABRs) with the normal threshold of ABRs (Milinkeviciute et al., 2021). Ephrin-A3 mutants, which lack a key axon guidance signaling factor, have degraded frequency-responsiveness tonotopy within the cochlear nucleus. These mice have deficits in signal conduction and frequency discrimination with a normal hearing threshold (Hoshino et al., 2021). Outside of genetic modifications, aging disrupts precise tonotopic organization from the cochlear nucleus to the auditory cortex as hearing function degrades (Caspary et al., 2005; de Villers-Sidani et al., 2010). It appears that sound input is required to establish and maintain tonotopy, which is required to maintain proper auditory processing. Thus, it is worthy to further examine whether $BDNF^{+/-}$ mice lacking tonotopy of MNTB neurons along the mediolateral axis have auditory processing deficits.

DATA AVAILABILITY STATEMENT

The raw data supporting the conclusions of this article will be made available by the authors, without undue reservation.

ETHICS STATEMENT

The animal study was reviewed and approved by the UT Health San Antonio Institutional Animal Care and Use Committee.

AUTHOR CONTRIBUTIONS

MW and JK contributed to the conception and design of the study. MW collected and analyzed the data. All authors contributed to the article and approved the submitted version.

FUNDING

This work was supported by a grant from the National Institute on Deafness and Other Communication Disorders (NIDCD; R01 DC018797) to JK and a pre-doctoral grant from the Biology of Aging Department at UT Health San Antonio (T32-AG021890-18) to MW.

ACKNOWLEDGMENTS

We would like to thank Dr. Manzoor Bhat for providing the β4-spectrin primary antibody. We also thank Drs. Eun Jung Kim and Elizabeth Gould for providing technical assistance. Confocal images were generated in the Core Optical Imaging Facility, which is supported by UT Health San Antonio and NIH-NCI P30 CA54174.

REFERENCES

Abidin, İ., Aydin-Abidin, S., and Mittmann, T. (2019). Neuronal excitability and spontaneous synaptic transmission in the entorhinal cortex of BDNF heterozygous mice. *Neurosci. Lett.* 690, 69–75. doi: 10.1016/j.neulet.2018.10.019

Akaneya, Y., Tsumoto, T., Kinoshita, S., and Hatanaka, H. (1997). Brain-derived neurotrophic factor enhances long-term potentiation in rat visual cortex. *J. Neurosci.* 17, 6707–6716. doi: 10.1523/JNEUROSCI.17-17-06707.1997

Akter, N., Adachi, R., Kato, A., Fukaya, R., and Kuba, H. (2018). Auditory input shapes tonotopic differentiation of Kv1.1 expression in avian cochlear nucleus during late development. *J. Neurosci.* 38, 2967–2980. doi: 10.1523/JNEUROSCI.2472-17.2018

Anomal, R., de Villers-Sidani, E., Merzenich, M. M., and Panizzutti, R. (2013). Manipulation of BDNF signaling modifies the experience-dependent plasticity induced by pure tone exposure during the critical period in the primary auditory cortex. *PLoS One* 8:e64208. doi: 10.1371/journal.pone.0064208

Babola, T. A., Li, S., Gribizis, A., Lee, B. J., Issa, J. B., Wang, H. C., et al. (2018). Homeostatic control of spontaneous activity in the developing auditory system. *Neuron* 99, 511–524.e5. doi: 10.1016/j.neuron.2018.07.004

Bengtsson, S. L., Nagy, Z., Skare, S., Forsman, L., Forssberg, H., and Ullén, F. (2005). Extensive piano practicing has regionally specific effects on white matter development. *Nat. Neurosci.* 8, 1148–1150. doi: 10.1038/nn1516

Caspary, D. M., Schatteman, T. A., and Hughes, L. F. (2005). Age-related changes in the inhibitory response properties of dorsal cochlear nucleus

output neurons: role of inhibitory inputs. *J. Neurosci.* 25, 10952–10959. doi: 10.1523/JNEUROSCI.2451-05.2005

de Villers-Sidani, E., Alzghoul, L., Zhou, X., Simpson, K. L., Lin, R. C., and Merzenich, M. M. (2010). Recovery of functional and structural age-related changes in the rat primary auditory cortex with operant training. *Proc. Natl. Acad. Sci. U S A* 107, 13900–13905. doi: 10.1073/pnas.1007885107

Grubb, M. S., and Burrone, J. (2010). Activity-dependent relocation of the axon initial segment fine-tunes neuronal excitability. *Nature* 465, 1070–1074. doi: 10.1038/nature09160

Guo, Y., Su, Z. J., Chen, Y. K., and Chai, Z. (2017). Brain-derived neurotrophic factor/neurotrophin 3 regulate axon initial segment location and affect neuronal excitability in cultured hippocampal neurons. *J. Neurochem.* 142, 260–271. doi: 10.1111/jnc.14050

Hafidi, A. (1999). Distribution of BDNF, NT-3 and NT-4 in the developing auditory brainstem. *Int. J. Dev. Neurosci.* 17, 285–294. doi: 10.1016/s0736-5748(99)00043-x

Holm, M. M., Nieto-Gonzalez, J. L., Vardya, I., Vaegter, C. B., Nykjaer, A., and Jensen, K. (2009). Mature BDNF, but not proBDNF, reduces excitability of fast-spiking interneurons in mouse dentate gyrus. *J. Neurosci.* 29, 12412–12418. doi: 10.1523/JNEUROSCI.2978-09.2009

Hoshino, N., Altarshan, Y., Alzein, A., Fernando, A. M., Nguyen, H. T., Majewski, E. F., et al. (2021). Ephrin-A3 is required for tonotopic map precision and auditory functions in the mouse auditory brainstem. *J. Comp. Neurol.* 529, 3633–3654. doi: 10.1002/cne.25213

Huber, K. M., Sawtell, N. B., and Bear, M. F. (1998). Brain-derived neurotrophic factor alters the synaptic modification threshold in visual cortex. *Neuropharmacology* 37, 571–579. doi: 10.1016/s0028-3908(98)00050-1

Jiao, Y., Zhang, Z., Zhang, C., Wang, X., Sakata, K., Lu, B., et al. (2011). A key mechanism underlying sensory experience-dependent maturation of neocortical GABAergic circuits *in vivo*. *Proc. Natl. Acad. Sci. U S A* 108, 12131–12136. doi: 10.1073/pnas.1105296108

Kandler, K., Clause, A., and Noh, J. (2009). Tonotopic reorganization of developing auditory brainstem circuits. *Nat. Neurosci.* 12, 711–717. doi: 10.1038/nn.2332

Karmakar, K., Narita, Y., Fadok, J., Ducret, S., Loche, A., Kitazawa, T., et al. (2017). Hox2 genes are required for tonotopic map precision and sound discrimination in the mouse auditory brainstem. *Cell Rep.* 18, 185–197. doi: 10.1016/j.celrep.2016.12.021

Kim, E. J., Feng, C., Santamaria, F., and Kim, J. H. (2019). Impact of auditory experience on the structural plasticity of the AIS in the mouse brainstem throughout the lifespan. *Front. Cell. Neurosci.* 13:456. doi: 10.3389/fncel.2019.00456

Korte, M., Carroll, P., Wolf, E., Brem, G., Thoenen, H., and Bonhoeffer, T. (1995). Hippocampal long-term potentiation is impaired in mice lacking brain-derived neurotrophic factor. *Proc. Natl. Acad. Sci. U S A* 92, 8856–8860. doi: 10.1073/pnas.92.19.8856

Kuba, H., Oichi, Y., and Ohmori, H. (2010). Presynaptic activity regulates Na(+) channel distribution at the axon initial segment. *Nature* 465, 1075–1078. doi: 10.1038/nature09087

Kuba, H., Adachi, R., and Ohmori, H. (2014). Activity-dependent and activity-independent development of the axon initial segment. *J. Neurosci.* 34, 3443–3453. doi: 10.1523/JNEUROSCI.4357-13.2014

Kuba, H., Ishii, T., and Ohmori, H. (2006). Axonal site of spike initiation enhances auditory coincidence detection. *Nature* 444, 1069–1072. doi: 10.1038/nature05347

Kuczewski, N., Langlois, A., Fiorentino, H., Bonnet, S., Marissal, T., Diabira, D., et al. (2008). Spontaneous glutamatergic activity induces a BDNF-dependent potentiation of GABAergic synapses in the newborn rat hippocampus. *J. Physiol.* 586, 5119–5128. doi: 10.1113/jphysiol.2008.158550

Leao, R. N., Sun, H., Svahn, K., Berntson, A., Youssoufian, M., Paolini, A. G., et al. (2006). Topographic organization in the auditory brainstem of juvenile mice is disrupted in congenital deafness. *J. Physiol.* 571, 563–578. doi: 10.1113/jphysiol.2005.098780

Li, W., Kaczmarek, L. K., and Perney, T. M. (2001). , Localization of two high-threshold potassium channel subunits in the rat central auditory system. *J. Comp. Neurol.* 437, 196–218. doi: 10.1002/cne.1279

Matt, L., Eckert, P., Panford-Walsh, R., Geisler, H. S., Bausch, A. E., Manthey, M., et al. (2018). Visualizing BDNF transcript usage during sound-induced memory linked plasticity. *Front. Mol. Neurosci.* 11:260. doi: 10.3389/fnmol.2018.00260

Milinkeviciute, G., Chokr, S. M., Castro, E. M., and Cramer, K. S. (2021). CX3CR1 mutation alters synaptic and astrocytic protein expression, topographic gradients and response latencies in the auditory brainstem. *J. Comp. Neurol.* 529, 3076–3097. doi: 10.1002/cne.25150

Nieto-Gonzalez, J. L., and Jensen, K. (2013). BDNF depresses excitability of parvalbumin-positive interneurons through an M-like current in rat dentate gyrus. *PLoS One* 8:e67318. doi: 10.1371/journal.pone.0067318

Parameshwaran, S., Carr, C. E., and Perney, T. M. (2001). Expression of the Kv3.1 potassium channel in the avian auditory brainstem. *J. Neurosci.* 21, 485–494. doi: 10.1523/JNEUROSCI.21-02-00485.2001

Patterson, S. L., Abel, T., Deuel, T. A., Martin, K. C., Rose, J. C., and Kandel, E. R. (1996). Recombinant BDNF rescues deficits in basal synaptic transmission and hippocampal LTP in BDNF knockout mice. *Neuron* 16, 1137–1145. doi: 10.1016/s0896-6273(00)80140-3

Schimmang, T., Tan, J., Müller, M., Zimmermann, U., Rohbock, K., Köpschall, I., et al. (2003). Lack of Bdnf and TrkB signalling in the postnatal cochlea leads to a spatial reshaping of innervation along the tonotopic axis and hearing loss. *Development* 130, 4741–4750. doi: 10.1242/dev.00676

Sonntag, M., Englitz, B., Kopp-Scheinpflug, C., and Rübsamen, R. (2009). Early postnatal development of spontaneous and acoustically evoked discharge activity of principal cells of the medial nucleus of the trapezoid body: an *in vivo* study in mice. *J. Neurosci.* 29, 9510–9520. doi: 10.1523/JNEUROSCI.1377-09.2009

von Hehn, C. A., Bhattacharjee, A., and Kaczmarek, L. K. (2004). Loss of Kv3.1 tonotopicity and alterations in cAMP response element-binding protein signaling in central auditory neurons of hearing impaired mice. *J. Neurosci.* 24, 1936–1940. doi: 10.1523/JNEUROSCI.4554-03.2004

Wang, H., Brozoski, T. J., Ling, L., Hughes, L. F., and Caspary, D. M. (2011). Impact of sound exposure and aging on brain-derived neurotrophic factor and tyrosine kinase B receptors levels in dorsal cochlear nucleus 80 days following sound exposure. *Neuroscience* 172, 453–459. doi: 10.1016/j.neuroscience.2010.10.056

Weatherstone, J. H., Kopp-Scheinpflug, C., Pilati, N., Wang, Y., Forsythe, I. D., Rubel, E. W., et al. (2017). Maintenance of neuronal size gradient in MNTB requires sound-evoked activity. *J. Neurophysiol.* 117, 756–766. doi: 10.1152/jn.00528.2016

Wiechers, B., Gestwa, G., Mack, A., Carroll, P., Zenner, H. P., and Knipper, M. (1999). A changing pattern of brain-derived neurotrophic factor expression correlates with the rearrangement of fibers during cochlear development of rats and mice. *J. Neurosci.* 19, 3033–3042. doi: 10.1523/JNEUROSCI.19-08-03033.1999

Zhang, Y. H., Chi, X. X., and Nicol, G. D. (2008). Brain-derived neurotrophic factor enhances the excitability of rat sensory neurons through activation of the p75 neurotrophin receptor and the sphingomyelin pathway. *J. physiol.* 586, 3113–3127. doi: 10.1113/jphysiol.2008.152439

Conflict of Interest: The authors declare that the research was conducted in the absence of any commercial or financial relationships that could be construed as a potential conflict of interest.

Publisher's Note: All claims expressed in this article are solely those of the authors and do not necessarily represent those of their affiliated organizations, or those of the publisher, the editors and the reviewers. Any product that may be evaluated in this article, or claim that may be made by its manufacturer, is not guaranteed or endorsed by the publisher.

Advantages of publishing in Frontiers

OPEN ACCESS
Articles are free to read for greatest visibility and readership

FAST PUBLICATION
Around 90 days from submission to decision

HIGH QUALITY PEER-REVIEW
Rigorous, collaborative, and constructive peer-review

TRANSPARENT PEER-REVIEW
Editors and reviewers acknowledged by name on published articles

Frontiers
Avenue du Tribunal-Fédéral 34
1005 Lausanne | Switzerland

Visit us: www.frontiersin.org
Contact us: frontiersin.org/about/contact

REPRODUCIBILITY OF RESEARCH
Support open data and methods to enhance research reproducibility

DIGITAL PUBLISHING
Articles designed for optimal readership across devices

FOLLOW US
@frontiersin

IMPACT METRICS
Advanced article metrics track visibility across digital media

EXTENSIVE PROMOTION
Marketing and promotion of impactful research

LOOP RESEARCH NETWORK
Our network increases your article's readership